

# Multiplicity Dependence of $\sigma_{\psi(2S)} / \sigma_{J/\psi}$ in $pp$ collision at $\sqrt{s} = 13$ TeV

Xianglei Zhu, Youen Kang, Li Xu, Chenzhi Dong.

*Tsinghua University*

## Abstract

Using a data sample with an integrated Luminosity of  $658 \text{ pb}^{-1}$  collected by the LHCb detector in the LHC operations in 2016, ratio of production cross section of  $\psi(2S)$  over  $J/\psi$  as a function of multiplicity was measured in proton-proton collisions at a centre-of-mass energy  $\sqrt{s} = 13$  TeV. A multiplicity-dependent modification of the ratio has been observed for prompt mesons when there is an overlap between the rapidity ranges where the multiplicity and the charmonia production are measured. No evident modification of same significance of that of prompt component was found for the mesons from  $b$ -hadron decay. Further calculations of different models needed to specify the sources of preferential suppression for  $\psi(2S)$ .



# 1 Contents

2	1 Introduction	2
3	2 Data and Monte Carlo samples	3
4	2.1 Data . . . . .	3
5	2.2 Monte Carlo . . . . .	3
6	3 Candidate Reconstruction and selection	4
7	3.1 Trigger and Turbo stream selection . . . . .	4
8	3.2 Offline Selection . . . . .	4
9	4 Ratio of Cross-Section Determination	7
10	4.1 Double Differential Cross-Section . . . . .	7
11	4.2 Ratio of Cross-Section . . . . .	8
12	5 Signal Extraction	9
13	5.1 Determination of the prompt and detached signal yields . . . . .	9
14	6 Efficiency determination	13
15	6.1 Geometrical acceptance . . . . .	14
16	6.2 Reconstruction-selection efficiency . . . . .	15
17	6.3 Muon identification efficiency . . . . .	17
18	6.4 Trigger efficiency . . . . .	19
19	6.5 Total efficiency . . . . .	19
20	6.6 Variation due do different reweight samples . . . . .	20
21	7 Systematic Uncertainties	21
22	7.1 Signal extraction . . . . .	22
23	7.1.1 Signal mass shape . . . . .	22
24	7.1.2 Fit to $t_z$ background . . . . .	23
25	7.1.3 Fit to $t_z$ signal . . . . .	24
26	7.2 Trigger efficiency . . . . .	24
27	7.3 Tracking efficiency . . . . .	26
28	7.4 MuonID efficiency . . . . .	27
29	7.5 MC sample size . . . . .	29
30	7.6 Other systematic uncertainties . . . . .	29
31	8 Bin Width Correction	30
32	9 Results	31
33	9.1 $\psi(2S)$ -to- $J/\psi$ ratio as functions of multiplicity . . . . .	31
34	9.2 $\psi(2S)$ -to- $J/\psi$ ratio in different $p_T$ regions . . . . .	33
35	9.3 $\psi(2S)$ -to- $J/\psi$ ratio in different $y$ regions . . . . .	35
36	10 Conclusion	37
37	References	173

# 38 1 Introduction

39 In normal matter, quarks and gluons are confined within particles called hadrons, such  
40 as protons and neutrons. However, at extremely high temperatures and densities, such  
41 as those that existed shortly after the Big Bang or in high-energy particle collisions, the  
42 strong force that binds quarks and gluons together becomes weaker. It results in the  
43 creation of a new form of matter Quark Gluon Plasma (QGP) in which the partons are  
44 evolving quasi freely. The measurement of quarkonia suppression is considered a probe of  
45 QGP. In such a hot and dense state, the existence of a large density of free color charges  
46 will lead to a color screening of quark and anti-quark binding, hence, the dissociation of  
47 quarkonium [1].

48 But before we interpret any phenomena observed in hot, dense QCD matter, baseline  
49 measurements need to be performed in the small system such as  $pp$  collisions in which  
50 no QGP is in principle produced. With the increasing charged-particle multiplicity, a  
51 transition from normal density to a relatively high-density environment serves as a probe  
52 for how quarkonium production suppression is affected by the charged particle multiplicity.

53 Quarkonia suppression can be detected by measuring nuclear modification factors.  
54 This factor is computed by measuring the Quarkonia yield in heavy-ion collisions and  
55 compared to the yield in from  $pp$  collisions scaled by the number of nucleons. The PHENIX  
56 collaboration measured the nuclear modification factor of  $J/\psi$  in dAu collisions at 200  
57 GeV [2] and observed a significative suppression while no QGP production is expected.  
58 More recent results by LHCb also confirm this suppression [3] in the nuclear modification  
59 factor measured using  $p\text{Pb}$  collisions. However, this suppression can be explained by  
60 different effects such as quarkonia energy loss [4] or interaction with co-moving particles [5].  
61 The latter effect would affect quarkonia from two excited states differently, as they have  
62 different binding energy, and would have a stronger influence when the multiplicity of the  
63 collisions is high. The effect governing heavy quark production is expected to be similar  
64 for charmonium with the same content.

65 As we mentioned above, quarkonia suppressions in  $pp$  collisions have been traditionally  
66 served as a baseline measurement when searching QGP. While more and more signatures  
67 of QGP has been observed in small systems such as high-multiplicity  $pp$  collisions. For  
68 examples, ALICE collaboration has reported a measurement of strangeness enhancement  
69 in high-multiplicity  $pp$  collisions at  $\sqrt{s} = 7$  TeV [6] and CMS collaboration found a high  
70 degree of collectivity flow in high-multiplicity  $pp$  collisions at  $\sqrt{s} = 13$  TeV [7]. The  
71 possible existence of QGP in high-multiplicity  $pp$  collisions could also have an effect on  
72 the suppressions of charmonia since color Debye Screening effect will prevent quark from  
73 forming a quarkonium with an anti-quark. Quarkonia with same content but different  
74 energy levels may dissociate at different temperatures. Those with higher energy levels  
75 have a weaker bound will dissociate first compared to the lower-levels in QGP, which  
76 will cause a similar effect on the ratio of  $\sigma_{\psi(2S)}/\sigma_{J/\psi}$ . Hence, a further calculation from  
77 co-mover model prediction is needed to verify the sources of different suppressions, if exist.

78 The analysis proceeds as follows: Samples of  $J/\psi$  and  $\psi(2S)$  are selected from 13 TeV  
79  $pp$  collisions data collected in 2016, by fitting the invariant mass spectrum of oppositely  
80 charged muons. Prompt and non-prompt components are separated by fitting the pseudo  
81 proper-time in multiple bins of multiplicity. Then the yields are corrected by the efficiencies  
82 from different sources. Then the ratio of production is calculated in each multiplicity  
83 bin to come to a final result. Three variables, PVNTRACKS, nForwardTracks and

84 nBackwardTracks, are used as proxy for the multiplicity of the  $pp$  collisions. PVNTRACKS  
85 is the number of tracks used to reconstruct the primary vertex, and nBackTracks is the  
86 number of tracks in the backward directions. PVNTRACKS is the global multiplicity of  
87 the  $pp$  collisions while nForwardTracks is the multiplicity measured in the same phase  
88 space as the two charmonia. Some correlations between the ratio and nForwardTracks  
89 can appear and due to that, the use of nBackTracks, allows to reduce this effect.

## 90 2 Data and Monte Carlo samples

### 91 2.1 Data

92 The study here uses  $pp$  collision data collected by the LHCb detector at a center-of-mass  
93 energy of 13 TeV in 2016 with a corresponding luminosity of  $658 \pm 13 \text{ pb}^{-1}$ . To enlarge  
94 the sample size, two different TCKs 0x1138160F and 0x11381612 of both MagUp and  
95 MagDown were used. In this analysis, only muon triggers are used, and both TCKs have  
96 identical criteria for muon selection. The bookkeeping paths for the mdst file for both  
97  $J/\psi$  and  $\psi(2S)$  are as follows:

- 98 • MagUp /LHCb/Collision16/Beam6500GeV-VeloClosed-MagUp/Real  
99 Data/Turbo03a/94000000/LEPTONS.MDST
- 100 • MagDown /LHCb/Collision16/Beam6500GeV-VeloClosed-MagDown/Real  
101 Data/Turbo03a/94000000/LEPTONS.MDST

### 102 2.2 Monte Carlo

103 To study the efficiency, full simulation Monte Carlo samples with about 20 M candidates  
104 for  $J/\psi$  and 10 M for  $\psi(2S)$ . The bookKeeping path for them are:

- 105 •  $J/\psi$ 
  - 106 – MagUp /MC/2016/24142001/Beam6500GeV-2016-MagUp-Nu1.6-25ns-  
107 Pythia8/Sim09b/Trig0x6138160F/Reco16/Turbo03/  
108 Stripping26NoPrescalingFlagged/ALLSTREAMS.DST
  - 109 – MagDown /MC/2016/24142001/Beam6500GeV-2016-MagDown-Nu1.6-25ns-  
110 Pythia8/Sim09b/Trig0x6138160F/Reco16/Turbo03/  
111 Stripping26NoPrescalingFlagged/ALLSTREAMS.DST
- 112 •  $\psi(2S)$ 
  - 113 – MagUp: /MC/2016/28142001/Beam6500GeV-2016-MagDown-Nu1.6-25ns-  
114 Pythia8/Sim09i/Trig0x6139160F/Reco16/Turbo03a/  
115 Stripping28r2NoPrescalingFlagged/ALLSTREAMS.DST
  - 116 – MagDown: /MC/2016/28142001/Beam6500GeV-2016-MagUp-Nu1.6-25ns-  
117 Pythia8/Sim09i/Trig0x6139160F/Reco16/Turbo03/  
118 Stripping28r2NoPrescalingFlagged/ALLSTREAMS.DST

In the simulation,  $pp$  collisions are generated using Pythia [8] with a specific LHCb configuration [9]. Decays of hadronic particles are described by EvtGen [10], in which final state radiation is generated using Photos [11]. The interaction of the generated particles with the detector and its response are implemented using the Geant4 toolkit [12] as described in Ref. [13]. The prompt charmonium production is simulated in Pythia with contributions from both the leading order color-singlet and color-octet mechanisms [9, 14], and the charmonium is generated without polarization. To study the geometrical acceptance, two samples of 100 k candidates generator level Monte Carlo are produced for both  $J/\psi$  and  $\psi(2S)$  respectively. Since the acceptance is only a function of kinematic variables, hence, it is universal for all multiplicity regions. Under the binning scheme in Sec 4, the sample size is fairly enough.

## 3 Candidate Reconstruction and selection

### 3.1 Trigger and Turbo stream selection

The reconstruction and preselection of  $J/\psi$  and  $\psi(2S)$  candidates for real data were based on the Turbo stream. The LHCb trigger system consists of three levels. The first level (L0) is designed to retain the instreaming data rate from detector read-outs up to 1 MHz, at which the LHC bunch crossing rate is 40 MHz. The L0-triggered data is input to the first stage of the software trigger (HLT1), which then performs a partial event reconstruction to filter out potentially signals of interest in the inflow data. The second stage of the software trigger (HLT2) performs a full event reconstruction to further remove backgrounds. This analysis is based on *L0Dimuon* and *Hlt1DiMuonHighMass* for both  $J/\psi$  and  $\psi(2S)$ . And *Hlt2DiMuonJPsiTrubo* for  $J/\psi$  and *Hlt2DiMuonPsi2STrubo* for  $\psi(2S)$ . The online selections for the trigger are summarized in Table 1 for both  $J/\psi$  and  $\psi(2S)$ .

Table 1: Summary of Trigger Lines

trigger line	main cuts
<i>L0Dimuon</i>	nSPDHits < 900
<i>Hlt1DiMuonHighMass</i>	track $p_T > 300$ MeV/ $c$ track $p > 6000$ MeV/ $c$ $M_{\mu^+\mu^-} > 2700$ MeV/ $c^2$ Muon ID: IsMuon
<i>Hlt2DiMuonJPsiTrubo</i> <i>Hlt2DiMuonPsi2STrubo</i>	$(3096.9 - 120)$ MeV/ $c < m_{J/\psi} < (3096.9 + 120)$ MeV/ $c$ $(3686.09 - 120)$ MeV/ $c < m_{J/\psi} < (3686.09 + 120)$ MeV/ $c$ track $\chi^2/\text{ndf} < 4$ vertex $\chi^2/\text{ndf} < 25$

141

### 3.2 Offline Selection

The offline selections are applied to both  $J/\psi$  and  $\psi(2S)$  candidates to reduce the combinatorial background to a reasonable level and ensure the good quality of the signal-extraction

fit. First, each event is required to have exactly one primary vertex (PV) reconstructed to avoid track contributions from multiple PVs that occur in the same beam crossing (pile-up).  $J/\psi$  and  $\psi(2S)$  candidates are formed from pairs of oppositely charged tracks reconstructed in the full tracking system (long tracks). We require the ghost probability for each track ( $\mu^+$  and  $\mu^-$ ) to be less than 0.3. Both two tracks must have a transverse momentum  $p_T$  above 1200 MeV/c, pass muon identification , and have a good quality of the track fit ( $\chi^2/\text{ndf} < 3$ ). The pseudo-rapidity of each muon is required to be in the range  $2.0 < \eta < 4.9$ . A Particle identification (PID) is performed to identify muon candidates ( $\text{DLLmu} > 2$ ). The two muons are required to form a good vertex by restricting the vertex fit quality  $\text{Prob}(\chi^2/\text{ndf}) > 0.5\%$ . The pseudo-proper time is defined as

$$t_z = \frac{(z_X - z_{\text{PV}}) \times m_X}{p_z}, \quad (1)$$

where  $X$  is  $J/\psi$  or  $\psi(2S)$ ,  $z_X$  is the z position of the decay vertex,  $z_{\text{PV}}$  that of the primary vertex,  $p_z$  the measured momentum along the beam axis z, and  $m_X$  the known mass for  $J/\psi$  and  $\psi(2S)$  [15]. This variable was found to give a good approximation of the b-hadron decay proper time: given that b-hadrons are not fully reconstructed, the momentums of  $J/\psi$  and  $\psi(2S)$  are used instead of the exact b-hadron momentum.  $t_z$  is calculated event by event with uncertainty no more than 0.3ps. In the analysis, it is required to be in the range  $-10 < t_z < 10$  ps. Prompt component and component-from-b can be separated by the different behaviors in the pseudo-proper time  $t_z$ . The full offline selection criteria are summarized in Table 2. The restriction of vertex  $\chi^2/\text{ndf} < 7.8794$  is chosen so that the

Table 2: Summary of Offline Selections

Quantity	Requirement
nPVs	= 1
$z_{\text{PV}}$	> -60 mm (for PVNTRACKS as multiplicity variable) > -30 mm (for nBackTracks as multiplicity variable)
vertex $\chi^2/\text{ndf}$	< 7.8794
mass window	$m_{J/\psi} \pm 120$ MeV/c $^2$ $m_{\psi(2S)} \pm 120$ MeV/c $^2$
PID	IsMuon, DLLmu > 2 probNNmu > 0.8
muon $\eta$	$2 < \eta < 4.9$
track ghost prob.	< 0.3
$t_z$	-10 ps < $t_z$ < 10 ps
$t_z$ uncertainty	< 0.3 ps

P-Value is exactly 0.005. For PID selection, we set  $\text{DLLmu} > 2$  to reduce combinatorial background for both  $J/\psi$  and  $\psi(2S)$ . And  $\text{probNNmu} > 0.8$  is further applied since it can largely reduce the combinatorial background for  $\psi(2S)$  at high multiplicity and low  $p_T$  bins. Here we restrict  $z_{\text{PV}}$  to be larger than -60 mm in order to maintain equivalent VELO acceptance. From Figure 1 we can see that for  $z_{\text{PV}} < -60$  mm (as indicated by the black, red, and green points), there is a clear deviation from the other curves toward

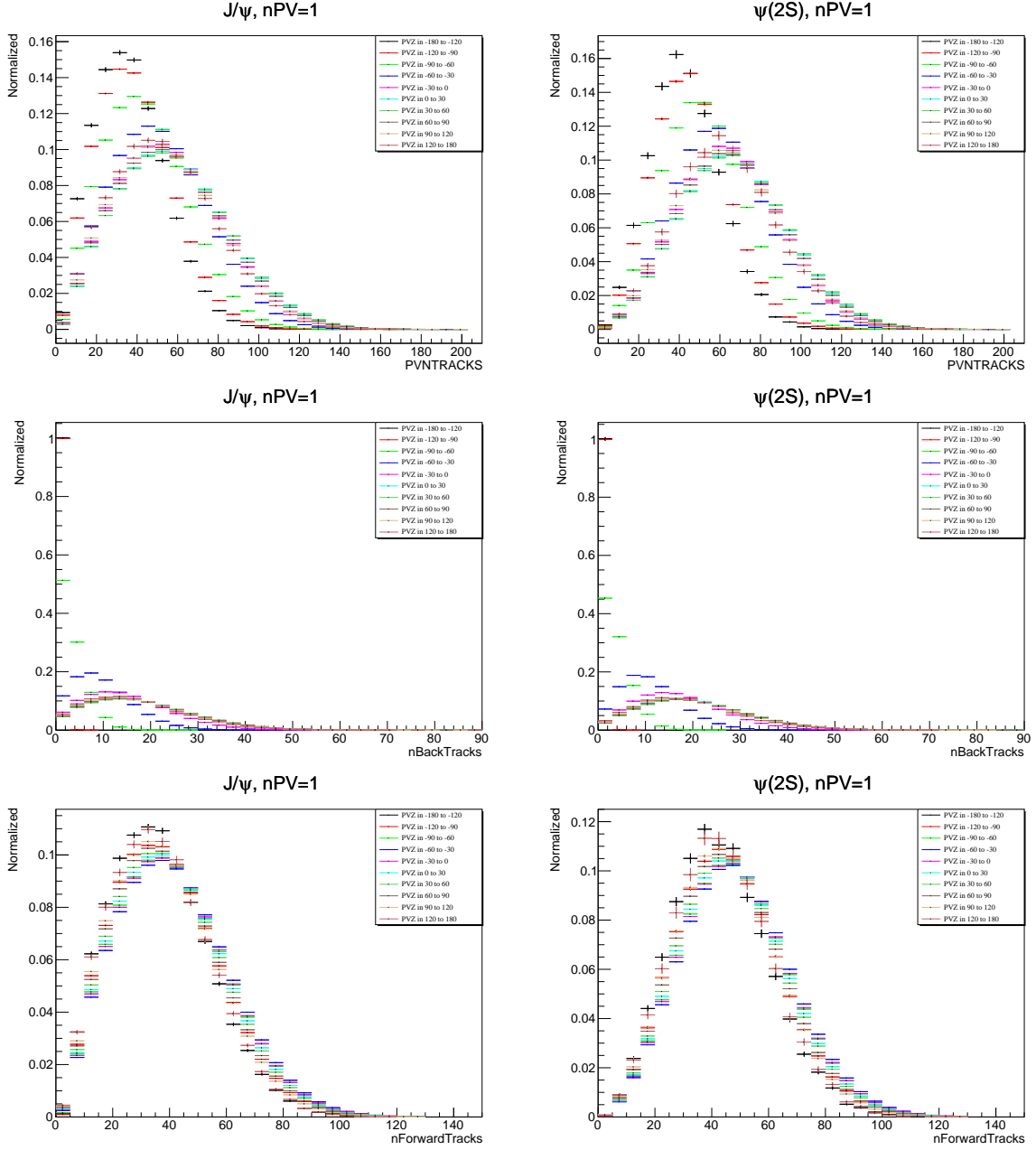


Figure 1: Distribution of PVNTRACKS, nBackTracks and nForwardTracks under  $nPVs = 1$  for  $J/\psi$  (left) and  $\psi(2S)$  (right). The clear deviation shows for  $z_{PV}$  smaller than a certain range so that we subtract that part of data for equivalence of VELO acceptance.

lower track multiplicity. This is due to events producing tracks that do not enter the VELO acceptance. Therefore, in this analysis, we restrict our primary vertex  $z$  range to  $z_{PV} > -60$  mm. If nBackTracks is used as multiplicity variables, the restriction is further modified to  $z_{PV} > -30$  mm, and no restriction needs to be made for nForwardTracks as multiplicity variable, which can be seen in Fig. 1.

## 175 4 Ratio of Cross-Section Determination

### 176 4.1 Double Differential Cross-Section

177 The determination of the double-differential production cross-section requires knowledge of  
 178 the numbers of prompt and non-prompt signals of  $J/\psi$  and  $\psi(2S)$  in bins of the kinematic  
 179 variables  $y$  and  $p_T$ , and multiplicity bin. This is done by performing a simultaneous fit  
 180 to the distributions of the dimuon invariant mass and the pseudo-proper time  $t_z$  in each  
 181 bin. The  $t_z$  of promptly produced signals has zero lifetime, while the  $t_z$  distribution for  
 182 the non-prompt signal is approximately exponential as seen from the simulation. The  
 183 pseudo-proper time  $t_z$  allows us to statistically separate the prompt signal from that  
 184 created in decays of b-hadrons. The double differential cross-section for prompt  $J/\psi$  and  
 185  $J/\psi$  from- $b$  production in a given ( $p_T$ ,  $y$ ) bin with multiplicity in a certain range is defined  
 186 as

$$\frac{d^2\sigma_{J/\psi}}{dydp_T} = \frac{N(J/\psi \rightarrow \mu^+\mu^-)}{\mathcal{L} \times \epsilon_{\text{tot}} \times \mathcal{B}(J/\psi \rightarrow \mu^+\mu^-) \times \Delta y \times \Delta p_T}. \quad (2)$$

187 And for  $\psi(2S)$

$$\frac{d^2\sigma_{\psi(2S)}}{dydp_T} = \frac{N(\psi(2S) \rightarrow \mu^+\mu^-)}{\mathcal{L} \times \epsilon_{\text{tot}} \times k \cdot \mathcal{B}(\psi(2S) \rightarrow e^+e^-) \times \Delta y \times \Delta p_T}. \quad (3)$$

188 where

- 189 •  $N$  is either the number of prompt  $\psi(2S)$  or  $\psi(2S)$  from  $b$ -hadron signals of  $J/\psi$  or  
 190  $\psi(2S)$  reconstructed through the dimuon decay channel. They are obtained by the  
 191 fits;
- 192 •  $\mathcal{L}$  is the integrated luminosity;
- 193 •  $\epsilon_{\text{tot}}$  is the total efficiency in that particular  $p_T - y$  bin with PVNTRACKS in a certain  
 194 range, for both prompt and non-prompt and both  $J/\psi$  and  $\psi(2S)$  respectively;
- 195 •  $k$  is the phase space factor which is assumed to be unit under the assumption of  
 196 lepton universality. The lepton universality is a reasonable assumption under the  
 197 current statistical precision;
- 198 •  $\mathcal{B}(J/\psi \rightarrow \mu^+\mu^-) = (5.961 \pm 0.033)\%$  is the branching fraction of the decay  $J/\psi \rightarrow$   
 199  $\mu^+\mu^-$ , quoted from the PDG 2022 review [15].
- 200 •  $\mathcal{B}(\psi(2S) \rightarrow e^+e^-) = (7.93 \pm 0.17) \times 10^{-3}$  is the branching fraction of the decay  
 201  $\psi(2S) \rightarrow e^+e^-$ , quoted from the PDG 2022 review [15]. The dielectron branching  
 202 fraction is used since it has a much smaller uncertainty than the dimuon one;
- 203 •  $\Delta p_T$  is the bin width of the transverse momentum;
- 204 •  $\Delta y$  is the bin width of the rapidity.

205 In the measurement of modification of  $b$  quark hadronization in high-multiplicity  $pp$   
 206 collision at  $\sqrt{s} = 13$  TeV shows that, ratio of cross sections  $\sigma_{B^0_s}/\sigma_{B^0}$  versus normalized  
 207 multiplicity behaves differently according to the choices of multiplicity variable [16]. That  
 208 motivates us to measure how the ratio changes with different multiplicity variables. The

following boundaries are used for the binning scheme of  $p_T$ ,  $y$  and different multiplicity variables. To remove the contribution from photon-production charmonium, we remove the production for  $p_T < 0.3 \text{ GeV}/c$ :

- $p_T$  boundaries [ GeV/c ]: 0.3, 2, 4, 6, 8, 20;
- $y$  boundaries: 2.0, 2.8, 3.5, 4.5;
- For multiplicity (each at a time)
  - PVNTRACKS: 4, 20, 45, 70, 95, 200. (At least 4 tracks required.)
  - nBackTracks: 0, 8, 15, 22, 30, 80.
  - nForwardTracks: 0, 12, 24, 36, 48, 130.

There is a wider bin in high  $p_T$  and multiplicity region, and the scheme of  $y$  is not exactly evenly distributed for the sake of significant signal numbers for fitting in each bin. And this binning scheme is common for both  $J/\psi$  and  $\psi(2S)$ . To see how charmonium suppression is affected by charged particle multiplicity, we normalize the ratio of production to see the trend. The multiplicity variables are normalized by their respective mean value from an unbiased data sample from the same year. Since the multiplicity distributions in high-energy hadron collisions is a KNO variable [17], which is, after normalized, the distribution of a certain collision system has the same distribution of a certain multiplicity variable. By scaling we change the multiplicity variable as a scale of how many times the mean number of charged particle multiplicity, so that the results are compatible with other results.

## 4.2 Ratio of Cross-Section

In each multiplicity region, we have defined the double differential cross-section in kinetic bin ( $p_T, y$ ) above. Then the ratio of double differential cross-section is determined as follows

$$\frac{\sigma(p_T, y)_{\psi(2S)}}{\sigma(p_T, y)_{J/\psi}} = \frac{N_{\psi(2S)}(p_T, y, )}{N_{J/\psi}(p_T, y, )} \times \frac{\epsilon_{\text{tot}, J/\psi}(p_T, y)}{\epsilon_{\text{tot}, \psi(2S)}(p_T, y)} \times \frac{\mathcal{B}_{J/\psi \rightarrow \mu^+ \mu^-}}{k \times \mathcal{B}_{\psi(2S) \rightarrow e^+ e^-}}, \quad (4)$$

where the bin widths for  $p_T$  and  $y$  are canceled out, so as the luminosity term. While when calculating the ratio of differential cross-section, the bin widths of  $p_T$  and  $y$  are no longer canceled out since the binning scheme is not uniform. Hence, the ratio of the cross-section is determined as follows,

$$\frac{\Sigma_{(p_T, y)} \sigma_{\psi(2S)}(p_T, y)}{\Sigma_{(p_T, y)} \sigma_{J/\psi}(p_T, y)} = \frac{\Sigma_{(p_T, y)} (\Delta p_T \times \Delta y \times N_{\psi(2S)}(p_T, y) / \epsilon_{\text{tot}, \psi(2S)}(p_T, y))}{\Sigma_{(p_T, y)} (\Delta p_T \times \Delta y \times N_{J/\psi}(p_T, y) / \epsilon_{\text{tot}, J/\psi}(p_T, y))} \times \frac{\mathcal{B}_{J/\psi \rightarrow \mu^+ \mu^-}}{k \times \mathcal{B}_{\psi(2S) \rightarrow e^+ e^-}}. \quad (5)$$

In a small kinetic bin, the efficiency  $\epsilon_{\text{tot}}$  is assumed to be constant, and thus a single number with corresponding uncertainty is provided. The efficiency for prompt non-prompt signals is calculated separately for  $J/\psi$  and  $\psi(2S)$ . And since our scheme is not significantly small, a re-weight in  $p_T$ - $y$  spectrum is performed when calculating the efficiency.

## 241 5 Signal Extraction

242 The total number of  $J/\psi$  and  $\psi(2S)$  signals is determined from an extended unbinned  
 243 maximum likelihood fit to the invariant mass distribution of the selected candidates. The  
 244 fit models for both  $J/\psi$  and  $\psi(2S)$  are the same, which we consider the previous studies of  
 245  $J/\psi$  production at 13 TeV [18] and  $\psi(2S)$  production at 13 TeV [19]. The only strategy  
 246 for both is as follows.

247 In the fit the component of the background is modelled with an exponential function

$$f_{\text{bkg}}(m) = a_0 e^{-p_0 \cdot m}. \quad (6)$$

248 The signal component is described by the sum of two Crystal Ball (CB) functions [20].

249 The CB function is defined as:

$$f_{\text{CB}}(m; \mu, \sigma, \alpha, n) = \begin{cases} \left(\frac{n}{|\alpha|}\right)^n e^{-\frac{1}{2}\alpha^2} \left(\frac{n}{|\alpha|} - |\alpha| - \frac{m-\mu}{\sigma}\right)^{-n} & \frac{m-\mu}{\sigma} < -|\alpha| \\ \exp\left(-\frac{1}{2}\left(\frac{m-\mu}{\sigma}\right)^2\right) & \frac{m-\mu}{\sigma} > -|\alpha|. \end{cases}, \quad (7)$$

250 which combines a Gaussian core (described by the parameters  $\mu$  and  $\sigma$ ) and one tail on  
 251 the left (described by the parameters  $\alpha$  and  $n$ ). The tails in CB functions are used to  
 252 model the radiative effects, which leads to more candidates with lower invariant masses.  
 253 Not all parameters of the CB functions are free when fitting data. Some parameters  
 254 are fixed or parameterized. For both  $J/\psi$  and  $\psi(2S)$ , the two CB functions share one  
 255 common mean value  $\mu$  and have different widths  $\sigma_1$  and  $\sigma_2$ , and  $\alpha$  is parameterized from  
 256 simulation as a function of the  $\sigma$ :  $\alpha = 2.066 \pm 0.0085\sigma - 0.00011\sigma^2$ , which applies to  
 257 both CB functions. Furthermore, for  $\psi(2S)$  only,  $\sigma_1$  and  $\sigma_2$  are parameterized as a linear  
 258 function:  $\sigma_2 = 25.7 + \sigma_1$  and the fraction of the narrower CB function is fixed at 0.96. For  
 259 the tail parameters,  $n$  is fixed to unity from physics [21]. Therefore, there are merely two  
 260 free parameters for the signal shape,  $\mu$  and  $\sigma_1$ . The strategy followed the previous study  
 261 of  $J/\psi$  and  $\psi(2S)$  production at 13 TeV [18, 19]. The invariant mass fit is performed in  
 262 each  $p_T - y$  and PVNTRACKS bin of the candidate.

### 263 5.1 Determination of the prompt and detached signal yields

264 To determine the signal yields of prompt and from- $b$  components separately, the  $t_z$   
 265 distribution is used. In each kinematic and multiplicity bin, an unbinned extended  
 266 maximum likelihood fit to the two-dimension distributions of invariant mass  $m(\mu^+\mu^-)$   
 267 and  $t_z$  is performed to separate prompt component from that from  $b$ .

268 At the generator level, the  $t_z$  distribution of the prompt component is a Dirac delta  
 269 function,  $\delta(t_z)$ , while that from  $b$  follows an exponential function as seen from simulation.  
 270 For  $J/\psi$  and  $\psi(2S)$  signals, the detector resolution is taken into account by convolving a  
 271 resolution function, which is described by the sum of two Gaussian functions,

$$f_{\text{resolution}}(t_z; \mu, S_1, S_2, \beta) = \frac{\beta}{\sqrt{2\pi}S_1\sigma} e^{-\frac{(t_z-\mu)^2}{2S_1^2\sigma^2}} + \frac{1-\beta}{\sqrt{2\pi}S_2\sigma} e^{-\frac{(t_z-\mu)^2}{2S_2^2\sigma^2}}. \quad (8)$$

272 The parameter  $\sigma$  is the event-by-event uncertainty of  $t_z$ , calculated by combining the esti-  
 273 mated uncertainties of the  $J/\psi$  and  $\psi(2S)$  decay vertex and the associated PV. Besides,  $S_1$

and  $S_2$  are two scale factors to correct the non-perfect estimation of the  $t_z$  uncertainty, the parameter  $\mu$  is the bias of the  $t_z$  measurement, and  $\beta$  is the fraction of one of the two Gaussians. In the fitting procedure, all the resolution parameters are floated. For some ( $p_T, y$ , PVNTRACKS) bin, the count for signal yield for  $\psi(2S)$  or  $J/\psi$  is significantly low that fit will fail for too many free parameters, and we may set  $\beta = 0$ , which is, only one Gaussian function is used to describe the resolution.

It is possible that the reconstructed candidate is associated with a "wrong" PV. This can happen either because the real PV that produces the candidate failed to be reconstructed, and the candidate was associated with the nearest reconstructed PV in the event, or because a wrong PV is accidentally close to the candidate. For the latter case, the positions of the reconstructed and the true PV are correlated, which results in a Gaussian-like  $t_z$  distribution with a width much larger than the detection resolution. This effect can be described by adding a third Gaussian with a much larger width than the resolution function. However, it is found from simulation that including the wide Gaussian in the resolution does not change the fitted parameters significantly because the fraction of this component is quite small,  $\leq 1\%$  as seen from studies in Ref. [18]. Therefore, the third wide Gaussian is not used in the fit function. For the former case that the true PV is not reconstructed, the true PV and wrongly associated PV are not correlated, which results in a long tail in the  $t_z$  distribution that can be modeled using the next-event method for both  $J/\psi$  and  $\psi(2S)$ . The next-event method is applied directly on data sample. The next-event pseudo-proper time,  $t_z^{\text{next}}$ , for each candidate, is calculated combining the candidate with the closest PV of another (next) event as

$$t_z^{\text{next}} = \frac{(z_{\mu\mu} - z_{\text{PV}}^{\text{next}}) \times m_{\mu\mu}}{p_z}, \quad (9)$$

where  $z_{\text{PV}}^{\text{next}}$  is the  $z$ -coordinate of the nearest PV of the next selected event. The tail distribution is extracted in each bin separately and not convolved with resolution functions since the distribution is much wider than the resolution and very smooth in the whole  $t_z$  region. It should be noted that since the requirement of PV reconstruction is loose, using at least 4 VELO tracks, the probability to reconstruct the true PV is very high ( $> 99\%$ ).

The candidates in the mass sidebands, where  $m_{\mu^+\mu^-}$  is at least 60 MeV/ $c$  away from the mass of  $J/\psi$  and  $\psi(2S)$ , are used as the background control sample to model the  $t_z$  distribution of the background. The background control sample consists of random combinations of muons from semi-leptonic  $b$  and  $c$  decays, which tend to produce positive  $t_z$  values, as well as mis-reconstructed tracks from decays-in-flight of kaons and pions, which contribute both to positive and negative  $t_z$  values. The  $t_z$  distribution of the background is therefore modeled with an empirical function, composed of a Dirac delta function and five exponentials (three for positive  $t_z$  and two for negative  $t_z$ , with one positive  $t_z$  and one negative sharing the same slope parameter). This function is convolved with the sum of two Gaussian functions as a resolution function, which has different

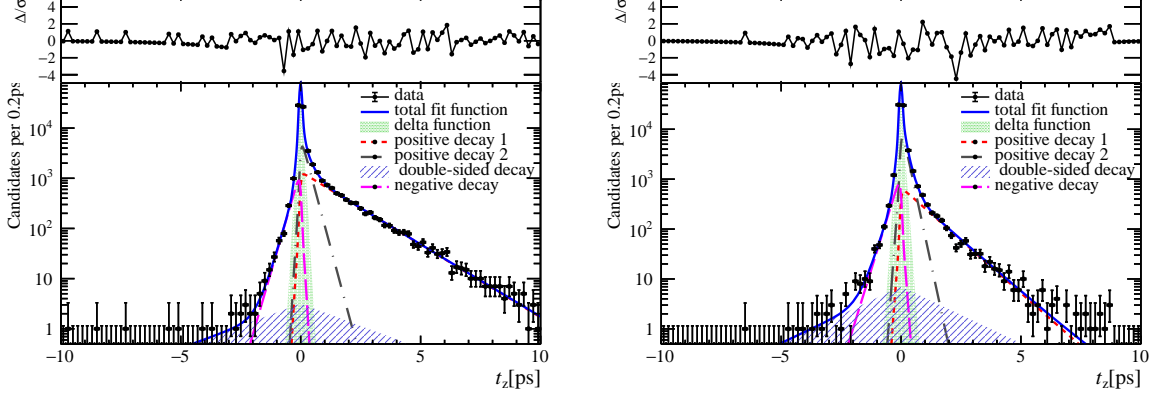


Figure 2:  $t_z$  background fit for PVNTRACKS from 20 to 40,  $y$  from 2 to 2.8, and  $p_T$  from 2 GeV/c to 4 GeV/c. The left is that of  $J/\psi$  and the right is of  $\psi(2S)$ .

311 parameters as for signals,<sup>1</sup> ,

$$f_{\text{background}} = \left[ (1 - f_1 - f_2 - f_3 - f_4) \delta(t_z) + \theta(t_z) \left( \frac{f_1}{\tau_1} e^{-t_z/\tau_1} + \frac{f_2}{\tau_2} e^{-t_z/\tau_2} \right) + \theta(-t_z) \left( \frac{f_3}{\tau_3} e^{t_z/\tau_3} + \frac{f_4}{2\tau_4} e^{-|t_z|/\tau_4} \right) \right] * \left( \frac{\beta'}{\sqrt{2\pi S'_1} \sigma} e^{-\frac{(t_z-\mu)^2}{2S'^2_1 \sigma^2}} + \frac{1-\beta'}{\sqrt{2\pi S'_2} \sigma} e^{-\frac{(t_z-\mu)^2}{2S'^2_2 \sigma^2}} \right). \quad (10)$$

312 The parameters in Eq. 10 are determined by fitting the  $t_z$  distribution of background  
 313 control sample defined above (in each kinematical bin of  $J/\psi$  and  $\psi(2S)$ ), and are fixed  
 314 for the final fits. In Fig. 2, the  $t_z$  distribution of the background in the kinematic range  
 315  $p_T \in [2, 4]$  GeV/c,  $y \in [2.0, 2.8]$  and PVNTRACKS  $\in [20, 40]$  is shown, superposed by a fit  
 316 using Eq. 10. In total, the eventual function for the  $t_z$  fit is:

$$F_{t_z}(t_z; n_{\text{prompt}}, n_{\text{tail}}, n_{\text{bdecay}}, n_{\text{bkg}}, \mu, S_1, S_2, \beta, \tau_b) \\ = \left( n_{\text{prompt}} \delta(t_z) + \frac{n_{\text{bdecay}}}{\tau_b} e^{-t_z/\tau_b} \right) * f_{\text{resolution}}(t_z; \mu, S_1, S_2, \beta) + n_{\text{tail}} f_{\text{tail}}(t_z) + n_{\text{bkg}} f_{\text{background}}(t_z), \quad (11)$$

317 where  $n_{\text{bkg}}$ ,  $n_{\text{prompt}}$ ,  $n_{\text{bdecay}}$  and  $n_{\text{tail}}$  are the number of background, prompt components,  
 318 components from  $b$  and wrong PV events, respectively.

319 Because the requirement of the PV reconstruction is loose, and the PV is not refitted  
 320 by removing the VELO segments of the muon tracks, it is reasonable to assume that  
 321 prompt components and components from  $b$  have equal probability to be assigned with  
 322 a wrong PV. Therefore, the fractions of the prompt and from  $b$  components in  $n_{\text{tail}}$  is  
 323 equal to the fraction  $\frac{n_{\text{prompt}}}{n_{\text{bdecay}}+n_{\text{prompt}}}$  and  $\frac{n_{\text{bdecay}}}{n_{\text{bdecay}}+n_{\text{prompt}}}$ . Even if the shape is extracted from  
 324 data including the background candidate, the fit result  $n_{\text{tail}}$  should only contain prompt  
 325 and non-prompt signals. First, the shape of the PDF due to the wrong-PV effect should  
 326 be the same no matter from which sample we extract it. Then, the wrong-PV effect for  
 327 background candidates should be merged in the background PDF, which means the  $n_{\text{tail}}$

<sup>1</sup>The uncertainty on the background vertex is usually worse than that for the signal vertex.

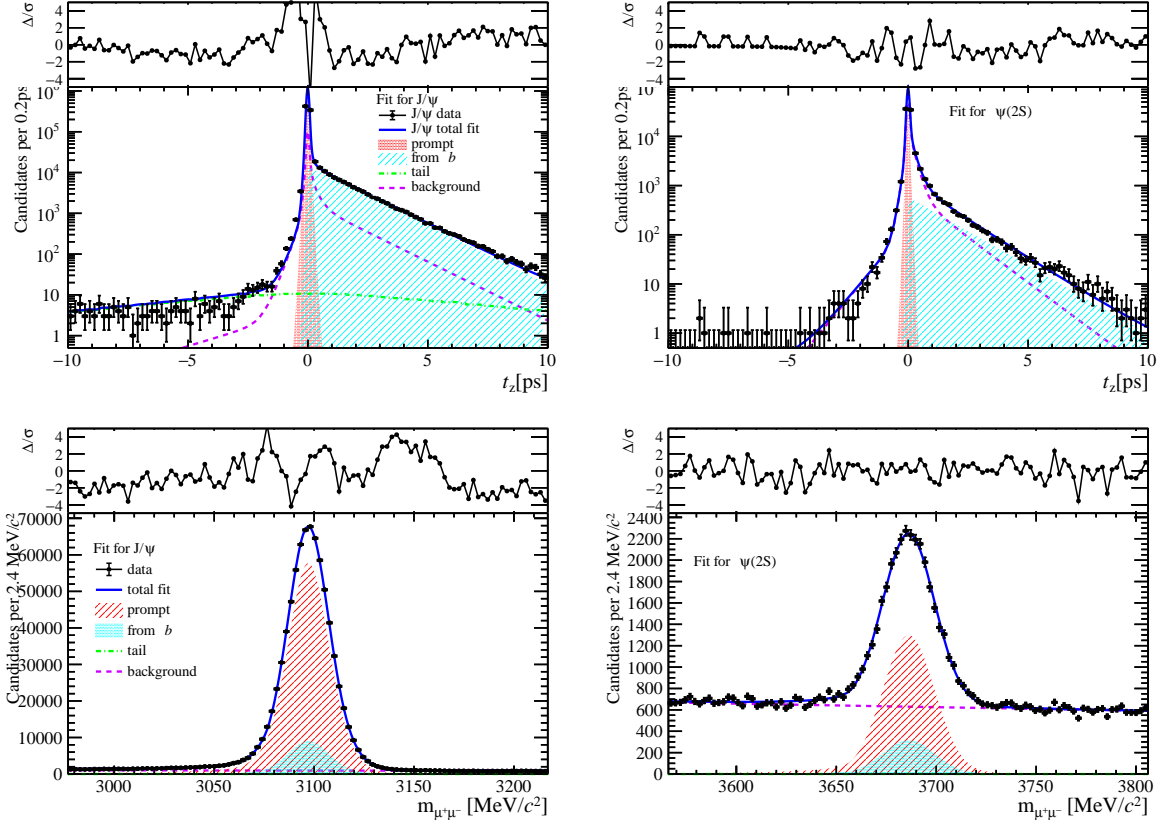


Figure 3: Projection in  $t_z$  and mass spectrum of  $t_z$ -mass fit for PVNTRACKS from 20 to 40,  $y$  from 2 to 2.8, and  $p_T$  from  $2 \text{ GeV}/c$  to  $4 \text{ GeV}/c$ . The left is that of  $J/\psi$  and the right is of  $\psi(2S)$ .

part in the total PDF should be specifically for signal candidates. And in this analysis, we only care about the ratio of prompt and from  $b$ , where  $n_{tail}$  in each kinetic bin and multiplicity bin accounts for about 0.1% of  $n_{b\text{decay}} + n_{\text{prompt}}$ , which results in an even more negligible influence on the ratio in Sec 4. In this case, we can ignore the subtle contribution to  $n_{b\text{decay}}$  and  $n_{\text{prompt}}$  from  $n_{tail}$ .

The two-dimensional fit to the invariant mass and the lifetime in the kinematic range  $4 \text{ GeV}/c < p_T < 6 \text{ GeV}/c$ ,  $2.0 < y < 2.8$  and multiplicity bin  $20 \leq \text{PVNTRACKS} \leq 40$  is shown in Fig. 3, with the red shaded area being prompt components, and the cyan shaded area being components from  $b$ , the dots with vertical error bar are data points, the violet dashed lines are the combinatorial background, the green dashed lines are the components by wrong PV (which are invisible in the graph of projection on mass) and the blue lines are the total fit functions. During the  $t_z$ -mass combined fitting procedure, the parameters of mass signal shape ( $\mu_{mass}$ ,  $\sigma_{mass}$ ,  $p_0$ ) are floated within a certain times of their uncertainties from the 1D mass fit for the final fits of  $J/\psi$ . While for  $\psi(2S)$ , due to the limitation of number of candidates, the parameters are fixed. According to the comparison of two fitting strategies upon  $J/\psi$ , no significant difference between errors of prompt and non-prompt signals are observed ( 0.1%).

## <sup>345</sup> 6 Efficiency determination

<sup>346</sup> The total efficiency  $\epsilon_{\text{tot}}$  is determined independently in each kinetic bin and multiplicity  
<sup>347</sup> bin. The expression is as follows,

$$\epsilon_{\text{tot}} = \epsilon_{\text{acc}} \times \epsilon_{\text{Reco\&Sel}} \times \epsilon_{\text{MuonID}} \times \epsilon_{\text{Trigger}}. \quad (12)$$

<sup>348</sup> The Monte Carlo samples for both prompt and non-prompt signals of  $J/\psi$  and  $\psi(2S)$  are  
<sup>349</sup> divided according to the multiplicity binning schemes in Sec. 4. For different multiplicity  
<sup>350</sup> regions based on division upon different multiplicity variables, efficiencies are calculated  
<sup>351</sup> in the same way as follows, which is calculated in the same binning scheme for kinematic  
<sup>352</sup> variables  $p_T$  and  $y$ . The truth-matching fail rates for both  $J/\psi$  and  $\psi(2S)$  are around 0.4%,  
<sup>353</sup> which is negligible compared to the statistical and systematic uncertainties after division  
<sup>354</sup> to get the ratio. And in the simulated sample, the efficiency of prompt components and  
<sup>355</sup> components from  $b$ -hadron decay is calculated separately. Since we have already separated  
<sup>356</sup> the data and MC in a multiplicity bin, the bin width of  $p_T$  and  $y$  is not significantly  
<sup>357</sup> small that the efficiency can be treated as constant in a certain kinetic bin, hence, all the  
<sup>358</sup> efficiencies are corrected by reweighting the distribution of  $p_T$ - $y$  spectrum of MC to that  
<sup>359</sup> of s-weighted data which contains only signal. Also, the effect due to the difference in  
<sup>360</sup> the distribution of multiplicity is corrected by reweighting the distribution of multiplicity  
<sup>361</sup> variables of MC to that of s-weighted data which contains only signal. Since there are  
<sup>362</sup> differences in the distribution of  $p_T$ - $y$  spectrum and multiplicity variables for prompt and  
<sup>363</sup> non-prompt signals, before calculating efficiencies, we reweight the  $p_T$ - $y$  and multiplicity  
<sup>364</sup> distributions separately for prompt and non-prompt signals, as shown in Figs 4.

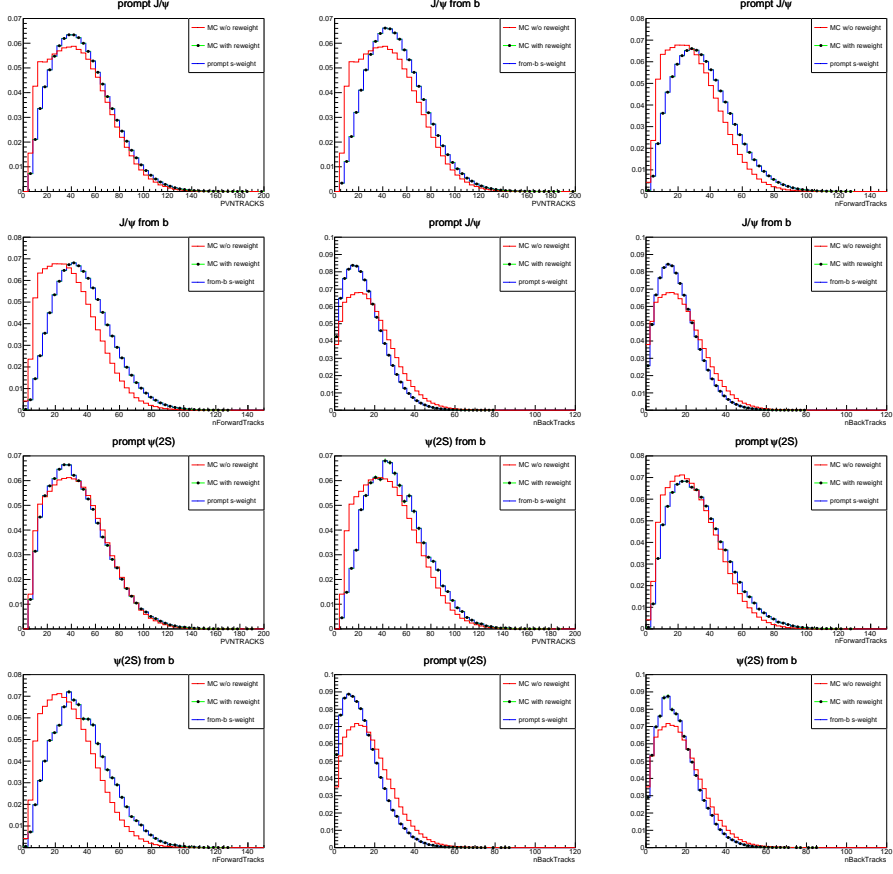


Figure 4: Reweighting the multiplicity distribution to match MC to s-weighted data. the right column is of  $\psi(2S)$ .

For  $J/\psi$   $p_T$ - $y$  reweight, the results cut in each  $y$  region for  $J/\psi$  is shown in Figs 5. And the result for  $\psi(2S)$  is shown in Figs 6.

## 6.1 Geometrical acceptance

The geometrical acceptance in each kinematic bin is defined as

$$\epsilon_{\text{acc}} \equiv \frac{N(p_T, y) \text{ with both } \mu \text{ in LHCb acceptance}}{N(p_T, y)}. \quad (13)$$

The LHCb acceptance means the polar angle  $[10, 400]$  mrad defined with respect to the direction of LHCb  $z$ -axis, before the effect of the magnetic field. The efficiency  $\epsilon_{\text{acc}}$  is determined using a simulated sample at the generator level. In Fig. 7, the efficiency in each  $p_T$  and  $y$  bin of  $J/\psi$  and  $\psi(2S)$  mesons for  $PVZ > -60\text{mm}$  and  $nPVs = 1$  are presented. The geometrical acceptances for prompt production and production from  $b$ -hadron decay are calculated separately for both  $J/\psi$  and  $\psi(2S)$ . And since the geometrical acceptance is only a function of kinematic variables, we assume that there is no difference between the geometrical acceptance between different multiplicity regions.

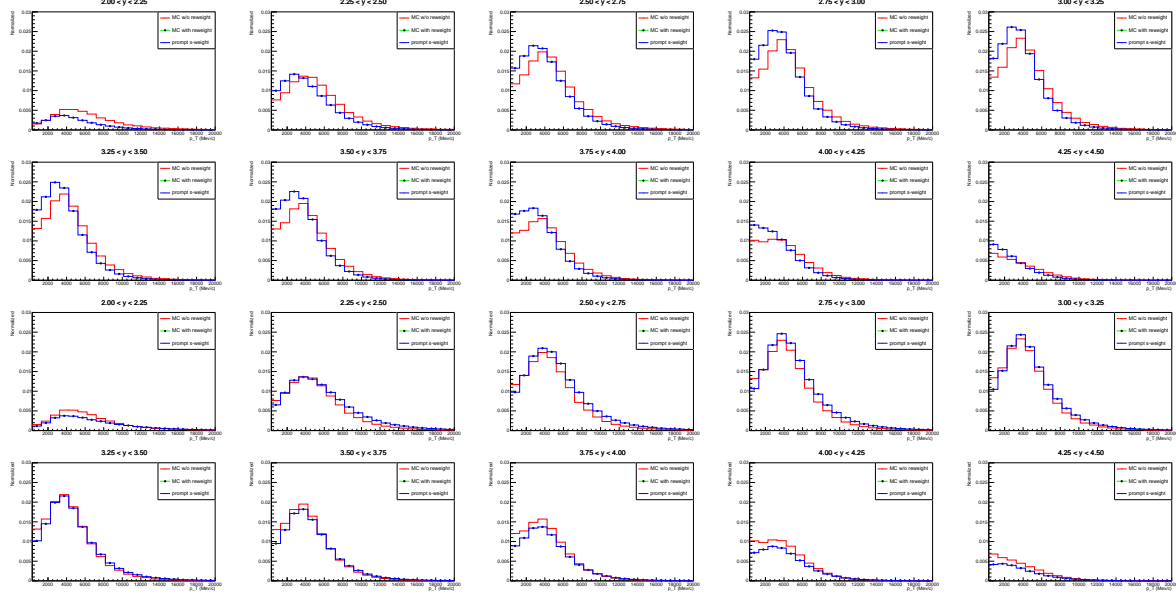


Figure 5: Reweight the  $p_T$ - $y$  distribution to match MC to s-weight data. The first two rows are results of prompt  $J/\psi$  and the rest two rows are that of non-prompt  $J/\psi$ .

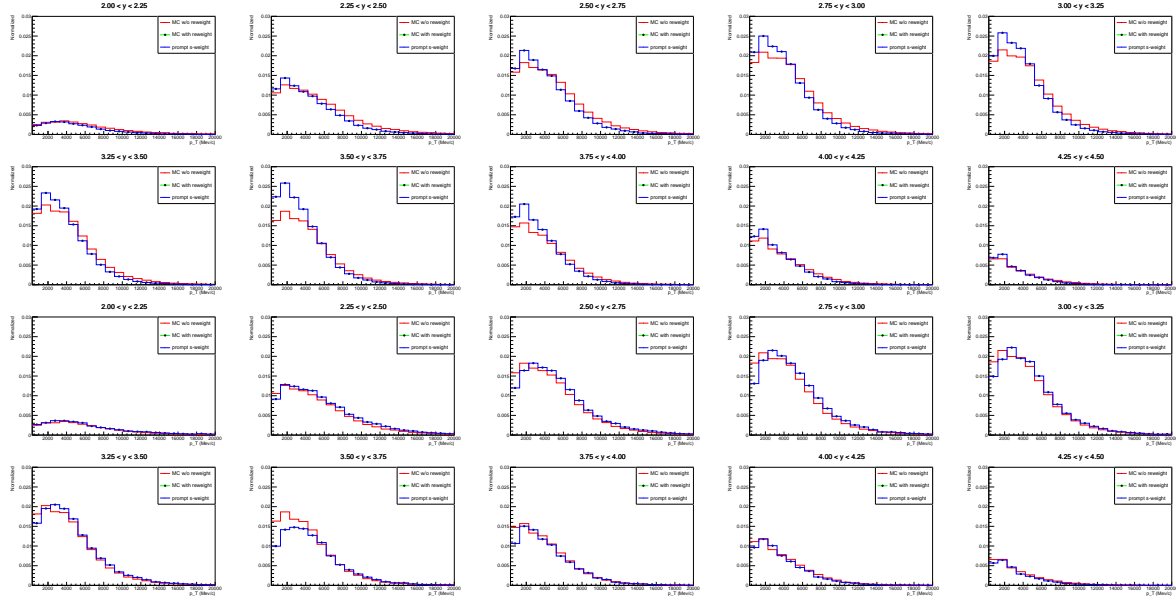


Figure 6: Reweight the  $p_T$ - $y$  distribution to match MC to s-weight data. The first two rows are results of prompt  $\psi(2S)$  and the rest two rows are that of non-prompt  $\psi(2S)$ .

## 377 6.2 Reconstruction-selection efficiency

378 The reconstruction and selection efficiency in each kinematic bin is estimated as

$$\epsilon_{\text{Reco\&Sel}} \equiv \frac{N(p_T, y) \text{ reconstructed and selected (w/o } \mu \text{ ID)}}{N(p_T, y) \text{ with both } \mu \text{ in LHCb acceptance}}. \quad (14)$$

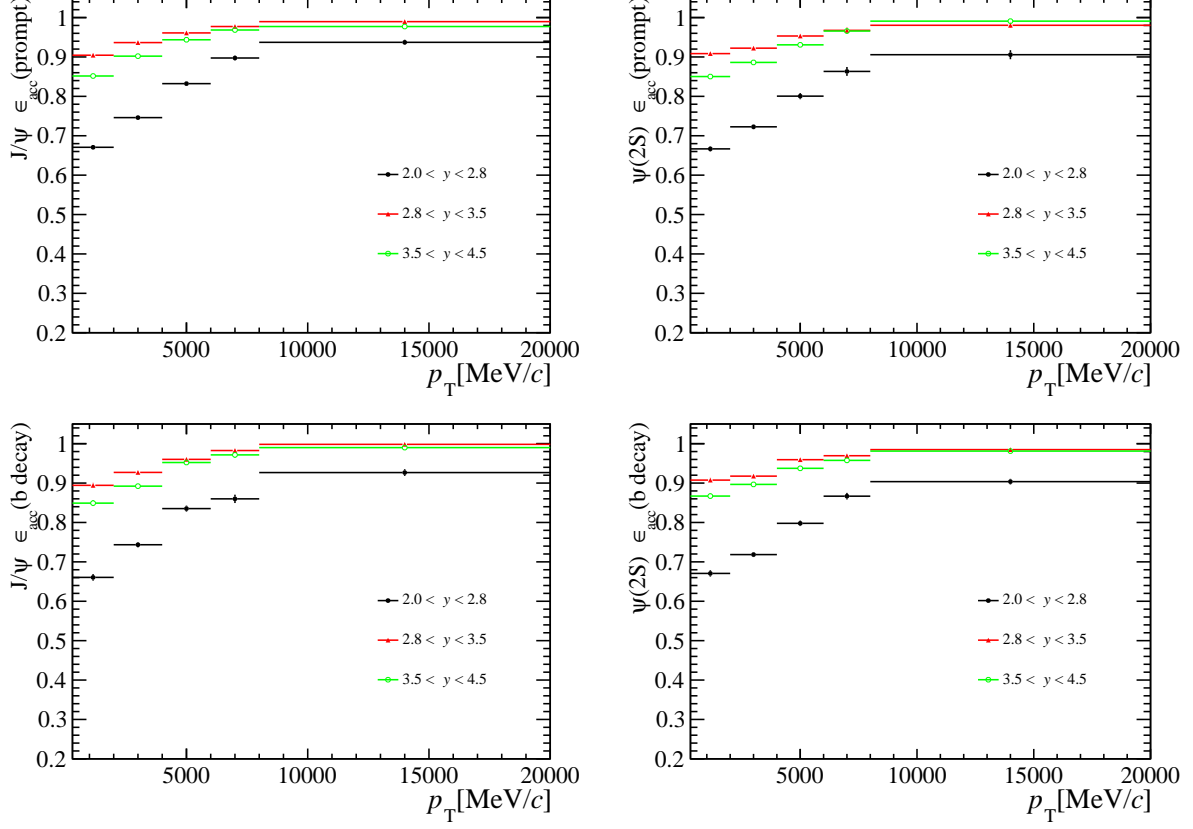


Figure 7: Efficiency of geometrical acceptance for both  $J/\psi$  and  $\psi(2S)$  for PVNTRACKS in 4 to 20, where the left is that of  $J/\psi$  and the right is of  $\psi(2S)$ . The first row is that of prompt signals and the second row is that of non-prompt signals.

379 It includes the efficiency of reconstructing the two muon tracks and the selection of the  
 380 signals, with the selection criteria listed in Table 2 (excluding muon identification and  
 381 the trigger). Then the reconstruction efficiency is further corrected using the data-over-  
 382 simulation single tracking efficiency ratio. The ratio of tracking efficiencies for a single  
 383 track in data and simulation determined with the Long Tag-Probe method [22] is shown  
 384 in Fig. 8, which was given by the tracking group.

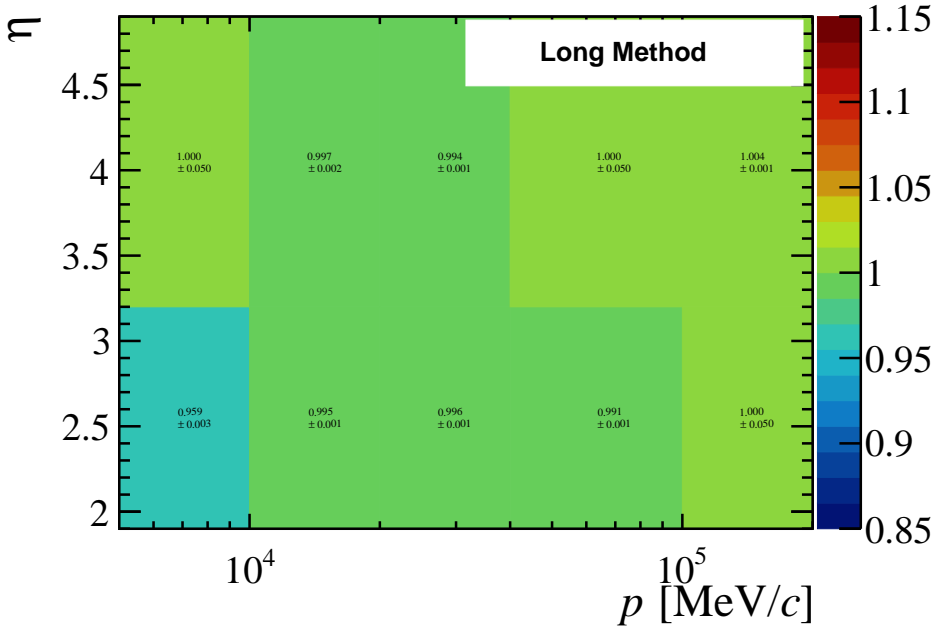


Figure 8: Tracking efficiency ratio between data and MC2016 simulation in bins of  $p_\mu$  and  $\eta_\mu$  of the muon.

For a given event the correction factor is determined by multiplying the efficiency ratios for each of the tracks in the final state. Since the event multiplicity distribution of prompt and non-prompt signals in simulation is quite similar compared to the event multiplicity difference between simulation and data, we assume prompt and non-prompt signals have the same efficiency corrections. For each  $p_T$  and  $y$  bin, the efficiency of  $\epsilon_{\text{Reco\&Sel}}$  is shown in Fig. 9 for PVNTRACKS between 4 to 20. Results in other multiplicity regions are shown in Sec 10.

### 6.3 Muon identification efficiency

The muon identification requirement used in this analysis is `IsMuon == 1&&DLLmu > 2&&ProbNNmu > 0.8`. The efficiency is introduced by

$$\epsilon_{\text{MuonID}} \equiv \frac{N(p_T, y) \text{ selected including } \mu\text{ID requirement}}{N(p_T, y) \text{ reconstructed and selected (w/o } \mu\text{ID)}}. \quad (15)$$

The Muon ID efficiency is obtained using simulated samples and calibrated with the data using the PIDCalib package. The full simulated samples used here are selected by all the selections except the muon ID and the trigger. The selected samples are the same as the ones used in the reconstruction and selection. As estimating the reconstruction and selection efficiency, we first reweight the nVeloClusters and  $p_T$ - $y$  spectrum. The muon ID efficiency in each  $(p_T, y)$  bin is then calculated by averaging the muon ID efficiency of each candidate in the bin, which is the product of the muon ID efficiencies of the two muons from the efficiency table, obtained from the PIDCalib package, according to their

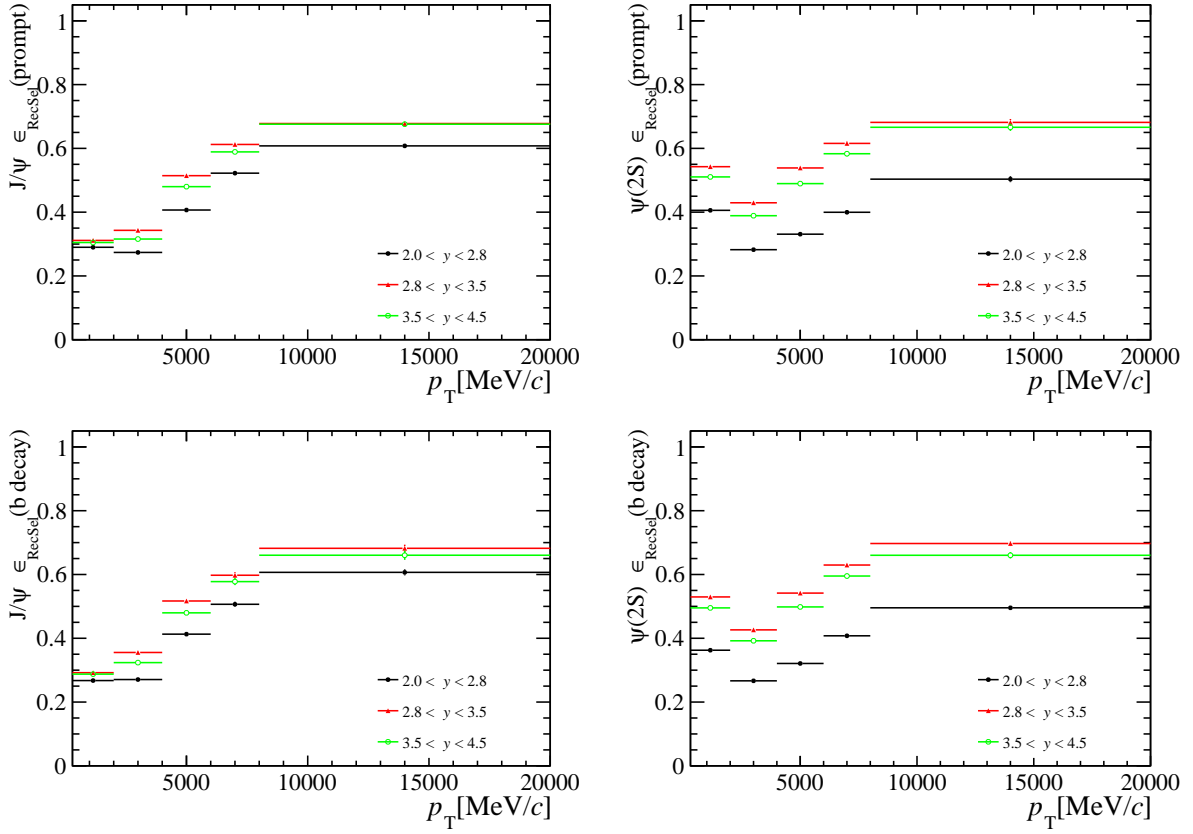


Figure 9: Efficiency of reconstruction and selection (excluding muon identification and the trigger) for both  $J/\psi$  and  $\psi(2S)$  for PVNTRACKS in 4 to 20, where the left is that of  $J/\psi$  and the right is of  $\psi(2S)$ . The first row is that of prompt signals and the second row is that of non-prompt signals.

403  $(p, \eta, \text{nSPDhits})$  values. The formula is

$$\bar{\epsilon}(p_T, y) = \frac{\sum \epsilon_{\mu^+}(p_{\mu^+}, \eta_{\mu^+}, \text{nSPDhits}) \epsilon_{\mu^-}(p_{\mu^-}, \eta_{\mu^-}, \text{nSPDhits})}{N_{\text{res\&sel}}}. \quad (16)$$

404 where  $\epsilon_{\mu^+}(p_{\mu^+}, \eta_{\mu^+}, \text{nSPDhits})$  and  $\epsilon_{\mu^-}(p_{\mu^-}, \eta_{\mu^-}, \text{nSPDhits})$  are the muon ID efficiencies  
 405 obtained from the efficiency table. The efficiency table we used here is from the calibration  
 406 sample which contains  $J/\psi$  candidates taken in the same period and the average efficiency  
 407 over the whole period is used. One 3-Dimensional efficiency table dedicated to the muon  
 408 ID selection is obtained from this calibration sample in bins of the muon  $(p, \eta, \text{nSPDhits})$   
 409 using the tag-and-probe method. The MagDown and MagUp efficiencies are calculated  
 410 separately. For the muon candidates whose  $(p, \eta, \text{nSPDhits})$  are out of the range of the  
 411 calibration sample, we simply set the value to be one due to the fact that the production  
 412 in those bins is significantly small. For each  $p_T$  and  $y$  bin, the efficiency of  $\epsilon_{\text{MuonID}}$  is  
 413 shown in Fig. 10. Results in other multiplicity regions are shown in Sec 10.

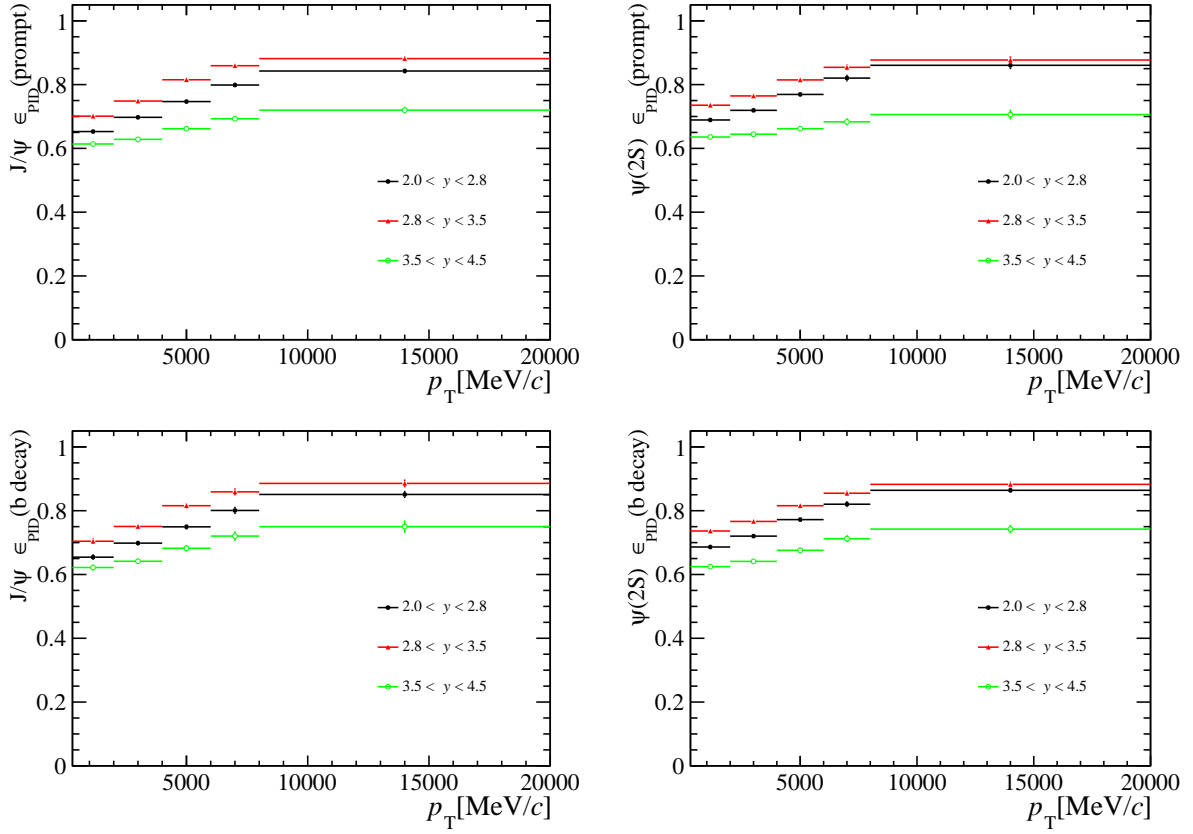


Figure 10: PID efficiencies for both  $J/\psi$  and  $\psi(2S)$  for PVNTRACKS in 4 to 20, where the left is that of  $J/\psi$  and the right is of  $\psi(2S)$ . The first row is that of prompt signals and the second row is that of non-prompt signals.

#### 414 6.4 Trigger efficiency

415 The trigger efficiency in each kinematic bin is defined as

$$\epsilon_{\text{Trigger}} \equiv \frac{N(p_T, y) \text{ triggered}}{N(p_T, y) \text{ selected including } \mu\text{ID requirement}} \quad (17)$$

416 Here the triggers include both TOS requirements of L0DiMuon, Hlt1DiMuonHighMass for  
417 both, and Hlt2DiMuonJPsiTurbo for  $J/\psi$  and Hlt2DiMuonPsi2STurbo for  $\psi(2S)$ , respec-  
418 tively. Only L0DiMuon and Hlt1DiMuonHighMass contribute actually to the efficiency  
419 because the Hlt2DiMuonJPsiTurbo and Hlt2DiMuonPsi2STurbo is almost fully efficient  
420 due to the facts that the offline selections are tighter. For each  $p_T$  and  $y$  bin, the efficiencies  
421 of  $\epsilon_{\text{Trigger}}$  for both  $J/\psi$  and  $\psi(2S)$  from different sources for PVNTRACKS between 4 to  
422 20 are shown in Fig. 11. Results in other multiplicity regions are shown in Sec 10.

#### 423 6.5 Total efficiency

424 The total efficiencies  $\epsilon_{\text{tot}}$  for  $J/\psi$  and  $\psi(2S)$  from different sources for PVNTRACKS  
425 between 4 to 20 are shown in Fig. 12. Results in other multiplicity regions are shown in  
426 Sec 10. The separate efficiencies for prompt and non-prompt signals are used to calculate  
427 the final cross-section.

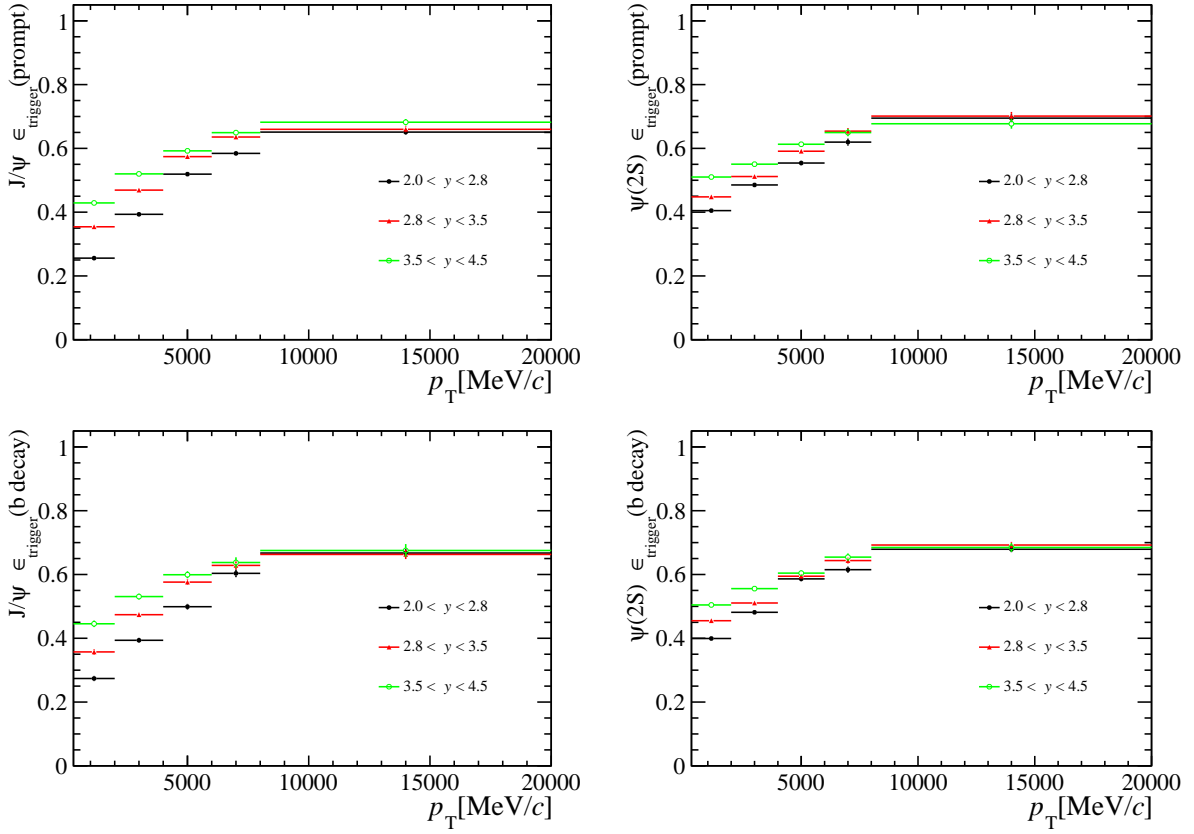


Figure 11: Trigger efficiencies for both  $J/\psi$  and  $\psi(2S)$  for PVNTRACKS in 4 to 20, where the left is that of  $J/\psi$  and the right is of  $\psi(2S)$ . The first row is that of prompt signals and the second row is that of non-prompt signals.

## 428 6.6 Variation due do different reweight samples

429 Since the multiplicity-dependent breakup effects may vary with  $(p_T, y)$ , the two-  
 430 dimensional  $(p_T, y)$  distribution may differ in different multiplicity region. To study  
 431 this effect, the  $(p_T, y)$  spectra are prepared for three different multiplicity classes: all  
 432 selections of PVNTRACKS as what we use to reweight previously, a high multiplicity  
 433 sample (defined as candidates from events with greater than the border line of last two  
 434  $p_T$  bin of PVNTRACKS 60) in red and a low multiplicity sample (PVNTRACKS<60) in  
 435 blue 13. With this two samples for  $(p_T, y)$  reweight, we can calculate the ratio of total  
 436 efficiencies for both prompt and non-prompt  $J/\psi$  and  $\psi(2S)$  in each multiplicity region.  
 437 And after comparing the newly calculated ratio of total efficiencies with the original one,  
 438 we record the variation in each  $(p_T, y, \text{PVNTRACKS})$  bin in form of a certain time of  
 439 statistical uncertainty in that bin. And the result is shown in Figs 14. It's clearly shown  
 440 that all the variations are within uncertainties, where the center values and uncertainties  
 441 for ratio of efficiencies are from the results reweighted by the full-multiplicity sample.

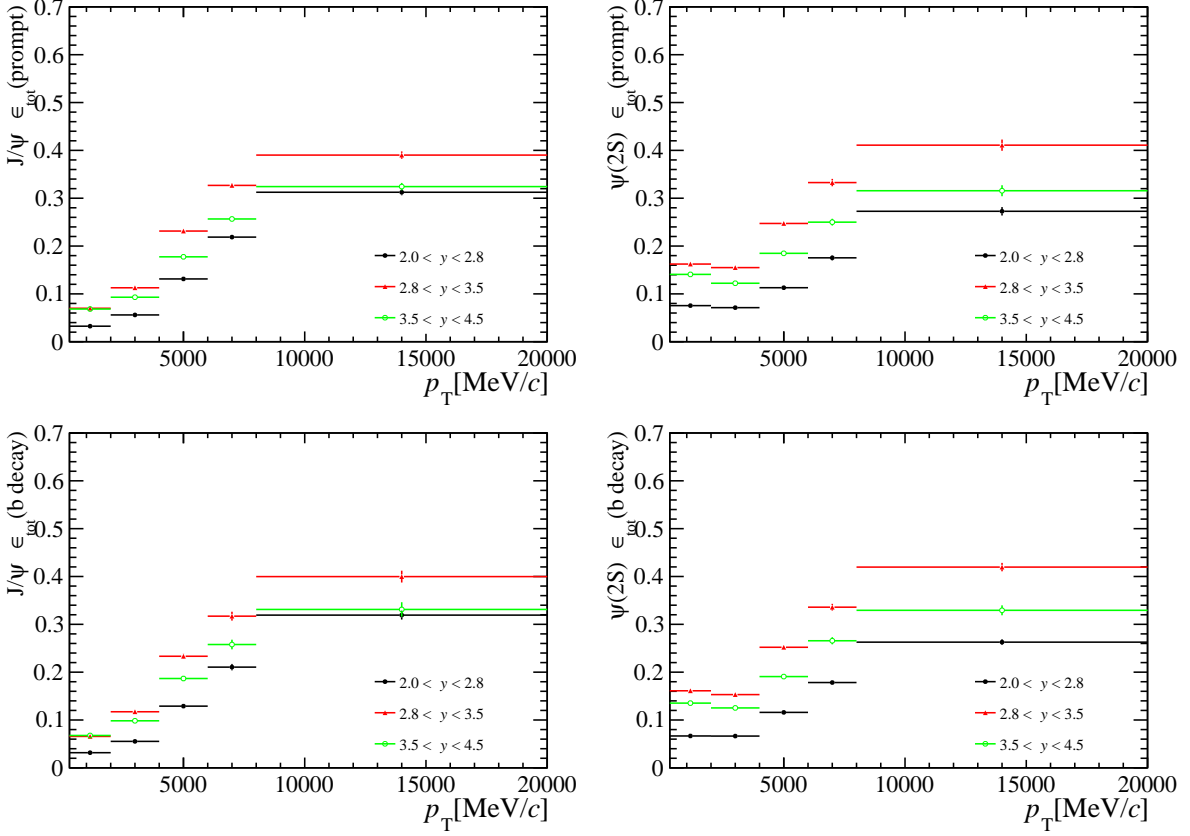


Figure 12: Total efficiencies for both  $J/\psi$  and  $\psi(2S)$  for PVNTRACKS in 4 to 20, where the left is that of  $J/\psi$  and the right is of  $\psi(2S)$ . The first row is that of prompt signals and the second row is that of non-prompt signals.

## 442 7 Systematic Uncertainties

443 The ratio of production of  $\psi(2S)$  to  $J/\psi$  in a certain  $(p_T, y)$  is defined in equation 4,  
 444 which is universal for both prompt components and components from  $b$ -hadron decay  
 445 in each multiplicity bin and Systematic uncertainties of various sources are combined  
 446 through the error propagation formula in each bin. While when calculating the systematic  
 447 uncertainties of the ratio of integrated production, the bin size is no more canceled and  
 448 we need to take into account the production as weight in each bin. The ratio of integrated  
 449 production is defined in equation 5. The form of expression for the ratio of integrated  
 450 production is not a simple production or division (it is a division of sums). So when  
 451 studying the systematic uncertainties, a simple and straightforward way is calculating the  
 452 uncertainties of  $\frac{\Sigma_{(p_T, y)} \sigma_{\psi(2S)}(p_T, y)}{\Sigma_{(p_T, y)} \sigma_{J/\psi}(p_T, y)}$  itself, which is for example, if we calculate the uncertainty  
 453 of the fit model, instead of combining the uncertainties from different bins, we directly  
 454 calculate how much  $\frac{\Sigma_{(p_T, y)} \sigma_{\psi(2S)}(p_T, y)}{\Sigma_{(p_T, y)} \sigma_{J/\psi}(p_T, y)}$  would vary when we change the fit model. For the  
 455 uncertainties which are independent of bins, we can combine them through the error  
 456 propagation formula, i.e. the Systematic uncertainty due to MC sample size. The following  
 457 sources of systematic uncertainties are considered. And the systematic uncertainties are  
 458 calculated separately in each multiplicity bin. For the rest of the part, we only show the  
 459 results for the first multiplicity bin, which is  $4 \leq \text{PVNTRACKS} < 20$ .

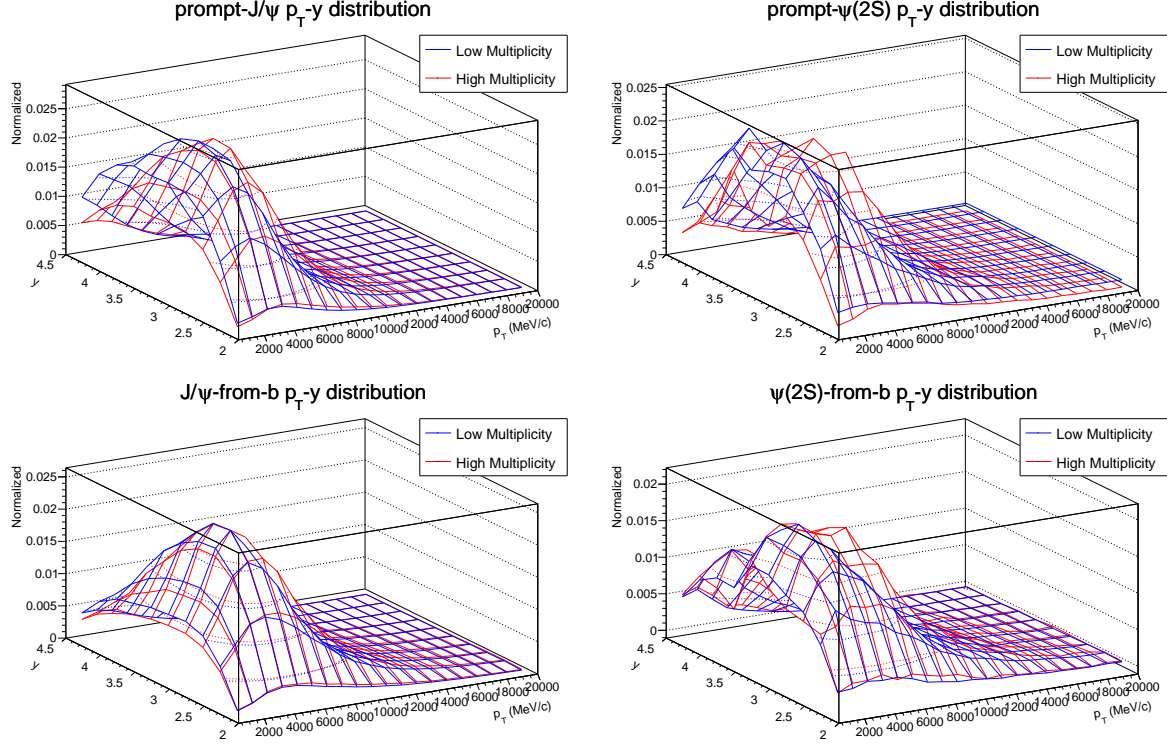


Figure 13: Two-dimensional ( $p_T$ ,  $y$ ) distribution for prompt and non-prompt  $J/\psi$  and  $\psi(2S)$  of different samples (high-multiplicity sample in red).

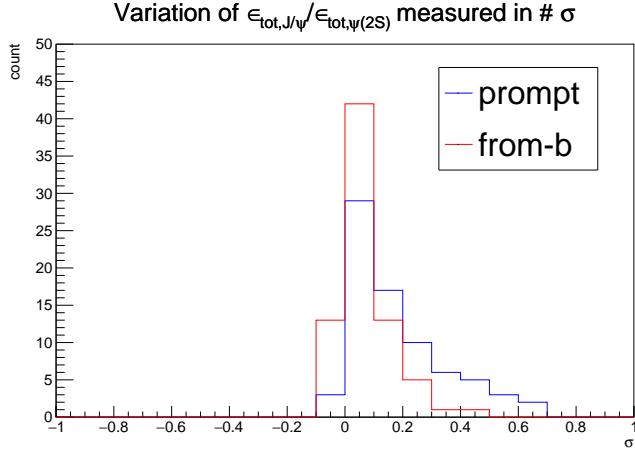


Figure 14: Distribution of the variation due to different reweight samples recorded in times of the statistical uncertainty.

## 460 7.1 Signal extraction

### 461 7.1.1 Signal mass shape

462 Using the sum of two Crystal Ball functions parametrized as described in Section 5 could  
 463 bias the signal yields. For an alternative, the signal invariant mass is also fitted with  
 464 the model which is extracted from the kernel-estimated distribution from the simulated

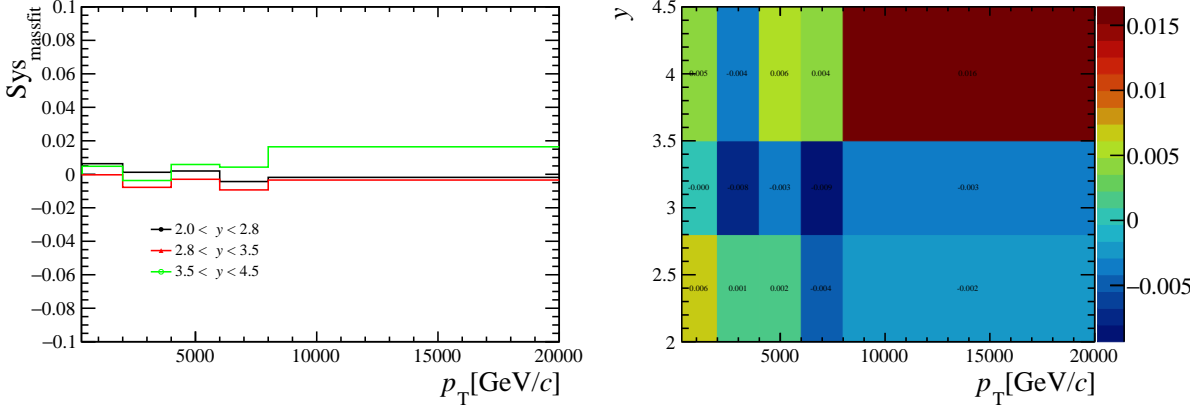


Figure 15: The systematic uncertainty of ratio of production due to the fit model in each bin for PVNTRACKS from 4 to 20. It is common for both prompt components and components from  $b$ -hadron decay.

sample bin dependently. In order to account for the resolution difference between data and simulation, a Gaussian function (all the parameters float during the fit procedure) is used to smear the shape of the signals. The study is performed in each kinematic bin, and the signal yields from the default fit and alternative fit are compared. For both  $J/\psi$  and  $\psi(2S)$ , we change the fit model to get uncertainties for both and then calculate the uncertainties through the error propagation formula. The detailed results of systematic uncertainty for ratio in each single  $p_T$  and  $y$  bin and PVNTRACKS from 4 to 20 are shown in Fig. 15. The result is common for both prompt components and components from  $b$ -hadron decay since when we fit the mass spectrum, we fit both components simultaneously. For the ratio of integrated production, we change the fit model and calculate a new value with equation 5. The variation between the new ratio and the original one is quoted as systematic uncertainty for ratio of integrated production due to mass fit model.

### 7.1.2 Fit to $t_z$ background

There are several scenarios that could deviate the fitted  $b$  fraction from its true value:

- Imperfect modeling of the detector resolution of  $t_z$ . Since the shape of prompt  $\psi(2S)$  is dominated by the resolution, a defective description of the resolution could make the prompt  $J/\psi$  and  $\psi(2S)$  distribution not fitted very well, and thus will affect the fitted fraction of components from  $b$ . To study this effect, a third wide Gaussian is added to the resolution function. It is found that the difference of the fitted  $F_b$  between the default fit and the new fit is negligible.
- Systematic uncertainty related to the background description. In the nominal procedure, the fit explicitly models the background distribution using the mass sidebands. As an alternative, the parameters of the  $t_z$  distribution for the background are obtained by the sPlot technique for both  $J/\psi$  and  $\psi(2S)$  and are fixed in the  $t_z$  fit.

For each  $p_T$  and  $y$  bin, the systematic uncertainties are calculated by combining the uncertainties from  $J/\psi$  and  $\psi(2S)$ . For the ratio of integrated production, similarly, as

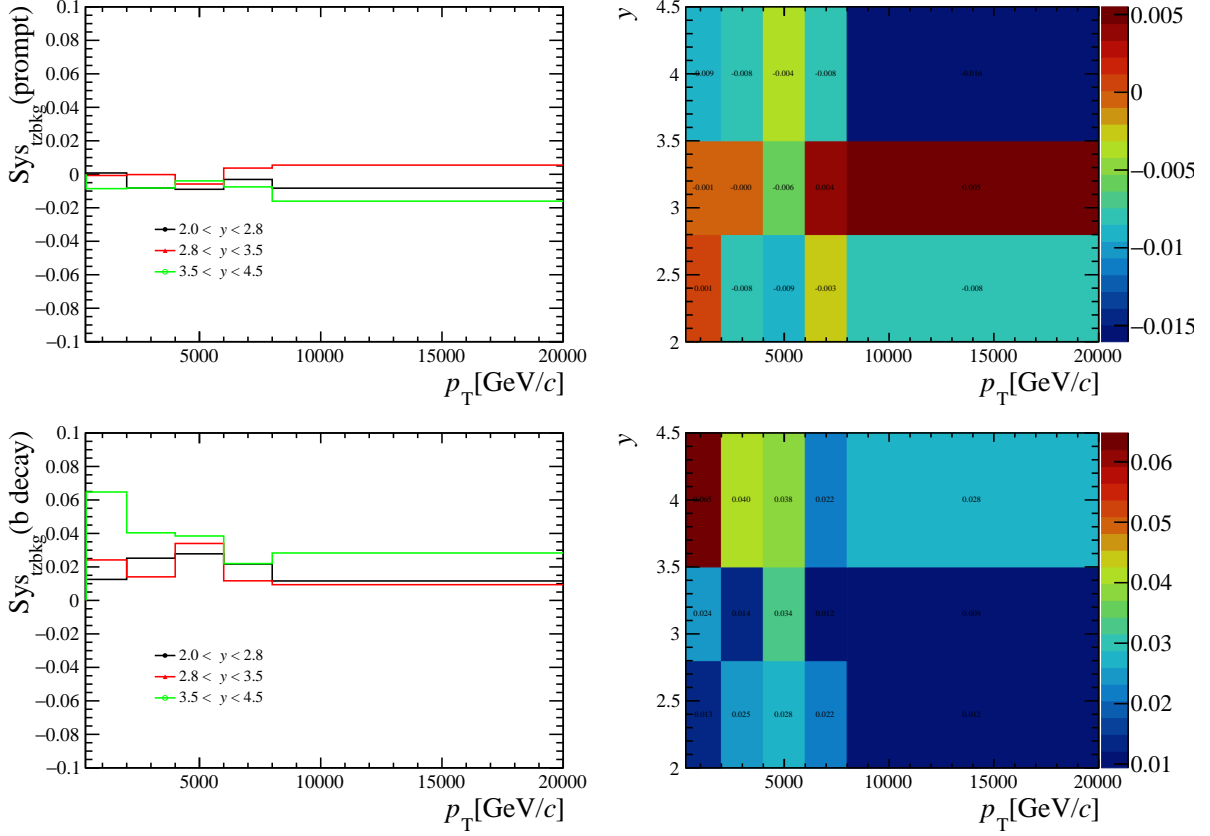


Figure 16: The systematic uncertainty of ratio of production due to  $t_z$  background fit model in each bin for PVNTRACKS from 4 to 20. The first row is that of prompt components and the second row is that of components from  $b$ -hadron decay.

above, we change the fit model for  $t_z$  background for both  $J/\psi$  and  $\psi(2S)$  to calculate a new value and quote the variation as a systematic uncertainty. The uncertainties for prompt components and components from  $b$ -hadron decay are calculated separately. The results in a single bin are shown in figure 16.

#### 7.1.3 Fit to $t_z$ signal

For the imperfect modeling of detector resolution, we fit the  $t_z$  spectrum on MC and then compare the yields of prompt components to the real counts in MC. The variation is quoted as systematic uncertainty due to imperfect modeling of the  $t_z$  signal model. When fitting the  $t_z$  spectrum on MC for  $J/\psi$  or  $\psi(2S)$ , we should take care that one or two Gaussian functions should be used depending on the number of Gaussian functions we are using when fitting  $t_z$  spectrum on data in a certain ( $p_T, y$ , PVNTRACKS) bin. The systematic uncertainties of ratio in different bins 17 are listed for PVNTRACKS from 4 to 20.

## 7.2 Trigger efficiency

The trigger efficiency in simulation is cross-checked with data, and the resulting difference in the ratio of production between simulation and data is quoted as a systematic uncertainty.

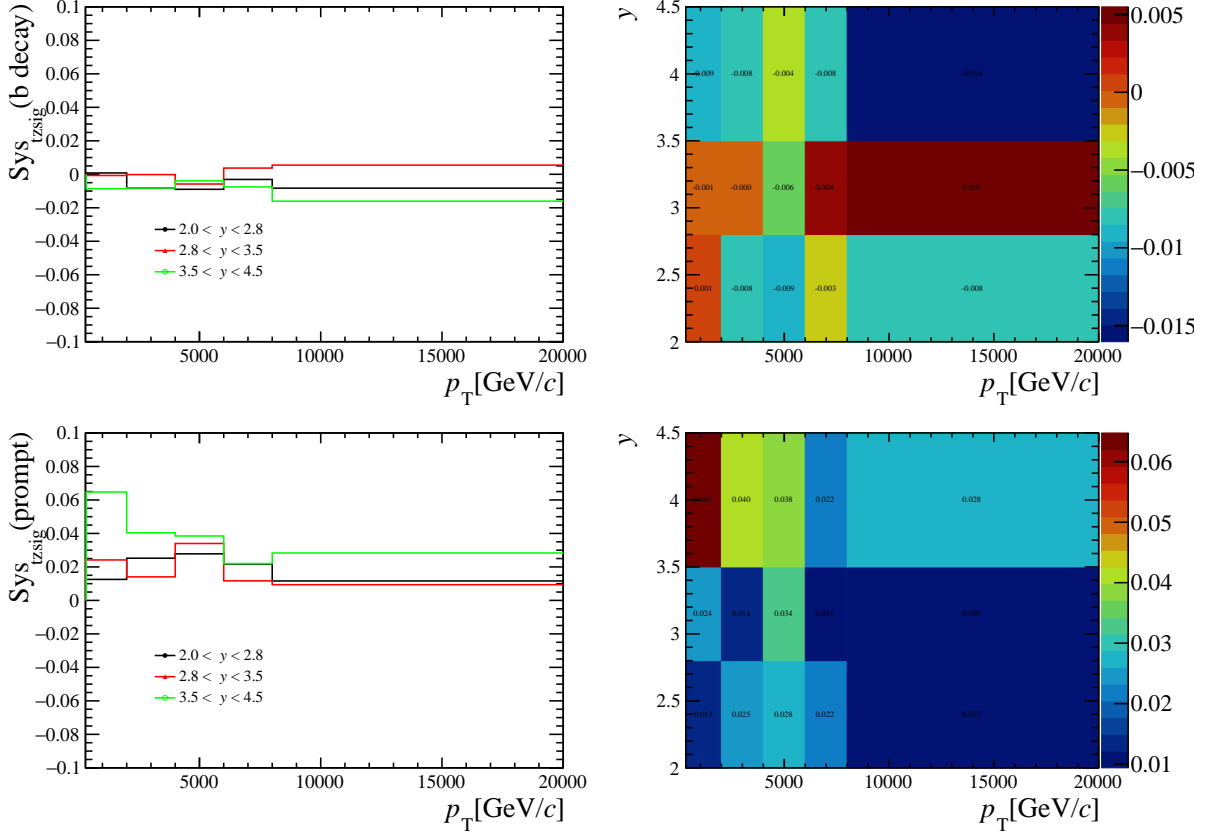


Figure 17: The systematic uncertainty of ratio of production due to  $t_z$  signal fit model in each bin for PVNTRACKS from 4 to 20. The first row is that of prompt components and the second row is that of components from  $b$ -hadron decay.

508 For both L0DiMuon and Hlt1DiMuonHighMass the TISTOS method is used to evaluate  
 509 the efficiency for L0DiMuon&&Hlt1DiMuonHighMass both in simulation and data. We  
 510 use L0Global and Hlt1Global as the TIS line. As the data sample size is limited by  
 511 the number of the TIS events of  $\psi(2S)$  sample, we only consider the uncertainty in  
 512 different  $p_T$  bins and assume the same value in different  $y$  bins and different multiplicity  
 513 regions. The systematic uncertainties of the ratio of production in each bin are calculated  
 514 for both prompt components and components from  $b$ -hadron decay together. While the  
 515 uncertainties of the ratio of integrated production for prompt components and components  
 516 from  $b$ -hadron decay are calculated separately since we need to take into account the  
 517 production in each bin, and it is different for prompt components and components from  
 518  $b$ -hadron decay. For any uncertainty of the ratio of integrated production where the  
 519 integrating region includes different  $y$  bins, the uncertainty is calculated. The uncertainty  
 520 of ratio due to the uncertainty of trigger efficiency in each bin is listed in Table 18.

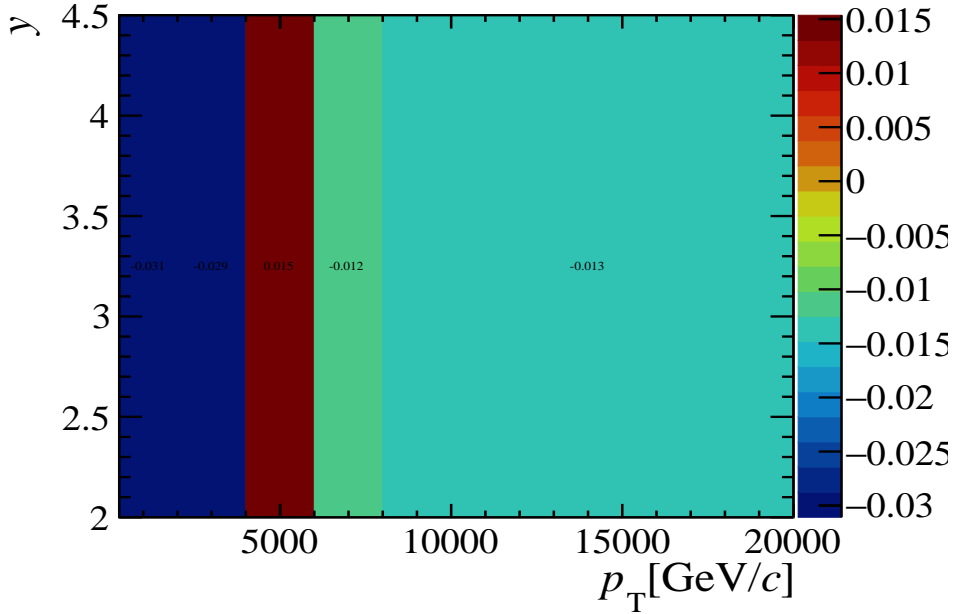


Figure 18: Summary of Systematic Uncertainties of ratio due to uncertainty of  $\epsilon_{\text{trigger}}$ .

### 521 7.3 Tracking efficiency

522 There are two sources of systematic uncertainties associated with the track reconstruction  
 523 efficiency.

524 One is the statistical uncertainty of the ratios due to the limited sample size used to  
 525 obtain the tracking correction table. This part could be obtained by toy studies: Two  
 526 hundred experiments were performed where the efficiency for each bin in the  $p$  and  $\eta$   
 527 was sampled from Fig. 8 by Gaussian distributions with the corresponding central value  
 528 as the mean and the uncertainty as the width; For each experiment, the reconstruction  
 529 and selection efficiency of prompt components and components from  $b$ -hadron decay in  
 530 different bins could be obtained with the sampled efficiency correction table, and hence  
 531 we can calculate two hundred values for ratio in a single bin or any integrated region;  
 532 Finally, using a gaussian function to fit the two hundred of results, and the sigma divided  
 533 by the mean value of the fit result is quoted as the relative uncertainty. The relative  
 534 uncertainty in each bin for prompt components and components from  $b$ -hadron decay for  
 535 PVNTRACKS from 4 to 20 is shown in figure 19.

536 Another one is the choice of event multiplicity variable. This systematic uncertainty  
 537 is provided by the tracking group. The tracking experts indicate that the choice of  
 538 the multiplicity variable (nTracks, nSPDHits, or others) is relevant for deciding the  
 539 systematics. They studied this effect and suggest 0.8% per track, as detailed in Ref. [23].  
 540 But when we calculate the ratio between  $J/\psi$  and  $\psi(2S)$ , the uncertainty due to the choice  
 541 of multiplicity variable is canceled out since we use the same table for calculating both  
 542  $J/\psi$  and  $\psi(2S)$ .

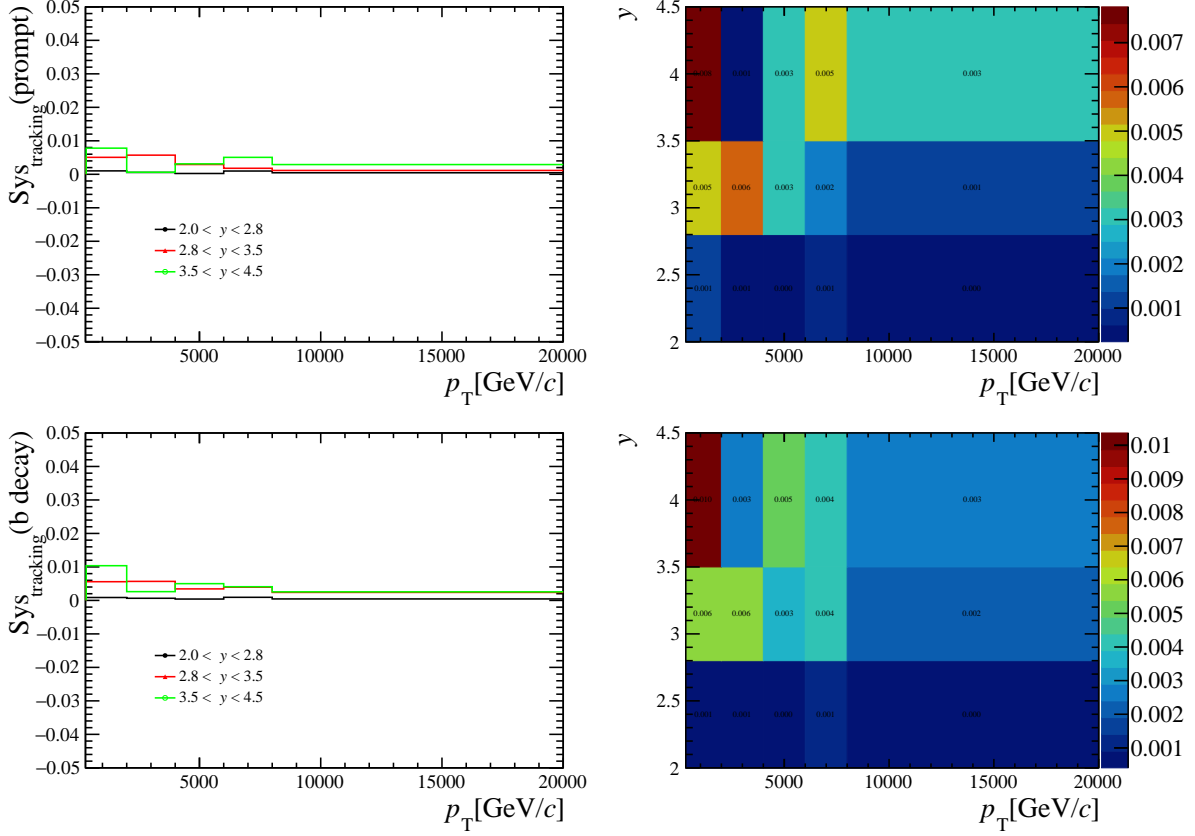


Figure 19: The systematic uncertainty of ratio of production due to the uncertainty of track table in each bin for PVNTRACKS from 4 to 20. The first row is that of prompt components and the second row is that of components from  $b$ -hadron decay.

## 543 7.4 MuonID efficiency

544 The systematic uncertainty due to MuonID includes the following contributions:

- 545 • The statistical uncertainty is due to the finite size of the calibration sample. To  
546 estimate the systematic uncertainty due to the limited calibration sample size, we  
547 first generate two hundred tables of efficiencies from the original table, where the  
548 efficiency in each bin of each table is randomly sampled from a Gaussian distribution  
549 using the central value as the mean and the uncertainty as the width. Then, we  
550 obtain two hundred efficiency values from the generated efficiency tables, hence, we  
551 calculated two hundred productions of  $J/\psi$  and  $\psi(2S)$  in each  $p_T$ - $y$  bin in different  
552 multiplicity region and their ratios. Finally, we fit the distribution of the two  
553 hundred ratios (in a single bin and integrated region) with a Gaussian function.  
554 The ratio between the width and the mean value of the fitted Gaussian function is  
555 quoted as a systematic uncertainty, which is summarized in figure 20.
- 556 • Uncertainty due to binning scheme of the calibration sample, studied by varying the  
557 binning method in  $p_\mu$ ,  $\eta_\mu$ , and nSPDHits respectively. The default one and the two  
558 alternative binning schemes could be found below. The nominal binning scheme of  
559 the muon ID efficiency for muons we use to calculate the muon ID efficiency of  $J/\psi$   
560 and  $\psi(2S)$  mesons is defined:

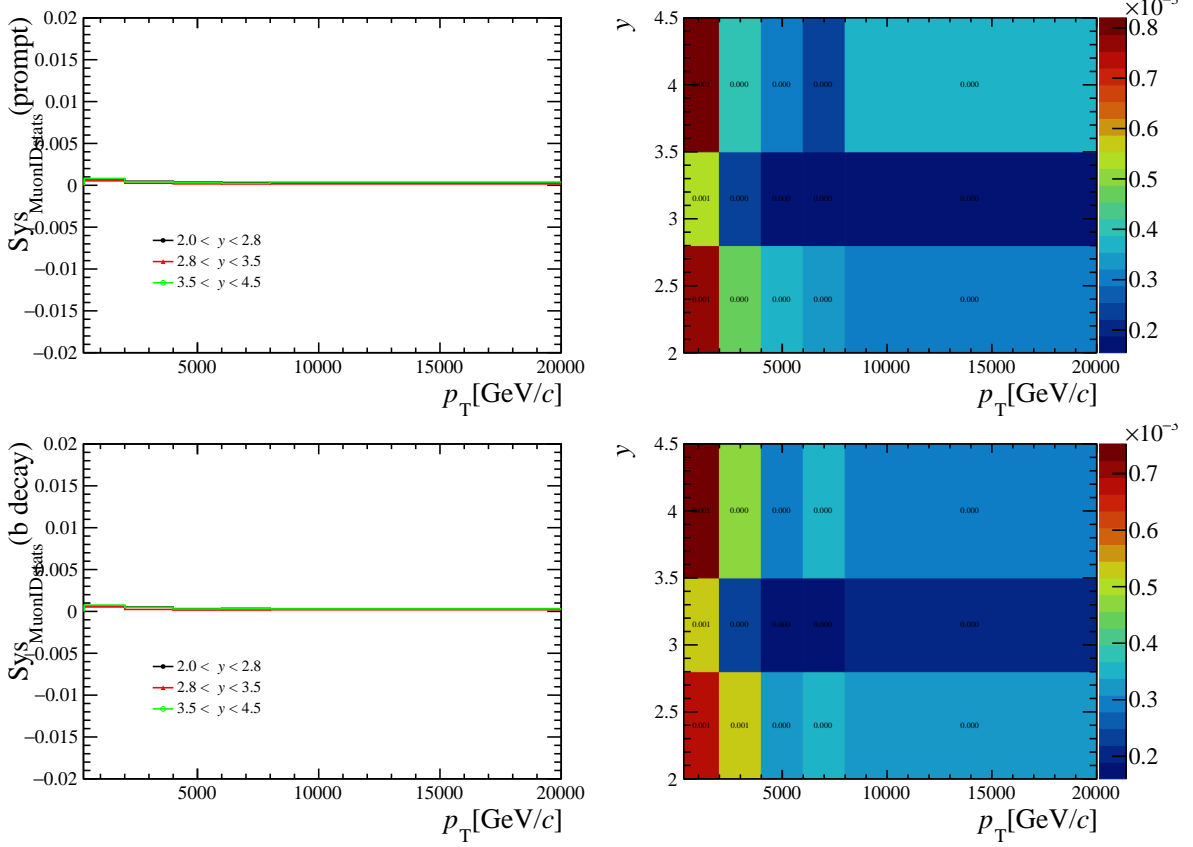


Figure 20: The systematic uncertainty of ratio of production due to the statistical uncertainty of PID efficiency in each bin for PVNTRACKS from 4 to 20. The first row is that of prompt components and the second row is that of components from  $b$ -hadron decay.

- 561     –  $p_\mu$  boundaries [ GeV/c ]: 3, 6, 8, 10, 12, 13, 14, 15, 16, 18, 20, 24, 28, 32, 40, 60,
- 562       70, 80, 90, 100, 200, 1000
- 563     –  $\eta$  boundaries: 2.0, 2.5, 3.0, 3.5, 4.0, 4.5, 4.9
- 564     – nSPDhits boundaries: 0, 200, 400, 1000.

565     One of the two alternative binning schemes is defined:

- 566     –  $p_\mu$  boundaries [ GeV/c ]: 5, 7, 9, 11, 12, 13, 14, 15, 17, 19, 23, 27, 32, 40, 55, 65,
- 567       75, 85, 95, 150, 200, 1000
- 568     –  $\eta$  boundaries: 2.0, 2.4, 2.9, 3.4, 3.9, 4.4, 4.9
- 569     – nSPDhits boundaries: 0, 300, 500, 1000.

570     The other one binning schemes is defined:

- 571     –  $p_\mu$  boundaries [ GeV/c ]: 3, 5.5, 7.5, 9.5, 11.5, 12.5, 13.5, 14.5, 15.5, 17.5, 19.5,
- 572       23.5, 27.5, 32, 38, 48, 58, 68, 78, 88, 98, 198, 1000
- 573     –  $\eta$  boundaries: 2.0, 2.6, 3.1, 3.6, 4.1, 4.6, 4.9
- 574     – nSPDhits boundaries: 0, 150, 480, 1000.

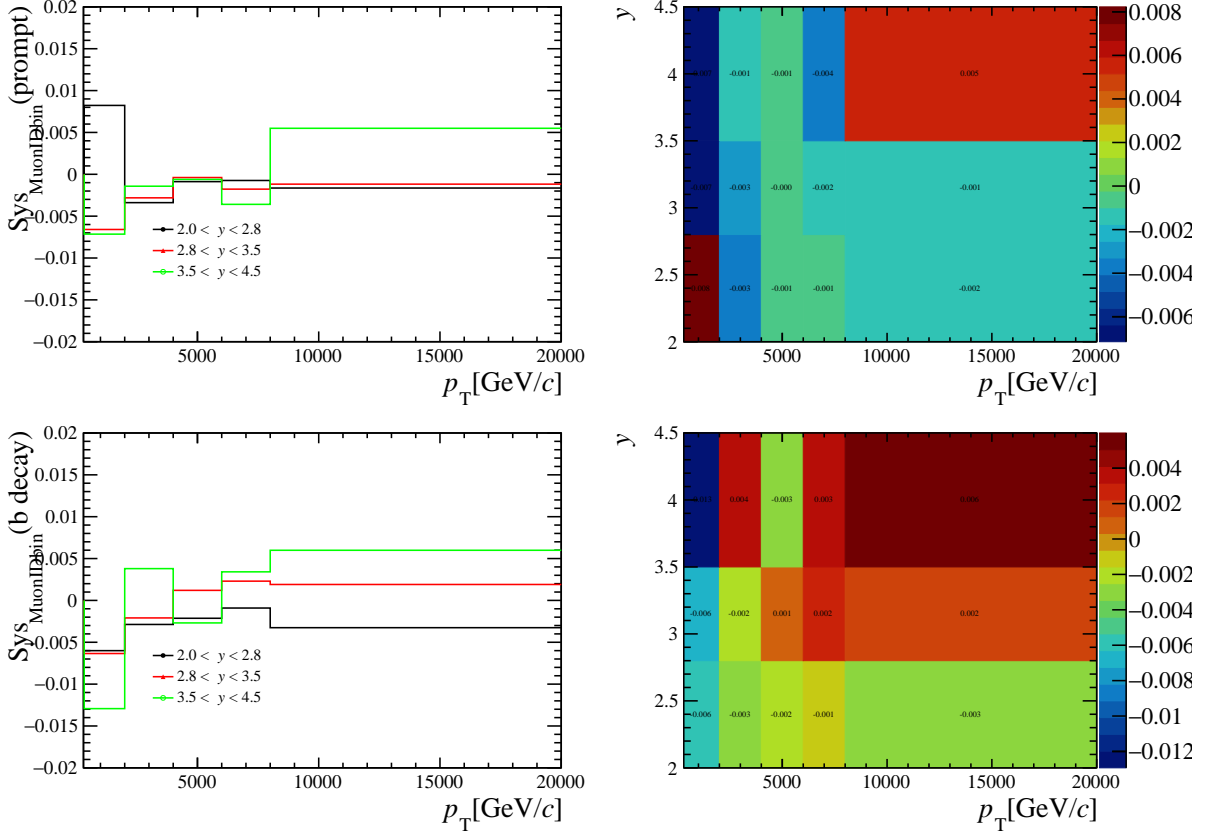


Figure 21: The systematic uncertainty of ratio of production due to the binning scheme of calibration sample in each bin for PVNTRACKS from 4 to 20. The first row is that of prompt components and the second row is that of components from  $b$ -hadron decay.

The maximum difference between the two new ratios calculated by new efficiency and the original ratio is quoted as the systematic uncertainty. The relative uncertainties for the ratio in each bin for PVNTRACKS from 4 to 20 are summarized in Fig 21.

## 578 7.5 MC sample size

579 The limited size of the simulation sample used to determine the efficiencies is a source of  
 580 systematic uncertainties. The uncertainty of ratio due to MC sample size in different bin  
 581 for PVNTRACKS from 4 to 20 are summarized in Fig 22.

## 582 7.6 Other systematic uncertainties

- 583 • The uncertainty of  $\mathcal{B}(J/\psi \rightarrow \mu^+\mu^-) = (5.961 \pm 0.033)\%$  and  $\mathcal{B}(\psi(2S) \rightarrow e^+e^-) = (7.93 \pm 0.17) \times 10^{-3}$  are canceled when we only care the normalized ratio.
- 585 • The relative uncertainty of the luminosity is canceled out when calculating the ratio  
 586 of production cross-section.
- 587 • A fraction of events is lost because of the QED radiative tail. But when calculating  
 588 the ratio of production, the effects for  $J/\psi$  and  $\psi(2S)$  are canceled out.

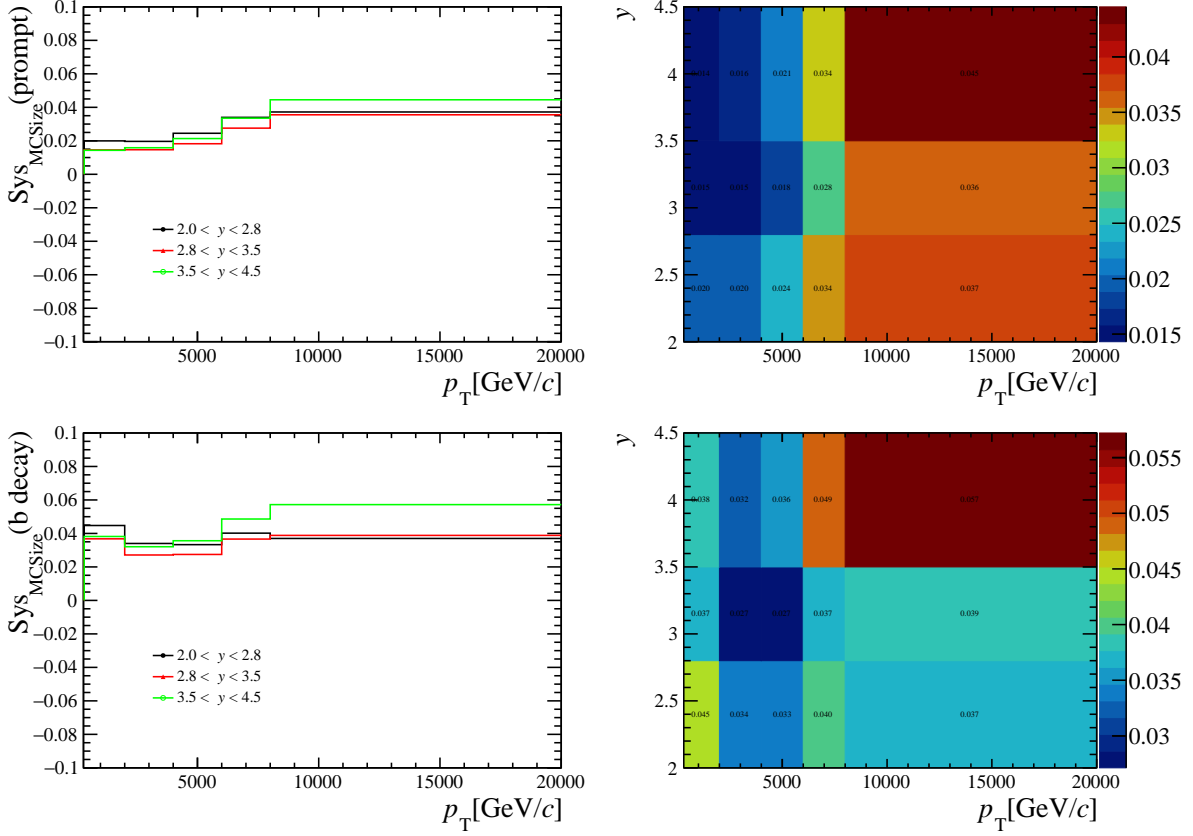


Figure 22: The systematic uncertainty of ratio of production due to limit sample size in each bin for PVNTRACKS from 4 to 20. The first row is that of prompt components and the second row is that of components from  $b$ -hadron decay.

## 589 8 Bin Width Correction

590 As shown in Fig. 4, the distributions of multiplicity skew a lot so that in a certain bin,  
 591 the center of the bin may not represent an ideal horizontal coordinate for plotting the  
 592 results, especially for the small and large multiplicity regions. To study the effect, 10000  
 593 fitting trials are done in Monte Carlo. In each trial, in a certain multiplicity region of the  
 594 three different binning schemes (PVNTRACKS, nForwardTracks, and nBackTracks), we  
 595 randomly sample the mean values of the multiplicity region from a Gaussian sampling,  
 596 within each bin, mean being the content of the bin and width being the error of the bin.  
 597 Then we fit the 10000 mean values with gaussian distribution to get the central values and  
 598 uncertainties. To choose a point at which to plot the data, we make the average value of  
 599 the central values we get from the fit. Since the data point is a ratio between two species,  
 600  $J/\psi$ , and  $\psi(2S)$ , the average value for the ratio is weighted by the inverse of the square of  
 601 the uncertainties (following the PDG weighted average procedure). An example is shown  
 602 in Fig. 23.

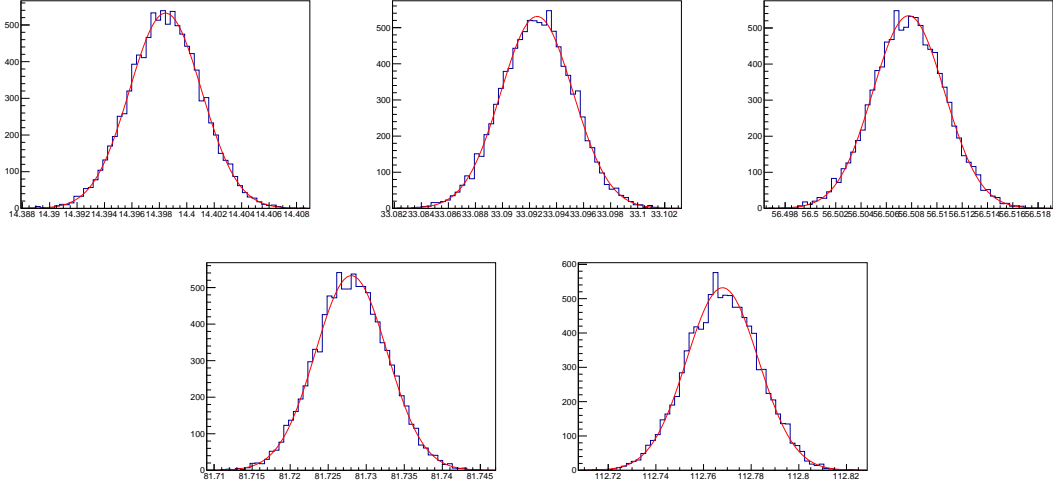


Figure 23: The distribution of mean value of PVNTRACKS for prompt  $J/\psi$  signal in each multiplicity region.

After finding the proper horizontal coordinates in each multiplicity region, they are further normalized by dividing the mean value of that into no-biased data. Finally, the horizontal coordinates for each species are summarized in Table 3.

Table 3: The horizontal coordinates for different binning schemes.

PVNTRACKS	4-20	20-45	45-70	70-100	100-200
prompt	0.4577	1.0524	1.7974	2.5996	3.5870
from $b$	0.4740	1.0685	1.8007	2.5989	3.5799
nForwardTracks	0-12	12-24	24-36	36-48	48-130
prompt	0.5395	1.1138	1.8132	2.5215	3.7005
from $b$	0.5416	1.1289	1.8183	2.5241	3.6952
nBackTracks	0-8	8-15	15-22	22-30	30-80
prompt	0.4622	1.1744	1.8746	2.6175	3.7706
from $b$	0.4937	1.1792	1.8767	2.6183	3.7707

## 9 Results

### 9.1 $\psi(2S)$ -to- $J/\psi$ ratio as functions of multiplicity

With the signal yields determined from the fitting to dimuon invariant mass distributions, the efficiencies estimated from simulation and calibrated control sample, and the systematic uncertainties, the ratio of  $\psi(2S)$  and  $J/\psi$  production cross-sections are measured in each kinematic and multiplicity bin. By integrating the double differential results over  $p_T$  ( $y$ ) one can obtain the ratio as functions of  $y(p_T)$ . And also the normalized ratio of total cross-sections as a function of normalized multiplicity can be obtained by integrating the double

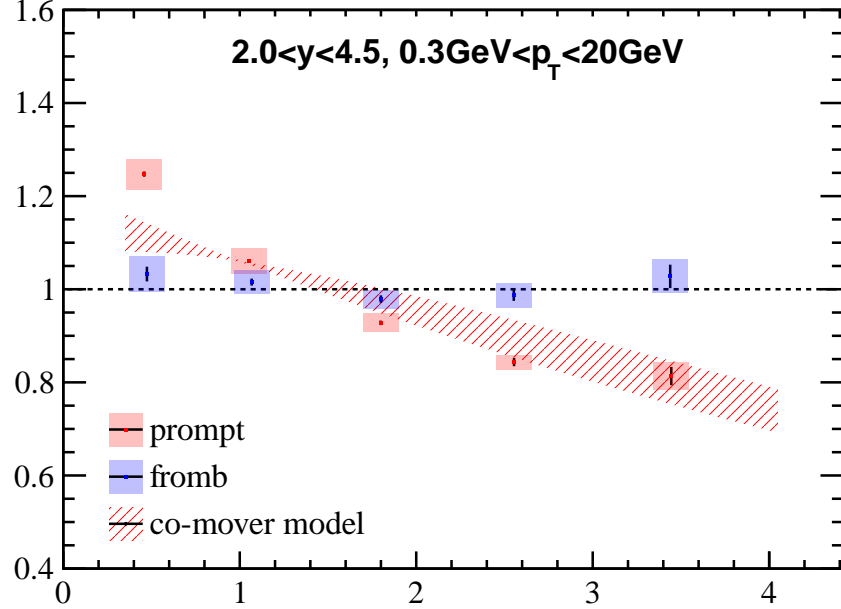


Figure 24: The ratio of integrated production over  $p_T$ - $y$  as a function of PVNTRACKS.

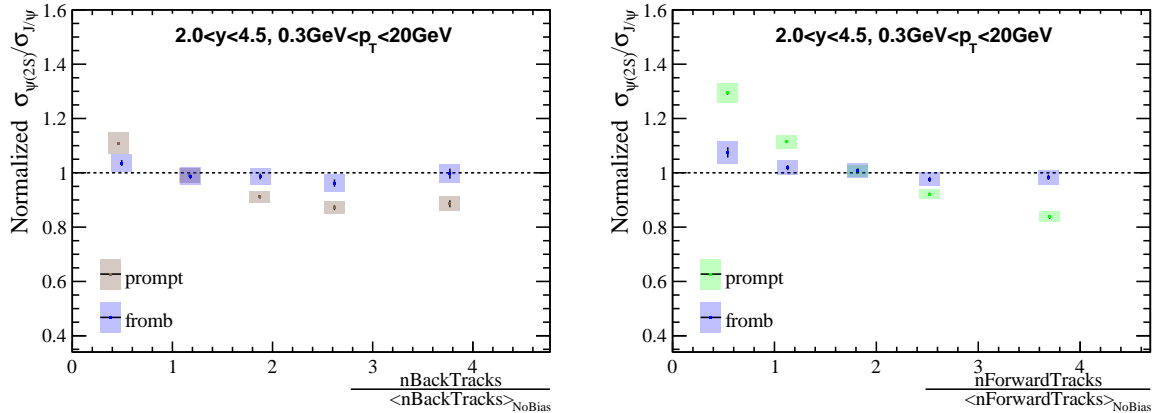


Figure 25: The ratio of integrated production over  $p_T$ - $y$  as a function of nBackTracks and nForwardTracks.

614 differential results over  $p_T$  and  $y$  bins. The normalized ratio of integrated production over  
 615  $p_T$ - $y$  as a function of PVNTRACKS is shown in Fig 24. We can see a decreasing trend  
 616 for the ratio of prompt production with multiplicity getting larger. While for the ratio  
 617 of production from  $b$ -hadron decay, no significantly decreasing trend is observed. The  
 618 ratio of production is also measured as a function of nBackTracks and nForwardTracks 25,  
 619 which are two mutual subsets of PVNTRACKS representing numbers of backward and  
 620 forward tracks respectively. The ratio of production from  $b$ -hadron decay is roughly  
 621 independent of multiplicity under three different kinds of schemes. The decreasing trend  
 622 for the ratio versus nBackTracks is much slower than the other two. This indicates

623 that the relative suppression is correlated with the local particle multiplicity since an  
 624 independent multiplicity variable leads to a slower decrease. It is within expectation since  
 625  $\psi(2S)$  has a larger radius and lower bounding energy so a preferential dissociation may  
 626 happen when interacting with the co-moving matters after the collisions. Theoretically,  
 627 nBackTracks is a multiplicity variable independent of the measured ratio, and the ratio  
 628 should roughly be the same in different multiplicity regions. But nBackTracks is not fully  
 629 independent since there is a correlation between nForwardTracks and nBackTracks with  
 630 a correlation factor of 0.54 for  $J/\psi$  and 0.51 for  $\psi(2S)$ . To study the effect produced by  
 631 the correlation between nBackTracks and nForwardTracks, we measure the mean values  
 632 of nForwardTracks in each nBackTracks bin for both prompt  $J/\psi$  and  $\psi(2S)$ . Then we  
 633 follow the procedures in Sec 8 to calculate the x-coordinates of nForwardTracks in each  
 634 nBackTracks bin. Finally, the normalized ratios in different nBackTracks bin is migrated  
 635 to the plot of nForwardTracks in Figs. 26. We find a good agreement on the decreasing  
 636 trend, which means the dependence of normalized  $\psi(2S)$ -to- $J/\psi$  ratio on nBackTracks  
 637 could result from the correlation between nBackTracks and nForwardTracks.

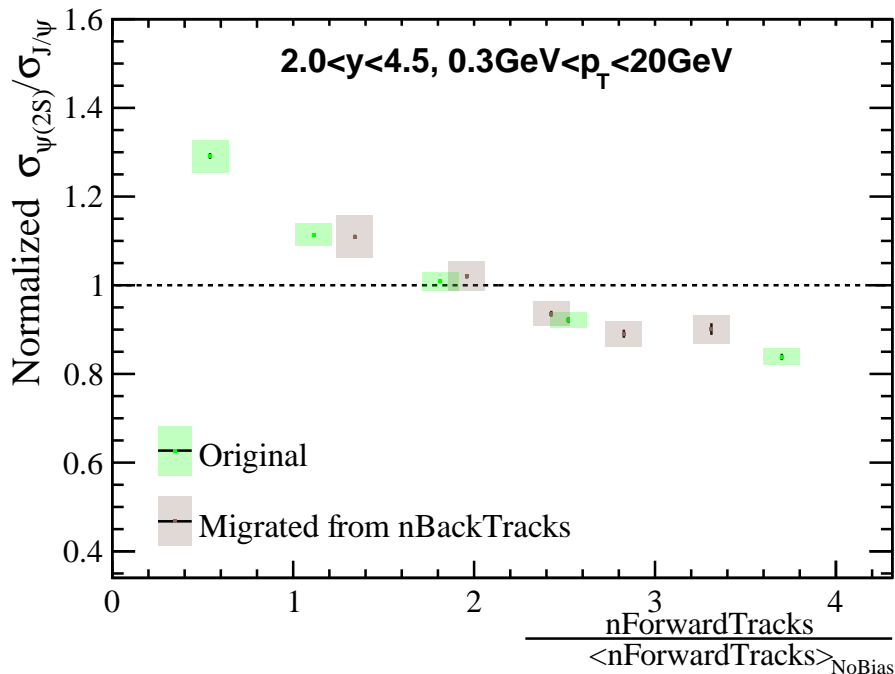


Figure 26: Data points on nBackTracks are migrated to plot of nForwardTracks by find the mean value of nForwardTracks in each nBackTracks bin.

## 638 9.2 $\psi(2S)$ -to- $J/\psi$ ratio in different $p_T$ regions

639 In Sec 8 we have discussed how to find appropriate horizontal coordinates for the  $\psi(2S)$ -to-  
 640  $J/\psi$  ratio in  $2.0 < y < 4.5$  and  $0.3 \text{ GeV}/c < p_T < 20 \text{ GeV}/c$ . The multiplicity distributions  
 641 in different  $p_T$  ranges are significantly different. Hence, for all the results in different  
 642  $p_T$  ranges, we need to repeat the procedures in Sec 8 to find appropriate horizontal  
 643 coordinates for plotting. And the final results in different  $p_T$  ranges are shown in Fig 27,  
 644 Fig 28 and Fig 29. In three binning schemes for multiplicity, the ratios share the same

645 property that, in low  $p_T$  region, the preferential suppression of  $\psi(2S)$  is higher than that  
 646 in higher  $p_T$  region.

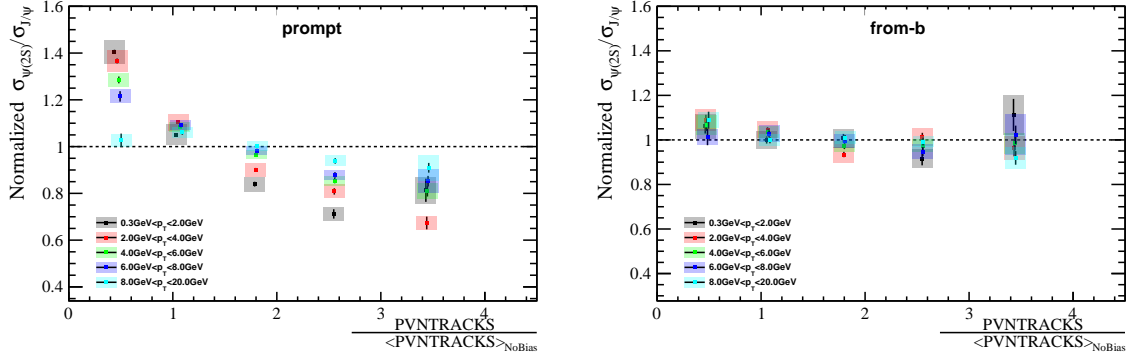


Figure 27: Ratio of  $\psi(2S)$  to  $J/\psi$  in different  $p_T$  region when multiplicity is divided by PVN-TRACKS

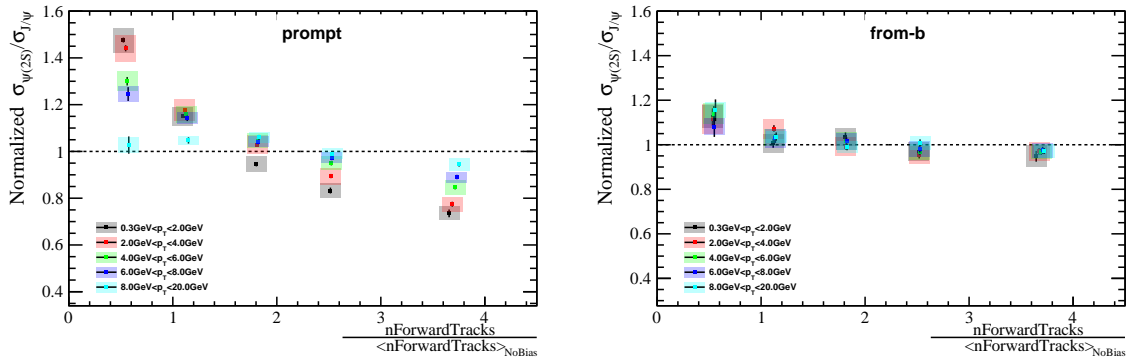


Figure 28: Ratio of  $\psi(2S)$  to  $J/\psi$  in different  $p_T$  region when multiplicity is divided by nForwardTracks

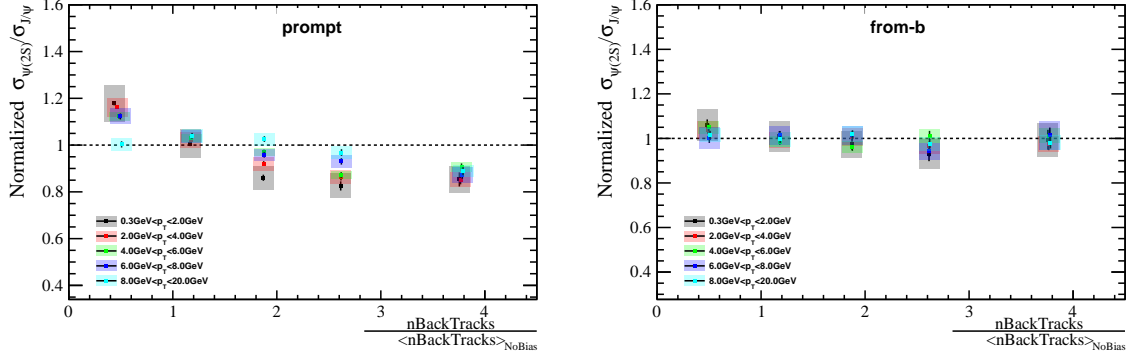


Figure 29: Ratio of  $\psi(2S)$  to  $J/\psi$  in different  $p_T$  region when multiplicity is divided by nBackTracks

### 9.3 $\psi(2S)$ -to- $J/\psi$ ratio in different $y$ regions

The results for ratio in different rapidity bins are given in Figs 30 when taking PVN-TRACKS as a multiplicity variable. And the results for nForwardTracks and nBackTracks are given in Figs 31 and Figs 32. The results show that there is no significant difference in different rapidity regions, for both prompt and non-prompt signals.

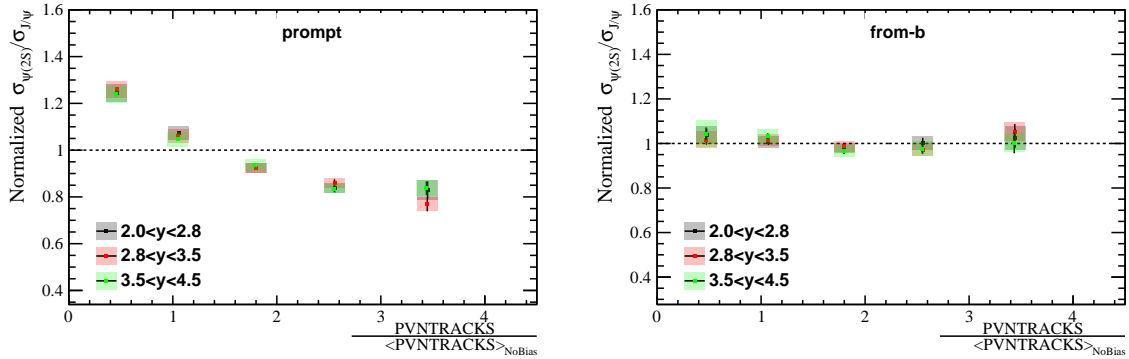


Figure 30: Ratio of  $\psi(2S)$  to  $J/\psi$  in different  $y$  region when multiplicity is divided by PVN-TRACKS

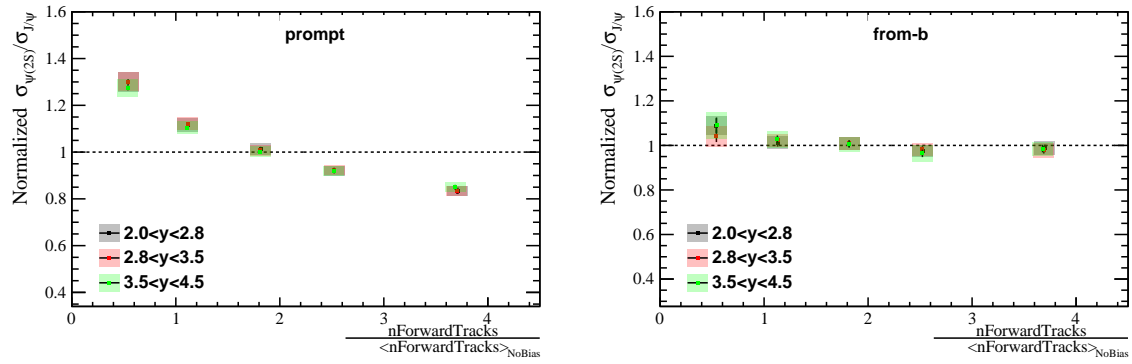


Figure 31: Ratio of  $\psi(2S)$  to  $J/\psi$  in different  $y$  region when multiplicity is divided by nForwardTracks

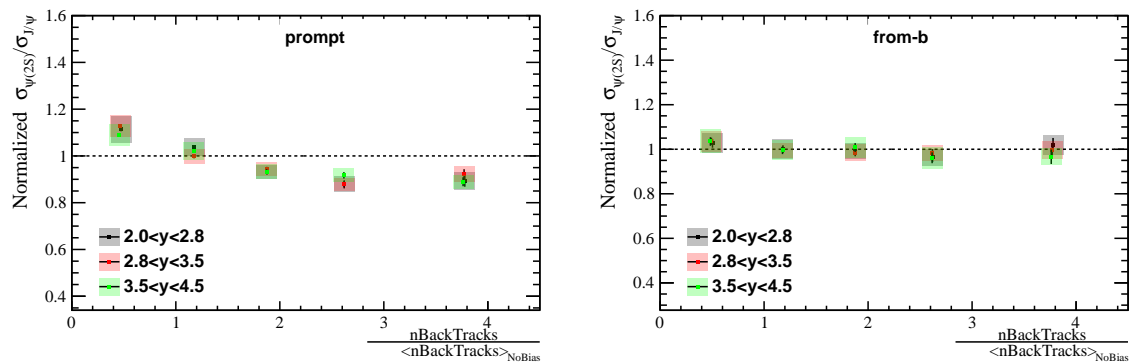


Figure 32: Ratio of  $\psi(2S)$  to  $J/\psi$  in different  $y$  region when multiplicity is divided by nBackTracks

## 652 10 Conclusion

653 The ratio of production cross-sections of  $\psi(2S)$  to  $J/\psi$  in proton-proton collisions at a  
654 center-of-mass energy  $\sqrt{s} = 13$  TeV are reported with a data sample corresponding to  
655 an integrated luminosity of  $658 \pm 13 \text{ pb}^{-1}$ , collected by the LHCb detector in 2016. The  
656 normalized ratio of  $\psi(2S)$ -to- $J/\psi$  production, as functions of  $p_T$  and  $y$  in different  $p_T$   
657 and  $y$  regions, are measured as well as in the total region of  $0 \text{ GeV} < p_T < 20 \text{ GeV}$  and  
658  $2.0 < y < 4.5$  for prompt production and production from  $b$ -hadron decay. We see an  
659 obvious decreasing trend for prompt production as a function of PVNTRACKS and  
660 nForwardTracks and a slower decrease as a function of nBackTracks. For the ratio of  
661 production from  $b$ -hadron decay, there is no independence shown.

## 662 A. Tables of ratio

### 663 A.1 Taking PVNTRACKS as multiplicity variable

Table 4: Ratio(%) of double differential production cross-section for prompt  $\psi(2S)$  to  $J/\psi$  in bins of  $(p_T, y)$ . The first uncertainties are statistical, the second are the systematic uncertainties, for  $0 \leq \text{PVNTRACKS} < 20$ .

prompt			
$p_T$ (GeV/c)	$2 < y < 2.8$	$2.8 < y < 3.5$	$3.5 < y < 4.5$
0-2	$14.95 \pm 0.19 \pm 0.64$	$15.18 \pm 0.15 \pm 0.56$	$15.54 \pm 0.15 \pm 0.60$
2-4	$20.45 \pm 0.30 \pm 0.82$	$18.97 \pm 0.22 \pm 0.66$	$19.49 \pm 0.24 \pm 0.68$
4-6	$29.18 \pm 0.60 \pm 0.93$	$23.22 \pm 0.39 \pm 0.59$	$22.75 \pm 0.45 \pm 0.67$
6-8	$34.60 \pm 1.08 \pm 1.32$	$26.74 \pm 0.76 \pm 0.85$	$27.89 \pm 0.93 \pm 1.05$
8-20	$33.05 \pm 1.39 \pm 1.41$	$27.67 \pm 1.19 \pm 1.04$	$29.83 \pm 1.65 \pm 1.62$
from $b$			
$p_T$ (GeV/c)	$2 < y < 2.8$	$2.8 < y < 3.5$	$3.5 < y < 4.5$
0-2	$21.88 \pm 1.19 \pm 1.26$	$19.99 \pm 0.91 \pm 1.10$	$21.04 \pm 1.16 \pm 1.80$
2-4	$28.29 \pm 1.17 \pm 1.48$	$27.02 \pm 0.90 \pm 1.21$	$27.60 \pm 1.11 \pm 1.65$
4-6	$32.89 \pm 1.53 \pm 1.53$	$29.53 \pm 1.13 \pm 1.39$	$33.70 \pm 1.57 \pm 1.91$
6-8	$34.89 \pm 2.10 \pm 1.78$	$31.70 \pm 1.69 \pm 1.30$	$32.33 \pm 2.23 \pm 1.87$
8-20	$43.93 \pm 2.36 \pm 1.82$	$39.96 \pm 2.16 \pm 1.63$	$39.78 \pm 2.95 \pm 2.71$

Table 5: Ratio(%) of double differential production cross-section for prompt  $\psi(2S)$  to  $J/\psi$  in bins of  $(p_T, y)$ . The first uncertainties are statistical, the second are the systematic uncertainties, for  $20 \leq \text{PVNTRACKS} < 45$ .

prompt			
$p_T$ (GeV/c)	$2 < y < 2.8$	$2.8 < y < 3.5$	$3.5 < y < 4.5$
0-2	$11.50 \pm 0.14 \pm 0.46$	$10.92 \pm 0.11 \pm 0.48$	$11.62 \pm 0.11 \pm 0.57$
2-4	$16.48 \pm 0.17 \pm 0.59$	$15.33 \pm 0.13 \pm 0.51$	$15.81 \pm 0.14 \pm 0.51$
4-6	$22.41 \pm 0.25 \pm 0.54$	$20.68 \pm 0.18 \pm 0.42$	$20.62 \pm 0.21 \pm 0.45$
6-8	$29.18 \pm 0.40 \pm 0.87$	$26.20 \pm 0.32 \pm 0.58$	$25.11 \pm 0.38 \pm 0.67$
8-20	$35.01 \pm 0.53 \pm 1.00$	$29.31 \pm 0.43 \pm 0.78$	$28.46 \pm 0.54 \pm 0.89$
from $b$			
$p_T$ (GeV/c)	$2 < y < 2.8$	$2.8 < y < 3.5$	$3.5 < y < 4.5$
0-2	$19.03 \pm 0.57 \pm 0.93$	$20.24 \pm 0.49 \pm 0.85$	$20.72 \pm 0.56 \pm 1.02$
2-4	$26.92 \pm 0.55 \pm 1.08$	$25.65 \pm 0.43 \pm 1.03$	$27.27 \pm 0.56 \pm 1.16$
4-6	$34.28 \pm 0.68 \pm 0.97$	$28.18 \pm 0.49 \pm 0.84$	$29.32 \pm 0.67 \pm 1.12$
6-8	$34.61 \pm 0.83 \pm 1.37$	$32.17 \pm 0.71 \pm 0.99$	$34.12 \pm 1.02 \pm 2.00$
8-20	$41.47 \pm 0.84 \pm 1.25$	$36.17 \pm 0.78 \pm 1.15$	$34.52 \pm 1.04 \pm 1.25$

Table 6: Ratio(%) of double differential production cross-section for prompt  $\psi(2S)$  to  $J/\psi$  in bins of  $(p_T, y)$ . The first uncertainties are statistical, the second are the systematic uncertainties, for  $45 \leq \text{PVNTRACKS} < 70$ .

prompt			
$p_T$ (GeV/c)	$2 < y < 2.8$	$2.8 < y < 3.5$	$3.5 < y < 4.5$
0-2	$9.04 \pm 0.22 \pm 0.38$	$8.79 \pm 0.18 \pm 0.33$	$9.42 \pm 0.16 \pm 0.40$
2-4	$13.03 \pm 0.21 \pm 0.46$	$12.38 \pm 0.16 \pm 0.41$	$13.53 \pm 0.17 \pm 0.47$
4-6	$20.18 \pm 0.28 \pm 0.57$	$17.62 \pm 0.21 \pm 0.39$	$18.83 \pm 0.23 \pm 0.49$
6-8	$25.17 \pm 0.38 \pm 0.70$	$23.94 \pm 0.31 \pm 0.54$	$23.65 \pm 0.37 \pm 0.62$
8-20	$31.32 \pm 0.43 \pm 0.87$	$29.02 \pm 0.41 \pm 0.75$	$27.94 \pm 0.50 \pm 0.90$

from $b$			
$p_T$ (GeV/c)	$2 < y < 2.8$	$2.8 < y < 3.5$	$3.5 < y < 4.5$
0-2	$20.93 \pm 0.68 \pm 1.03$	$18.99 \pm 0.56 \pm 0.98$	$19.55 \pm 0.62 \pm 0.91$
2-4	$23.54 \pm 0.54 \pm 0.93$	$24.22 \pm 0.45 \pm 0.94$	$23.76 \pm 0.55 \pm 1.08$
4-6	$31.83 \pm 0.66 \pm 0.90$	$26.85 \pm 0.49 \pm 0.84$	$27.46 \pm 0.67 \pm 1.21$
6-8	$32.65 \pm 0.77 \pm 1.05$	$31.71 \pm 0.69 \pm 1.04$	$34.16 \pm 0.96 \pm 1.56$
8-20	$39.44 \pm 0.74 \pm 1.16$	$37.75 \pm 0.73 \pm 1.17$	$38.58 \pm 1.07 \pm 1.73$

Table 7: Ratio(%) of double differential production cross-section for prompt  $\psi(2S)$  to  $J/\psi$  in bins of  $(p_T, y)$ . The first uncertainties are statistical, the second are the systematic uncertainties, for  $70 \leq \text{PVNTRACKS} < 95$ .

prompt			
$p_T$ (GeV/c)	$2 < y < 2.8$	$2.8 < y < 3.5$	$3.5 < y < 4.5$
0-2	$7.71 \pm 0.44 \pm 0.36$	$7.89 \pm 0.34 \pm 0.33$	$7.55 \pm 0.28 \pm 0.56$
2-4	$11.29 \pm 0.37 \pm 0.47$	$11.58 \pm 0.31 \pm 0.43$	$12.18 \pm 0.30 \pm 0.57$
4-6	$17.92 \pm 0.43 \pm 0.62$	$15.68 \pm 0.31 \pm 0.41$	$16.52 \pm 0.36 \pm 0.53$
6-8	$23.07 \pm 0.54 \pm 0.83$	$20.16 \pm 0.43 \pm 0.62$	$21.77 \pm 0.52 \pm 0.79$
8-20	$29.65 \pm 0.59 \pm 1.20$	$27.43 \pm 0.55 \pm 1.01$	$25.27 \pm 0.66 \pm 1.05$

from $b$			
$p_T$ (GeV/c)	$2 < y < 2.8$	$2.8 < y < 3.5$	$3.5 < y < 4.5$
0-2	$17.74 \pm 1.03 \pm 1.20$	$17.59 \pm 0.80 \pm 0.93$	$19.41 \pm 0.99 \pm 1.03$
2-4	$26.99 \pm 0.92 \pm 1.23$	$24.29 \pm 0.69 \pm 1.01$	$25.62 \pm 0.89 \pm 1.43$
4-6	$32.36 \pm 0.99 \pm 1.15$	$26.84 \pm 0.71 \pm 0.98$	$26.85 \pm 0.95 \pm 1.25$
6-8	$31.96 \pm 1.12 \pm 1.29$	$31.70 \pm 1.01 \pm 1.32$	$28.69 \pm 1.32 \pm 1.63$
8-20	$41.22 \pm 1.06 \pm 1.33$	$35.64 \pm 1.01 \pm 1.42$	$34.33 \pm 1.47 \pm 1.63$

Table 8: Ratio(%) of double differential production cross-section for prompt  $\psi(2S)$  to  $J/\psi$  in bins of  $(p_T, y)$ . The first uncertainties are statistical, the second are the systematic uncertainties, for  $95 \leq \text{PVNTRACKS} < 200$ .

prompt			
$p_T$ (GeV/c)	$2 < y < 2.8$	$2.8 < y < 3.5$	$3.5 < y < 4.5$
0-2	$9.91 \pm 1.05 \pm 0.88$	$7.13 \pm 0.79 \pm 0.51$	$8.93 \pm 0.77 \pm 0.74$
2-4	$9.18 \pm 0.74 \pm 0.61$	$9.23 \pm 0.59 \pm 0.47$	$10.99 \pm 0.61 \pm 0.59$
4-6	$17.20 \pm 0.86 \pm 1.04$	$14.79 \pm 0.61 \pm 0.69$	$15.31 \pm 0.66 \pm 1.10$
6-8	$22.16 \pm 1.04 \pm 1.89$	$19.04 \pm 0.78 \pm 1.61$	$22.02 \pm 1.00 \pm 1.61$
8-20	$28.98 \pm 1.05 \pm 3.44$	$26.00 \pm 0.93 \pm 1.54$	$24.66 \pm 1.17 \pm 1.85$
from $b$			
$p_T$ (GeV/c)	$2 < y < 2.8$	$2.8 < y < 3.5$	$3.5 < y < 4.5$
0-2	$23.68 \pm 2.65 \pm 3.14$	$20.28 \pm 1.84 \pm 1.76$	$21.47 \pm 2.45 \pm 2.14$
2-4	$24.12 \pm 1.55 \pm 2.00$	$25.31 \pm 1.39 \pm 1.47$	$24.29 \pm 1.61 \pm 1.82$
4-6	$30.40 \pm 1.81 \pm 4.43$	$28.96 \pm 1.41 \pm 1.87$	$28.78 \pm 1.85 \pm 2.27$
6-8	$35.56 \pm 2.30 \pm 3.37$	$36.19 \pm 1.99 \pm 4.03$	$25.80 \pm 2.46 \pm 2.30$
8-20	$35.20 \pm 1.79 \pm 2.75$	$33.68 \pm 1.78 \pm 1.75$	$37.92 \pm 2.77 \pm 3.22$

## 664 A.2 Taking nBackTracks as multiplicity variable

Table 9: Ratio(%) of double differential production cross-section for prompt  $\psi(2S)$  to  $J/\psi$  in bins of  $(p_T, y)$ . The first uncertainties are statistical, the second are the systematic uncertainties, for  $0 \leq \text{nBackTracks} < 8$ .

prompt			
$p_T$ (GeV/c)	$2 < y < 2.8$	$2.8 < y < 3.5$	$3.5 < y < 4.5$
0-2	$12.78 \pm 0.18 \pm 1.00$	$12.48 \pm 0.14 \pm 0.79$	$12.88 \pm 0.13 \pm 0.88$
2-4	$17.26 \pm 0.23 \pm 0.72$	$16.40 \pm 0.18 \pm 0.58$	$16.36 \pm 0.18 \pm 0.56$
4-6	$23.45 \pm 0.36 \pm 0.68$	$21.17 \pm 0.26 \pm 0.44$	$20.84 \pm 0.29 \pm 0.49$
6-8	$30.78 \pm 0.62 \pm 1.28$	$26.87 \pm 0.47 \pm 0.90$	$26.21 \pm 0.53 \pm 0.99$
8-20	$32.25 \pm 0.71 \pm 1.28$	$28.28 \pm 0.60 \pm 1.05$	$27.93 \pm 0.76 \pm 1.11$
from $b$			
$p_T$ (GeV/c)	$2 < y < 2.8$	$2.8 < y < 3.5$	$3.5 < y < 4.5$
0-2	$21.71 \pm 0.88 \pm 2.51$	$20.83 \pm 0.72 \pm 1.56$	$21.28 \pm 0.82 \pm 1.83$
2-4	$26.41 \pm 0.79 \pm 1.18$	$26.46 \pm 0.63 \pm 1.16$	$26.41 \pm 0.75 \pm 1.23$
4-6	$34.65 \pm 1.00 \pm 1.18$	$29.13 \pm 0.71 \pm 0.93$	$30.13 \pm 0.95 \pm 1.32$
6-8	$33.39 \pm 1.23 \pm 1.87$	$31.37 \pm 1.02 \pm 1.54$	$33.99 \pm 1.40 \pm 2.37$
8-20	$41.81 \pm 1.26 \pm 1.45$	$36.94 \pm 1.11 \pm 1.56$	$35.45 \pm 1.45 \pm 1.75$

Table 10: Ratio(%) of double differential production cross-section for prompt  $\psi(2S)$  to  $J/\psi$  in bins of  $(p_T, y)$ . The first uncertainties are statistical, the second are the systematic uncertainties, for  $8 \leq n_{\text{BackTracks}} < 15$ .

prompt			
$p_T$ (GeV/c)	$2 < y < 2.8$	$2.8 < y < 3.5$	$3.5 < y < 4.5$
0-2	$10.88 \pm 0.21 \pm 0.71$	$10.31 \pm 0.17 \pm 0.60$	$11.35 \pm 0.16 \pm 0.74$
2-4	$15.30 \pm 0.24 \pm 0.60$	$13.74 \pm 0.18 \pm 0.47$	$14.85 \pm 0.19 \pm 0.51$
4-6	$21.98 \pm 0.33 \pm 0.56$	$18.69 \pm 0.23 \pm 0.39$	$19.23 \pm 0.27 \pm 0.43$
6-8	$27.76 \pm 0.49 \pm 1.04$	$25.11 \pm 0.38 \pm 0.74$	$24.65 \pm 0.47 \pm 0.91$
8-20	$33.44 \pm 0.60 \pm 1.22$	$28.62 \pm 0.51 \pm 0.88$	$29.46 \pm 0.66 \pm 1.36$

from $b$			
$p_T$ (GeV/c)	$2 < y < 2.8$	$2.8 < y < 3.5$	$3.5 < y < 4.5$
0-2	$21.38 \pm 0.82 \pm 1.64$	$19.44 \pm 0.63 \pm 1.32$	$19.59 \pm 0.71 \pm 1.55$
2-4	$25.22 \pm 0.68 \pm 1.10$	$24.62 \pm 0.53 \pm 0.97$	$26.11 \pm 0.70 \pm 1.06$
4-6	$32.12 \pm 0.80 \pm 1.00$	$27.71 \pm 0.60 \pm 0.78$	$28.15 \pm 0.81 \pm 1.17$
6-8	$33.65 \pm 0.99 \pm 1.49$	$33.25 \pm 0.88 \pm 1.29$	$32.86 \pm 1.20 \pm 2.28$
8-20	$39.68 \pm 0.95 \pm 1.50$	$37.19 \pm 0.94 \pm 1.34$	$35.36 \pm 1.31 \pm 1.92$

Table 11: Ratio(%) of double differential production cross-section for prompt  $\psi(2S)$  to  $J/\psi$  in bins of  $(p_T, y)$ . The first uncertainties are statistical, the second are the systematic uncertainties, for  $15 \leq n_{\text{BackTracks}} < 22$ .

prompt			
$p_T$ (GeV/c)	$2 < y < 2.8$	$2.8 < y < 3.5$	$3.5 < y < 4.5$
0-2	$8.97 \pm 0.27 \pm 0.55$	$9.42 \pm 0.23 \pm 0.57$	$9.58 \pm 0.21 \pm 0.61$
2-4	$13.41 \pm 0.28 \pm 0.50$	$12.68 \pm 0.22 \pm 0.44$	$13.57 \pm 0.24 \pm 0.51$
4-6	$20.29 \pm 0.38 \pm 0.54$	$17.52 \pm 0.27 \pm 0.37$	$18.62 \pm 0.33 \pm 0.46$
6-8	$25.76 \pm 0.52 \pm 0.95$	$23.21 \pm 0.41 \pm 0.74$	$22.37 \pm 0.49 \pm 0.82$
8-20	$32.96 \pm 0.62 \pm 1.26$	$28.41 \pm 0.55 \pm 0.93$	$28.58 \pm 0.73 \pm 1.05$

from $b$			
$p_T$ (GeV/c)	$2 < y < 2.8$	$2.8 < y < 3.5$	$3.5 < y < 4.5$
0-2	$18.28 \pm 0.84 \pm 1.29$	$19.54 \pm 0.74 \pm 1.33$	$21.70 \pm 0.89 \pm 1.48$
2-4	$26.99 \pm 0.78 \pm 1.15$	$24.53 \pm 0.61 \pm 1.07$	$24.61 \pm 0.76 \pm 1.33$
4-6	$31.88 \pm 0.91 \pm 1.00$	$25.95 \pm 0.64 \pm 1.09$	$27.80 \pm 0.93 \pm 1.11$
6-8	$35.26 \pm 1.08 \pm 1.53$	$31.24 \pm 0.93 \pm 1.34$	$32.19 \pm 1.34 \pm 2.00$
8-20	$40.96 \pm 1.06 \pm 1.59$	$36.60 \pm 1.00 \pm 1.43$	$37.63 \pm 1.47 \pm 1.94$

Table 12: Ratio(%) of double differential production cross-section for prompt  $\psi(2S)$  to  $J/\psi$  in bins of  $(p_T, y)$ . The first uncertainties are statistical, the second are the systematic uncertainties, for  $22 \leq n\text{BackTracks} < 30$ .

prompt			
$p_T$ (GeV/c)	$2 < y < 2.8$	$2.8 < y < 3.5$	$3.5 < y < 4.5$
0-2	$8.84 \pm 0.42 \pm 0.59$	$8.44 \pm 0.31 \pm 0.52$	$9.44 \pm 0.30 \pm 0.79$
2-4	$12.34 \pm 0.39 \pm 0.57$	$11.70 \pm 0.29 \pm 0.42$	$13.21 \pm 0.32 \pm 0.50$
4-6	$17.14 \pm 0.46 \pm 0.54$	$16.60 \pm 0.35 \pm 0.41$	$17.25 \pm 0.42 \pm 0.50$
6-8	$24.94 \pm 0.65 \pm 1.08$	$21.02 \pm 0.49 \pm 0.73$	$23.60 \pm 0.66 \pm 1.00$
8-20	$30.78 \pm 0.71 \pm 1.18$	$27.47 \pm 0.66 \pm 0.98$	$26.57 \pm 0.84 \pm 1.43$

from $b$			
$p_T$ (GeV/c)	$2 < y < 2.8$	$2.8 < y < 3.5$	$3.5 < y < 4.5$
0-2	$19.08 \pm 1.06 \pm 1.52$	$18.33 \pm 0.91 \pm 1.33$	$18.24 \pm 1.04 \pm 1.80$
2-4	$24.53 \pm 0.93 \pm 1.12$	$24.59 \pm 0.75 \pm 0.97$	$24.82 \pm 0.98 \pm 1.20$
4-6	$34.04 \pm 1.14 \pm 1.17$	$27.68 \pm 0.83 \pm 0.96$	$28.05 \pm 1.18 \pm 1.51$
6-8	$30.65 \pm 1.25 \pm 1.30$	$30.66 \pm 1.13 \pm 1.39$	$31.91 \pm 1.65 \pm 2.05$
8-20	$38.03 \pm 1.20 \pm 1.30$	$36.79 \pm 1.24 \pm 1.53$	$35.96 \pm 1.79 \pm 2.24$

Table 13: Ratio(%) of double differential production cross-section for prompt  $\psi(2S)$  to  $J/\psi$  in bins of  $(p_T, y)$ . The first uncertainties are statistical, the second are the systematic uncertainties, for  $30 \leq n\text{BackTracks} < 80$ .

prompt			
$p_T$ (GeV/c)	$2 < y < 2.8$	$2.8 < y < 3.5$	$3.5 < y < 4.5$
0-2	$10.05 \pm 0.65 \pm 0.85$	$8.74 \pm 0.49 \pm 0.54$	$8.60 \pm 0.43 \pm 0.57$
2-4	$11.00 \pm 0.52 \pm 0.47$	$12.93 \pm 0.46 \pm 0.66$	$13.28 \pm 0.44 \pm 0.50$
4-6	$19.54 \pm 0.67 \pm 0.67$	$15.82 \pm 0.44 \pm 0.39$	$17.01 \pm 0.52 \pm 0.66$
6-8	$21.82 \pm 0.78 \pm 1.09$	$21.98 \pm 0.68 \pm 1.17$	$21.93 \pm 0.79 \pm 0.89$
8-20	$28.63 \pm 0.87 \pm 1.21$	$25.73 \pm 0.78 \pm 0.94$	$22.99 \pm 0.96 \pm 1.02$

from $b$			
$p_T$ (GeV/c)	$2 < y < 2.8$	$2.8 < y < 3.5$	$3.5 < y < 4.5$
0-2	$20.03 \pm 1.60 \pm 2.02$	$19.62 \pm 1.20 \pm 1.47$	$20.23 \pm 1.49 \pm 1.54$
2-4	$26.02 \pm 1.26 \pm 1.18$	$23.62 \pm 1.01 \pm 1.00$	$24.16 \pm 1.25 \pm 1.08$
4-6	$33.55 \pm 1.45 \pm 1.22$	$28.41 \pm 1.07 \pm 1.06$	$27.64 \pm 1.44 \pm 1.63$
6-8	$35.20 \pm 1.81 \pm 1.99$	$34.75 \pm 1.62 \pm 2.77$	$27.33 \pm 2.10 \pm 2.31$
8-20	$40.75 \pm 1.57 \pm 1.67$	$33.67 \pm 1.46 \pm 1.21$	$34.87 \pm 2.28 \pm 1.78$

665 **A.3 Taking nForwardTracks as multiplicity variable**

Table 14: Ratio(%) of double differential production cross-section for prompt  $\psi(2S)$  to  $J/\psi$  in bins of  $(p_T, y)$ . The first uncertainties are statistical, the second are the systematic uncertainties, for  $0 \leq \text{nForwardTracks} < 12$ .

prompt			
$p_T$ (GeV/c)	$2 < y < 2.8$	$2.8 < y < 3.5$	$3.5 < y < 4.5$
0-2	$16.01 \pm 0.22 \pm 0.66$	$15.86 \pm 0.18 \pm 0.58$	$16.07 \pm 0.18 \pm 0.60$
2-4	$21.67 \pm 0.37 \pm 0.98$	$19.67 \pm 0.27 \pm 0.82$	$20.59 \pm 0.31 \pm 0.86$
4-6	$28.37 \pm 0.70 \pm 1.08$	$24.31 \pm 0.51 \pm 0.89$	$23.25 \pm 0.58 \pm 0.91$
6-8	$34.96 \pm 1.38 \pm 1.39$	$27.17 \pm 1.00 \pm 1.01$	$28.99 \pm 1.26 \pm 1.18$
8-20	$33.65 \pm 1.77 \pm 1.53$	$27.14 \pm 1.59 \pm 1.10$	$28.53 \pm 2.28 \pm 1.78$
from $b$			
$p_T$ (GeV/c)	$2 < y < 2.8$	$2.8 < y < 3.5$	$3.5 < y < 4.5$
0-2	$22.02 \pm 1.35 \pm 1.24$	$21.28 \pm 1.08 \pm 1.24$	$23.51 \pm 1.43 \pm 1.45$
2-4	$29.87 \pm 1.36 \pm 1.87$	$26.89 \pm 1.03 \pm 1.47$	$27.32 \pm 1.33 \pm 2.22$
4-6	$35.66 \pm 1.82 \pm 1.57$	$30.86 \pm 1.42 \pm 1.72$	$35.67 \pm 1.97 \pm 2.05$
6-8	$36.27 \pm 2.50 \pm 1.78$	$35.57 \pm 2.18 \pm 1.76$	$34.00 \pm 2.92 \pm 1.86$
8-20	$48.13 \pm 3.00 \pm 1.93$	$40.55 \pm 2.76 \pm 1.67$	$39.03 \pm 3.58 \pm 2.79$

Table 15: Ratio(%) of double differential production cross-section for prompt  $\psi(2S)$  to  $J/\psi$  in bins of  $(p_T, y)$ . The first uncertainties are statistical, the second are the systematic uncertainties, for  $12 \leq \text{nForwardTracks} < 24$ .

prompt			
$p_T$ (GeV/c)	$2 < y < 2.8$	$2.8 < y < 3.5$	$3.5 < y < 4.5$
0-2	$12.52 \pm 0.16 \pm 0.48$	$12.00 \pm 0.12 \pm 0.42$	$12.79 \pm 0.12 \pm 0.48$
2-4	$17.29 \pm 0.20 \pm 0.74$	$16.64 \pm 0.15 \pm 0.66$	$16.81 \pm 0.16 \pm 0.67$
4-6	$24.11 \pm 0.32 \pm 0.83$	$21.80 \pm 0.23 \pm 0.70$	$22.20 \pm 0.27 \pm 0.73$
6-8	$30.99 \pm 0.54 \pm 1.00$	$27.27 \pm 0.42 \pm 0.68$	$25.82 \pm 0.50 \pm 0.74$
8-20	$34.20 \pm 0.69 \pm 0.96$	$28.33 \pm 0.59 \pm 0.79$	$28.99 \pm 0.77 \pm 0.94$
from $b$			
$p_T$ (GeV/c)	$2 < y < 2.8$	$2.8 < y < 3.5$	$3.5 < y < 4.5$
0-2	$19.02 \pm 0.69 \pm 0.96$	$20.54 \pm 0.60 \pm 0.86$	$20.53 \pm 0.69 \pm 1.01$
2-4	$27.70 \pm 0.70 \pm 1.24$	$26.41 \pm 0.55 \pm 1.22$	$27.35 \pm 0.69 \pm 1.27$
4-6	$33.87 \pm 0.87 \pm 1.24$	$28.73 \pm 0.63 \pm 1.12$	$28.92 \pm 0.85 \pm 1.57$
6-8	$34.24 \pm 1.10 \pm 1.67$	$31.66 \pm 0.95 \pm 1.18$	$36.00 \pm 1.40 \pm 1.73$
8-20	$42.40 \pm 1.14 \pm 1.20$	$36.58 \pm 1.06 \pm 1.10$	$37.08 \pm 1.47 \pm 1.55$

Table 16: Ratio(%) of double differential production cross-section for prompt  $\psi(2S)$  to  $J/\psi$  in bins of  $(p_T, y)$ . The first uncertainties are statistical, the second are the systematic uncertainties, for  $24 \leq n\text{ForwardTracks} < 36$ .

prompt			
$p_T$ (GeV/c)	$2 < y < 2.8$	$2.8 < y < 3.5$	$3.5 < y < 4.5$
0-2	$10.25 \pm 0.19 \pm 0.41$	$9.94 \pm 0.15 \pm 0.36$	$10.47 \pm 0.14 \pm 0.39$
2-4	$15.01 \pm 0.21 \pm 0.68$	$14.06 \pm 0.16 \pm 0.57$	$15.27 \pm 0.17 \pm 0.62$
4-6	$22.14 \pm 0.30 \pm 0.77$	$19.72 \pm 0.21 \pm 0.64$	$19.45 \pm 0.24 \pm 0.65$
6-8	$27.15 \pm 0.43 \pm 0.85$	$24.99 \pm 0.34 \pm 0.61$	$24.87 \pm 0.42 \pm 0.80$
8-20	$34.19 \pm 0.55 \pm 0.97$	$29.95 \pm 0.48 \pm 0.72$	$28.70 \pm 0.59 \pm 1.03$

from $b$			
$p_T$ (GeV/c)	$2 < y < 2.8$	$2.8 < y < 3.5$	$3.5 < y < 4.5$
0-2	$20.86 \pm 0.70 \pm 0.97$	$19.55 \pm 0.57 \pm 0.90$	$20.70 \pm 0.66 \pm 0.99$
2-4	$24.64 \pm 0.59 \pm 1.21$	$25.44 \pm 0.49 \pm 1.12$	$25.49 \pm 0.61 \pm 1.14$
4-6	$33.39 \pm 0.75 \pm 1.36$	$28.38 \pm 0.55 \pm 1.21$	$28.53 \pm 0.75 \pm 1.33$
6-8	$34.21 \pm 0.91 \pm 1.31$	$32.26 \pm 0.78 \pm 1.08$	$33.53 \pm 1.12 \pm 2.10$
8-20	$39.71 \pm 0.87 \pm 1.18$	$36.66 \pm 0.85 \pm 1.12$	$34.49 \pm 1.16 \pm 1.56$

Table 17: Ratio(%) of double differential production cross-section for prompt  $\psi(2S)$  to  $J/\psi$  in bins of  $(p_T, y)$ . The first uncertainties are statistical, the second are the systematic uncertainties, for  $36 \leq n\text{ForwardTracks} < 48$ .

prompt			
$p_T$ (GeV/c)	$2 < y < 2.8$	$2.8 < y < 3.5$	$3.5 < y < 4.5$
0-2	$8.97 \pm 0.27 \pm 0.39$	$8.91 \pm 0.21 \pm 0.34$	$9.18 \pm 0.19 \pm 0.41$
2-4	$12.98 \pm 0.25 \pm 0.56$	$12.24 \pm 0.20 \pm 0.51$	$13.34 \pm 0.21 \pm 0.57$
4-6	$19.67 \pm 0.33 \pm 0.75$	$17.34 \pm 0.24 \pm 0.57$	$18.71 \pm 0.27 \pm 0.70$
6-8	$25.22 \pm 0.45 \pm 0.81$	$24.19 \pm 0.37 \pm 0.66$	$22.53 \pm 0.43 \pm 0.85$
8-20	$30.83 \pm 0.52 \pm 1.01$	$29.39 \pm 0.48 \pm 0.84$	$26.80 \pm 0.58 \pm 0.97$

from $b$			
$p_T$ (GeV/c)	$2 < y < 2.8$	$2.8 < y < 3.5$	$3.5 < y < 4.5$
0-2	$19.55 \pm 0.82 \pm 1.03$	$18.95 \pm 0.68 \pm 0.98$	$18.66 \pm 0.73 \pm 1.06$
2-4	$24.04 \pm 0.66 \pm 1.13$	$24.03 \pm 0.55 \pm 1.12$	$24.57 \pm 0.67 \pm 1.22$
4-6	$32.21 \pm 0.79 \pm 1.31$	$26.33 \pm 0.56 \pm 0.95$	$27.16 \pm 0.79 \pm 1.45$
6-8	$32.09 \pm 0.91 \pm 1.27$	$33.16 \pm 0.85 \pm 1.19$	$31.59 \pm 1.13 \pm 1.97$
8-20	$38.94 \pm 0.89 \pm 1.25$	$37.14 \pm 0.87 \pm 1.26$	$39.10 \pm 1.30 \pm 1.72$

Table 18: Ratio(%) of double differential production cross-section for prompt  $\psi(2S)$  to  $J/\psi$  in bins of  $(p_T, y)$ . The first uncertainties are statistical, the second are the systematic uncertainties, for  $48 \leq n\text{ForwardTracks} < 130$ .

prompt			
$p_T$ (GeV/c)	$2 < y < 2.8$	$2.8 < y < 3.5$	$3.5 < y < 4.5$
0-2	$7.83 \pm 0.35 \pm 0.38$	$7.63 \pm 0.28 \pm 0.38$	$8.44 \pm 0.25 \pm 0.35$
2-4	$10.93 \pm 0.30 \pm 0.52$	$10.96 \pm 0.24 \pm 0.48$	$11.58 \pm 0.23 \pm 0.50$
4-6	$18.12 \pm 0.35 \pm 0.79$	$15.04 \pm 0.24 \pm 0.53$	$16.48 \pm 0.28 \pm 0.74$
6-8	$23.28 \pm 0.44 \pm 0.87$	$19.97 \pm 0.32 \pm 0.58$	$22.83 \pm 0.42 \pm 0.86$
8-20	$29.91 \pm 0.46 \pm 0.98$	$27.16 \pm 0.41 \pm 1.04$	$25.68 \pm 0.51 \pm 1.07$

from $b$			
$p_T$ (GeV/c)	$2 < y < 2.8$	$2.8 < y < 3.5$	$3.5 < y < 4.5$
0-2	$19.00 \pm 0.87 \pm 1.22$	$17.31 \pm 0.66 \pm 1.12$	$19.72 \pm 0.79 \pm 1.03$
2-4	$24.67 \pm 0.68 \pm 1.21$	$24.22 \pm 0.55 \pm 1.11$	$24.98 \pm 0.68 \pm 1.22$
4-6	$30.68 \pm 0.76 \pm 1.27$	$27.65 \pm 0.57 \pm 1.19$	$27.95 \pm 0.74 \pm 1.34$
6-8	$32.93 \pm 0.89 \pm 1.26$	$32.79 \pm 0.78 \pm 1.27$	$29.56 \pm 1.01 \pm 1.62$
8-20	$39.20 \pm 0.79 \pm 1.35$	$35.10 \pm 0.75 \pm 1.30$	$34.72 \pm 1.11 \pm 1.71$

<sup>666</sup> **B Efficiency tables**

<sup>667</sup> **B.1 Geometrical Acceptance (Universal for three multiplicity bin-**  
<sup>668</sup> **ning schemes)**

Table 19: The efficiency  $\epsilon_{\text{acc}}$  in different bins of  $p_{\text{T}}$  and  $y$  for prompt  $J/\psi$  mesons for PVZ>-60mm.

$p_{\text{T}}$ ( GeV/c )	$2 < y < 2.8$	$2.8 < y < 3.5$	$3.5 < y < 4.5$
0-2	$0.671 \pm 0.004$	$0.904 \pm 0.003$	$0.852 \pm 0.003$
2-4	$0.746 \pm 0.004$	$0.936 \pm 0.002$	$0.902 \pm 0.003$
4-6	$0.832 \pm 0.005$	$0.961 \pm 0.003$	$0.944 \pm 0.003$
6-8	$0.897 \pm 0.006$	$0.977 \pm 0.004$	$0.968 \pm 0.004$
8-20	$0.937 \pm 0.007$	$0.990 \pm 0.003$	$0.977 \pm 0.005$

Table 20: The efficiency  $\epsilon_{\text{acc}}$  in different bins of  $p_{\text{T}}$  and  $y$  for prompt  $\psi(2S)$  mesons for PVZ>-60mm.

$p_{\text{T}}$ ( GeV/c )	$2 < y < 2.8$	$2.8 < y < 3.5$	$3.5 < y < 4.5$
0-2	$0.667 \pm 0.007$	$0.908 \pm 0.005$	$0.850 \pm 0.005$
2-4	$0.723 \pm 0.006$	$0.922 \pm 0.004$	$0.886 \pm 0.005$
4-6	$0.801 \pm 0.008$	$0.953 \pm 0.005$	$0.931 \pm 0.006$
6-8	$0.863 \pm 0.011$	$0.967 \pm 0.007$	$0.966 \pm 0.007$
8-20	$0.906 \pm 0.011$	$0.980 \pm 0.006$	$0.991 \pm 0.005$

Table 21: The efficiency  $\epsilon_{\text{acc}}$  in different bins of  $p_{\text{T}}$  and  $y$  for  $J/\psi$  from b hardron decay mesons for PVZ>-60mm.

$p_{\text{T}}$ ( GeV/c )	$2 < y < 2.8$	$2.8 < y < 3.5$	$3.5 < y < 4.5$
0-2	$0.661 \pm 0.008$	$0.894 \pm 0.006$	$0.849 \pm 0.007$
2-4	$0.743 \pm 0.007$	$0.927 \pm 0.005$	$0.892 \pm 0.006$
4-6	$0.835 \pm 0.008$	$0.960 \pm 0.005$	$0.952 \pm 0.006$
6-8	$0.860 \pm 0.011$	$0.983 \pm 0.005$	$0.972 \pm 0.007$
8-20	$0.927 \pm 0.008$	$0.998 \pm 0.002$	$0.990 \pm 0.005$

Table 22: The efficiency  $\epsilon_{\text{acc}}$  in different bins of  $p_{\text{T}}$  and  $y$  for  $\psi(2S)$  from b hardron decay mesons for PVZ>-60mm.

$p_{\text{T}}$ ( GeV/c )	$2 < y < 2.8$	$2.8 < y < 3.5$	$3.5 < y < 4.5$
0-2	$0.671 \pm 0.008$	$0.908 \pm 0.006$	$0.867 \pm 0.007$
2-4	$0.718 \pm 0.006$	$0.918 \pm 0.005$	$0.897 \pm 0.005$
4-6	$0.798 \pm 0.007$	$0.959 \pm 0.004$	$0.937 \pm 0.006$
6-8	$0.867 \pm 0.008$	$0.969 \pm 0.005$	$0.958 \pm 0.007$
8-20	$0.904 \pm 0.007$	$0.985 \pm 0.004$	$0.981 \pm 0.005$

## 669 B.2 Efficiency of reconstruction and selection

670 In different PVNTRACKS region:

Table 23: The efficiency  $\epsilon_{\text{MuonID}}$  for prompt signals in different  $(p_{\text{T}}, y)$  bins.

$0 \leq \text{PVNTRACKS} < 20$					
$p_{\text{T}}$ ( GeV/c )	0-2	2-4	4-6	6-8	8-20
$2.0 < y < 2.8$	$0.653 \pm 0.003$	$0.697 \pm 0.003$	$0.747 \pm 0.004$	$0.799 \pm 0.006$	$0.843 \pm 0.008$
$2.8 < y < 3.5$	$0.701 \pm 0.003$	$0.748 \pm 0.003$	$0.815 \pm 0.004$	$0.859 \pm 0.006$	$0.881 \pm 0.008$
$3.5 < y < 4.5$	$0.614 \pm 0.003$	$0.628 \pm 0.003$	$0.662 \pm 0.004$	$0.693 \pm 0.007$	$0.720 \pm 0.010$
$20 \leq \text{PVNTRACKS} < 45$					
$p_{\text{T}}$ ( GeV/c )	0-2	2-4	4-6	6-8	8-20
$2.0 < y < 2.8$	$0.651 \pm 0.002$	$0.696 \pm 0.002$	$0.748 \pm 0.003$	$0.799 \pm 0.004$	$0.843 \pm 0.004$
$2.8 < y < 3.5$	$0.699 \pm 0.002$	$0.747 \pm 0.002$	$0.814 \pm 0.002$	$0.860 \pm 0.003$	$0.882 \pm 0.004$
$3.5 < y < 4.5$	$0.613 \pm 0.002$	$0.626 \pm 0.002$	$0.659 \pm 0.003$	$0.688 \pm 0.004$	$0.715 \pm 0.005$
$45 \leq \text{PVNTRACKS} < 70$					
$p_{\text{T}}$ ( GeV/c )	0-2	2-4	4-6	6-8	8-20
$2.0 < y < 2.8$	$0.634 \pm 0.003$	$0.685 \pm 0.003$	$0.741 \pm 0.003$	$0.794 \pm 0.004$	$0.839 \pm 0.004$
$2.8 < y < 3.5$	$0.681 \pm 0.003$	$0.734 \pm 0.002$	$0.806 \pm 0.003$	$0.852 \pm 0.004$	$0.877 \pm 0.004$
$3.5 < y < 4.5$	$0.599 \pm 0.002$	$0.618 \pm 0.002$	$0.652 \pm 0.003$	$0.681 \pm 0.004$	$0.708 \pm 0.005$
$70 \leq \text{PVNTRACKS} < 95$					
$p_{\text{T}}$ ( GeV/c )	0-2	2-4	4-6	6-8	8-20
$2.0 < y < 2.8$	$0.610 \pm 0.004$	$0.667 \pm 0.004$	$0.729 \pm 0.004$	$0.785 \pm 0.006$	$0.831 \pm 0.006$
$2.8 < y < 3.5$	$0.655 \pm 0.004$	$0.716 \pm 0.003$	$0.792 \pm 0.004$	$0.842 \pm 0.005$	$0.869 \pm 0.006$
$3.5 < y < 4.5$	$0.579 \pm 0.004$	$0.602 \pm 0.003$	$0.642 \pm 0.004$	$0.671 \pm 0.006$	$0.696 \pm 0.007$
$95 \leq \text{PVNTRACKS} < 200$					
$p_{\text{T}}$ ( GeV/c )	0-2	2-4	4-6	6-8	8-20
$2.0 < y < 2.8$	$0.588 \pm 0.008$	$0.652 \pm 0.008$	$0.720 \pm 0.009$	$0.776 \pm 0.011$	$0.827 \pm 0.011$
$2.8 < y < 3.5$	$0.632 \pm 0.008$	$0.698 \pm 0.007$	$0.779 \pm 0.008$	$0.833 \pm 0.010$	$0.863 \pm 0.011$
$3.5 < y < 4.5$	$0.560 \pm 0.007$	$0.591 \pm 0.007$	$0.628 \pm 0.008$	$0.660 \pm 0.012$	$0.688 \pm 0.014$

Table 24: The efficiency  $\epsilon_{\text{MuonID}}$  for prompt signals in different  $(p_T, y)$  bins.

$0 \leq \text{PVNTRACKS} < 20$					
$p_T$ ( GeV/c )	0-2	2-4	4-6	6-8	8-20
$2.0 < y < 2.8$	$0.689 \pm 0.004$	$0.719 \pm 0.005$	$0.769 \pm 0.007$	$0.820 \pm 0.011$	$0.861 \pm 0.012$
$2.8 < y < 3.5$	$0.735 \pm 0.003$	$0.764 \pm 0.004$	$0.815 \pm 0.006$	$0.854 \pm 0.009$	$0.877 \pm 0.012$
$3.5 < y < 4.5$	$0.636 \pm 0.003$	$0.644 \pm 0.004$	$0.662 \pm 0.006$	$0.683 \pm 0.011$	$0.706 \pm 0.016$
$20 \leq \text{PVNTRACKS} < 45$					
$p_T$ ( GeV/c )	0-2	2-4	4-6	6-8	8-20
$2.0 < y < 2.8$	$0.687 \pm 0.003$	$0.719 \pm 0.004$	$0.771 \pm 0.005$	$0.819 \pm 0.006$	$0.861 \pm 0.006$
$2.8 < y < 3.5$	$0.734 \pm 0.003$	$0.764 \pm 0.003$	$0.813 \pm 0.004$	$0.854 \pm 0.005$	$0.878 \pm 0.006$
$3.5 < y < 4.5$	$0.634 \pm 0.003$	$0.644 \pm 0.003$	$0.661 \pm 0.004$	$0.684 \pm 0.006$	$0.710 \pm 0.008$
$45 \leq \text{PVNTRACKS} < 70$					
$p_T$ ( GeV/c )	0-2	2-4	4-6	6-8	8-20
$2.0 < y < 2.8$	$0.674 \pm 0.004$	$0.709 \pm 0.004$	$0.763 \pm 0.005$	$0.816 \pm 0.007$	$0.857 \pm 0.007$
$2.8 < y < 3.5$	$0.720 \pm 0.003$	$0.752 \pm 0.003$	$0.804 \pm 0.004$	$0.850 \pm 0.006$	$0.874 \pm 0.006$
$3.5 < y < 4.5$	$0.625 \pm 0.003$	$0.635 \pm 0.004$	$0.652 \pm 0.005$	$0.671 \pm 0.007$	$0.699 \pm 0.008$
$70 \leq \text{PVNTRACKS} < 95$					
$p_T$ ( GeV/c )	0-2	2-4	4-6	6-8	8-20
$2.0 < y < 2.8$	$0.654 \pm 0.007$	$0.692 \pm 0.007$	$0.751 \pm 0.008$	$0.806 \pm 0.010$	$0.850 \pm 0.010$
$2.8 < y < 3.5$	$0.698 \pm 0.005$	$0.735 \pm 0.006$	$0.792 \pm 0.007$	$0.837 \pm 0.009$	$0.865 \pm 0.009$
$3.5 < y < 4.5$	$0.605 \pm 0.005$	$0.622 \pm 0.006$	$0.642 \pm 0.007$	$0.666 \pm 0.010$	$0.697 \pm 0.012$
$95 \leq \text{PVNTRACKS} < 200$					
$p_T$ ( GeV/c )	0-2	2-4	4-6	6-8	8-20
$2.0 < y < 2.8$	$0.636 \pm 0.014$	$0.679 \pm 0.015$	$0.742 \pm 0.018$	$0.800 \pm 0.022$	$0.846 \pm 0.019$
$2.8 < y < 3.5$	$0.679 \pm 0.012$	$0.723 \pm 0.012$	$0.784 \pm 0.014$	$0.833 \pm 0.018$	$0.854 \pm 0.017$
$3.5 < y < 4.5$	$0.589 \pm 0.012$	$0.613 \pm 0.012$	$0.631 \pm 0.015$	$0.663 \pm 0.021$	$0.681 \pm 0.023$

Table 25: The efficiency  $\epsilon_{\text{MuonID}}$  for from b signals in different  $(p_T, y)$  bins.

$0 \leq \text{PVNTRACKS} < 20$					
$p_T$ ( GeV/c )	0-2	2-4	4-6	6-8	8-20
$2.0 < y < 2.8$	$0.654 \pm 0.009$	$0.698 \pm 0.008$	$0.749 \pm 0.008$	$0.801 \pm 0.011$	$0.851 \pm 0.011$
$2.8 < y < 3.5$	$0.704 \pm 0.009$	$0.751 \pm 0.007$	$0.816 \pm 0.008$	$0.859 \pm 0.011$	$0.886 \pm 0.012$
$3.5 < y < 4.5$	$0.622 \pm 0.009$	$0.642 \pm 0.008$	$0.682 \pm 0.010$	$0.720 \pm 0.015$	$0.750 \pm 0.020$
$20 \leq \text{PVNTRACKS} < 45$					
$p_T$ ( GeV/c )	0-2	2-4	4-6	6-8	8-20
$2.0 < y < 2.8$	$0.650 \pm 0.005$	$0.696 \pm 0.004$	$0.748 \pm 0.005$	$0.799 \pm 0.006$	$0.848 \pm 0.005$
$2.8 < y < 3.5$	$0.700 \pm 0.005$	$0.748 \pm 0.004$	$0.815 \pm 0.004$	$0.859 \pm 0.005$	$0.883 \pm 0.005$
$3.5 < y < 4.5$	$0.620 \pm 0.005$	$0.637 \pm 0.004$	$0.676 \pm 0.005$	$0.713 \pm 0.007$	$0.742 \pm 0.008$
$45 \leq \text{PVNTRACKS} < 70$					
$p_T$ ( GeV/c )	0-2	2-4	4-6	6-8	8-20
$2.0 < y < 2.8$	$0.632 \pm 0.006$	$0.684 \pm 0.005$	$0.740 \pm 0.005$	$0.793 \pm 0.006$	$0.843 \pm 0.005$
$2.8 < y < 3.5$	$0.678 \pm 0.006$	$0.733 \pm 0.004$	$0.805 \pm 0.004$	$0.851 \pm 0.006$	$0.876 \pm 0.005$
$3.5 < y < 4.5$	$0.602 \pm 0.006$	$0.626 \pm 0.005$	$0.668 \pm 0.005$	$0.706 \pm 0.007$	$0.732 \pm 0.008$
$70 \leq \text{PVNTRACKS} < 95$					
$p_T$ ( GeV/c )	0-2	2-4	4-6	6-8	8-20
$2.0 < y < 2.8$	$0.609 \pm 0.009$	$0.668 \pm 0.007$	$0.729 \pm 0.007$	$0.784 \pm 0.008$	$0.839 \pm 0.007$
$2.8 < y < 3.5$	$0.652 \pm 0.008$	$0.714 \pm 0.006$	$0.792 \pm 0.006$	$0.842 \pm 0.008$	$0.870 \pm 0.008$
$3.5 < y < 4.5$	$0.585 \pm 0.008$	$0.609 \pm 0.007$	$0.663 \pm 0.008$	$0.698 \pm 0.010$	$0.721 \pm 0.011$
$95 \leq \text{PVNTRACKS} < 200$					
$p_T$ ( GeV/c )	0-2	2-4	4-6	6-8	8-20
$2.0 < y < 2.8$	$0.589 \pm 0.017$	$0.649 \pm 0.013$	$0.719 \pm 0.013$	$0.778 \pm 0.016$	$0.833 \pm 0.012$
$2.8 < y < 3.5$	$0.629 \pm 0.016$	$0.699 \pm 0.012$	$0.782 \pm 0.012$	$0.830 \pm 0.015$	$0.861 \pm 0.013$
$3.5 < y < 4.5$	$0.568 \pm 0.016$	$0.598 \pm 0.013$	$0.649 \pm 0.015$	$0.684 \pm 0.019$	$0.712 \pm 0.020$

Table 26: The efficiency  $\epsilon_{\text{MuonID}}$  for from b signals in different  $(p_T, y)$  bins.

$0 \leq \text{PVNTRACKS} < 20$					
$p_T$ ( GeV/c )	0-2	2-4	4-6	6-8	8-20
$2.0 < y < 2.8$	$0.686 \pm 0.007$	$0.720 \pm 0.007$	$0.772 \pm 0.007$	$0.820 \pm 0.009$	$0.864 \pm 0.008$
$2.8 < y < 3.5$	$0.736 \pm 0.006$	$0.766 \pm 0.006$	$0.816 \pm 0.006$	$0.855 \pm 0.008$	$0.883 \pm 0.009$
$3.5 < y < 4.5$	$0.625 \pm 0.007$	$0.641 \pm 0.006$	$0.676 \pm 0.008$	$0.712 \pm 0.011$	$0.742 \pm 0.013$
$20 \leq \text{PVNTRACKS} < 45$					
$p_T$ ( GeV/c )	0-2	2-4	4-6	6-8	8-20
$2.0 < y < 2.8$	$0.684 \pm 0.004$	$0.719 \pm 0.004$	$0.770 \pm 0.004$	$0.820 \pm 0.005$	$0.865 \pm 0.004$
$2.8 < y < 3.5$	$0.734 \pm 0.004$	$0.764 \pm 0.003$	$0.815 \pm 0.003$	$0.855 \pm 0.004$	$0.881 \pm 0.004$
$3.5 < y < 4.5$	$0.623 \pm 0.004$	$0.640 \pm 0.004$	$0.668 \pm 0.004$	$0.701 \pm 0.006$	$0.739 \pm 0.006$
$45 \leq \text{PVNTRACKS} < 70$					
$p_T$ ( GeV/c )	0-2	2-4	4-6	6-8	8-20
$2.0 < y < 2.8$	$0.668 \pm 0.005$	$0.707 \pm 0.004$	$0.762 \pm 0.004$	$0.815 \pm 0.005$	$0.859 \pm 0.004$
$2.8 < y < 3.5$	$0.717 \pm 0.004$	$0.749 \pm 0.004$	$0.805 \pm 0.004$	$0.846 \pm 0.004$	$0.874 \pm 0.004$
$3.5 < y < 4.5$	$0.610 \pm 0.004$	$0.627 \pm 0.004$	$0.659 \pm 0.005$	$0.689 \pm 0.006$	$0.730 \pm 0.006$
$70 \leq \text{PVNTRACKS} < 95$					
$p_T$ ( GeV/c )	0-2	2-4	4-6	6-8	8-20
$2.0 < y < 2.8$	$0.649 \pm 0.007$	$0.691 \pm 0.007$	$0.751 \pm 0.007$	$0.805 \pm 0.008$	$0.852 \pm 0.006$
$2.8 < y < 3.5$	$0.696 \pm 0.006$	$0.735 \pm 0.005$	$0.792 \pm 0.006$	$0.838 \pm 0.007$	$0.865 \pm 0.006$
$3.5 < y < 4.5$	$0.589 \pm 0.007$	$0.617 \pm 0.006$	$0.651 \pm 0.007$	$0.681 \pm 0.009$	$0.713 \pm 0.009$
$95 \leq \text{PVNTRACKS} < 200$					
$p_T$ ( GeV/c )	0-2	2-4	4-6	6-8	8-20
$2.0 < y < 2.8$	$0.632 \pm 0.015$	$0.680 \pm 0.013$	$0.740 \pm 0.014$	$0.800 \pm 0.015$	$0.846 \pm 0.011$
$2.8 < y < 3.5$	$0.679 \pm 0.013$	$0.721 \pm 0.011$	$0.780 \pm 0.011$	$0.829 \pm 0.013$	$0.859 \pm 0.012$
$3.5 < y < 4.5$	$0.579 \pm 0.013$	$0.605 \pm 0.012$	$0.641 \pm 0.014$	$0.664 \pm 0.017$	$0.705 \pm 0.017$

671 In different nBackTracks region:

Table 27: The efficiency  $\epsilon_{\text{Trigger}}$  for prompt signals in different  $(p_T, y)$  bins.

$0 \leq n_{\text{BackTracks}} < 8$					
$p_T$ (GeV/c)	0-2	2-4	4-6	6-8	8-20
$2.0 < y < 2.8$	$0.259 \pm 0.003$	$0.395 \pm 0.003$	$0.518 \pm 0.004$	$0.595 \pm 0.006$	$0.659 \pm 0.007$
$2.8 < y < 3.5$	$0.356 \pm 0.003$	$0.473 \pm 0.003$	$0.579 \pm 0.004$	$0.649 \pm 0.006$	$0.662 \pm 0.007$
$3.5 < y < 4.5$	$0.428 \pm 0.003$	$0.523 \pm 0.003$	$0.600 \pm 0.004$	$0.650 \pm 0.006$	$0.675 \pm 0.008$
$8 \leq n_{\text{BackTracks}} < 15$					
$p_T$ (GeV/c)	0-2	2-4	4-6	6-8	8-20
$2.0 < y < 2.8$	$0.269 \pm 0.003$	$0.406 \pm 0.003$	$0.527 \pm 0.004$	$0.596 \pm 0.005$	$0.650 \pm 0.006$
$2.8 < y < 3.5$	$0.361 \pm 0.003$	$0.475 \pm 0.003$	$0.583 \pm 0.003$	$0.636 \pm 0.005$	$0.678 \pm 0.006$
$3.5 < y < 4.5$	$0.440 \pm 0.003$	$0.524 \pm 0.003$	$0.597 \pm 0.004$	$0.652 \pm 0.005$	$0.685 \pm 0.007$
$15 \leq n_{\text{BackTracks}} < 22$					
$p_T$ (GeV/c)	0-2	2-4	4-6	6-8	8-20
$2.0 < y < 2.8$	$0.266 \pm 0.003$	$0.408 \pm 0.003$	$0.524 \pm 0.004$	$0.592 \pm 0.005$	$0.668 \pm 0.006$
$2.8 < y < 3.5$	$0.375 \pm 0.003$	$0.477 \pm 0.003$	$0.589 \pm 0.003$	$0.648 \pm 0.005$	$0.676 \pm 0.006$
$3.5 < y < 4.5$	$0.434 \pm 0.004$	$0.528 \pm 0.003$	$0.607 \pm 0.004$	$0.647 \pm 0.006$	$0.682 \pm 0.007$
$22 \leq n_{\text{BackTracks}} < 30$					
$p_T$ (GeV/c)	0-2	2-4	4-6	6-8	8-20
$2.0 < y < 2.8$	$0.278 \pm 0.004$	$0.409 \pm 0.004$	$0.535 \pm 0.004$	$0.601 \pm 0.006$	$0.661 \pm 0.006$
$2.8 < y < 3.5$	$0.374 \pm 0.004$	$0.486 \pm 0.003$	$0.584 \pm 0.004$	$0.642 \pm 0.006$	$0.681 \pm 0.007$
$3.5 < y < 4.5$	$0.441 \pm 0.004$	$0.529 \pm 0.004$	$0.599 \pm 0.004$	$0.647 \pm 0.006$	$0.685 \pm 0.008$
$30 \leq n_{\text{BackTracks}} < 80$					
$p_T$ (GeV/c)	0-2	2-4	4-6	6-8	8-20
$2.0 < y < 2.8$	$0.282 \pm 0.004$	$0.413 \pm 0.004$	$0.541 \pm 0.005$	$0.601 \pm 0.006$	$0.668 \pm 0.007$
$2.8 < y < 3.5$	$0.377 \pm 0.004$	$0.495 \pm 0.004$	$0.591 \pm 0.004$	$0.655 \pm 0.006$	$0.692 \pm 0.007$
$3.5 < y < 4.5$	$0.431 \pm 0.005$	$0.537 \pm 0.004$	$0.607 \pm 0.005$	$0.647 \pm 0.007$	$0.663 \pm 0.008$

Table 28: The efficiency  $\epsilon_{\text{Trigger}}$  for prompt signals in different  $(p_T, y)$  bins.

$0 \leq n_{\text{BackTracks}} < 8$					
$p_T$ (GeV/c)	0-2	2-4	4-6	6-8	8-20
$2.0 < y < 2.8$	$0.404 \pm 0.004$	$0.489 \pm 0.005$	$0.571 \pm 0.007$	$0.629 \pm 0.010$	$0.699 \pm 0.011$
$2.8 < y < 3.5$	$0.454 \pm 0.004$	$0.513 \pm 0.004$	$0.593 \pm 0.006$	$0.640 \pm 0.009$	$0.694 \pm 0.010$
$3.5 < y < 4.5$	$0.513 \pm 0.004$	$0.561 \pm 0.005$	$0.615 \pm 0.006$	$0.643 \pm 0.010$	$0.681 \pm 0.012$
$8 \leq n_{\text{BackTracks}} < 15$					
$p_T$ (GeV/c)	0-2	2-4	4-6	6-8	8-20
$2.0 < y < 2.8$	$0.410 \pm 0.005$	$0.498 \pm 0.005$	$0.573 \pm 0.007$	$0.636 \pm 0.009$	$0.683 \pm 0.009$
$2.8 < y < 3.5$	$0.459 \pm 0.004$	$0.523 \pm 0.004$	$0.602 \pm 0.005$	$0.634 \pm 0.008$	$0.680 \pm 0.009$
$3.5 < y < 4.5$	$0.517 \pm 0.004$	$0.563 \pm 0.005$	$0.612 \pm 0.006$	$0.667 \pm 0.009$	$0.673 \pm 0.011$
$15 \leq n_{\text{BackTracks}} < 22$					
$p_T$ (GeV/c)	0-2	2-4	4-6	6-8	8-20
$2.0 < y < 2.8$	$0.425 \pm 0.005$	$0.491 \pm 0.006$	$0.581 \pm 0.007$	$0.636 \pm 0.009$	$0.678 \pm 0.009$
$2.8 < y < 3.5$	$0.464 \pm 0.004$	$0.526 \pm 0.005$	$0.597 \pm 0.006$	$0.639 \pm 0.008$	$0.679 \pm 0.009$
$3.5 < y < 4.5$	$0.516 \pm 0.005$	$0.554 \pm 0.005$	$0.614 \pm 0.007$	$0.648 \pm 0.009$	$0.673 \pm 0.011$
$22 \leq n_{\text{BackTracks}} < 30$					
$p_T$ (GeV/c)	0-2	2-4	4-6	6-8	8-20
$2.0 < y < 2.8$	$0.416 \pm 0.006$	$0.490 \pm 0.007$	$0.593 \pm 0.008$	$0.640 \pm 0.011$	$0.697 \pm 0.010$
$2.8 < y < 3.5$	$0.460 \pm 0.005$	$0.526 \pm 0.005$	$0.596 \pm 0.007$	$0.652 \pm 0.009$	$0.683 \pm 0.010$
$3.5 < y < 4.5$	$0.518 \pm 0.006$	$0.548 \pm 0.006$	$0.603 \pm 0.008$	$0.637 \pm 0.011$	$0.674 \pm 0.012$
$30 \leq n_{\text{BackTracks}} < 80$					
$p_T$ (GeV/c)	0-2	2-4	4-6	6-8	8-20
$2.0 < y < 2.8$	$0.424 \pm 0.007$	$0.499 \pm 0.008$	$0.587 \pm 0.009$	$0.650 \pm 0.011$	$0.703 \pm 0.011$
$2.8 < y < 3.5$	$0.456 \pm 0.006$	$0.523 \pm 0.006$	$0.605 \pm 0.007$	$0.645 \pm 0.010$	$0.690 \pm 0.011$
$3.5 < y < 4.5$	$0.513 \pm 0.007$	$0.561 \pm 0.007$	$0.616 \pm 0.009$	$0.663 \pm 0.012$	$0.704 \pm 0.013$

Table 29: The efficiency  $\epsilon_{\text{Trigger}}$  for from b signals in different  $(p_T, y)$  bins.

$0 \leq n\text{BackTracks} < 8$					
$p_T$ ( GeV/c )	0-2	2-4	4-6	6-8	8-20
$2.0 < y < 2.8$	$0.268 \pm 0.008$	$0.404 \pm 0.007$	$0.520 \pm 0.008$	$0.605 \pm 0.010$	$0.674 \pm 0.009$
$2.8 < y < 3.5$	$0.353 \pm 0.008$	$0.478 \pm 0.007$	$0.595 \pm 0.007$	$0.628 \pm 0.010$	$0.667 \pm 0.011$
$3.5 < y < 4.5$	$0.438 \pm 0.009$	$0.526 \pm 0.008$	$0.609 \pm 0.009$	$0.653 \pm 0.012$	$0.666 \pm 0.014$
$8 \leq n\text{BackTracks} < 15$					
$p_T$ ( GeV/c )	0-2	2-4	4-6	6-8	8-20
$2.0 < y < 2.8$	$0.274 \pm 0.007$	$0.407 \pm 0.006$	$0.530 \pm 0.007$	$0.608 \pm 0.008$	$0.676 \pm 0.007$
$2.8 < y < 3.5$	$0.373 \pm 0.007$	$0.477 \pm 0.006$	$0.586 \pm 0.006$	$0.643 \pm 0.008$	$0.685 \pm 0.008$
$3.5 < y < 4.5$	$0.428 \pm 0.008$	$0.536 \pm 0.007$	$0.605 \pm 0.008$	$0.654 \pm 0.010$	$0.691 \pm 0.011$
$15 \leq n\text{BackTracks} < 22$					
$p_T$ ( GeV/c )	0-2	2-4	4-6	6-8	8-20
$2.0 < y < 2.8$	$0.274 \pm 0.007$	$0.405 \pm 0.006$	$0.528 \pm 0.007$	$0.606 \pm 0.008$	$0.687 \pm 0.007$
$2.8 < y < 3.5$	$0.389 \pm 0.008$	$0.487 \pm 0.006$	$0.587 \pm 0.006$	$0.642 \pm 0.008$	$0.683 \pm 0.009$
$3.5 < y < 4.5$	$0.438 \pm 0.009$	$0.527 \pm 0.007$	$0.611 \pm 0.008$	$0.666 \pm 0.011$	$0.692 \pm 0.012$
$22 \leq n\text{BackTracks} < 30$					
$p_T$ ( GeV/c )	0-2	2-4	4-6	6-8	8-20
$2.0 < y < 2.8$	$0.263 \pm 0.008$	$0.407 \pm 0.007$	$0.536 \pm 0.007$	$0.608 \pm 0.009$	$0.667 \pm 0.008$
$2.8 < y < 3.5$	$0.378 \pm 0.009$	$0.485 \pm 0.007$	$0.588 \pm 0.007$	$0.650 \pm 0.009$	$0.683 \pm 0.009$
$3.5 < y < 4.5$	$0.432 \pm 0.010$	$0.535 \pm 0.008$	$0.601 \pm 0.009$	$0.662 \pm 0.012$	$0.672 \pm 0.012$
$30 \leq n\text{BackTracks} < 80$					
$p_T$ ( GeV/c )	0-2	2-4	4-6	6-8	8-20
$2.0 < y < 2.8$	$0.273 \pm 0.009$	$0.422 \pm 0.007$	$0.534 \pm 0.008$	$0.611 \pm 0.010$	$0.687 \pm 0.008$
$2.8 < y < 3.5$	$0.387 \pm 0.009$	$0.496 \pm 0.007$	$0.597 \pm 0.007$	$0.659 \pm 0.009$	$0.671 \pm 0.009$
$3.5 < y < 4.5$	$0.445 \pm 0.011$	$0.532 \pm 0.009$	$0.603 \pm 0.010$	$0.664 \pm 0.012$	$0.686 \pm 0.013$

Table 30: The efficiency  $\epsilon_{\text{Trigger}}$  for from b signals in different  $(p_T, y)$  bins.

$0 \leq n_{\text{BackTracks}} < 8$					
$p_T$ ( GeV/c )	0-2	2-4	4-6	6-8	8-20
$2.0 < y < 2.8$	$0.396 \pm 0.007$	$0.497 \pm 0.006$	$0.592 \pm 0.007$	$0.627 \pm 0.008$	$0.684 \pm 0.007$
$2.8 < y < 3.5$	$0.449 \pm 0.006$	$0.506 \pm 0.005$	$0.594 \pm 0.006$	$0.648 \pm 0.008$	$0.686 \pm 0.008$
$3.5 < y < 4.5$	$0.519 \pm 0.007$	$0.567 \pm 0.006$	$0.603 \pm 0.007$	$0.648 \pm 0.010$	$0.692 \pm 0.010$
$8 \leq n_{\text{BackTracks}} < 15$					
$p_T$ ( GeV/c )	0-2	2-4	4-6	6-8	8-20
$2.0 < y < 2.8$	$0.404 \pm 0.006$	$0.499 \pm 0.006$	$0.594 \pm 0.006$	$0.640 \pm 0.007$	$0.699 \pm 0.006$
$2.8 < y < 3.5$	$0.464 \pm 0.005$	$0.517 \pm 0.005$	$0.594 \pm 0.005$	$0.636 \pm 0.006$	$0.688 \pm 0.006$
$3.5 < y < 4.5$	$0.519 \pm 0.006$	$0.559 \pm 0.006$	$0.620 \pm 0.006$	$0.659 \pm 0.008$	$0.681 \pm 0.008$
$15 \leq n_{\text{BackTracks}} < 22$					
$p_T$ ( GeV/c )	0-2	2-4	4-6	6-8	8-20
$2.0 < y < 2.8$	$0.419 \pm 0.006$	$0.506 \pm 0.006$	$0.584 \pm 0.006$	$0.659 \pm 0.007$	$0.696 \pm 0.006$
$2.8 < y < 3.5$	$0.457 \pm 0.006$	$0.521 \pm 0.005$	$0.601 \pm 0.005$	$0.647 \pm 0.007$	$0.683 \pm 0.006$
$3.5 < y < 4.5$	$0.526 \pm 0.007$	$0.562 \pm 0.006$	$0.612 \pm 0.007$	$0.643 \pm 0.008$	$0.675 \pm 0.008$
$22 \leq n_{\text{BackTracks}} < 30$					
$p_T$ ( GeV/c )	0-2	2-4	4-6	6-8	8-20
$2.0 < y < 2.8$	$0.417 \pm 0.007$	$0.510 \pm 0.007$	$0.595 \pm 0.007$	$0.651 \pm 0.008$	$0.686 \pm 0.006$
$2.8 < y < 3.5$	$0.465 \pm 0.007$	$0.523 \pm 0.006$	$0.597 \pm 0.006$	$0.650 \pm 0.007$	$0.690 \pm 0.007$
$3.5 < y < 4.5$	$0.531 \pm 0.008$	$0.563 \pm 0.007$	$0.619 \pm 0.007$	$0.658 \pm 0.009$	$0.686 \pm 0.009$
$30 \leq n_{\text{BackTracks}} < 80$					
$p_T$ ( GeV/c )	0-2	2-4	4-6	6-8	8-20
$2.0 < y < 2.8$	$0.400 \pm 0.008$	$0.502 \pm 0.007$	$0.586 \pm 0.008$	$0.640 \pm 0.008$	$0.706 \pm 0.007$
$2.8 < y < 3.5$	$0.475 \pm 0.007$	$0.527 \pm 0.006$	$0.596 \pm 0.007$	$0.646 \pm 0.008$	$0.679 \pm 0.007$
$3.5 < y < 4.5$	$0.521 \pm 0.008$	$0.568 \pm 0.008$	$0.613 \pm 0.008$	$0.636 \pm 0.010$	$0.672 \pm 0.010$

672 In different nForwardTracks region:

Table 31: The efficiency  $\epsilon_{\text{tot}}$  for prompt signals in different  $(p_{\text{T}}, y)$  bins.

<u>0≤nForwardTracks&lt;12</u>					
$p_{\text{T}}$ ( GeV/c )	0-2	2-4	4-6	6-8	8-20
$2.0 < y < 2.8$	$0.032 \pm 0.000$	$0.056 \pm 0.001$	$0.131 \pm 0.002$	$0.218 \pm 0.004$	$0.307 \pm 0.006$
$2.8 < y < 3.5$	$0.070 \pm 0.001$	$0.112 \pm 0.001$	$0.231 \pm 0.002$	$0.330 \pm 0.005$	$0.392 \pm 0.008$
$3.5 < y < 4.5$	$0.068 \pm 0.001$	$0.093 \pm 0.001$	$0.176 \pm 0.002$	$0.252 \pm 0.005$	$0.325 \pm 0.008$
<u>12≤nForwardTracks&lt;24</u>					
$p_{\text{T}}$ ( GeV/c )	0-2	2-4	4-6	6-8	8-20
$2.0 < y < 2.8$	$0.033 \pm 0.000$	$0.057 \pm 0.001$	$0.132 \pm 0.001$	$0.224 \pm 0.003$	$0.314 \pm 0.004$
$2.8 < y < 3.5$	$0.070 \pm 0.001$	$0.116 \pm 0.001$	$0.235 \pm 0.002$	$0.325 \pm 0.003$	$0.396 \pm 0.005$
$3.5 < y < 4.5$	$0.068 \pm 0.001$	$0.095 \pm 0.001$	$0.178 \pm 0.001$	$0.258 \pm 0.003$	$0.319 \pm 0.005$
<u>24≤nForwardTracks&lt;36</u>					
$p_{\text{T}}$ ( GeV/c )	0-2	2-4	4-6	6-8	8-20
$2.0 < y < 2.8$	$0.033 \pm 0.000$	$0.057 \pm 0.001$	$0.133 \pm 0.001$	$0.218 \pm 0.003$	$0.317 \pm 0.004$
$2.8 < y < 3.5$	$0.071 \pm 0.001$	$0.115 \pm 0.001$	$0.230 \pm 0.002$	$0.328 \pm 0.003$	$0.401 \pm 0.004$
$3.5 < y < 4.5$	$0.067 \pm 0.001$	$0.094 \pm 0.001$	$0.178 \pm 0.002$	$0.254 \pm 0.003$	$0.314 \pm 0.004$
<u>36≤nForwardTracks&lt;48</u>					
$p_{\text{T}}$ ( GeV/c )	0-2	2-4	4-6	6-8	8-20
$2.0 < y < 2.8$	$0.032 \pm 0.000$	$0.055 \pm 0.001$	$0.128 \pm 0.001$	$0.215 \pm 0.003$	$0.306 \pm 0.004$
$2.8 < y < 3.5$	$0.070 \pm 0.001$	$0.114 \pm 0.001$	$0.232 \pm 0.002$	$0.325 \pm 0.004$	$0.397 \pm 0.005$
$3.5 < y < 4.5$	$0.066 \pm 0.001$	$0.094 \pm 0.001$	$0.176 \pm 0.002$	$0.247 \pm 0.003$	$0.306 \pm 0.005$
<u>48≤nForwardTracks&lt;130</u>					
$p_{\text{T}}$ ( GeV/c )	0-2	2-4	4-6	6-8	8-20
$2.0 < y < 2.8$	$0.031 \pm 0.001$	$0.054 \pm 0.001$	$0.129 \pm 0.002$	$0.214 \pm 0.003$	$0.305 \pm 0.005$
$2.8 < y < 3.5$	$0.066 \pm 0.001$	$0.109 \pm 0.001$	$0.223 \pm 0.002$	$0.310 \pm 0.004$	$0.392 \pm 0.005$
$3.5 < y < 4.5$	$0.063 \pm 0.001$	$0.090 \pm 0.001$	$0.169 \pm 0.002$	$0.239 \pm 0.004$	$0.303 \pm 0.005$

Table 32: The efficiency  $\epsilon_{\text{tot}}$  for prompt signals in different  $(p_{\text{T}}, y)$  bins.

<u>0≤nForwardTracks&lt;12</u>					
$p_{\text{T}}$ ( GeV/c )	0-2	2-4	4-6	6-8	8-20
$2.0 < y < 2.8$	$0.075 \pm 0.001$	$0.071 \pm 0.001$	$0.116 \pm 0.003$	$0.170 \pm 0.005$	$0.272 \pm 0.009$
$2.8 < y < 3.5$	$0.163 \pm 0.002$	$0.155 \pm 0.002$	$0.246 \pm 0.004$	$0.334 \pm 0.008$	$0.413 \pm 0.013$
$3.5 < y < 4.5$	$0.140 \pm 0.002$	$0.122 \pm 0.002$	$0.183 \pm 0.004$	$0.246 \pm 0.008$	$0.313 \pm 0.013$
<u>12≤nForwardTracks&lt;24</u>					
$p_{\text{T}}$ ( GeV/c )	0-2	2-4	4-6	6-8	8-20
$2.0 < y < 2.8$	$0.075 \pm 0.001$	$0.072 \pm 0.001$	$0.118 \pm 0.002$	$0.185 \pm 0.004$	$0.264 \pm 0.006$
$2.8 < y < 3.5$	$0.167 \pm 0.002$	$0.157 \pm 0.002$	$0.245 \pm 0.003$	$0.329 \pm 0.005$	$0.409 \pm 0.007$
$3.5 < y < 4.5$	$0.143 \pm 0.002$	$0.124 \pm 0.001$	$0.184 \pm 0.003$	$0.255 \pm 0.005$	$0.317 \pm 0.007$
<u>24≤nForwardTracks&lt;36</u>					
$p_{\text{T}}$ ( GeV/c )	0-2	2-4	4-6	6-8	8-20
$2.0 < y < 2.8$	$0.074 \pm 0.001$	$0.071 \pm 0.001$	$0.113 \pm 0.002$	$0.183 \pm 0.004$	$0.260 \pm 0.006$
$2.8 < y < 3.5$	$0.163 \pm 0.002$	$0.155 \pm 0.002$	$0.241 \pm 0.003$	$0.320 \pm 0.005$	$0.396 \pm 0.007$
$3.5 < y < 4.5$	$0.141 \pm 0.002$	$0.122 \pm 0.001$	$0.186 \pm 0.003$	$0.241 \pm 0.005$	$0.309 \pm 0.006$
<u>36≤nForwardTracks&lt;48</u>					
$p_{\text{T}}$ ( GeV/c )	0-2	2-4	4-6	6-8	8-20
$2.0 < y < 2.8$	$0.075 \pm 0.001$	$0.071 \pm 0.001$	$0.113 \pm 0.002$	$0.182 \pm 0.005$	$0.263 \pm 0.006$
$2.8 < y < 3.5$	$0.161 \pm 0.002$	$0.154 \pm 0.002$	$0.242 \pm 0.003$	$0.315 \pm 0.006$	$0.384 \pm 0.007$
$3.5 < y < 4.5$	$0.137 \pm 0.002$	$0.120 \pm 0.002$	$0.177 \pm 0.003$	$0.245 \pm 0.005$	$0.310 \pm 0.007$
<u>48≤nForwardTracks&lt;130</u>					
$p_{\text{T}}$ ( GeV/c )	0-2	2-4	4-6	6-8	8-20
$2.0 < y < 2.8$	$0.073 \pm 0.002$	$0.067 \pm 0.001$	$0.113 \pm 0.003$	$0.171 \pm 0.005$	$0.255 \pm 0.006$
$2.8 < y < 3.5$	$0.155 \pm 0.003$	$0.147 \pm 0.002$	$0.237 \pm 0.004$	$0.320 \pm 0.007$	$0.385 \pm 0.008$
$3.5 < y < 4.5$	$0.132 \pm 0.002$	$0.118 \pm 0.002$	$0.172 \pm 0.003$	$0.229 \pm 0.006$	$0.307 \pm 0.008$

Table 33: The efficiency  $\epsilon_{\text{tot}}$  for from b signals in different  $(p_T, y)$  bins.

<u>0≤nForwardTracks&lt;12</u>					
$p_T$ ( GeV/c )	0-2	2-4	4-6	6-8	8-20
$2.0 < y < 2.8$	$0.033 \pm 0.001$	$0.055 \pm 0.001$	$0.131 \pm 0.003$	$0.211 \pm 0.007$	$0.318 \pm 0.009$
$2.8 < y < 3.5$	$0.066 \pm 0.002$	$0.114 \pm 0.003$	$0.235 \pm 0.005$	$0.314 \pm 0.009$	$0.415 \pm 0.013$
$3.5 < y < 4.5$	$0.070 \pm 0.002$	$0.095 \pm 0.003$	$0.190 \pm 0.005$	$0.268 \pm 0.011$	$0.311 \pm 0.016$
<u>12≤nForwardTracks&lt;24</u>					
$p_T$ ( GeV/c )	0-2	2-4	4-6	6-8	8-20
$2.0 < y < 2.8$	$0.029 \pm 0.001$	$0.057 \pm 0.001$	$0.133 \pm 0.002$	$0.208 \pm 0.004$	$0.327 \pm 0.006$
$2.8 < y < 3.5$	$0.067 \pm 0.001$	$0.120 \pm 0.002$	$0.234 \pm 0.003$	$0.328 \pm 0.005$	$0.406 \pm 0.007$
$3.5 < y < 4.5$	$0.065 \pm 0.001$	$0.099 \pm 0.002$	$0.186 \pm 0.003$	$0.269 \pm 0.006$	$0.322 \pm 0.008$
<u>24≤nForwardTracks&lt;36</u>					
$p_T$ ( GeV/c )	0-2	2-4	4-6	6-8	8-20
$2.0 < y < 2.8$	$0.031 \pm 0.001$	$0.056 \pm 0.001$	$0.134 \pm 0.002$	$0.212 \pm 0.004$	$0.317 \pm 0.005$
$2.8 < y < 3.5$	$0.068 \pm 0.001$	$0.118 \pm 0.002$	$0.237 \pm 0.003$	$0.324 \pm 0.005$	$0.408 \pm 0.006$
$3.5 < y < 4.5$	$0.064 \pm 0.001$	$0.097 \pm 0.002$	$0.188 \pm 0.003$	$0.263 \pm 0.005$	$0.328 \pm 0.007$
<u>36≤nForwardTracks&lt;48</u>					
$p_T$ ( GeV/c )	0-2	2-4	4-6	6-8	8-20
$2.0 < y < 2.8$	$0.029 \pm 0.001$	$0.054 \pm 0.001$	$0.126 \pm 0.002$	$0.204 \pm 0.004$	$0.317 \pm 0.005$
$2.8 < y < 3.5$	$0.070 \pm 0.002$	$0.118 \pm 0.002$	$0.222 \pm 0.003$	$0.325 \pm 0.006$	$0.400 \pm 0.006$
$3.5 < y < 4.5$	$0.063 \pm 0.002$	$0.096 \pm 0.002$	$0.184 \pm 0.003$	$0.253 \pm 0.006$	$0.335 \pm 0.007$
<u>48≤nForwardTracks&lt;130</u>					
$p_T$ ( GeV/c )	0-2	2-4	4-6	6-8	8-20
$2.0 < y < 2.8$	$0.028 \pm 0.001$	$0.054 \pm 0.001$	$0.126 \pm 0.003$	$0.202 \pm 0.005$	$0.309 \pm 0.006$
$2.8 < y < 3.5$	$0.063 \pm 0.002$	$0.110 \pm 0.002$	$0.225 \pm 0.004$	$0.309 \pm 0.006$	$0.382 \pm 0.007$
$3.5 < y < 4.5$	$0.060 \pm 0.002$	$0.094 \pm 0.002$	$0.173 \pm 0.004$	$0.247 \pm 0.006$	$0.306 \pm 0.007$

Table 34: The efficiency  $\epsilon_{\text{tot}}$  for from b signals in different  $(p_T, y)$  bins.

<u>0≤nForwardTracks&lt;12</u>					
$p_T$ ( GeV/c )	0-2	2-4	4-6	6-8	8-20
$2.0 < y < 2.8$	$0.067 \pm 0.002$	$0.067 \pm 0.001$	$0.117 \pm 0.003$	$0.184 \pm 0.005$	$0.263 \pm 0.006$
$2.8 < y < 3.5$	$0.157 \pm 0.003$	$0.154 \pm 0.003$	$0.246 \pm 0.004$	$0.326 \pm 0.007$	$0.422 \pm 0.009$
$3.5 < y < 4.5$	$0.136 \pm 0.003$	$0.126 \pm 0.003$	$0.197 \pm 0.004$	$0.266 \pm 0.008$	$0.345 \pm 0.011$
<u>12≤nForwardTracks&lt;24</u>					
$p_T$ ( GeV/c )	0-2	2-4	4-6	6-8	8-20
$2.0 < y < 2.8$	$0.068 \pm 0.001$	$0.070 \pm 0.001$	$0.116 \pm 0.002$	$0.183 \pm 0.003$	$0.266 \pm 0.004$
$2.8 < y < 3.5$	$0.159 \pm 0.002$	$0.157 \pm 0.002$	$0.249 \pm 0.003$	$0.329 \pm 0.004$	$0.413 \pm 0.005$
$3.5 < y < 4.5$	$0.137 \pm 0.002$	$0.127 \pm 0.002$	$0.188 \pm 0.003$	$0.251 \pm 0.004$	$0.329 \pm 0.006$
<u>24≤nForwardTracks&lt;36</u>					
$p_T$ ( GeV/c )	0-2	2-4	4-6	6-8	8-20
$2.0 < y < 2.8$	$0.067 \pm 0.001$	$0.070 \pm 0.001$	$0.115 \pm 0.002$	$0.181 \pm 0.003$	$0.269 \pm 0.004$
$2.8 < y < 3.5$	$0.158 \pm 0.002$	$0.152 \pm 0.002$	$0.245 \pm 0.003$	$0.321 \pm 0.004$	$0.408 \pm 0.004$
$3.5 < y < 4.5$	$0.135 \pm 0.002$	$0.123 \pm 0.002$	$0.186 \pm 0.003$	$0.250 \pm 0.004$	$0.322 \pm 0.005$
<u>36≤nForwardTracks&lt;48</u>					
$p_T$ ( GeV/c )	0-2	2-4	4-6	6-8	8-20
$2.0 < y < 2.8$	$0.066 \pm 0.002$	$0.068 \pm 0.001$	$0.113 \pm 0.002$	$0.184 \pm 0.003$	$0.266 \pm 0.004$
$2.8 < y < 3.5$	$0.153 \pm 0.003$	$0.153 \pm 0.002$	$0.244 \pm 0.003$	$0.314 \pm 0.005$	$0.394 \pm 0.005$
$3.5 < y < 4.5$	$0.132 \pm 0.002$	$0.123 \pm 0.002$	$0.180 \pm 0.003$	$0.246 \pm 0.005$	$0.313 \pm 0.006$
<u>48≤nForwardTracks&lt;130</u>					
$p_T$ ( GeV/c )	0-2	2-4	4-6	6-8	8-20
$2.0 < y < 2.8$	$0.064 \pm 0.002$	$0.065 \pm 0.001$	$0.109 \pm 0.002$	$0.174 \pm 0.004$	$0.261 \pm 0.004$
$2.8 < y < 3.5$	$0.152 \pm 0.003$	$0.147 \pm 0.002$	$0.237 \pm 0.003$	$0.303 \pm 0.005$	$0.385 \pm 0.005$
$3.5 < y < 4.5$	$0.125 \pm 0.003$	$0.119 \pm 0.002$	$0.180 \pm 0.003$	$0.238 \pm 0.005$	$0.304 \pm 0.006$

673 **C Fitting plots in each kinematic bin**

674 **C.1 Separated by PVNTRACKS**

675 For each kinematic bin of  $J/\psi$  and  $\psi(2S)$  candidates, the two-dimensional fit to the  
 676 invariant mass and the lifetime are shown below. The left is the invariant mass and the  
 677 right is pseudo-proper decay time fit results. The first row in each figure set is that of  $J/\psi$   
 678 and the second row is that of  $\psi(2S)$ .

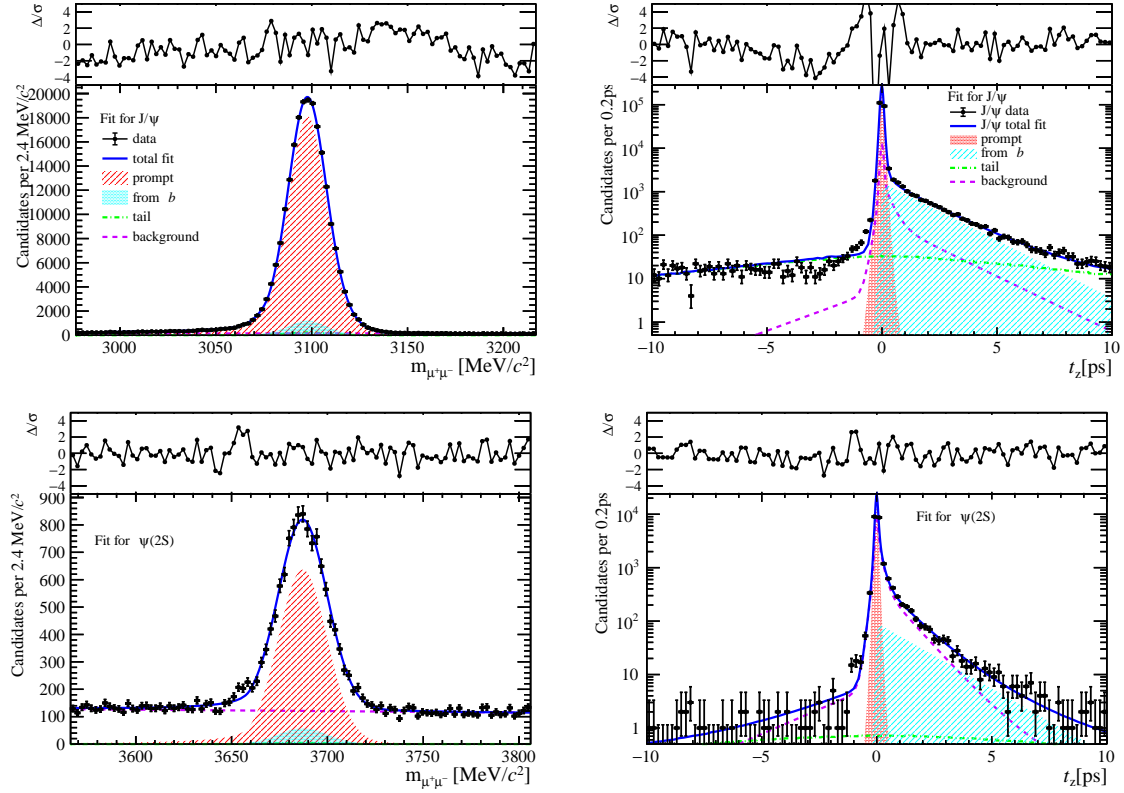


Figure 33: Fit results in  $0 \text{ GeV}/c < p_T < 2 \text{ GeV}/c$ ,  $2.0 < y < 2.8$  and  $0 \leq \text{PVNTRACKS} < 20$ .

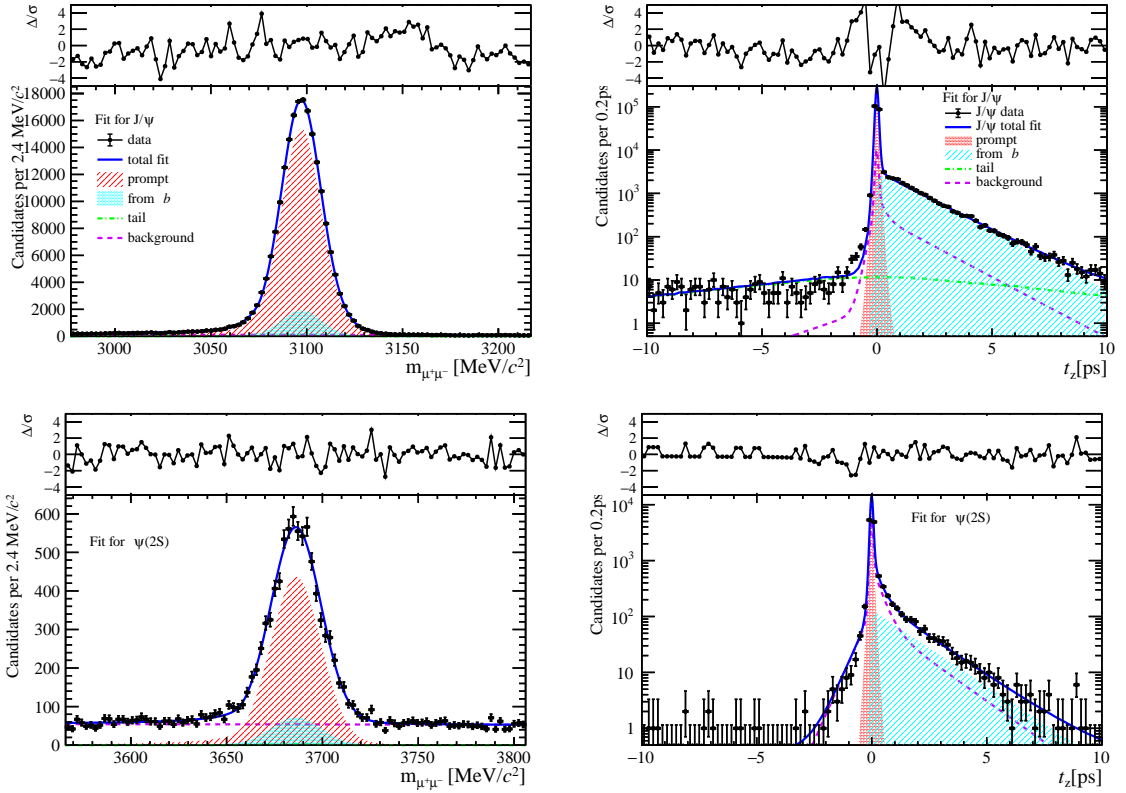


Figure 34: Fit results in  $2 \text{ GeV}/c < p_T < 4 \text{ GeV}/c$ ,  $2.0 < y < 2.8$  and  $0 \leq \text{PVNTRACKS} < 20$ .

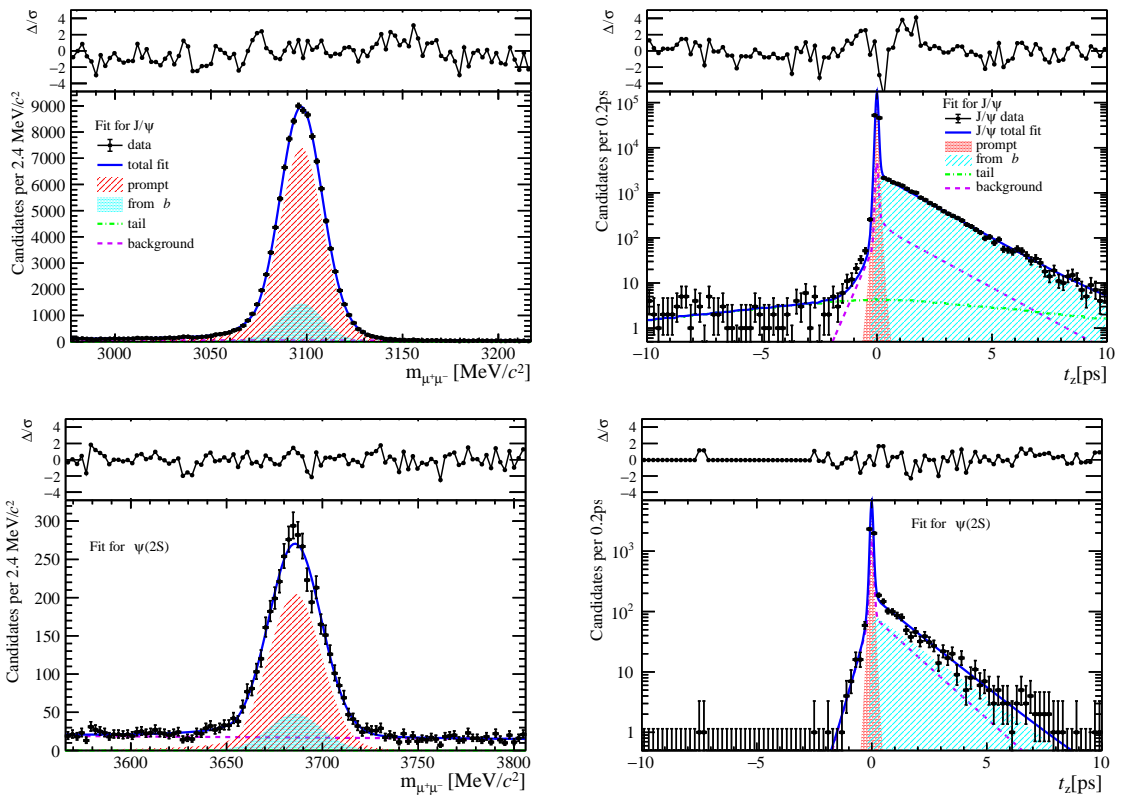


Figure 35: Fit results in  $4 \text{ GeV}/c < p_T < 6 \text{ GeV}/c$ ,  $2.0 < y < 2.8$  and  $0 \leq \text{PVNTRACKS} < 20$ .

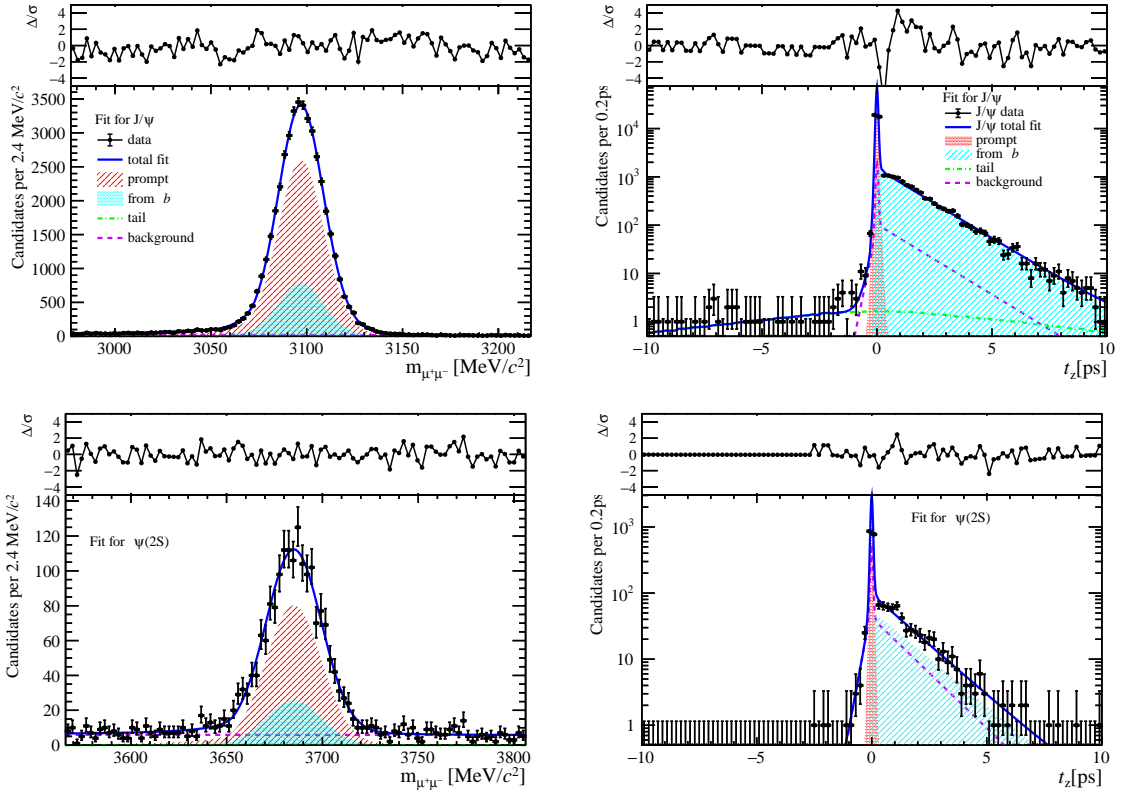


Figure 36: Fit results in  $6 \text{ GeV}/c < p_T < 8 \text{ GeV}/c$ ,  $2.0 < y < 2.8$  and  $0 \leq \text{PVNTRACKS} < 20$ .

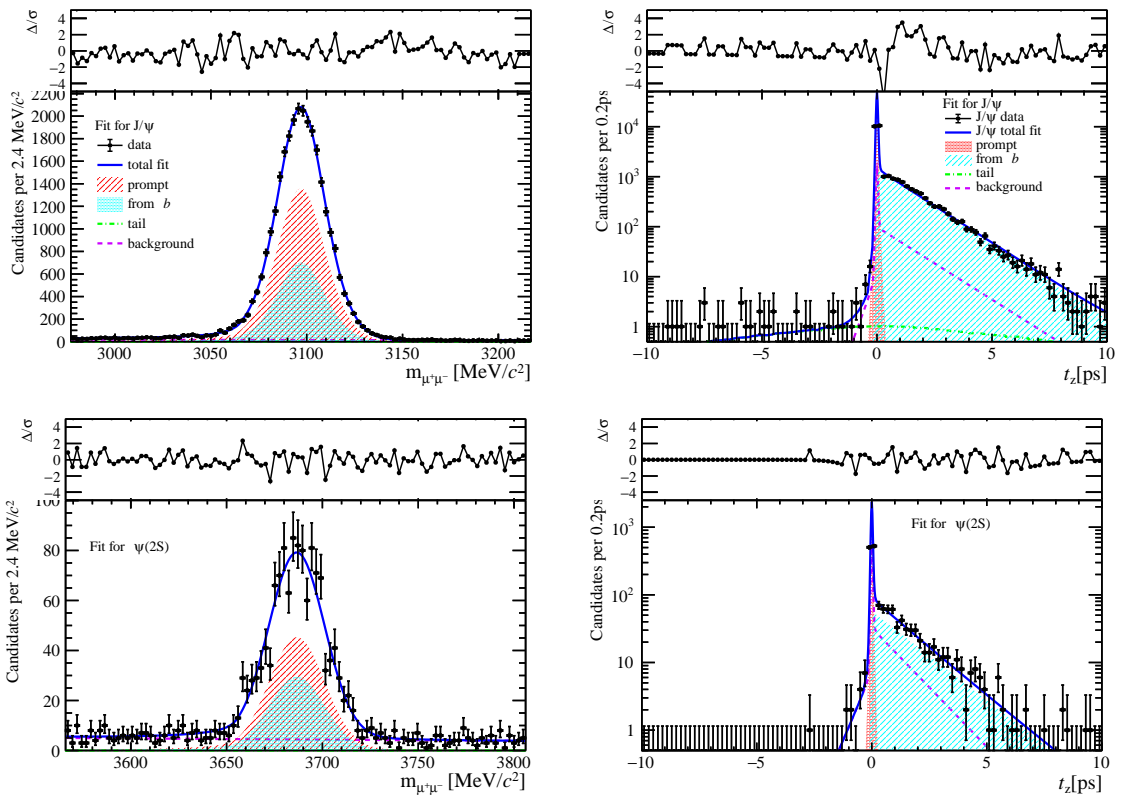


Figure 37: Fit results in  $8 \text{ GeV}/c < p_T < 20 \text{ GeV}/c$ ,  $2.0 < y < 2.8$  and  $0 \leq \text{PVNTRACKS} < 20$ .

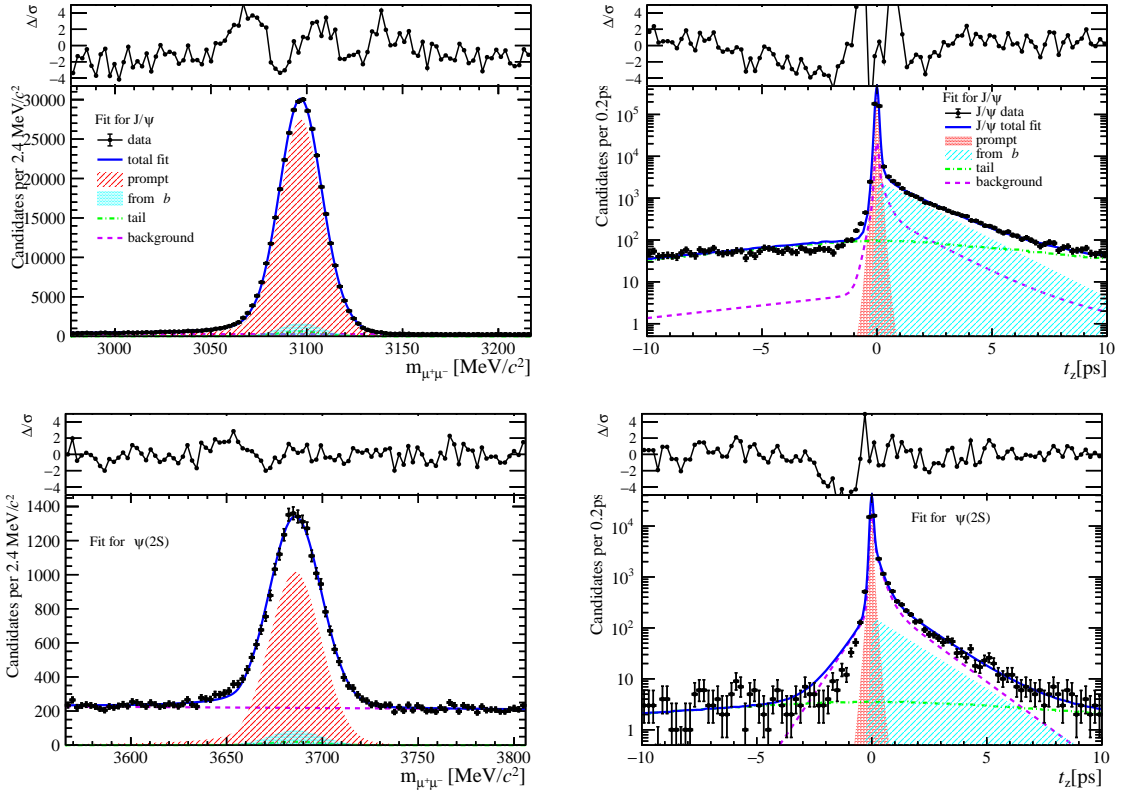


Figure 38: Fit results in  $0 \text{ GeV}/c < p_T < 2 \text{ GeV}/c$ ,  $2.8 < y < 3.5$  and  $0 \leq \text{PVNTRACKS} < 20$ .

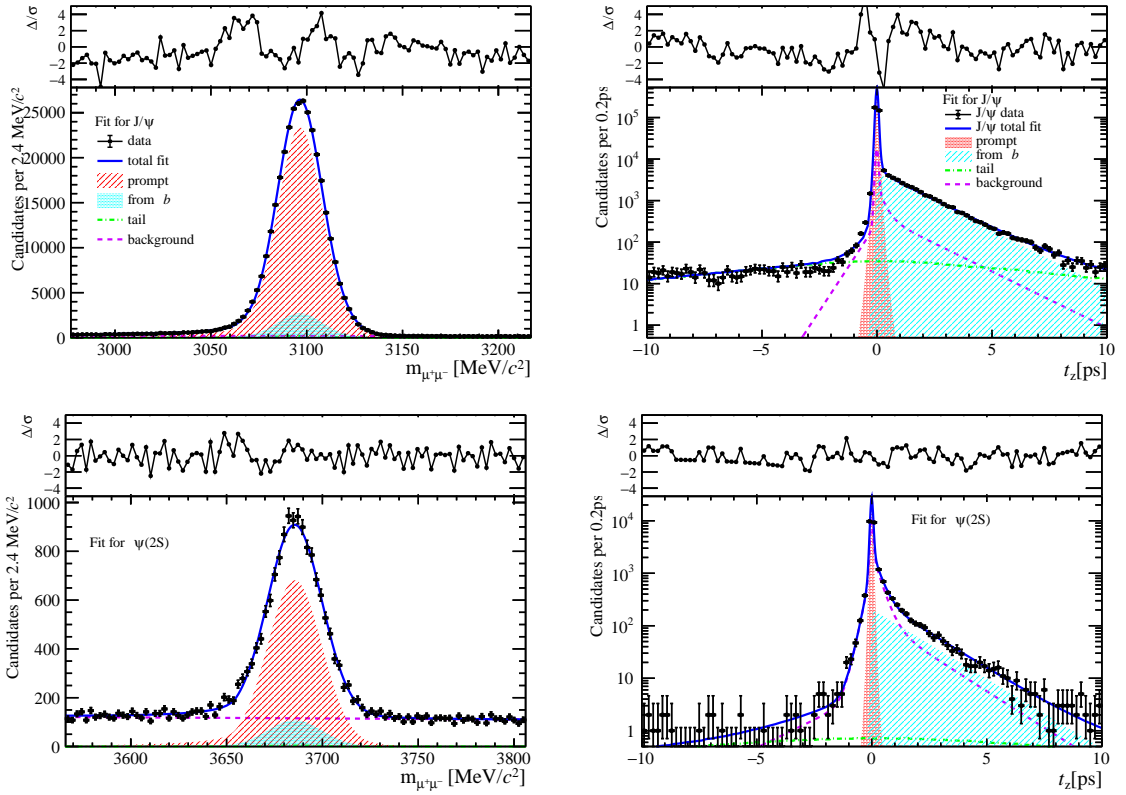


Figure 39: Fit results in  $2 \text{ GeV}/c < p_T < 4 \text{ GeV}/c$ ,  $2.8 < y < 3.5$  and  $0 \leq \text{PVNTRACKS} < 20$ .

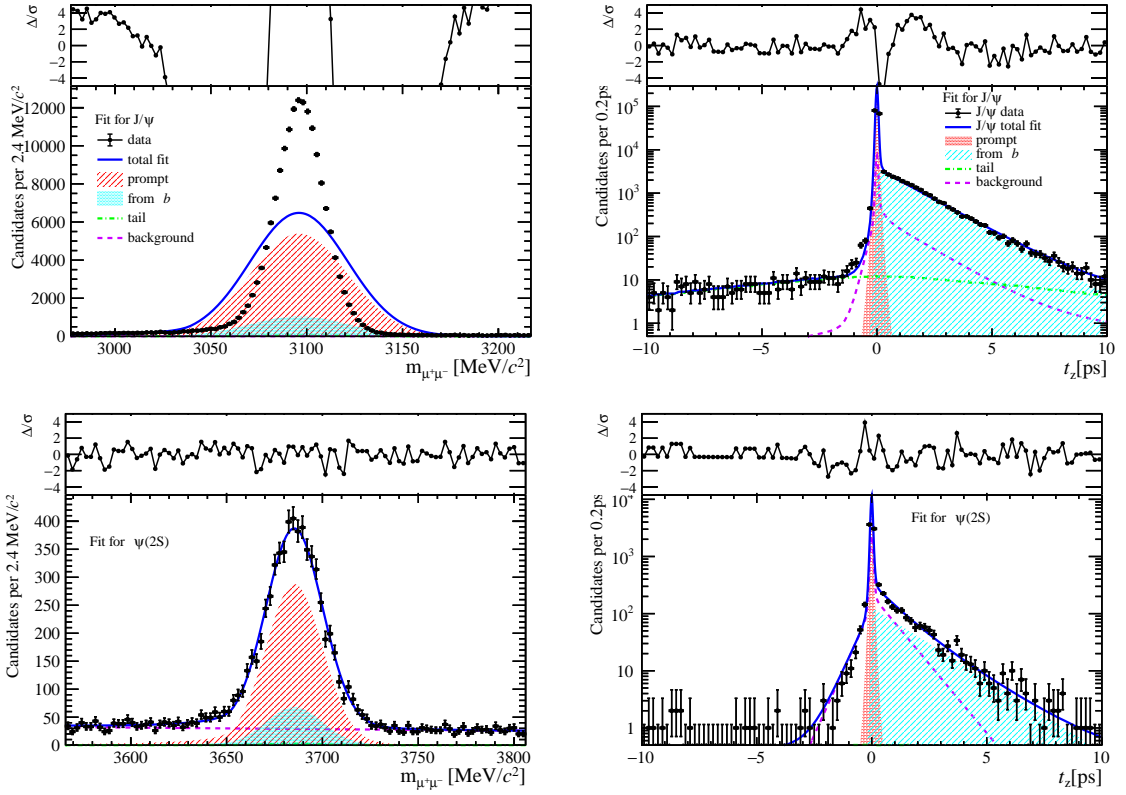


Figure 40: Fit results in  $4 \text{ GeV}/c < p_T < 6 \text{ GeV}/c$ ,  $2.8 < y < 3.5$  and  $0 \leq \text{PVNTRACKS} < 20$ .

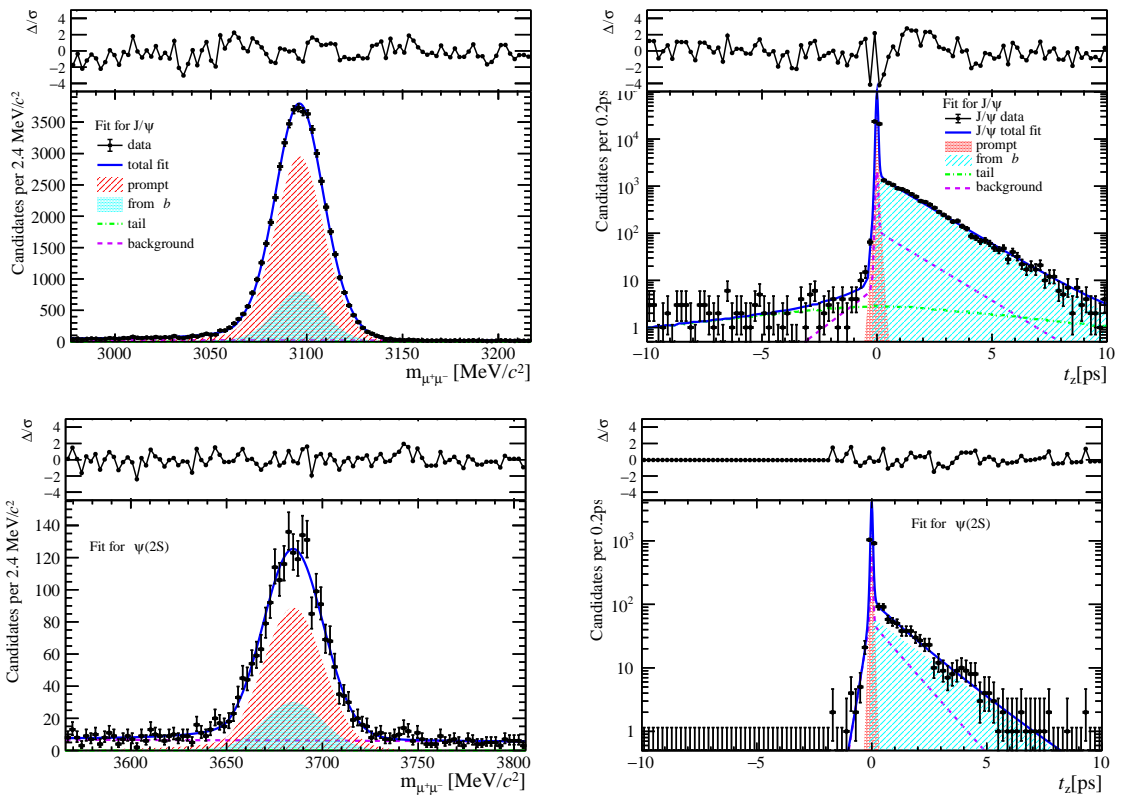


Figure 41: Fit results in  $6 \text{ GeV}/c < p_T < 8 \text{ GeV}/c$ ,  $2.8 < y < 3.5$  and  $0 \leq \text{PVNTRACKS} < 20$ .

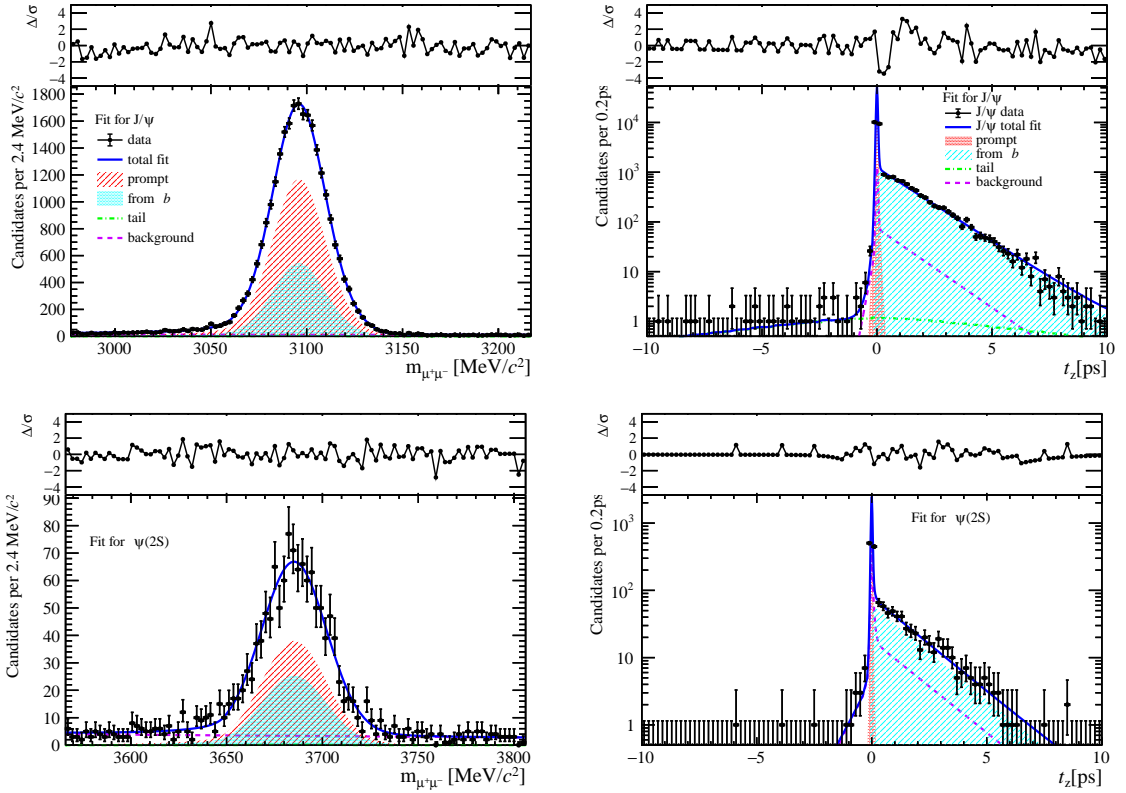


Figure 42: Fit results in  $8 \text{ GeV}/c < p_T < 20 \text{ GeV}/c$ ,  $2.8 < y < 3.5$  and  $0 \leq \text{PVNTRACKS} < 20$ .

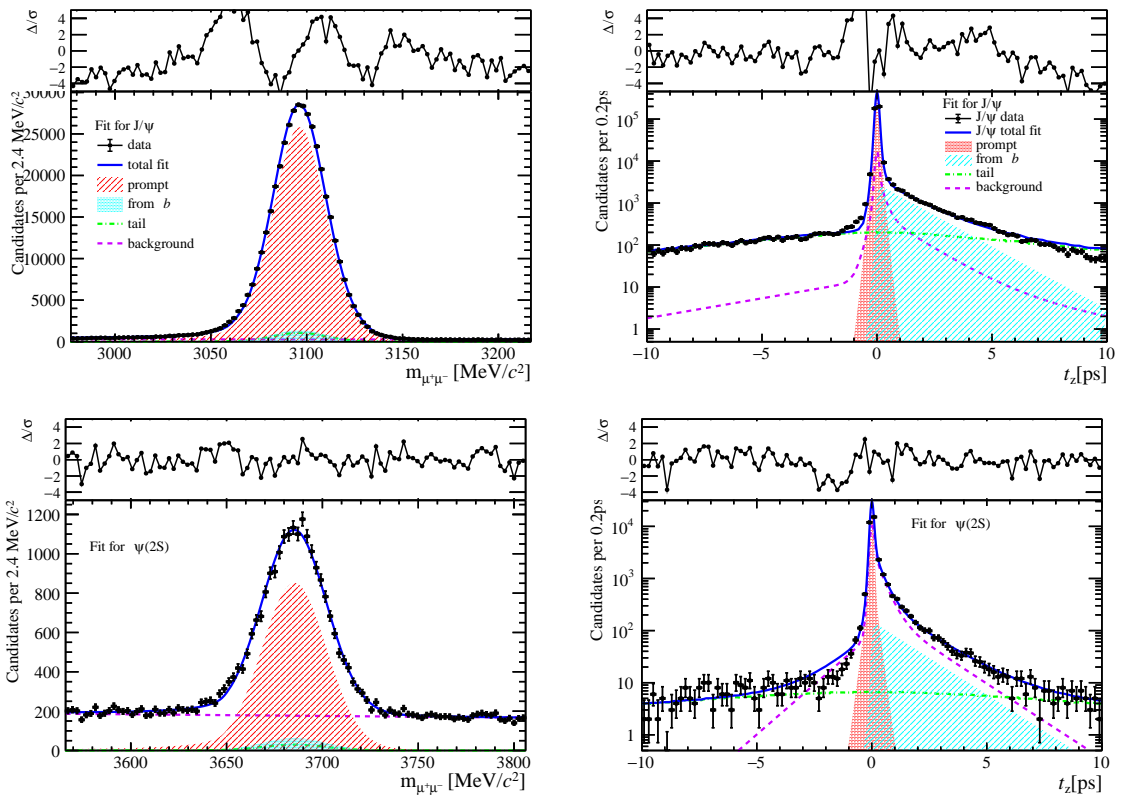


Figure 43: Fit results in  $0 \text{ GeV}/c < p_T < 2 \text{ GeV}/c$ ,  $3.5 < y < 4.5$  and  $0 \leq \text{PVNTRACKS} < 20$ .

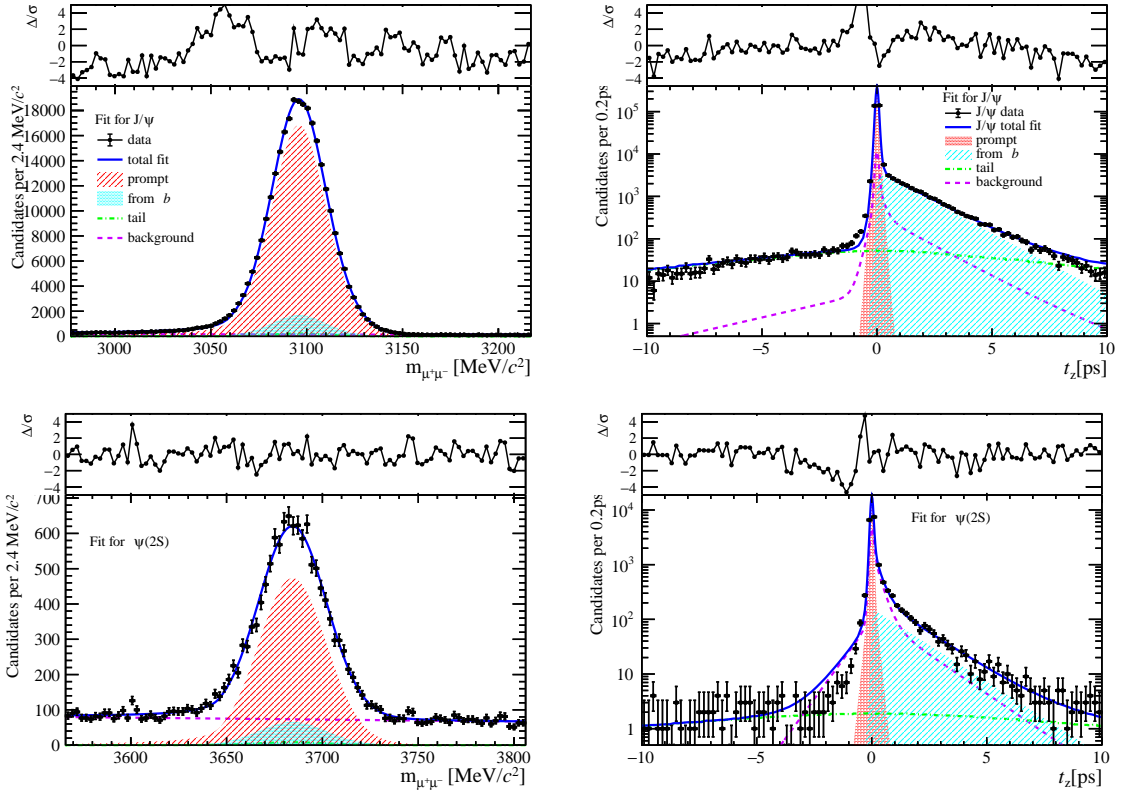


Figure 44: Fit results in  $2 \text{ GeV}/c < p_T < 4 \text{ GeV}/c$ ,  $3.5 < y < 4.5$  and  $0 \leq \text{PVNTRACKS} < 20$ .

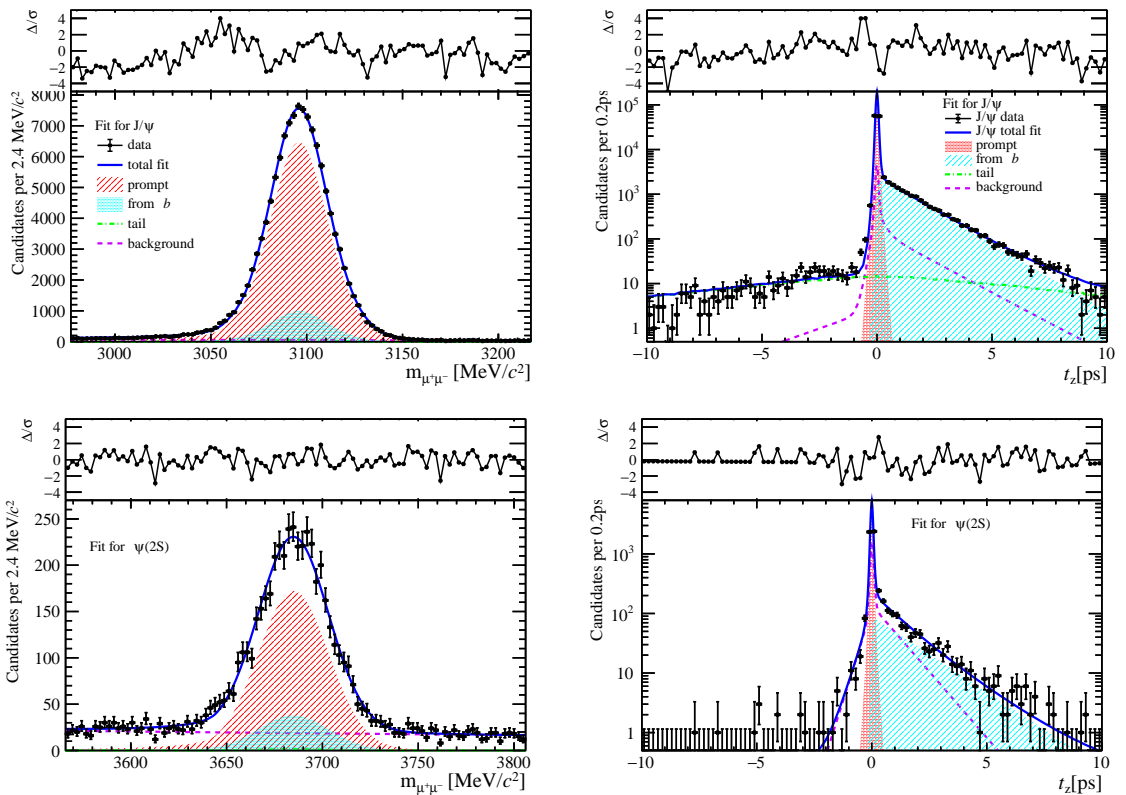


Figure 45: Fit results in  $4 \text{ GeV}/c < p_T < 6 \text{ GeV}/c$ ,  $3.5 < y < 4.5$  and  $0 \leq \text{PVNTRACKS} < 20$ .

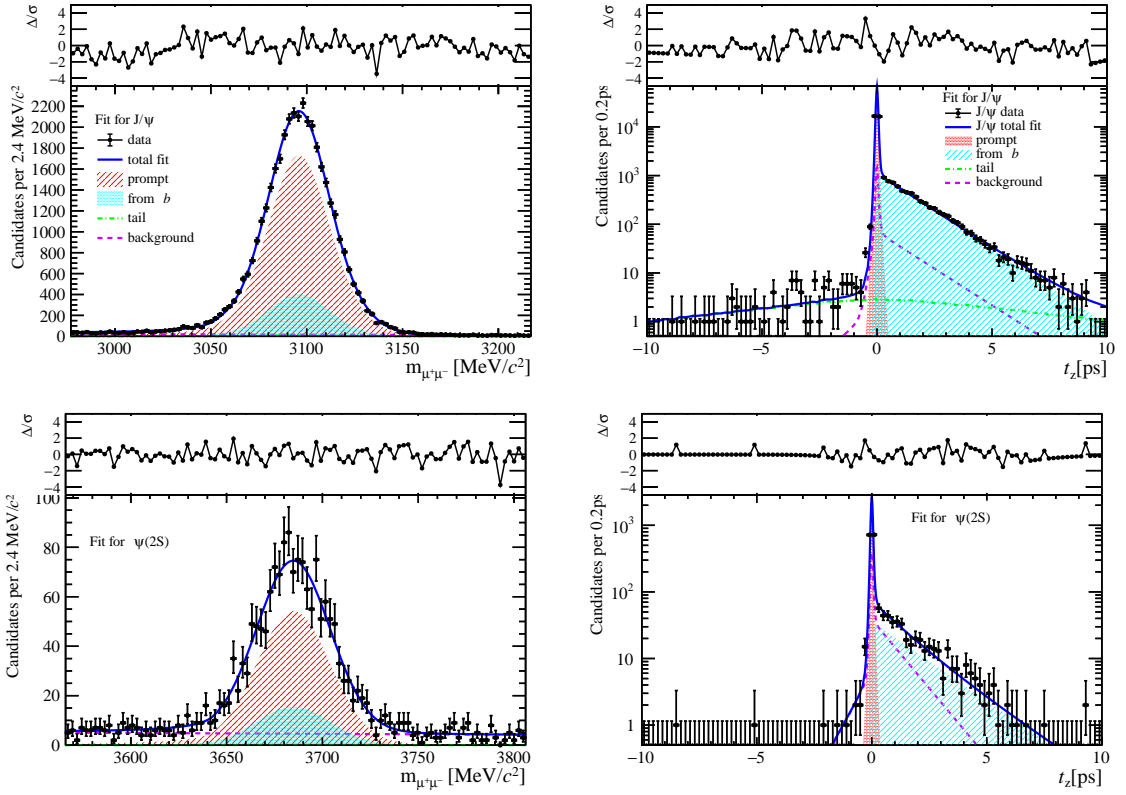


Figure 46: Fit results in  $6 \text{ GeV}/c < p_T < 8 \text{ GeV}/c$ ,  $3.5 < y < 4.5$  and  $0 \leq \text{PVNTRACKS} < 20$ .

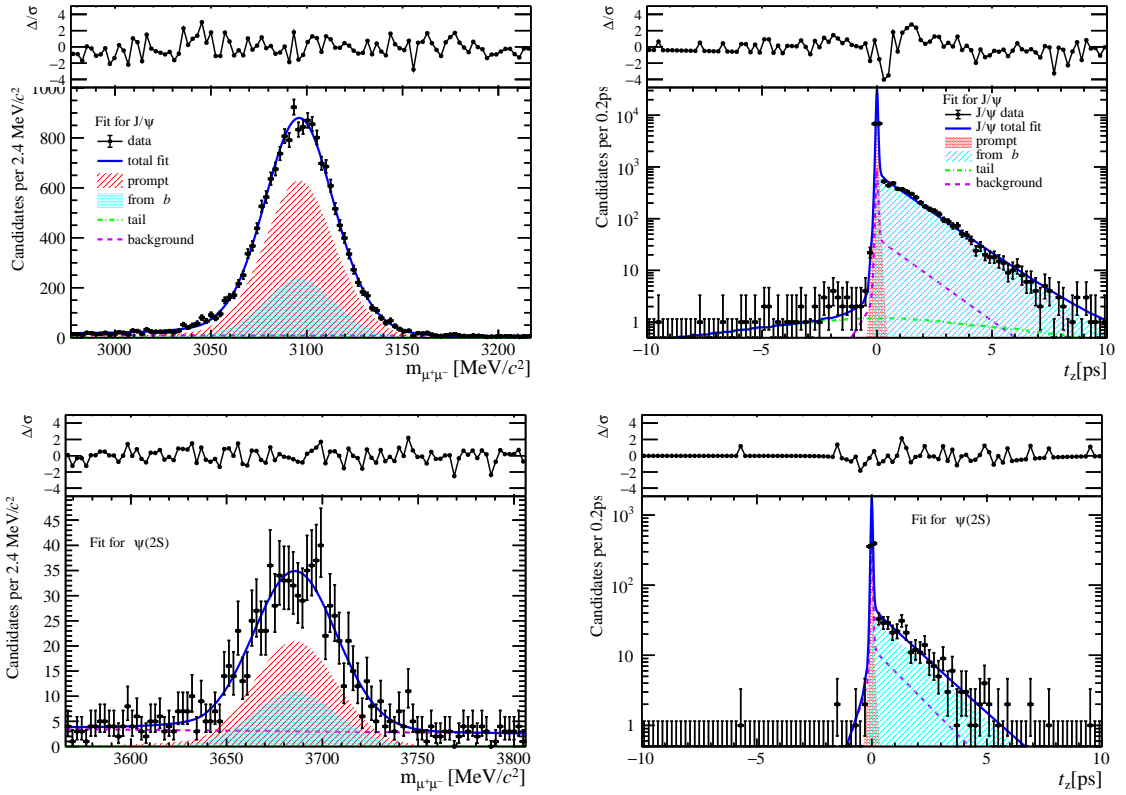


Figure 47: Fit results in  $8 \text{ GeV}/c < p_T < 20 \text{ GeV}/c$ ,  $3.5 < y < 4.5$  and  $0 \leq \text{PVNTRACKS} < 20$ .

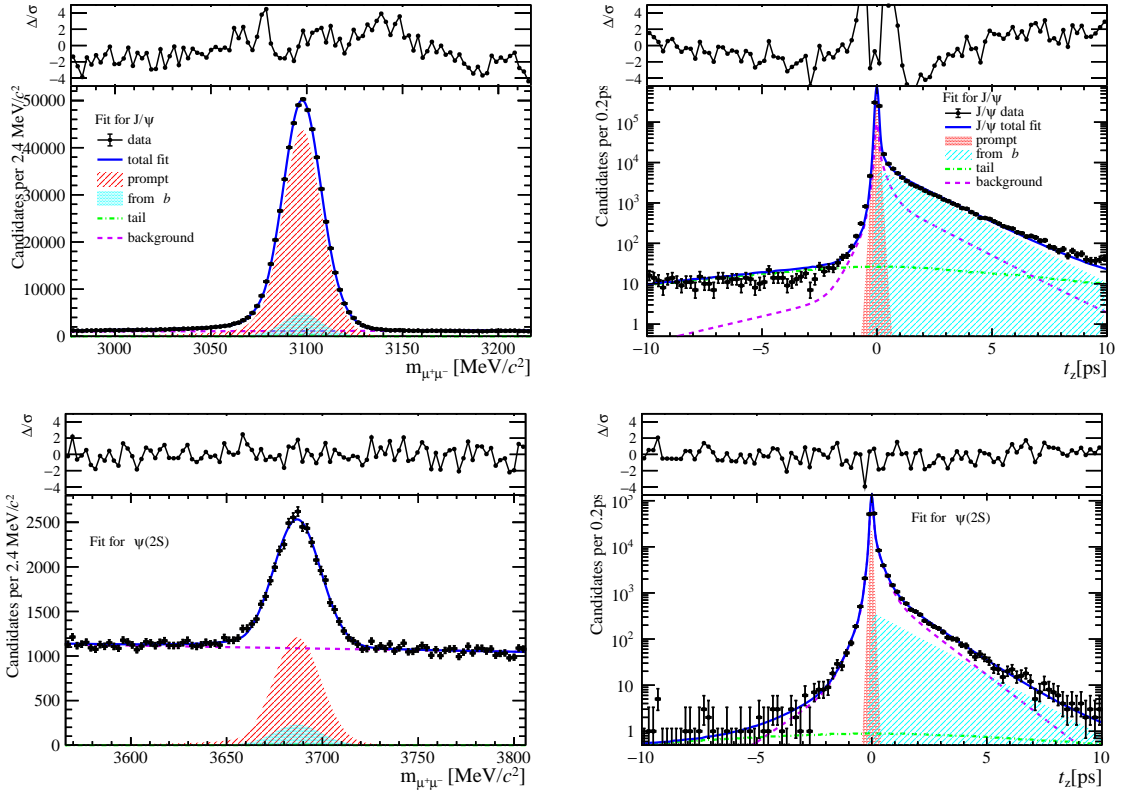


Figure 48: Fit results in  $0 \text{ GeV}/c < p_T < 2 \text{ GeV}/c$ ,  $2.0 < y < 2.8$  and  $20 \leq \text{PVNTRACKS} < 45$ .

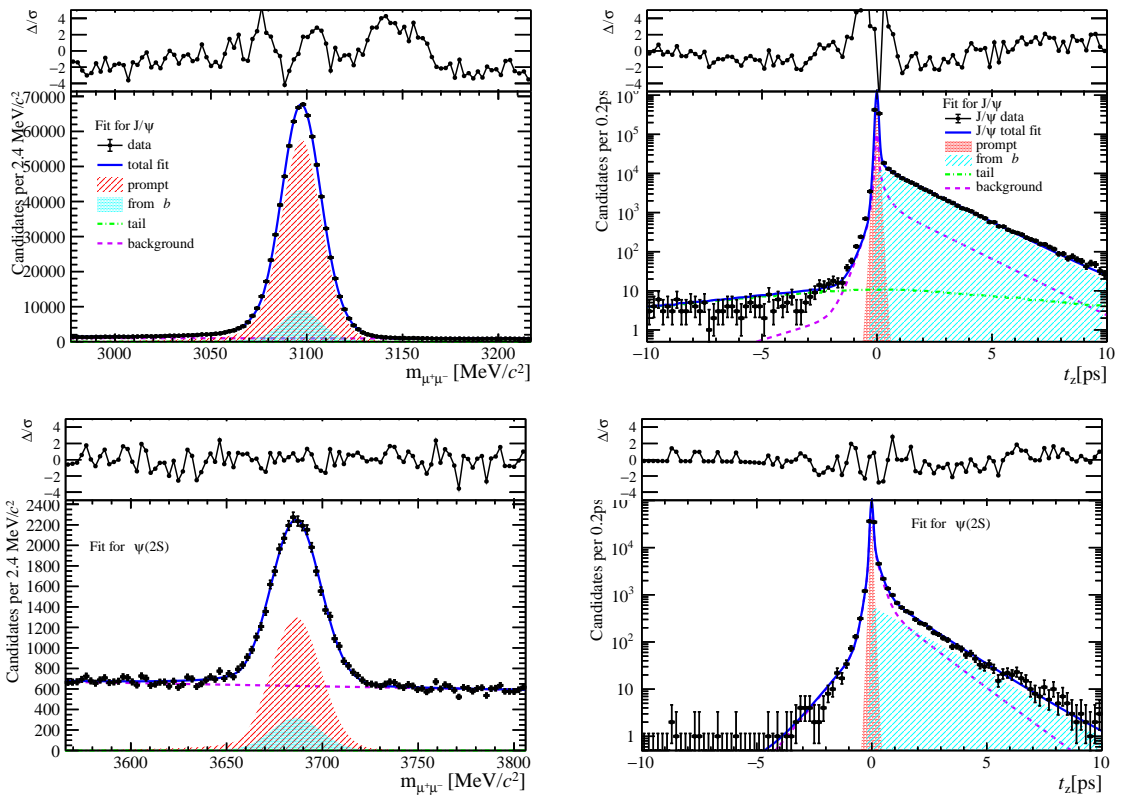


Figure 49: Fit results in  $2 \text{ GeV}/c < p_T < 4 \text{ GeV}/c$ ,  $2.0 < y < 2.8$  and  $20 \leq \text{PVNTRACKS} < 45$ .

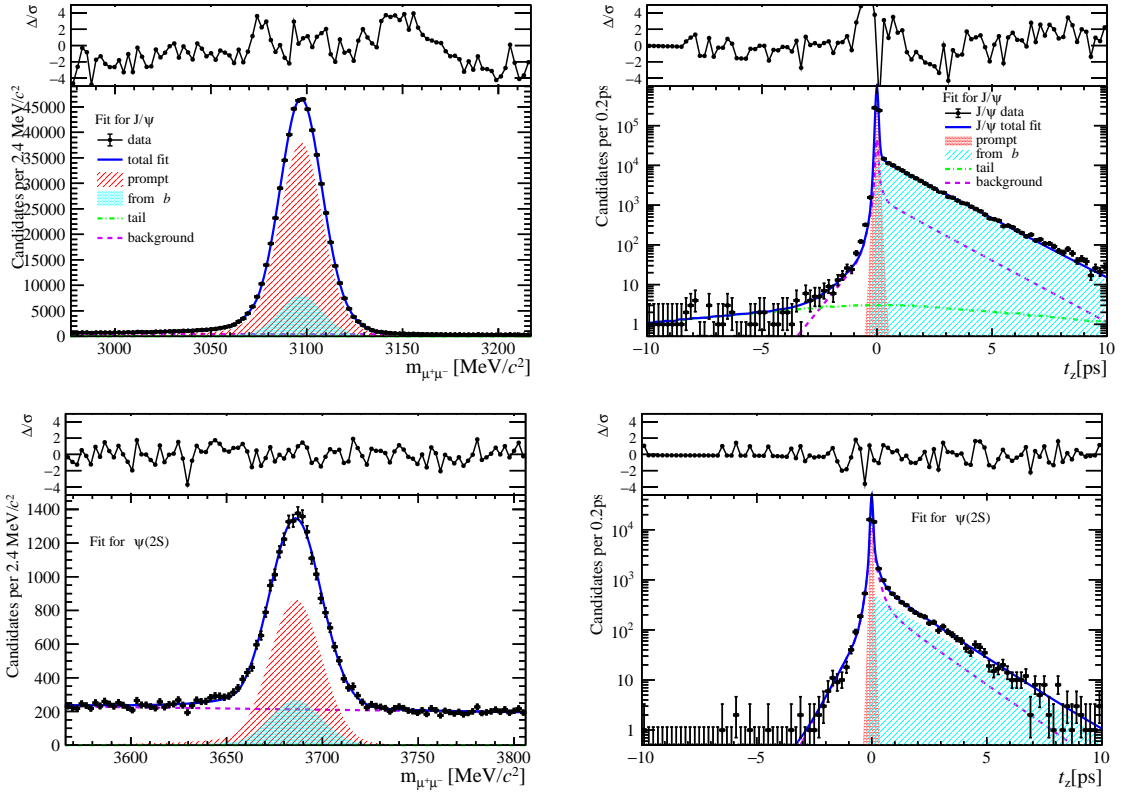


Figure 50: Fit results in  $4 \text{ GeV}/c < p_T < 6 \text{ GeV}/c$ ,  $2.0 < y < 2.8$  and  $20 \leq \text{PVNTRACKS} < 45$ .

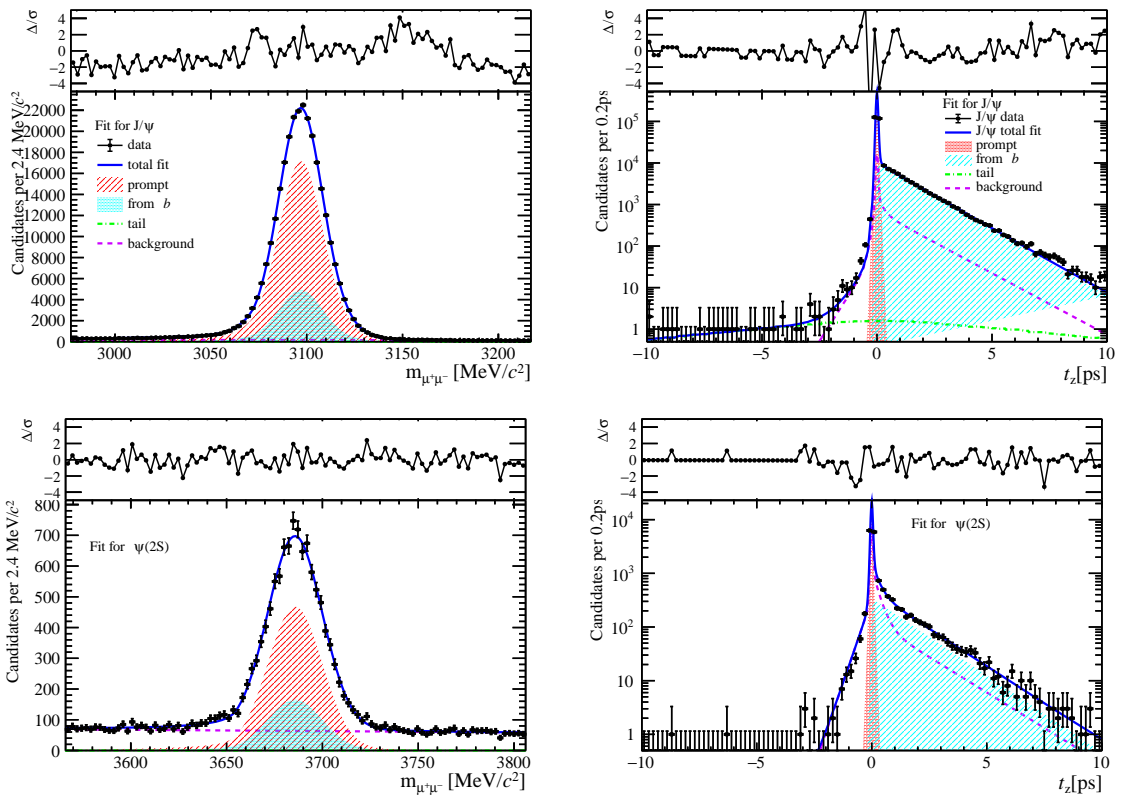


Figure 51: Fit results in  $6 \text{ GeV}/c < p_T < 8 \text{ GeV}/c$ ,  $2.0 < y < 2.8$  and  $20 \leq \text{PVNTRACKS} < 45$ .

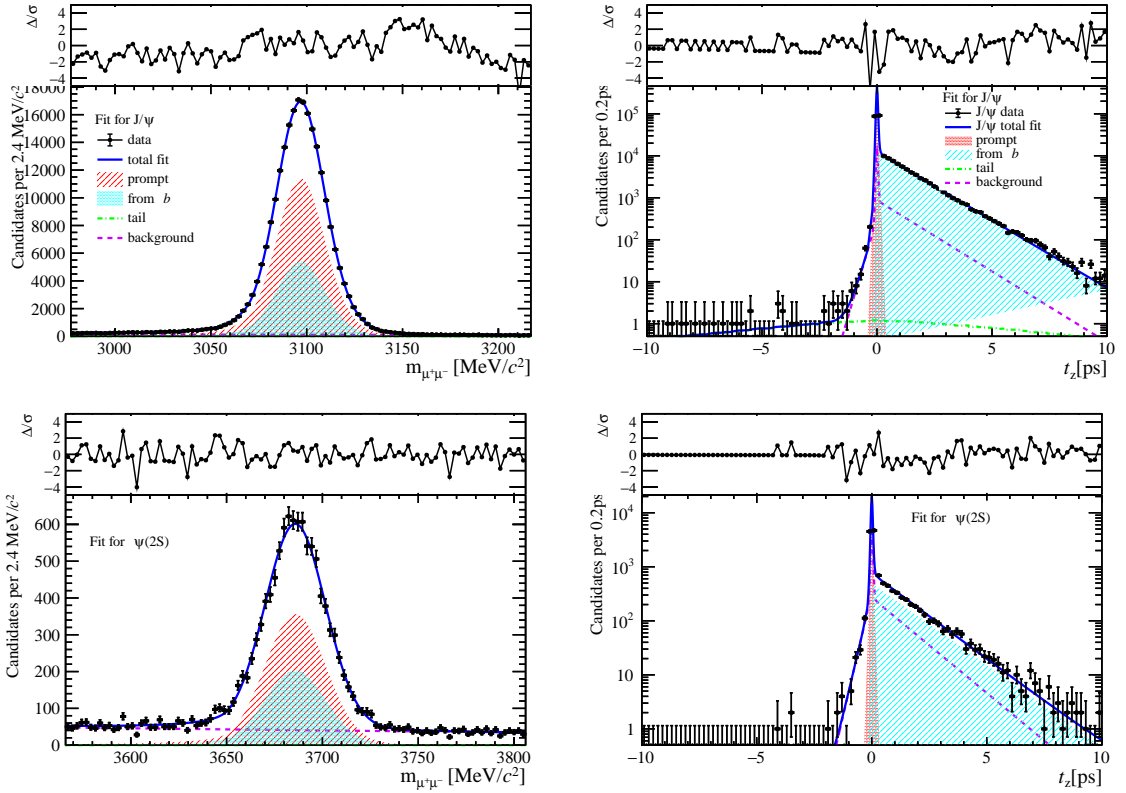


Figure 52: Fit results in  $8 \text{ GeV}/c < p_T < 20 \text{ GeV}/c$ ,  $2.0 < y < 2.8$  and  $20 \leq \text{PVNTRACKS} < 45$ .

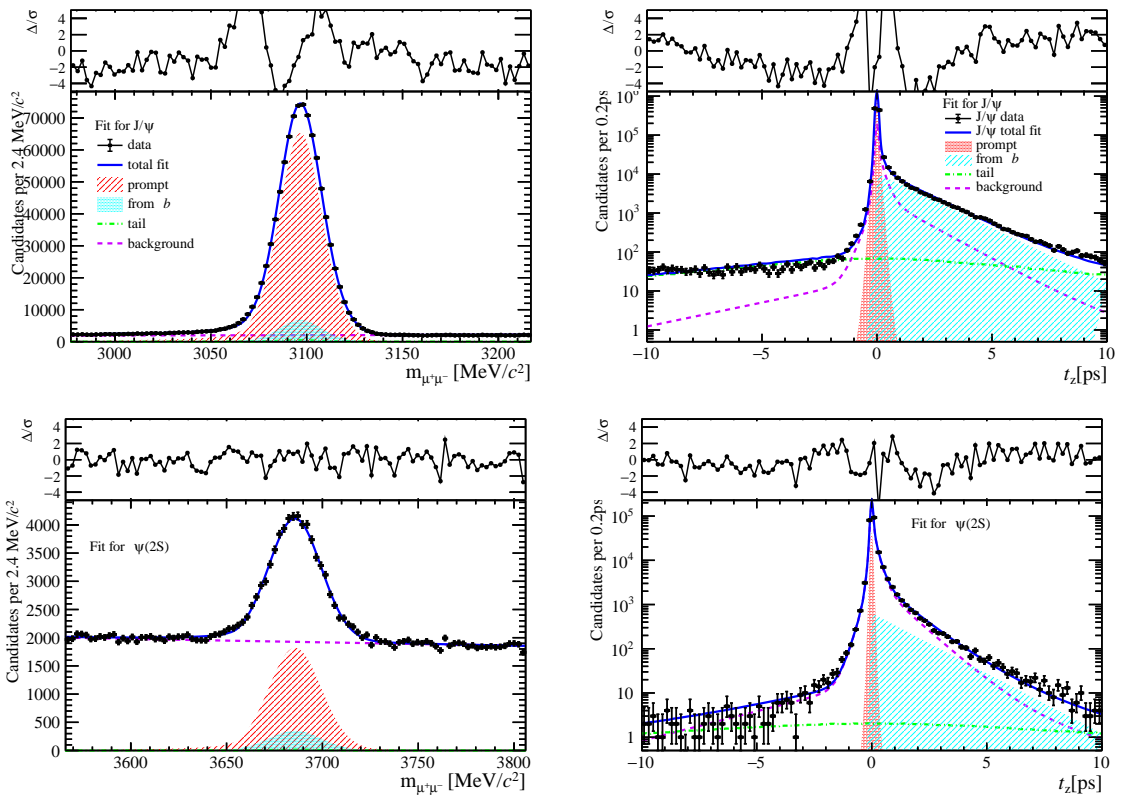


Figure 53: Fit results in  $0 \text{ GeV}/c < p_T < 2 \text{ GeV}/c$ ,  $2.8 < y < 3.5$  and  $20 \leq \text{PVNTRACKS} < 45$ .

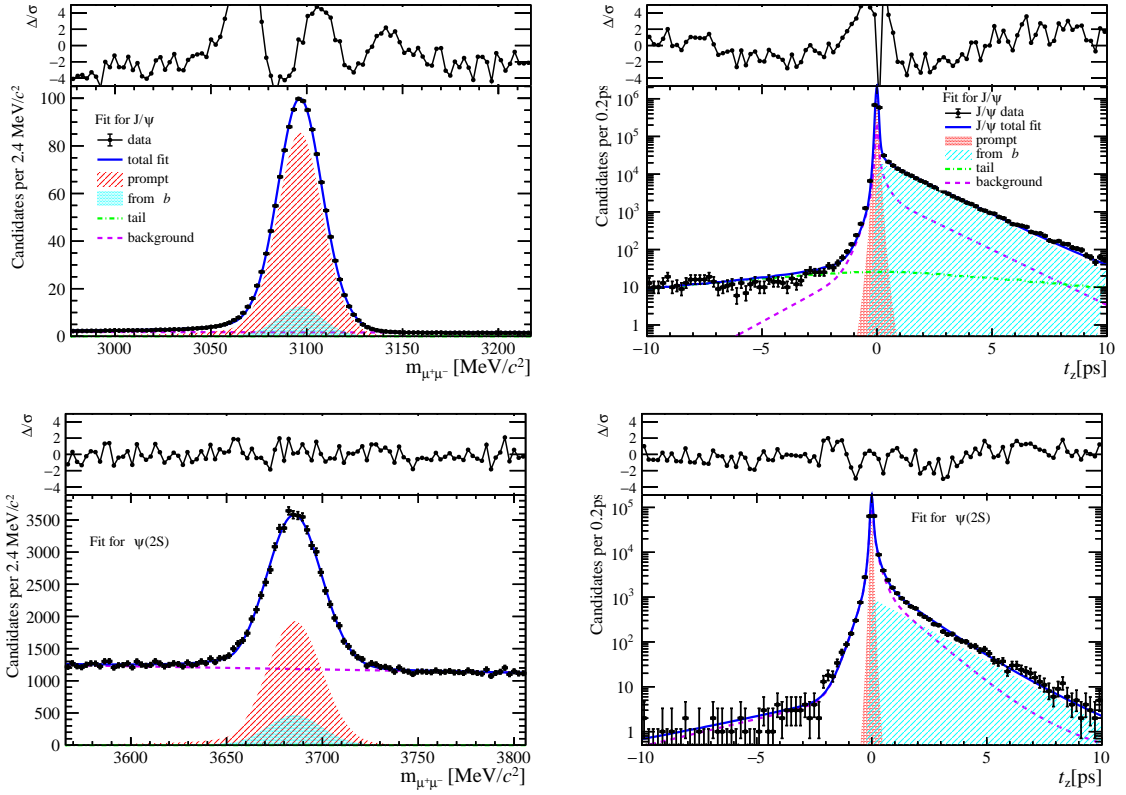


Figure 54: Fit results in  $2 \text{ GeV}/c < p_T < 4 \text{ GeV}/c$ ,  $2.8 < y < 3.5$  and  $20 \leq \text{PVNTRACKS} < 45$ .

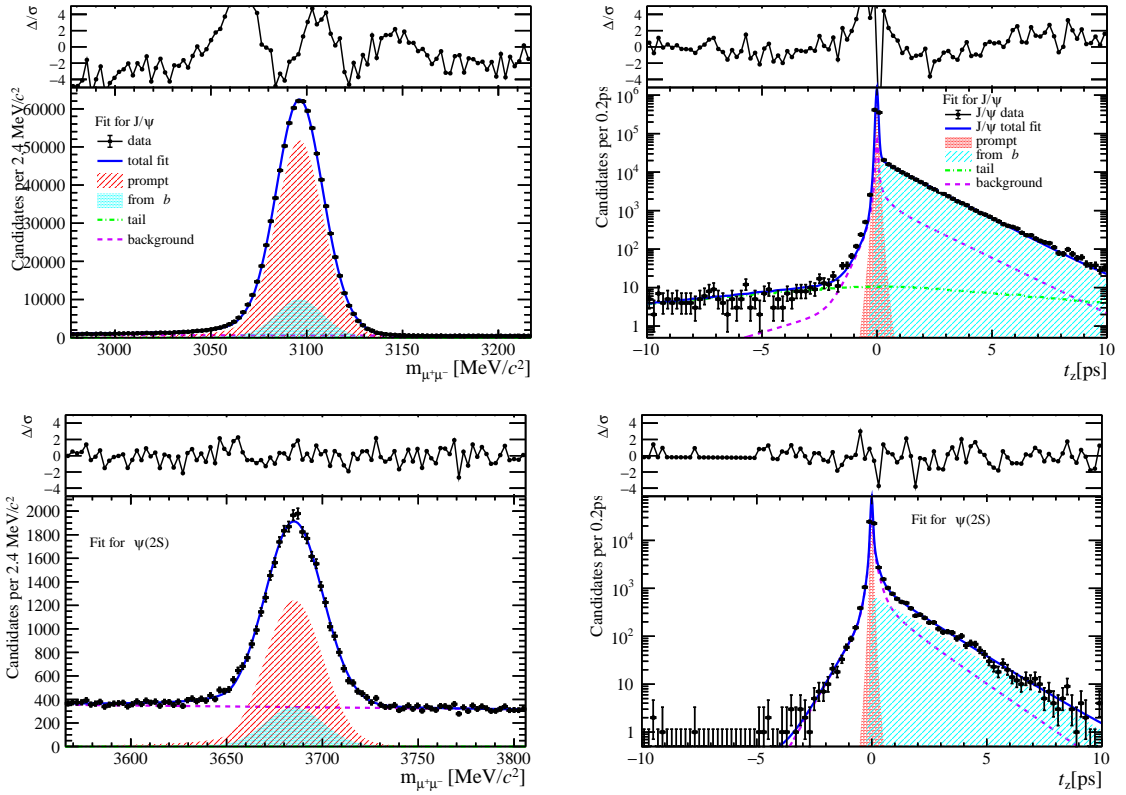


Figure 55: Fit results in  $4 \text{ GeV}/c < p_T < 6 \text{ GeV}/c$ ,  $2.8 < y < 3.5$  and  $20 \leq \text{PVNTRACKS} < 45$ .

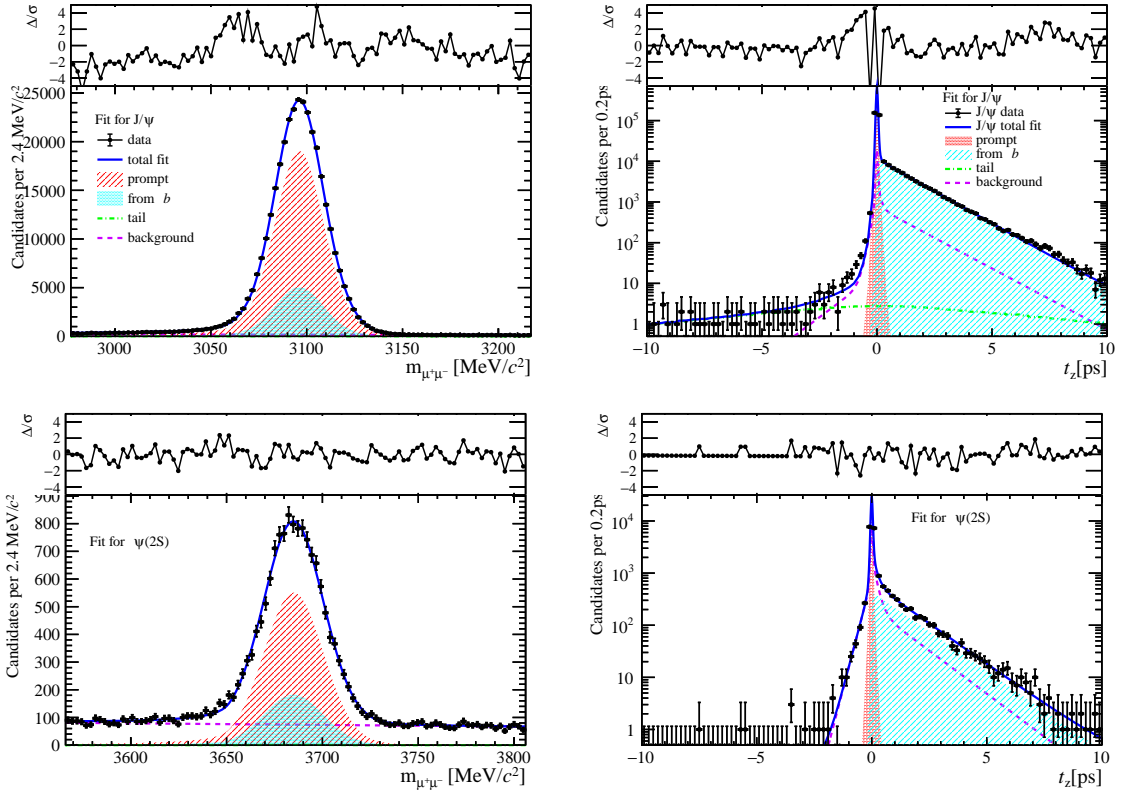


Figure 56: Fit results in  $6 \text{ GeV}/c < p_T < 8 \text{ GeV}/c$ ,  $2.8 < y < 3.5$  and  $20 \leq \text{PVNTRACKS} < 45$ .

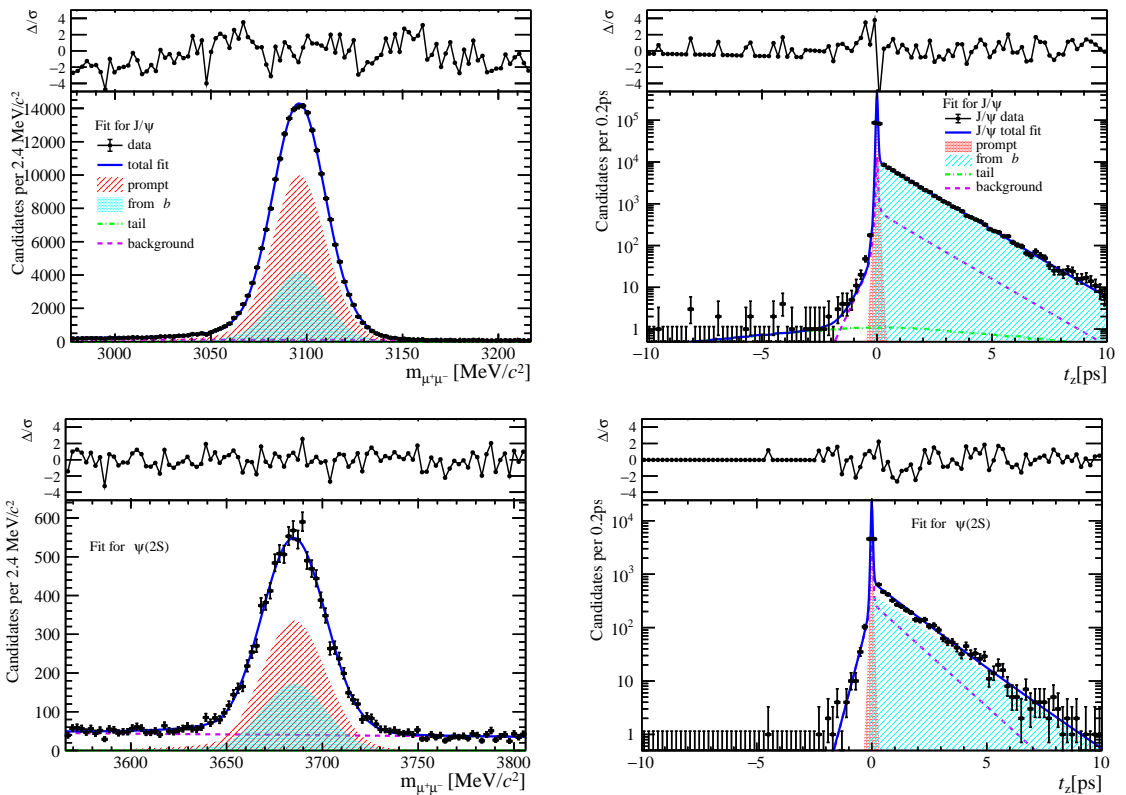


Figure 57: Fit results in  $8 \text{ GeV}/c < p_T < 20 \text{ GeV}/c$ ,  $2.8 < y < 3.5$  and  $20 \leq \text{PVNTRACKS} < 45$ .

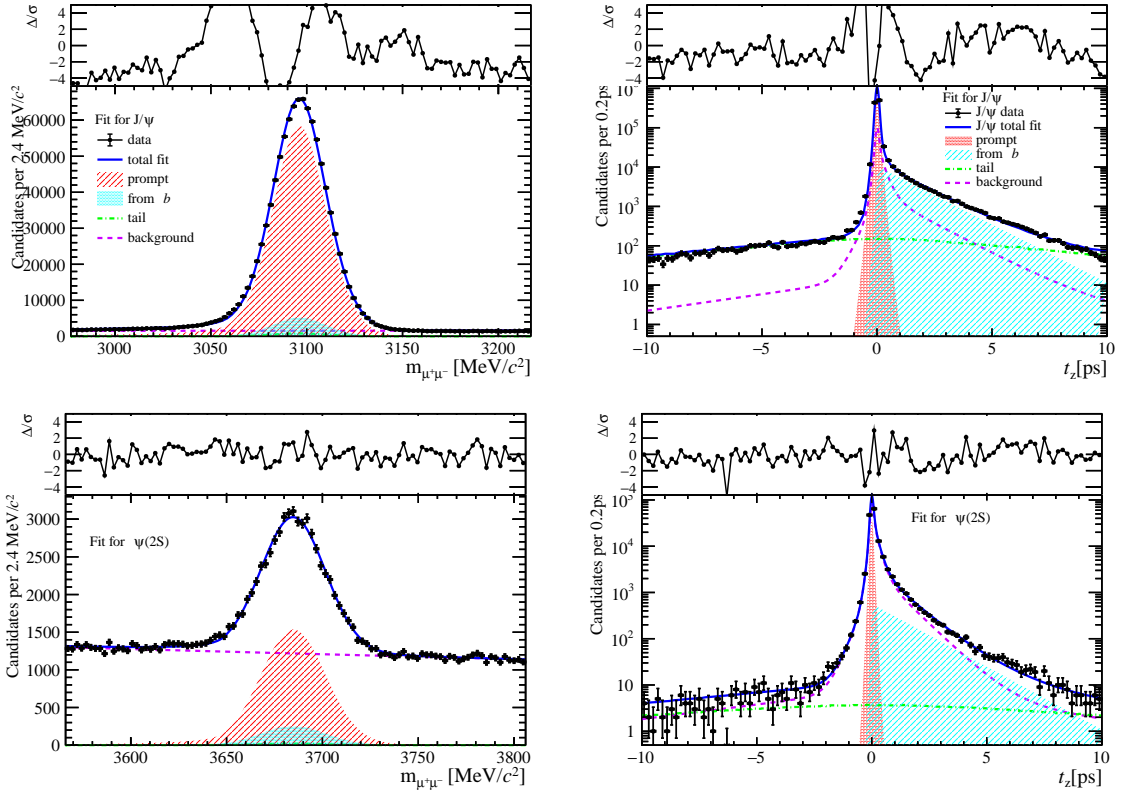


Figure 58: Fit results in  $0 \text{ GeV}/c < p_T < 2 \text{ GeV}/c$ ,  $3.5 < y < 4.5$  and  $20 \leq \text{PVNTRACKS} < 45$ .

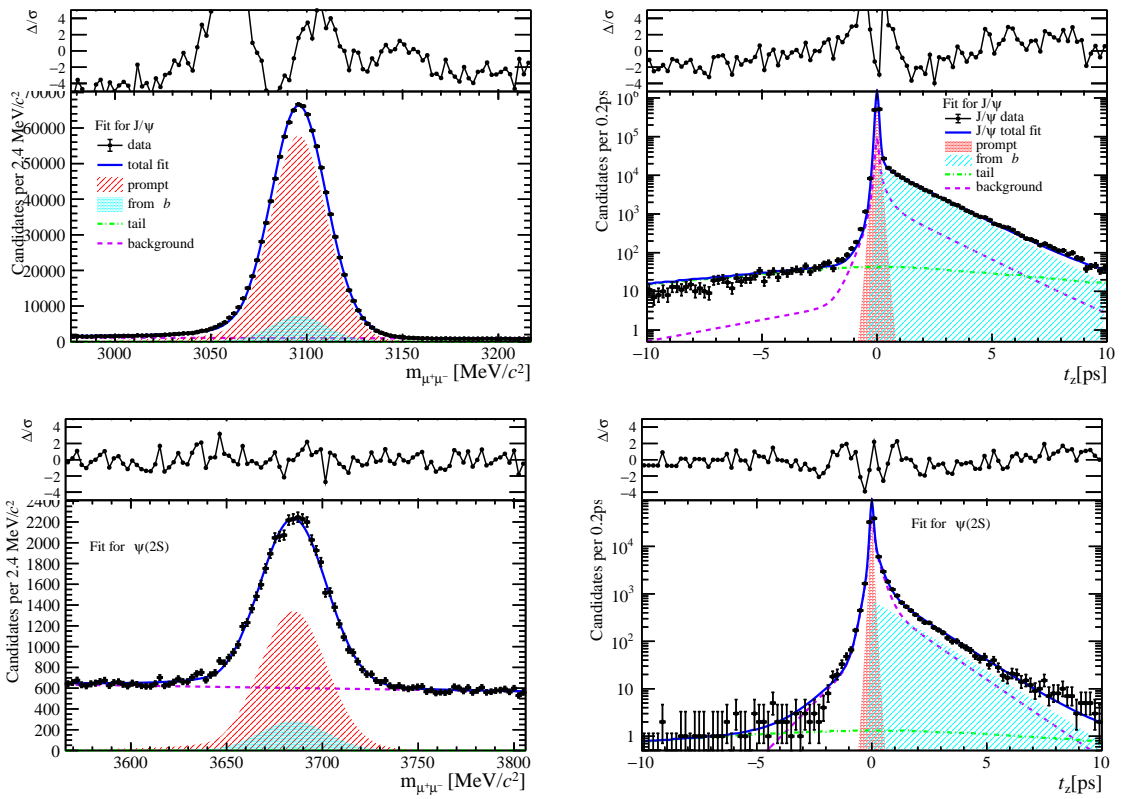


Figure 59: Fit results in  $2 \text{ GeV}/c < p_T < 4 \text{ GeV}/c$ ,  $3.5 < y < 4.5$  and  $20 \leq \text{PVNTRACKS} < 45$ .

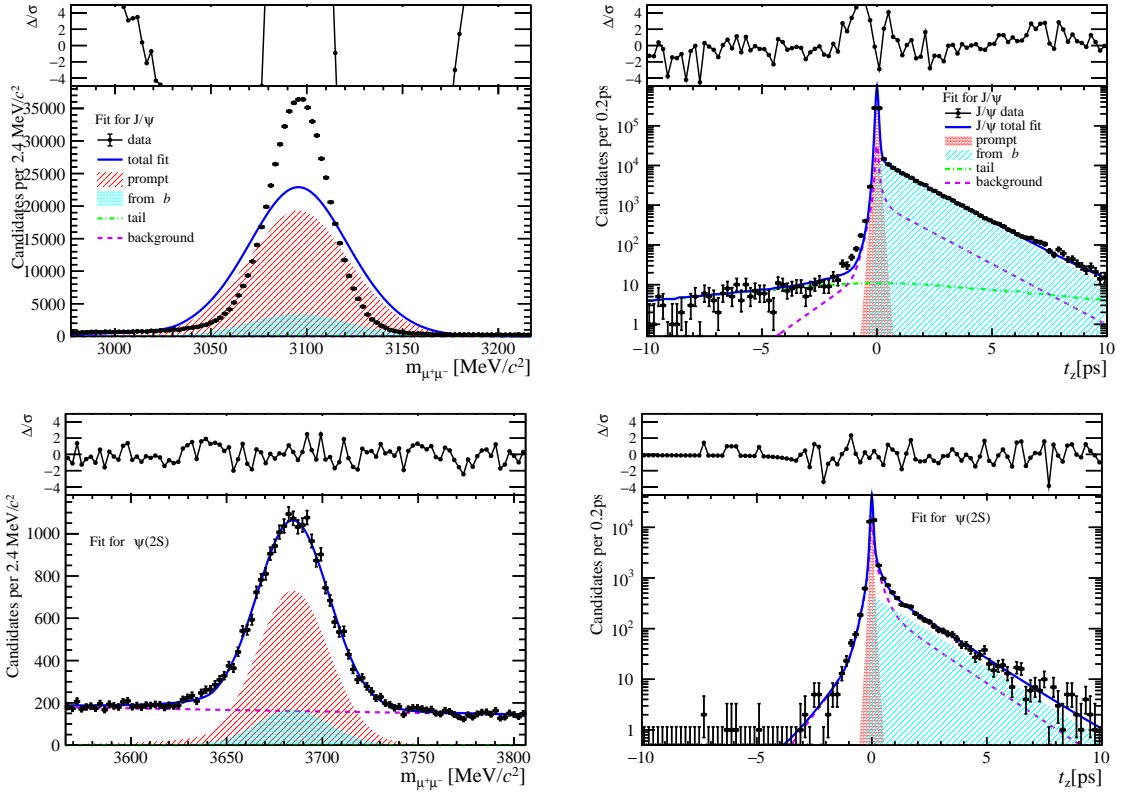


Figure 60: Fit results in  $4 \text{ GeV}/c < p_T < 6 \text{ GeV}/c$ ,  $3.5 < y < 4.5$  and  $20 \leq \text{PVNTRACKS} < 45$ .

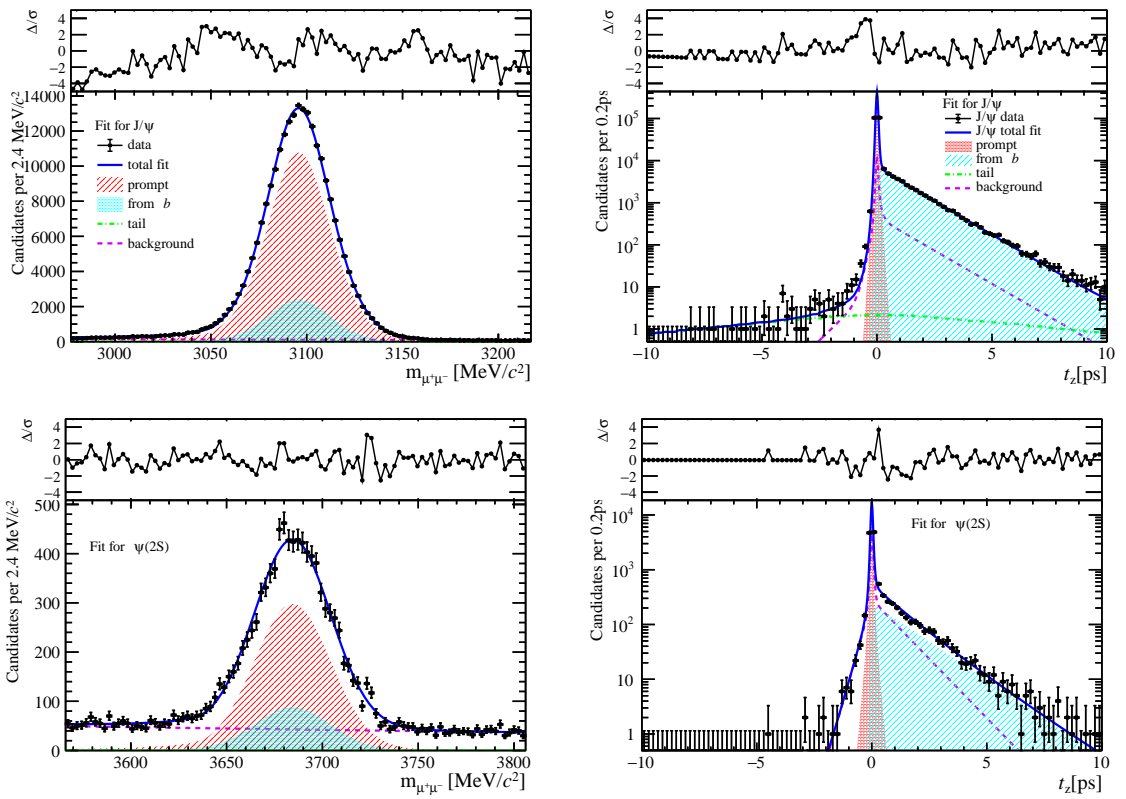


Figure 61: Fit results in  $6 \text{ GeV}/c < p_T < 8 \text{ GeV}/c$ ,  $3.5 < y < 4.5$  and  $20 \leq \text{PVNTRACKS} < 45$ .

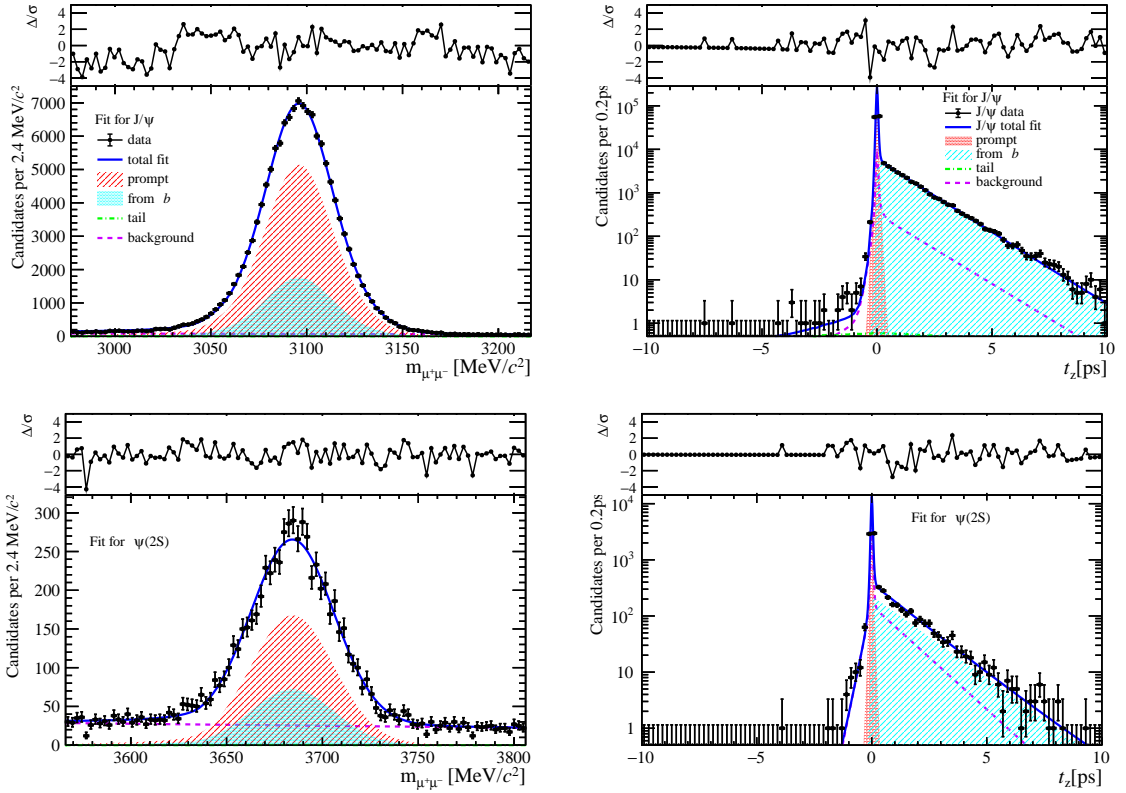


Figure 62: Fit results in  $8 \text{ GeV}/c < p_T < 20 \text{ GeV}/c$ ,  $3.5 < y < 4.5$  and  $20 \leq \text{PVNTRACKS} < 45$ .

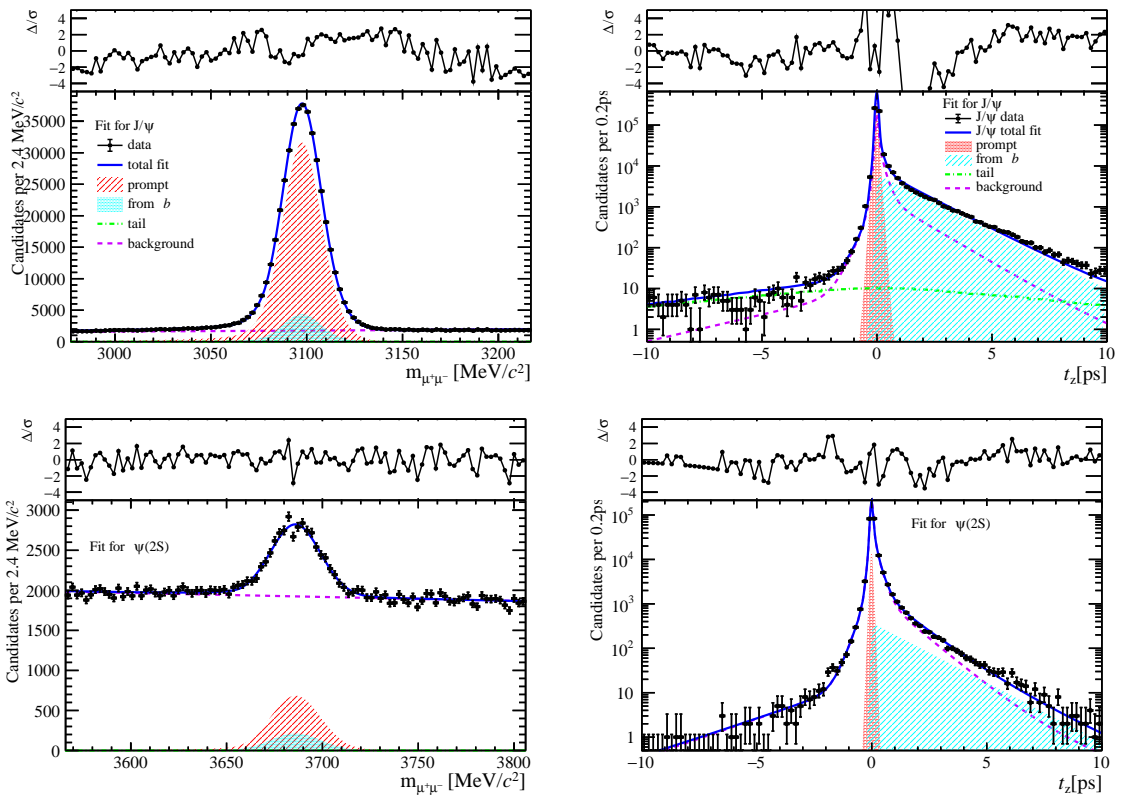


Figure 63: Fit results in  $0 \text{ GeV}/c < p_T < 2 \text{ GeV}/c$ ,  $2.0 < y < 2.8$  and  $45 \leq \text{PVNTRACKS} < 70$ .

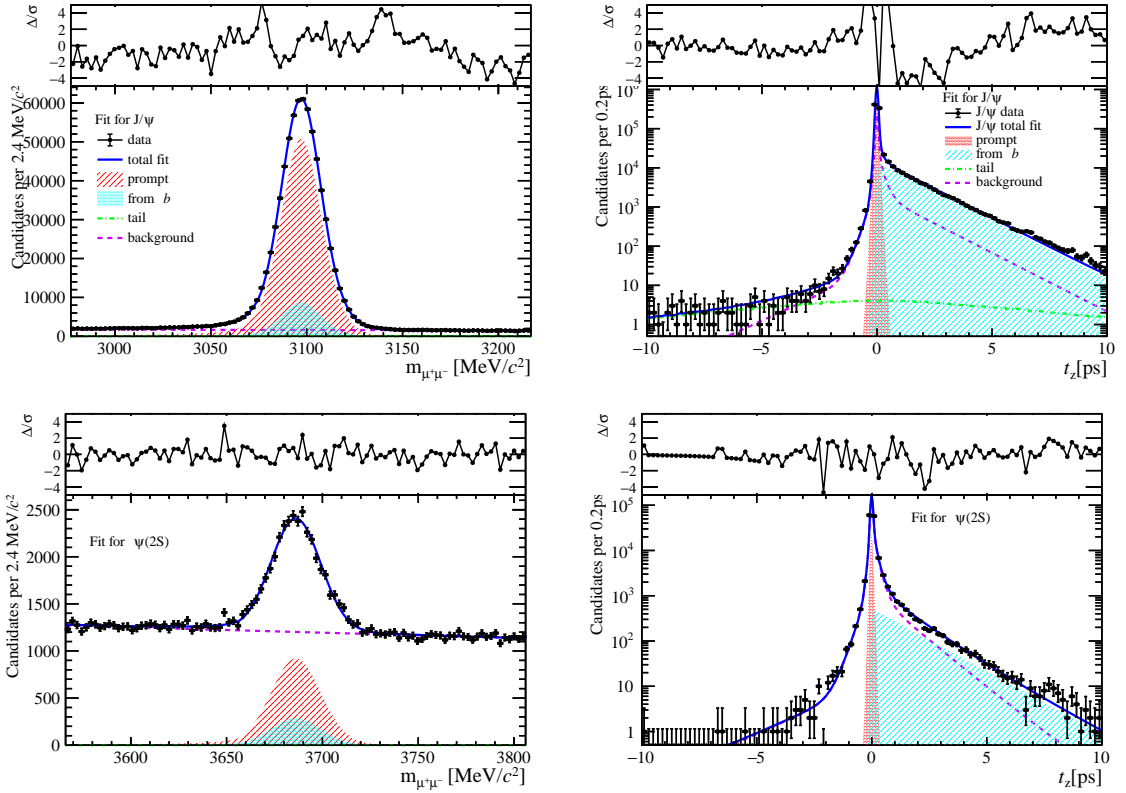


Figure 64: Fit results in  $2 \text{ GeV}/c < p_T < 4 \text{ GeV}/c$ ,  $2.0 < y < 2.8$  and  $45 \leq \text{PVNTRACKS} < 70$ .

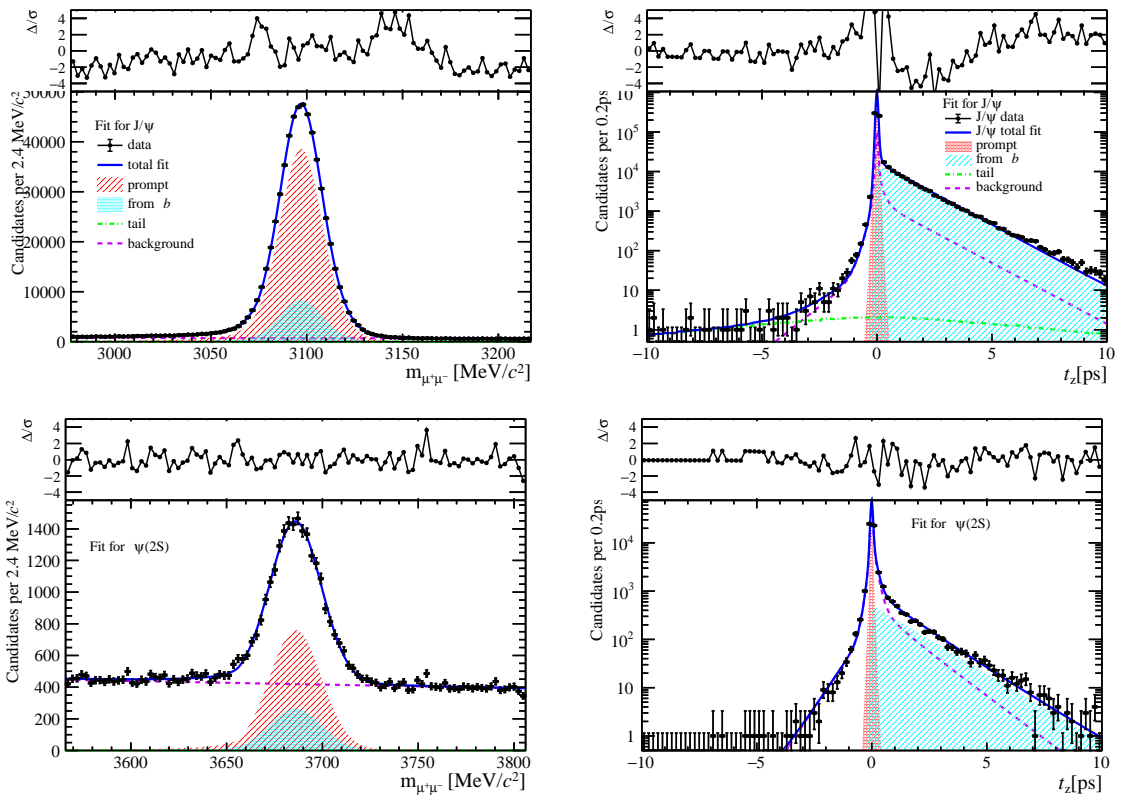


Figure 65: Fit results in  $4 \text{ GeV}/c < p_T < 6 \text{ GeV}/c$ ,  $2.0 < y < 2.8$  and  $45 \leq \text{PVNTRACKS} < 70$ .

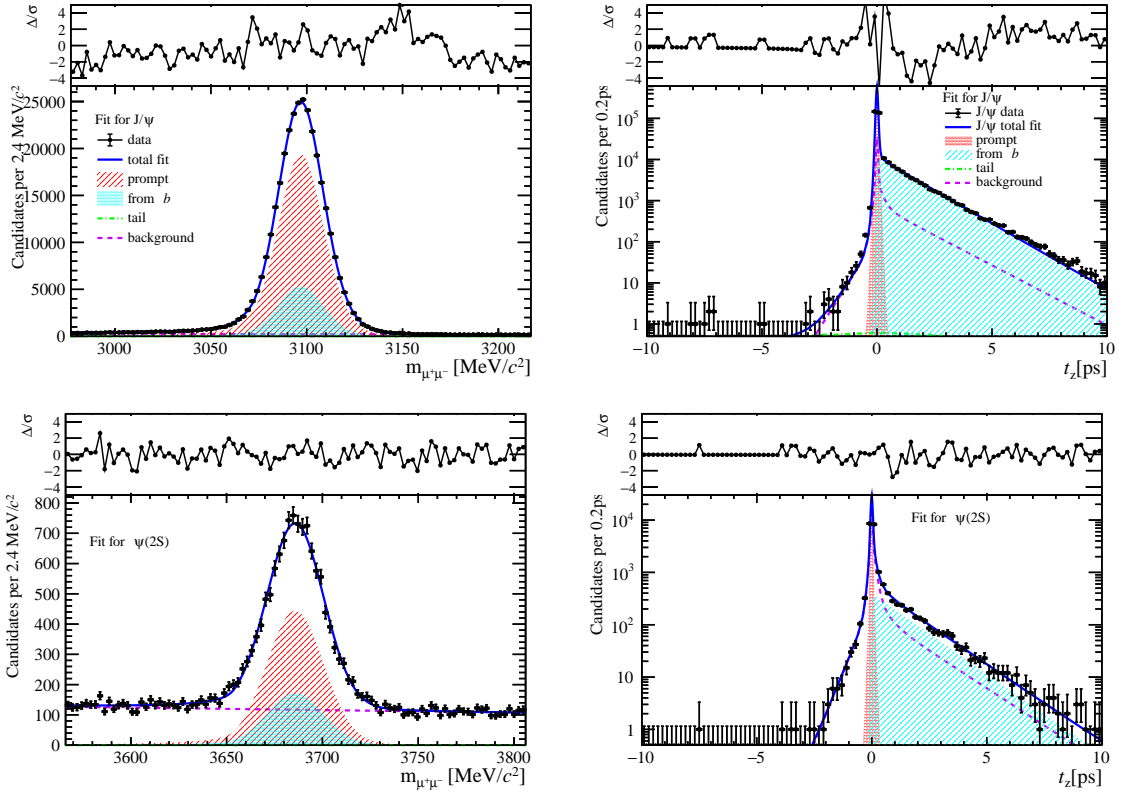


Figure 66: Fit results in  $6 \text{ GeV}/c < p_T < 8 \text{ GeV}/c$ ,  $2.0 < y < 2.8$  and  $45 \leq \text{PVNTRACKS} < 70$ .

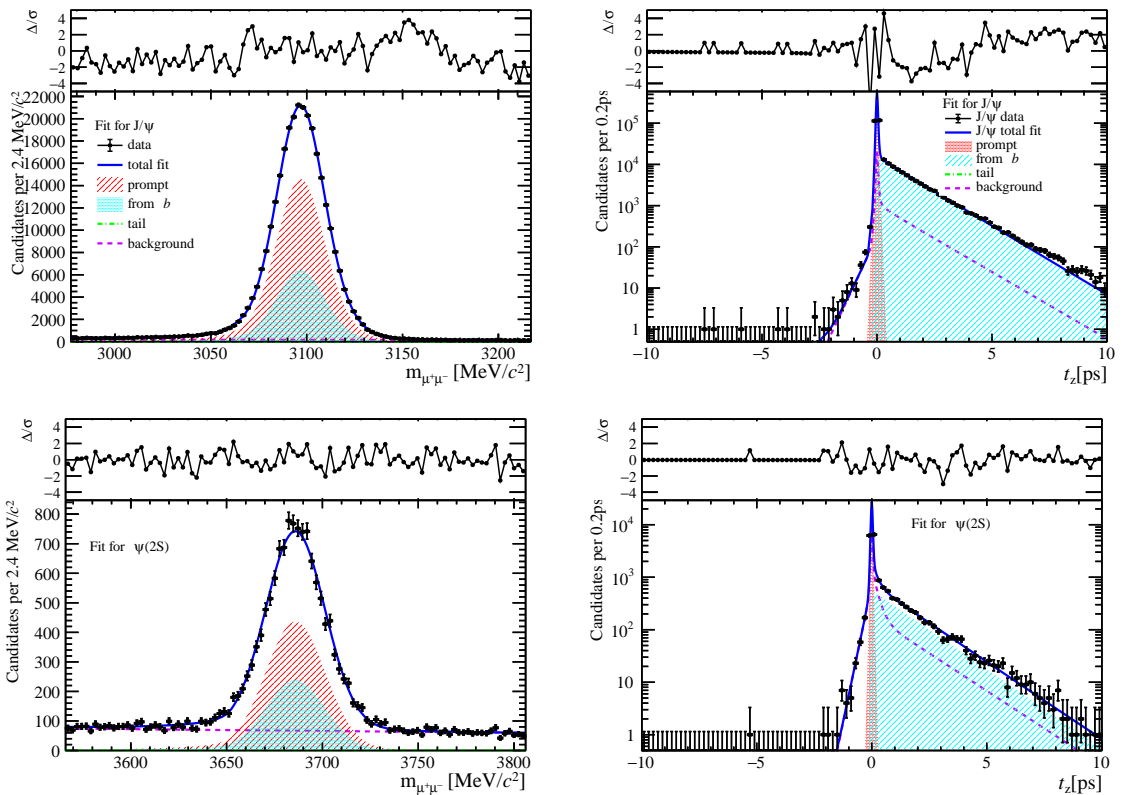


Figure 67: Fit results in  $8 \text{ GeV}/c < p_T < 20 \text{ GeV}/c$ ,  $2.0 < y < 2.8$  and  $45 \leq \text{PVNTRACKS} < 70$ .

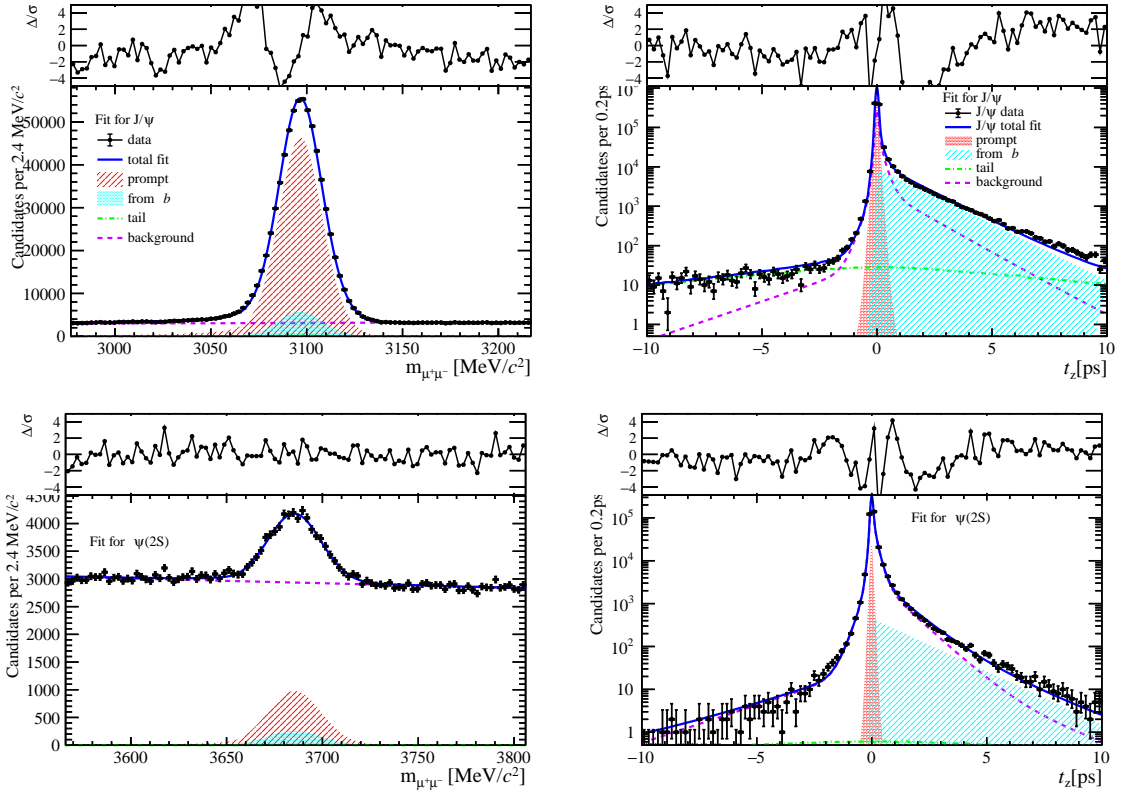


Figure 68: Fit results in  $0 \text{ GeV}/c < p_T < 2 \text{ GeV}/c$ ,  $2.8 < y < 3.5$  and  $45 \leq \text{PVNTRACKS} < 70$ .

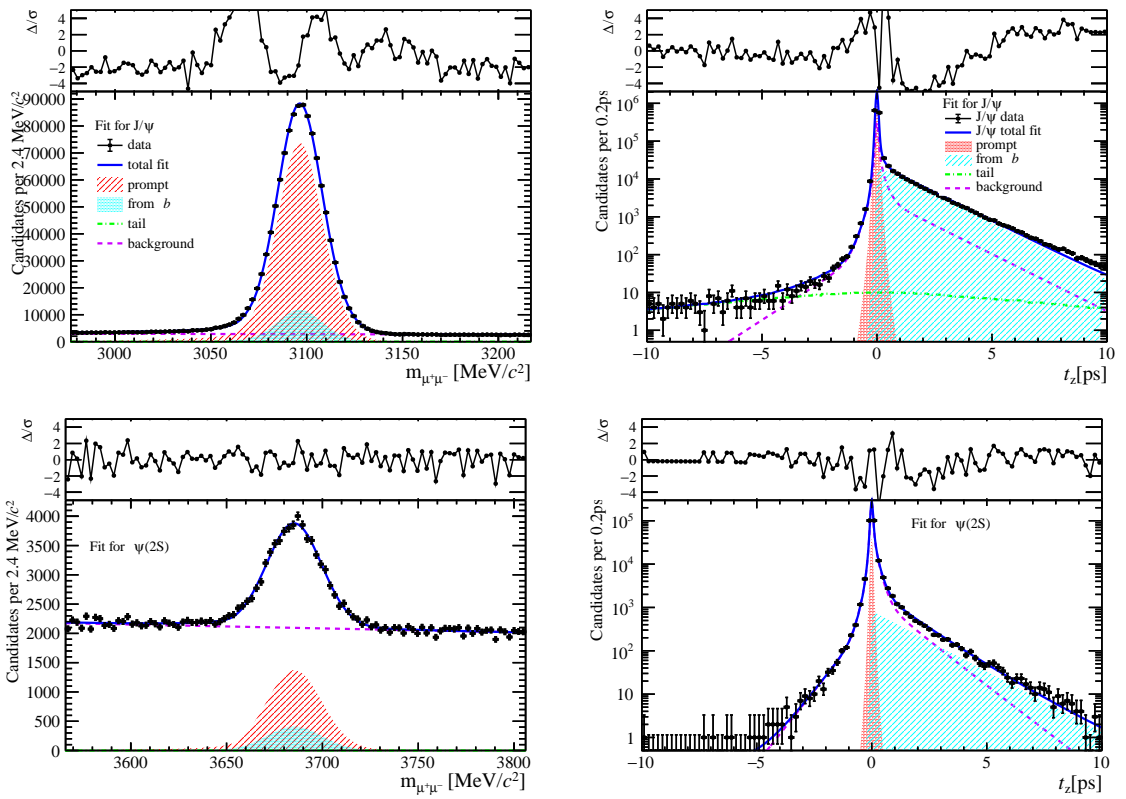


Figure 69: Fit results in  $2 \text{ GeV}/c < p_T < 4 \text{ GeV}/c$ ,  $2.8 < y < 3.5$  and  $45 \leq \text{PVNTRACKS} < 70$ .

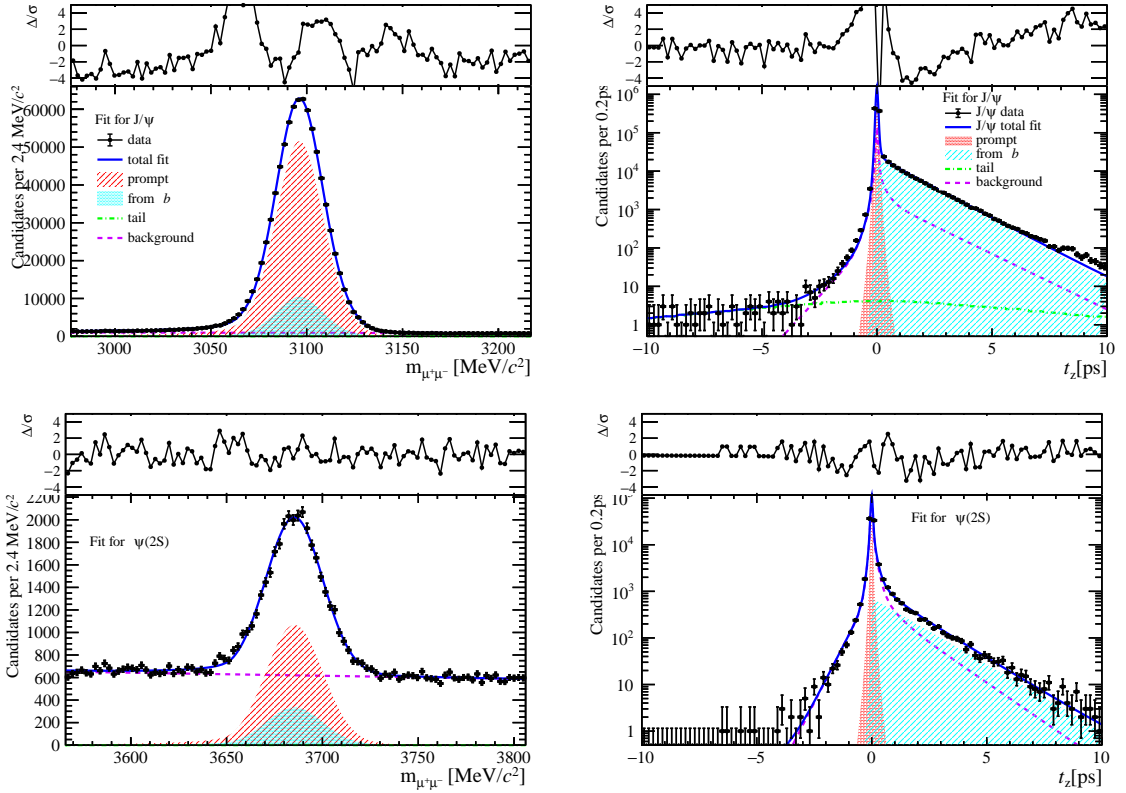


Figure 70: Fit results in  $4 \text{ GeV}/c < p_T < 6 \text{ GeV}/c$ ,  $2.8 < y < 3.5$  and  $45 \leq \text{PVNTRACKS} < 70$ .

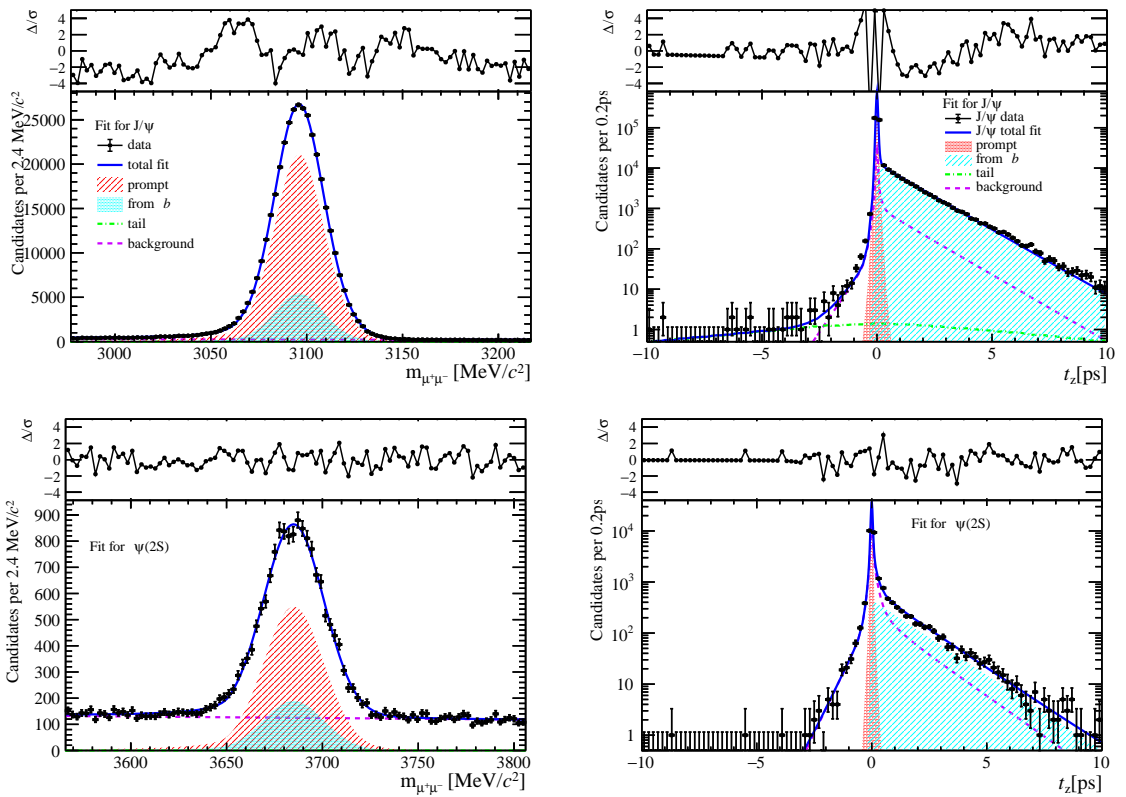


Figure 71: Fit results in  $6 \text{ GeV}/c < p_T < 8 \text{ GeV}/c$ ,  $2.8 < y < 3.5$  and  $45 \leq \text{PVNTRACKS} < 70$ .

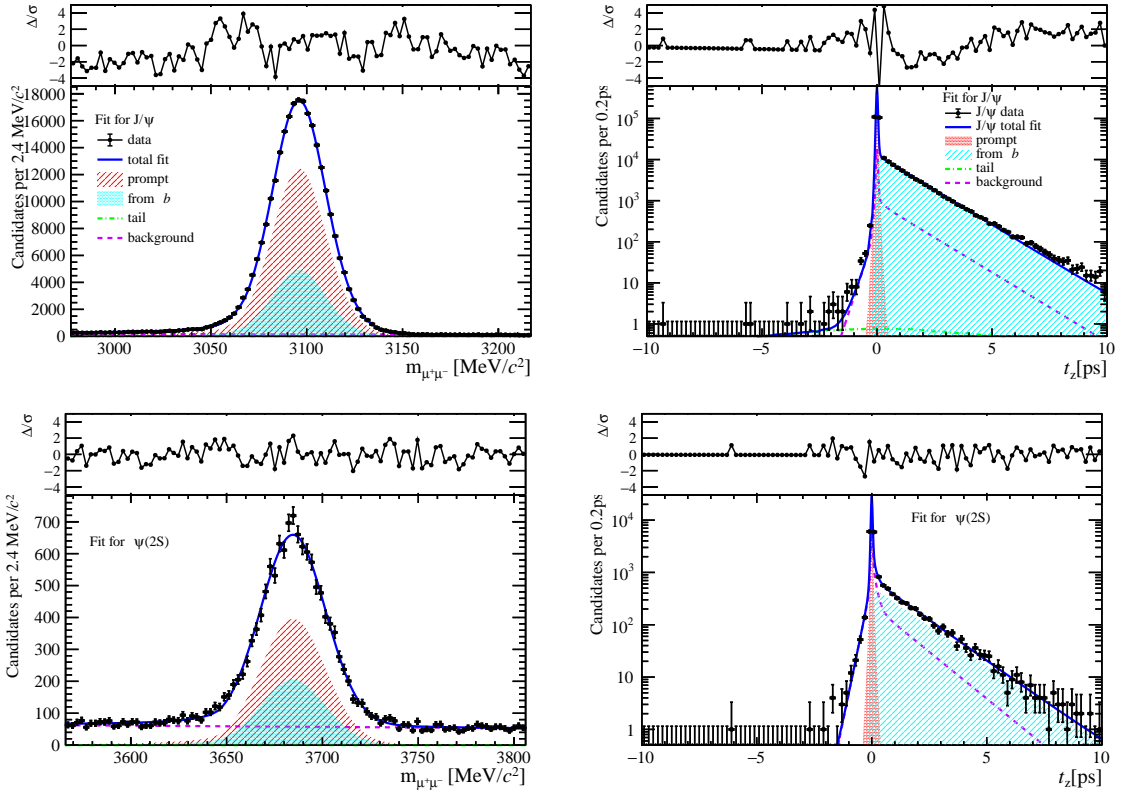


Figure 72: Fit results in  $8 \text{ GeV}/c < p_T < 20 \text{ GeV}/c$ ,  $2.8 < y < 3.5$  and  $45 \leq \text{PVNTRACKS} < 70$ .

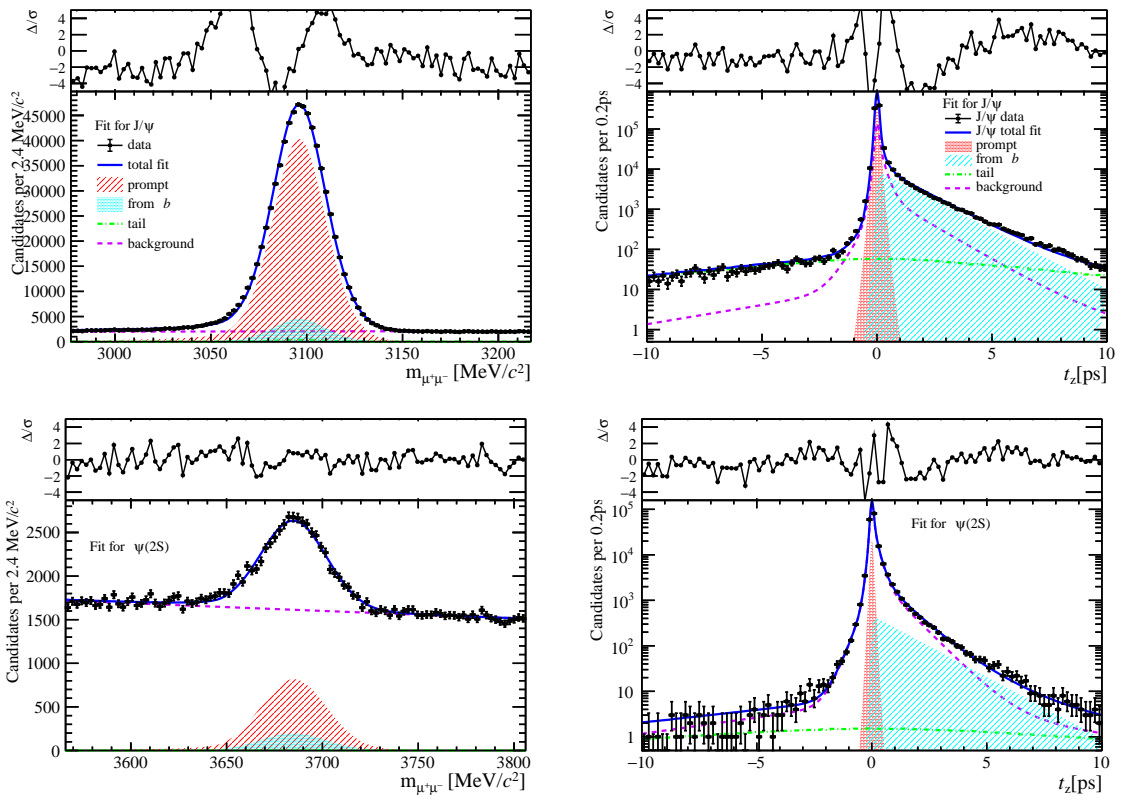


Figure 73: Fit results in  $0 \text{ GeV}/c < p_T < 2 \text{ GeV}/c$ ,  $3.5 < y < 4.5$  and  $45 \leq \text{PVNTRACKS} < 70$ .

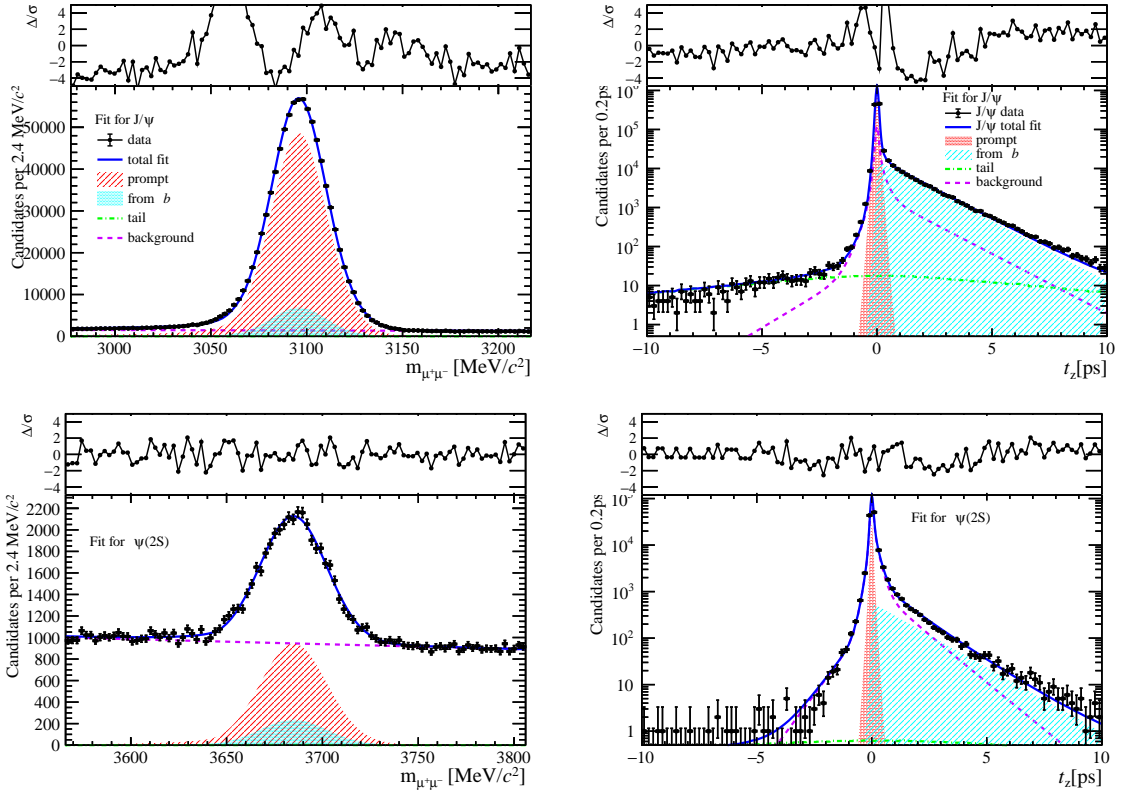


Figure 74: Fit results in  $2 \text{ GeV}/c < p_T < 4 \text{ GeV}/c$ ,  $3.5 < y < 4.5$  and  $45 \leq \text{PVNTRACKS} < 70$ .

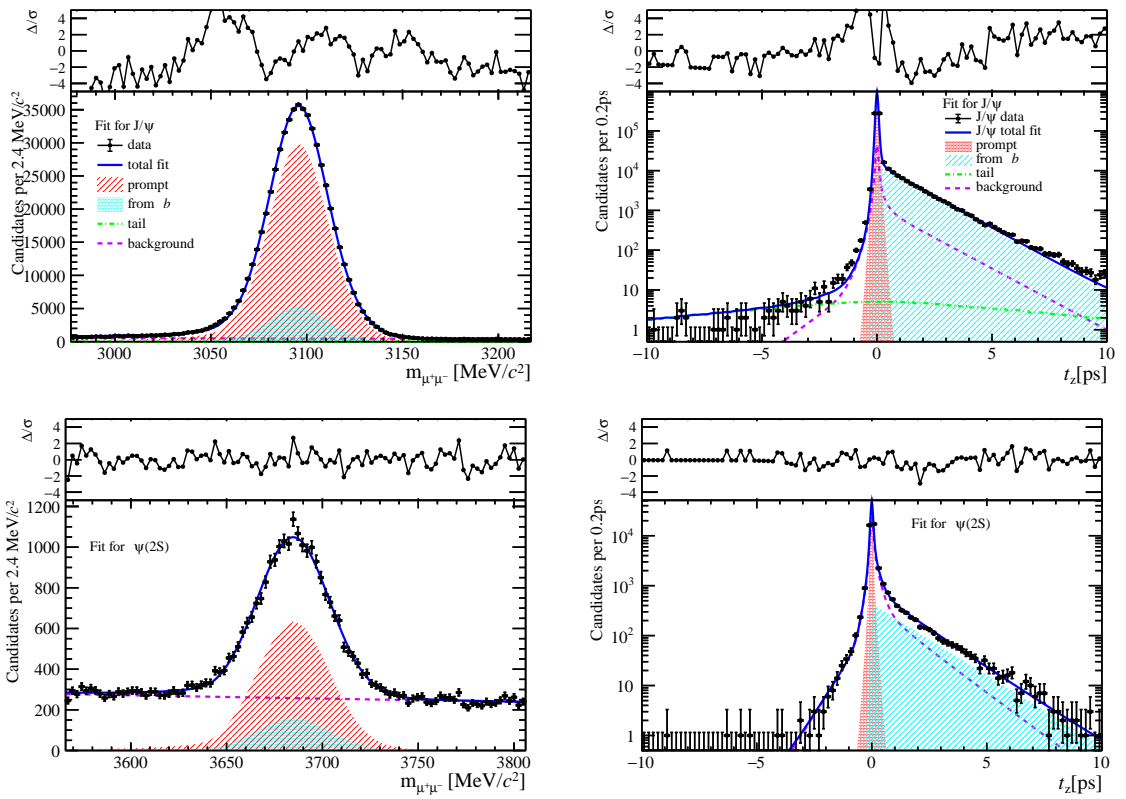


Figure 75: Fit results in  $4 \text{ GeV}/c < p_T < 6 \text{ GeV}/c$ ,  $3.5 < y < 4.5$  and  $45 \leq \text{PVNTRACKS} < 70$ .

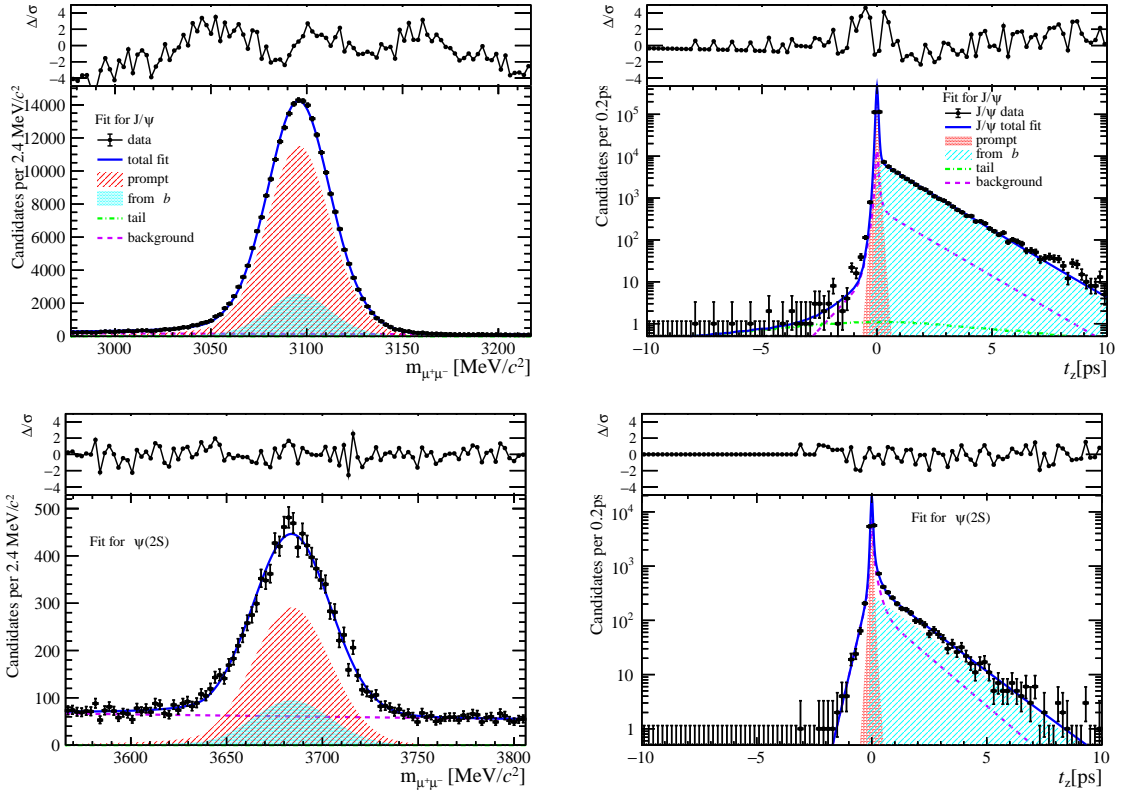


Figure 76: Fit results in  $6 \text{ GeV}/c < p_T < 8 \text{ GeV}/c$ ,  $3.5 < y < 4.5$  and  $45 \leq \text{PVNTRACKS} < 70$ .

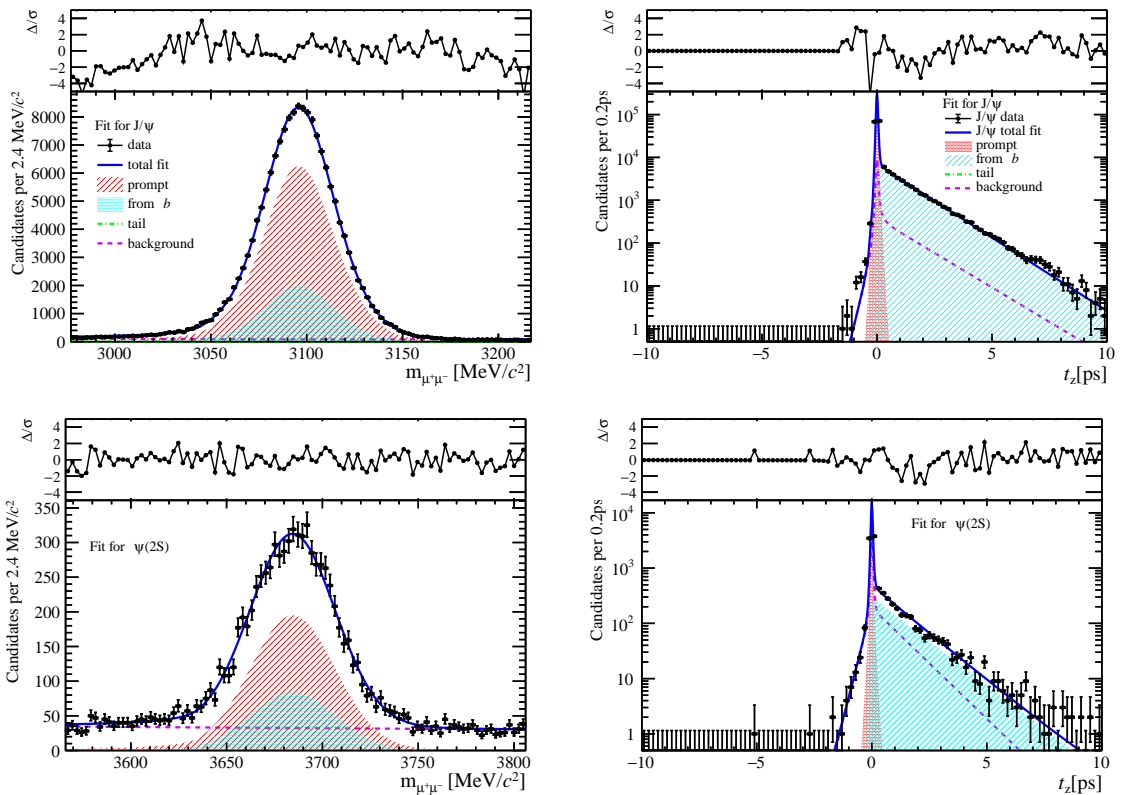


Figure 77: Fit results in  $8 \text{ GeV}/c < p_T < 20 \text{ GeV}/c$ ,  $3.5 < y < 4.5$  and  $45 \leq \text{PVNTRACKS} < 70$ .

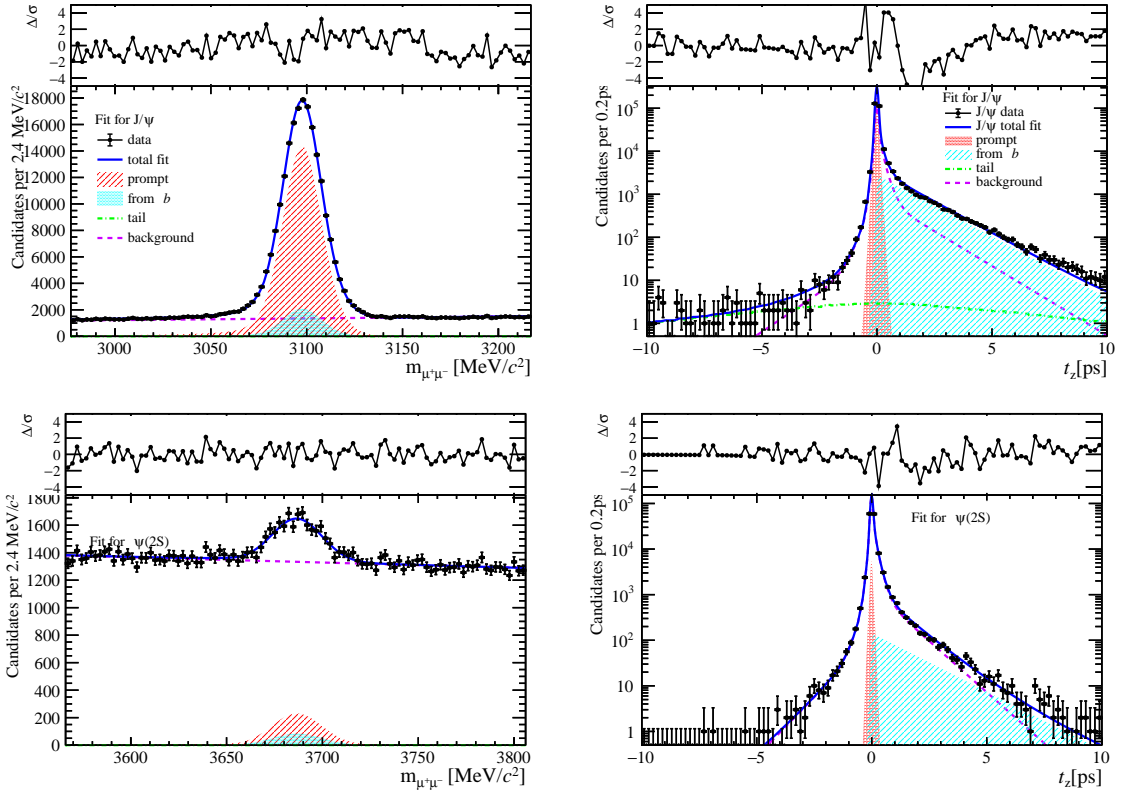


Figure 78: Fit results in  $0 \text{ GeV}/c < p_T < 2 \text{ GeV}/c$ ,  $2.0 < y < 2.8$  and  $70 \leq \text{PVNTRACKS} < 95$ .

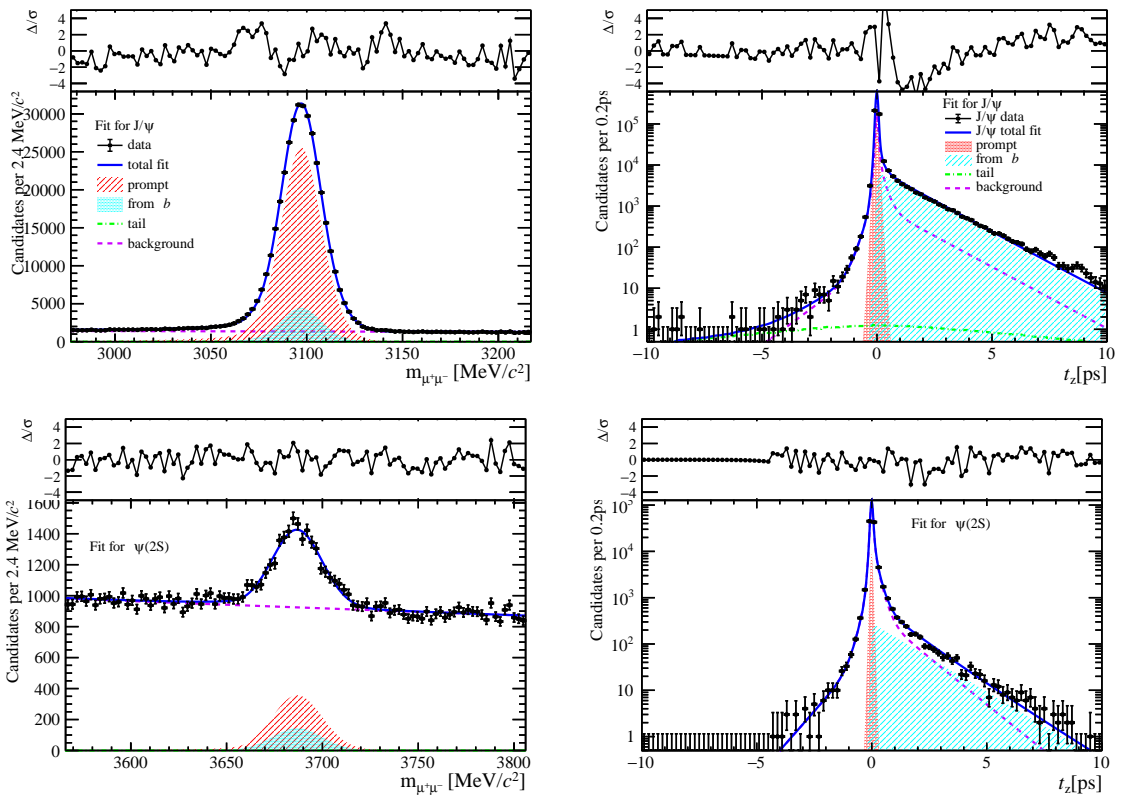


Figure 79: Fit results in  $2 \text{ GeV}/c < p_T < 4 \text{ GeV}/c$ ,  $2.0 < y < 2.8$  and  $70 \leq \text{PVNTRACKS} < 95$ .

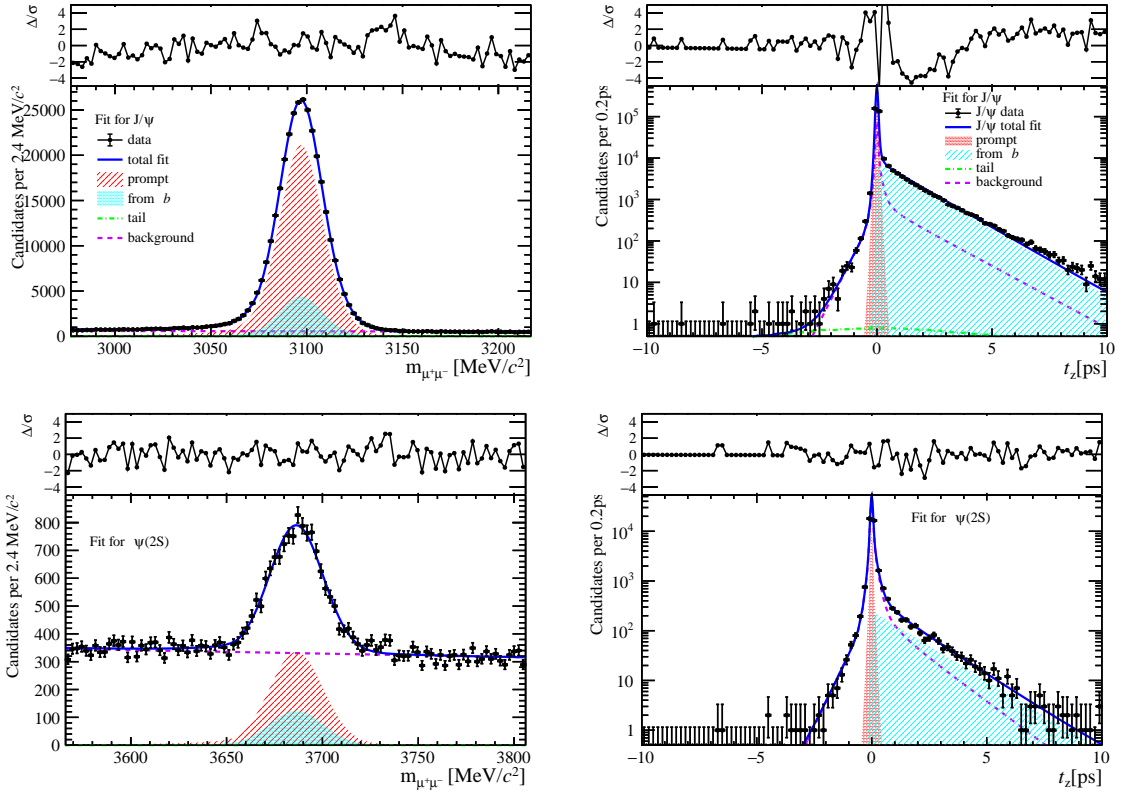


Figure 80: Fit results in  $4 \text{ GeV}/c < p_T < 6 \text{ GeV}/c$ ,  $2.0 < y < 2.8$  and  $70 \leq \text{PVNTRACKS} < 95$ .

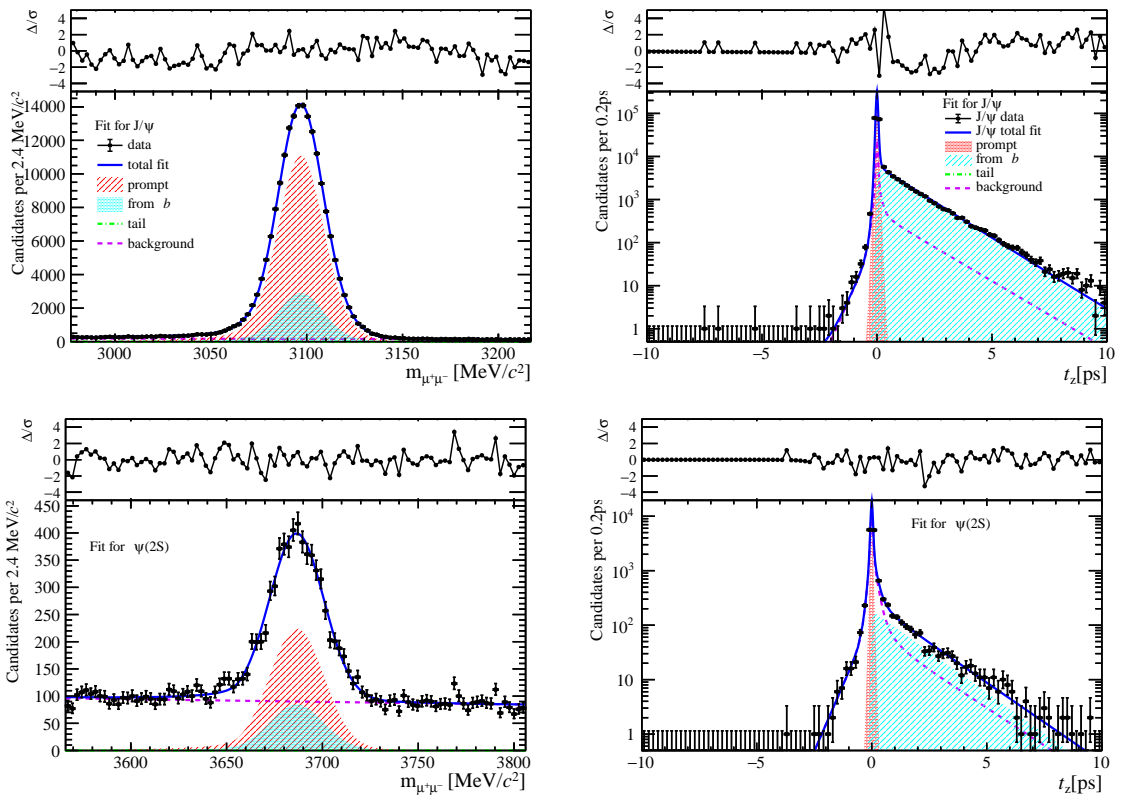


Figure 81: Fit results in  $6 \text{ GeV}/c < p_T < 8 \text{ GeV}/c$ ,  $2.0 < y < 2.8$  and  $70 \leq \text{PVNTRACKS} < 95$ .

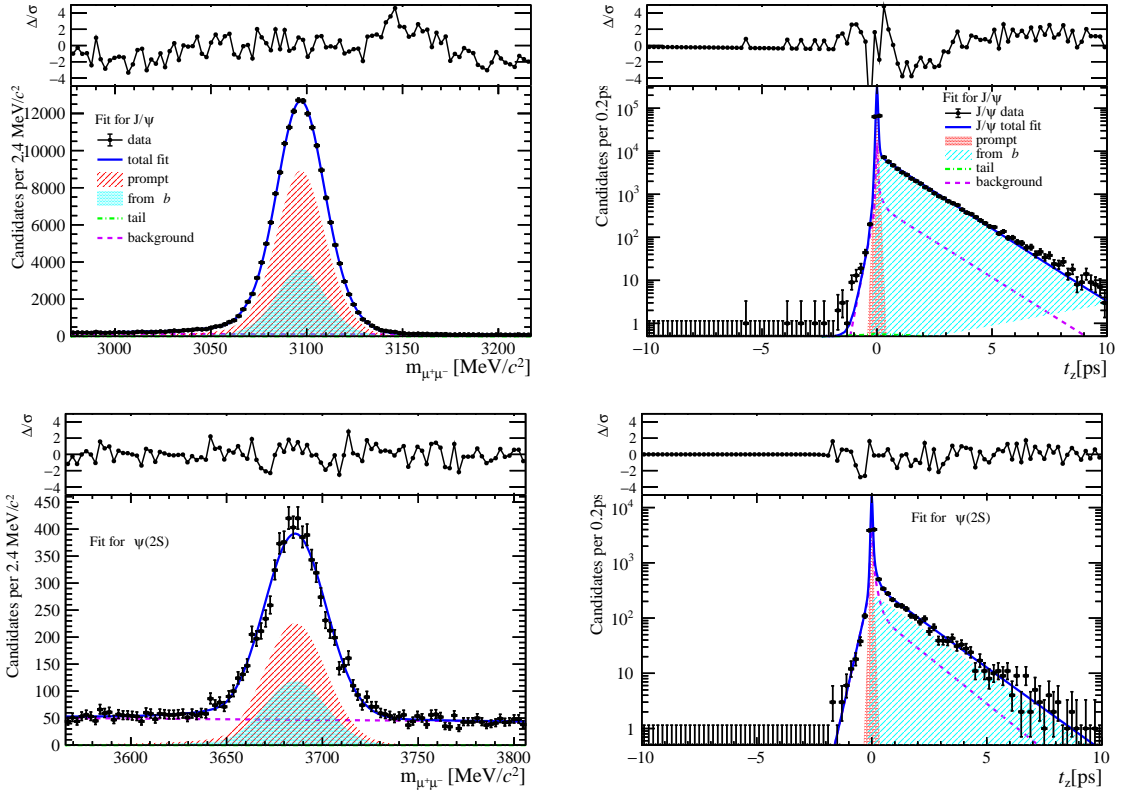


Figure 82: Fit results in  $8 \text{ GeV}/c < p_T < 20 \text{ GeV}/c$ ,  $2.0 < y < 2.8$  and  $70 \leq \text{PVNTRACKS} < 95$ .

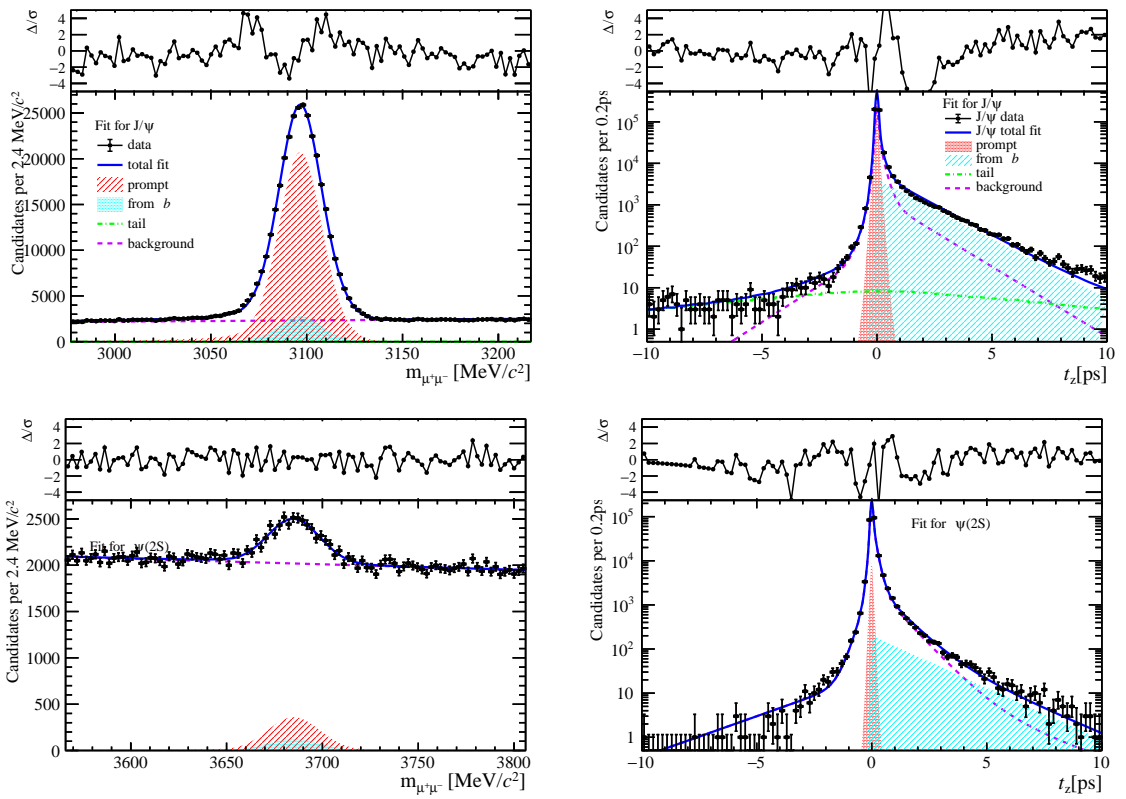


Figure 83: Fit results in  $0 \text{ GeV}/c < p_T < 2 \text{ GeV}/c$ ,  $2.8 < y < 3.5$  and  $70 \leq \text{PVNTRACKS} < 95$ .

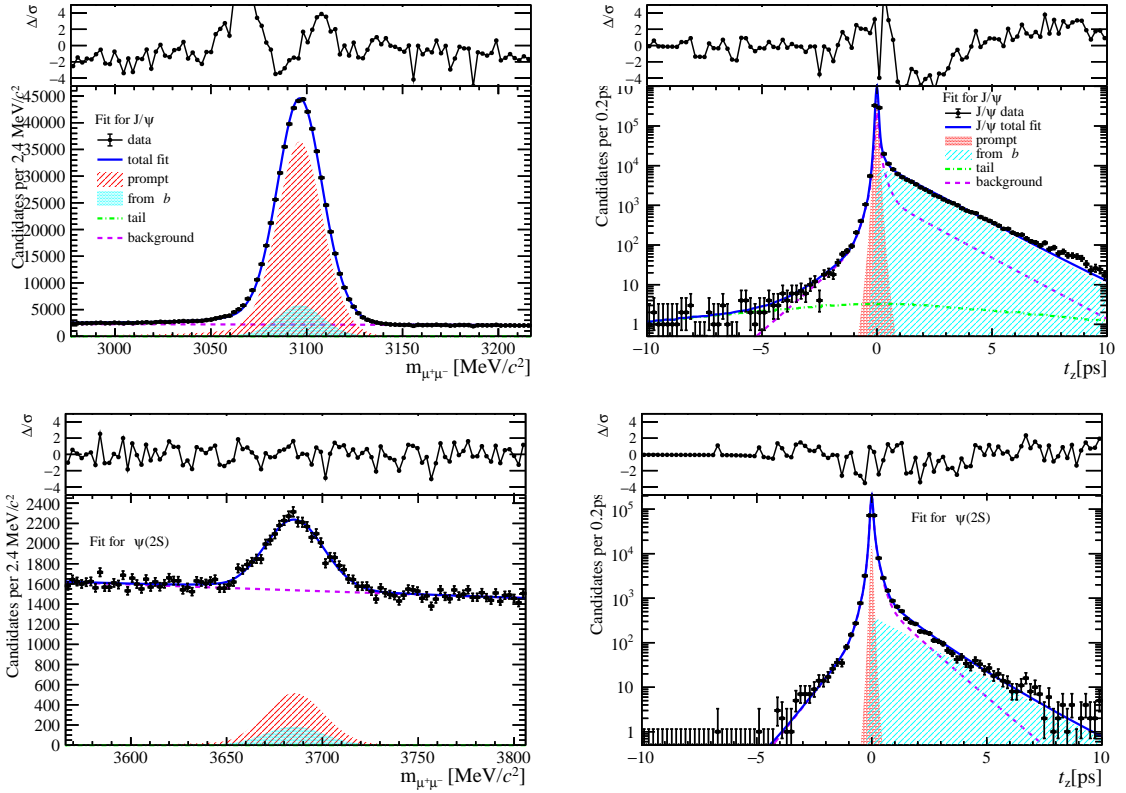


Figure 84: Fit results in  $2 \text{ GeV}/c < p_T < 4 \text{ GeV}/c$ ,  $2.8 < y < 3.5$  and  $70 \leq \text{PVNTRACKS} < 95$ .

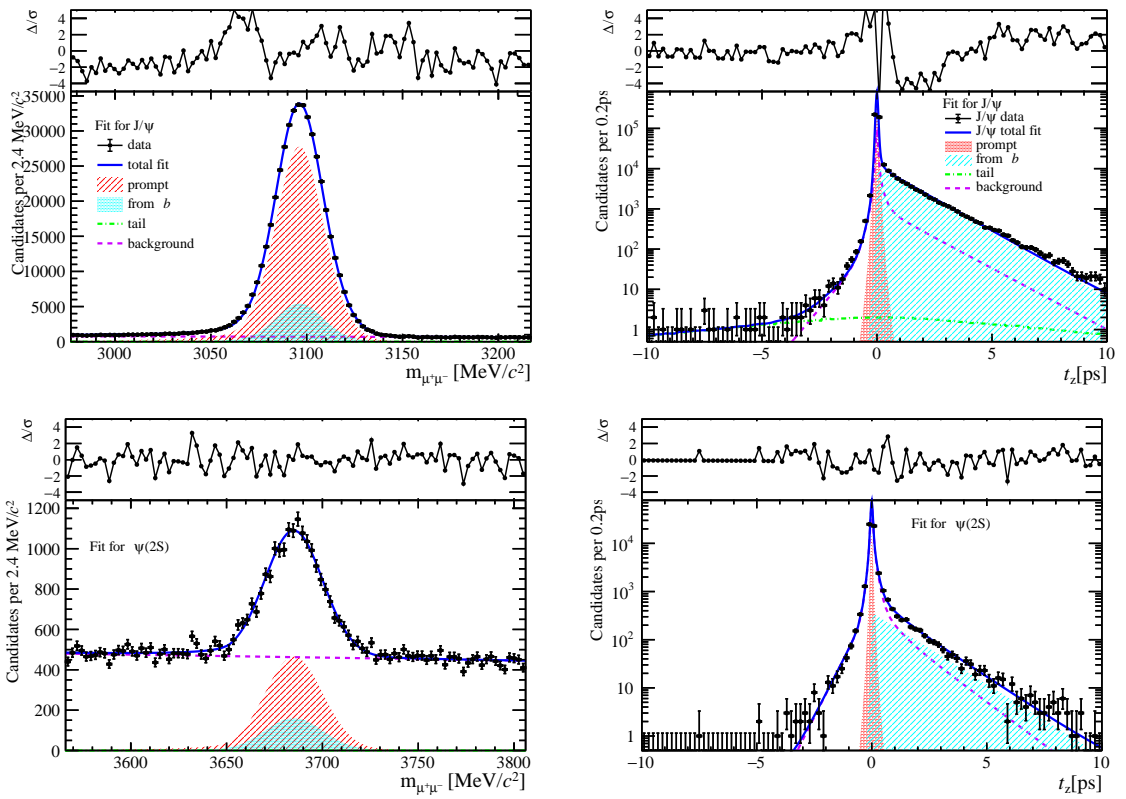


Figure 85: Fit results in  $4 \text{ GeV}/c < p_T < 6 \text{ GeV}/c$ ,  $2.8 < y < 3.5$  and  $70 \leq \text{PVNTRACKS} < 95$ .

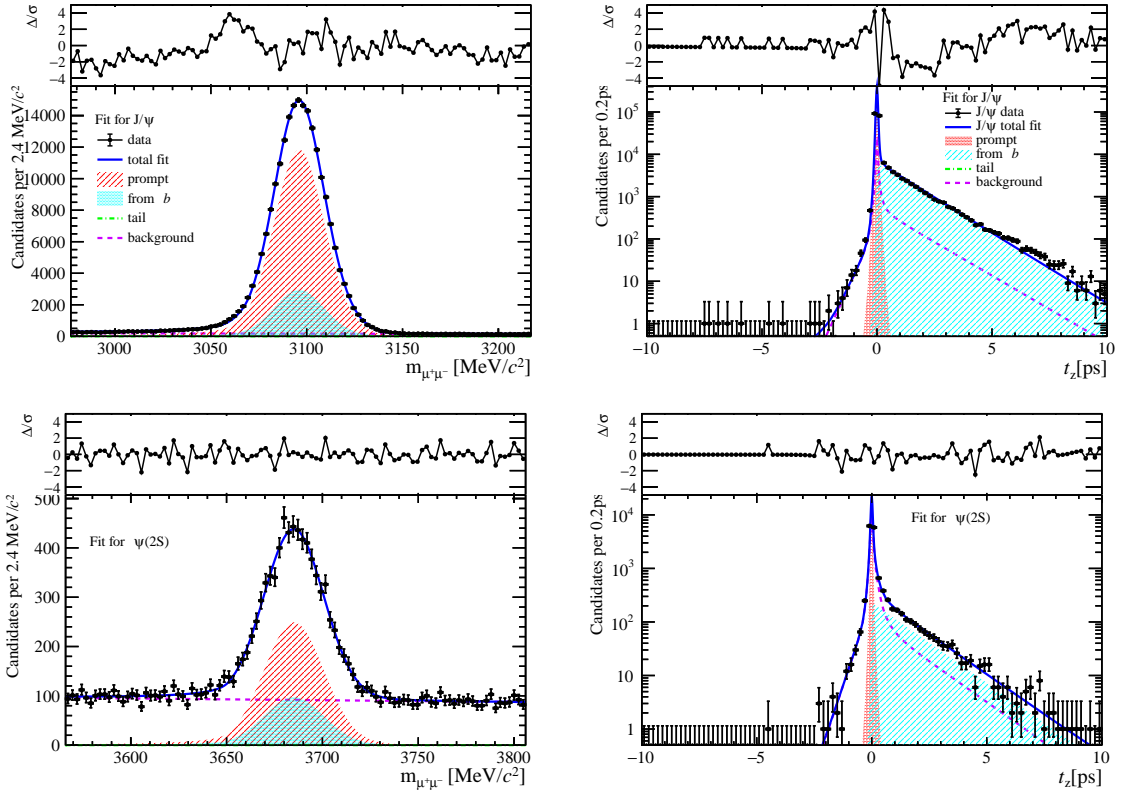


Figure 86: Fit results in  $6 \text{ GeV}/c < p_T < 8 \text{ GeV}/c$ ,  $2.8 < y < 3.5$  and  $70 \leq \text{PVNTRACKS} < 95$ .

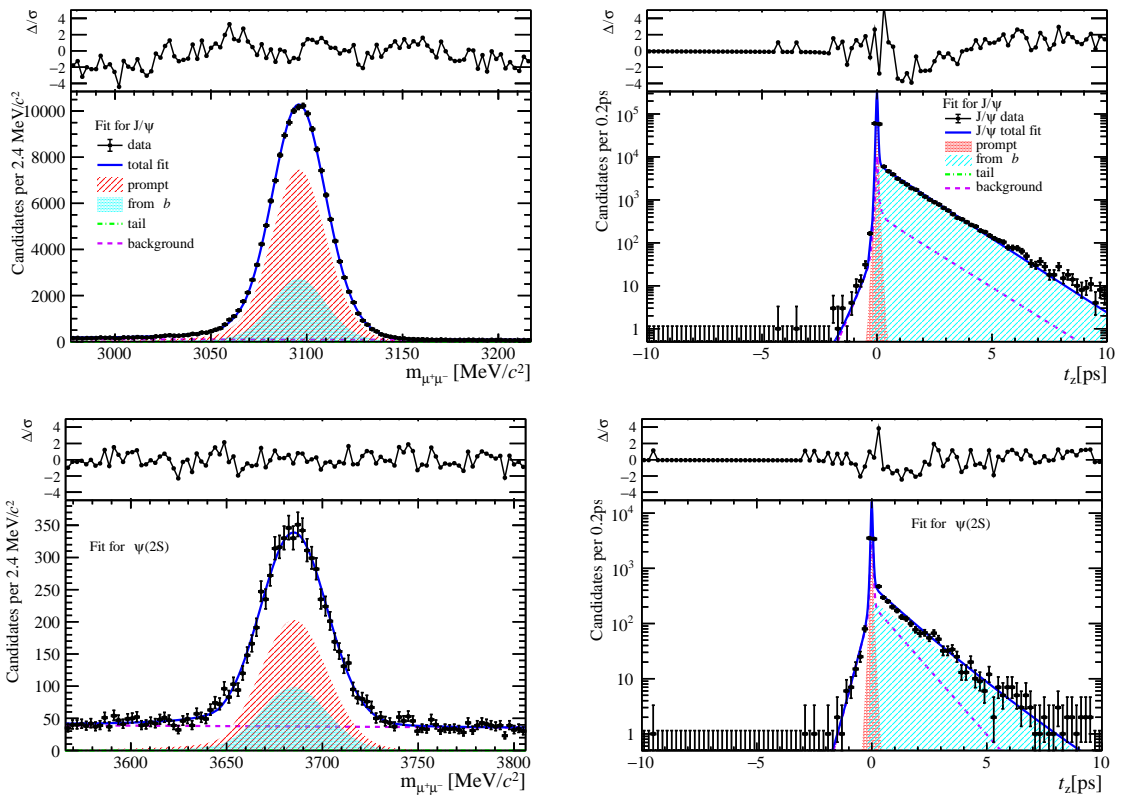


Figure 87: Fit results in  $8 \text{ GeV}/c < p_T < 20 \text{ GeV}/c$ ,  $2.8 < y < 3.5$  and  $70 \leq \text{PVNTRACKS} < 95$ .

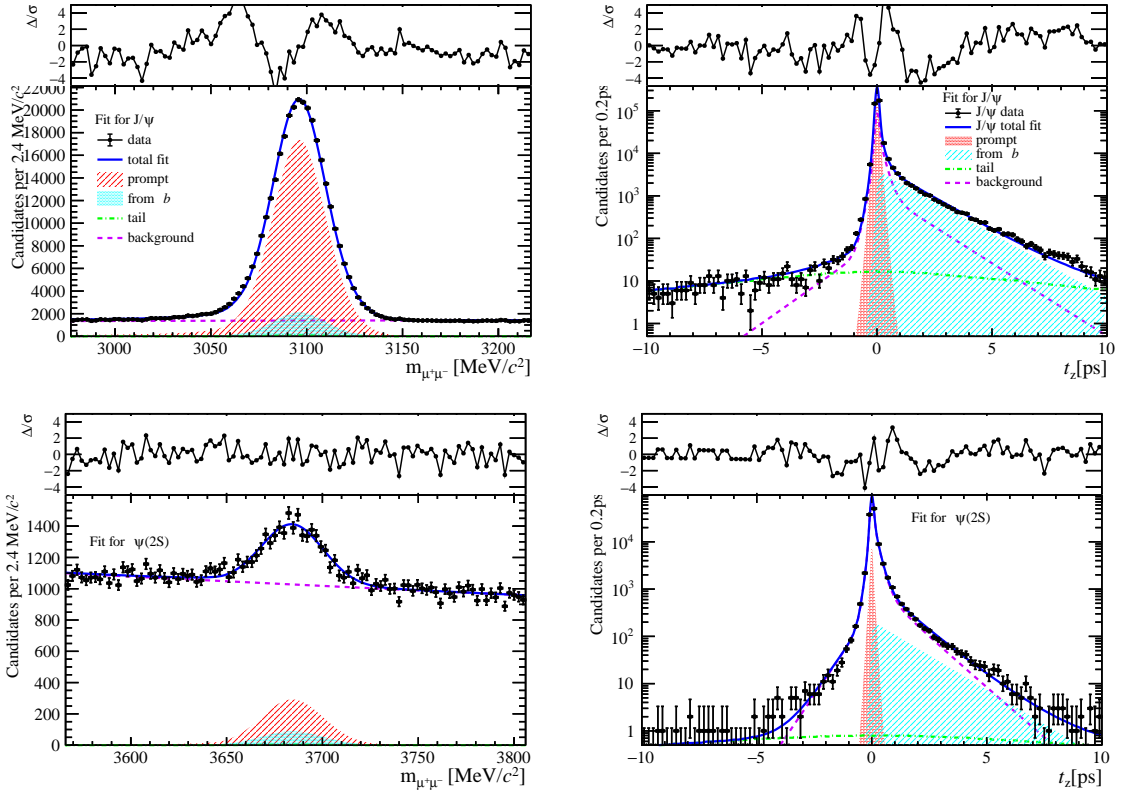


Figure 88: Fit results in  $0 \text{ GeV}/c < p_T < 2 \text{ GeV}/c$ ,  $3.5 < y < 4.5$  and  $70 \leq \text{PVNTRACKS} < 95$ .

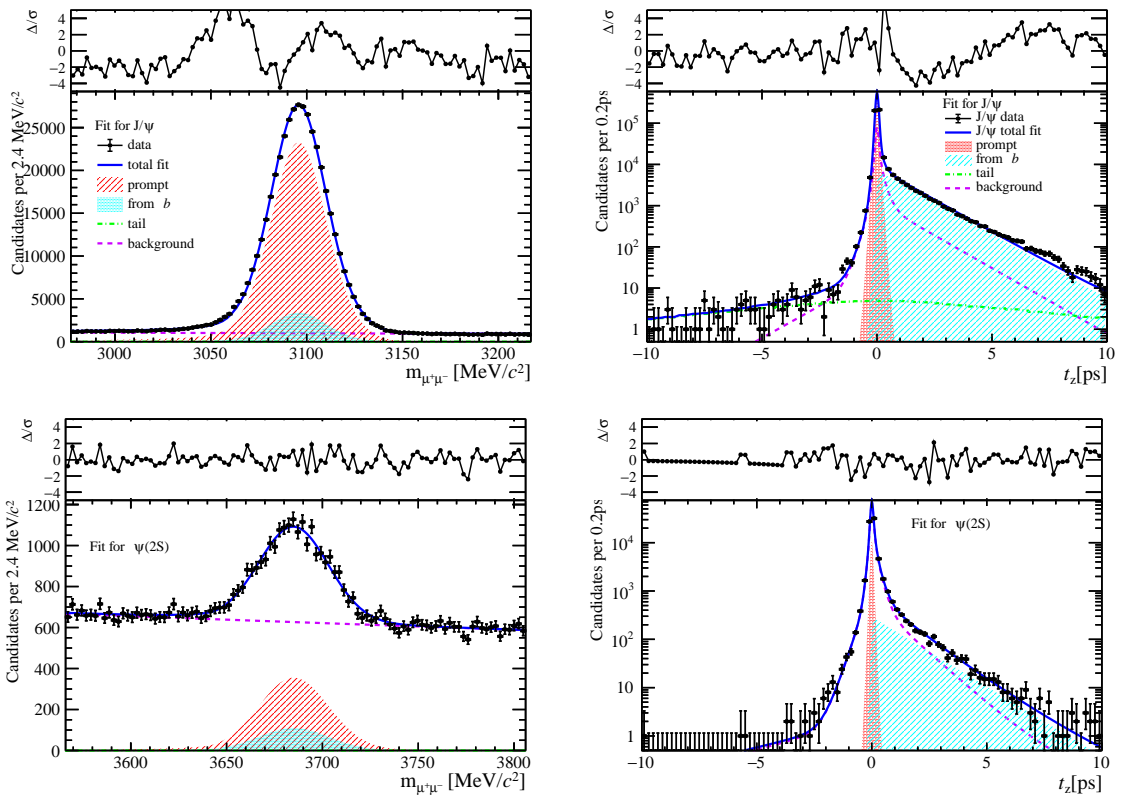


Figure 89: Fit results in  $2 \text{ GeV}/c < p_T < 4 \text{ GeV}/c$ ,  $3.5 < y < 4.5$  and  $70 \leq \text{PVNTRACKS} < 95$ .

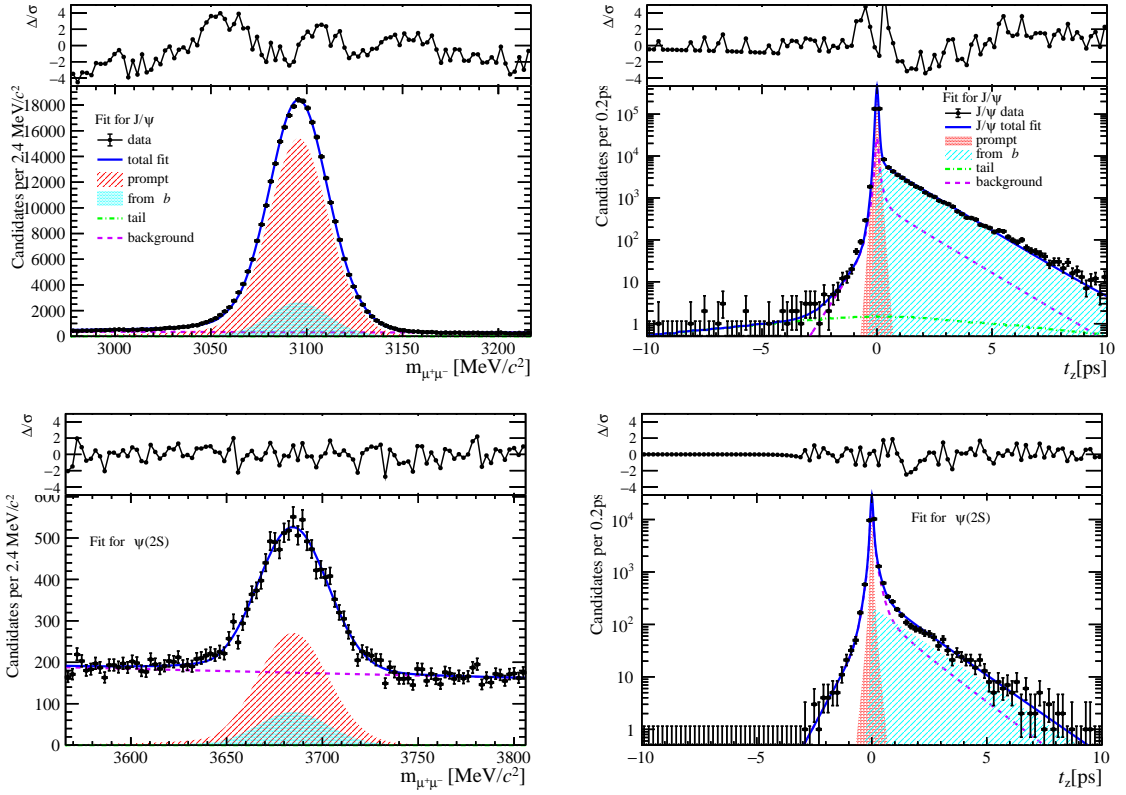


Figure 90: Fit results in  $4 \text{ GeV}/c < p_T < 6 \text{ GeV}/c$ ,  $3.5 < y < 4.5$  and  $70 \leq \text{PVNTRACKS} < 95$ .

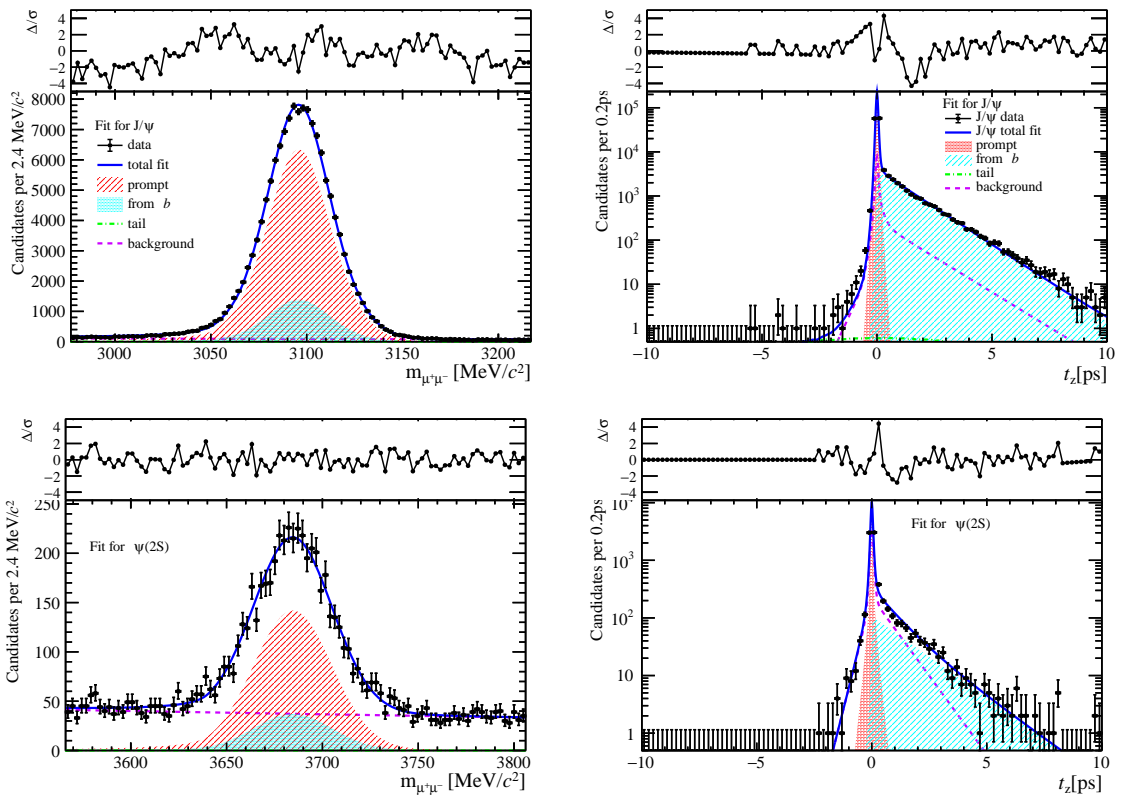


Figure 91: Fit results in  $6 \text{ GeV}/c < p_T < 8 \text{ GeV}/c$ ,  $3.5 < y < 4.5$  and  $70 \leq \text{PVNTRACKS} < 95$ .

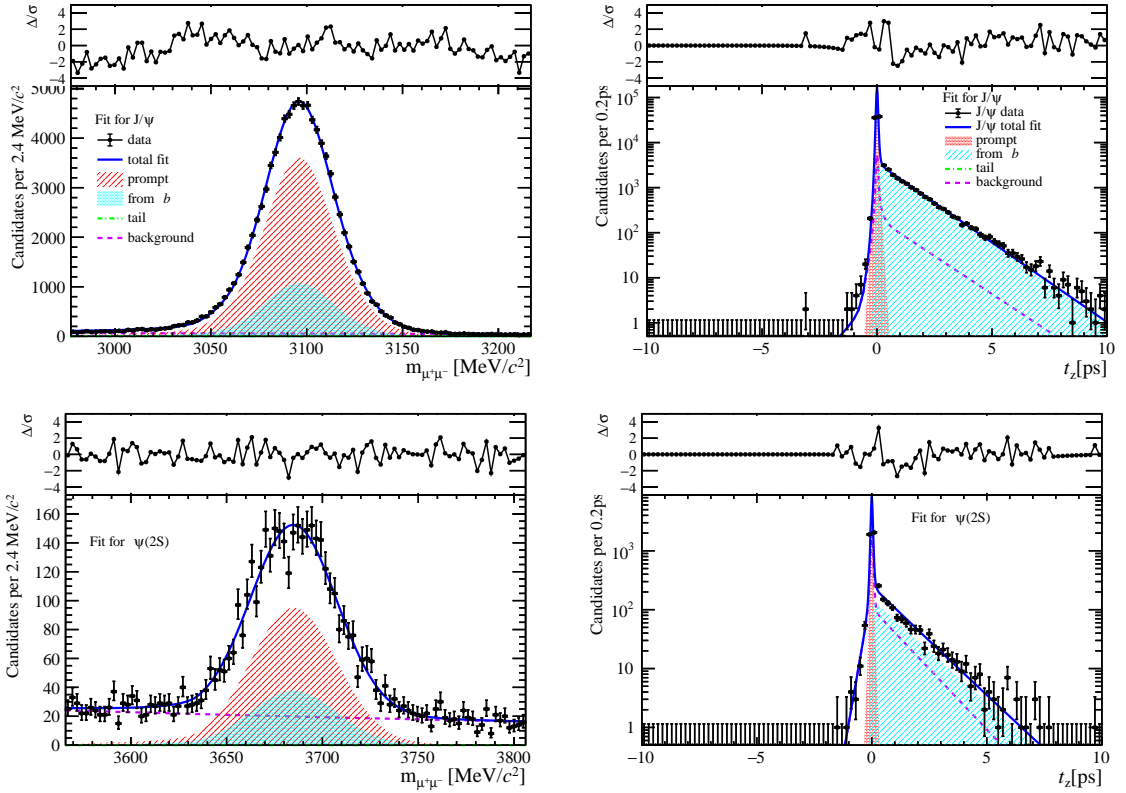


Figure 92: Fit results in  $8 \text{ GeV}/c < p_T < 20 \text{ GeV}/c$ ,  $3.5 < y < 4.5$  and  $70 \leq \text{PVNTRACKS} < 95$ .

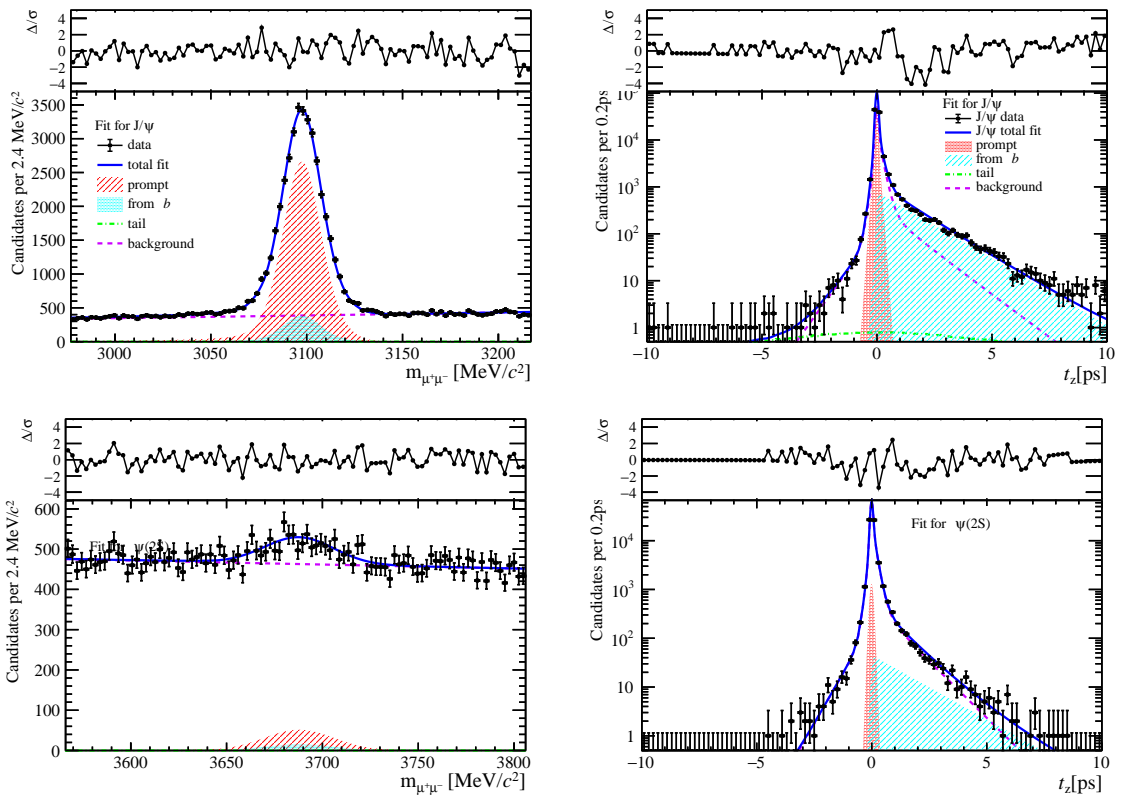


Figure 93: Fit results in  $0 \text{ GeV}/c < p_T < 2 \text{ GeV}/c$ ,  $2.0 < y < 2.8$  and  $95 \leq \text{PVNTRACKS} < 200$ .

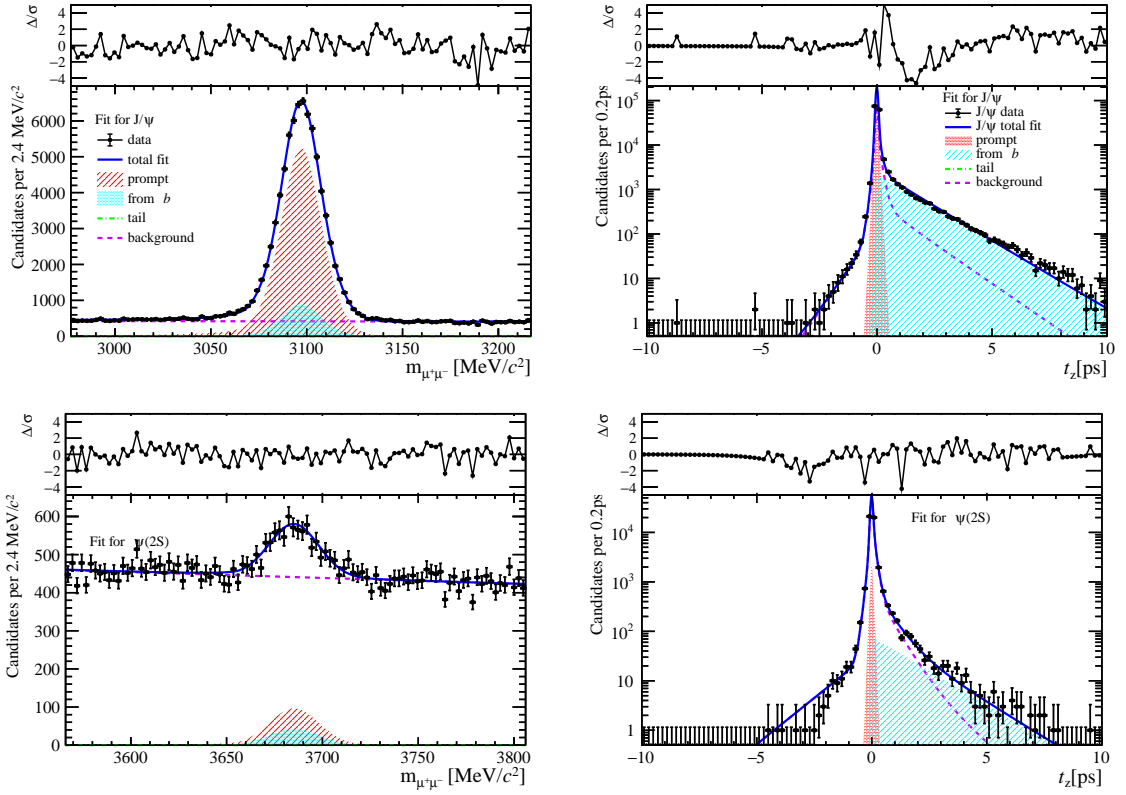


Figure 94: Fit results in  $2 \text{ GeV}/c < p_T < 4 \text{ GeV}/c$ ,  $2.0 < y < 2.8$  and  $95 \leq \text{PVNTRACKS} < 200$ .

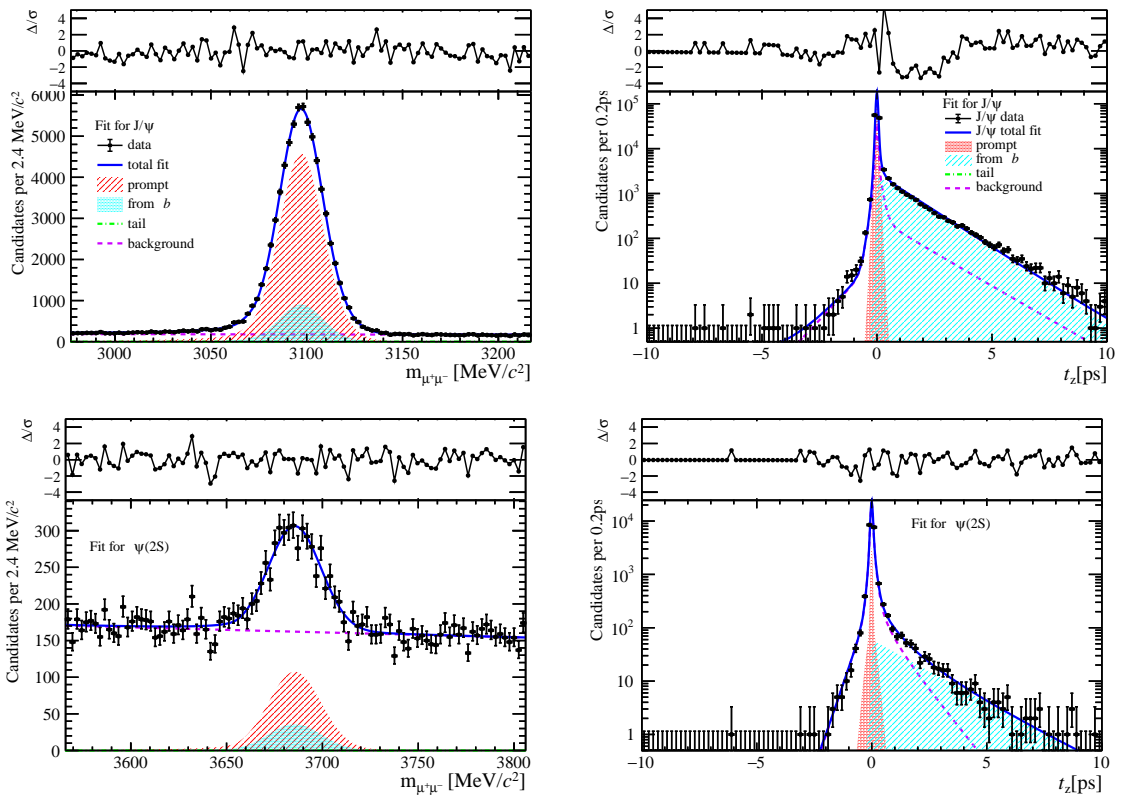


Figure 95: Fit results in  $4 \text{ GeV}/c < p_T < 6 \text{ GeV}/c$ ,  $2.0 < y < 2.8$  and  $95 \leq \text{PVNTRACKS} < 200$ .

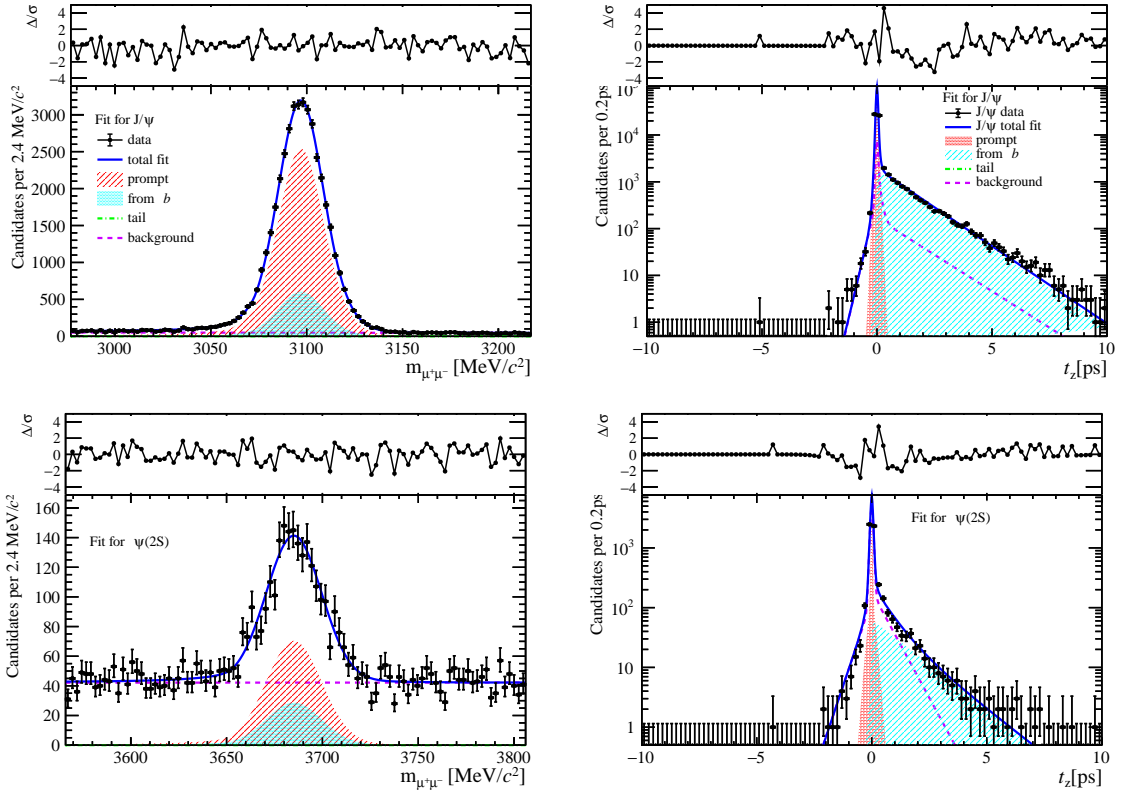


Figure 96: Fit results in  $6 \text{ GeV}/c < p_T < 8 \text{ GeV}/c$ ,  $2.0 < y < 2.8$  and  $95 \leq \text{PVNTRACKS} < 200$ .

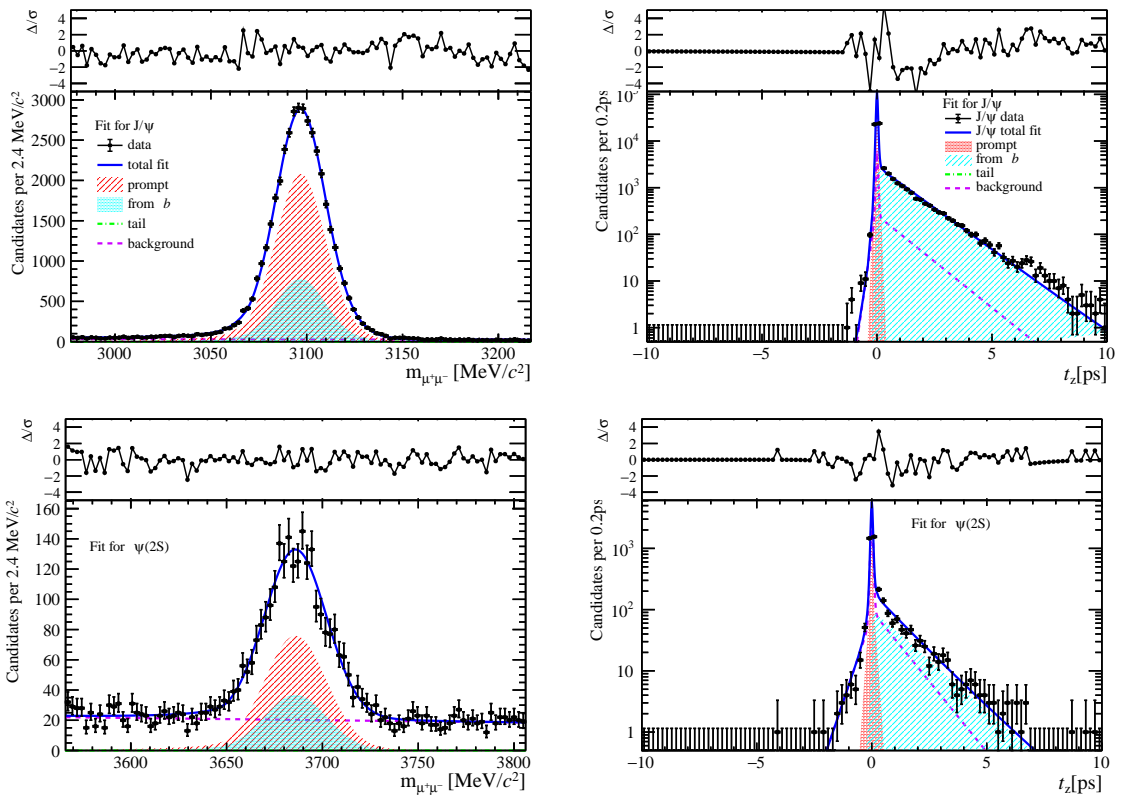


Figure 97: Fit results in  $8 \text{ GeV}/c < p_T < 20 \text{ GeV}/c$ ,  $2.0 < y < 2.8$  and  $95 \leq \text{PVNTRACKS} < 200$ .

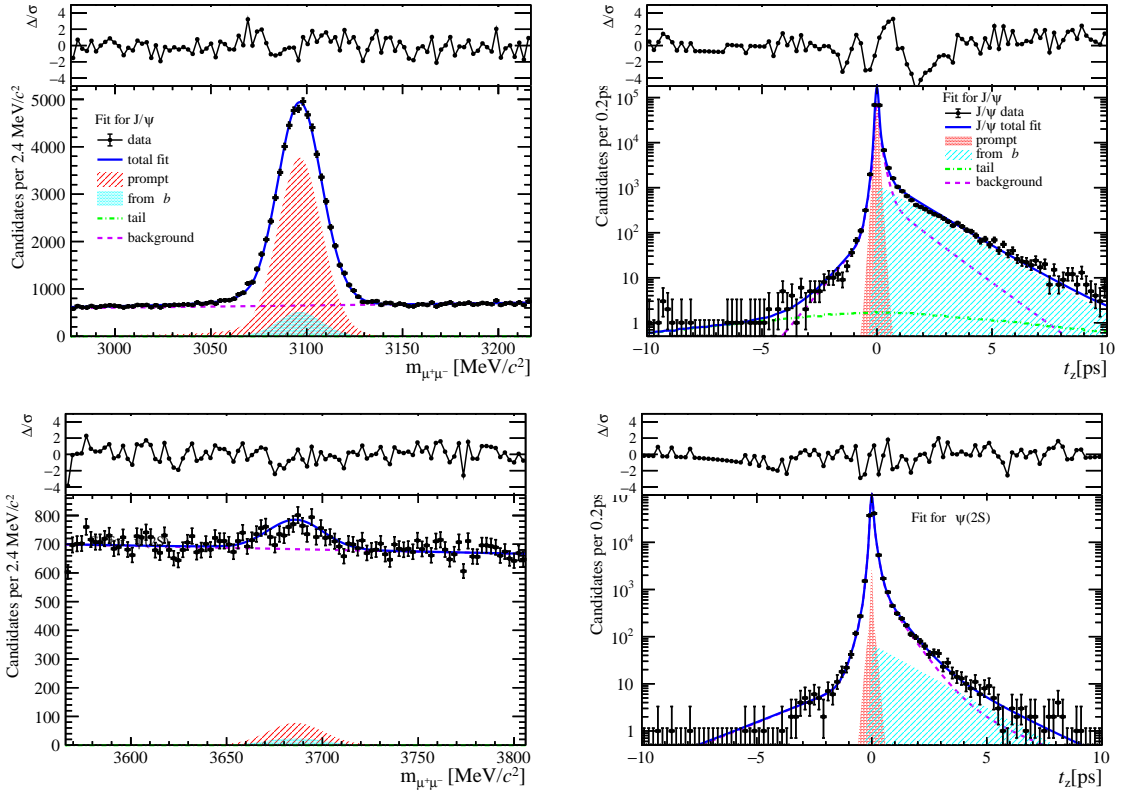


Figure 98: Fit results in  $0 \text{ GeV}/c < p_T < 2 \text{ GeV}/c$ ,  $2.8 < y < 3.5$  and  $95 \leq \text{PVNTRACKS} < 200$ .

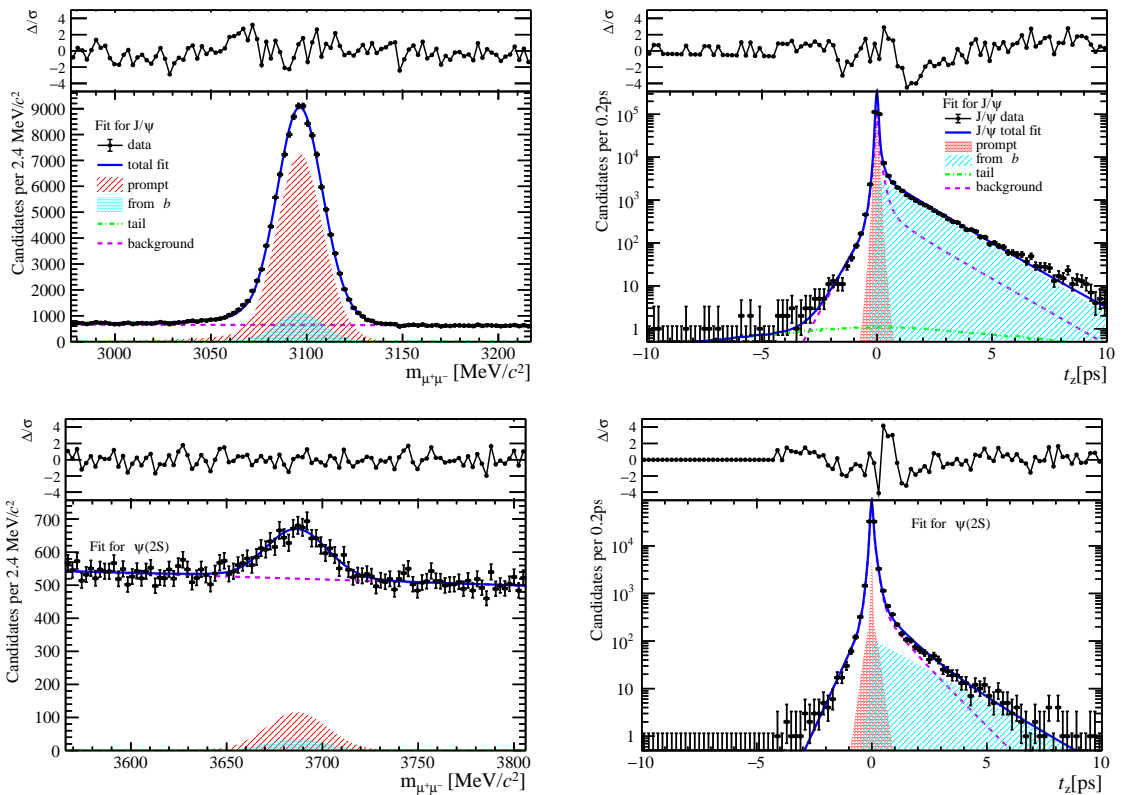


Figure 99: Fit results in  $2 \text{ GeV}/c < p_T < 4 \text{ GeV}/c$ ,  $2.8 < y < 3.5$  and  $95 \leq \text{PVNTRACKS} < 200$ .

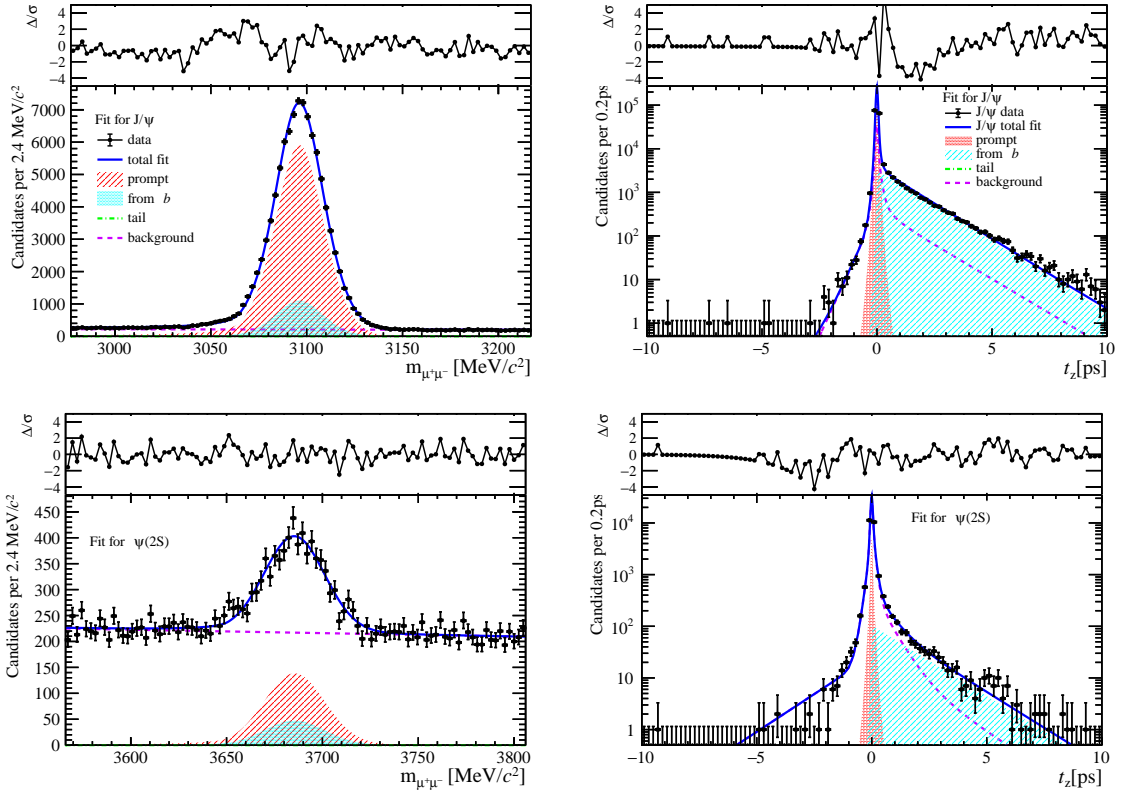


Figure 100: Fit results in  $4 \text{ GeV}/c < p_T < 6 \text{ GeV}/c$ ,  $2.8 < y < 3.5$  and  $95 \leq \text{PVNTRACKS} < 200$ .

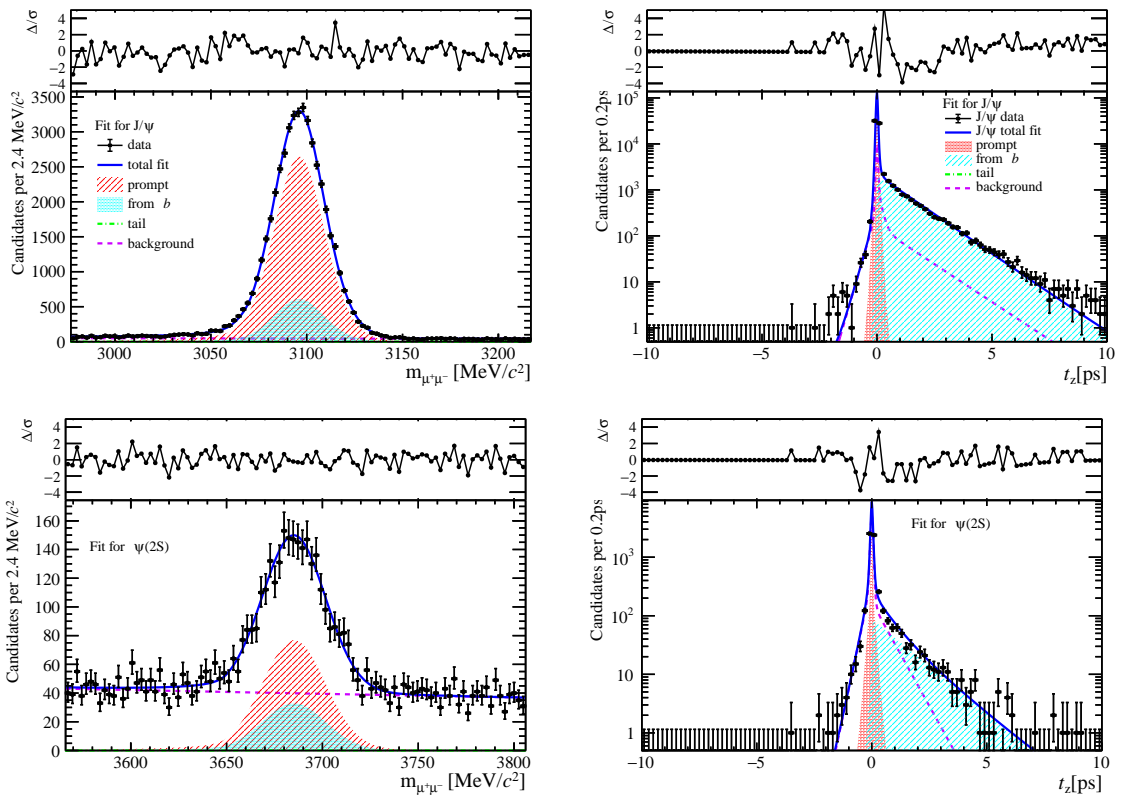


Figure 101: Fit results in  $6 \text{ GeV}/c < p_T < 8 \text{ GeV}/c$ ,  $2.8 < y < 3.5$  and  $95 \leq \text{PVNTRACKS} < 200$ .

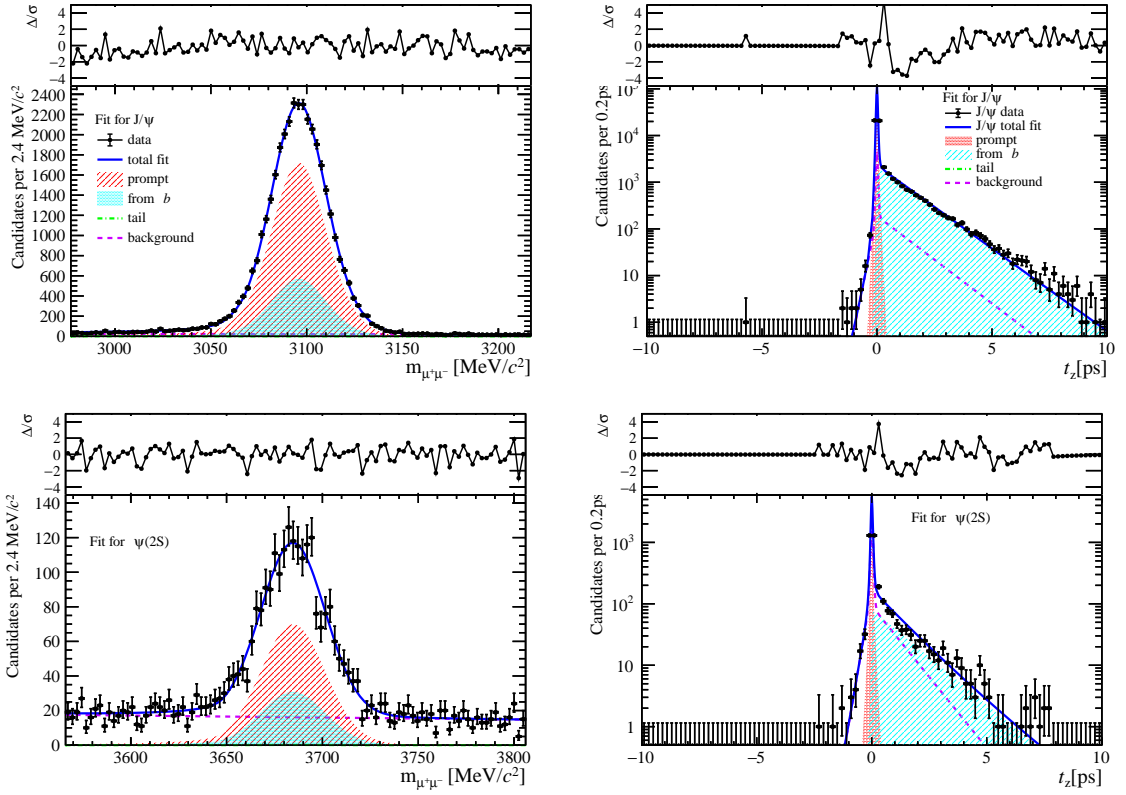


Figure 102: Fit results in  $8 \text{ GeV}/c < p_T < 20 \text{ GeV}/c$ ,  $2.8 < y < 3.5$  and  $95 \leq \text{PVNTRACKS} < 200$ .

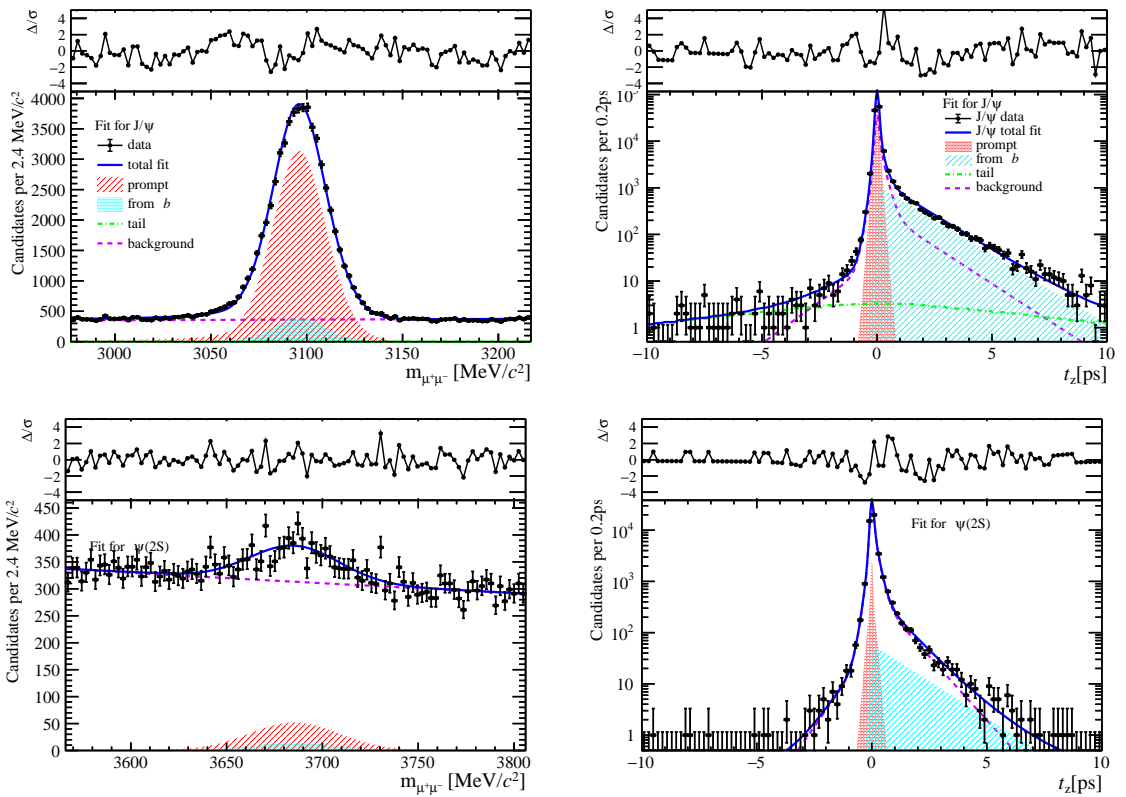


Figure 103: Fit results in  $0 \text{ GeV}/c < p_T < 2 \text{ GeV}/c$ ,  $3.5 < y < 4.5$  and  $95 \leq \text{PVNTRACKS} < 200$ .

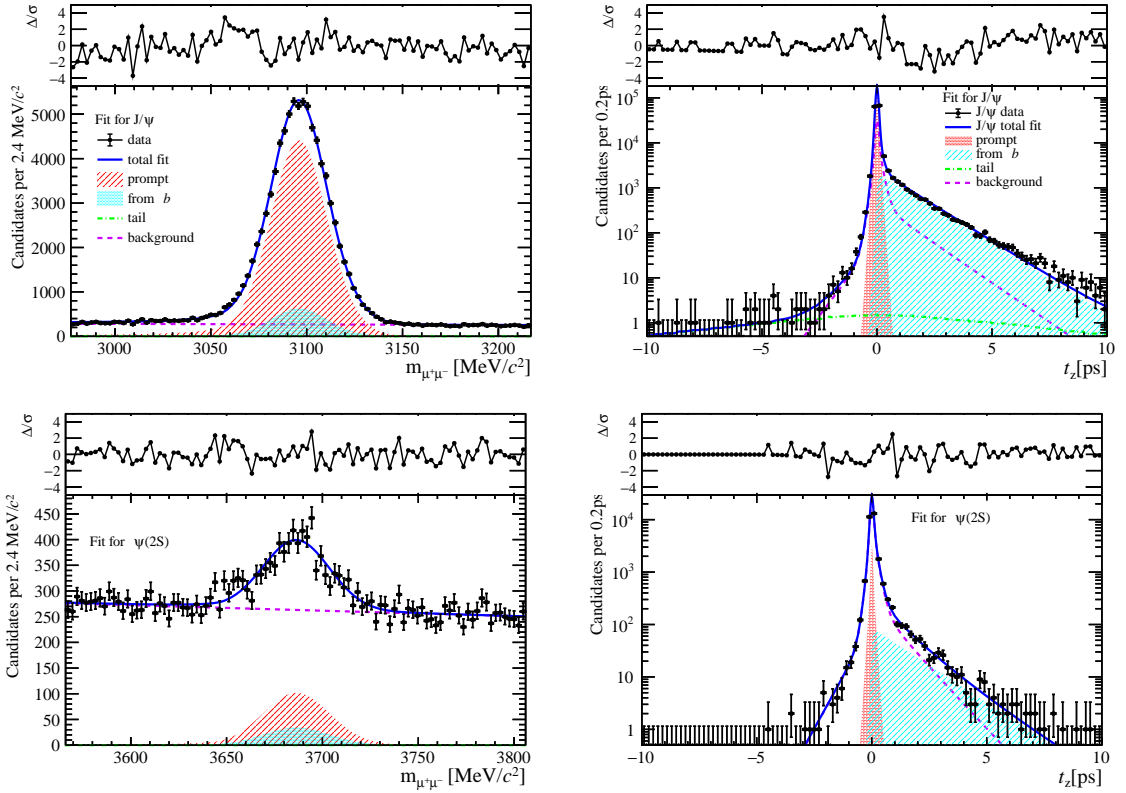


Figure 104: Fit results in  $2 \text{ GeV}/c < p_T < 4 \text{ GeV}/c$ ,  $3.5 < y < 4.5$  and  $95 \leq \text{PVNTRACKS} < 200$ .

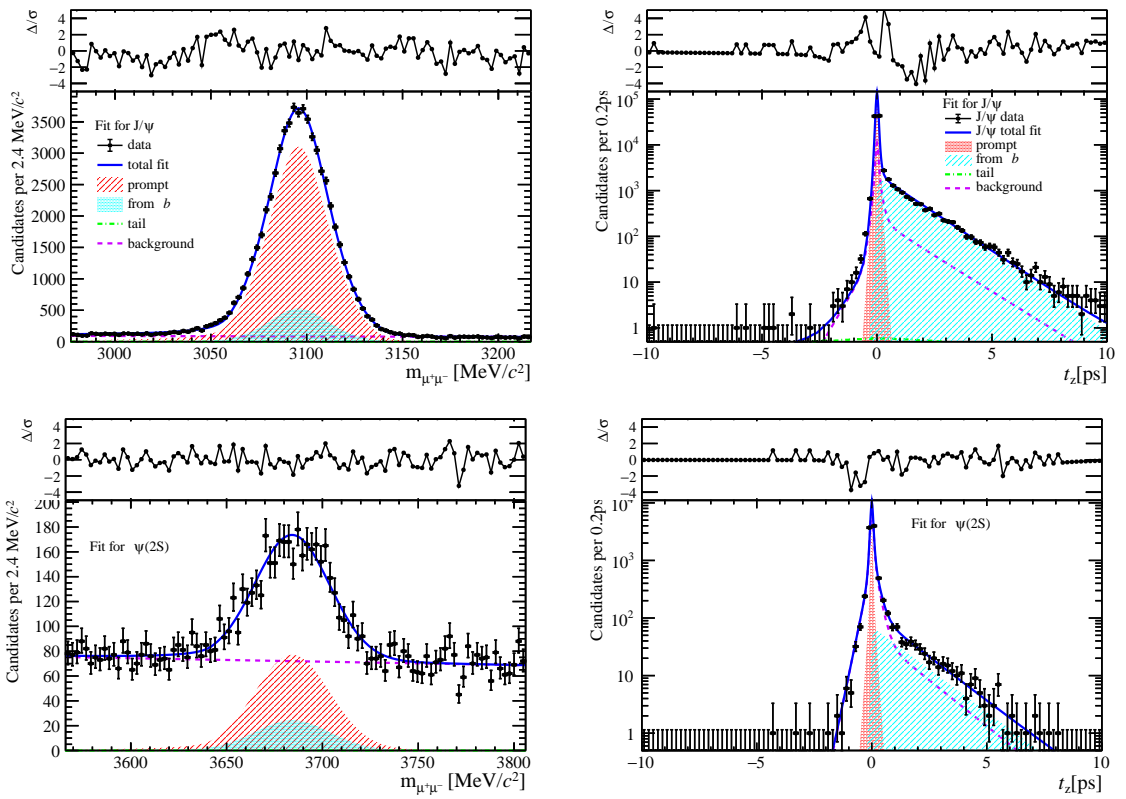


Figure 105: Fit results in  $4 \text{ GeV}/c < p_T < 6 \text{ GeV}/c$ ,  $3.5 < y < 4.5$  and  $95 \leq \text{PVNTRACKS} < 200$ .

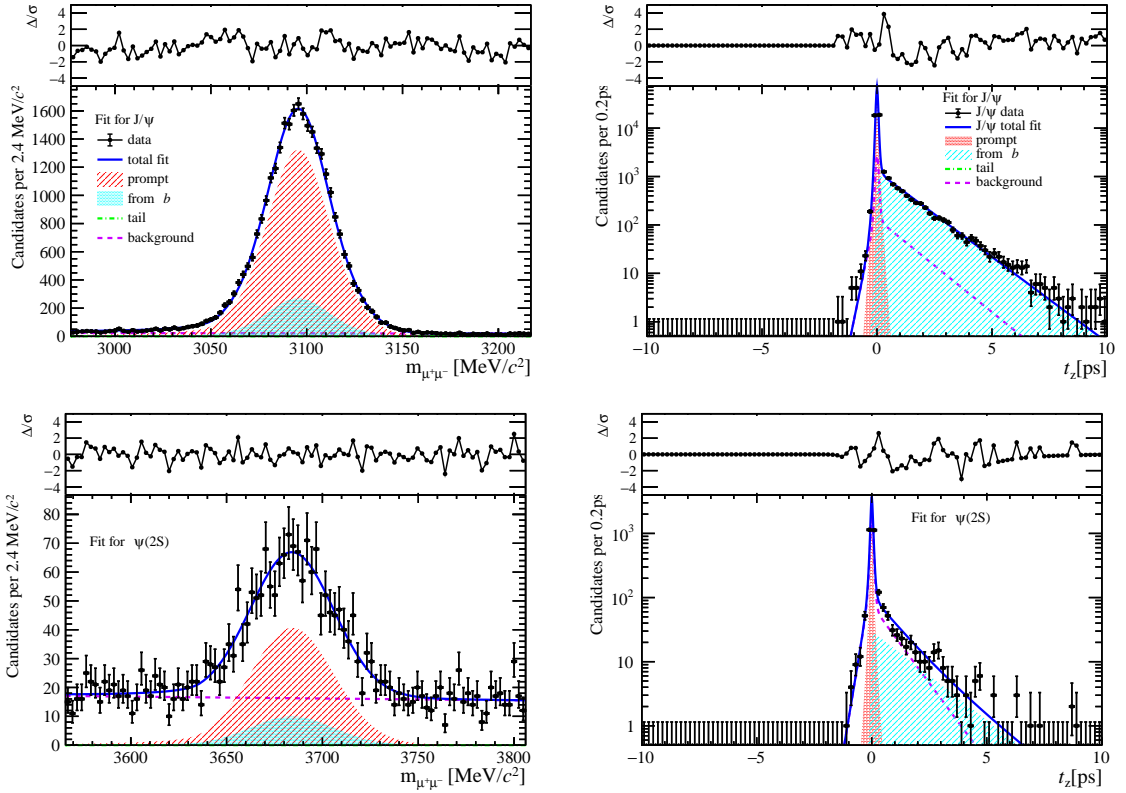


Figure 106: Fit results in  $6 \text{ GeV}/c < p_T < 8 \text{ GeV}/c$ ,  $3.5 < y < 4.5$  and  $95 \leq \text{PVNTRACKS} < 200$ .

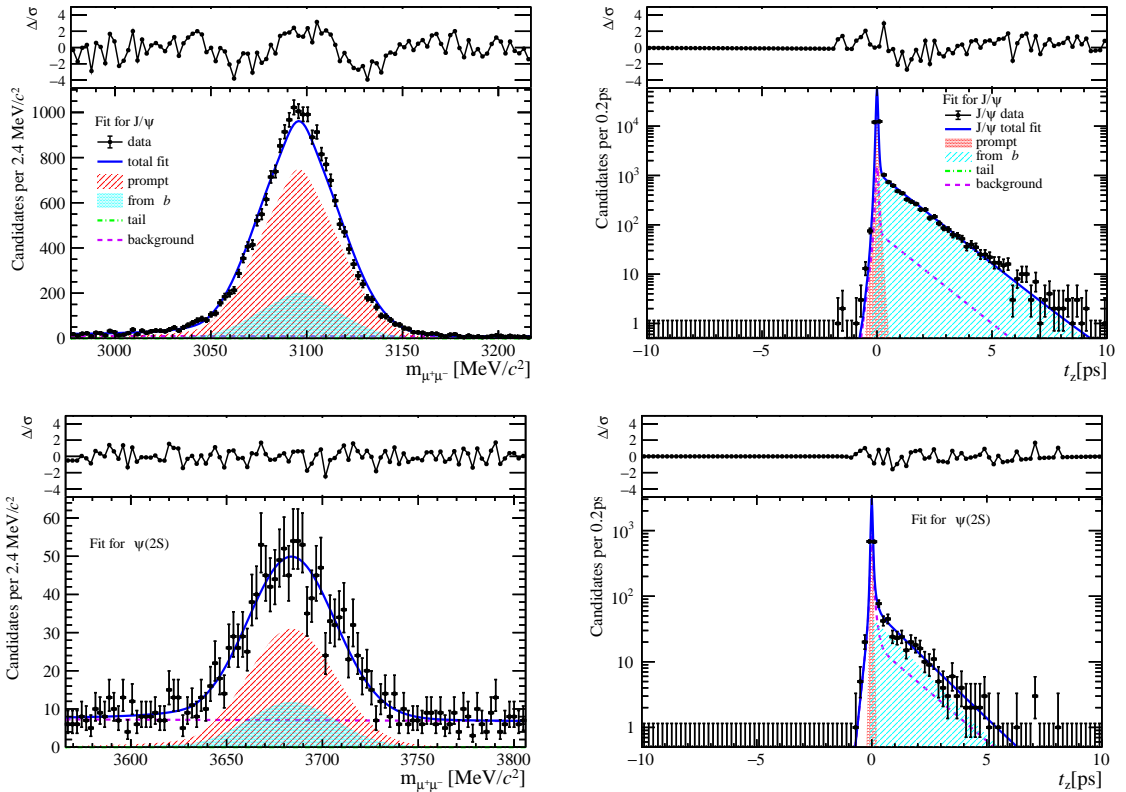


Figure 107: Fit results in  $8 \text{ GeV}/c < p_T < 20 \text{ GeV}/c$ ,  $3.5 < y < 4.5$  and  $95 \leq \text{PVNTRACKS} < 200$ .

679 C.2 Separated by nBackTracks

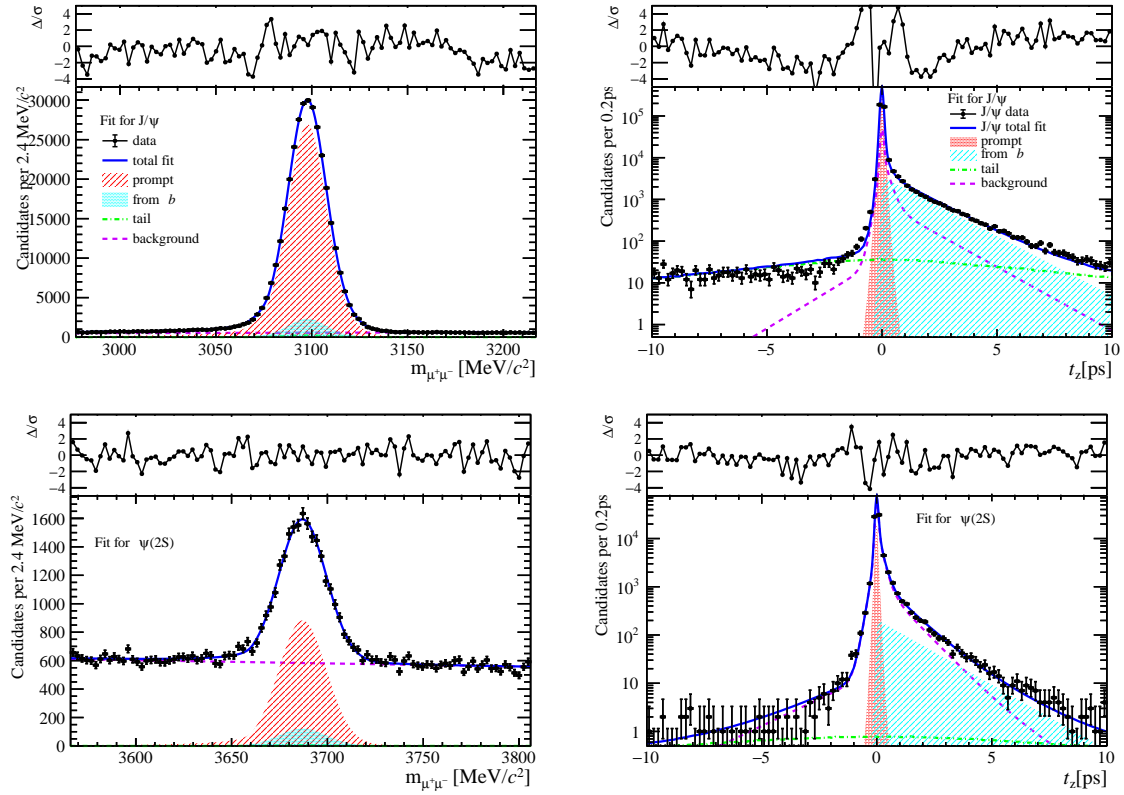


Figure 108: Fit results in  $0 \text{ GeV}/c < p_T < 2 \text{ GeV}/c$ ,  $2.0 < y < 2.8$  and  $0 \leq \text{nBackTracks} < 8$ .

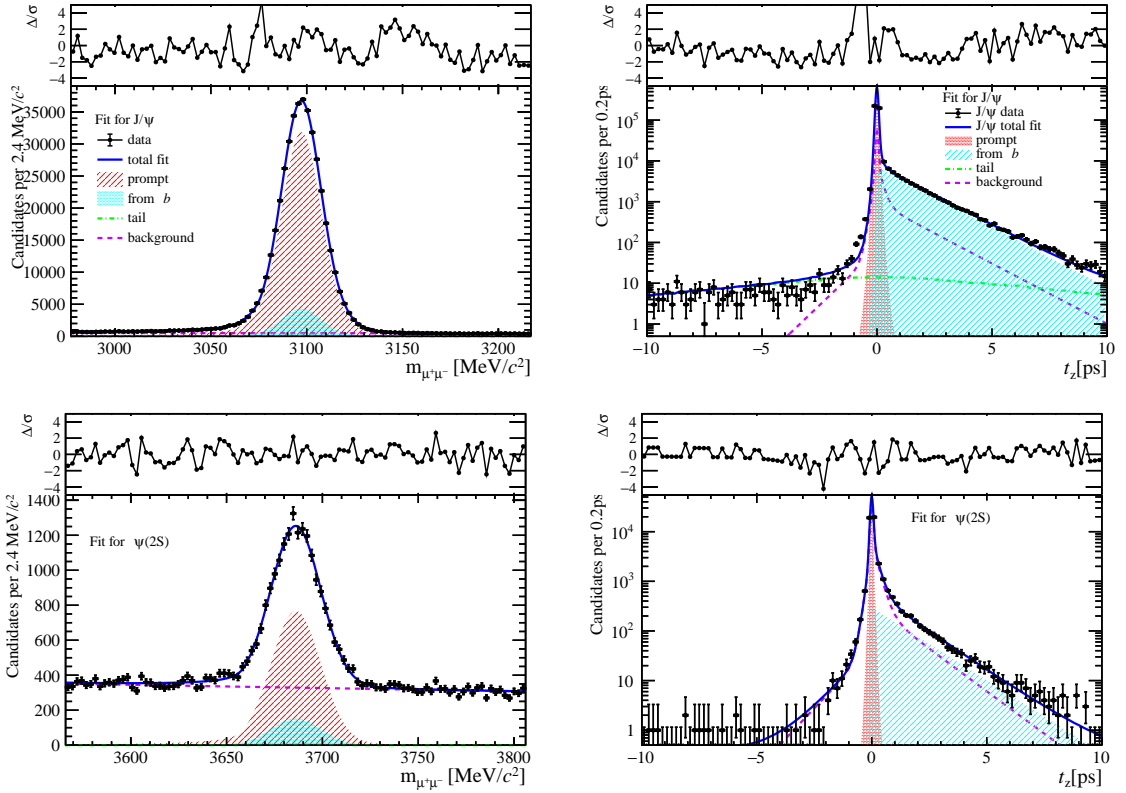


Figure 109: Fit results in  $2 \text{ GeV}/c < p_T < 4 \text{ GeV}/c$ ,  $2.0 < y < 2.8$  and  $0 \leq \text{nBackTracks} < 8$ .

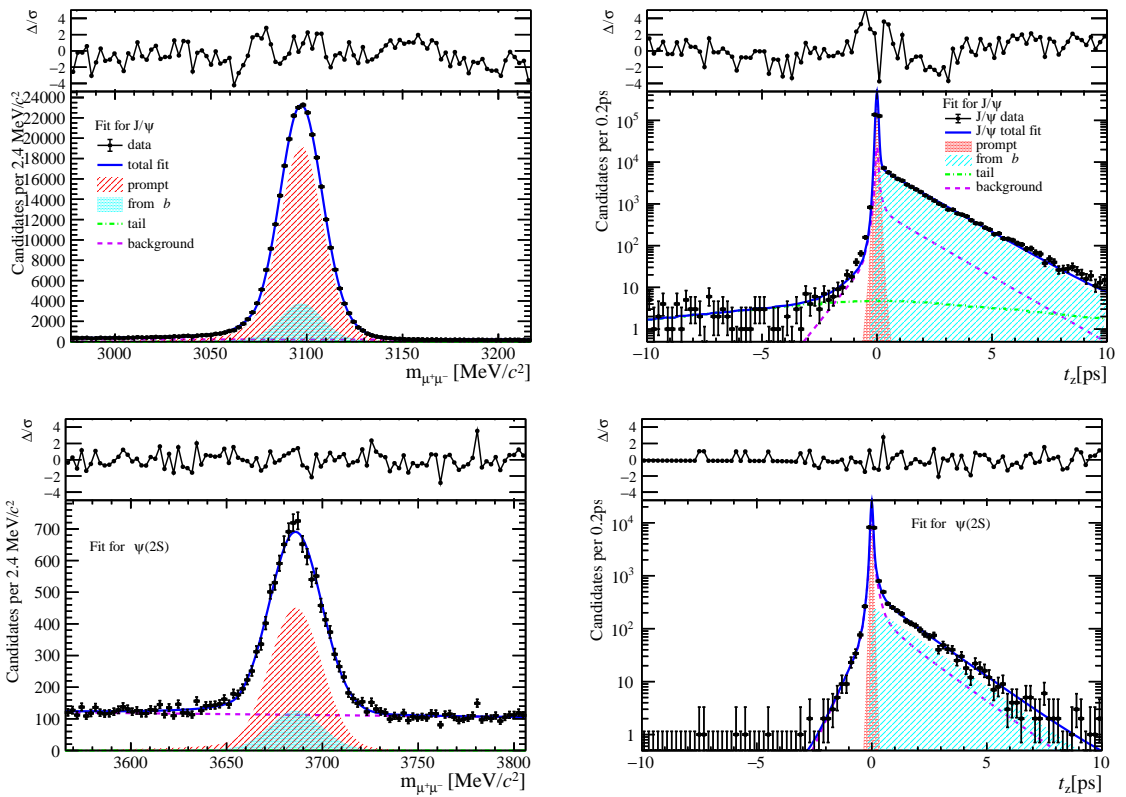


Figure 110: Fit results in  $4 \text{ GeV}/c < p_T < 6 \text{ GeV}/c$ ,  $2.0 < y < 2.8$  and  $0 \leq \text{nBackTracks} < 8$ .

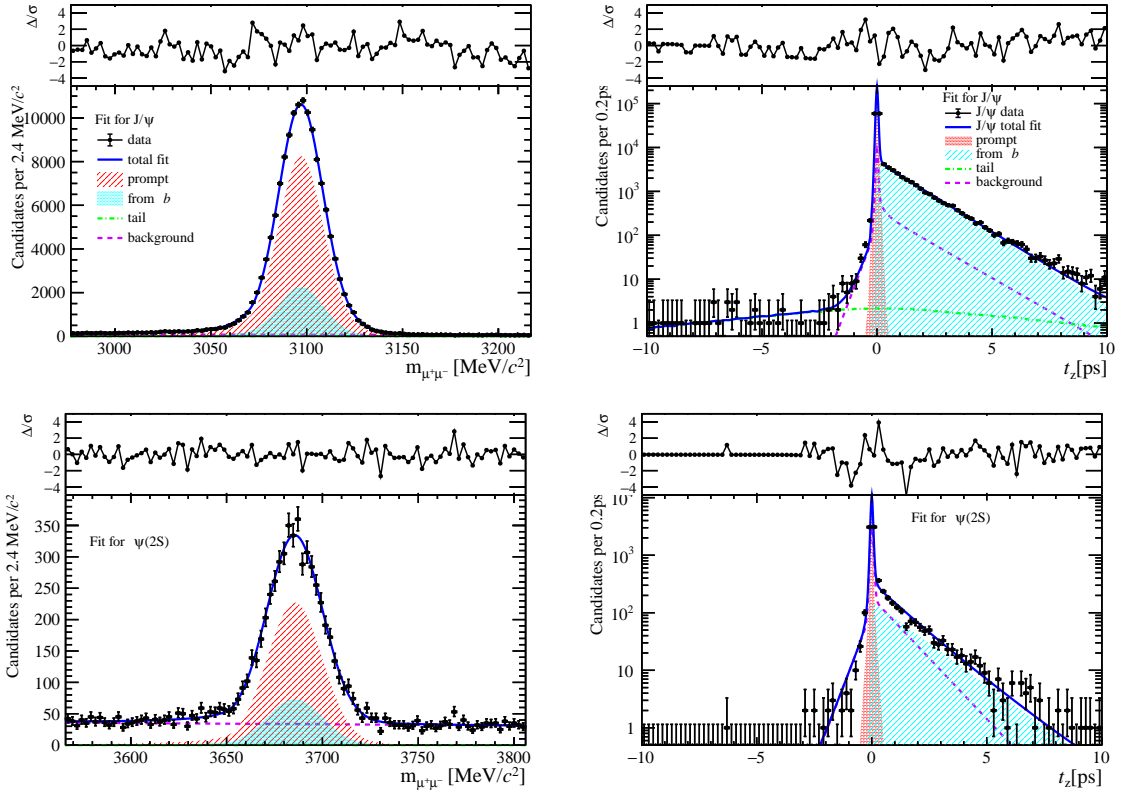


Figure 111: Fit results in  $6 \text{ GeV}/c < p_T < 8 \text{ GeV}/c$ ,  $2.0 < y < 2.8$  and  $0 \leq \text{nBackTracks} < 8$ .

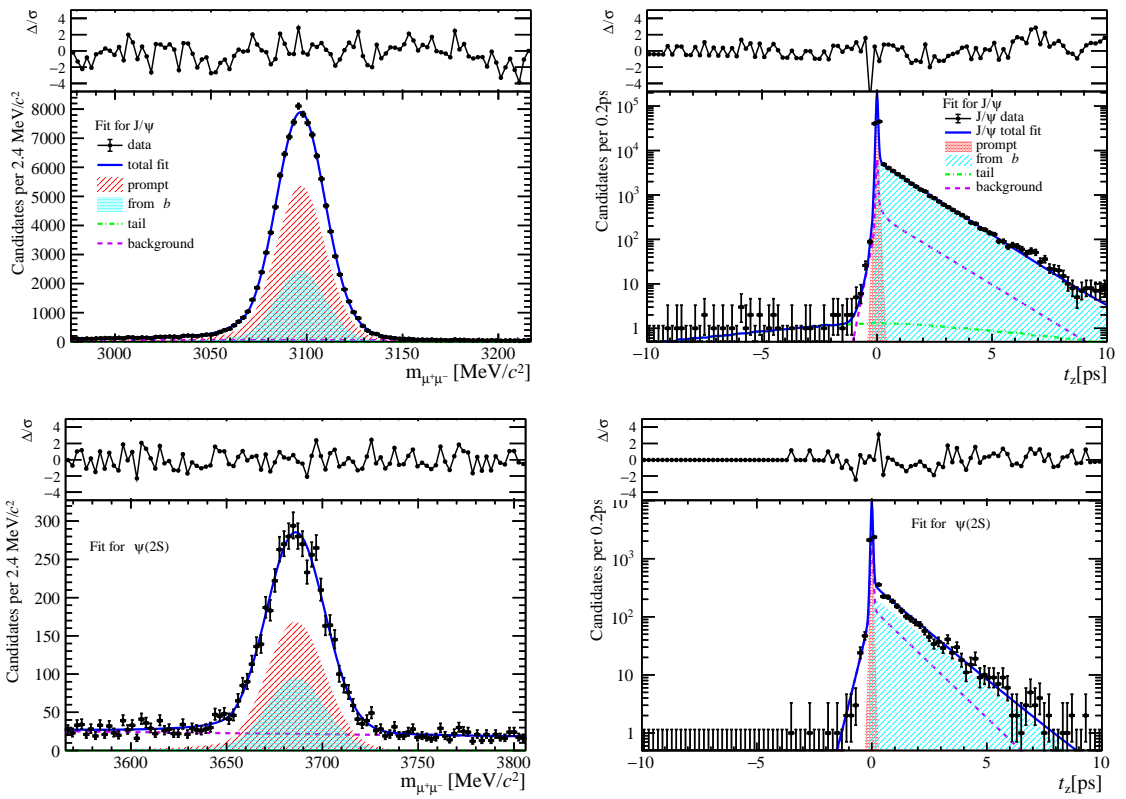


Figure 112: Fit results in  $8 \text{ GeV}/c < p_T < 20 \text{ GeV}/c$ ,  $2.0 < y < 2.8$  and  $0 \leq \text{nBackTracks} < 8$ .

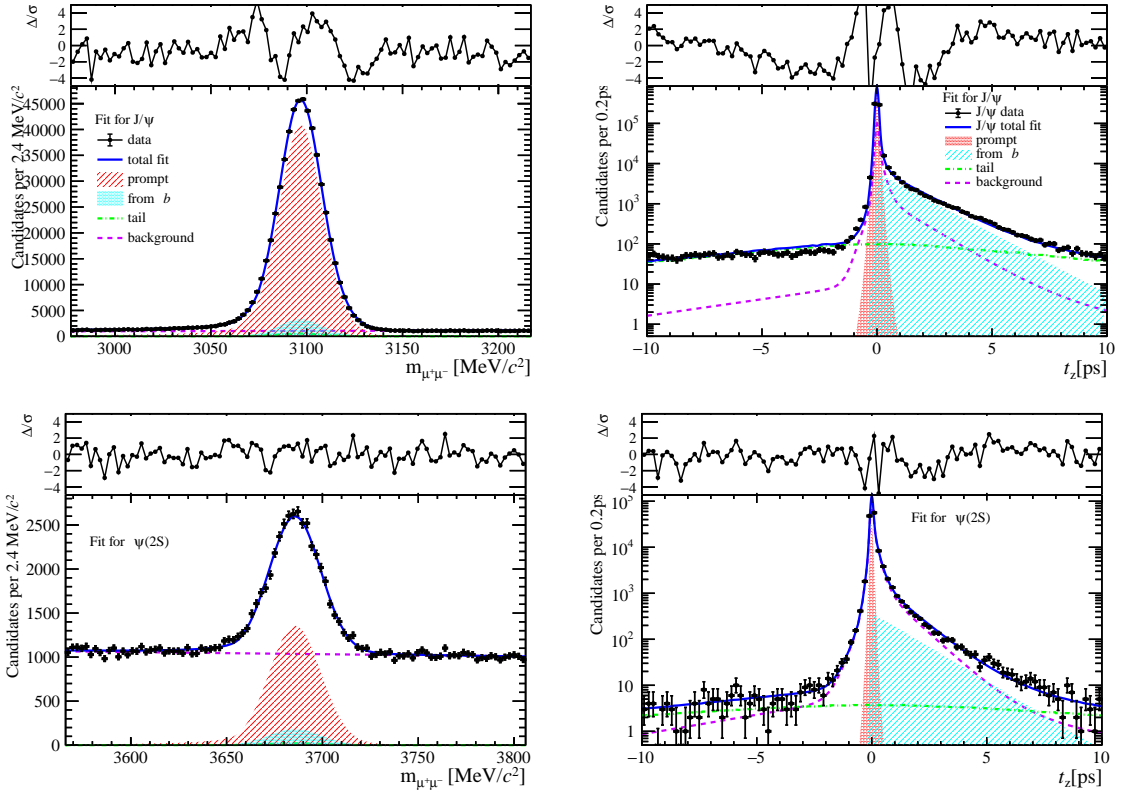


Figure 113: Fit results in  $0 \text{ GeV}/c < p_T < 2 \text{ GeV}/c$ ,  $2.8 < y < 3.5$  and  $0 \leq \text{nBackTracks} < 8$ .

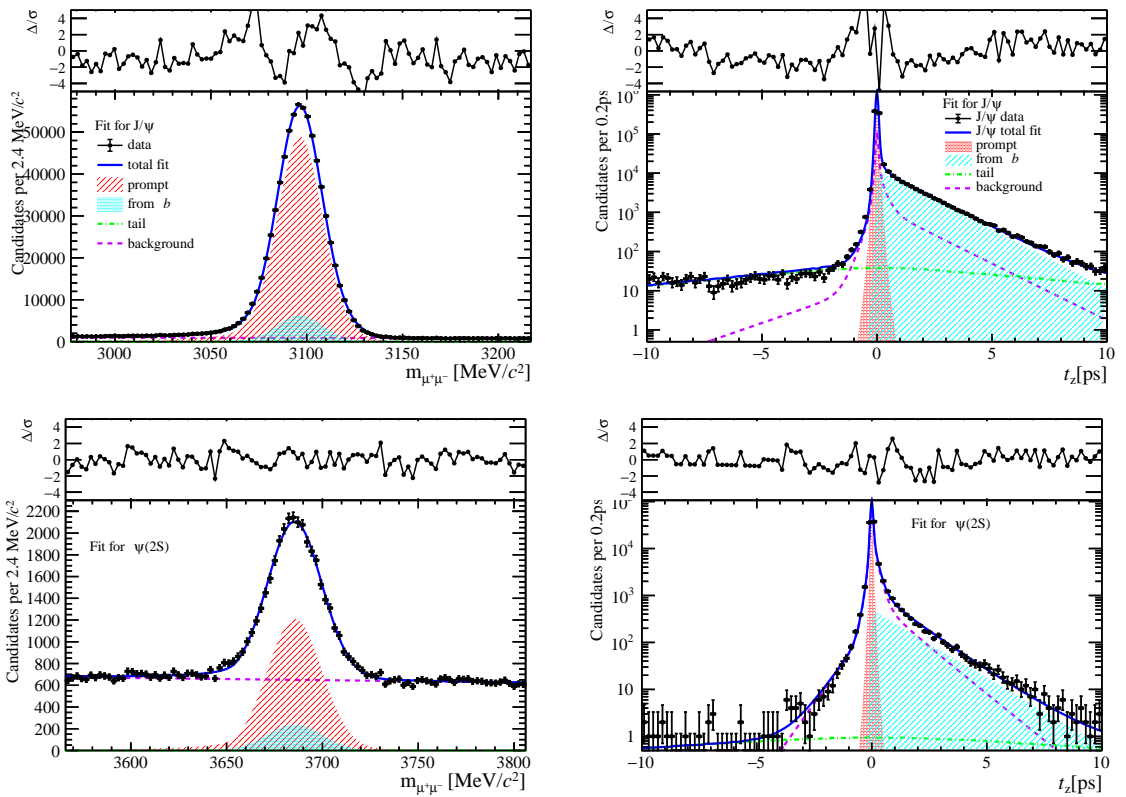


Figure 114: Fit results in  $2 \text{ GeV}/c < p_T < 4 \text{ GeV}/c$ ,  $2.8 < y < 3.5$  and  $0 \leq \text{nBackTracks} < 8$ .

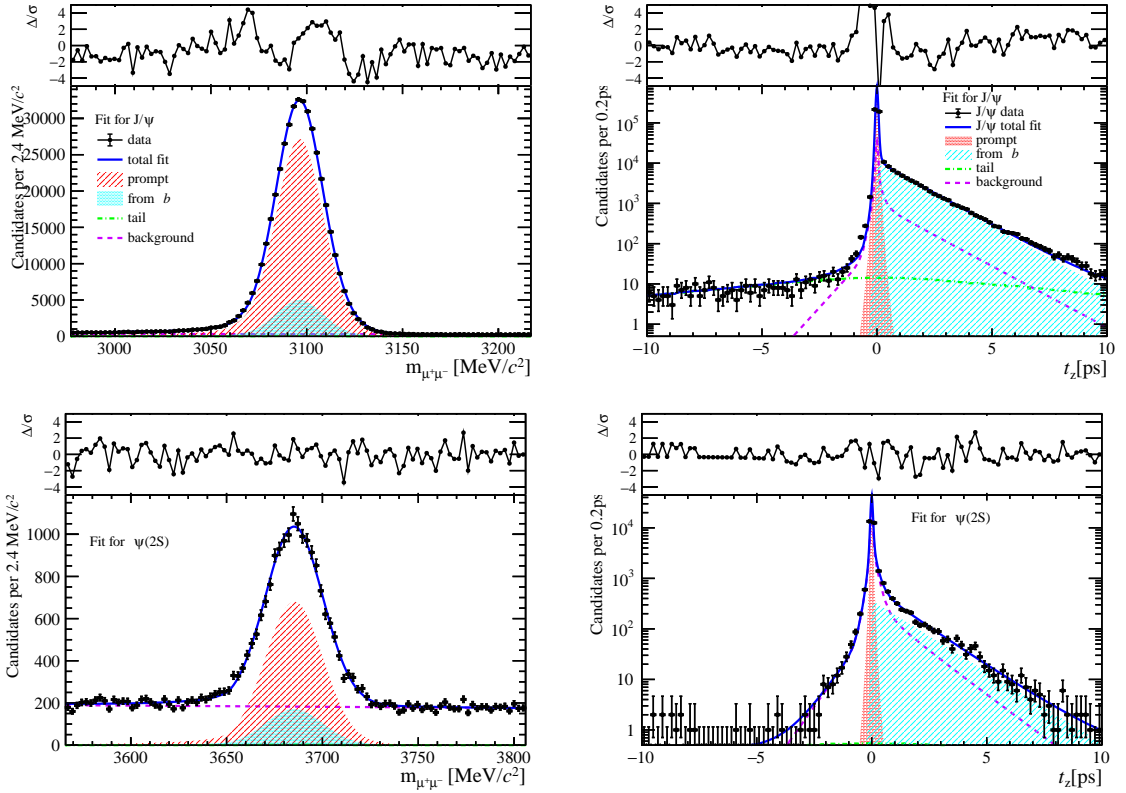


Figure 115: Fit results in  $4 \text{ GeV}/c < p_T < 6 \text{ GeV}/c$ ,  $2.8 < y < 3.5$  and  $0 \leq \text{nBackTracks} < 8$ .

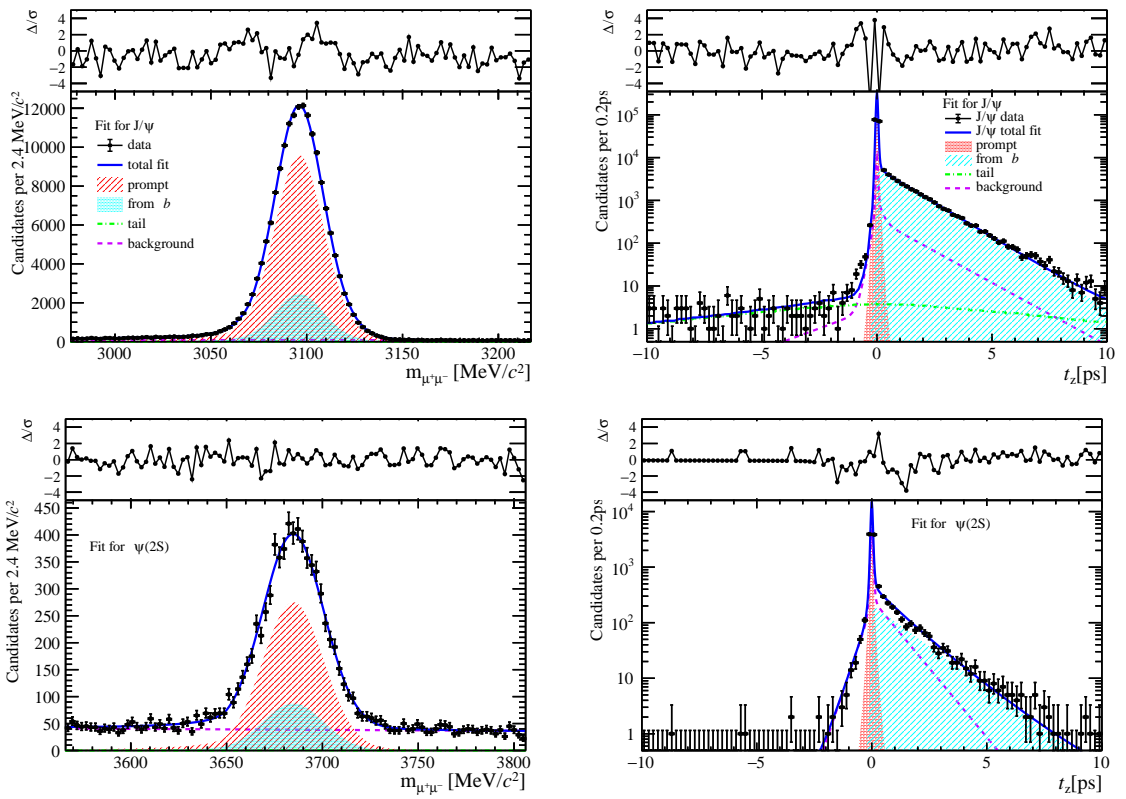


Figure 116: Fit results in  $6 \text{ GeV}/c < p_T < 8 \text{ GeV}/c$ ,  $2.8 < y < 3.5$  and  $0 \leq \text{nBackTracks} < 8$ .

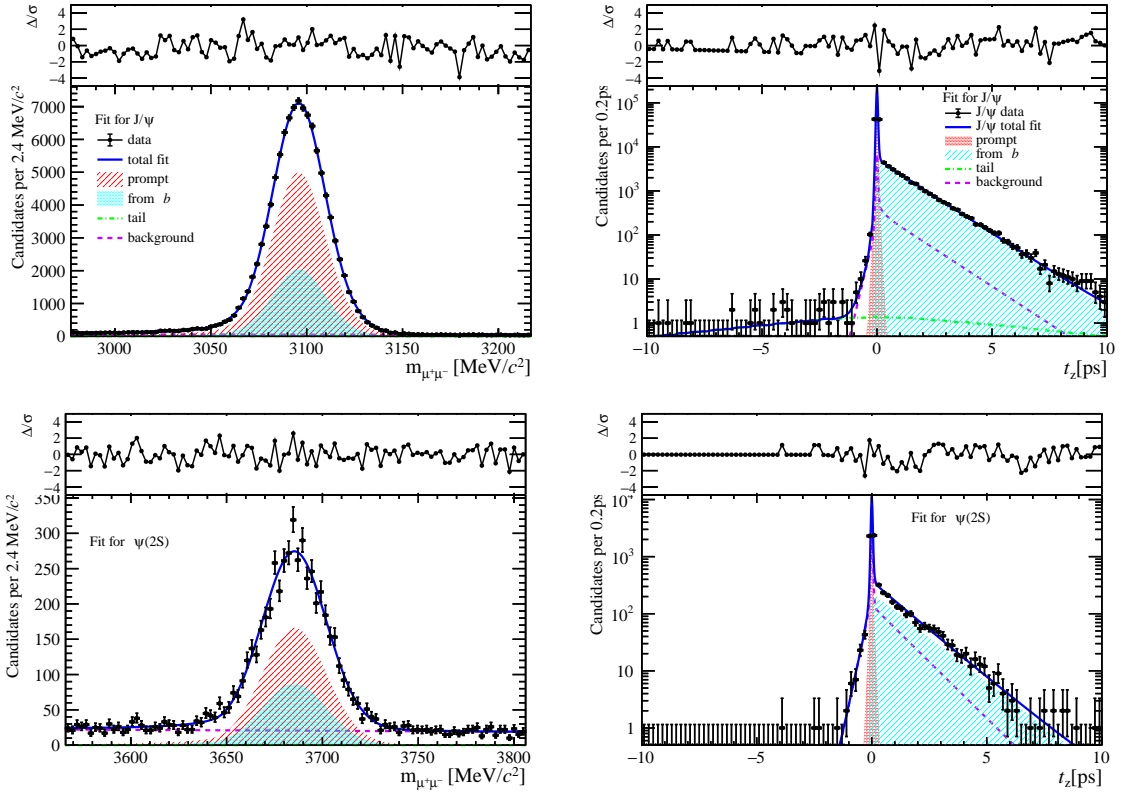


Figure 117: Fit results in  $8 \text{ GeV}/c < p_T < 20 \text{ GeV}/c$ ,  $2.8 < y < 3.5$  and  $0 \leq \text{nBackTracks} < 8$ .

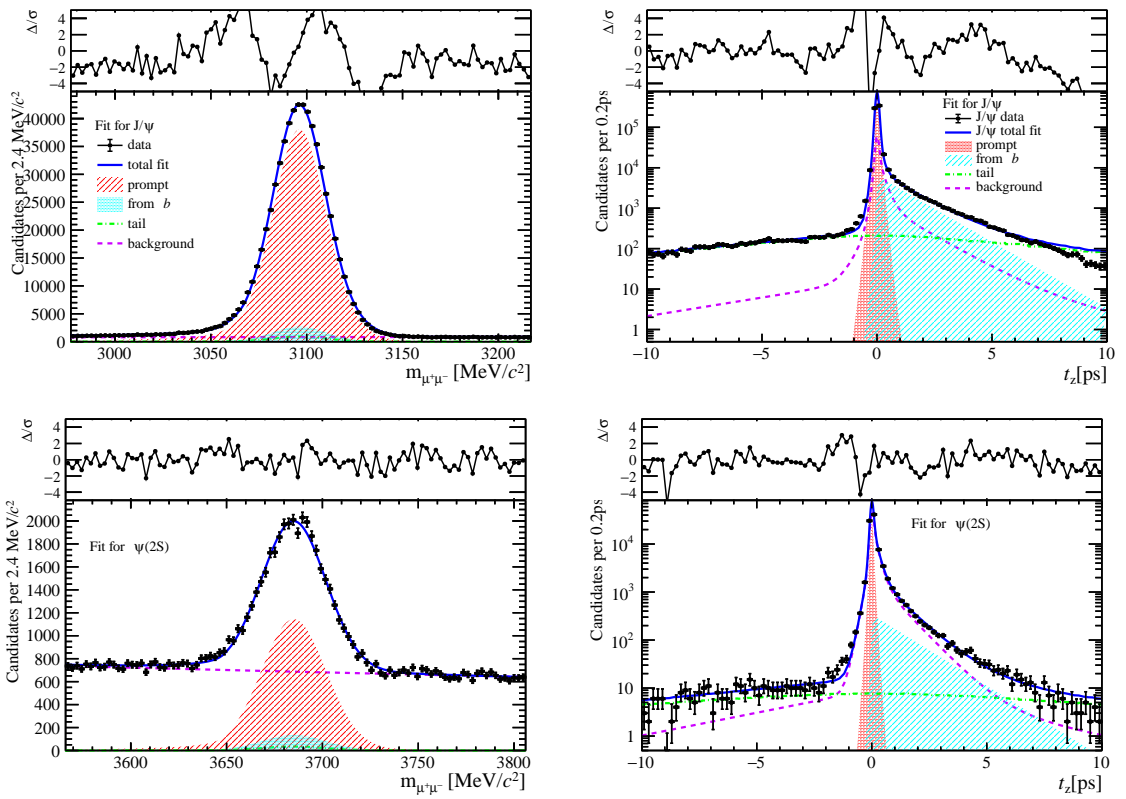


Figure 118: Fit results in  $0 \text{ GeV}/c < p_T < 2 \text{ GeV}/c$ ,  $3.5 < y < 4.5$  and  $0 \leq \text{nBackTracks} < 8$ .

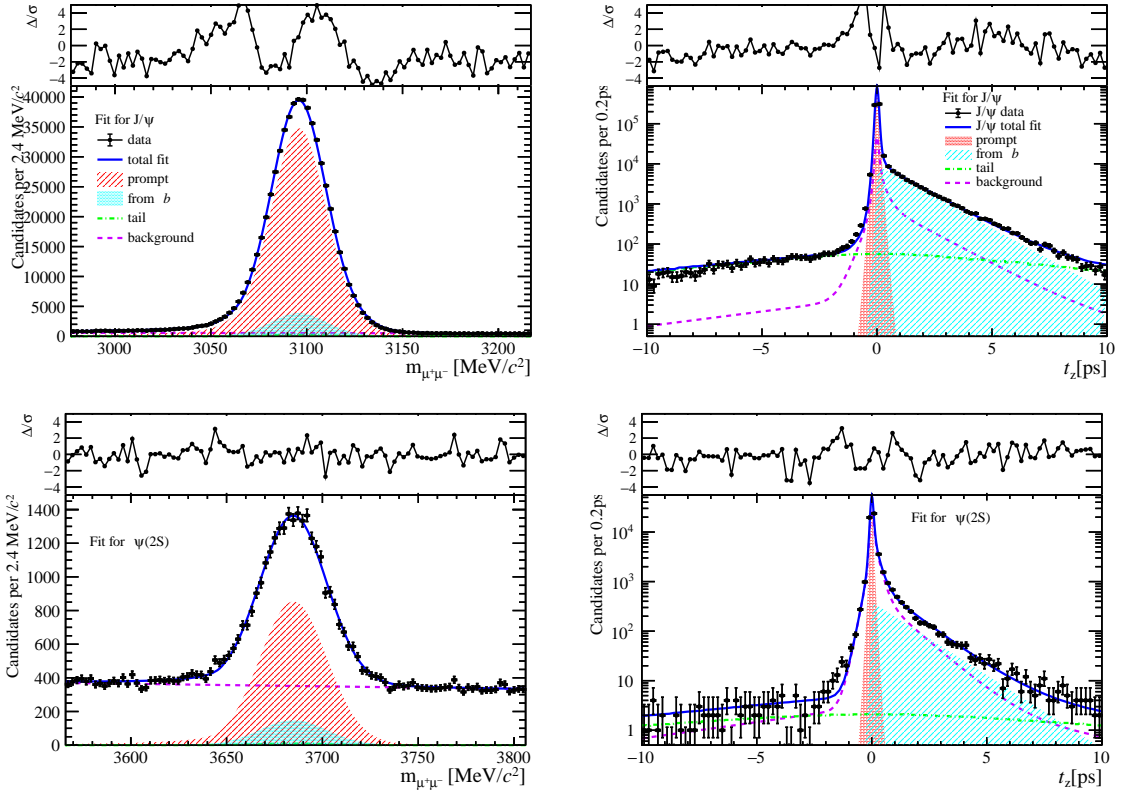


Figure 119: Fit results in  $2 \text{ GeV}/c < p_T < 4 \text{ GeV}/c$ ,  $3.5 < y < 4.5$  and  $0 \leq \text{nBackTracks} < 8$ .

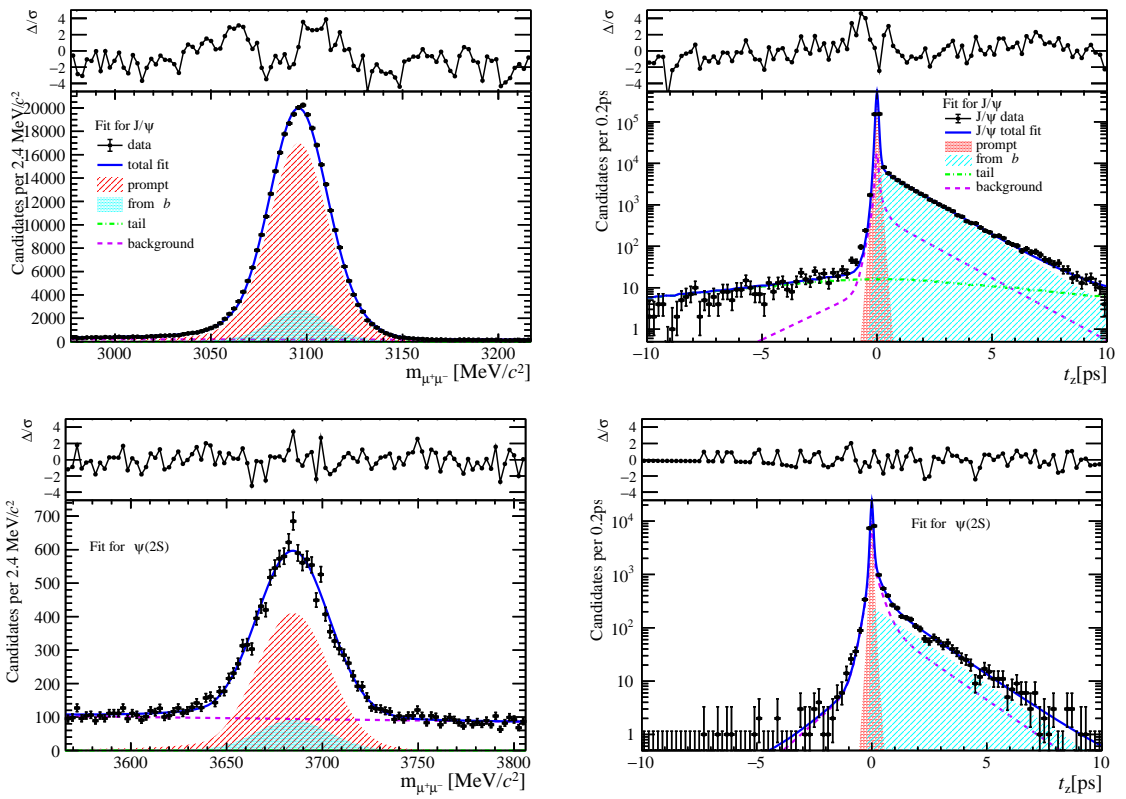


Figure 120: Fit results in  $4 \text{ GeV}/c < p_T < 6 \text{ GeV}/c$ ,  $3.5 < y < 4.5$  and  $0 \leq \text{nBackTracks} < 8$ .

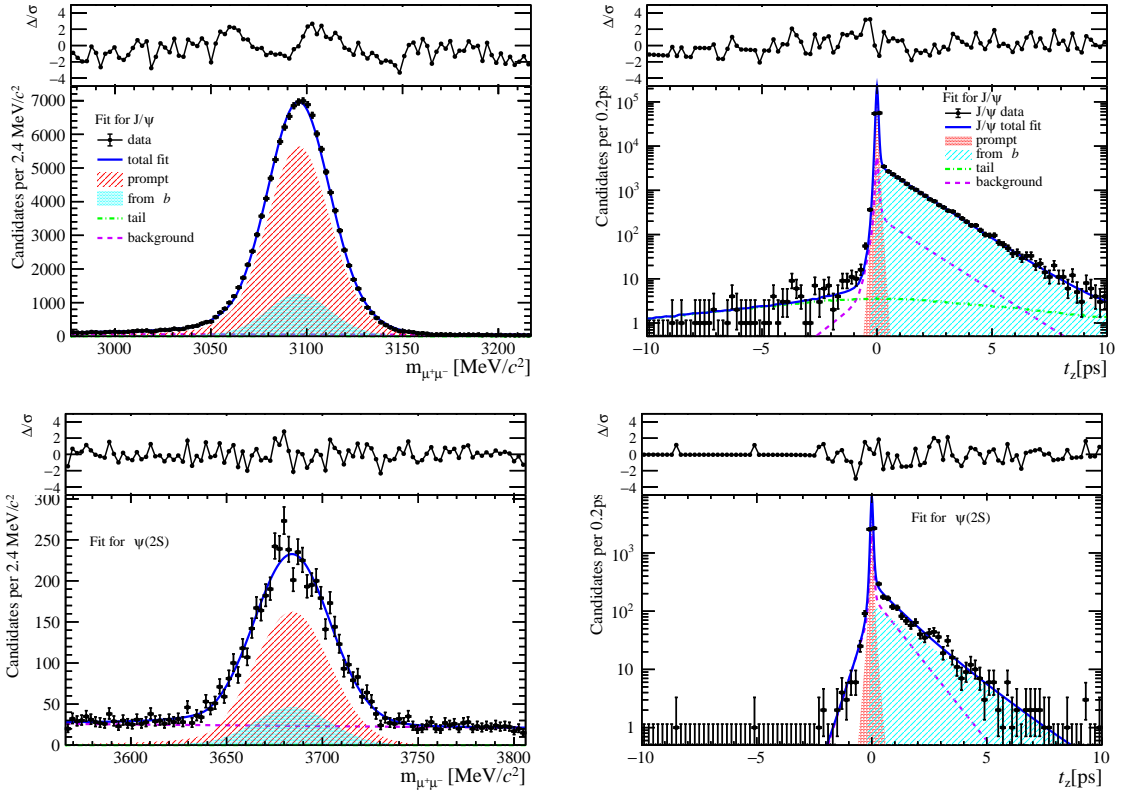


Figure 121: Fit results in  $6 \text{ GeV}/c < p_T < 8 \text{ GeV}/c$ ,  $3.5 < y < 4.5$  and  $0 \leq \text{nBackTracks} < 8$ .

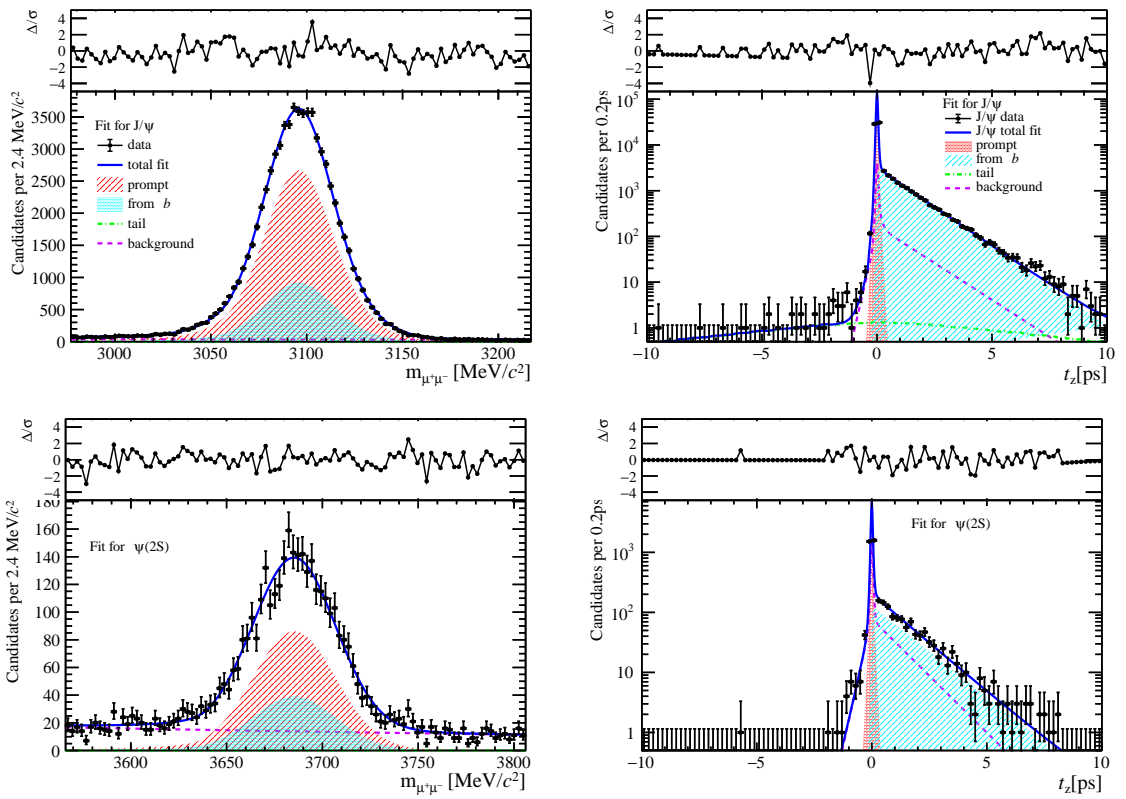


Figure 122: Fit results in  $8 \text{ GeV}/c < p_T < 20 \text{ GeV}/c$ ,  $3.5 < y < 4.5$  and  $0 \leq \text{nBackTracks} < 8$ .

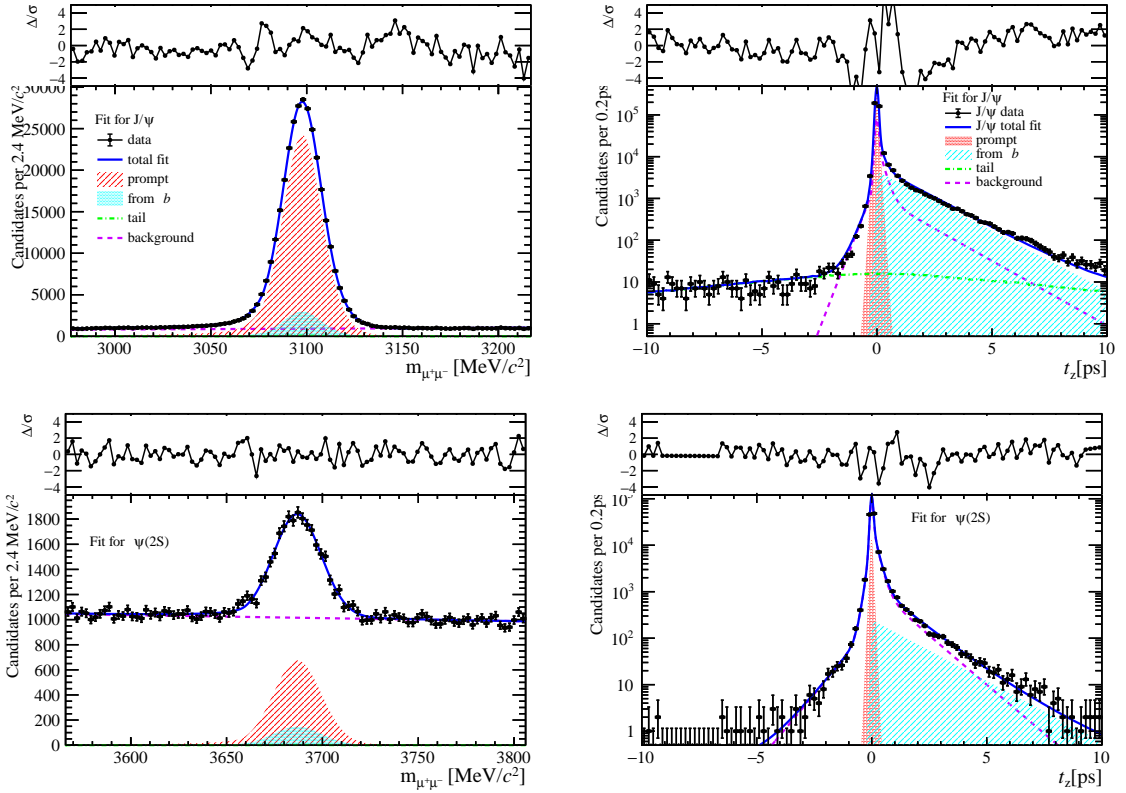


Figure 123: Fit results in  $0 \text{ GeV}/c < p_T < 2 \text{ GeV}/c$ ,  $2.0 < y < 2.8$  and  $8 \leq n\text{BackTracks} < 15$ .

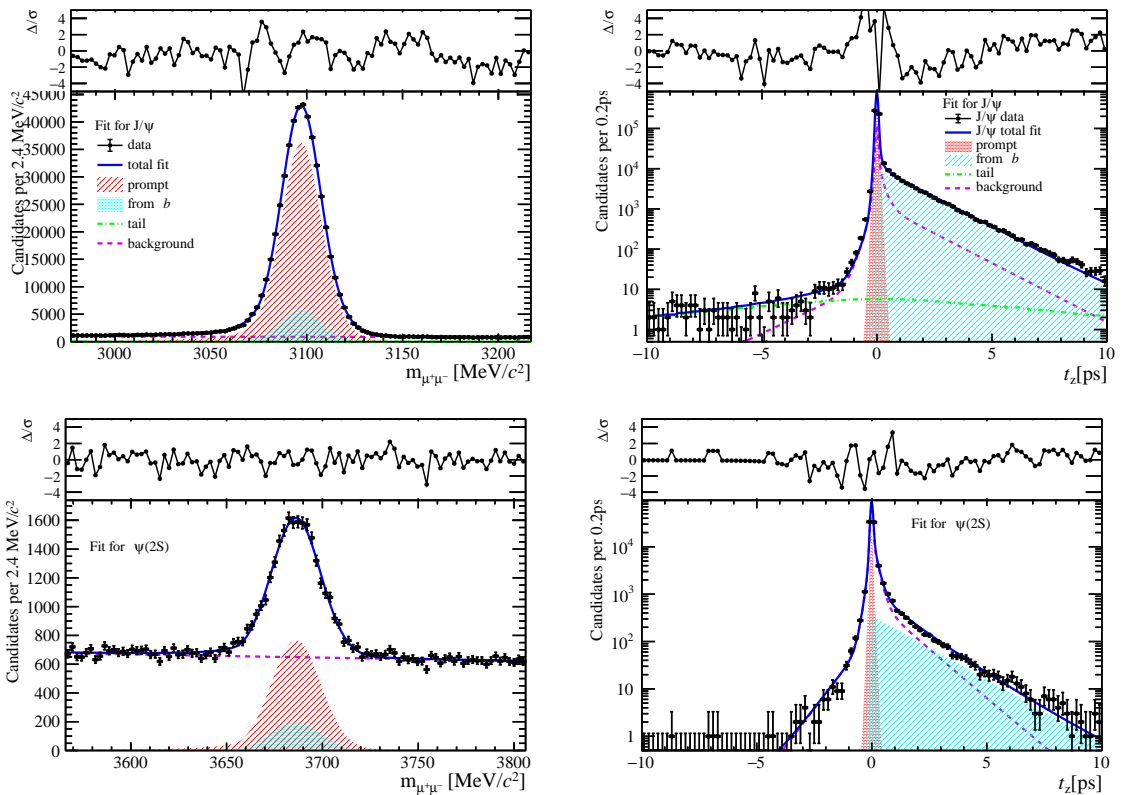


Figure 124: Fit results in  $2 \text{ GeV}/c < p_T < 4 \text{ GeV}/c$ ,  $2.0 < y < 2.8$  and  $8 \leq n\text{BackTracks} < 15$ .

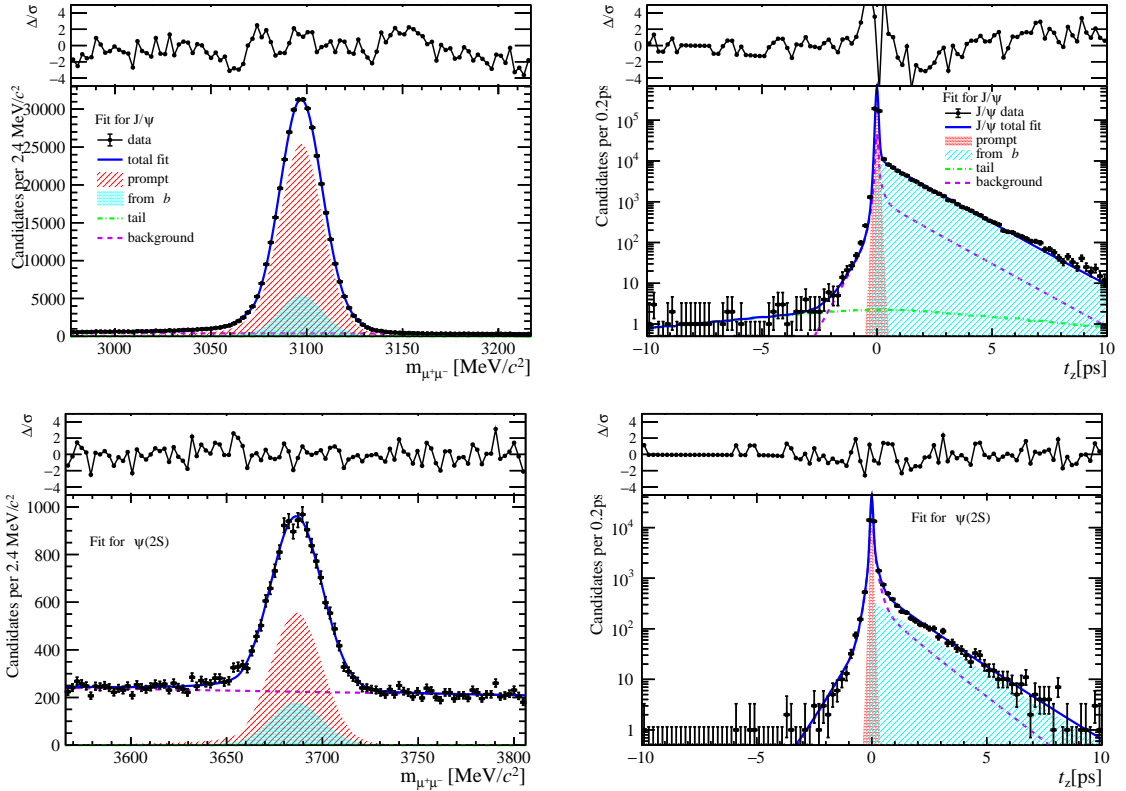


Figure 125: Fit results in  $4 \text{ GeV}/c < p_T < 6 \text{ GeV}/c$ ,  $2.0 < y < 2.8$  and  $8 \leq \text{nBackTracks} < 15$ .

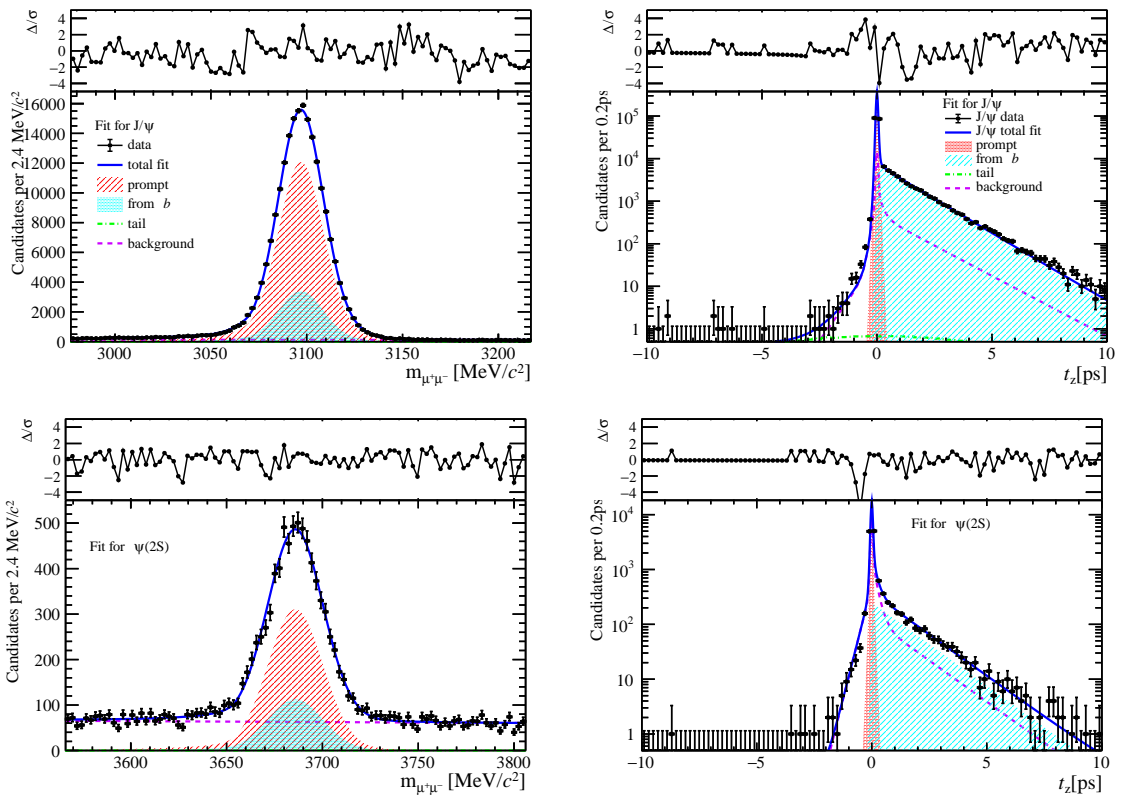


Figure 126: Fit results in  $6 \text{ GeV}/c < p_T < 8 \text{ GeV}/c$ ,  $2.0 < y < 2.8$  and  $8 \leq \text{nBackTracks} < 15$ .

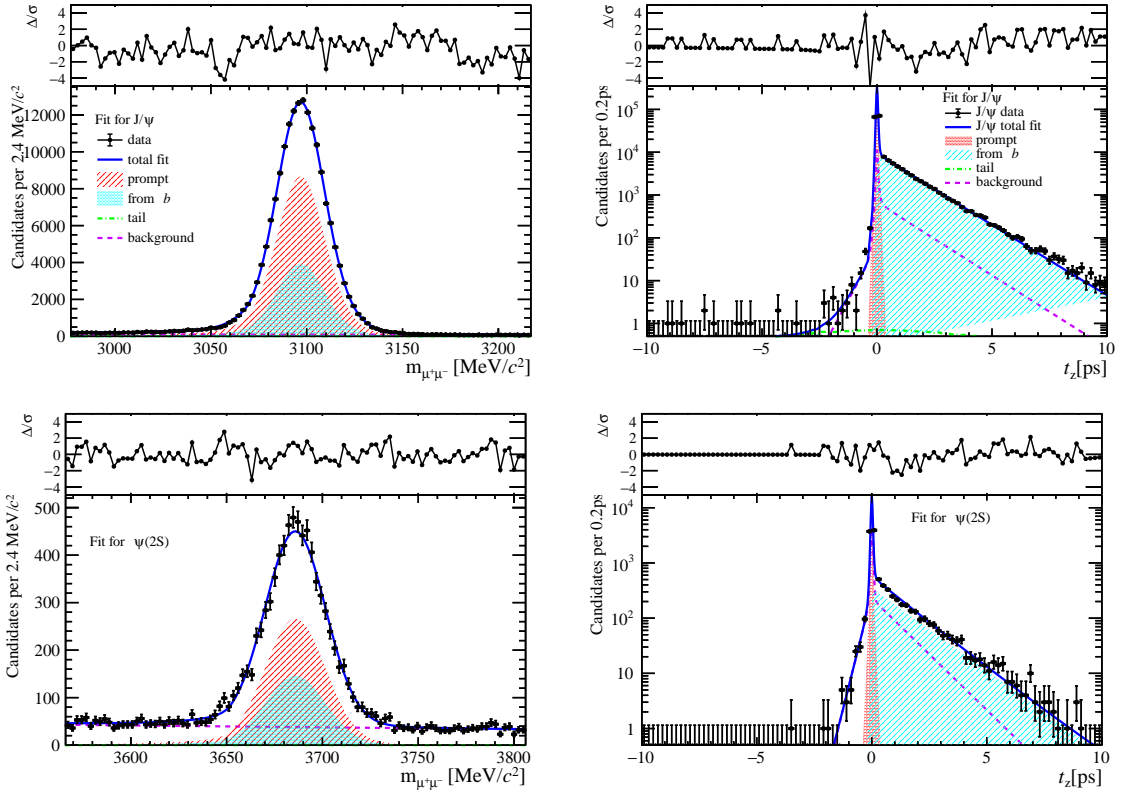


Figure 127: Fit results in  $8 \text{ GeV}/c < p_T < 20 \text{ GeV}/c$ ,  $2.0 < y < 2.8$  and  $8 \leq \text{nBackTracks} < 15$ .

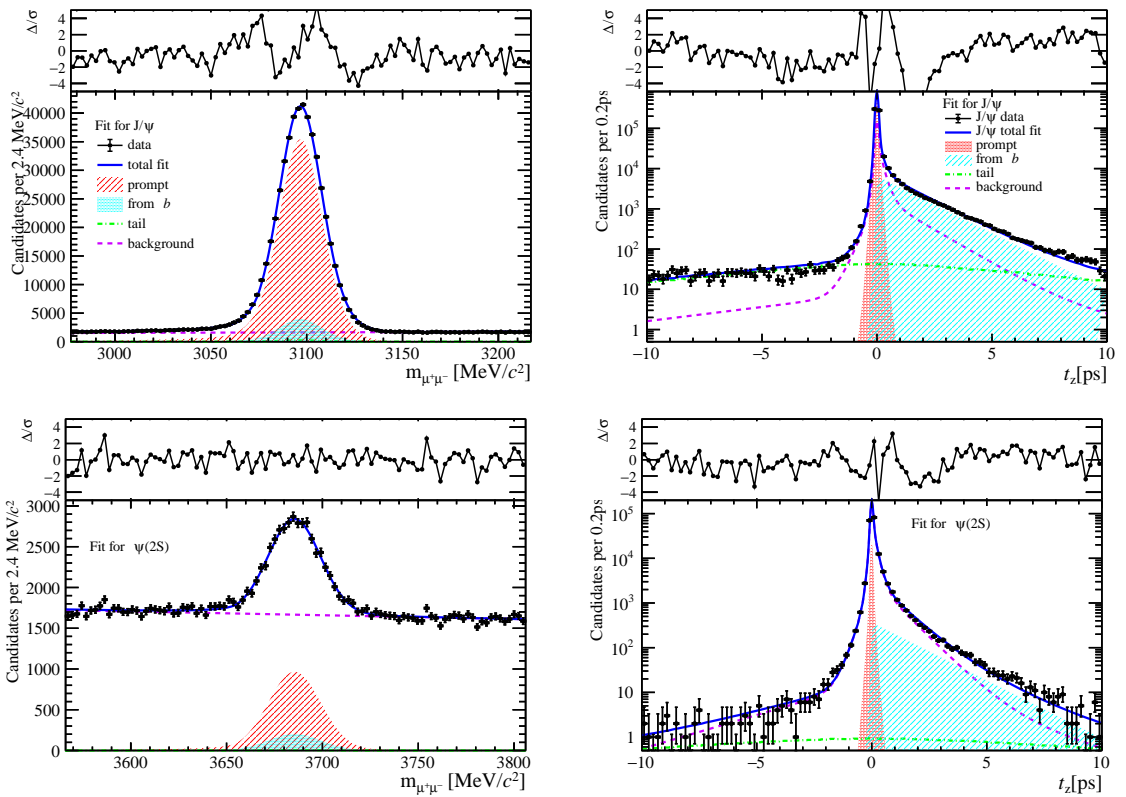


Figure 128: Fit results in  $0 \text{ GeV}/c < p_T < 2 \text{ GeV}/c$ ,  $2.8 < y < 3.5$  and  $8 \leq \text{nBackTracks} < 15$ .

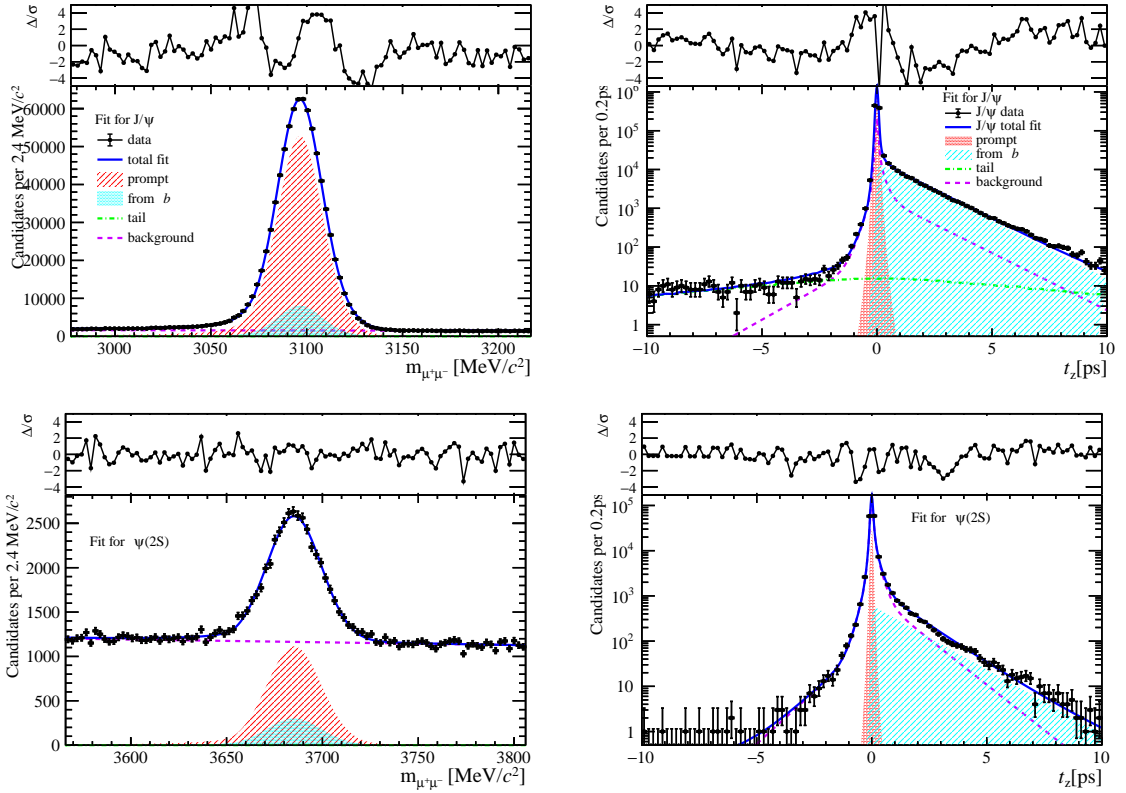


Figure 129: Fit results in  $2 \text{ GeV}/c < p_T < 4 \text{ GeV}/c$ ,  $2.8 < y < 3.5$  and  $8 \leq \text{nBackTracks} < 15$ .

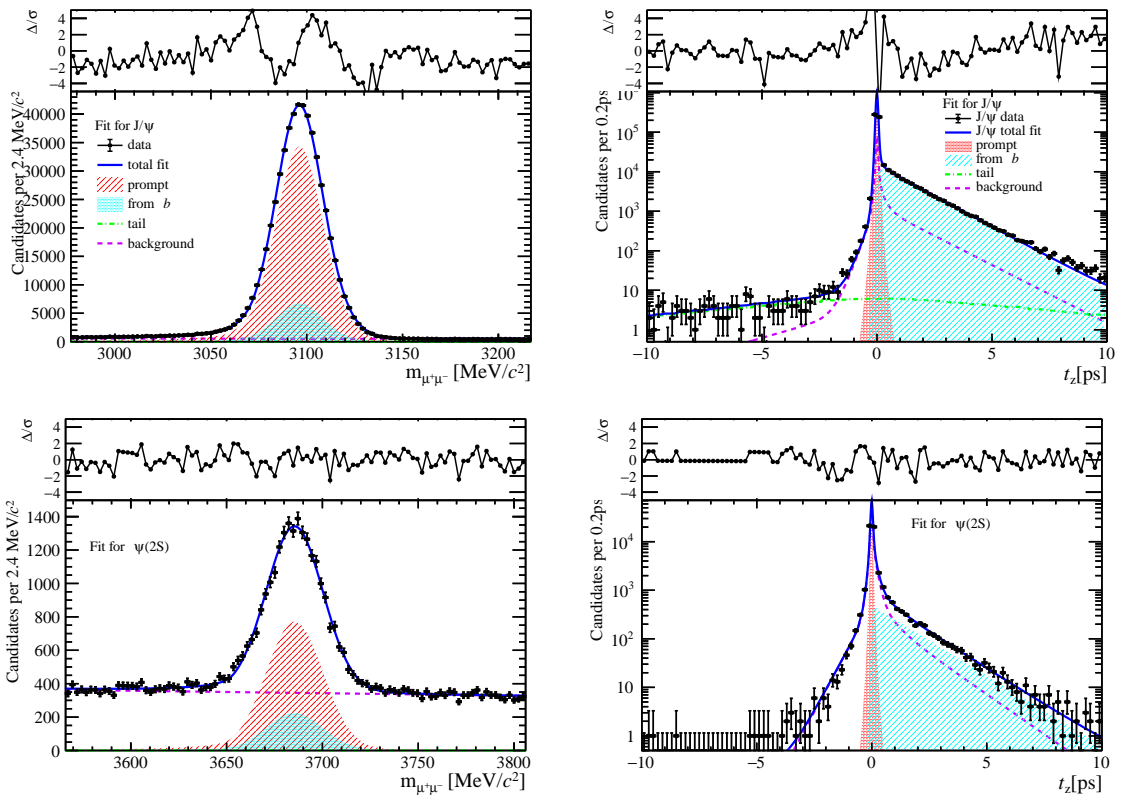


Figure 130: Fit results in  $4 \text{ GeV}/c < p_T < 6 \text{ GeV}/c$ ,  $2.8 < y < 3.5$  and  $8 \leq \text{nBackTracks} < 15$ .

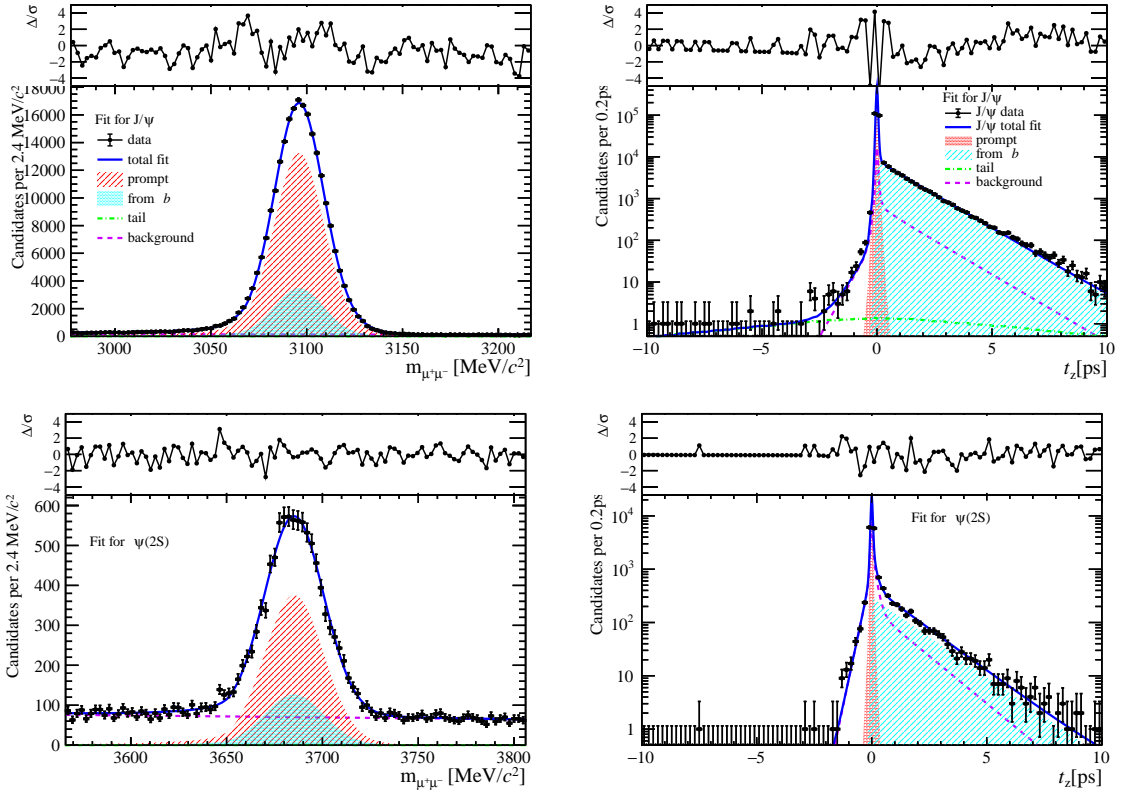


Figure 131: Fit results in  $6 \text{ GeV}/c < p_T < 8 \text{ GeV}/c$ ,  $2.8 < y < 3.5$  and  $8 \leq n\text{BackTracks} < 15$ .

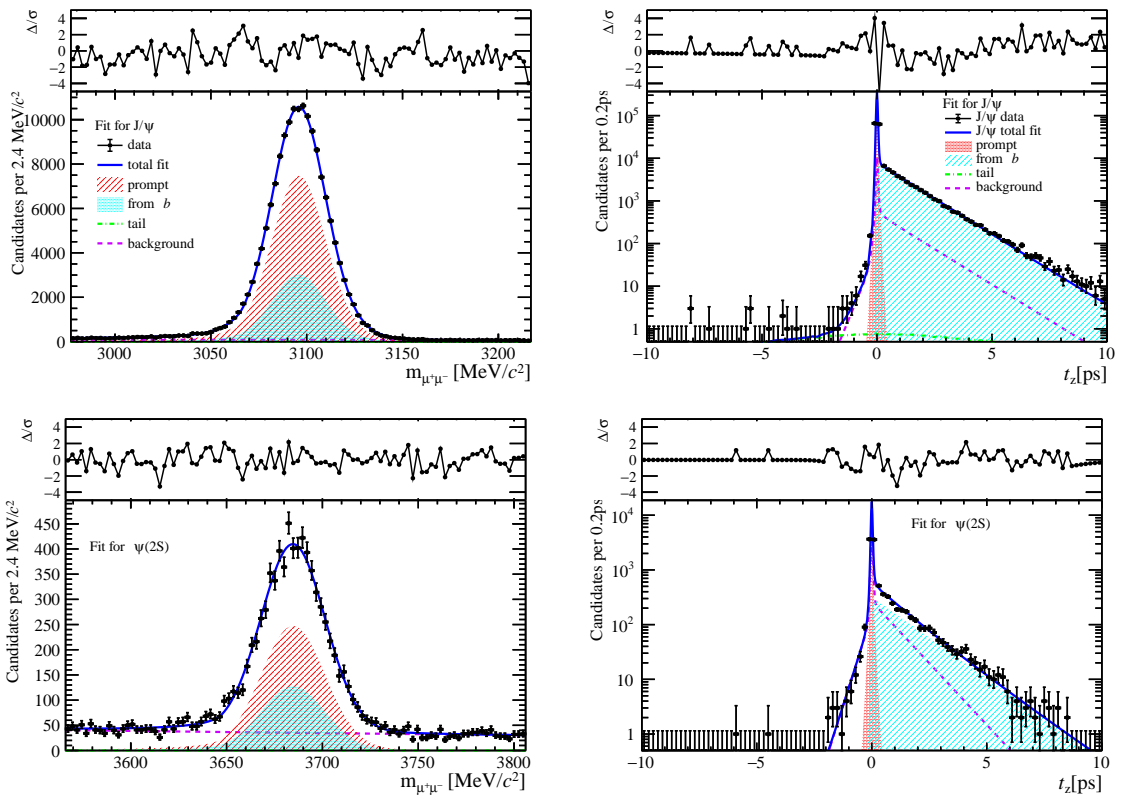


Figure 132: Fit results in  $8 \text{ GeV}/c < p_T < 20 \text{ GeV}/c$ ,  $2.8 < y < 3.5$  and  $8 \leq n\text{BackTracks} < 15$ .

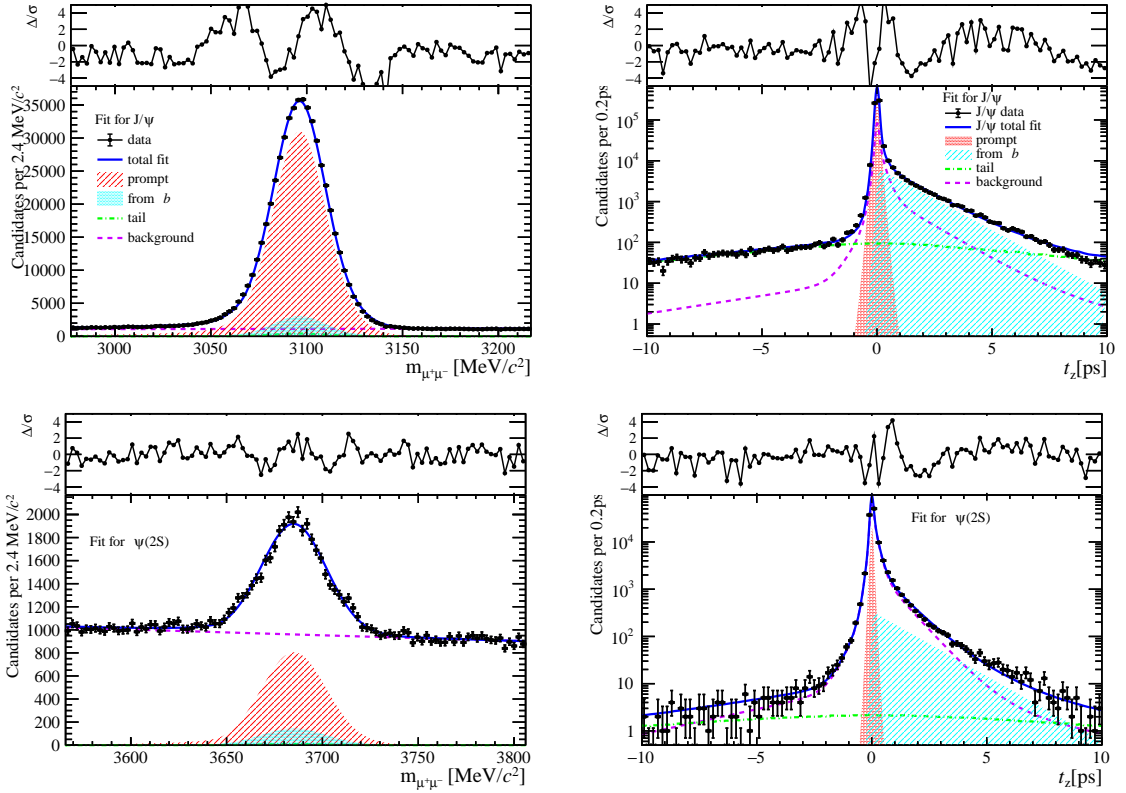


Figure 133: Fit results in  $0 \text{ GeV}/c < p_T < 2 \text{ GeV}/c$ ,  $3.5 < y < 4.5$  and  $8 \leq n\text{BackTracks} < 15$ .

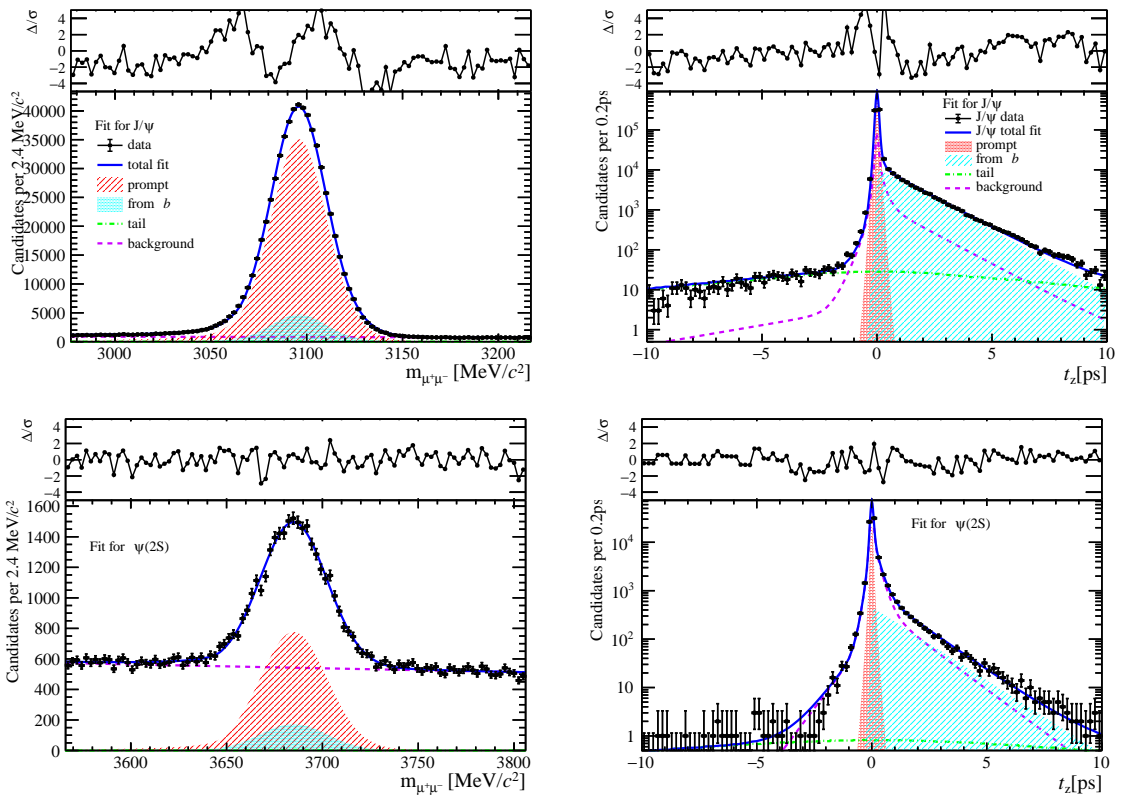


Figure 134: Fit results in  $2 \text{ GeV}/c < p_T < 4 \text{ GeV}/c$ ,  $3.5 < y < 4.5$  and  $8 \leq n\text{BackTracks} < 15$ .

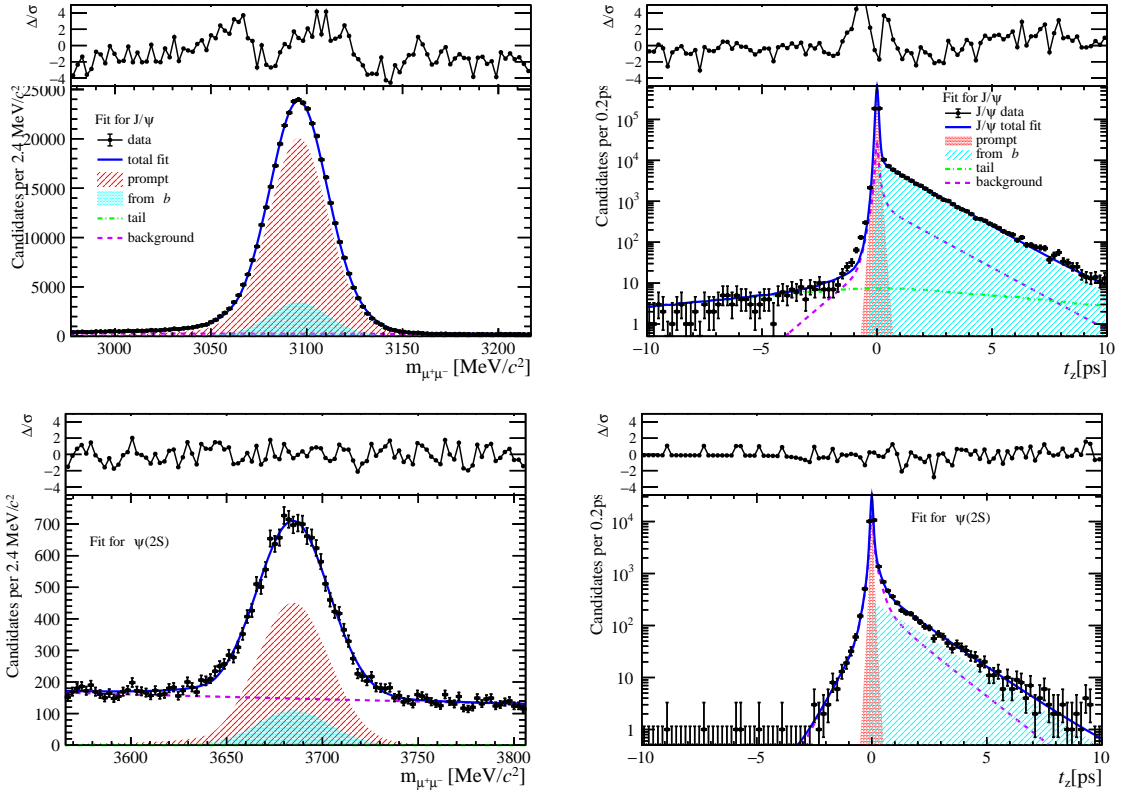


Figure 135: Fit results in  $4 \text{ GeV}/c < p_T < 6 \text{ GeV}/c$ ,  $3.5 < y < 4.5$  and  $8 \leq n\text{BackTracks} < 15$ .

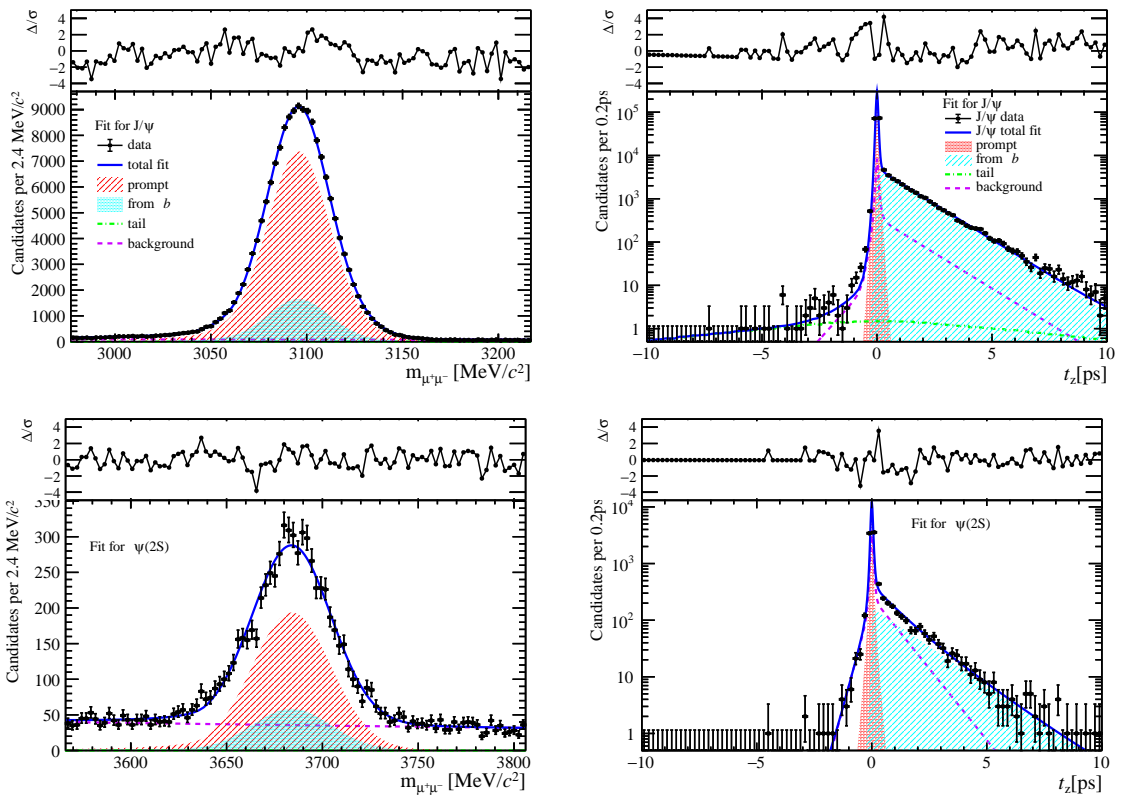


Figure 136: Fit results in  $6 \text{ GeV}/c < p_T < 8 \text{ GeV}/c$ ,  $3.5 < y < 4.5$  and  $8 \leq n\text{BackTracks} < 15$ .

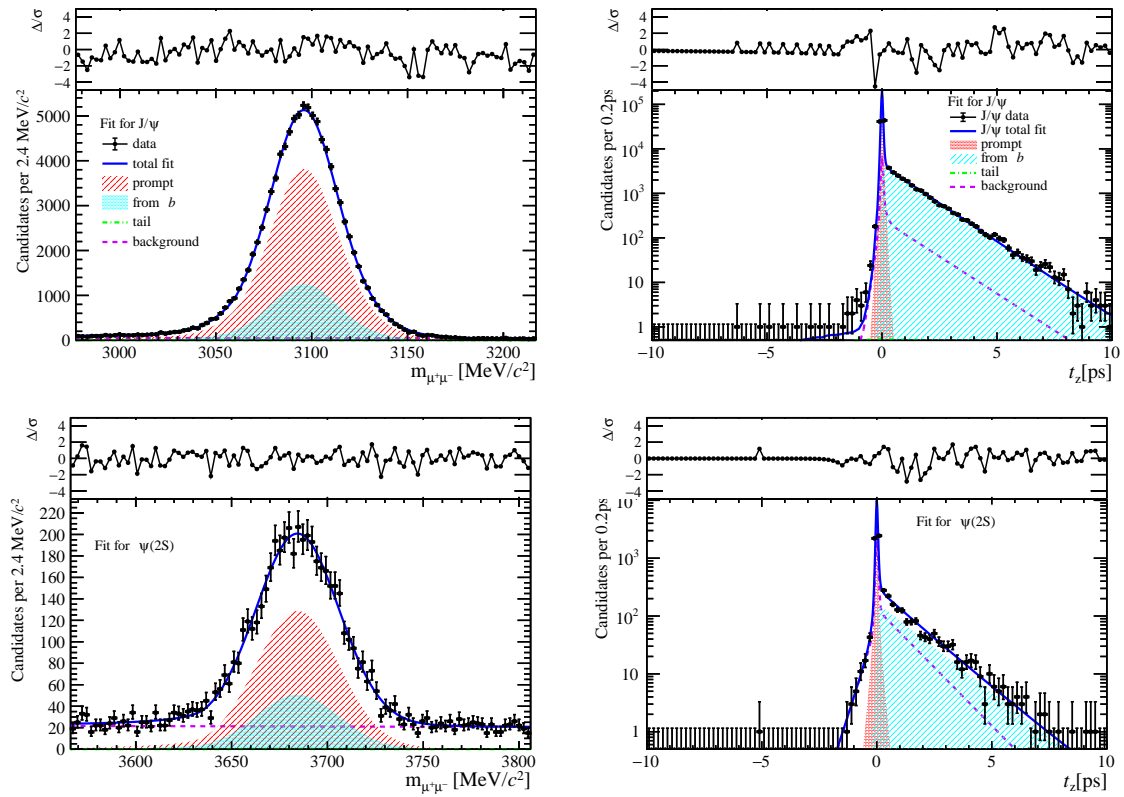


Figure 137: Fit results in  $8 \text{ GeV}/c < p_T < 20 \text{ GeV}/c$ ,  $3.5 < y < 4.5$  and  $8 \leq \text{nBackTracks} < 15$ .

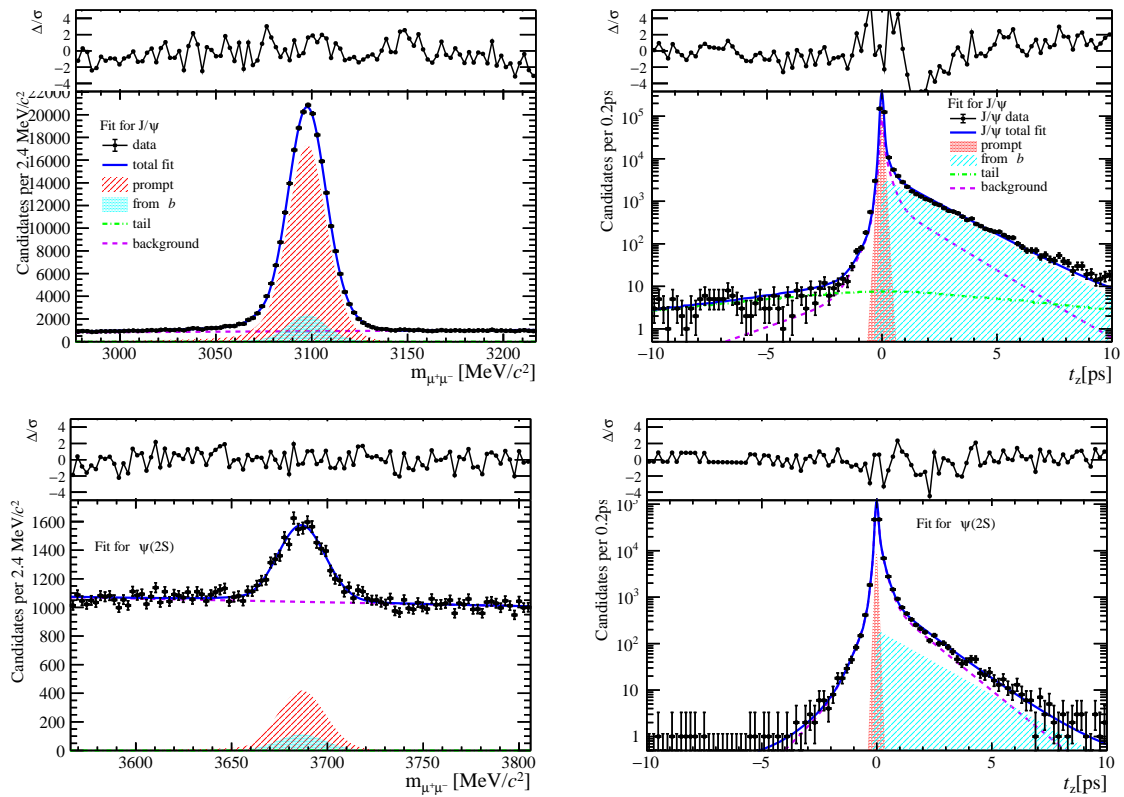


Figure 138: Fit results in  $0 \text{ GeV}/c < p_T < 2 \text{ GeV}/c$ ,  $2.0 < y < 2.8$  and  $15 \leq \text{nBackTracks} < 22$ .

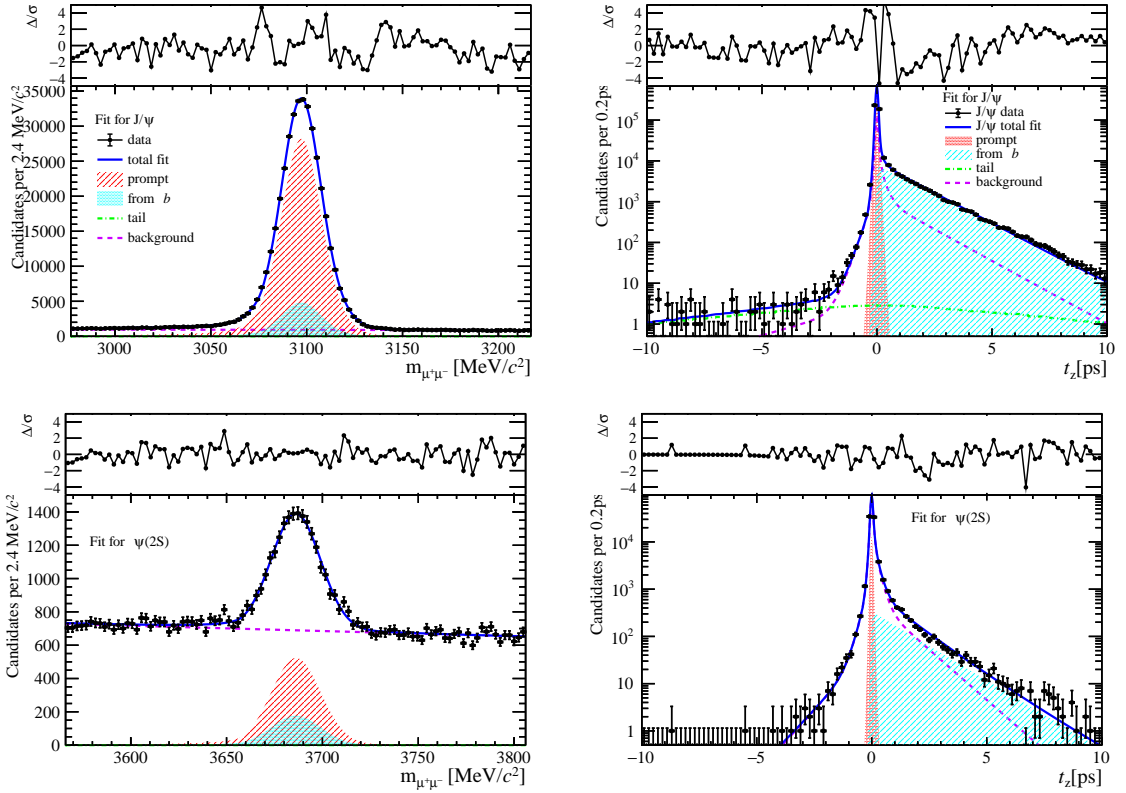


Figure 139: Fit results in  $2 \text{ GeV}/c < p_T < 4 \text{ GeV}/c$ ,  $2.0 < y < 2.8$  and  $15 \leq \text{nBackTracks} < 22$ .

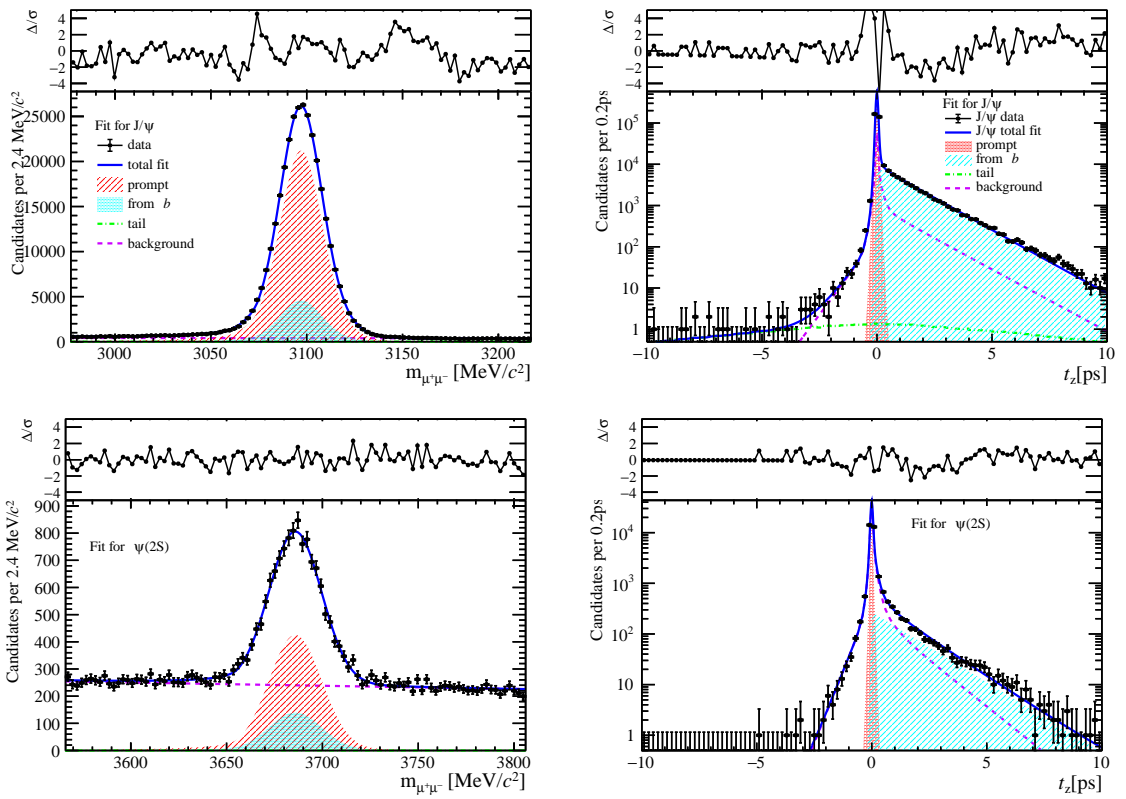


Figure 140: Fit results in  $4 \text{ GeV}/c < p_T < 6 \text{ GeV}/c$ ,  $2.0 < y < 2.8$  and  $15 \leq \text{nBackTracks} < 22$ .

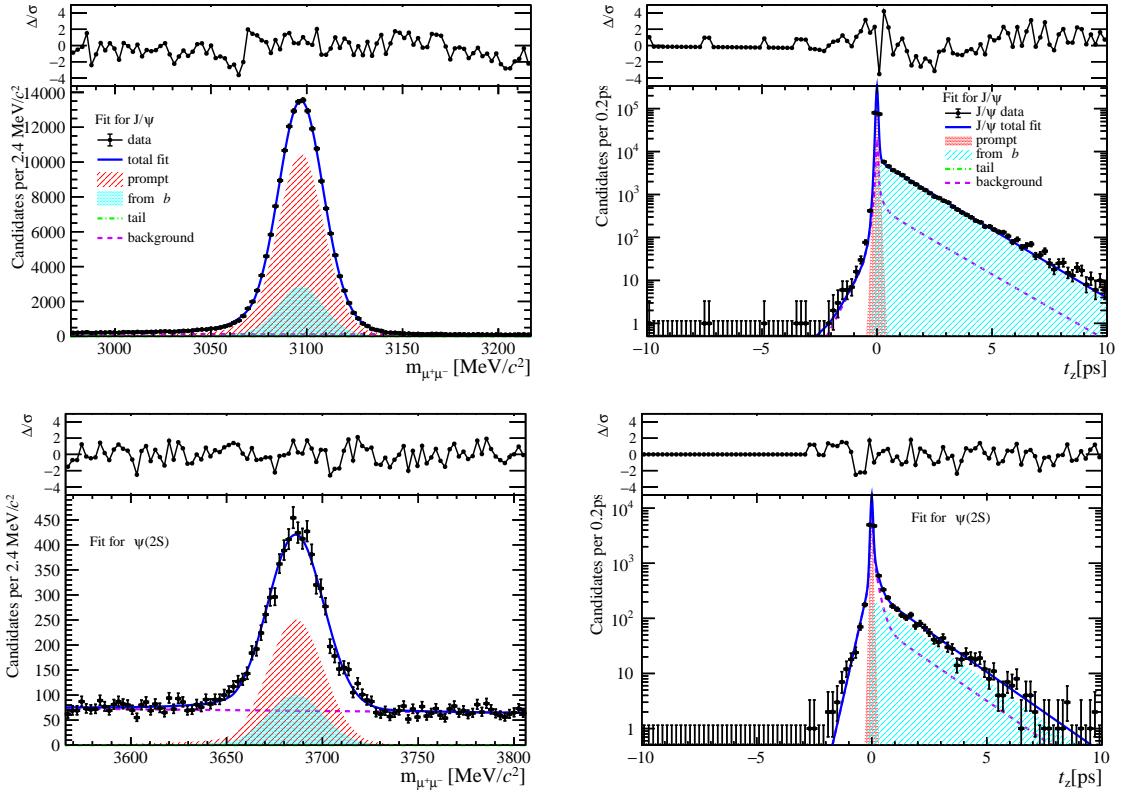


Figure 141: Fit results in  $6 \text{ GeV}/c < p_T < 8 \text{ GeV}/c$ ,  $2.0 < y < 2.8$  and  $15 \leq n\text{BackTracks} < 22$ .

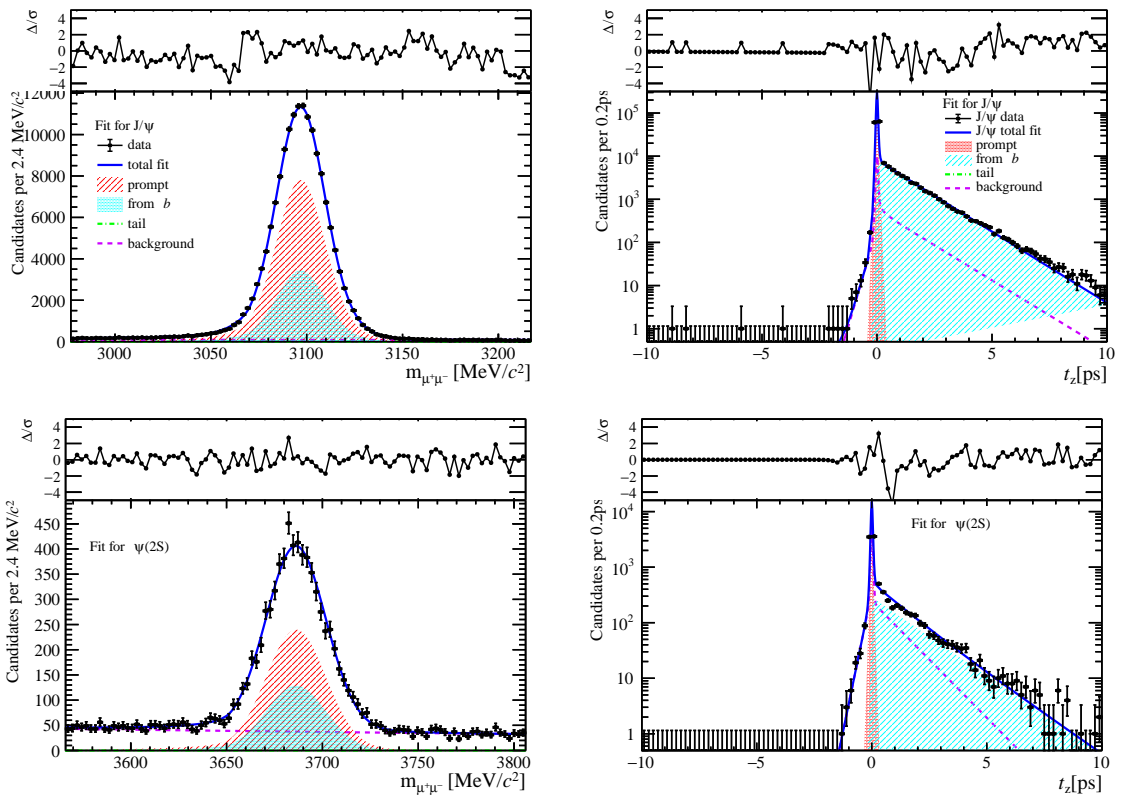


Figure 142: Fit results in  $8 \text{ GeV}/c < p_T < 20 \text{ GeV}/c$ ,  $2.0 < y < 2.8$  and  $15 \leq n\text{BackTracks} < 22$ .

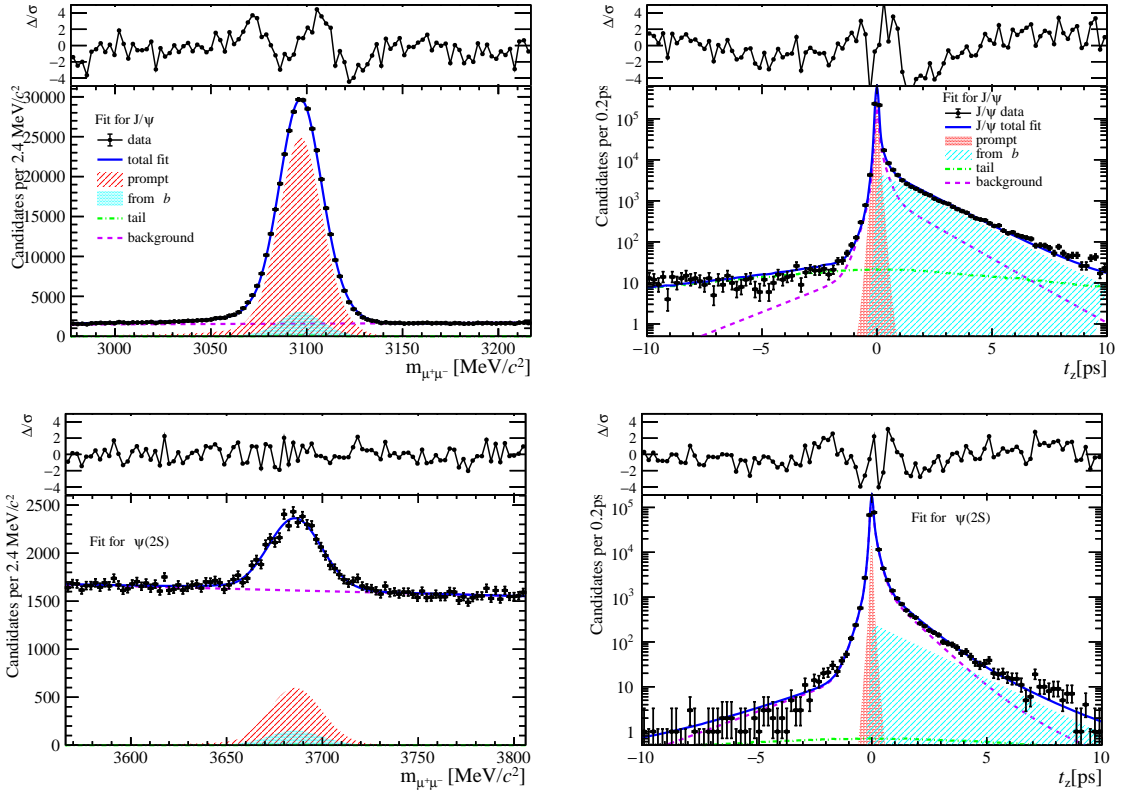


Figure 143: Fit results in  $0 \text{ GeV}/c < p_T < 2 \text{ GeV}/c$ ,  $2.8 < y < 3.5$  and  $15 \leq \text{nBackTracks} < 22$ .

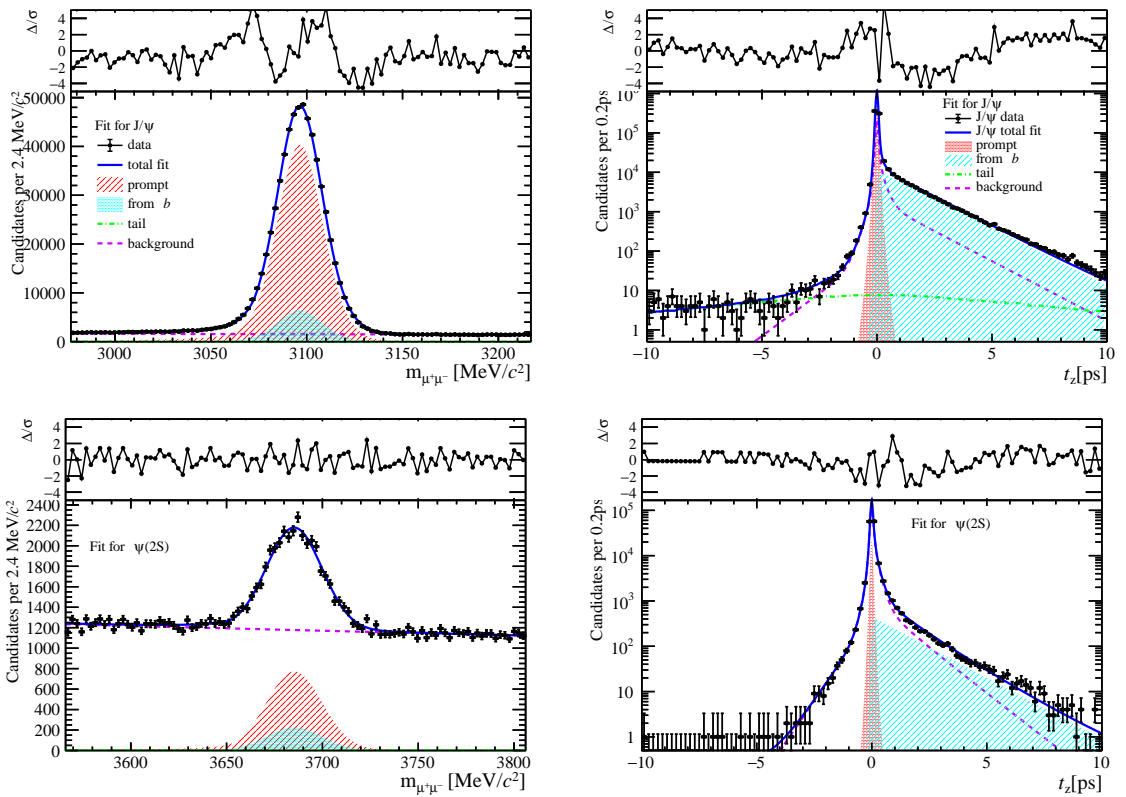


Figure 144: Fit results in  $2 \text{ GeV}/c < p_T < 4 \text{ GeV}/c$ ,  $2.8 < y < 3.5$  and  $15 \leq \text{nBackTracks} < 22$ .

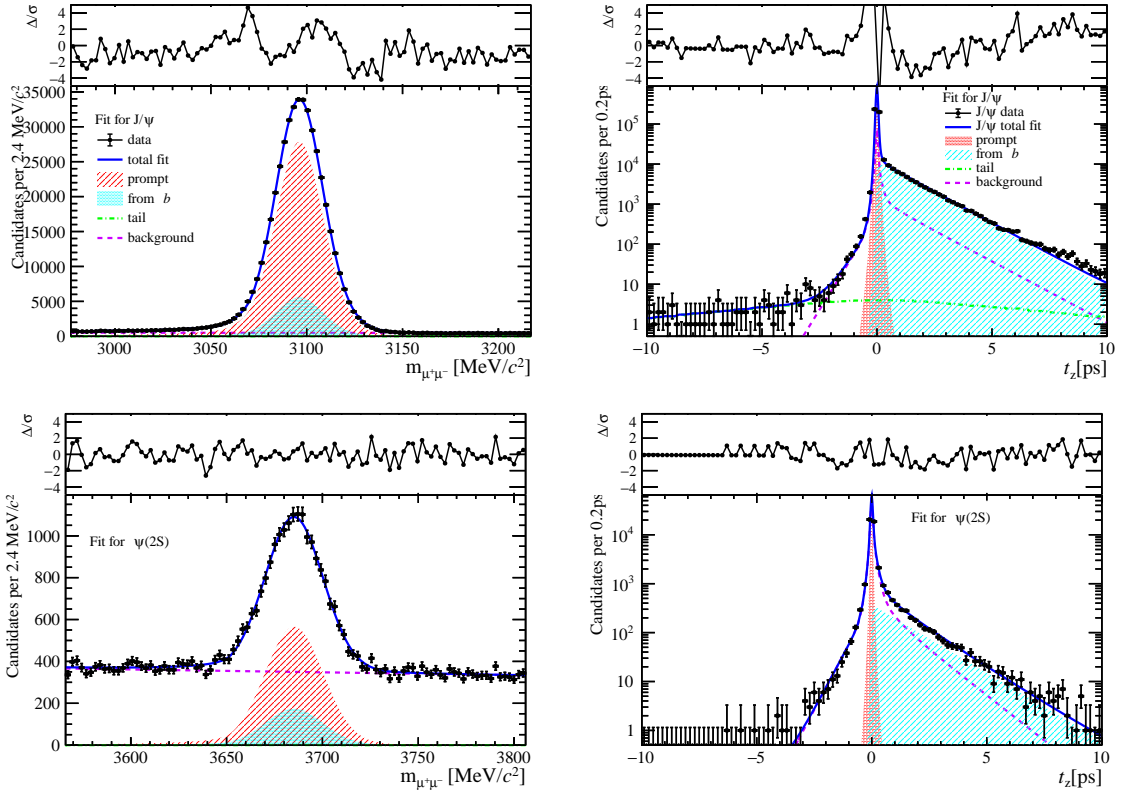


Figure 145: Fit results in  $4 \text{ GeV}/c < p_T < 6 \text{ GeV}/c$ ,  $2.8 < y < 3.5$  and  $15 \leq \text{nBackTracks} < 22$ .

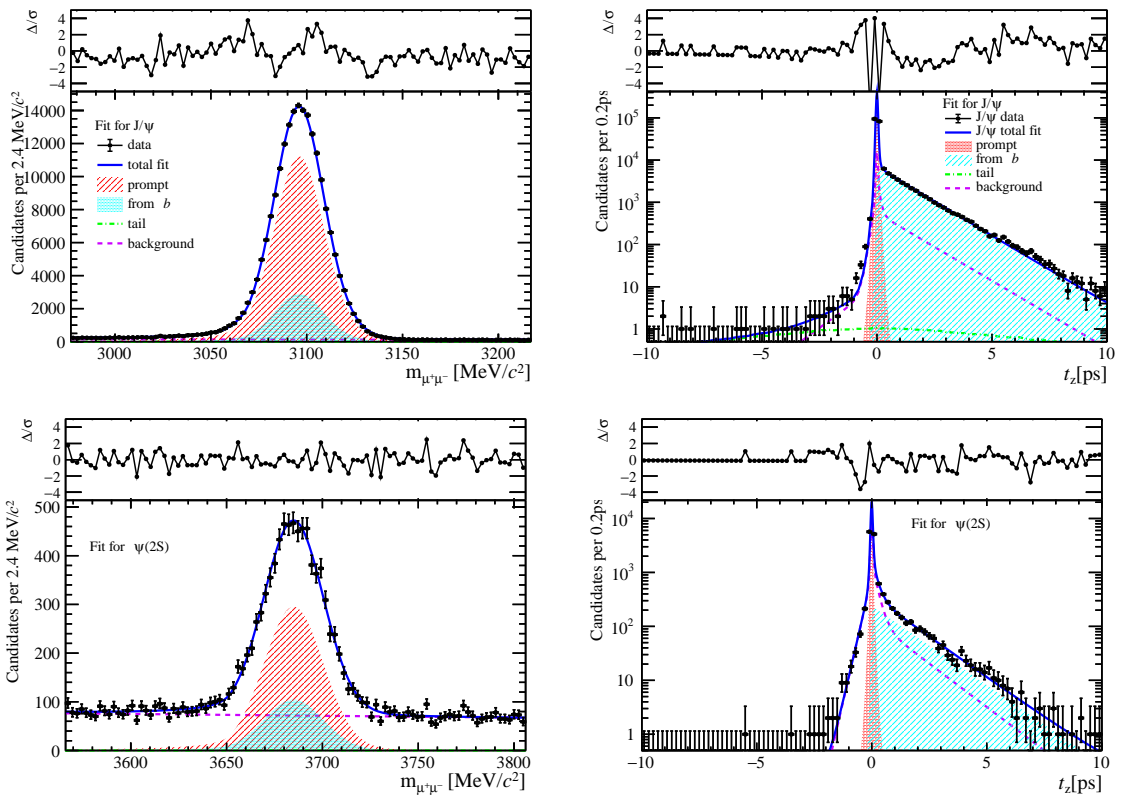


Figure 146: Fit results in  $6 \text{ GeV}/c < p_T < 8 \text{ GeV}/c$ ,  $2.8 < y < 3.5$  and  $15 \leq \text{nBackTracks} < 22$ .

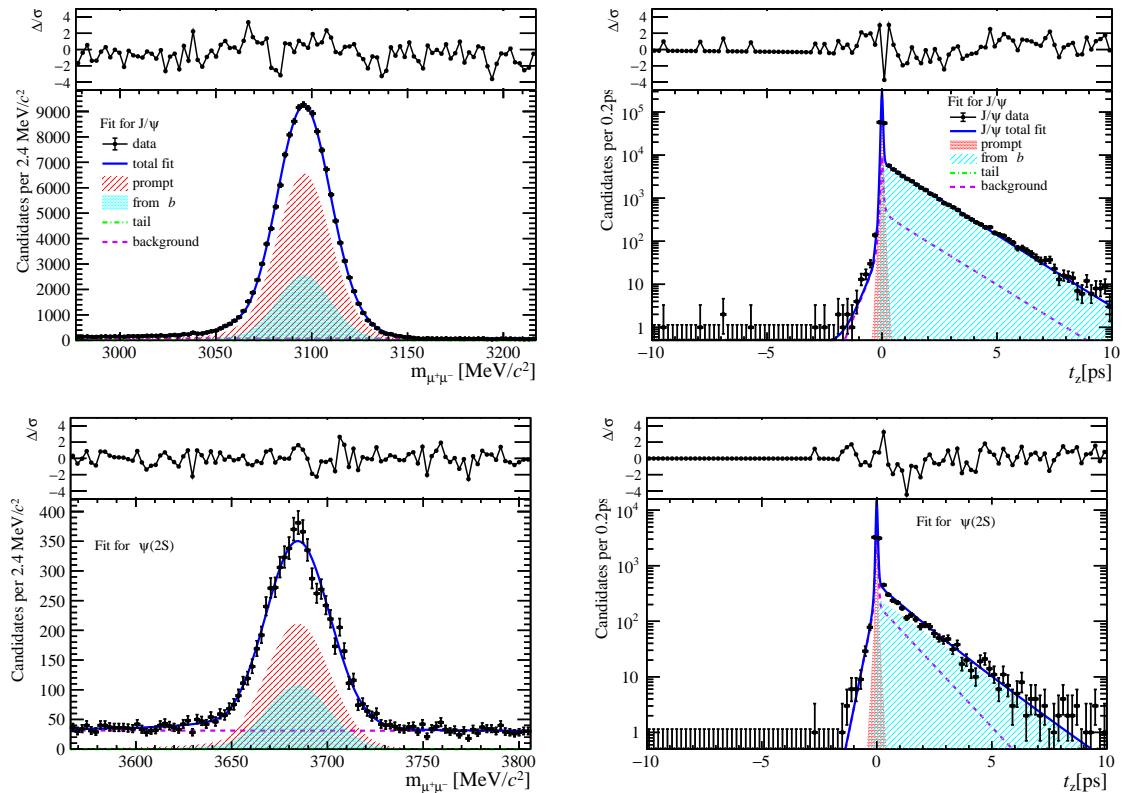


Figure 147: Fit results in  $8 \text{ GeV}/c < p_T < 20 \text{ GeV}/c$ ,  $2.8 < y < 3.5$  and  $15 \leq \text{nBackTracks} < 22$ .

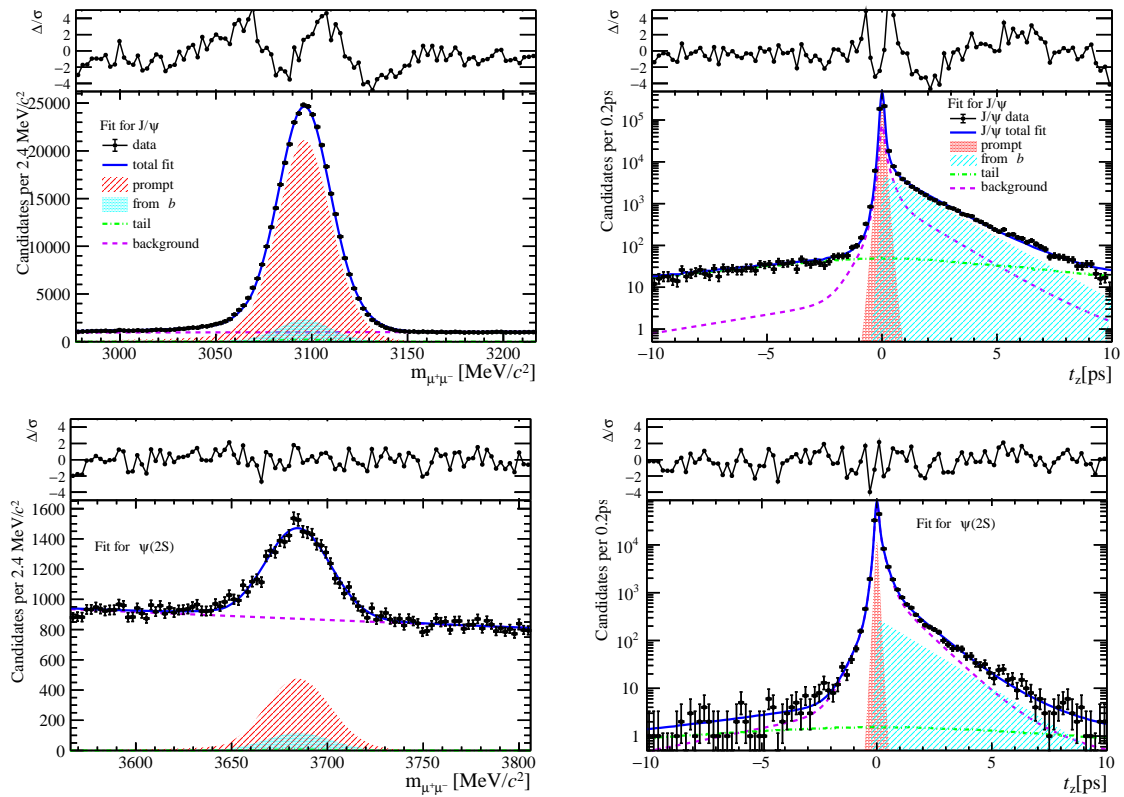


Figure 148: Fit results in  $0 \text{ GeV}/c < p_T < 2 \text{ GeV}/c$ ,  $3.5 < y < 4.5$  and  $15 \leq \text{nBackTracks} < 22$ .

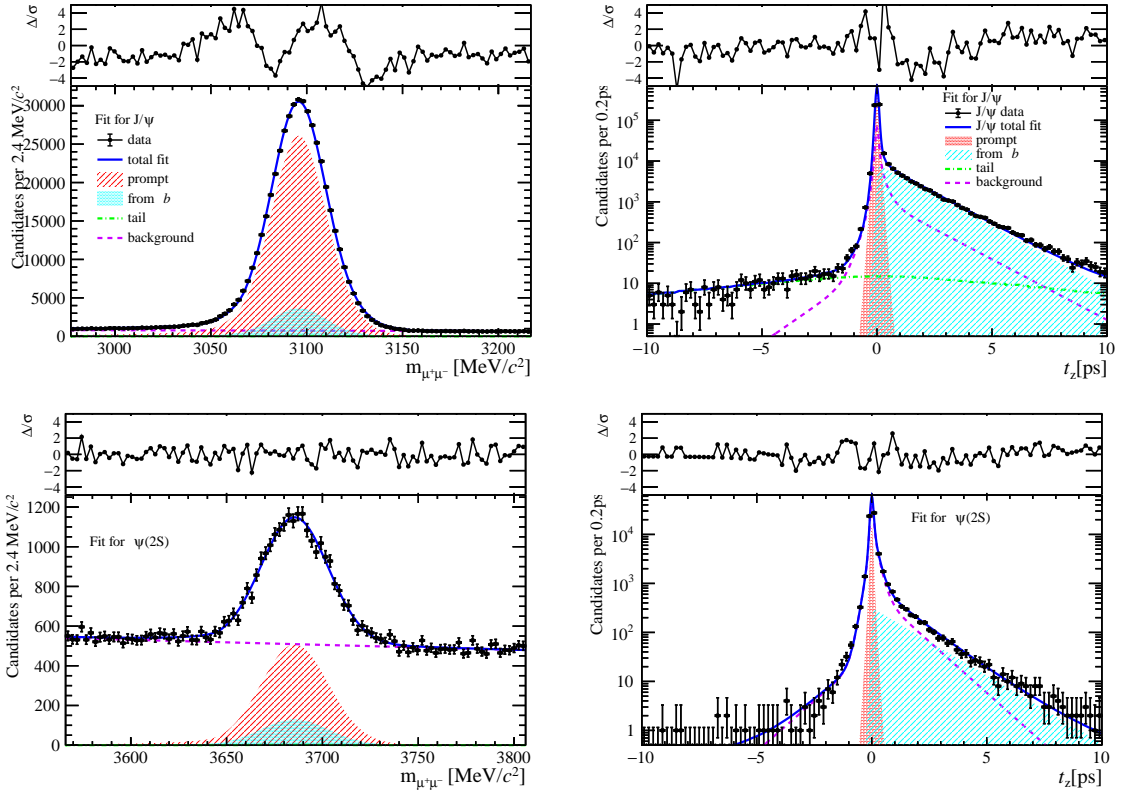


Figure 149: Fit results in  $2 \text{ GeV}/c < p_T < 4 \text{ GeV}/c$ ,  $3.5 < y < 4.5$  and  $15 \leq \text{nBackTracks} < 22$ .

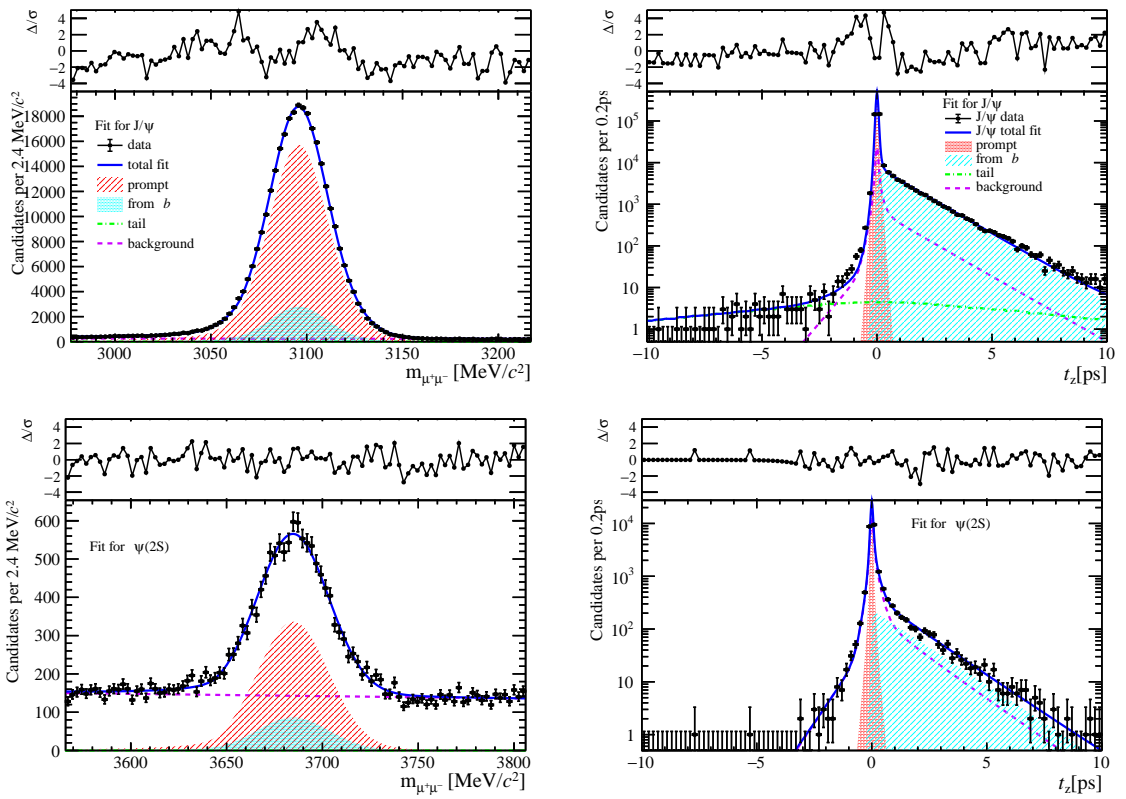


Figure 150: Fit results in  $4 \text{ GeV}/c < p_T < 6 \text{ GeV}/c$ ,  $3.5 < y < 4.5$  and  $15 \leq \text{nBackTracks} < 22$ .

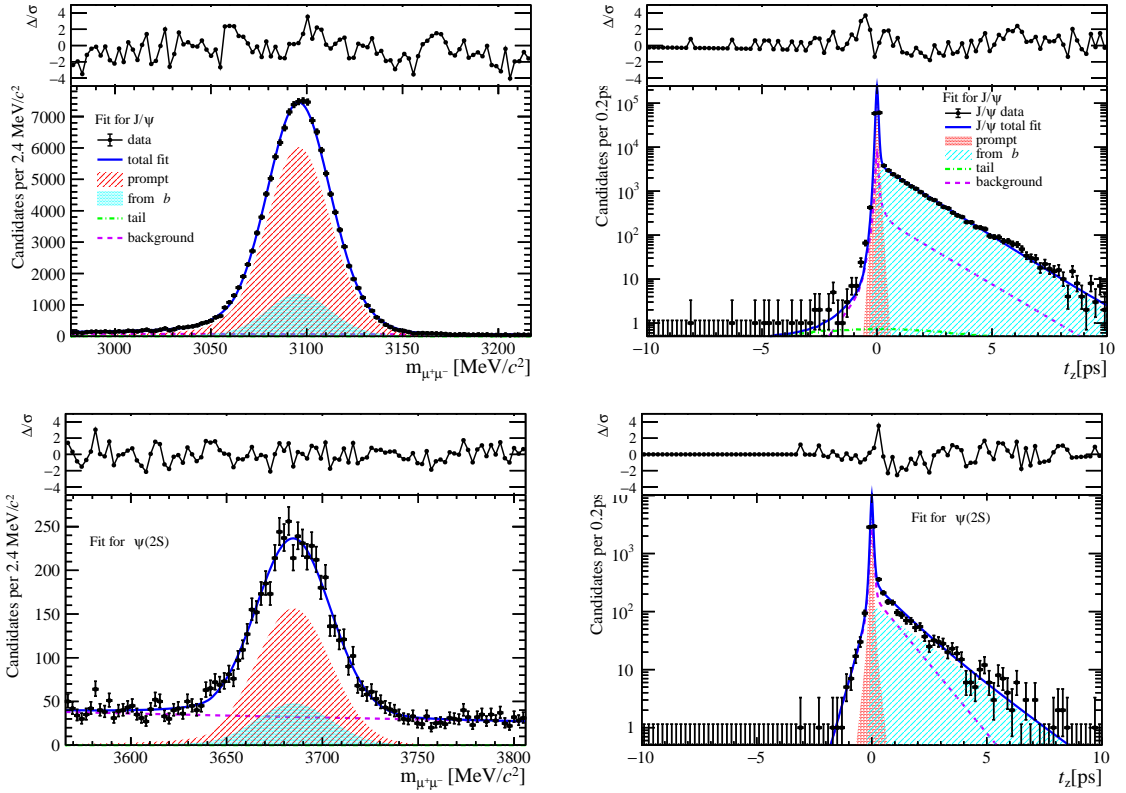


Figure 151: Fit results in  $6 \text{ GeV}/c < p_T < 8 \text{ GeV}/c$ ,  $3.5 < y < 4.5$  and  $15 \leq \text{nBackTracks} < 22$ .

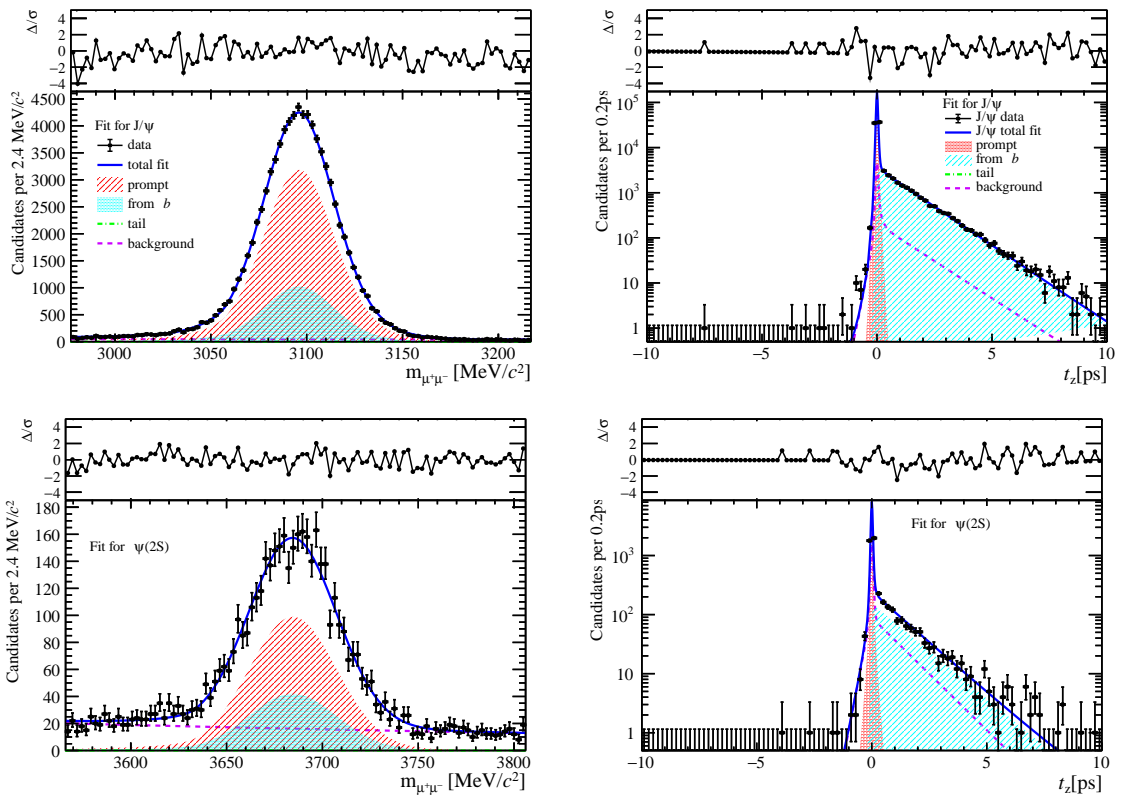


Figure 152: Fit results in  $8 \text{ GeV}/c < p_T < 20 \text{ GeV}/c$ ,  $3.5 < y < 4.5$  and  $15 \leq \text{nBackTracks} < 22$ .

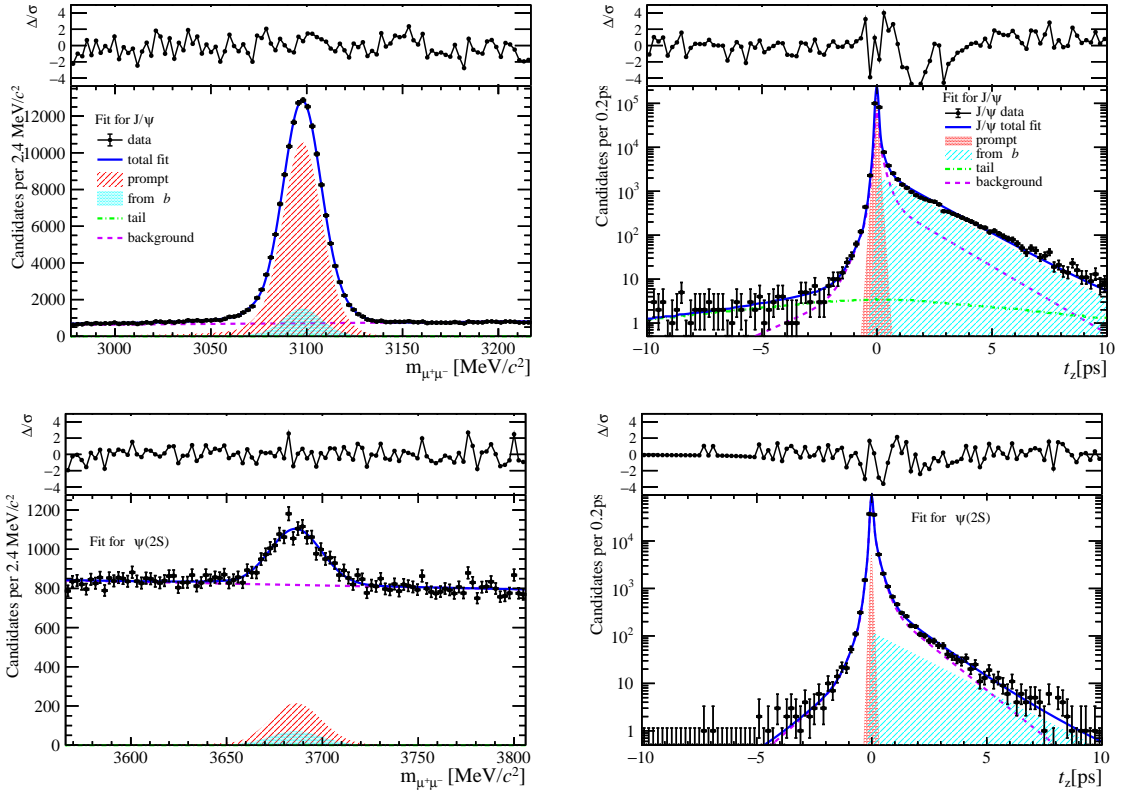


Figure 153: Fit results in  $0 \text{ GeV}/c < p_T < 2 \text{ GeV}/c$ ,  $2.0 < y < 2.8$  and  $22 \leq n\text{BackTracks} < 30$ .

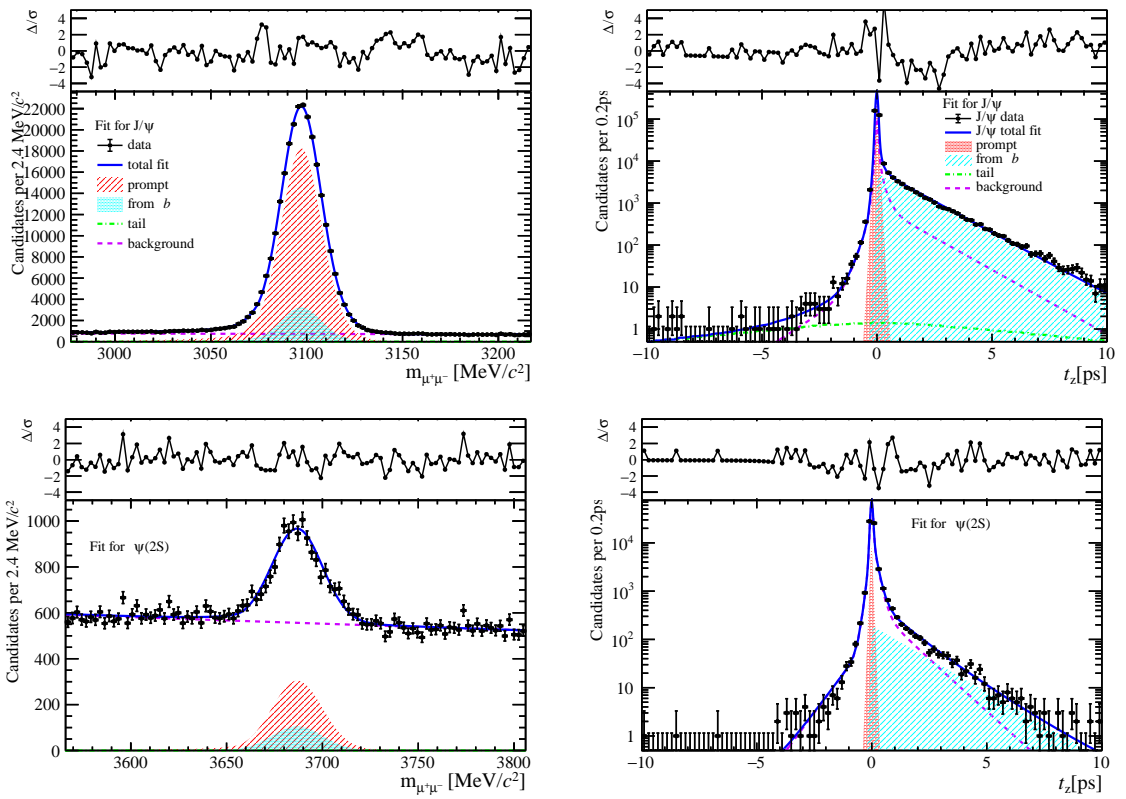


Figure 154: Fit results in  $2 \text{ GeV}/c < p_T < 4 \text{ GeV}/c$ ,  $2.0 < y < 2.8$  and  $22 \leq n\text{BackTracks} < 30$ .

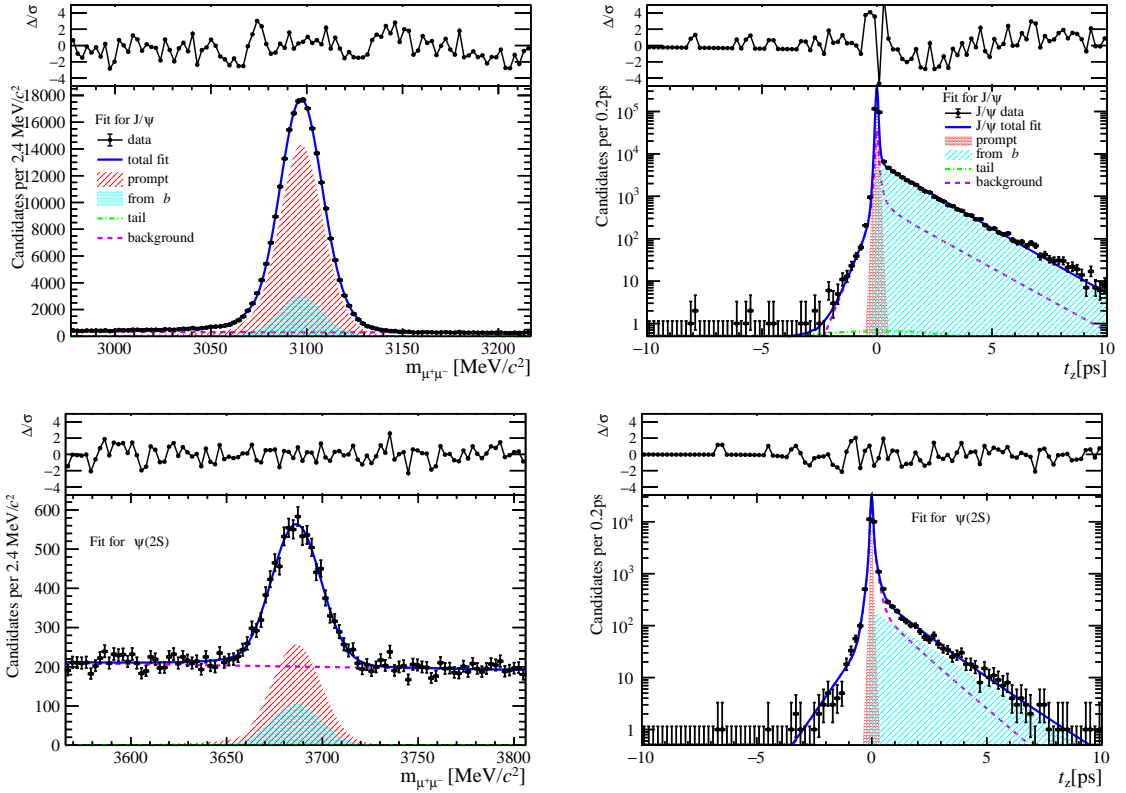


Figure 155: Fit results in  $4 \text{ GeV}/c < p_T < 6 \text{ GeV}/c$ ,  $2.0 < y < 2.8$  and  $22 \leq \text{nBackTracks} < 30$ .

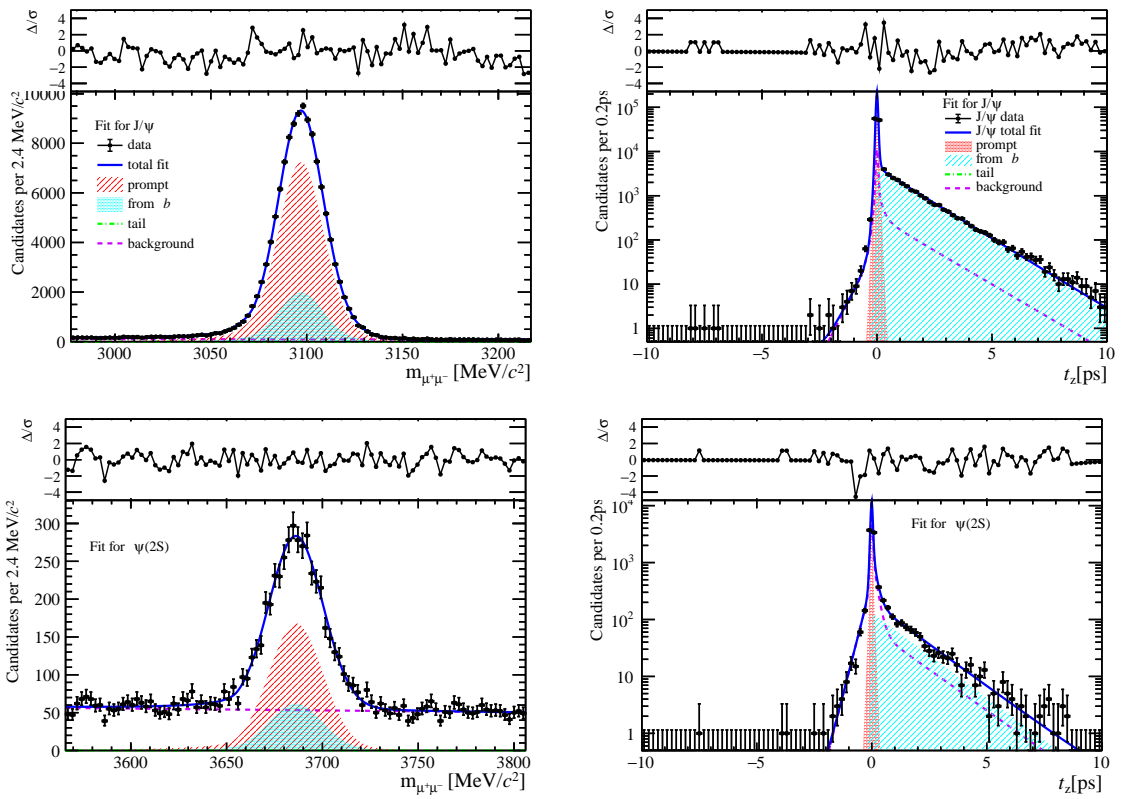


Figure 156: Fit results in  $6 \text{ GeV}/c < p_T < 8 \text{ GeV}/c$ ,  $2.0 < y < 2.8$  and  $22 \leq \text{nBackTracks} < 30$ .

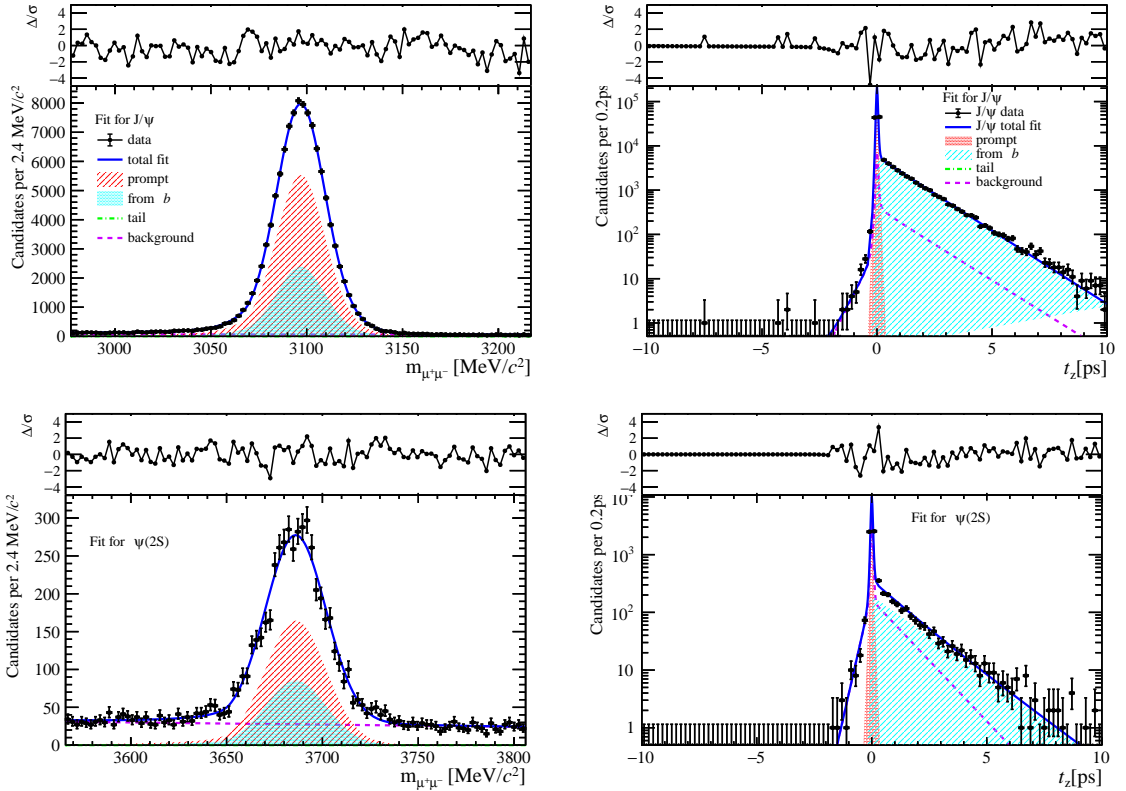


Figure 157: Fit results in  $8 \text{ GeV}/c < p_T < 20 \text{ GeV}/c$ ,  $2.0 < y < 2.8$  and  $22 \leq \text{nBackTracks} < 30$ .

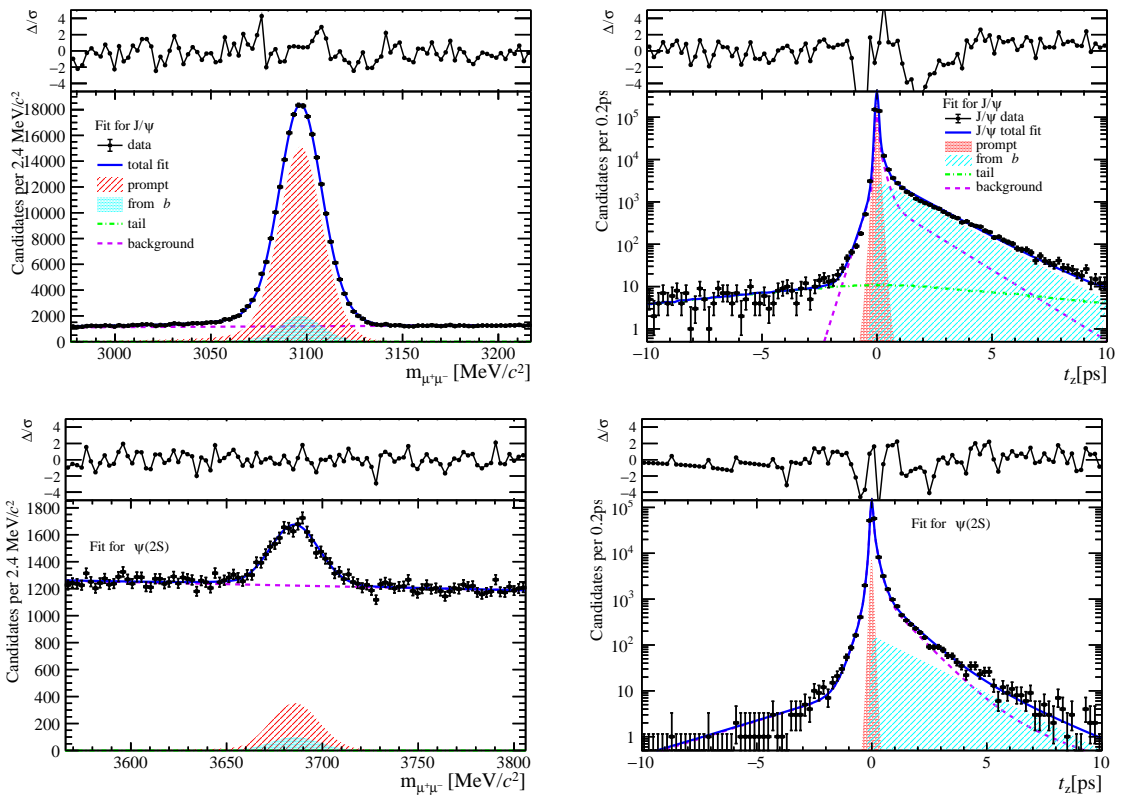


Figure 158: Fit results in  $0 \text{ GeV}/c < p_T < 2 \text{ GeV}/c$ ,  $2.8 < y < 3.5$  and  $22 \leq \text{nBackTracks} < 30$ .

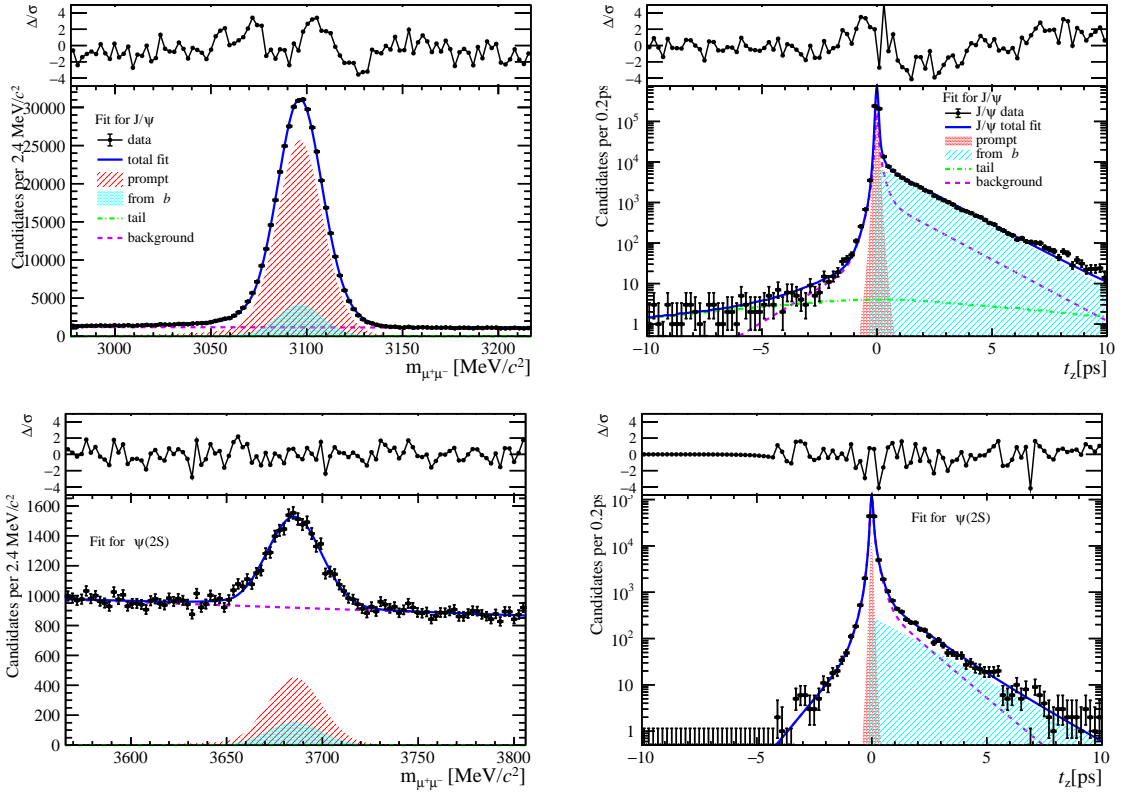


Figure 159: Fit results in  $2 \text{ GeV}/c < p_T < 4 \text{ GeV}/c$ ,  $2.8 < y < 3.5$  and  $22 \leq \text{nBackTracks} < 30$ .

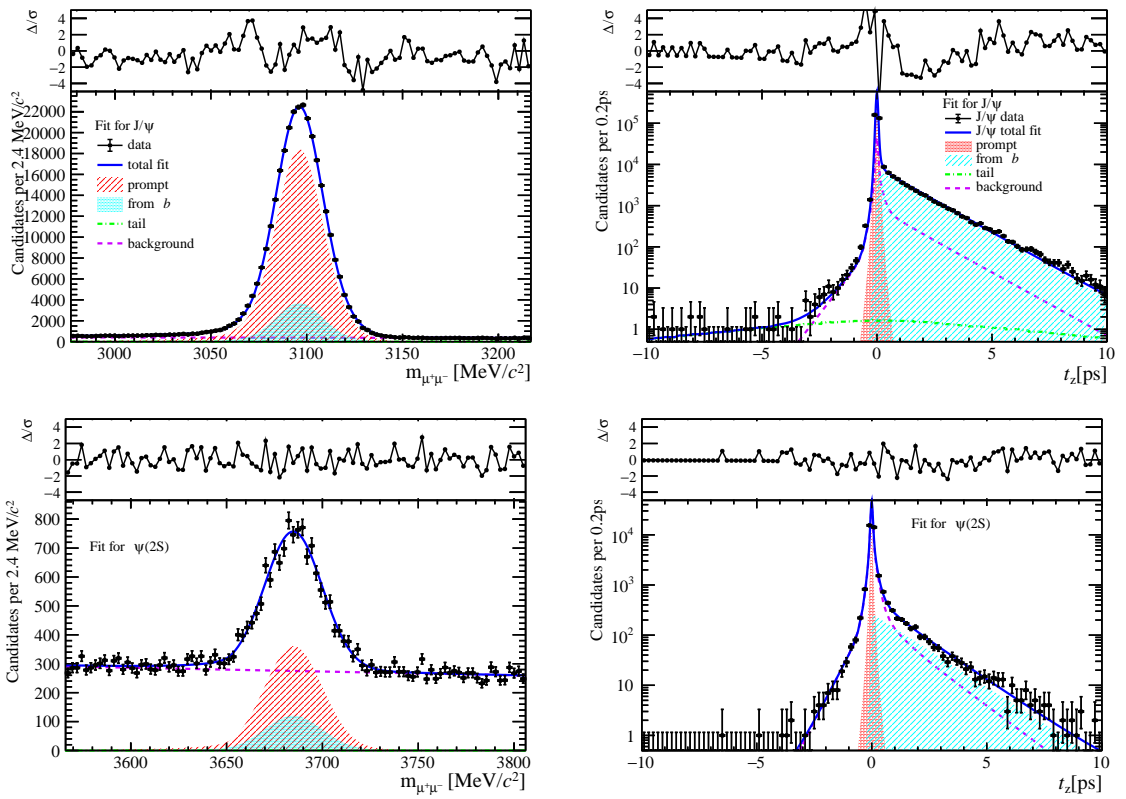


Figure 160: Fit results in  $4 \text{ GeV}/c < p_T < 6 \text{ GeV}/c$ ,  $2.8 < y < 3.5$  and  $22 \leq \text{nBackTracks} < 30$ .

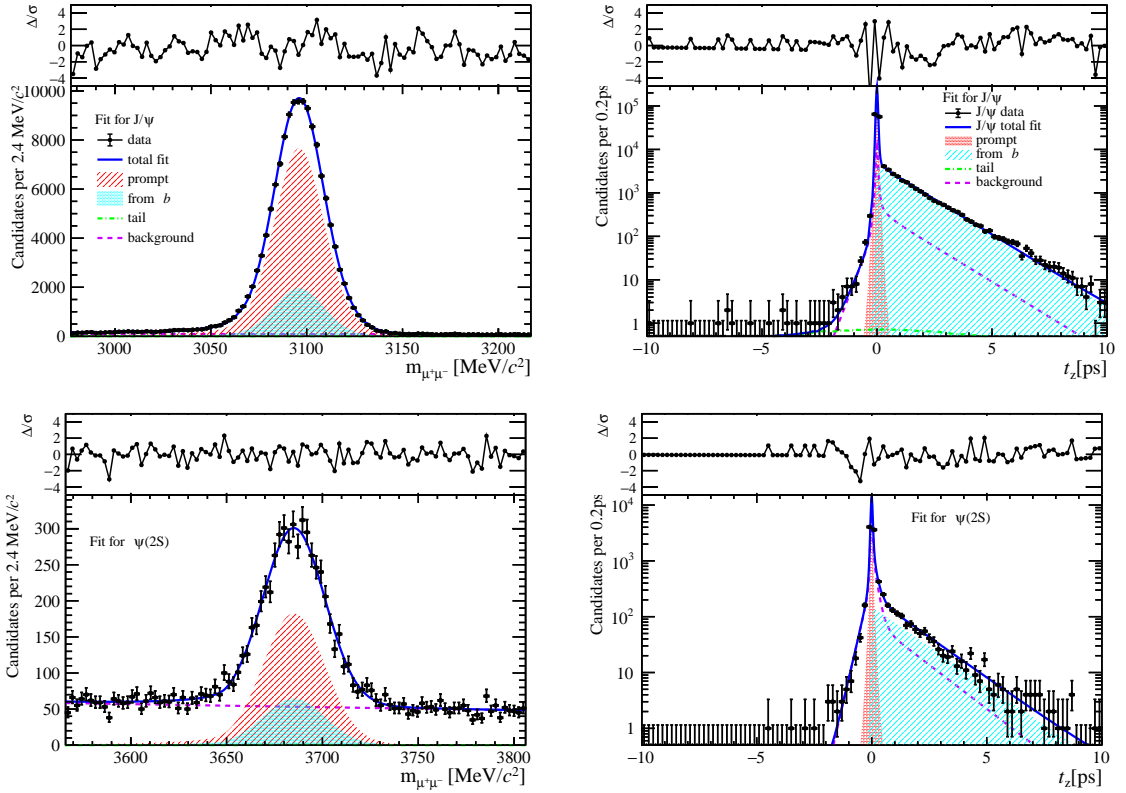


Figure 161: Fit results in  $6 \text{ GeV}/c < p_T < 8 \text{ GeV}/c$ ,  $2.8 < y < 3.5$  and  $22 \leq \text{nBackTracks} < 30$ .

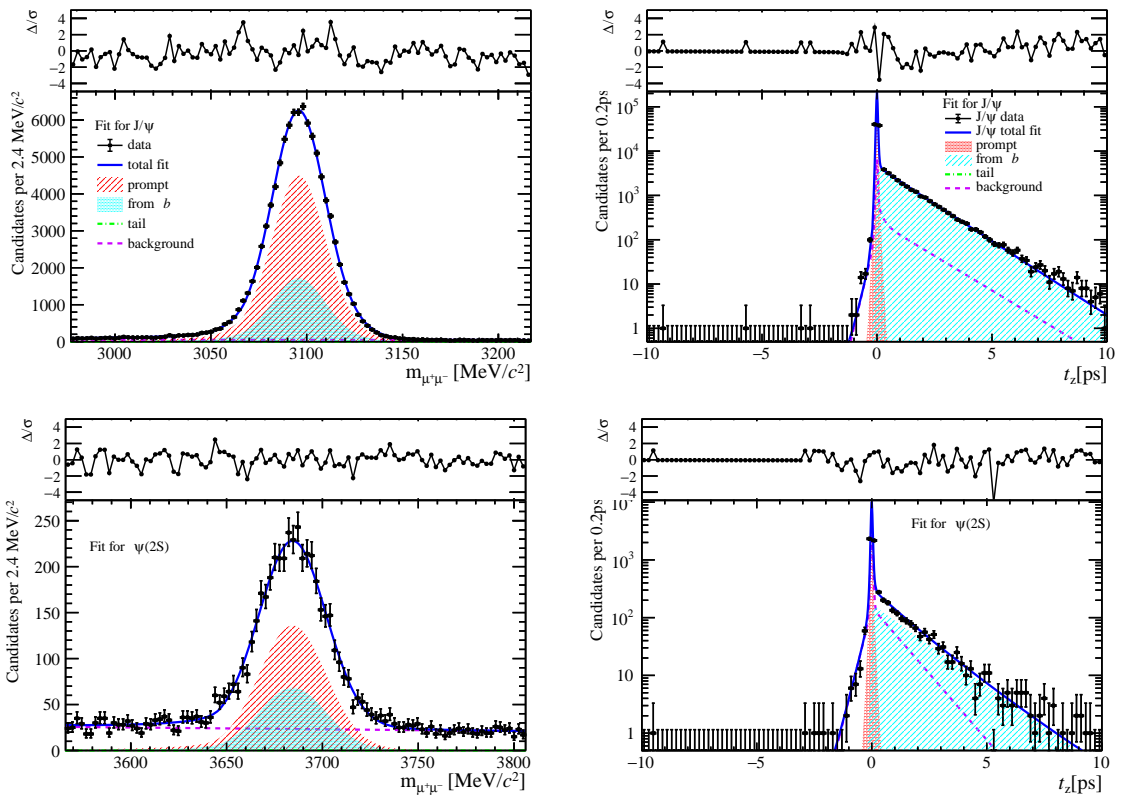


Figure 162: Fit results in  $8 \text{ GeV}/c < p_T < 20 \text{ GeV}/c$ ,  $2.8 < y < 3.5$  and  $22 \leq \text{nBackTracks} < 30$ .

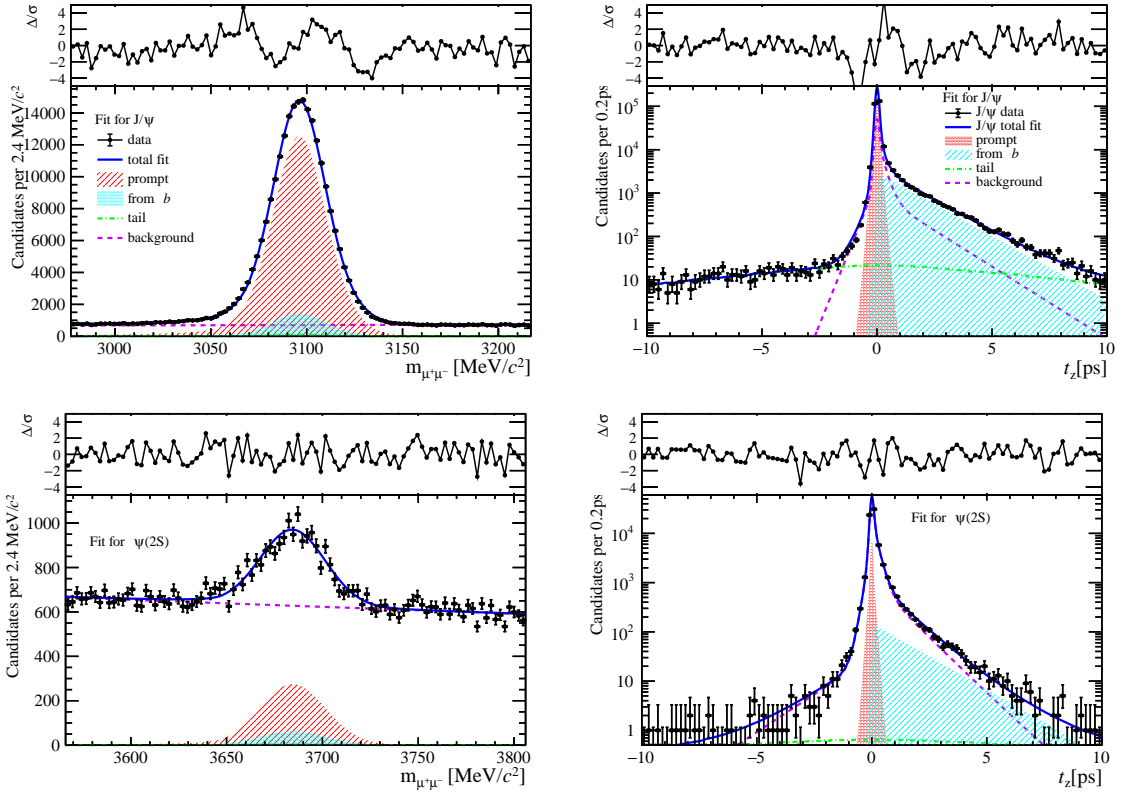


Figure 163: Fit results in  $0 \text{ GeV}/c < p_T < 2 \text{ GeV}/c$ ,  $3.5 < y < 4.5$  and  $22 \leq \text{nBackTracks} < 30$ .

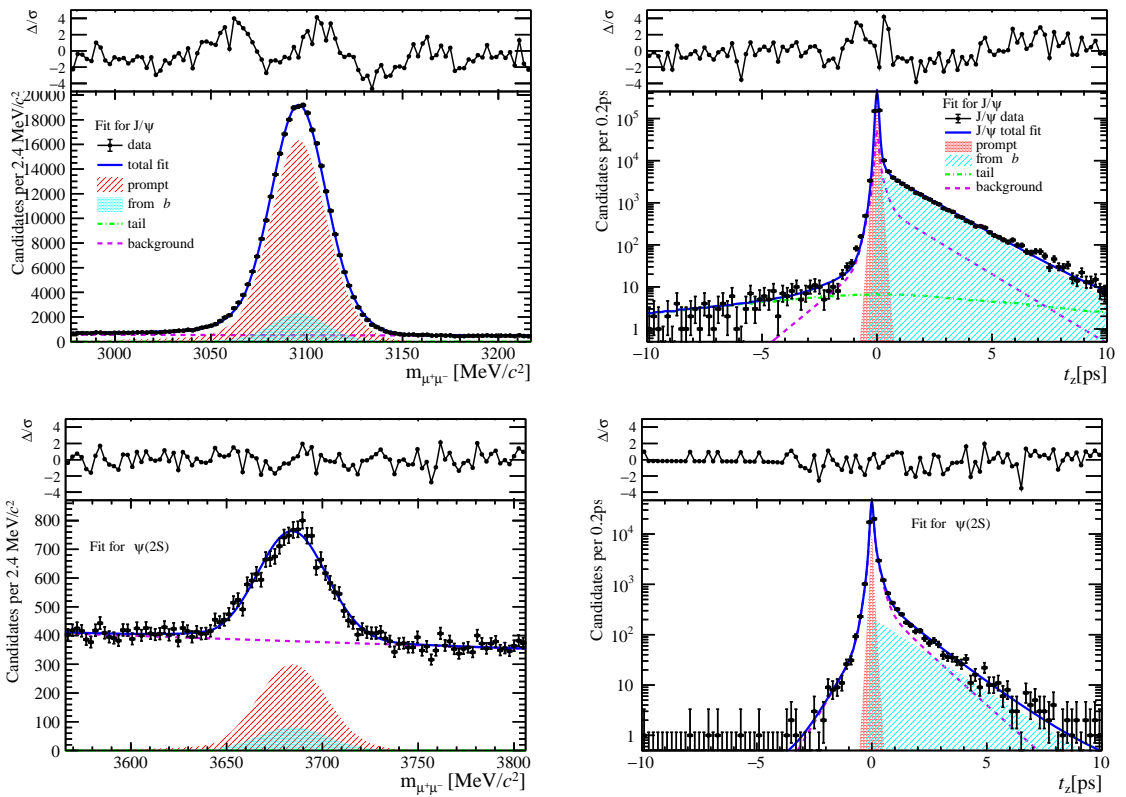


Figure 164: Fit results in  $2 \text{ GeV}/c < p_T < 4 \text{ GeV}/c$ ,  $3.5 < y < 4.5$  and  $22 \leq \text{nBackTracks} < 30$ .

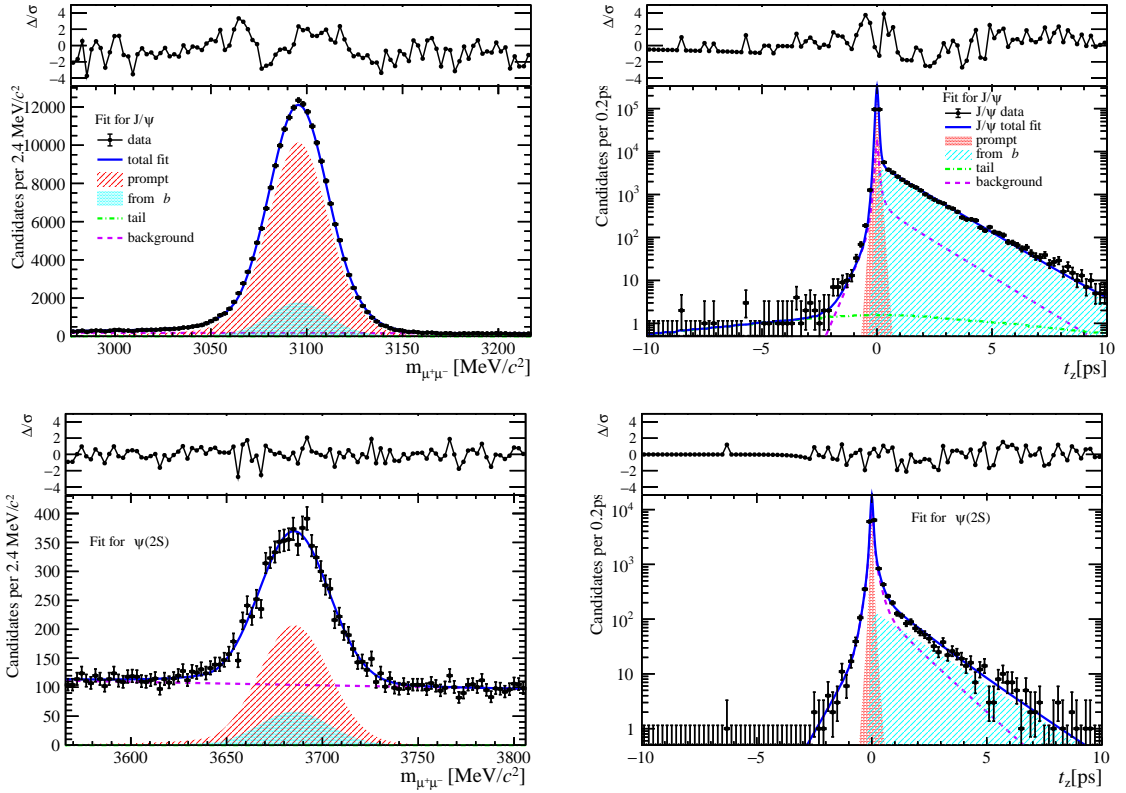


Figure 165: Fit results in  $4 \text{ GeV}/c < p_T < 6 \text{ GeV}/c$ ,  $3.5 < y < 4.5$  and  $22 \leq \text{nBackTracks} < 30$ .

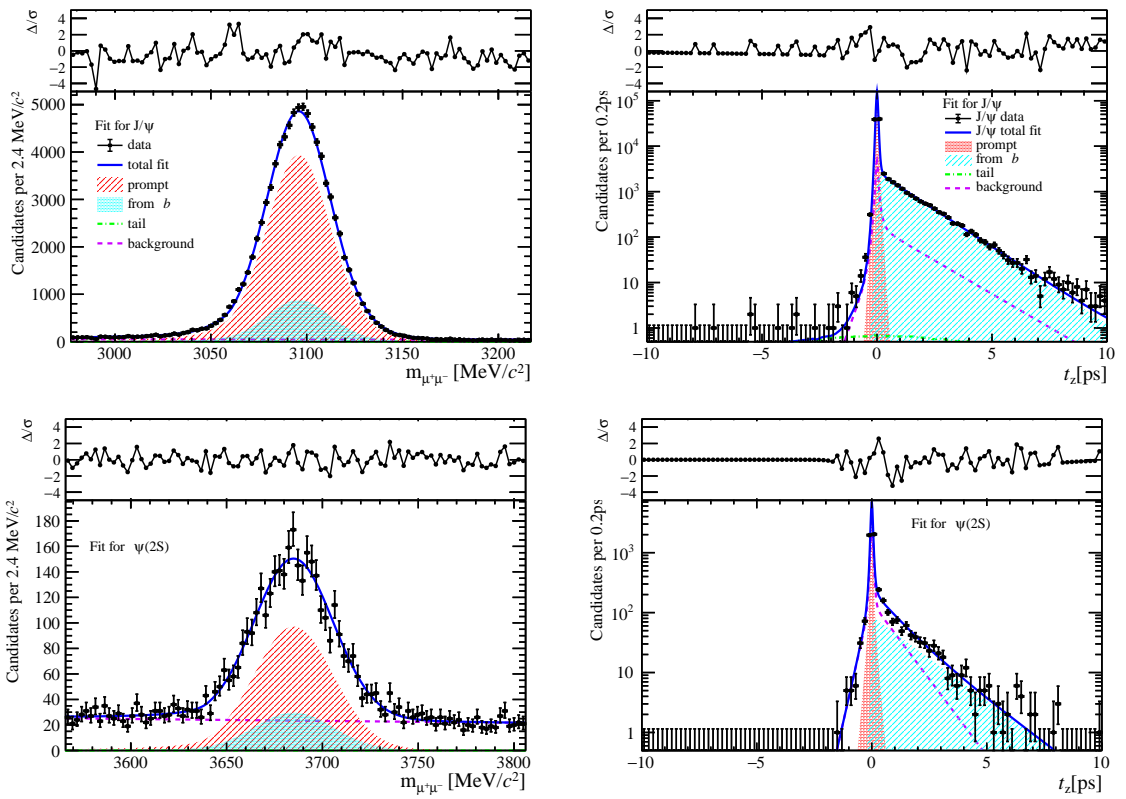


Figure 166: Fit results in  $6 \text{ GeV}/c < p_T < 8 \text{ GeV}/c$ ,  $3.5 < y < 4.5$  and  $22 \leq \text{nBackTracks} < 30$ .

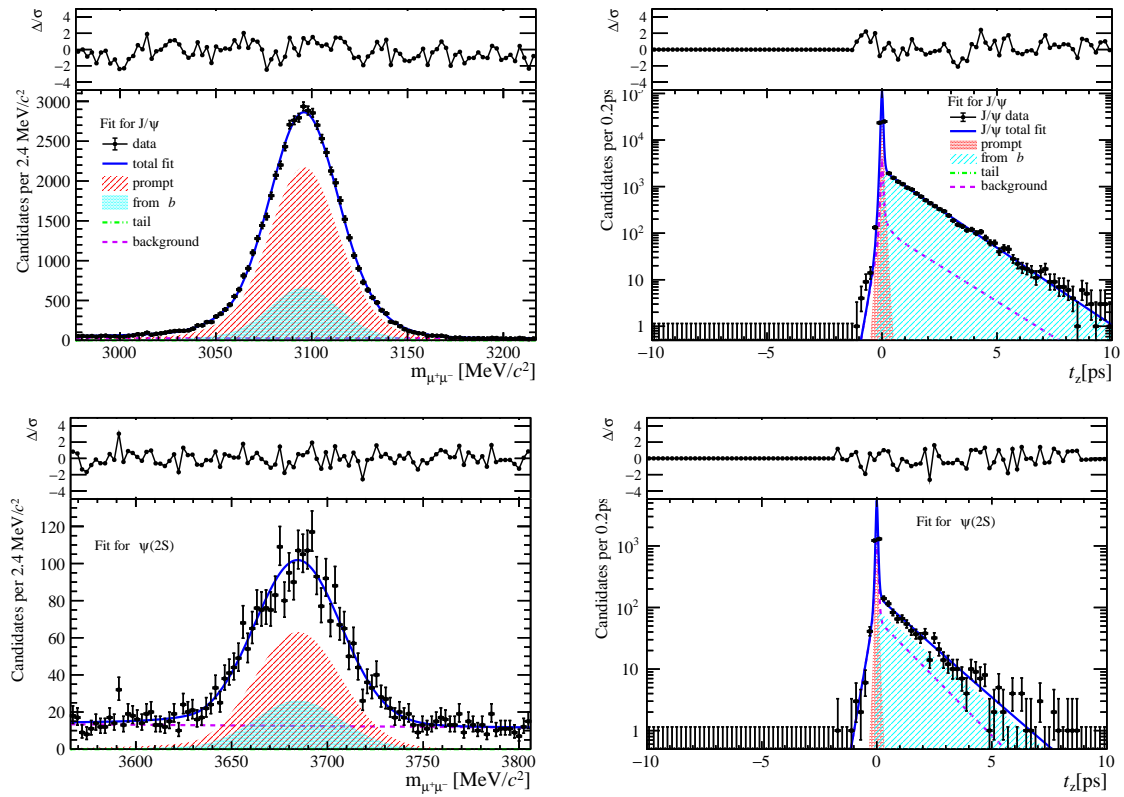


Figure 167: Fit results in  $8 \text{ GeV}/c < p_T < 20 \text{ GeV}/c$ ,  $3.5 < y < 4.5$  and  $22 \leq \text{nBackTracks} < 30$ .

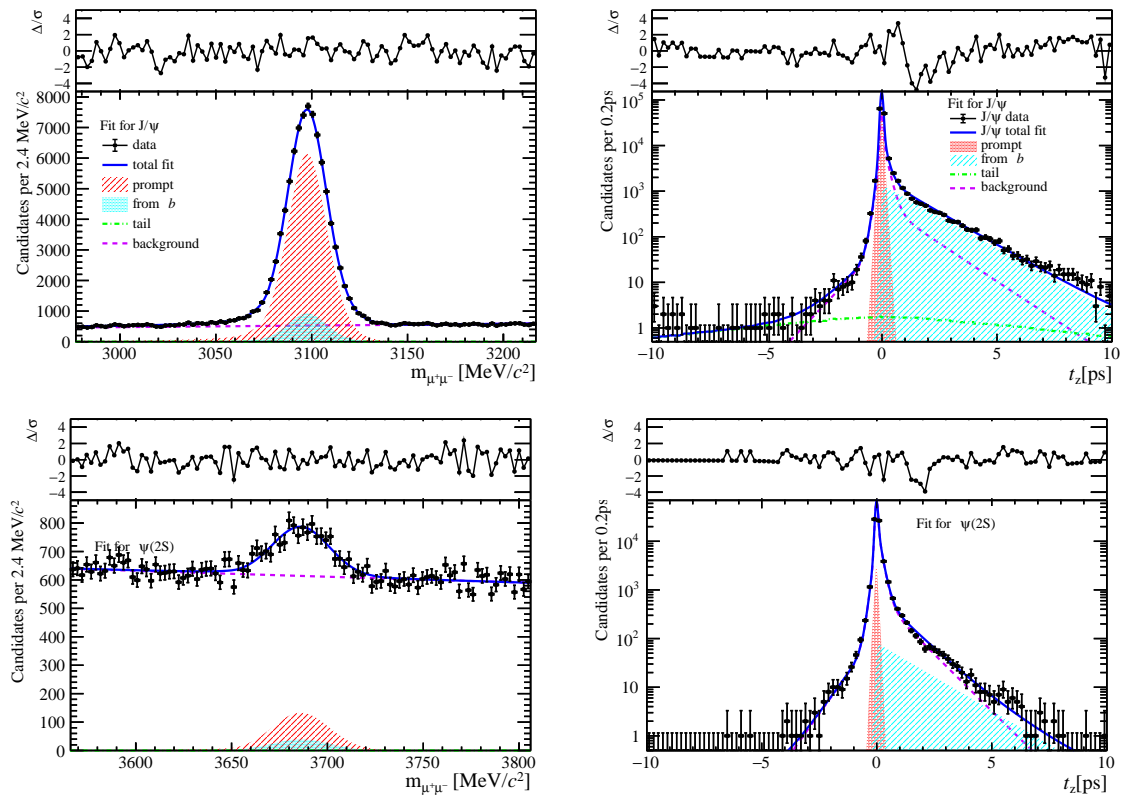


Figure 168: Fit results in  $0 \text{ GeV}/c < p_T < 2 \text{ GeV}/c$ ,  $2.0 < y < 2.8$  and  $30 \leq \text{nBackTracks} < 80$ .

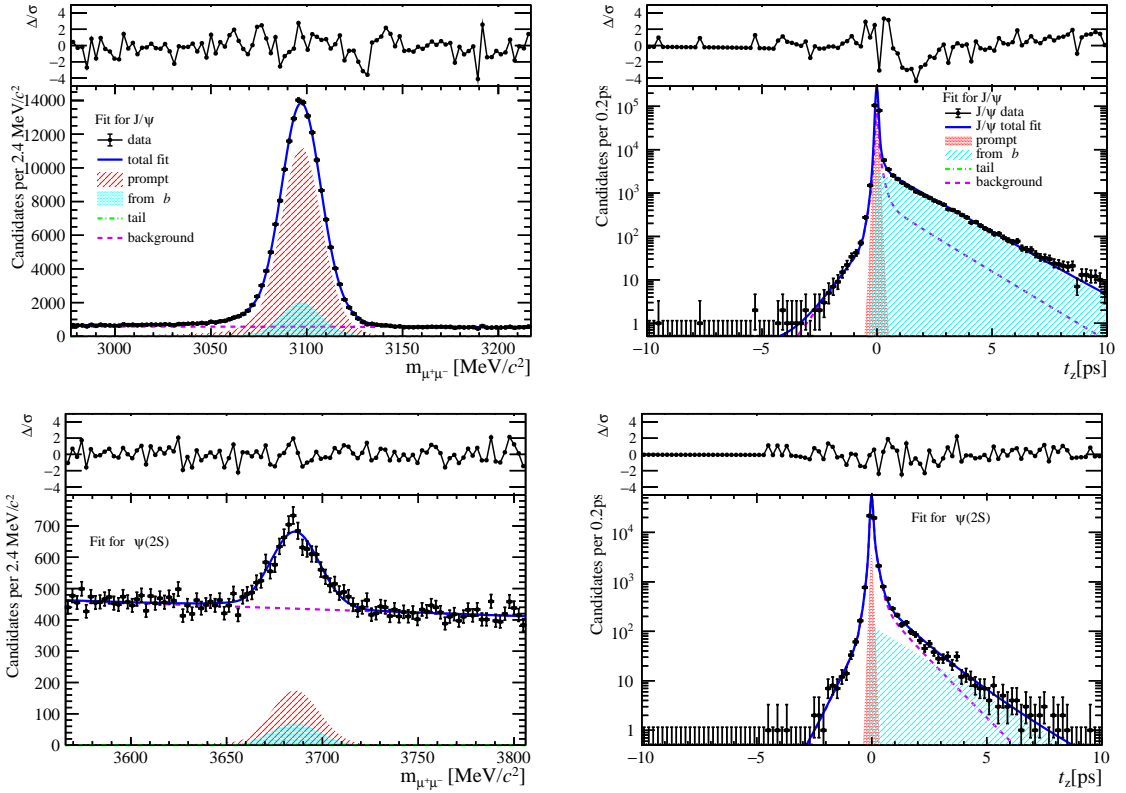


Figure 169: Fit results in  $2 \text{ GeV}/c < p_T < 4 \text{ GeV}/c$ ,  $2.0 < y < 2.8$  and  $30 \leq \text{nBackTracks} < 80$ .

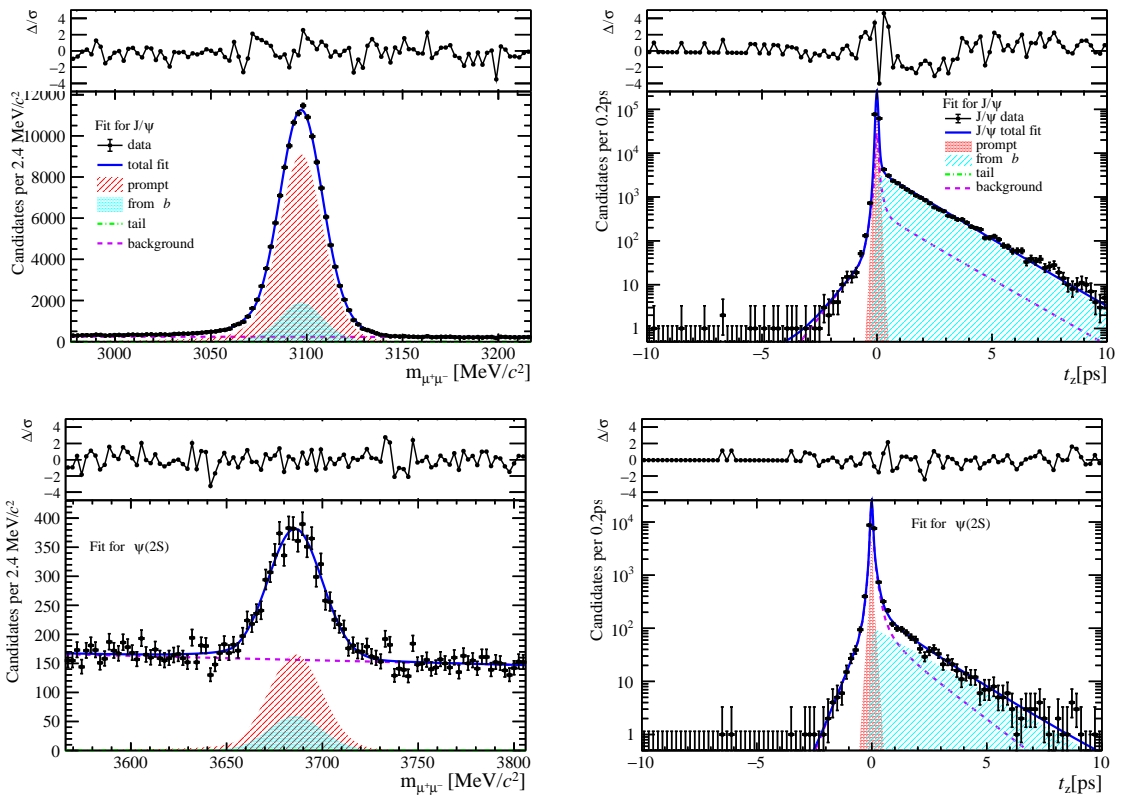


Figure 170: Fit results in  $4 \text{ GeV}/c < p_T < 6 \text{ GeV}/c$ ,  $2.0 < y < 2.8$  and  $30 \leq \text{nBackTracks} < 80$ .

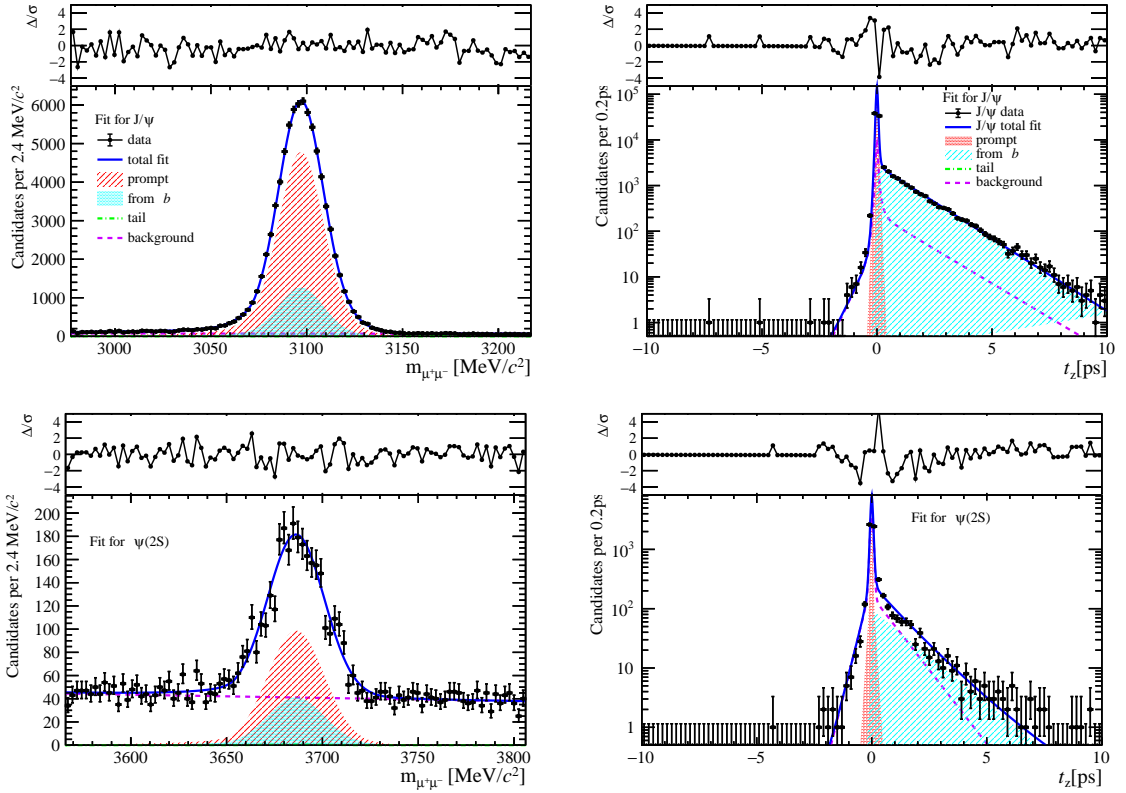


Figure 171: Fit results in  $6 \text{ GeV}/c < p_T < 8 \text{ GeV}/c$ ,  $2.0 < y < 2.8$  and  $30 \leq \text{nBackTracks} < 80$ .

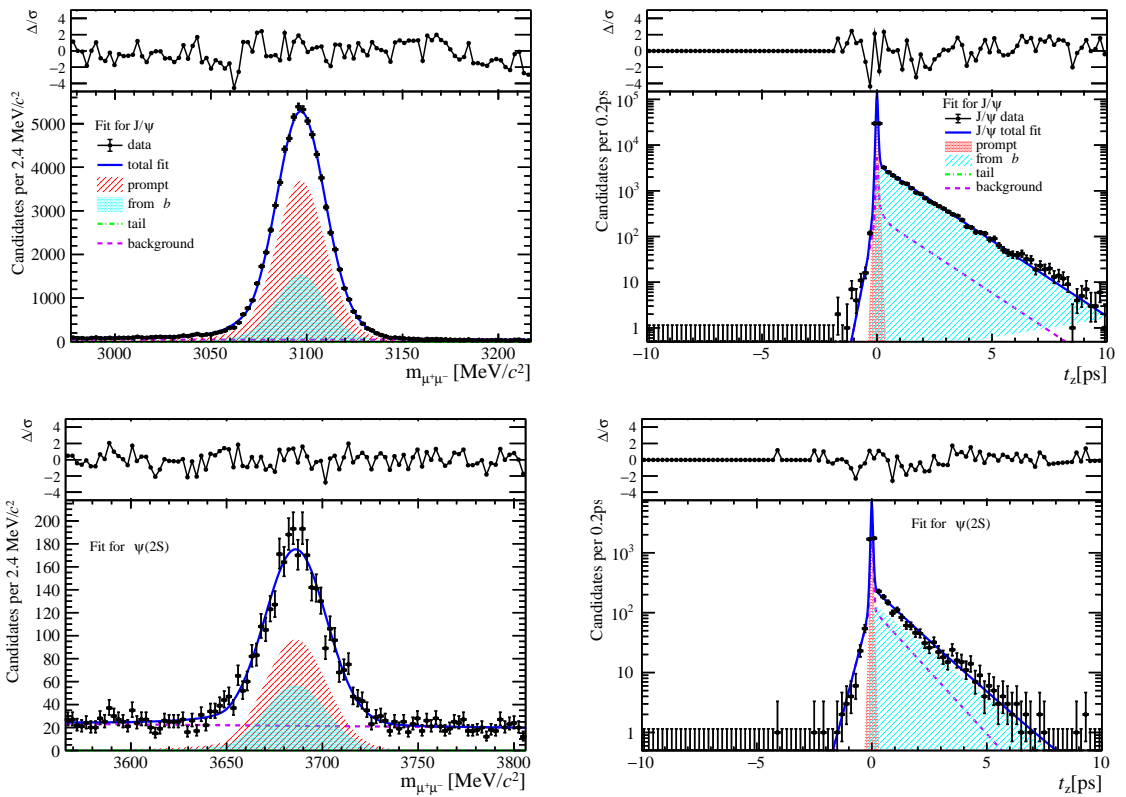


Figure 172: Fit results in  $8 \text{ GeV}/c < p_T < 20 \text{ GeV}/c$ ,  $2.0 < y < 2.8$  and  $30 \leq \text{nBackTracks} < 80$ .

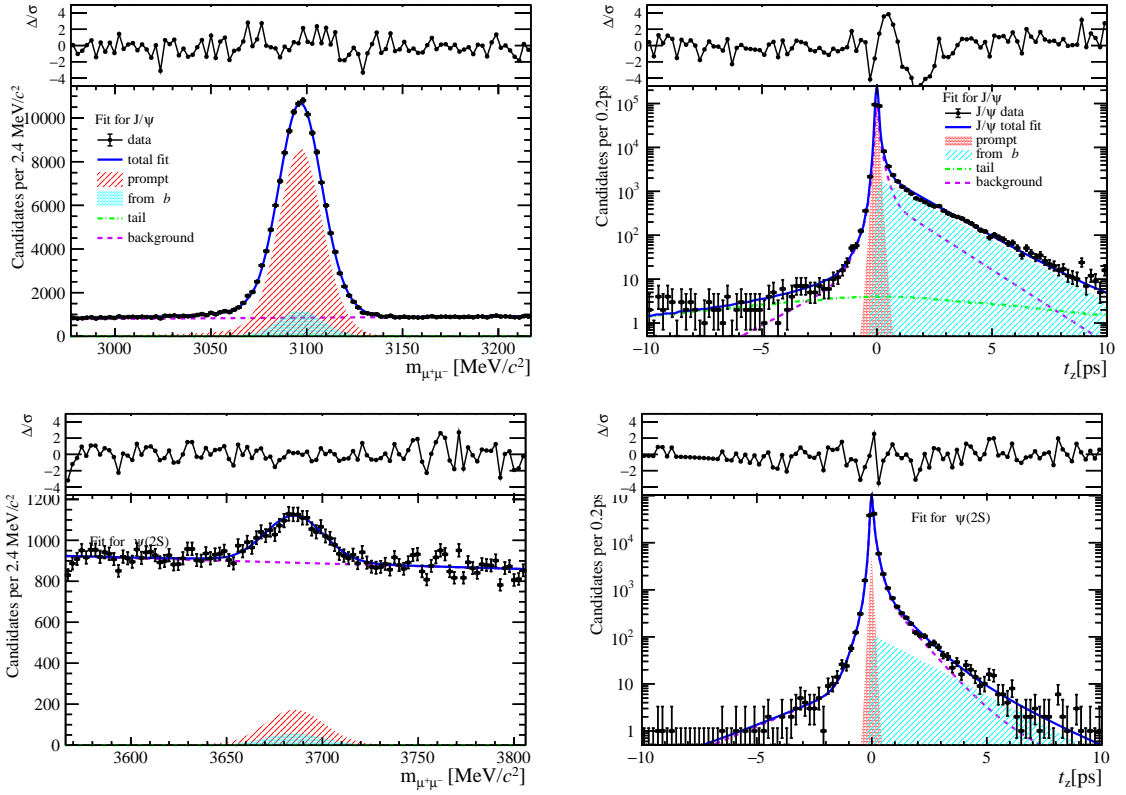


Figure 173: Fit results in  $0 \text{ GeV}/c < p_T < 2 \text{ GeV}/c$ ,  $2.8 < y < 3.5$  and  $30 \leq n\text{BackTracks} < 80$ .

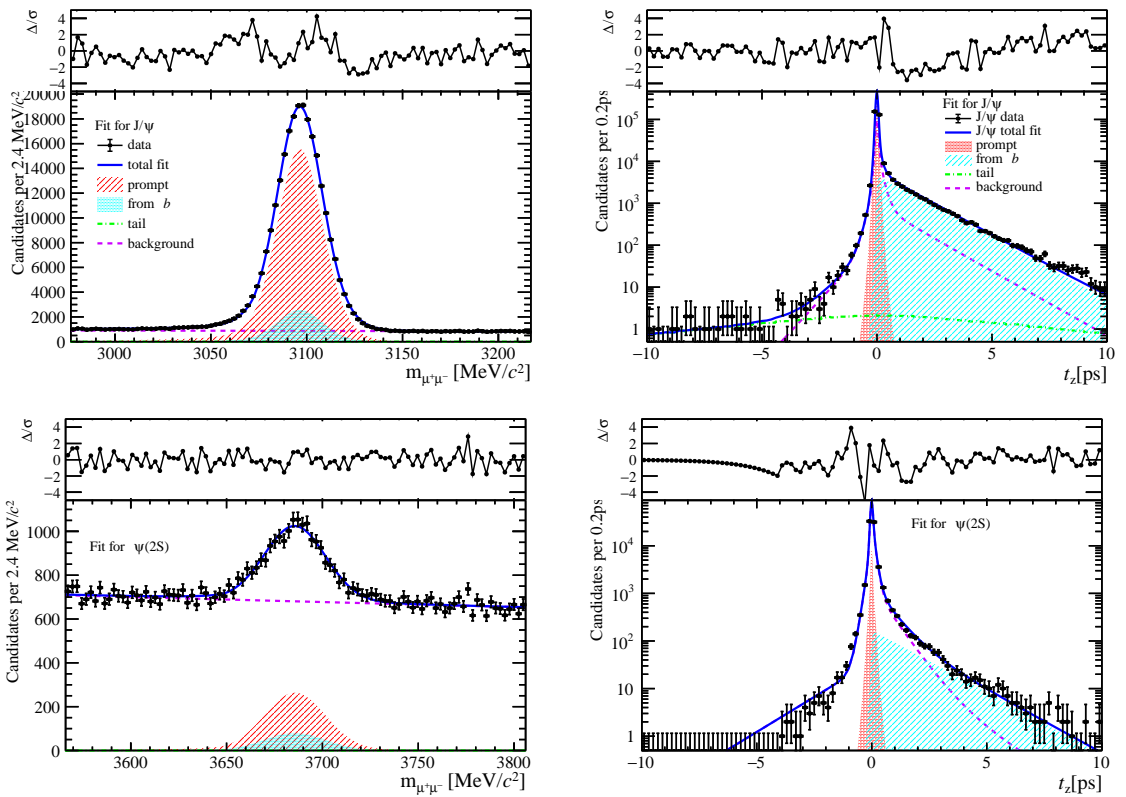


Figure 174: Fit results in  $2 \text{ GeV}/c < p_T < 4 \text{ GeV}/c$ ,  $2.8 < y < 3.5$  and  $30 \leq n\text{BackTracks} < 80$ .

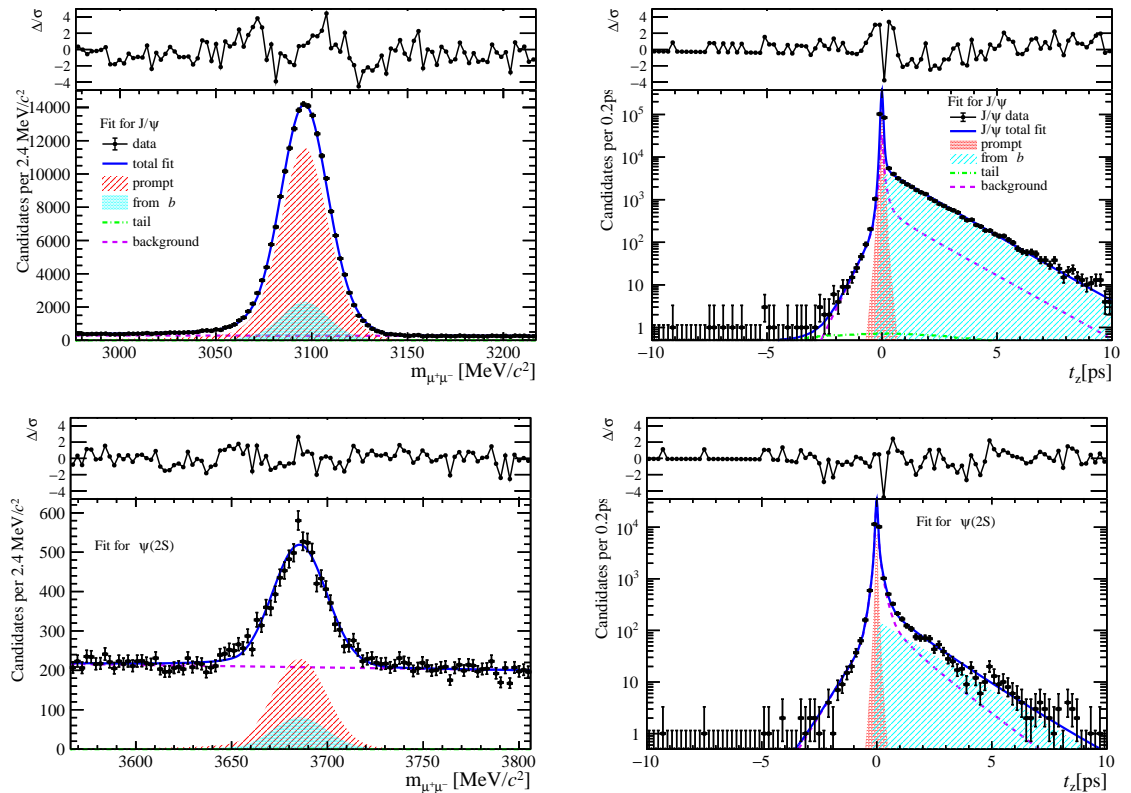


Figure 175: Fit results in  $4 \text{ GeV}/c < p_T < 6 \text{ GeV}/c$ ,  $2.8 < y < 3.5$  and  $30 \leq \text{nBackTracks} < 80$ .

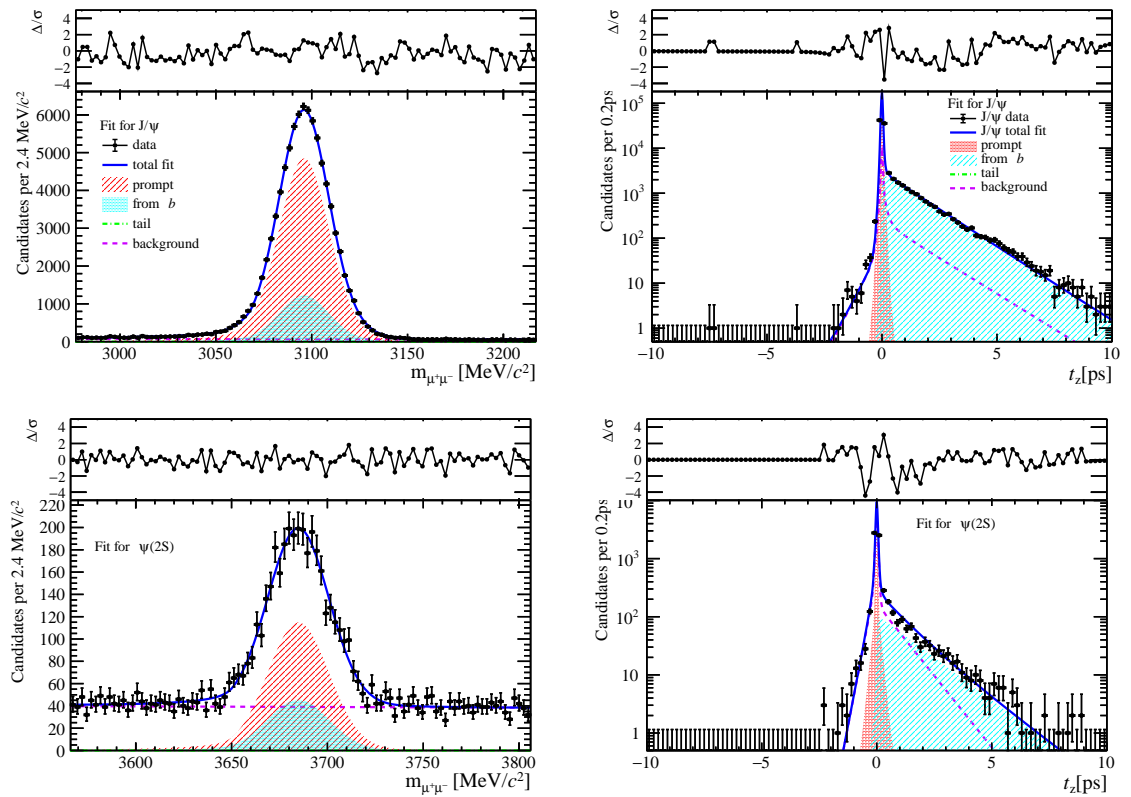


Figure 176: Fit results in  $6 \text{ GeV}/c < p_T < 8 \text{ GeV}/c$ ,  $2.8 < y < 3.5$  and  $30 \leq \text{nBackTracks} < 80$ .

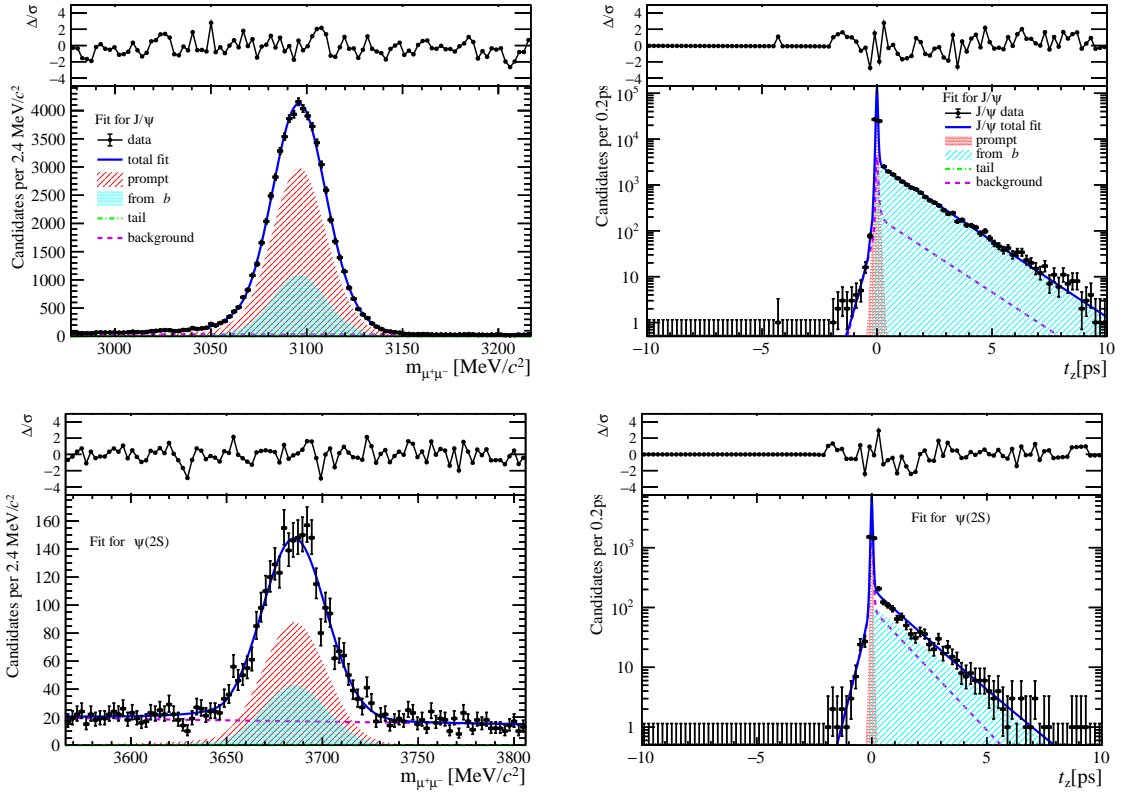


Figure 177: Fit results in  $8 \text{ GeV}/c < p_T < 20 \text{ GeV}/c$ ,  $2.8 < y < 3.5$  and  $30 \leq \text{nBackTracks} < 80$ .

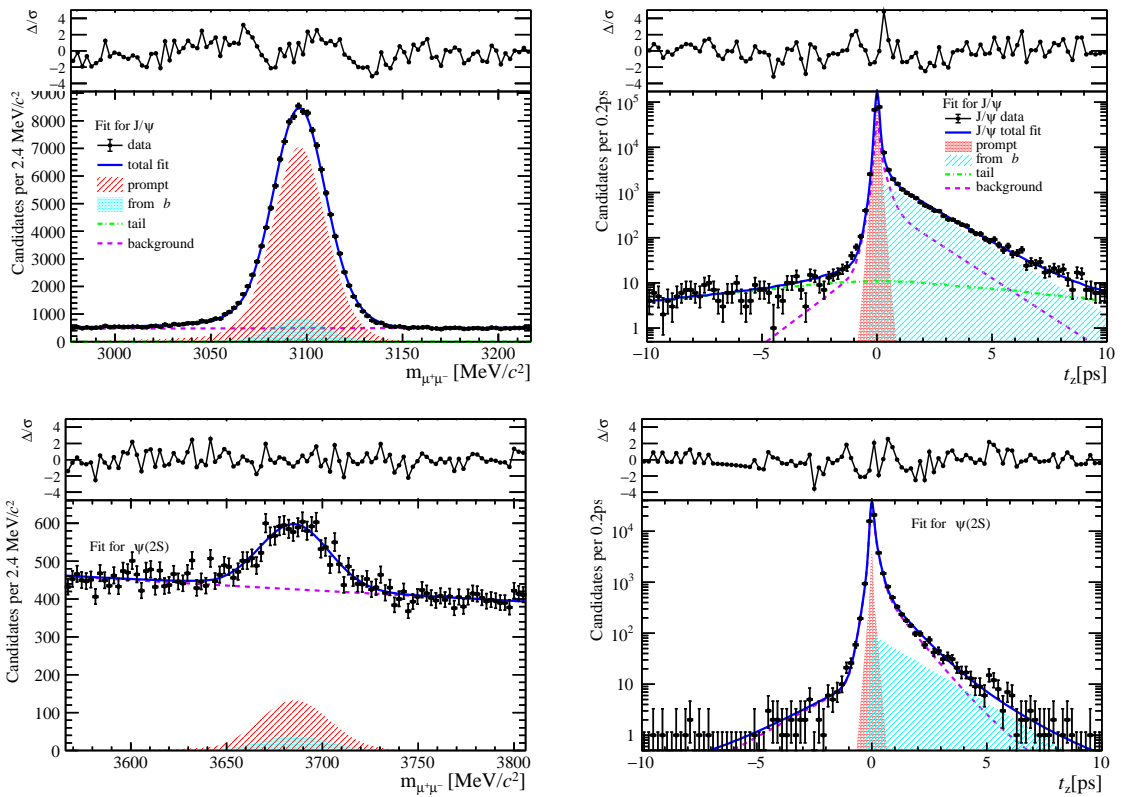


Figure 178: Fit results in  $0 \text{ GeV}/c < p_T < 2 \text{ GeV}/c$ ,  $3.5 < y < 4.5$  and  $30 \leq \text{nBackTracks} < 80$ .

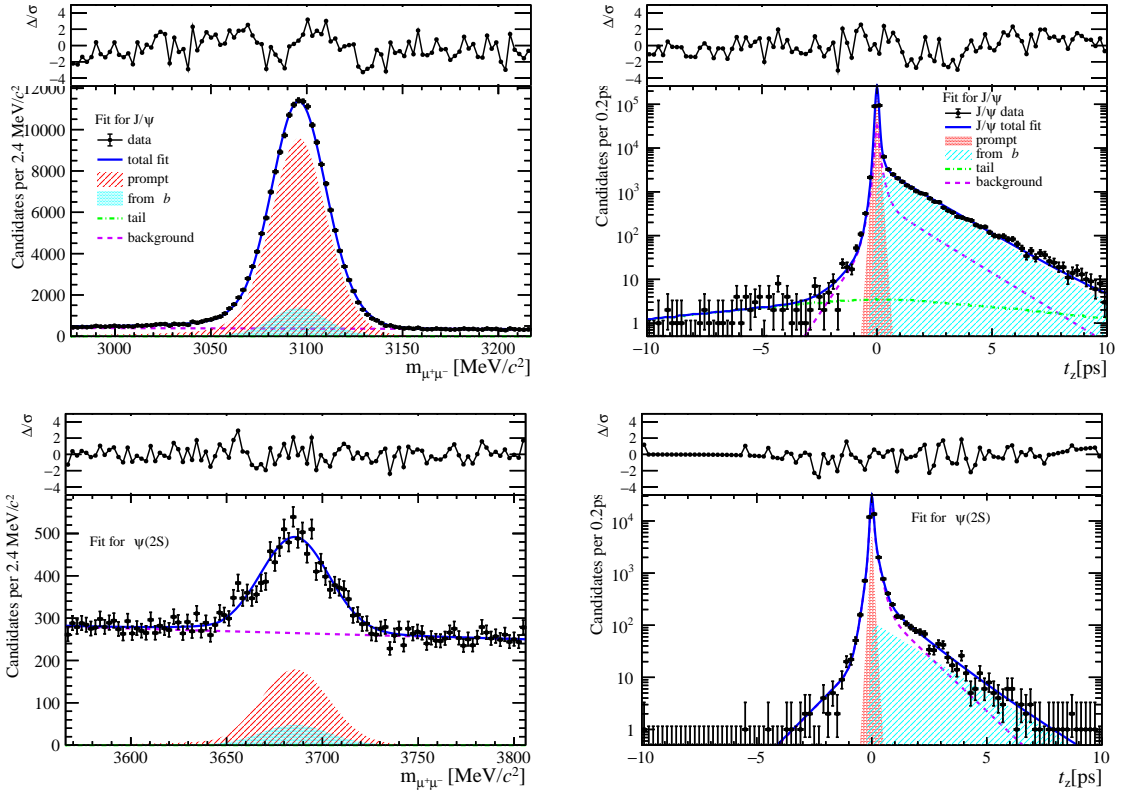


Figure 179: Fit results in  $2 \text{ GeV}/c < p_{\text{T}} < 4 \text{ GeV}/c$ ,  $3.5 < y < 4.5$  and  $30 \leq \text{nBackTracks} < 80$ .

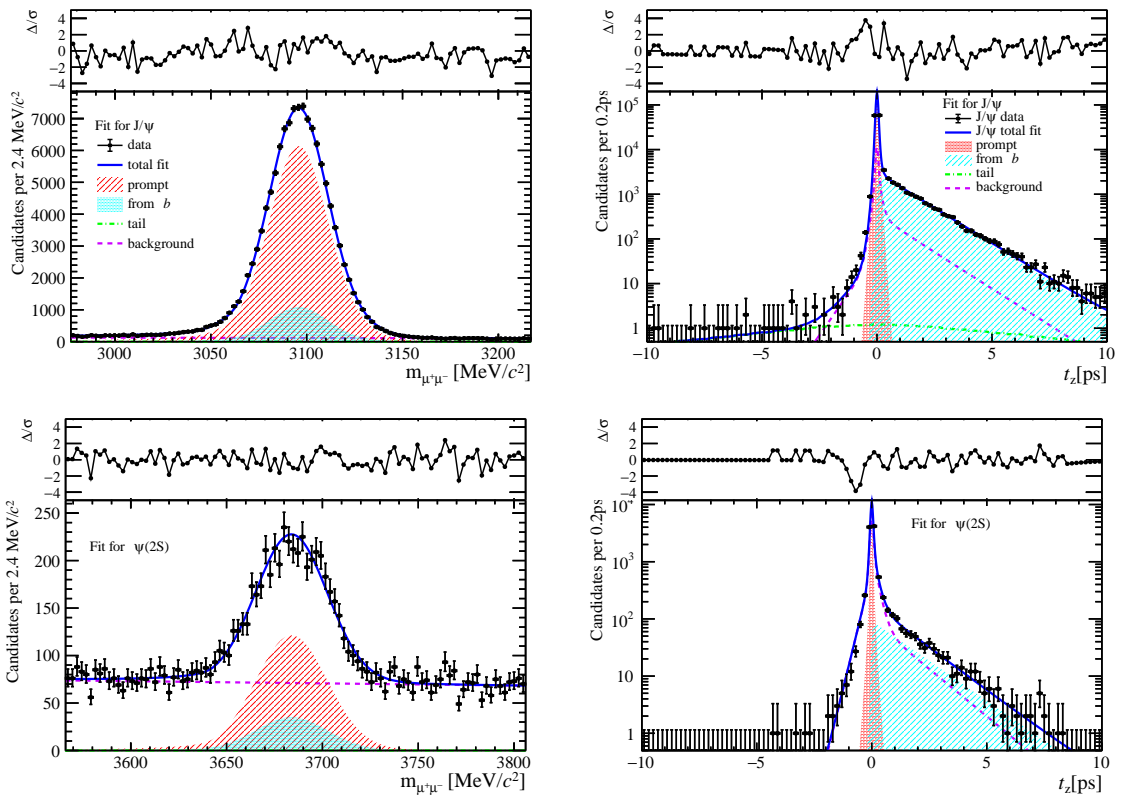


Figure 180: Fit results in  $4 \text{ GeV}/c < p_{\text{T}} < 6 \text{ GeV}/c$ ,  $3.5 < y < 4.5$  and  $30 \leq \text{nBackTracks} < 80$ .

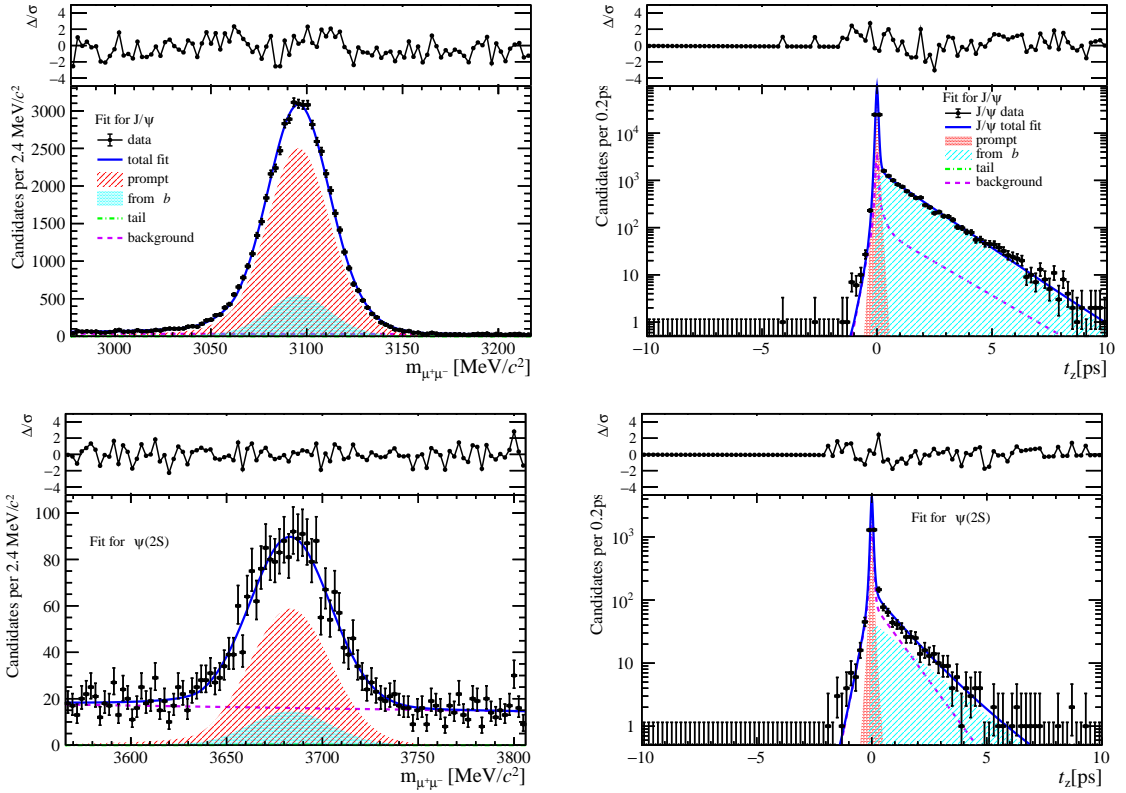


Figure 181: Fit results in  $6 \text{ GeV}/c < p_T < 8 \text{ GeV}/c$ ,  $3.5 < y < 4.5$  and  $30 \leq \text{nBackTracks} < 80$ .

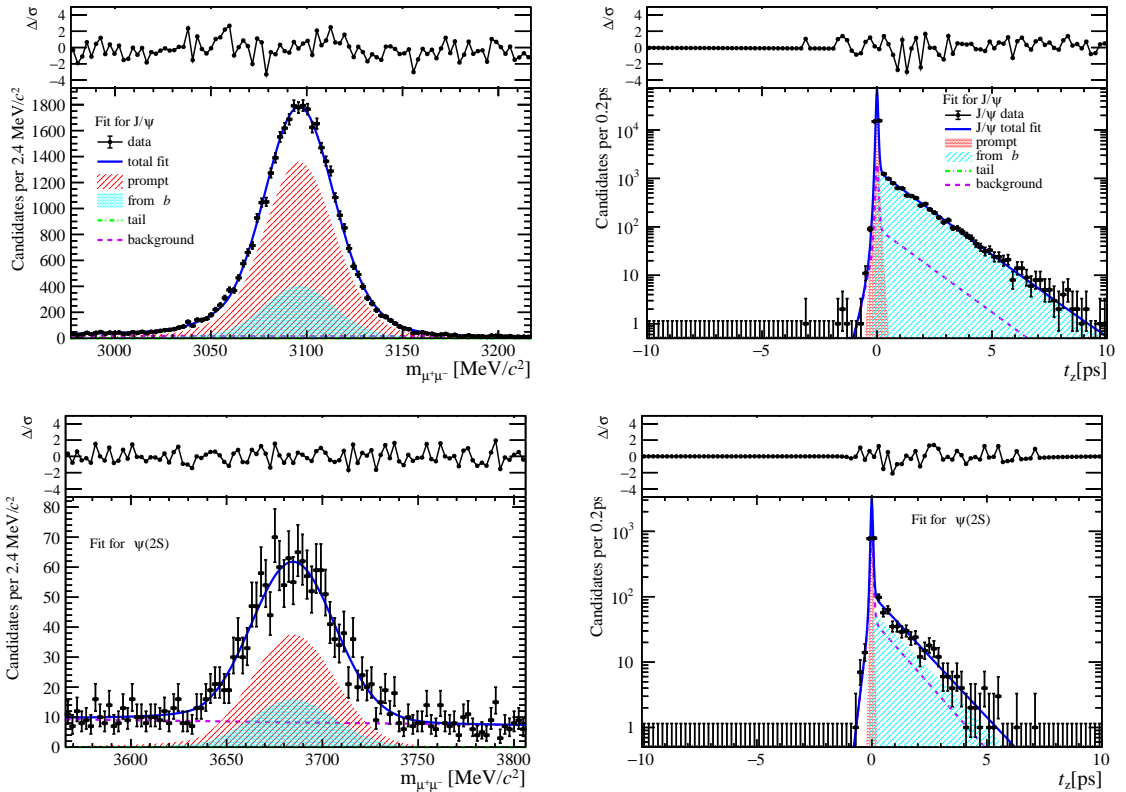


Figure 182: Fit results in  $8 \text{ GeV}/c < p_T < 20 \text{ GeV}/c$ ,  $3.5 < y < 4.5$  and  $30 \leq \text{nBackTracks} < 80$ .

680 C.3 Separated by nForwardTracks

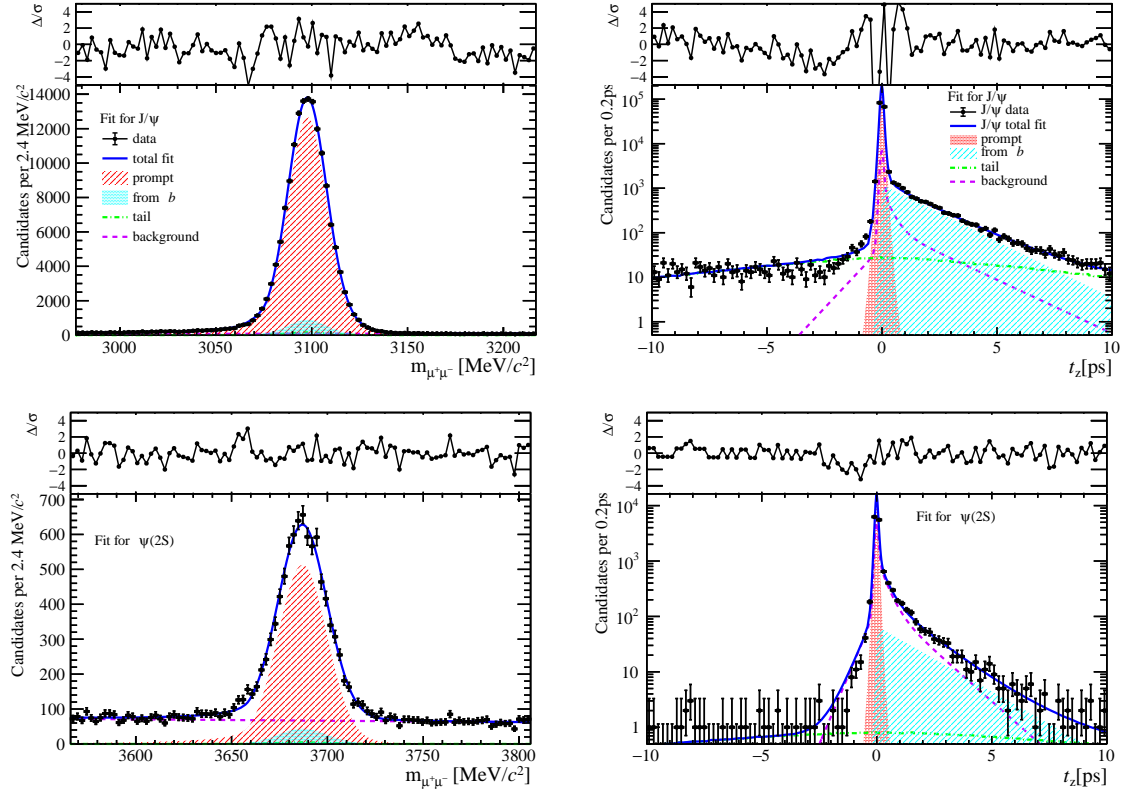


Figure 183: Fit results in  $0 \text{ GeV}/c < p_T < 2 \text{ GeV}/c$ ,  $2.0 < y < 2.8$  and  $0 \leq \text{nForwardTracks} < 12$ .

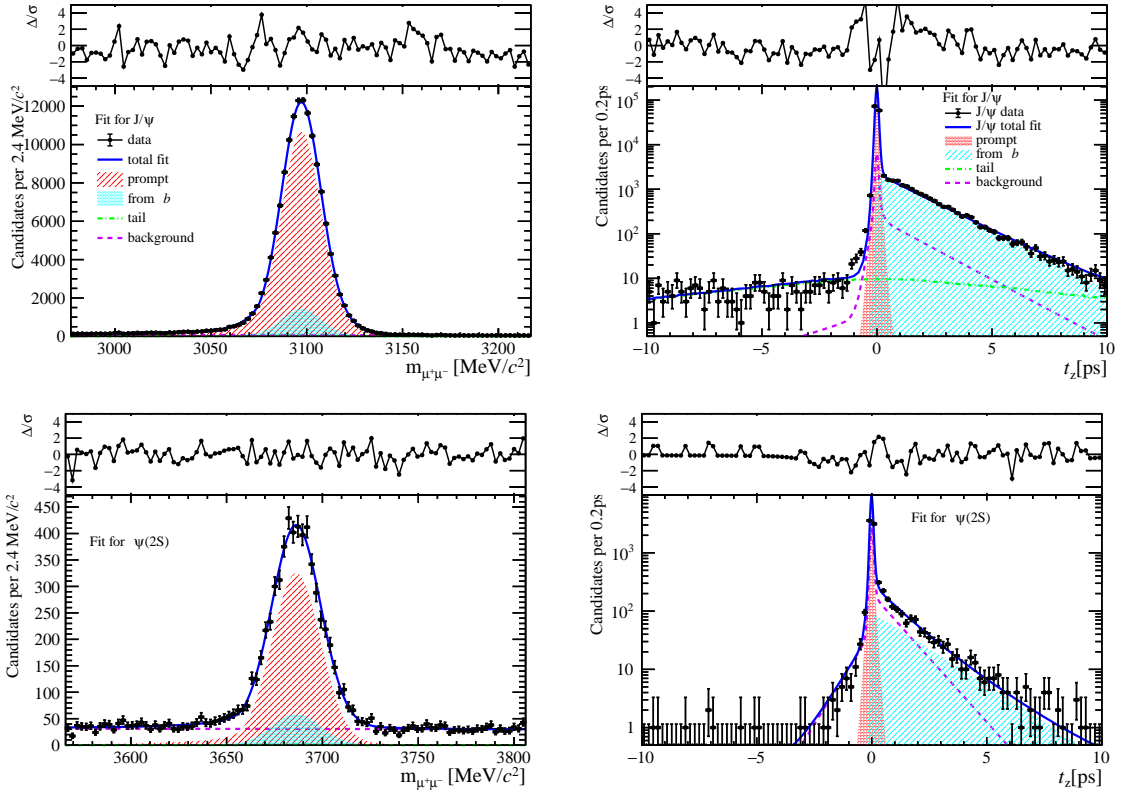


Figure 184: Fit results in  $2 \text{ GeV}/c < p_T < 4 \text{ GeV}/c$ ,  $2.0 < y < 2.8$  and  $0 \leq \text{nForwardTracks} < 12$ .

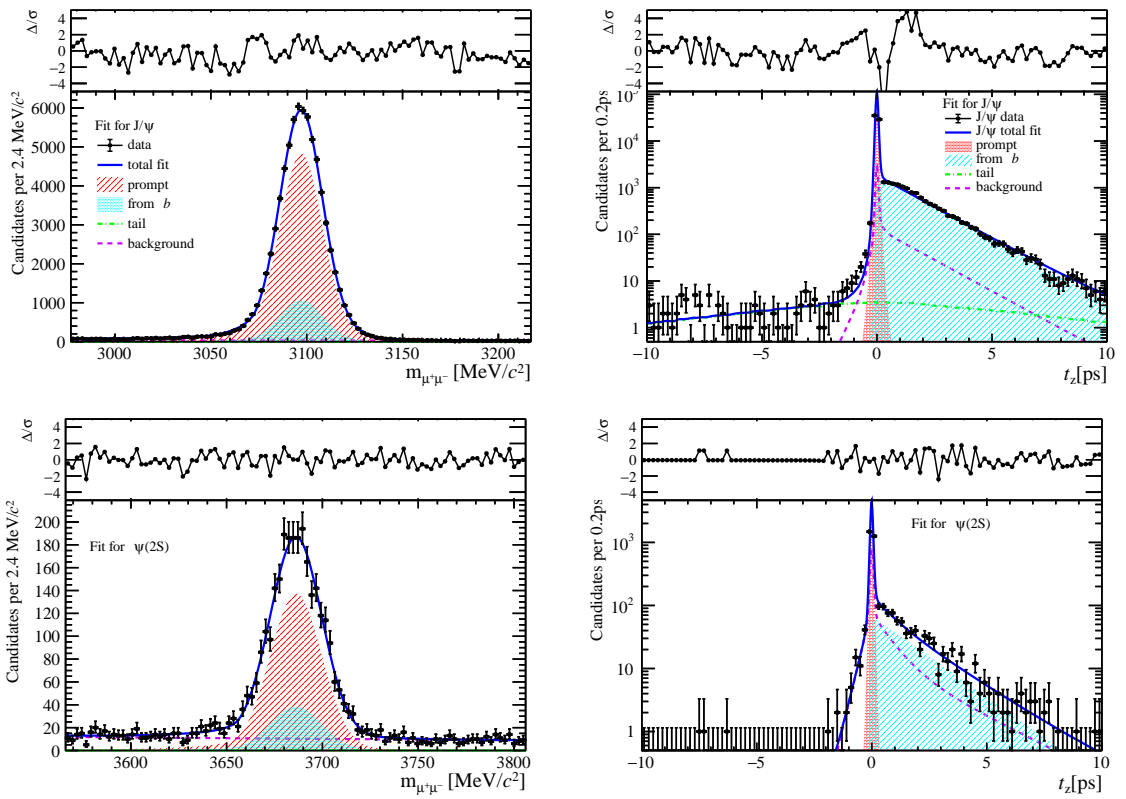


Figure 185: Fit results in  $4 \text{ GeV}/c < p_T < 6 \text{ GeV}/c$ ,  $2.0 < y < 2.8$  and  $0 \leq \text{nForwardTracks} < 12$ .

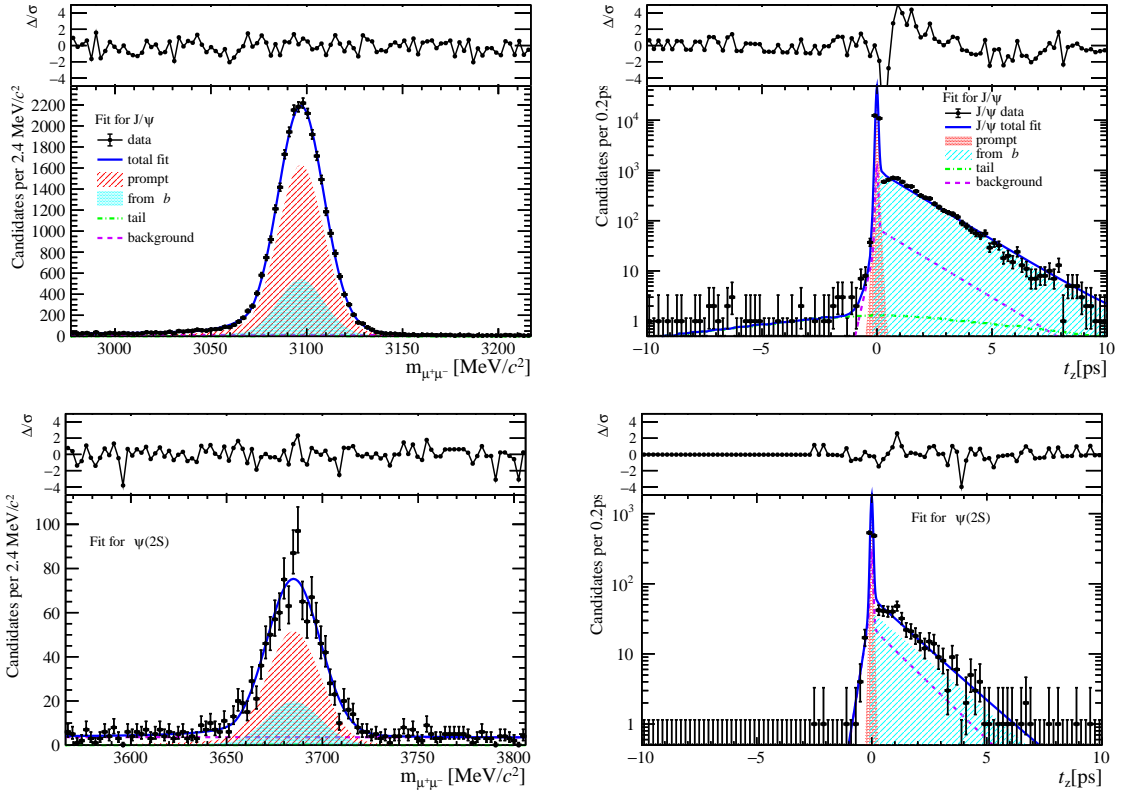


Figure 186: Fit results in  $6 \text{ GeV}/c < p_T < 8 \text{ GeV}/c$ ,  $2.0 < y < 2.8$  and  $0 \leq \text{nForwardTracks} < 12$ .

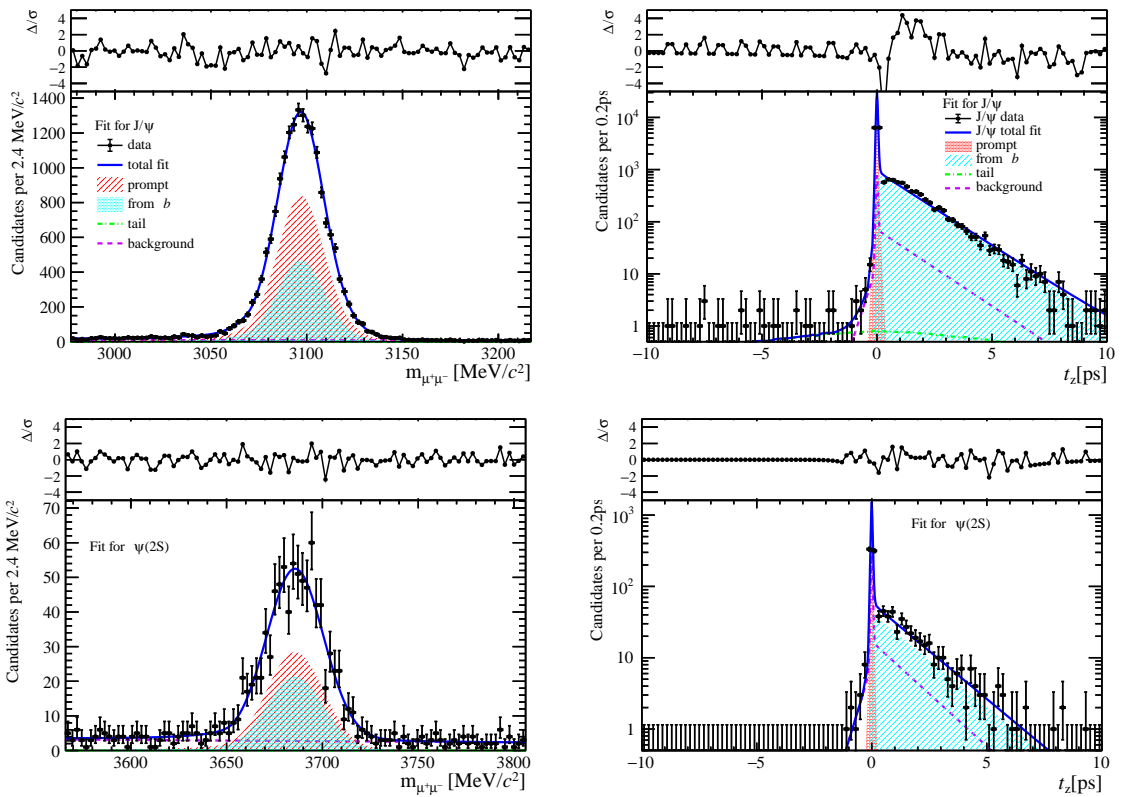


Figure 187: Fit results in  $8 \text{ GeV}/c < p_T < 20 \text{ GeV}/c$ ,  $2.0 < y < 2.8$  and  $0 \leq \text{nForwardTracks} < 12$ .

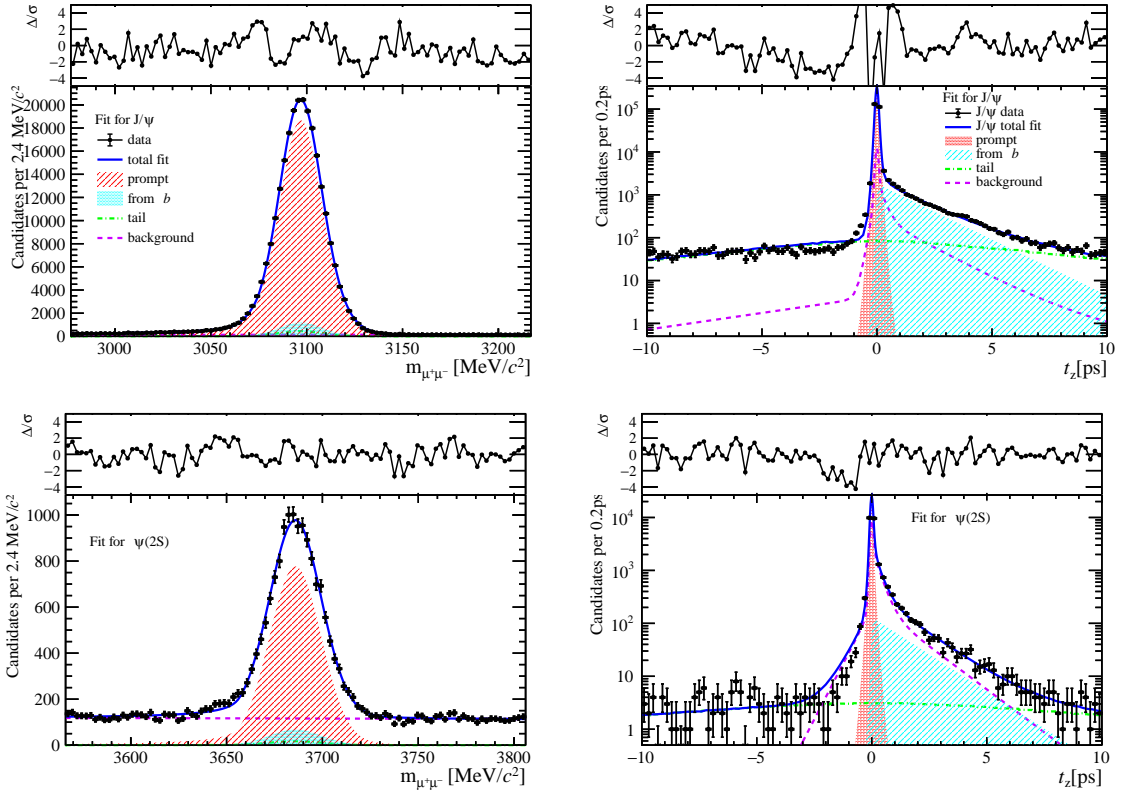


Figure 188: Fit results in  $0 \text{ GeV}/c < p_T < 2 \text{ GeV}/c$ ,  $2.8 < y < 3.5$  and  $0 \leq \text{nForwardTracks} < 12$ .

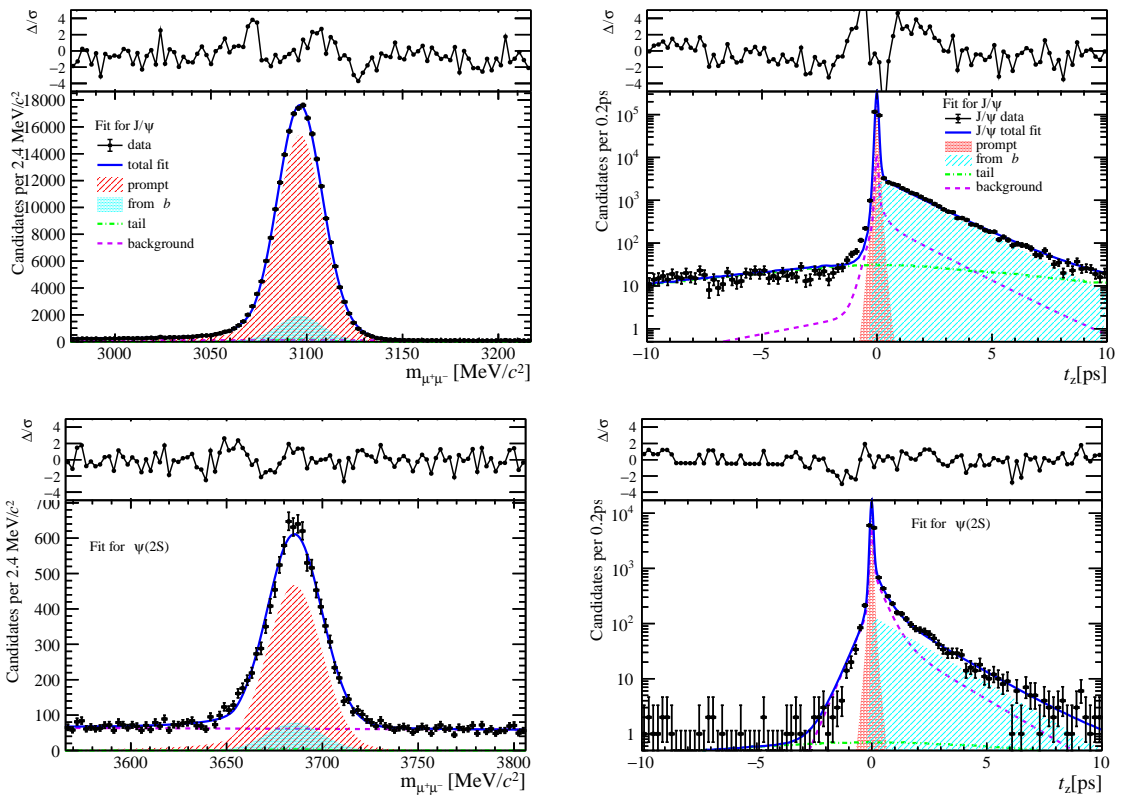


Figure 189: Fit results in  $2 \text{ GeV}/c < p_T < 4 \text{ GeV}/c$ ,  $2.8 < y < 3.5$  and  $0 \leq \text{nForwardTracks} < 12$ .

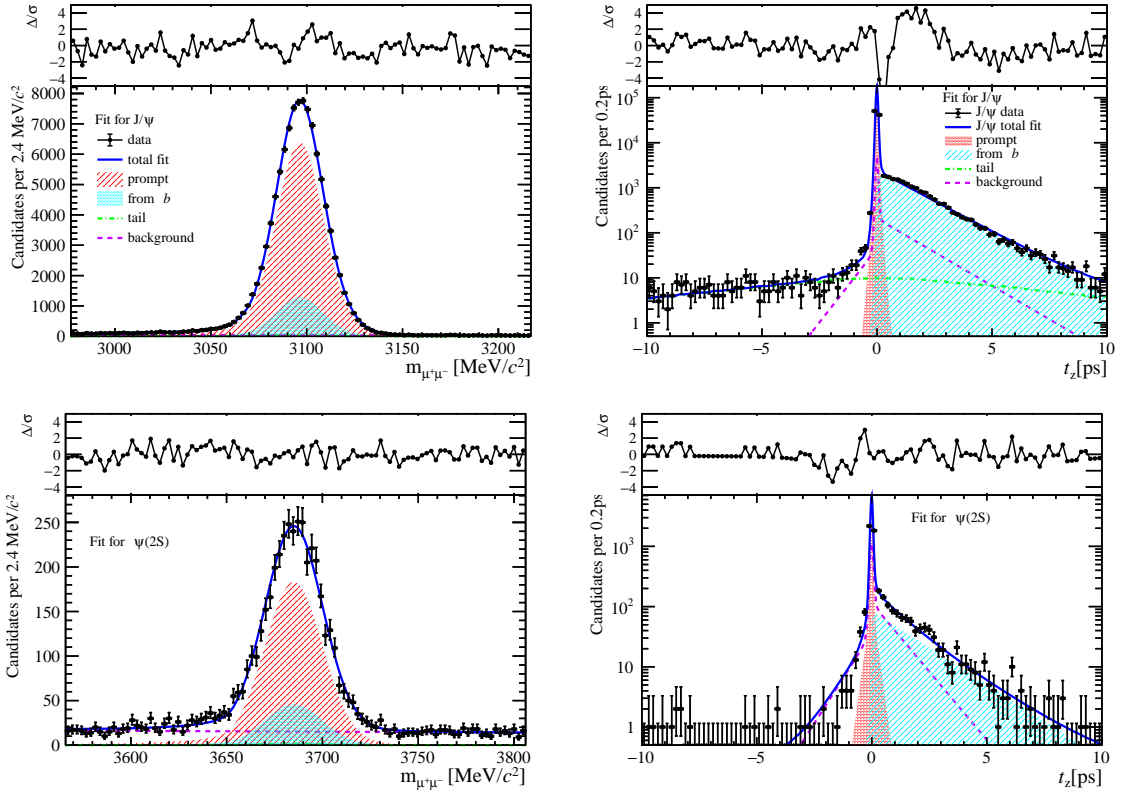


Figure 190: Fit results in  $4 \text{ GeV}/c < p_T < 6 \text{ GeV}/c$ ,  $2.8 < y < 3.5$  and  $0 \leq \text{nForwardTracks} < 12$ .

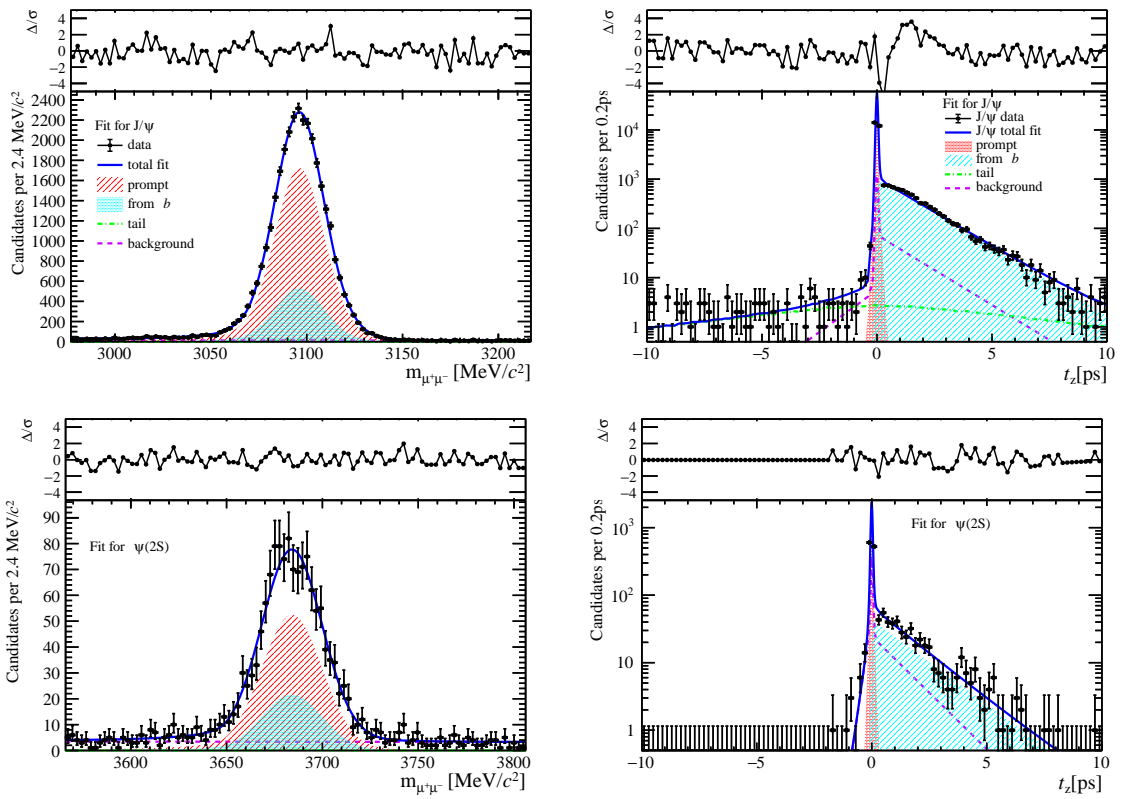


Figure 191: Fit results in  $6 \text{ GeV}/c < p_T < 8 \text{ GeV}/c$ ,  $2.8 < y < 3.5$  and  $0 \leq \text{nForwardTracks} < 12$ .

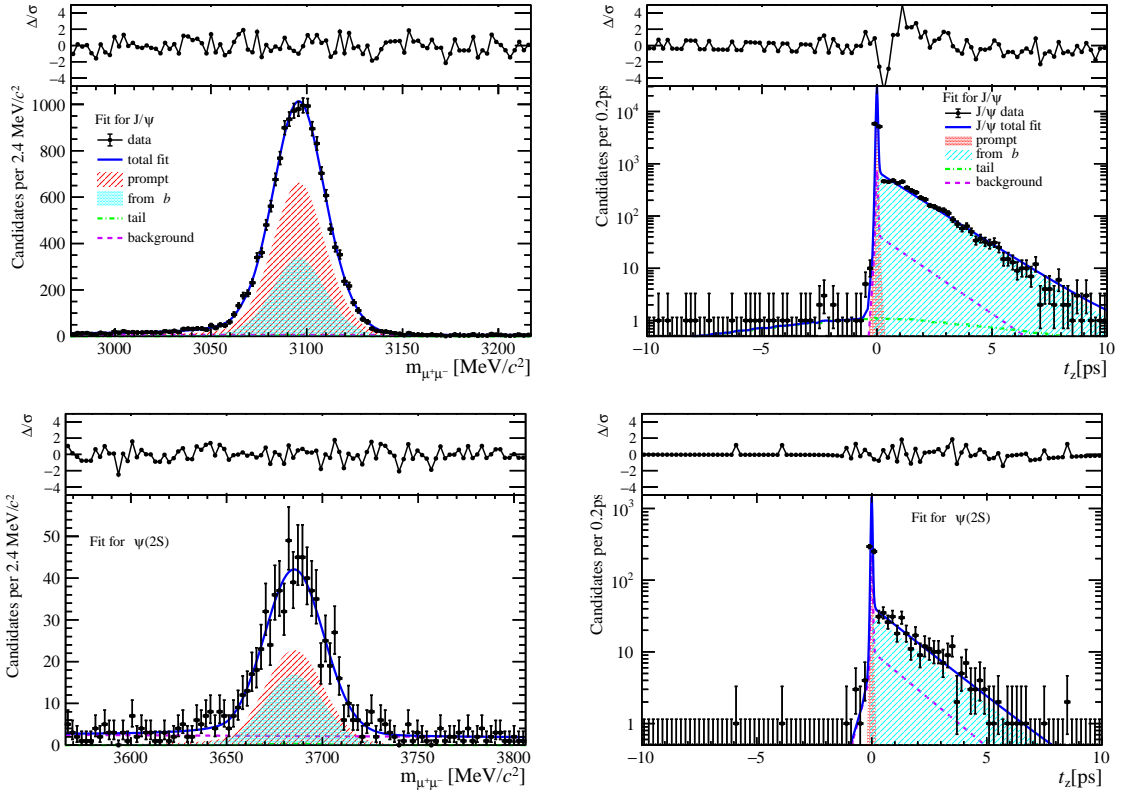


Figure 192: Fit results in  $8 \text{ GeV}/c < p_T < 20 \text{ GeV}/c$ ,  $2.8 < y < 3.5$  and  $0 \leq \text{nForwardTracks} < 12$ .

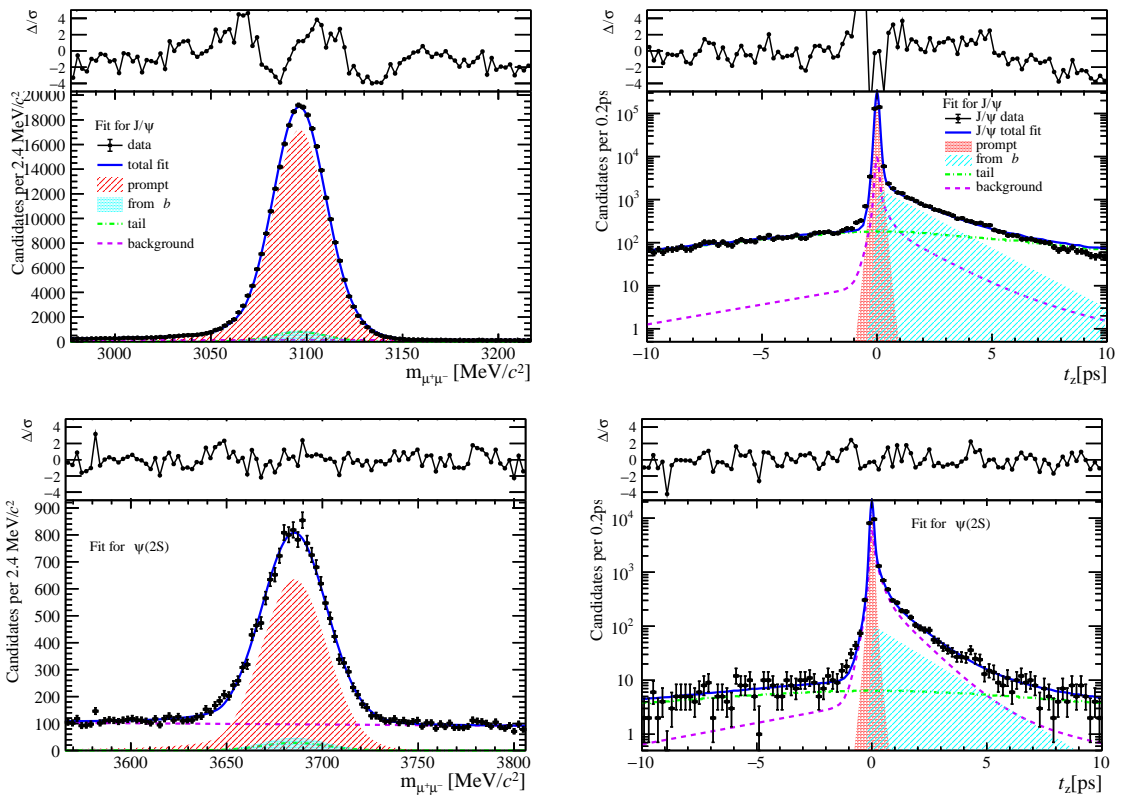


Figure 193: Fit results in  $0 \text{ GeV}/c < p_T < 2 \text{ GeV}/c$ ,  $3.5 < y < 4.5$  and  $0 \leq \text{nForwardTracks} < 12$ .

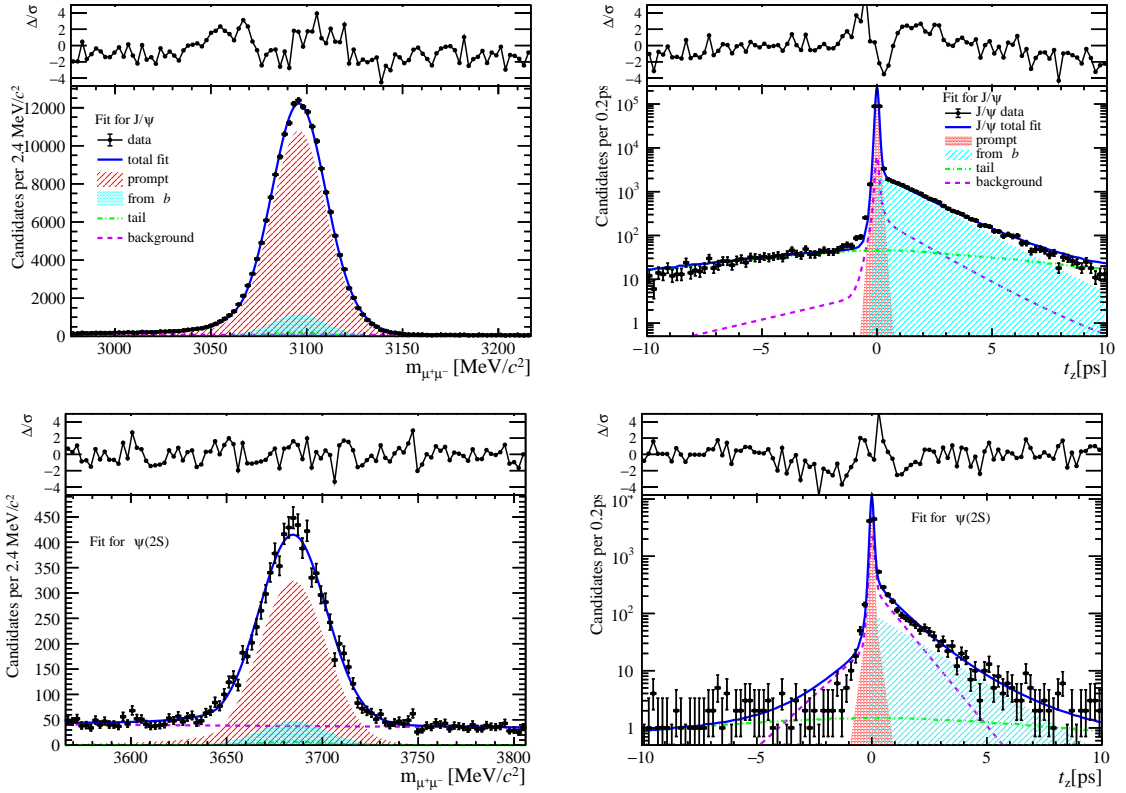


Figure 194: Fit results in  $2 \text{ GeV}/c < p_T < 4 \text{ GeV}/c$ ,  $3.5 < y < 4.5$  and  $0 \leq \text{nForwardTracks} < 12$ .

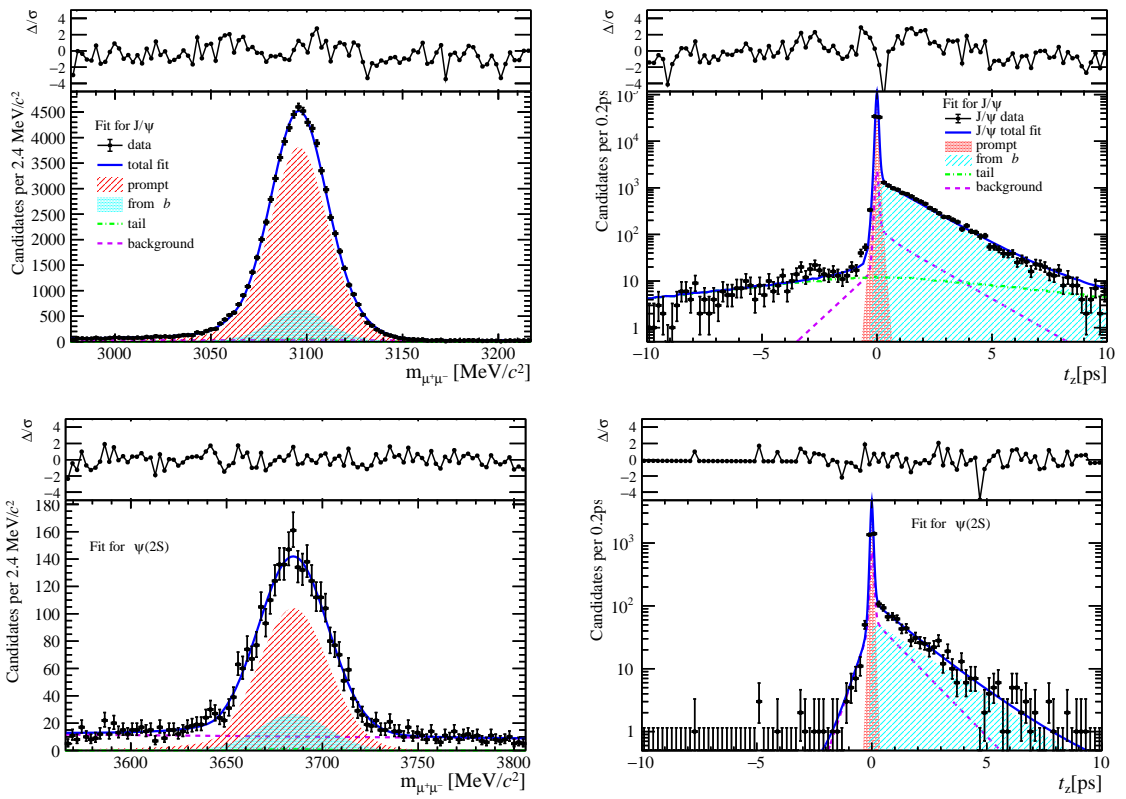


Figure 195: Fit results in  $4 \text{ GeV}/c < p_T < 6 \text{ GeV}/c$ ,  $3.5 < y < 4.5$  and  $0 \leq \text{nForwardTracks} < 12$ .

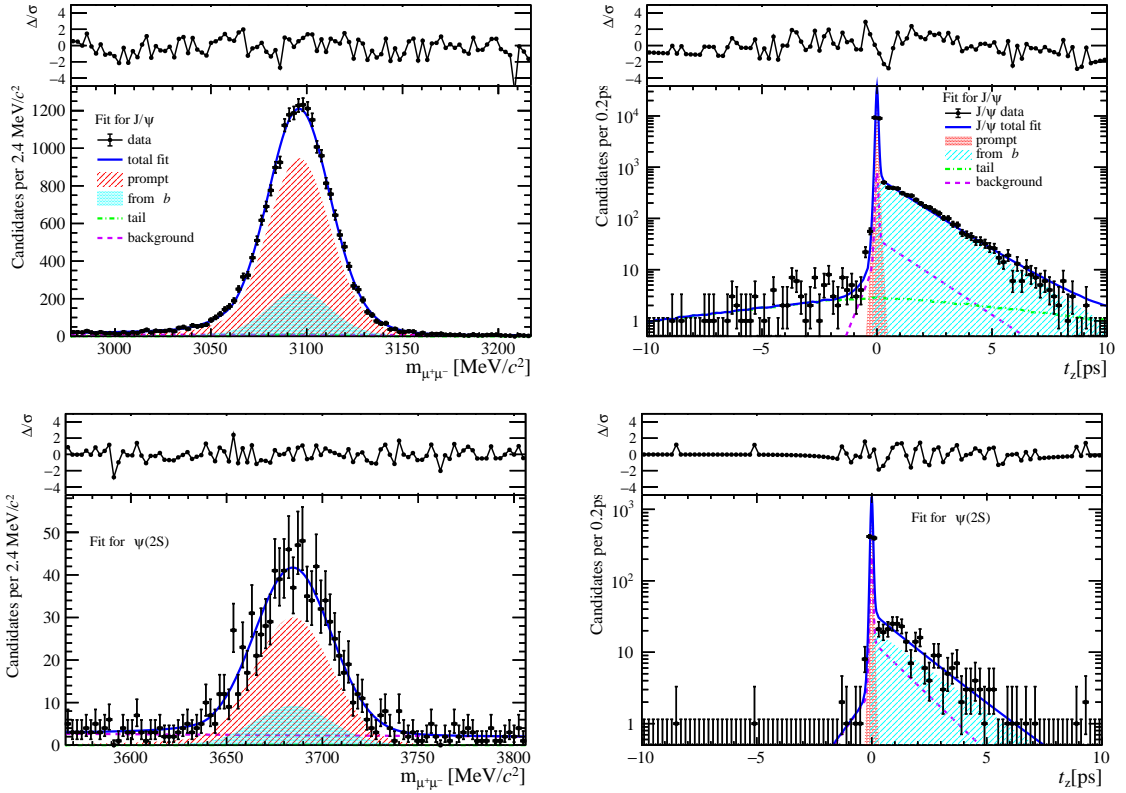


Figure 196: Fit results in  $6 \text{ GeV}/c < p_T < 8 \text{ GeV}/c$ ,  $3.5 < y < 4.5$  and  $0 \leq \text{nForwardTracks} < 12$ .

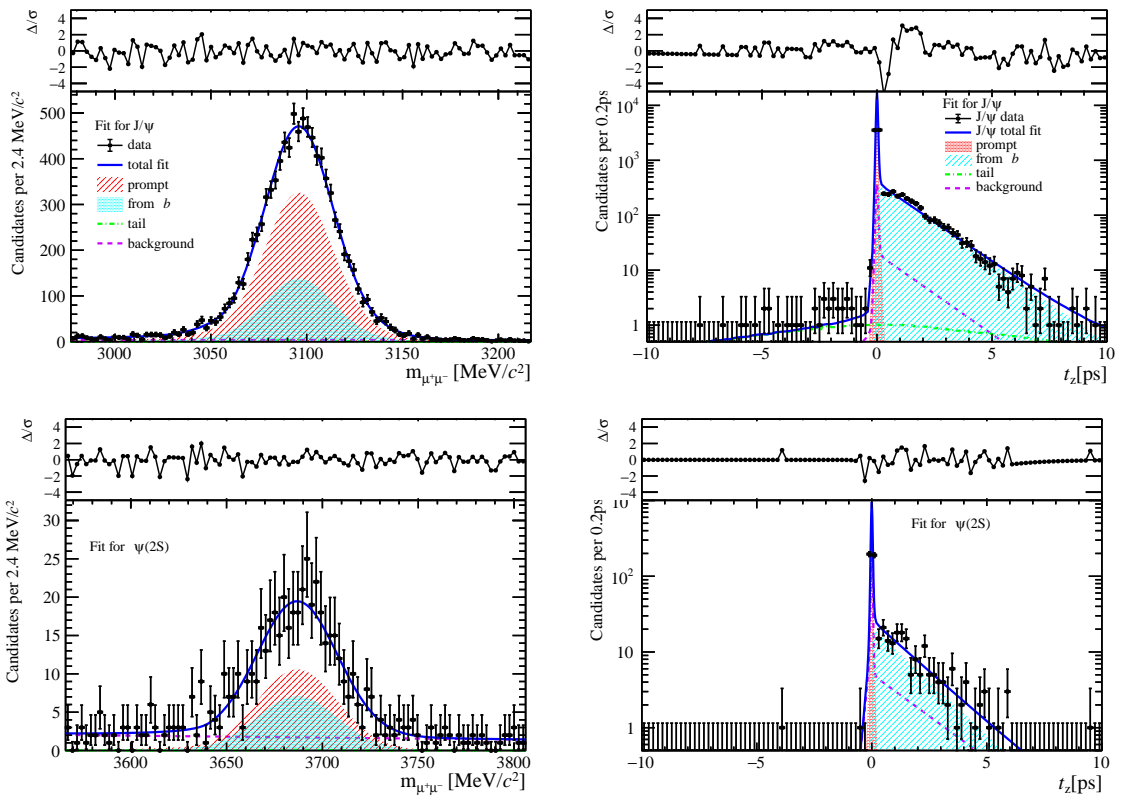


Figure 197: Fit results in  $8 \text{ GeV}/c < p_T < 20 \text{ GeV}/c$ ,  $3.5 < y < 4.5$  and  $0 \leq \text{nForwardTracks} < 12$ .

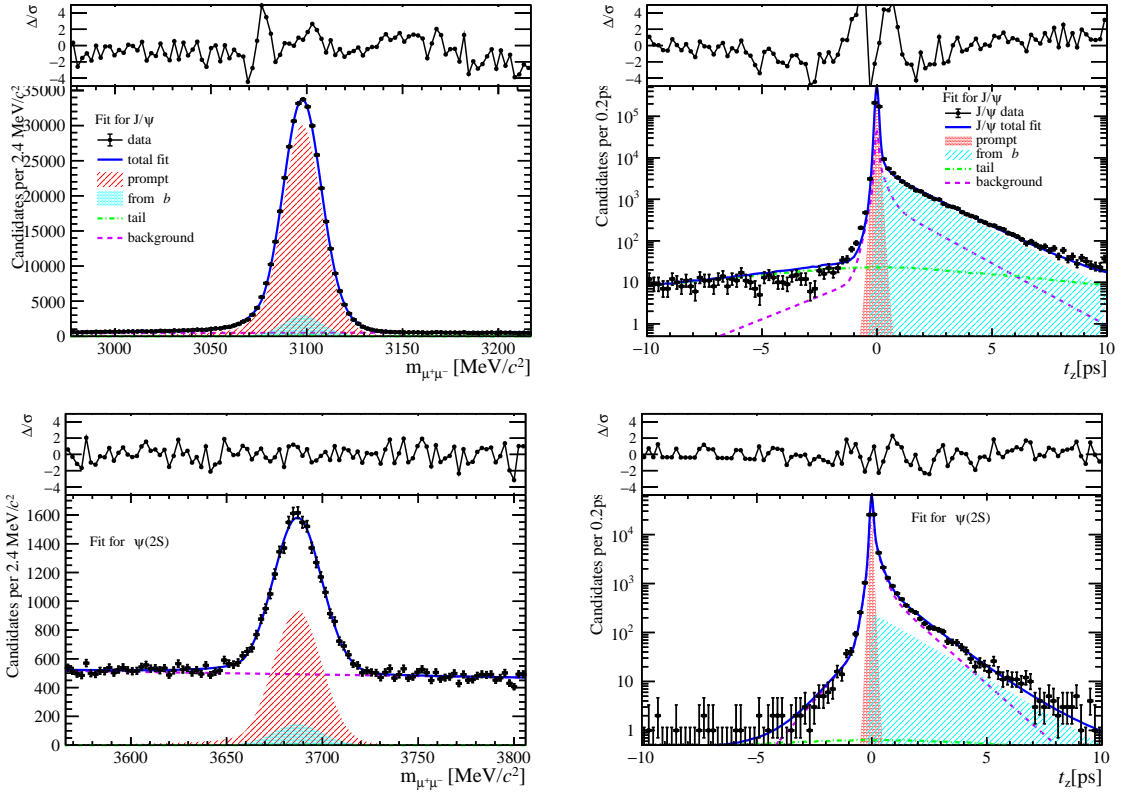


Figure 198: Fit results in  $0 \text{ GeV}/c < p_T < 2 \text{ GeV}/c$ ,  $2.0 < y < 2.8$  and  $12 \leq \text{nForwardTracks} < 24$ .

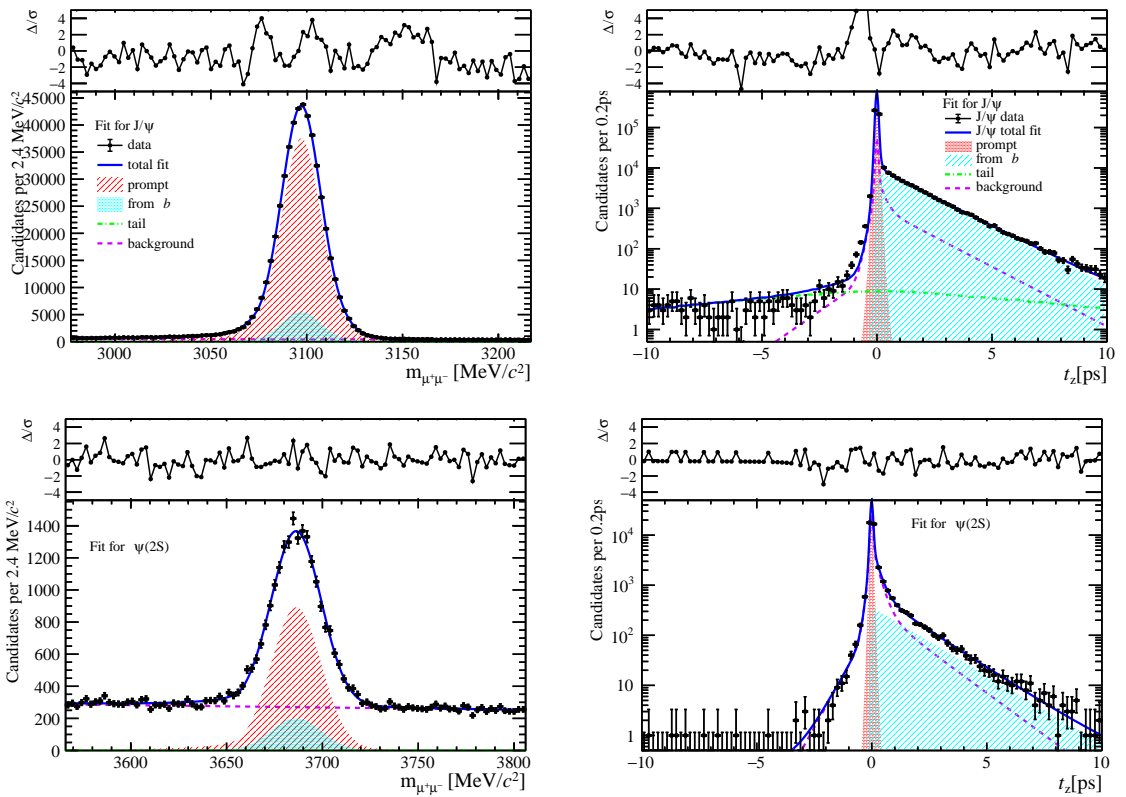


Figure 199: Fit results in  $2 \text{ GeV}/c < p_T < 4 \text{ GeV}/c$ ,  $2.0 < y < 2.8$  and  $12 \leq \text{nForwardTracks} < 24$ .

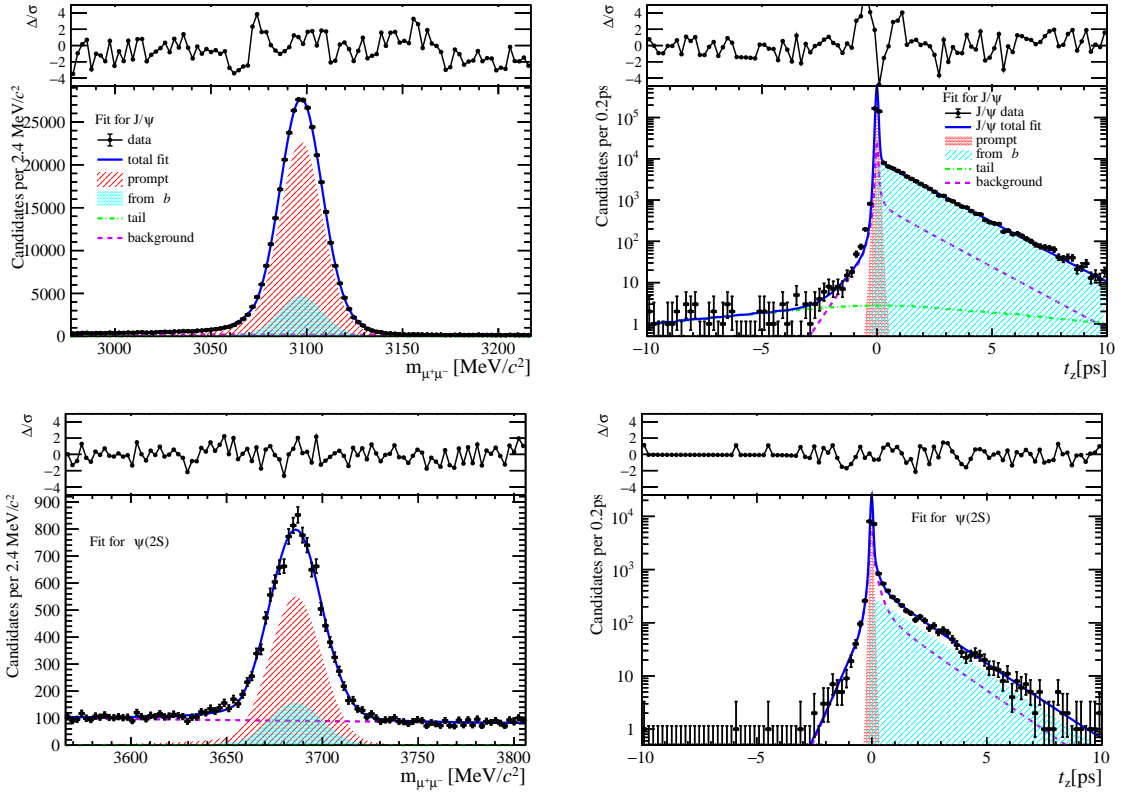


Figure 200: Fit results in  $4 \text{ GeV}/c < p_T < 6 \text{ GeV}/c$ ,  $2.0 < y < 2.8$  and  $12 \leq \text{nForwardTracks} < 24$ .

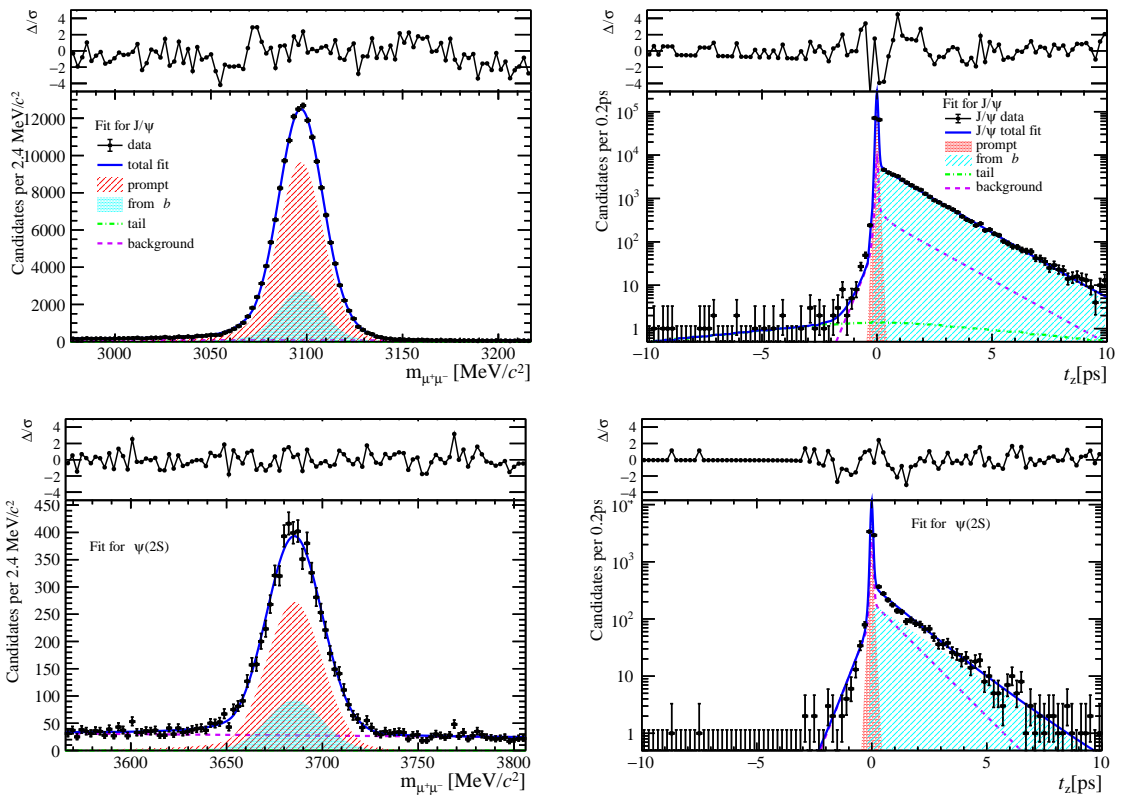


Figure 201: Fit results in  $6 \text{ GeV}/c < p_T < 8 \text{ GeV}/c$ ,  $2.0 < y < 2.8$  and  $12 \leq \text{nForwardTracks} < 24$ .

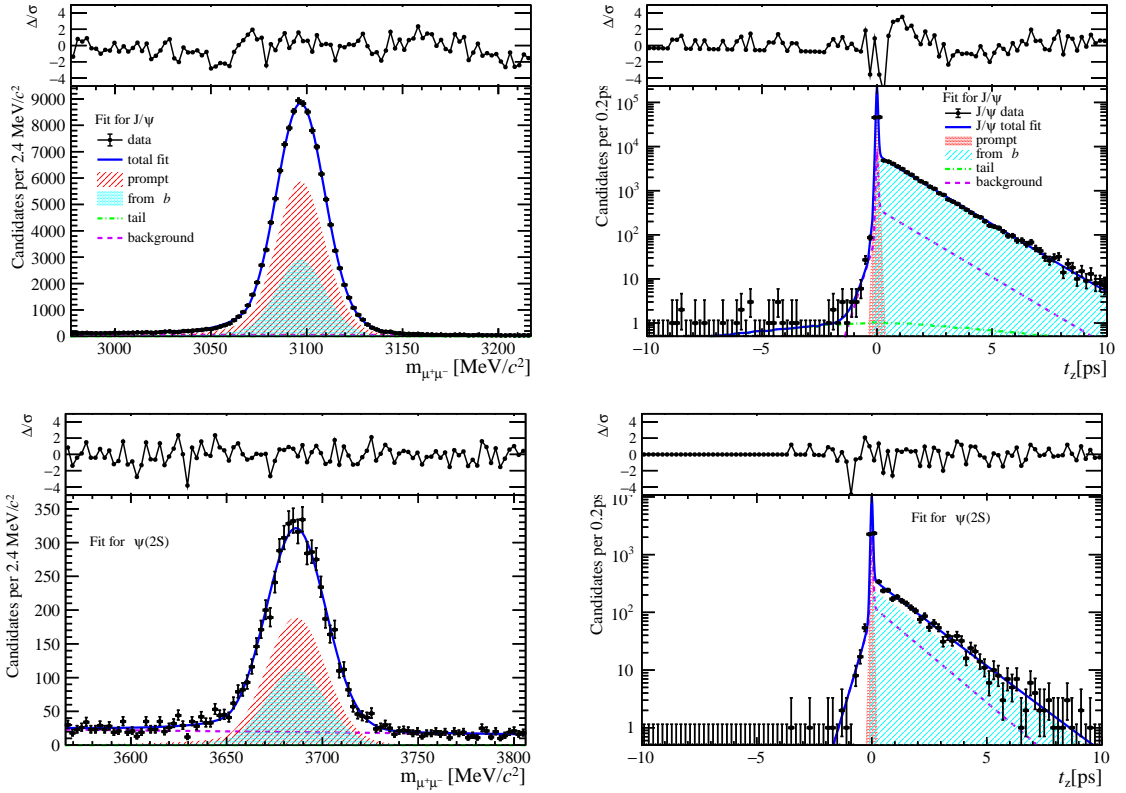


Figure 202: Fit results in  $8 \text{ GeV}/c < p_T < 20 \text{ GeV}/c$ ,  $2.0 < y < 2.8$  and  $12 \leq \text{nForwardTracks} < 24$ .

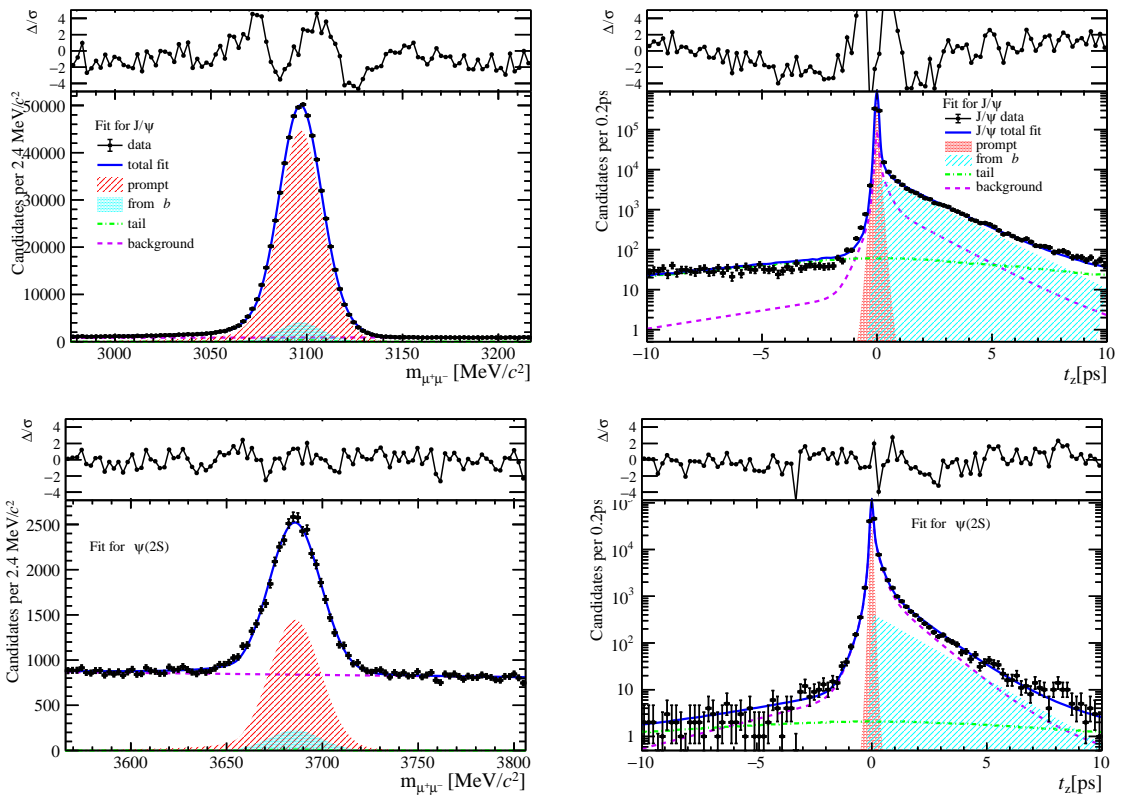


Figure 203: Fit results in  $0 \text{ GeV}/c < p_T < 2 \text{ GeV}/c$ ,  $2.8 < y < 3.5$  and  $12 \leq \text{nForwardTracks} < 24$ .

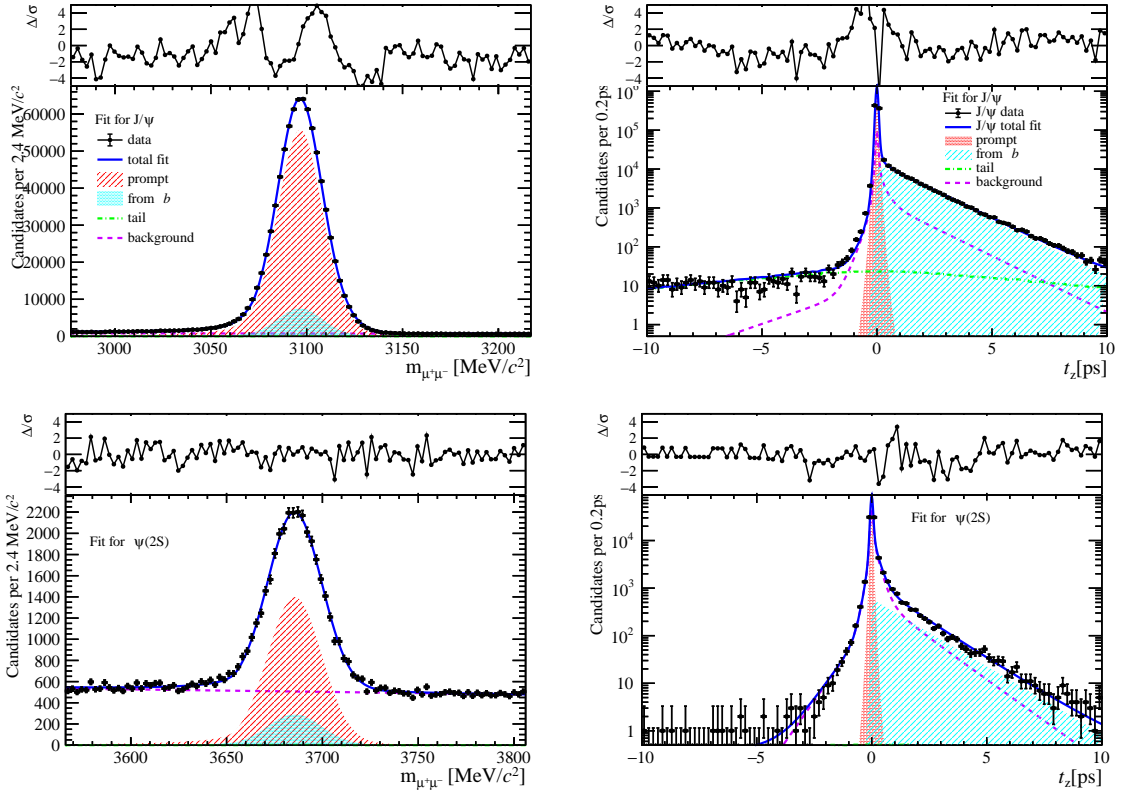


Figure 204: Fit results in  $2 \text{ GeV}/c < p_T < 4 \text{ GeV}/c$ ,  $2.8 < y < 3.5$  and  $12 \leq \text{nForwardTracks} < 24$ .

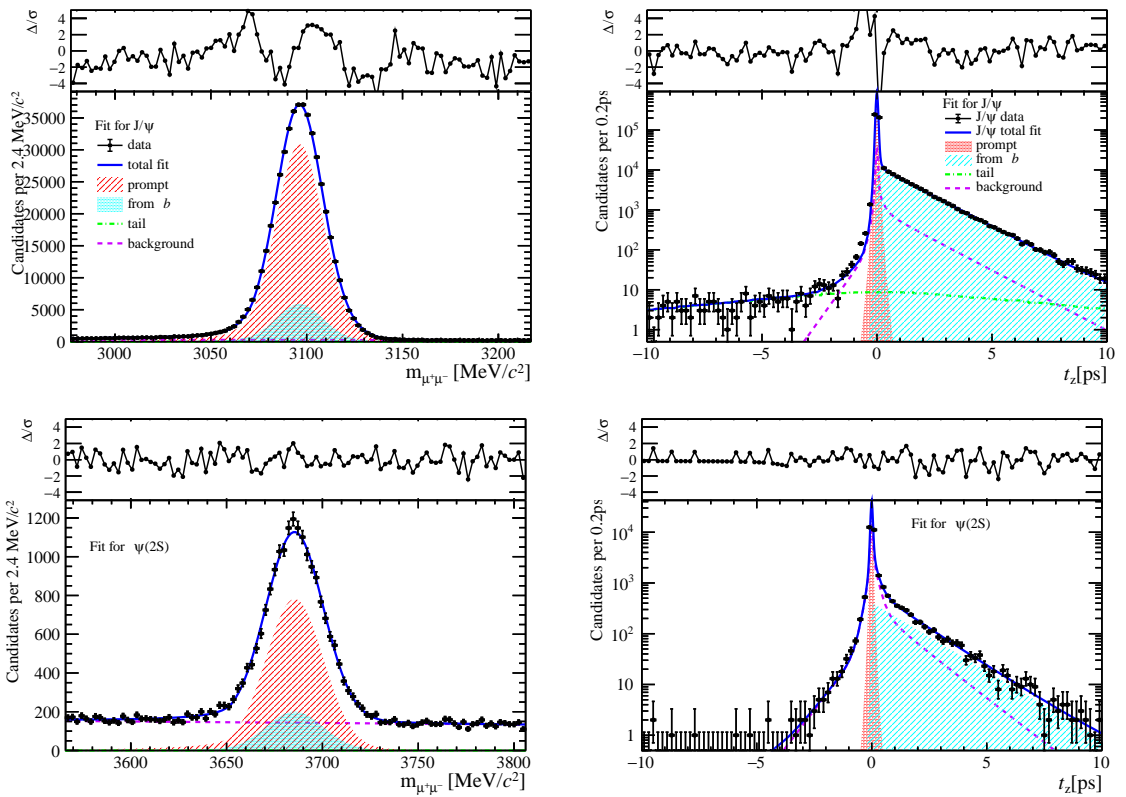


Figure 205: Fit results in  $4 \text{ GeV}/c < p_T < 6 \text{ GeV}/c$ ,  $2.8 < y < 3.5$  and  $12 \leq \text{nForwardTracks} < 24$ .

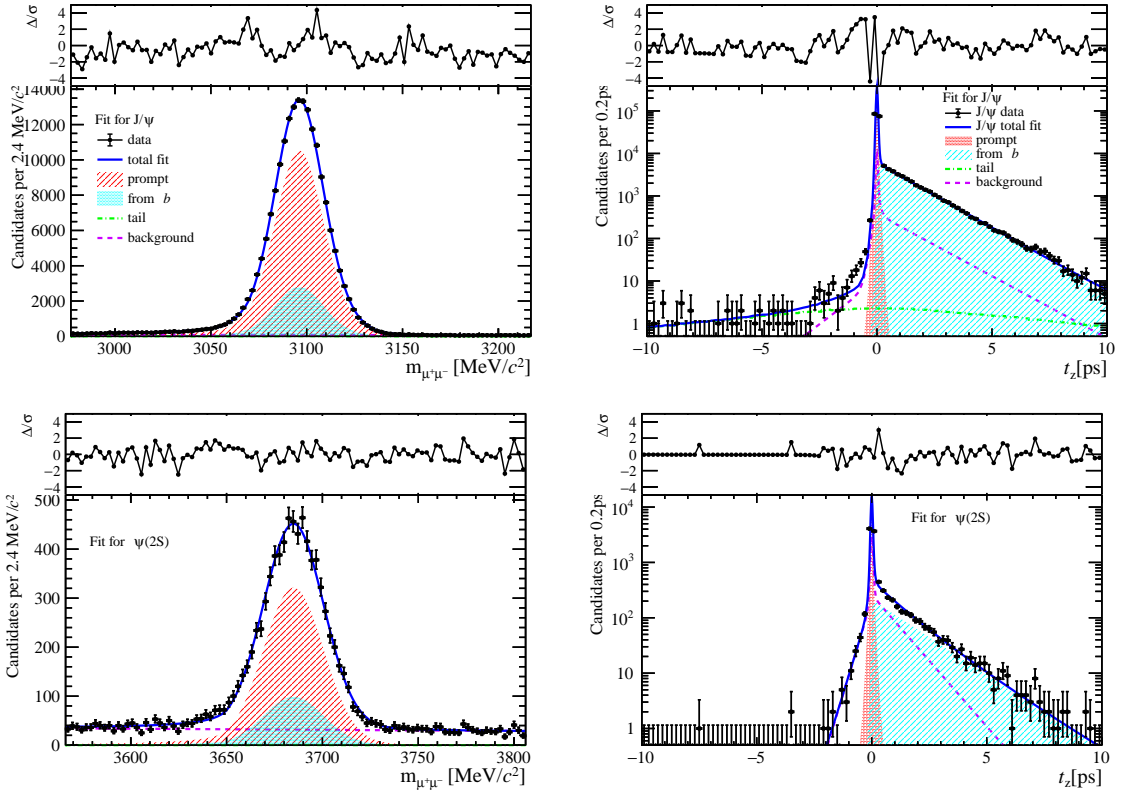


Figure 206: Fit results in  $6 \text{ GeV}/c < p_T < 8 \text{ GeV}/c$ ,  $2.8 < y < 3.5$  and  $12 \leq \text{nForwardTracks} < 24$ .

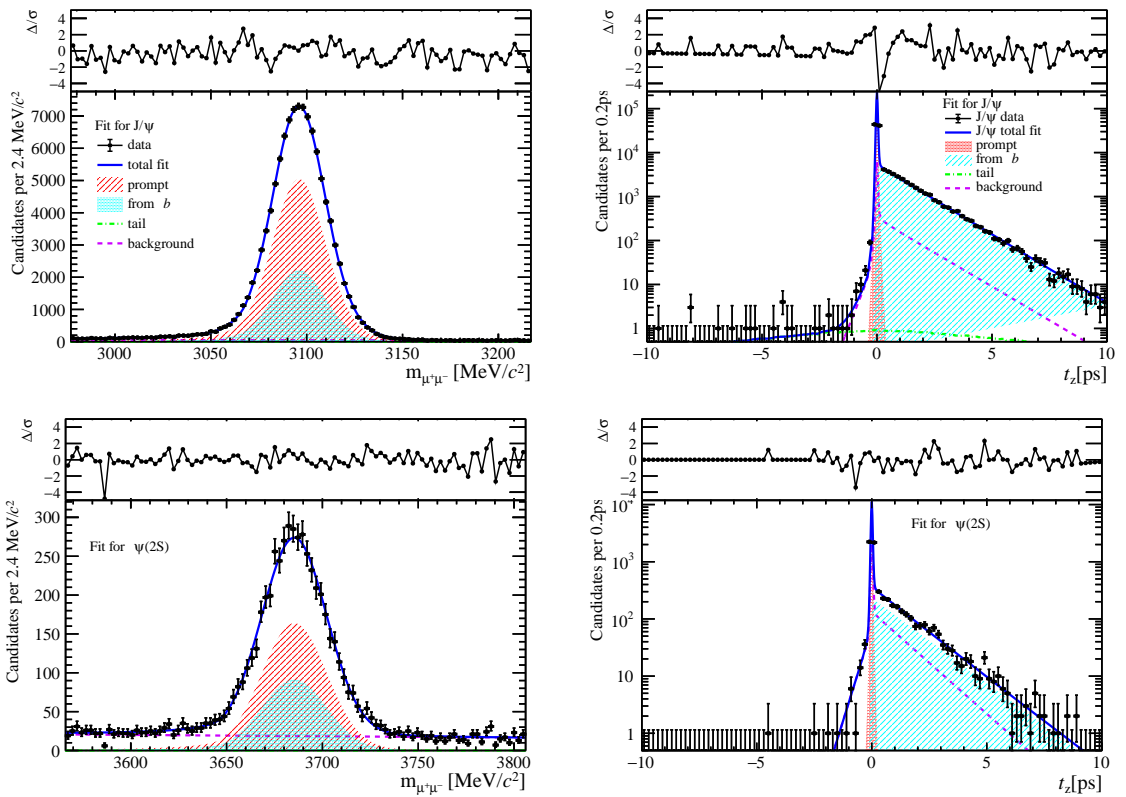


Figure 207: Fit results in  $8 \text{ GeV}/c < p_T < 20 \text{ GeV}/c$ ,  $2.8 < y < 3.5$  and  $12 \leq \text{nForwardTracks} < 24$ .

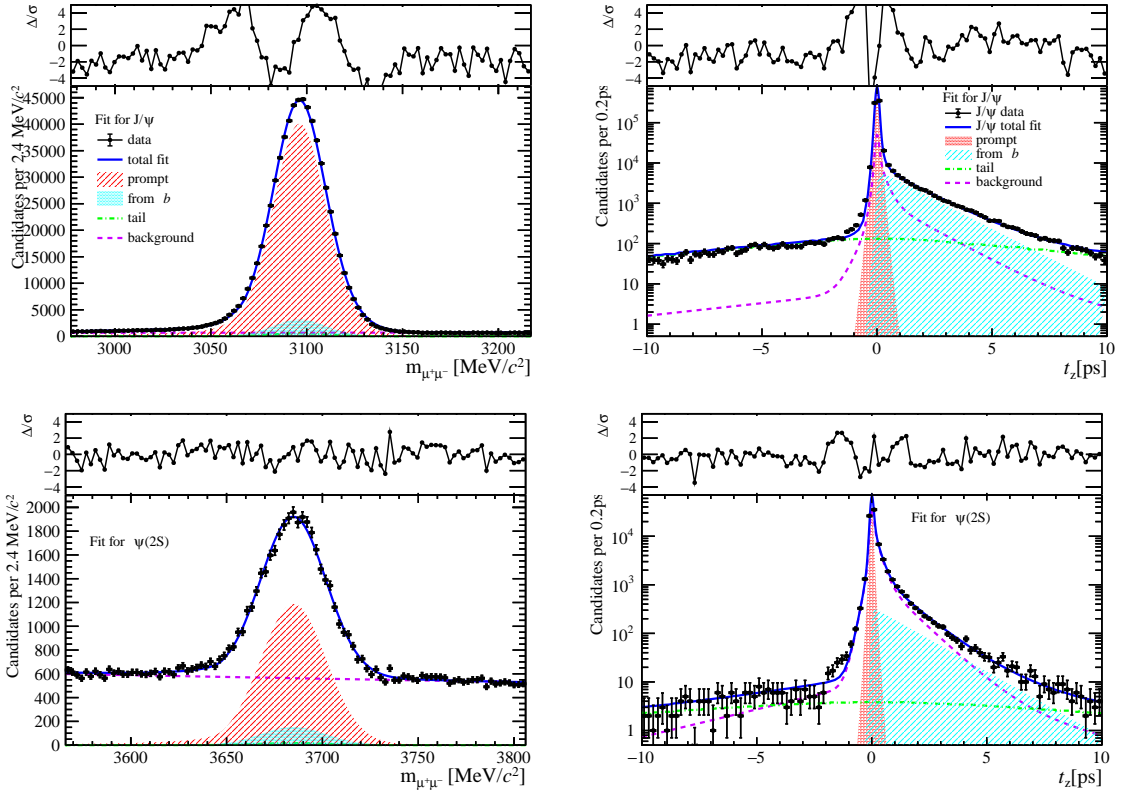


Figure 208: Fit results in  $0 \text{ GeV}/c < p_T < 2 \text{ GeV}/c$ ,  $3.5 < y < 4.5$  and  $12 \leq \text{nForwardTracks} < 24$ .

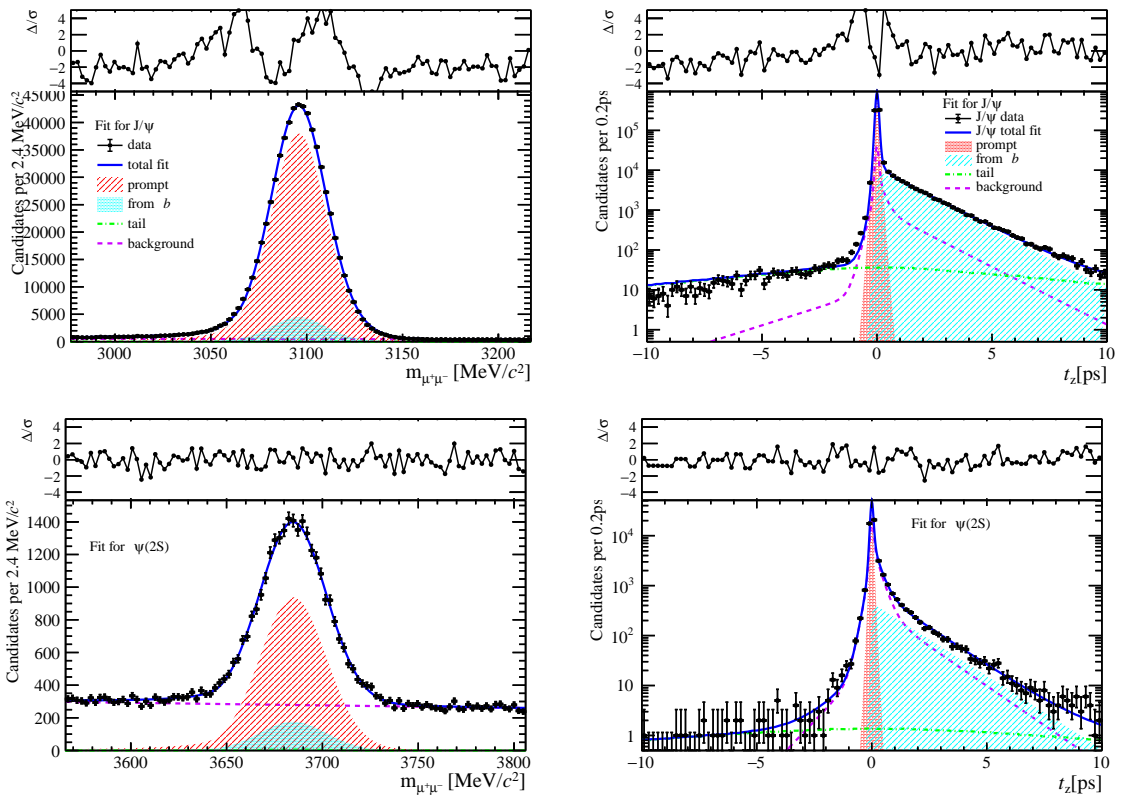


Figure 209: Fit results in  $2 \text{ GeV}/c < p_T < 4 \text{ GeV}/c$ ,  $3.5 < y < 4.5$  and  $12 \leq \text{nForwardTracks} < 24$ .

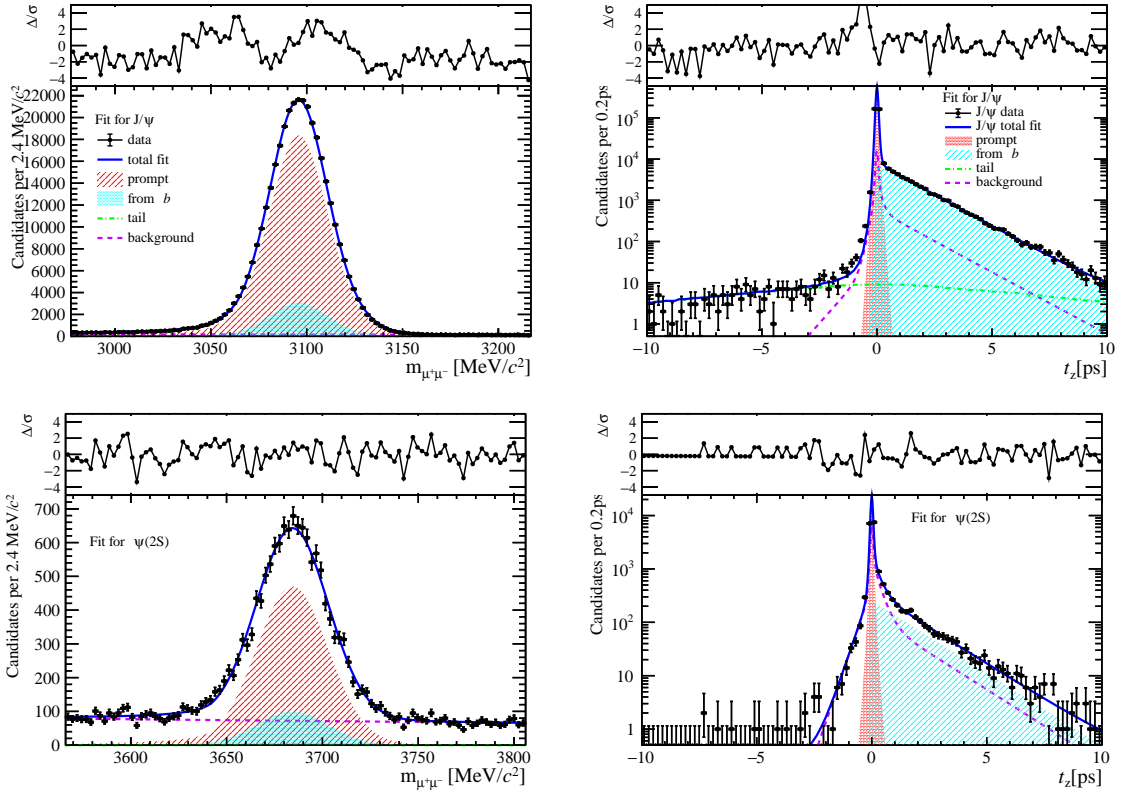


Figure 210: Fit results in  $4 \text{ GeV}/c < p_T < 6 \text{ GeV}/c$ ,  $3.5 < y < 4.5$  and  $12 \leq \text{nForwardTracks} < 24$ .

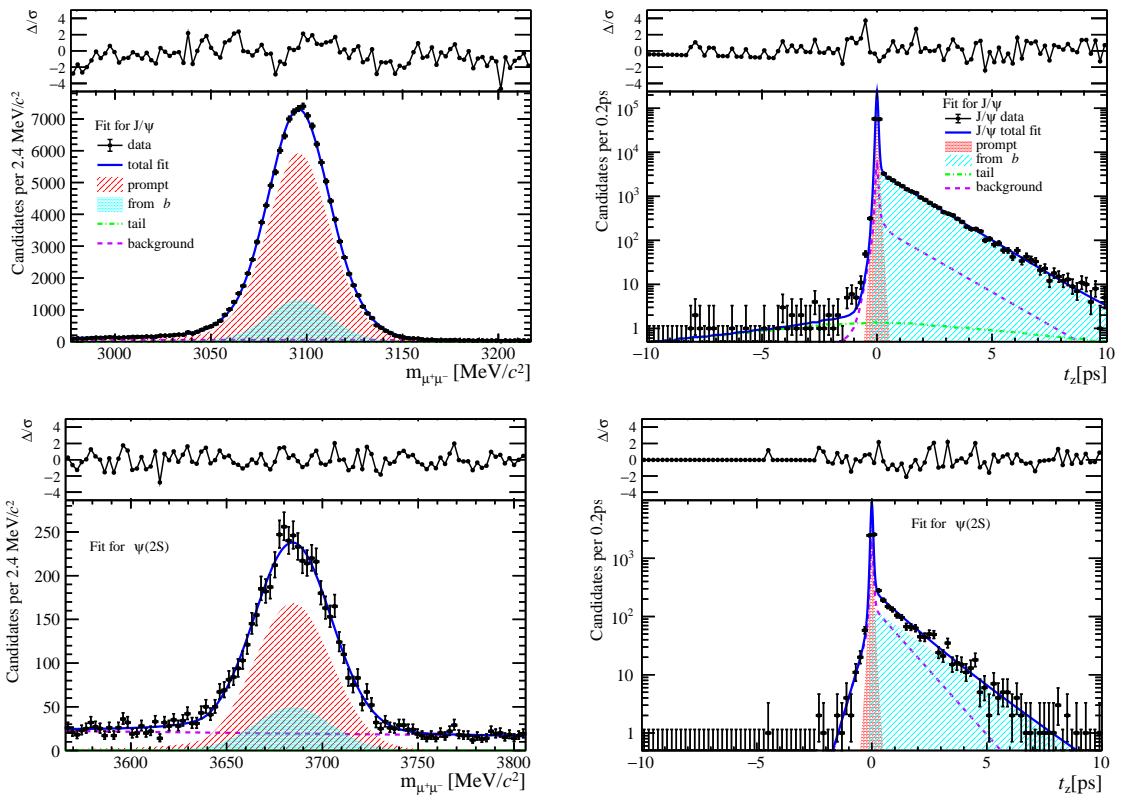


Figure 211: Fit results in  $6 \text{ GeV}/c < p_T < 8 \text{ GeV}/c$ ,  $3.5 < y < 4.5$  and  $12 \leq \text{nForwardTracks} < 24$ .

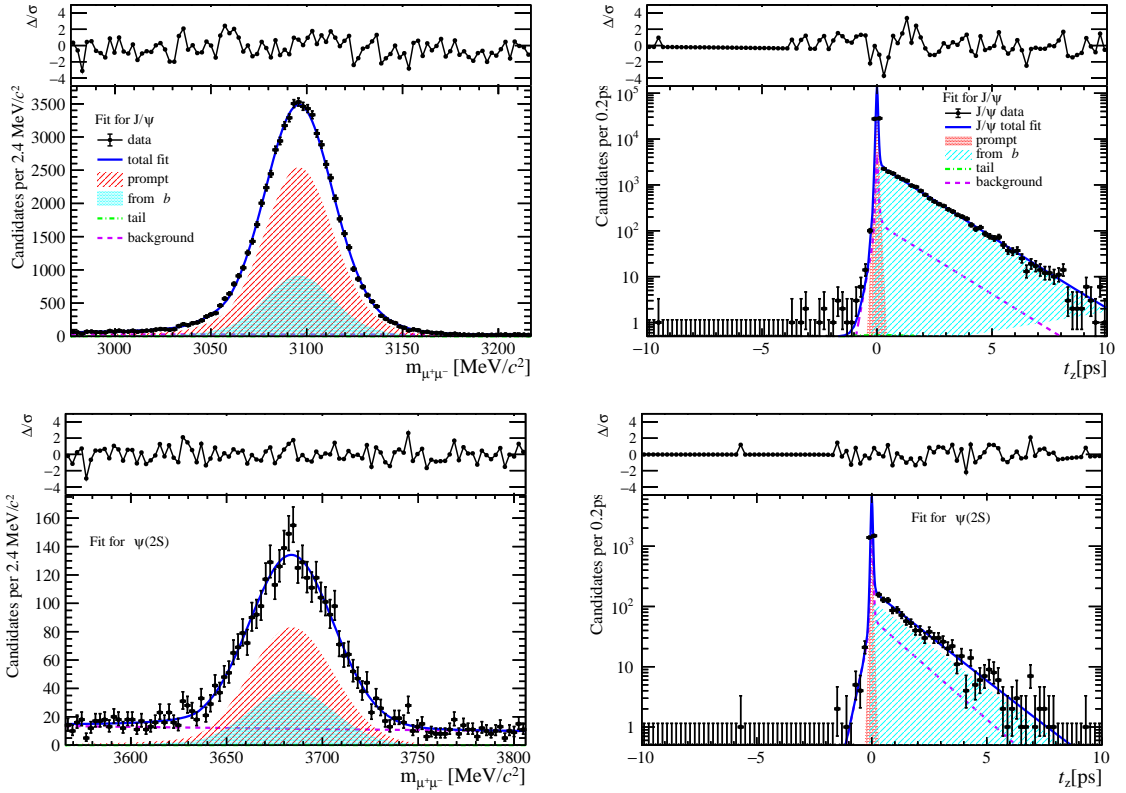


Figure 212: Fit results in  $8 \text{ GeV}/c < p_T < 20 \text{ GeV}/c$ ,  $3.5 < y < 4.5$  and  $12 \leq \text{nForwardTracks} < 24$ .

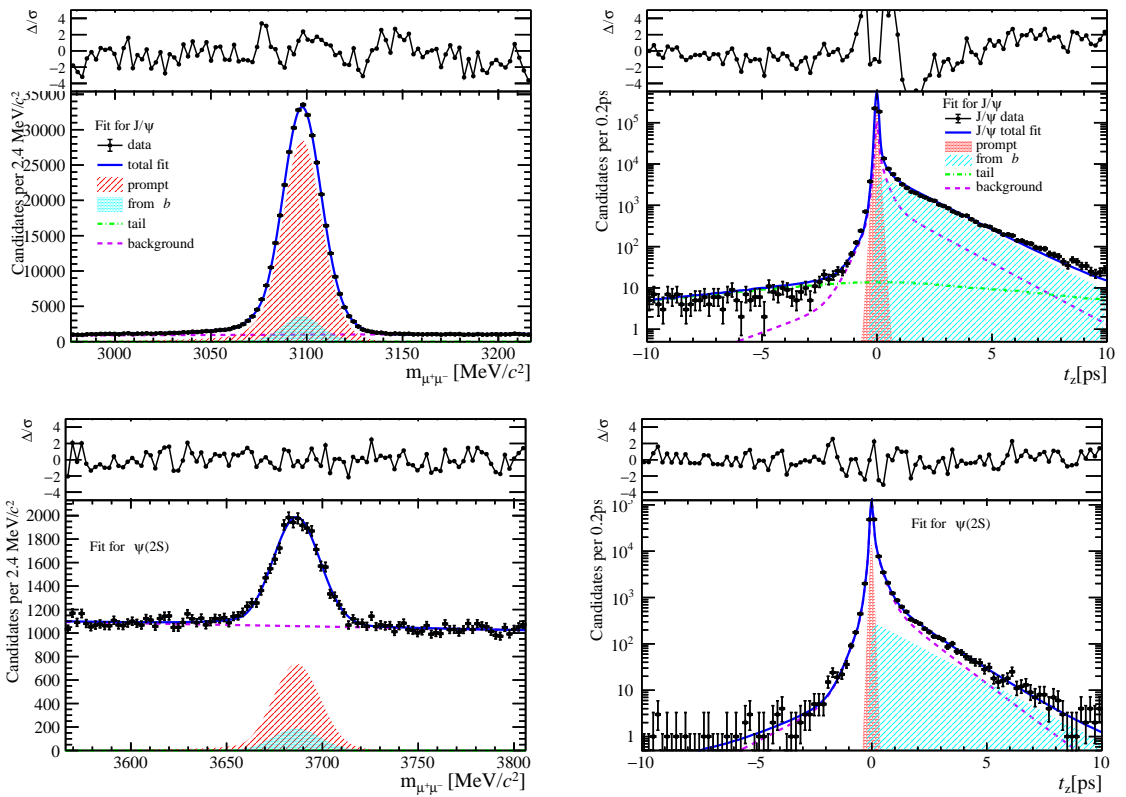


Figure 213: Fit results in  $0 \text{ GeV}/c < p_T < 2 \text{ GeV}/c$ ,  $2.0 < y < 2.8$  and  $24 \leq \text{nForwardTracks} < 36$ .

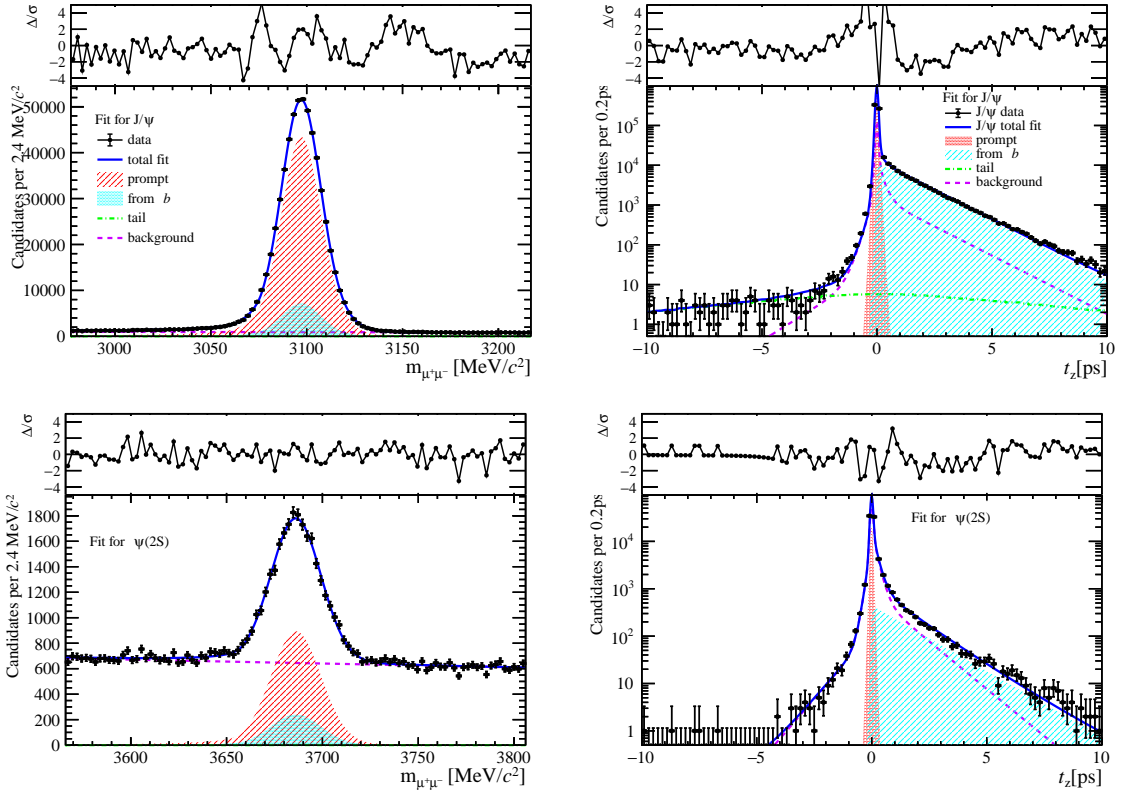


Figure 214: Fit results in  $2 \text{ GeV}/c < p_T < 4 \text{ GeV}/c$ ,  $2.0 < y < 2.8$  and  $24 \leq \text{nForwardTracks} < 36$ .

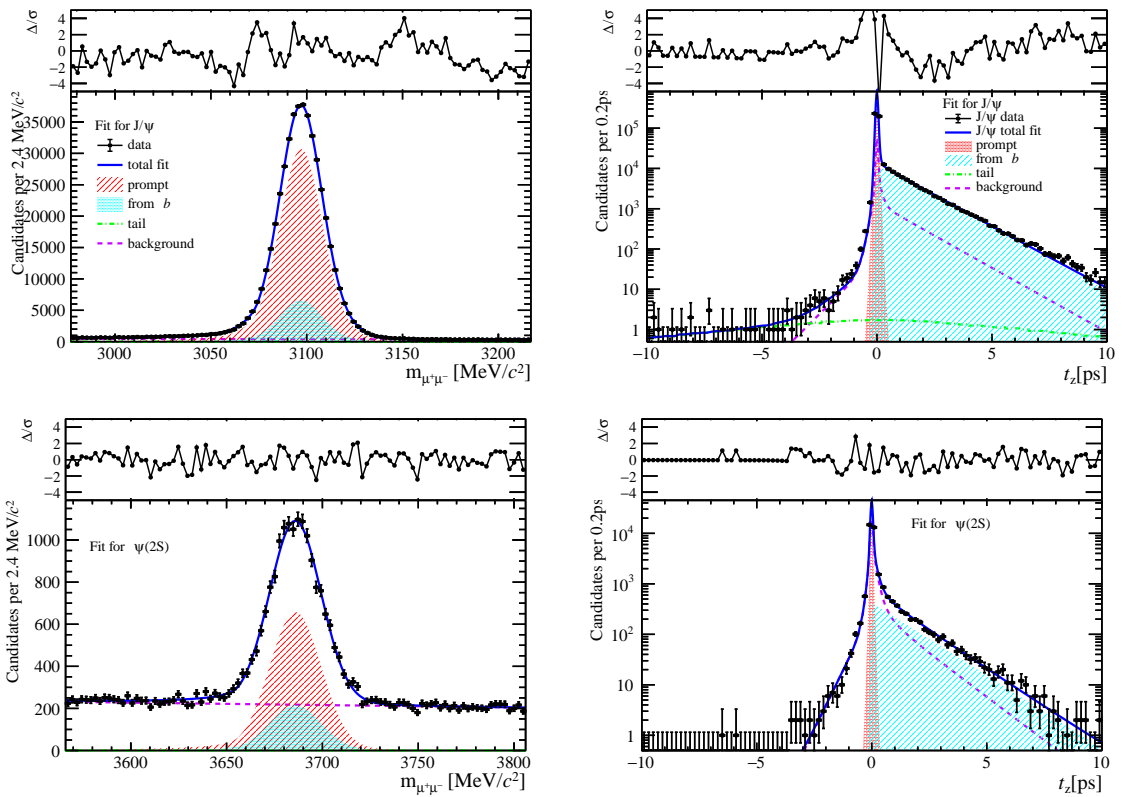


Figure 215: Fit results in  $4 \text{ GeV}/c < p_T < 6 \text{ GeV}/c$ ,  $2.0 < y < 2.8$  and  $24 \leq \text{nForwardTracks} < 36$ .

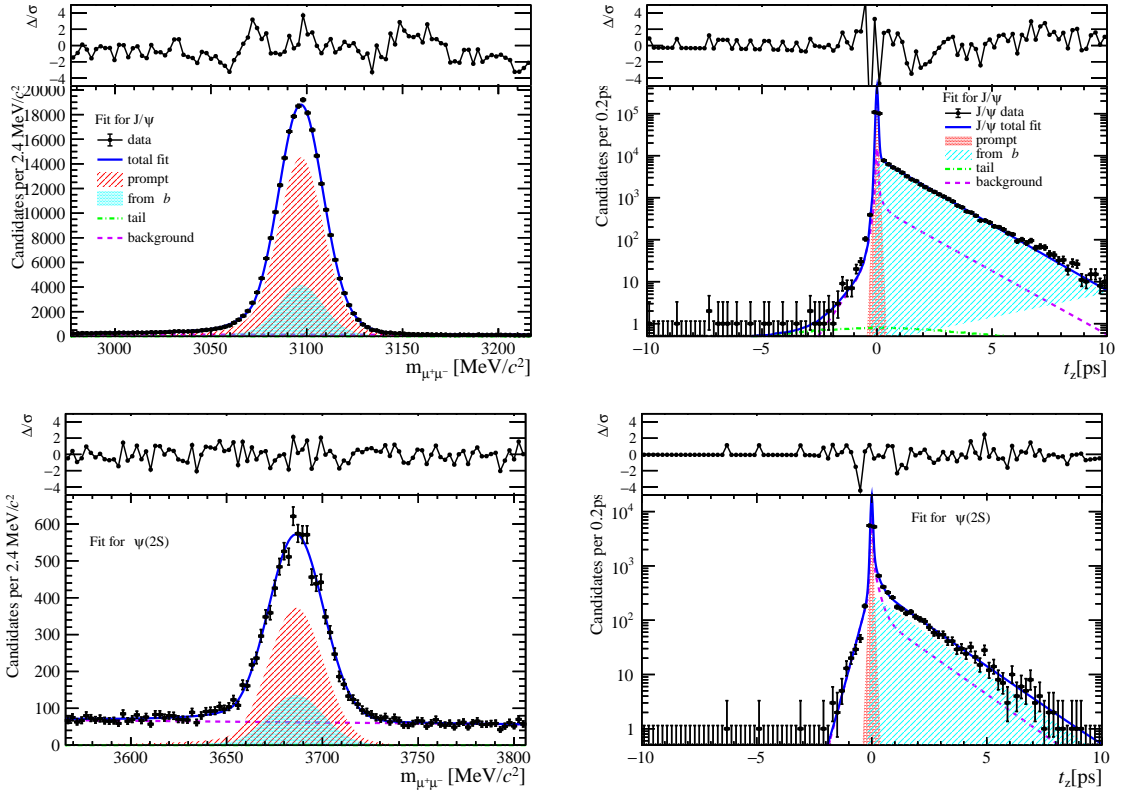


Figure 216: Fit results in  $6 \text{ GeV}/c < p_T < 8 \text{ GeV}/c$ ,  $2.0 < y < 2.8$  and  $24 \leq \text{nForwardTracks} < 36$ .

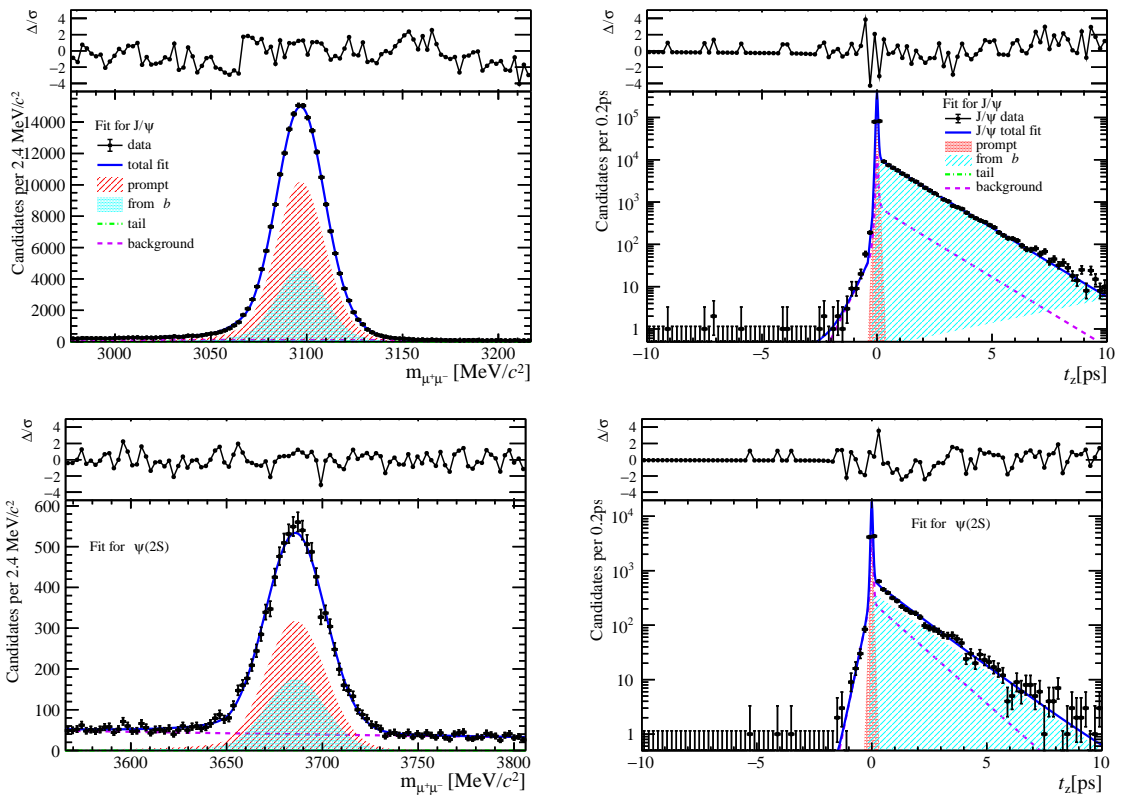


Figure 217: Fit results in  $8 \text{ GeV}/c < p_T < 20 \text{ GeV}/c$ ,  $2.0 < y < 2.8$  and  $24 \leq \text{nForwardTracks} < 36$ .

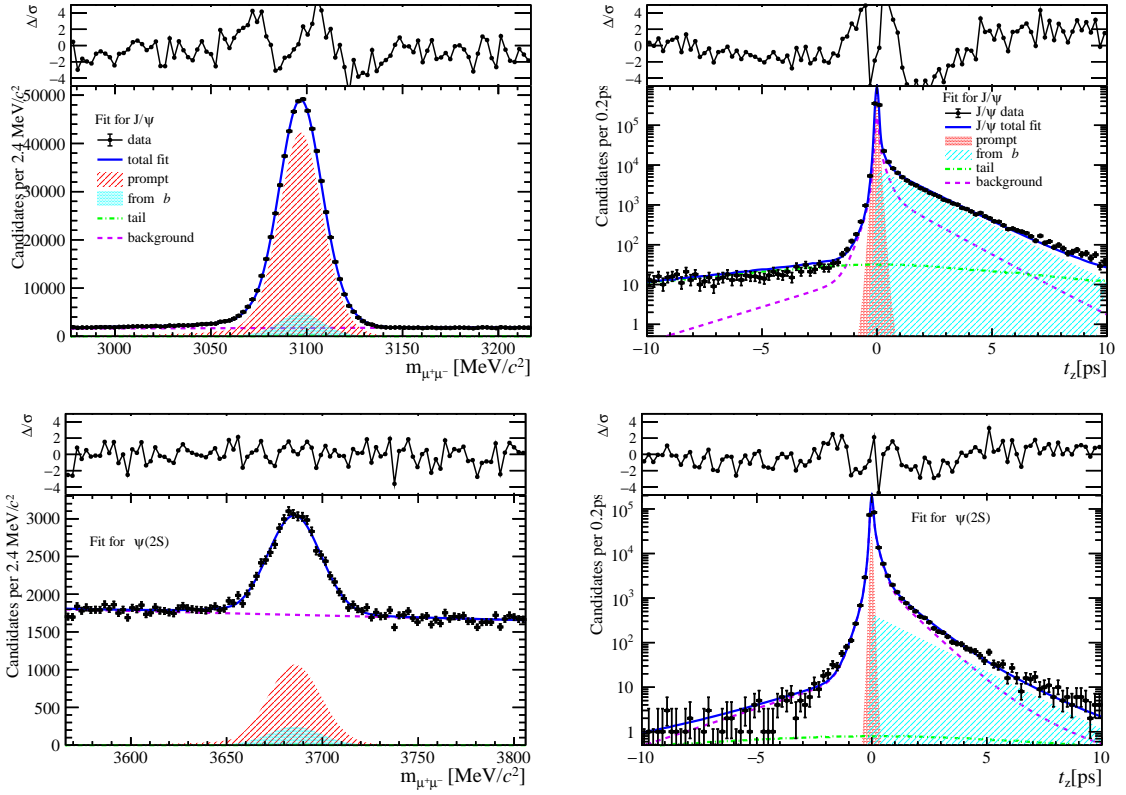


Figure 218: Fit results in  $0 \text{ GeV}/c < p_T < 2 \text{ GeV}/c$ ,  $2.8 < y < 3.5$  and  $24 \leq \text{nForwardTracks} < 36$ .

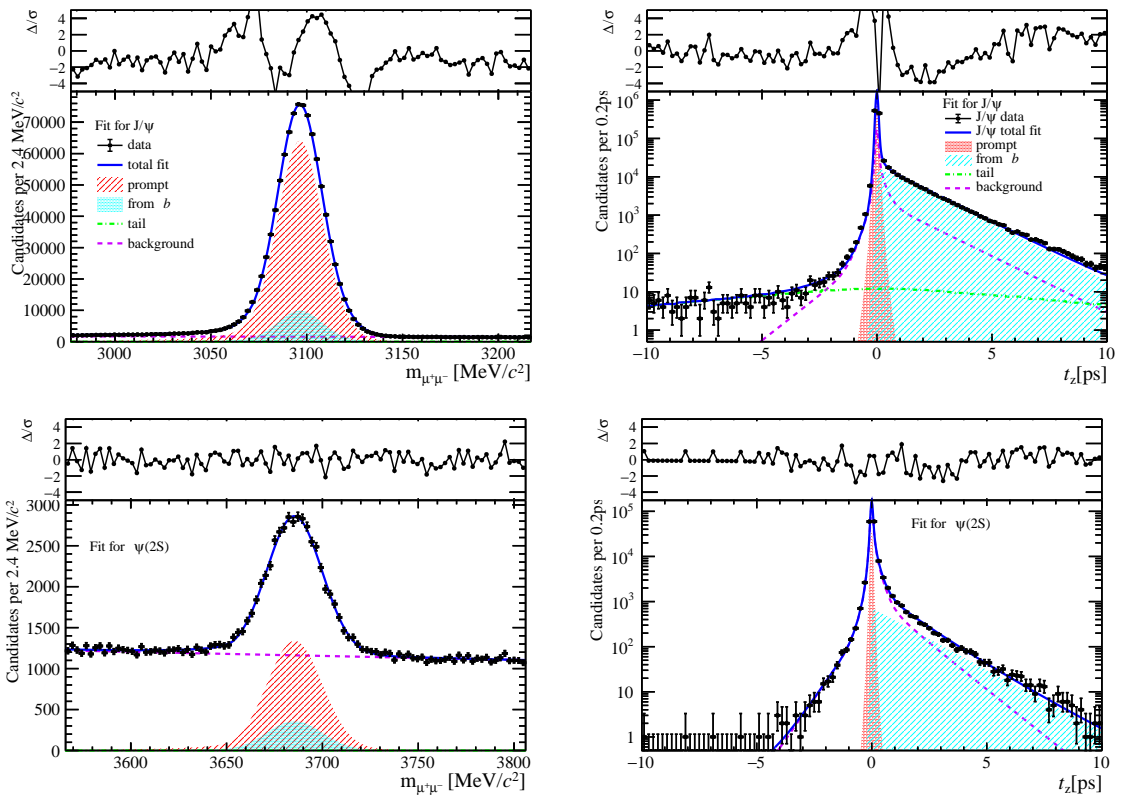


Figure 219: Fit results in  $2 \text{ GeV}/c < p_T < 4 \text{ GeV}/c$ ,  $2.8 < y < 3.5$  and  $24 \leq \text{nForwardTracks} < 36$ .

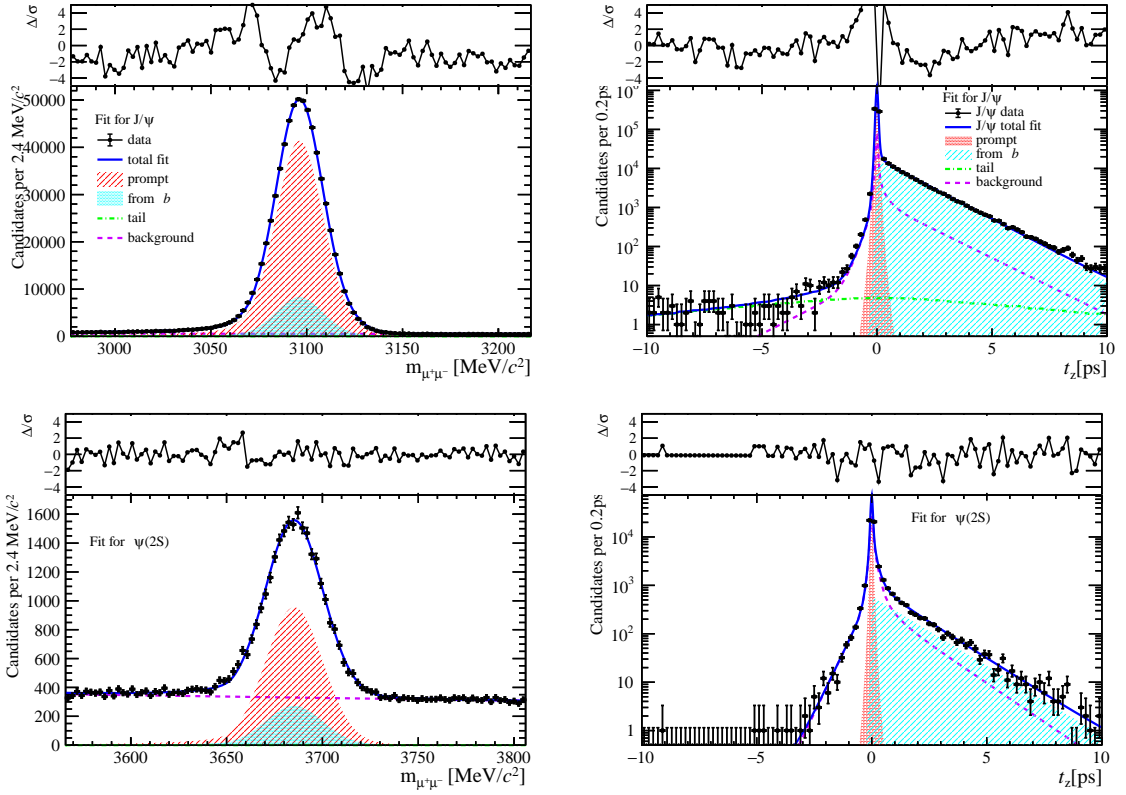


Figure 220: Fit results in  $4 \text{ GeV}/c < p_T < 6 \text{ GeV}/c$ ,  $2.8 < y < 3.5$  and  $24 \leq \text{nForwardTracks} < 36$ .

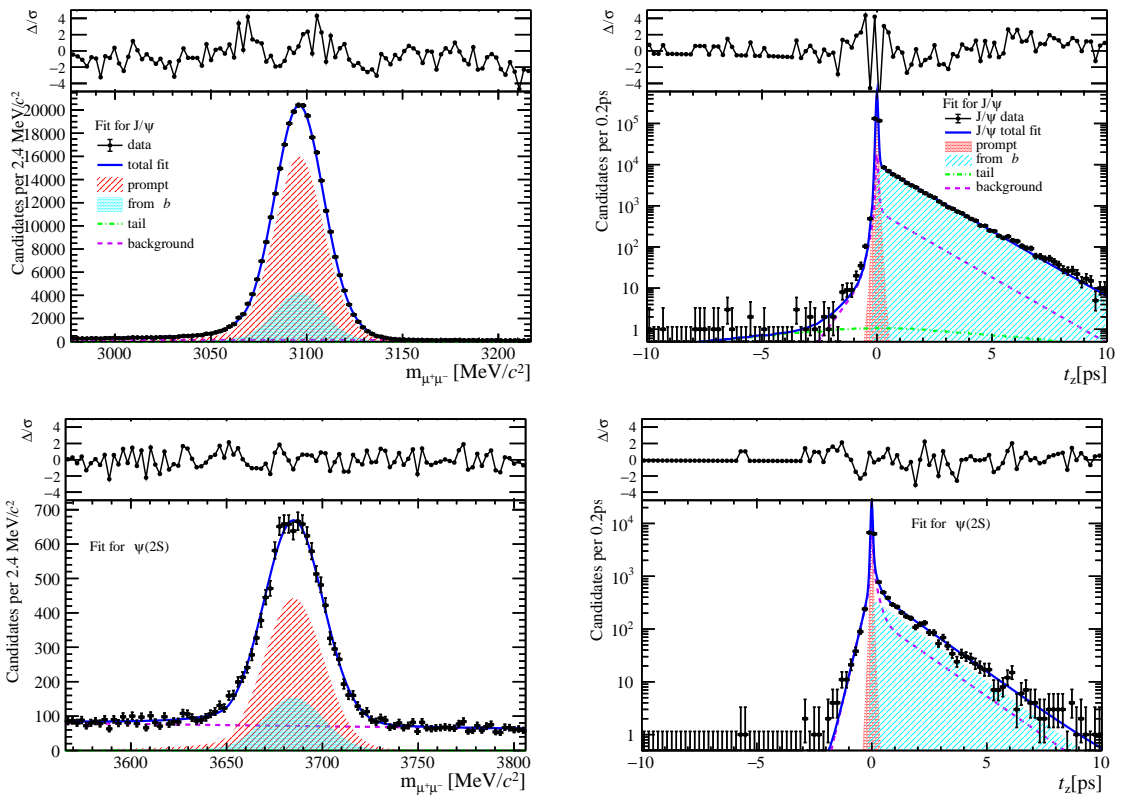


Figure 221: Fit results in  $6 \text{ GeV}/c < p_T < 8 \text{ GeV}/c$ ,  $2.8 < y < 3.5$  and  $24 \leq \text{nForwardTracks} < 36$ .

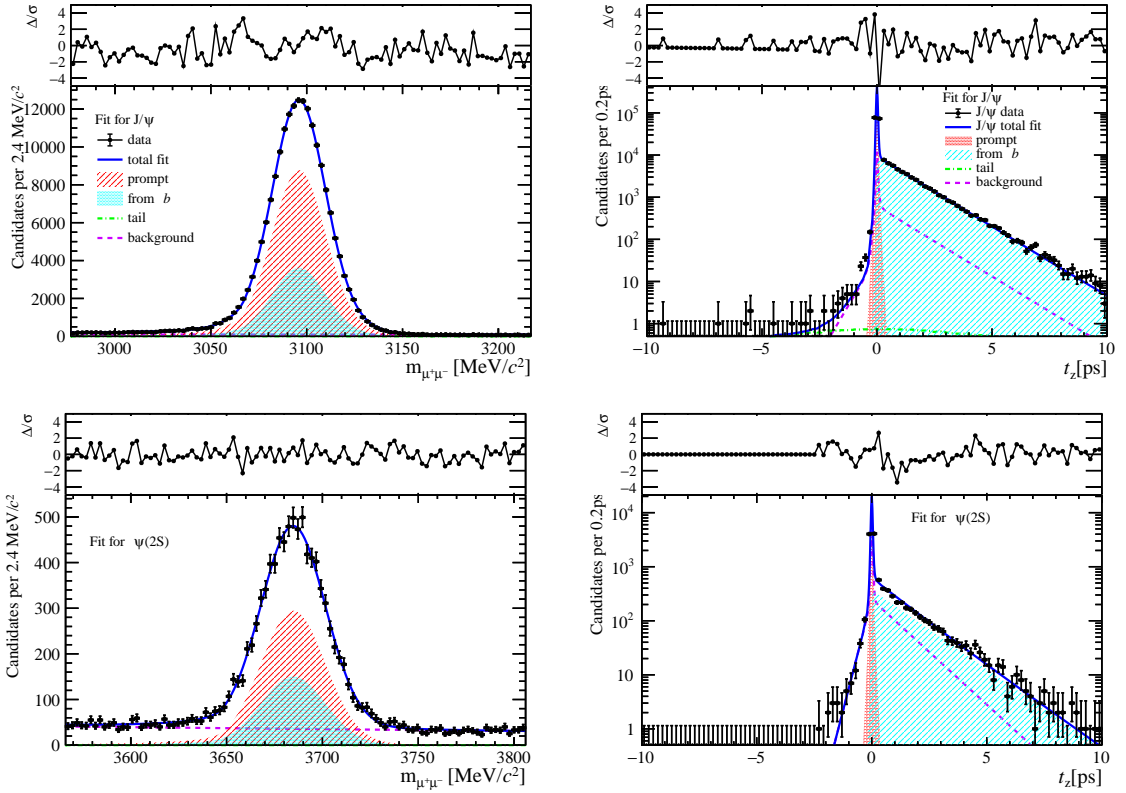


Figure 222: Fit results in  $8 \text{ GeV}/c < p_T < 20 \text{ GeV}/c$ ,  $2.8 < y < 3.5$  and  $24 \leq \text{nForwardTracks} < 36$ .

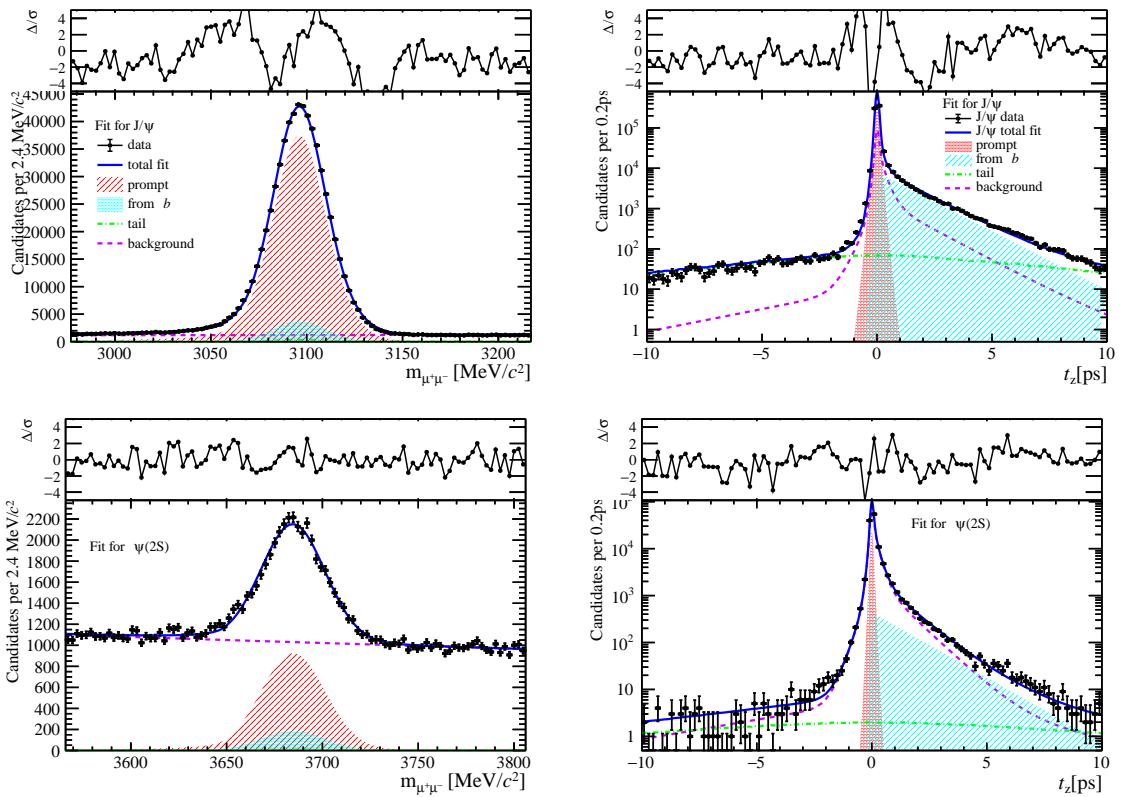


Figure 223: Fit results in  $0 \text{ GeV}/c < p_T < 2 \text{ GeV}/c$ ,  $3.5 < y < 4.5$  and  $24 \leq \text{nForwardTracks} < 36$ .

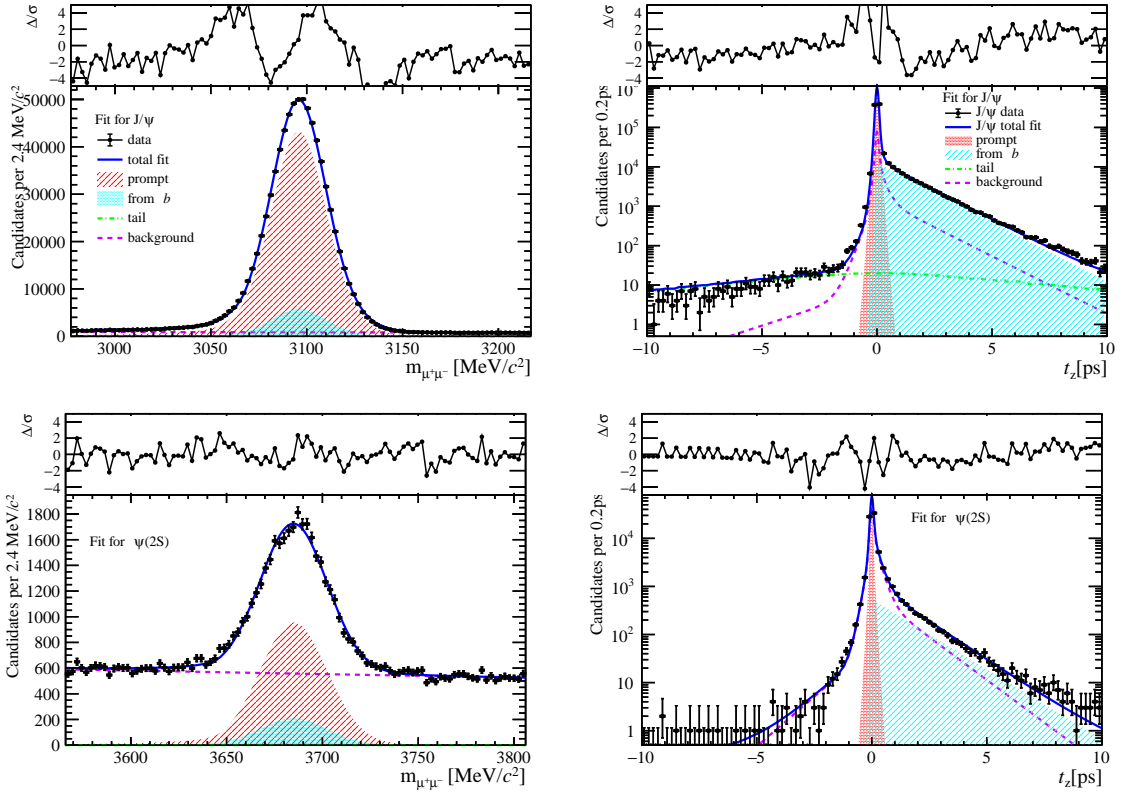


Figure 224: Fit results in  $2 \text{ GeV}/c < p_T < 4 \text{ GeV}/c$ ,  $3.5 < y < 4.5$  and  $24 \leq \text{nForwardTracks} < 36$ .

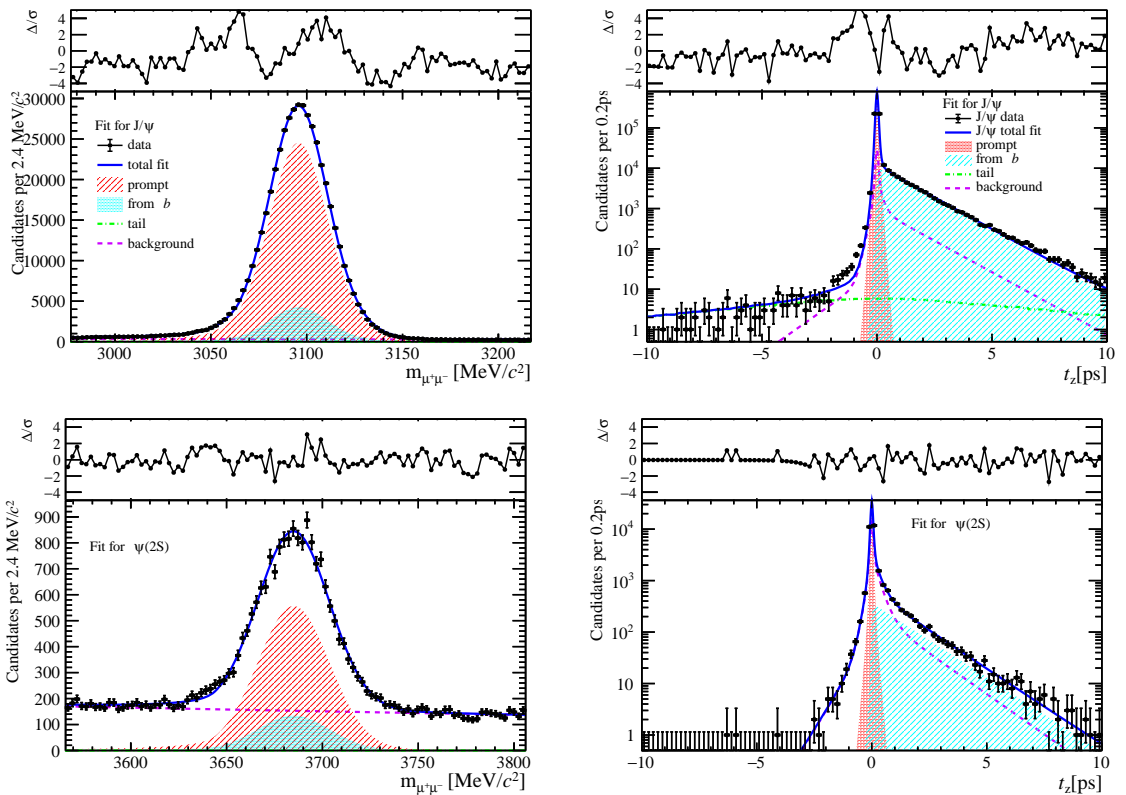


Figure 225: Fit results in  $4 \text{ GeV}/c < p_T < 6 \text{ GeV}/c$ ,  $3.5 < y < 4.5$  and  $24 \leq \text{nForwardTracks} < 36$ .

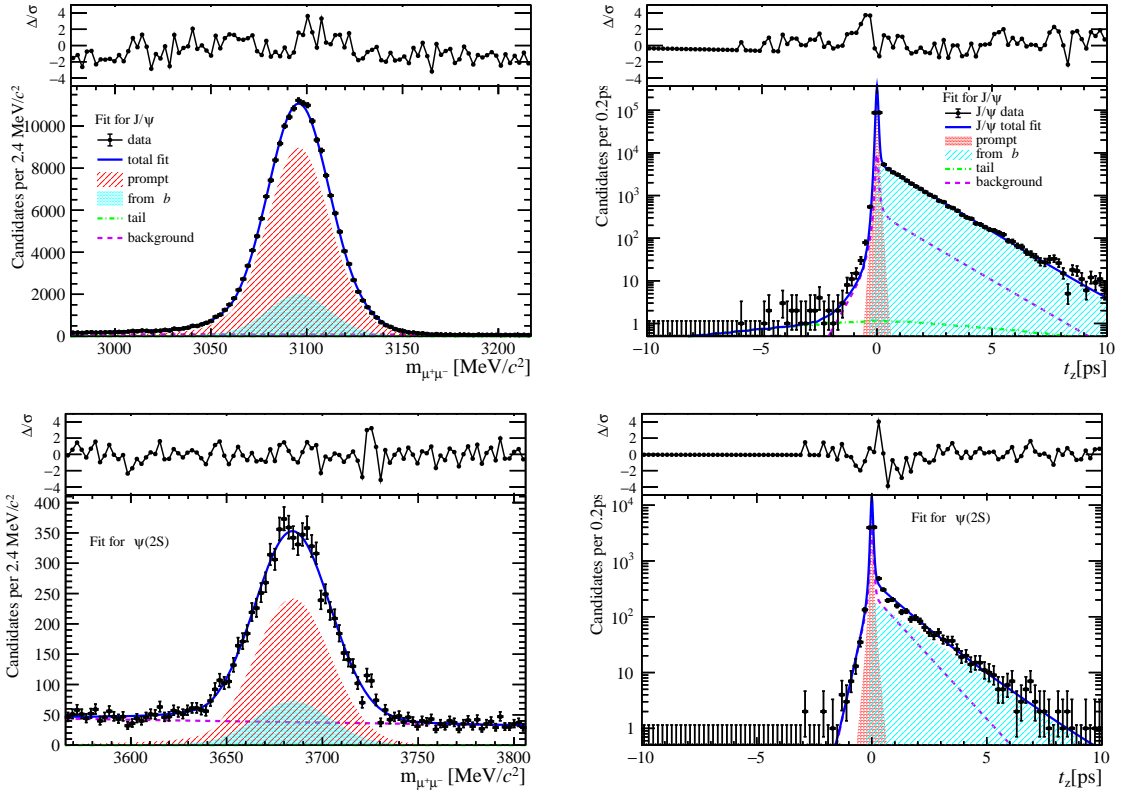


Figure 226: Fit results in  $6 \text{ GeV}/c < p_T < 8 \text{ GeV}/c$ ,  $3.5 < y < 4.5$  and  $24 \leq \text{nForwardTracks} < 36$ .

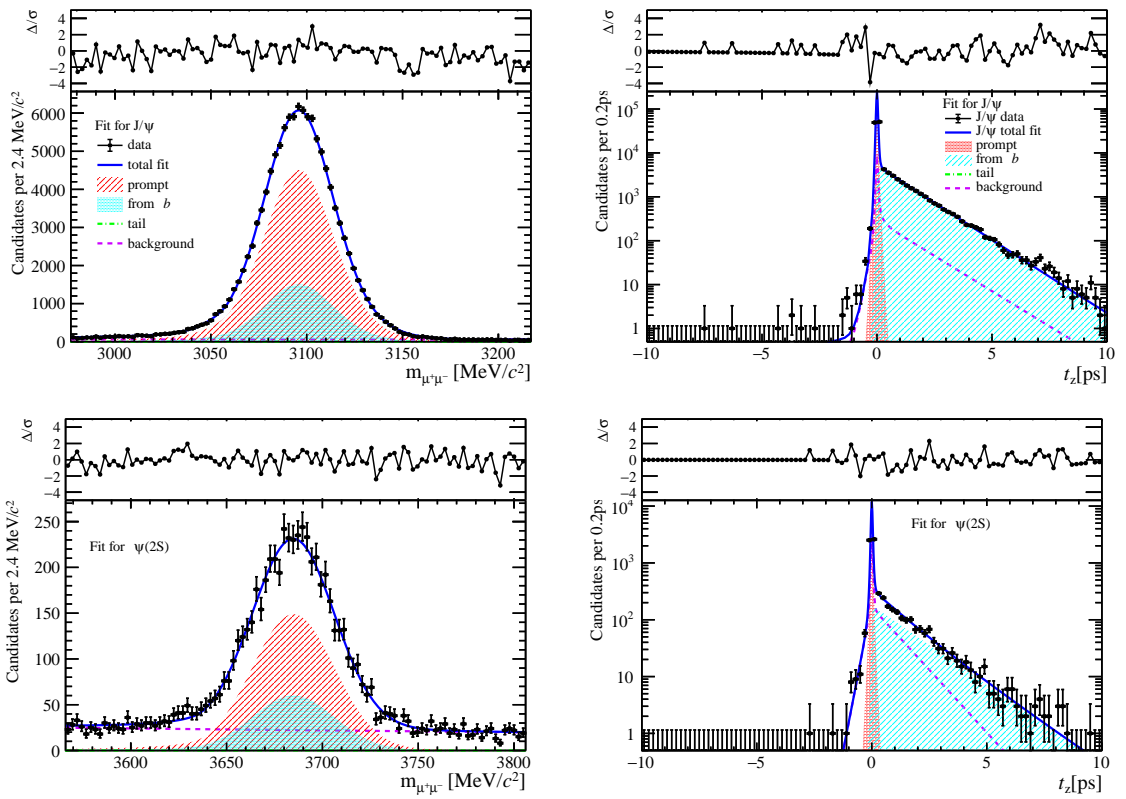


Figure 227: Fit results in  $8 \text{ GeV}/c < p_T < 20 \text{ GeV}/c$ ,  $3.5 < y < 4.5$  and  $24 \leq \text{nForwardTracks} < 36$ .

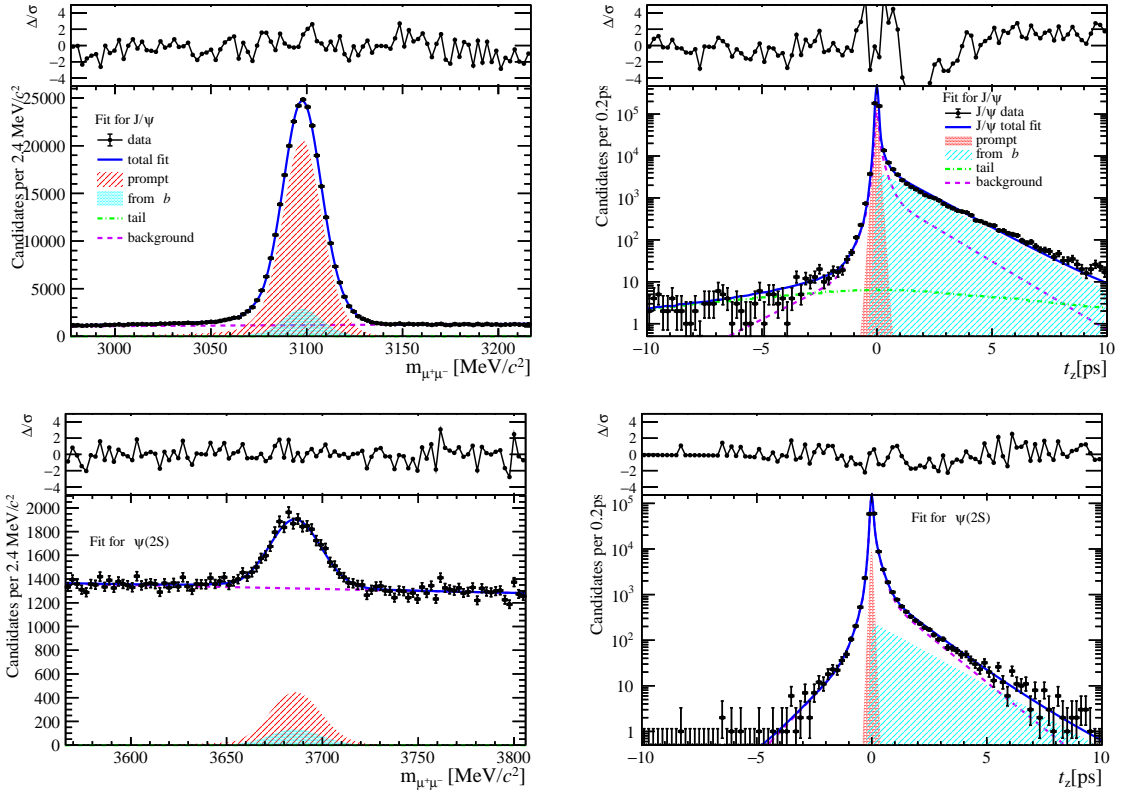


Figure 228: Fit results in  $0 \text{ GeV}/c < p_T < 2 \text{ GeV}/c$ ,  $2.0 < y < 2.8$  and  $36 \leq \text{nForwardTracks} < 48$ .

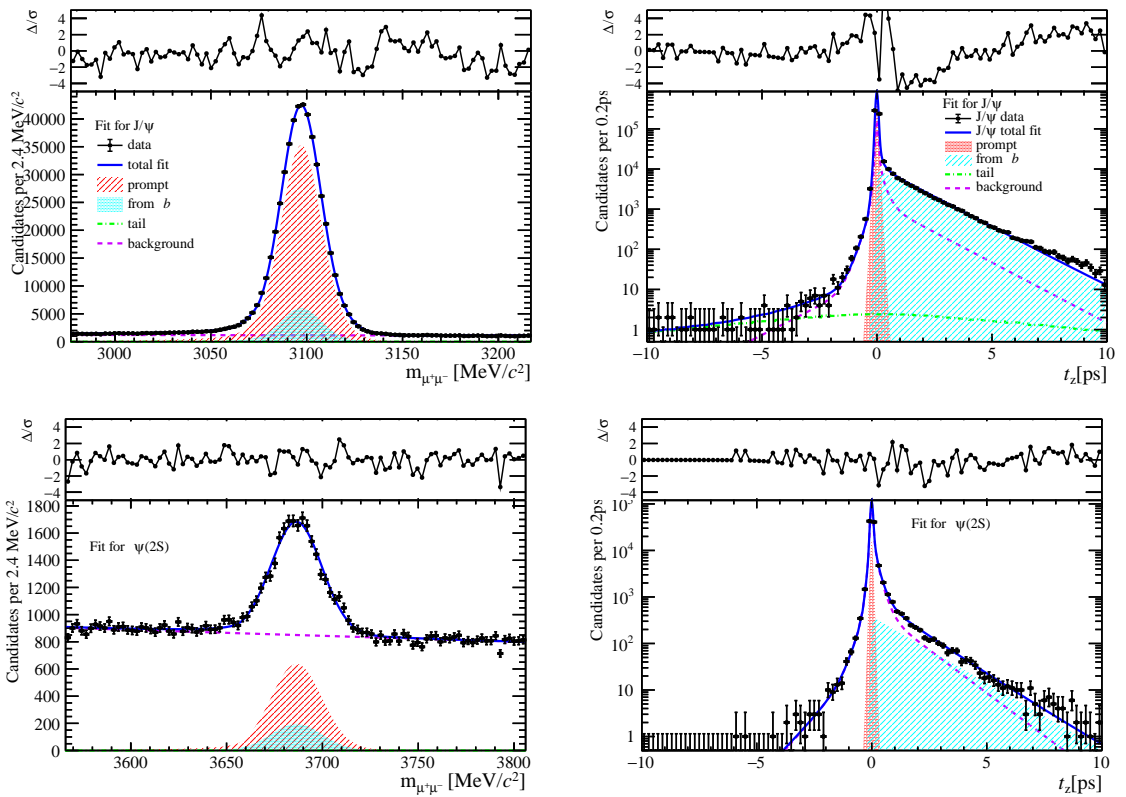


Figure 229: Fit results in  $2 \text{ GeV}/c < p_T < 4 \text{ GeV}/c$ ,  $2.0 < y < 2.8$  and  $36 \leq \text{nForwardTracks} < 48$ .

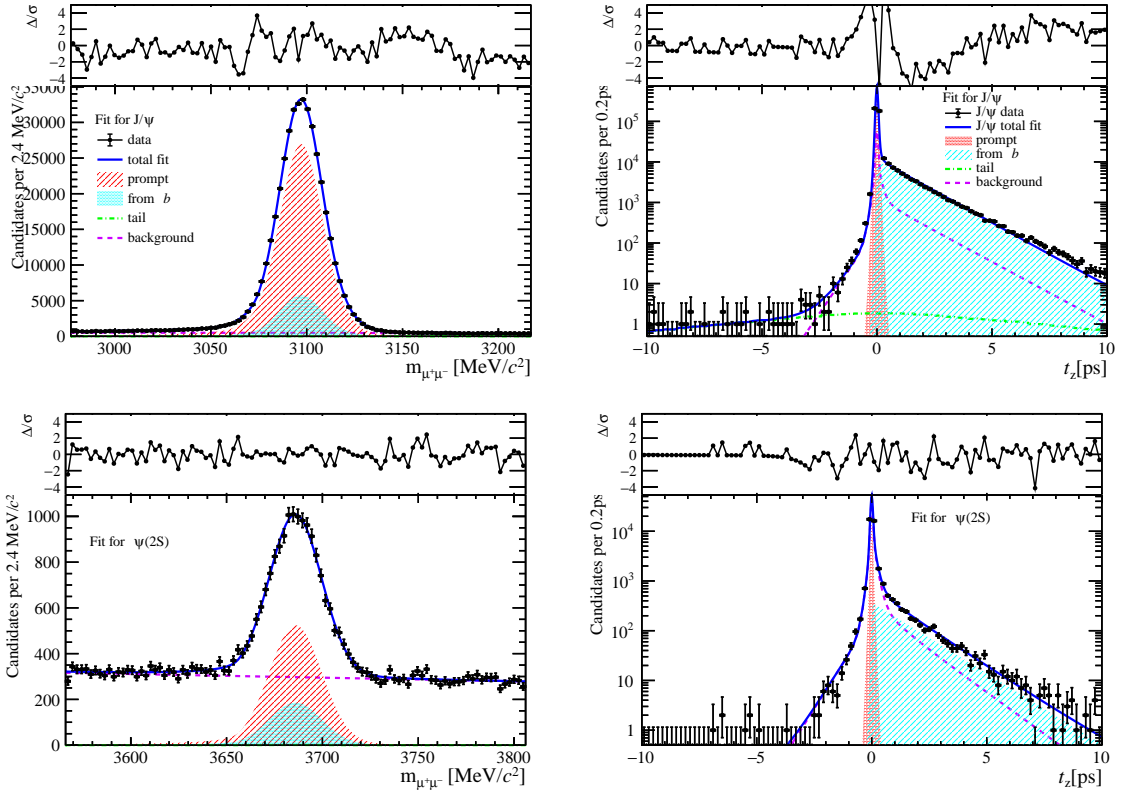


Figure 230: Fit results in  $4 \text{ GeV}/c < p_T < 6 \text{ GeV}/c$ ,  $2.0 < y < 2.8$  and  $36 \leq \text{nForwardTracks} < 48$ .

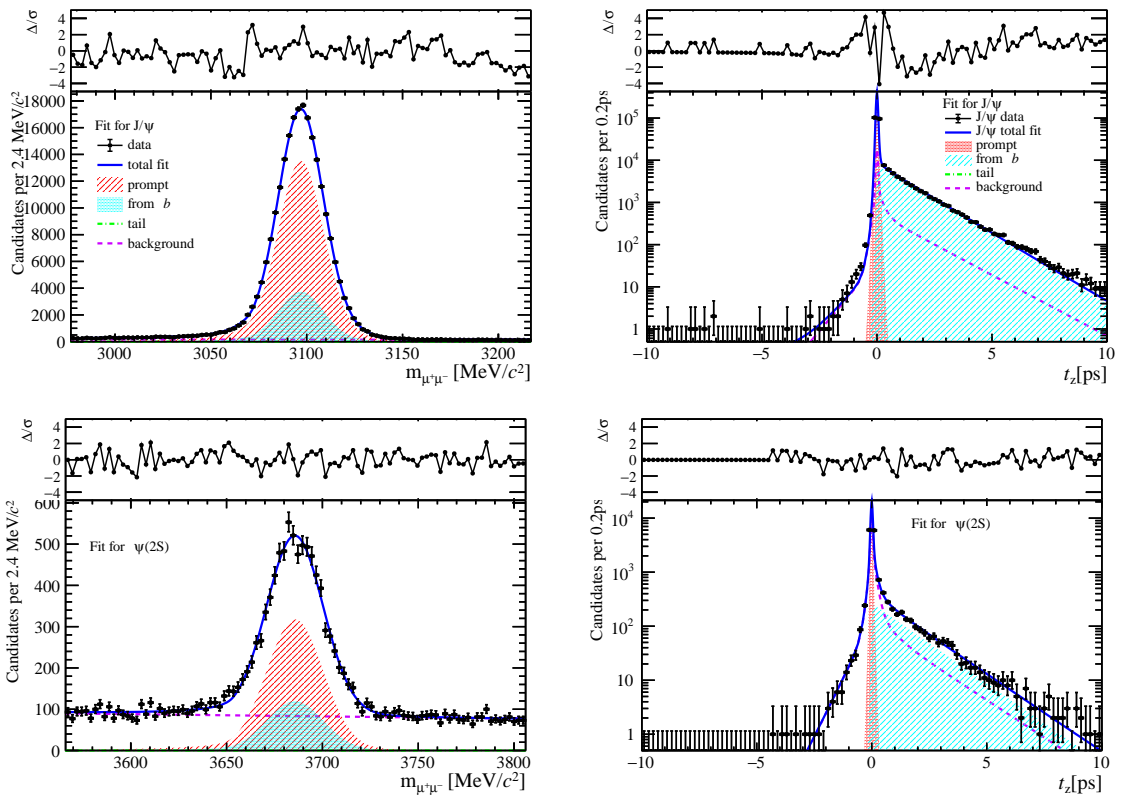


Figure 231: Fit results in  $6 \text{ GeV}/c < p_T < 8 \text{ GeV}/c$ ,  $2.0 < y < 2.8$  and  $36 \leq \text{nForwardTracks} < 48$ .

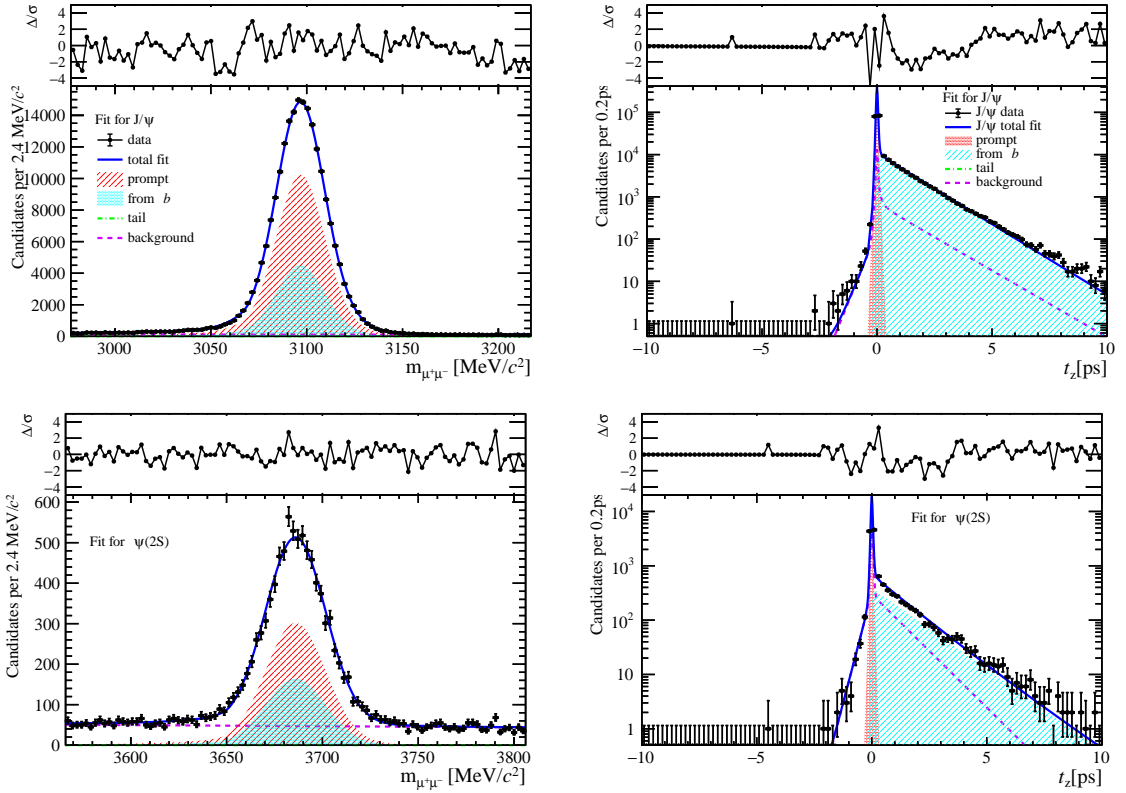


Figure 232: Fit results in  $8 \text{ GeV}/c < p_T < 20 \text{ GeV}/c$ ,  $2.0 < y < 2.8$  and  $36 \leq \text{nForwardTracks} < 48$ .

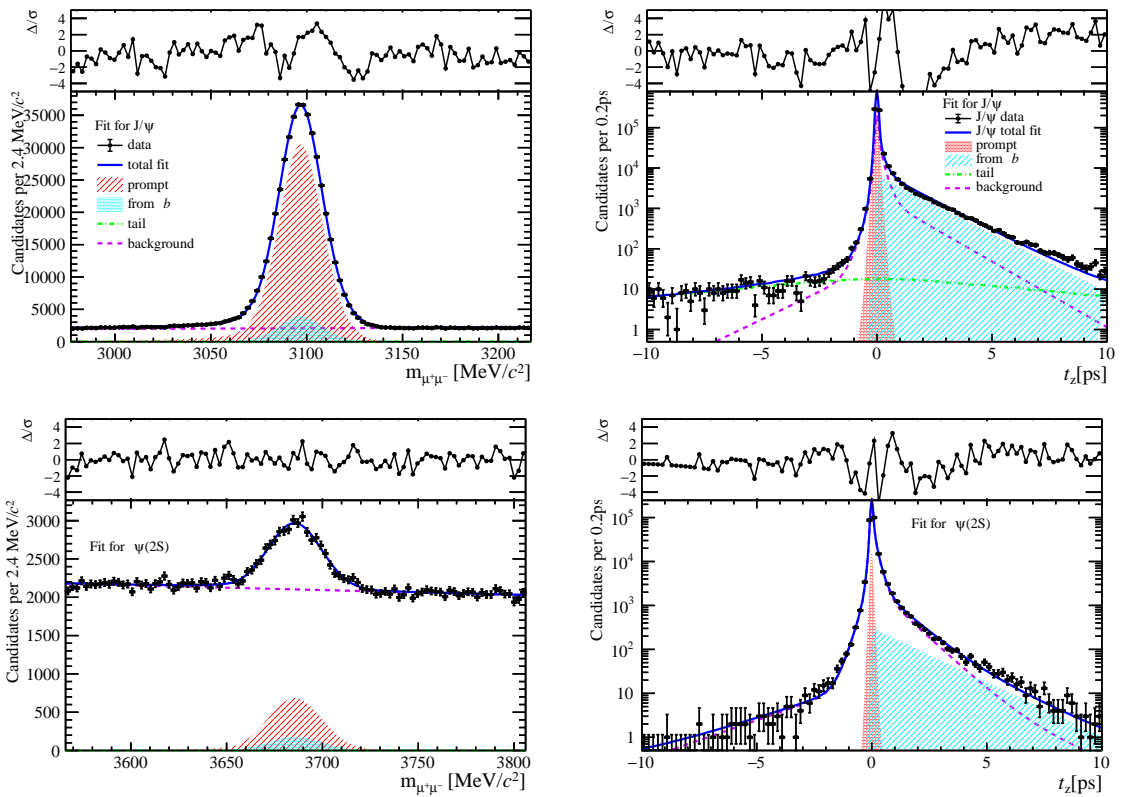


Figure 233: Fit results in  $0 \text{ GeV}/c < p_T < 2 \text{ GeV}/c$ ,  $2.8 < y < 3.5$  and  $36 \leq \text{nForwardTracks} < 48$ .

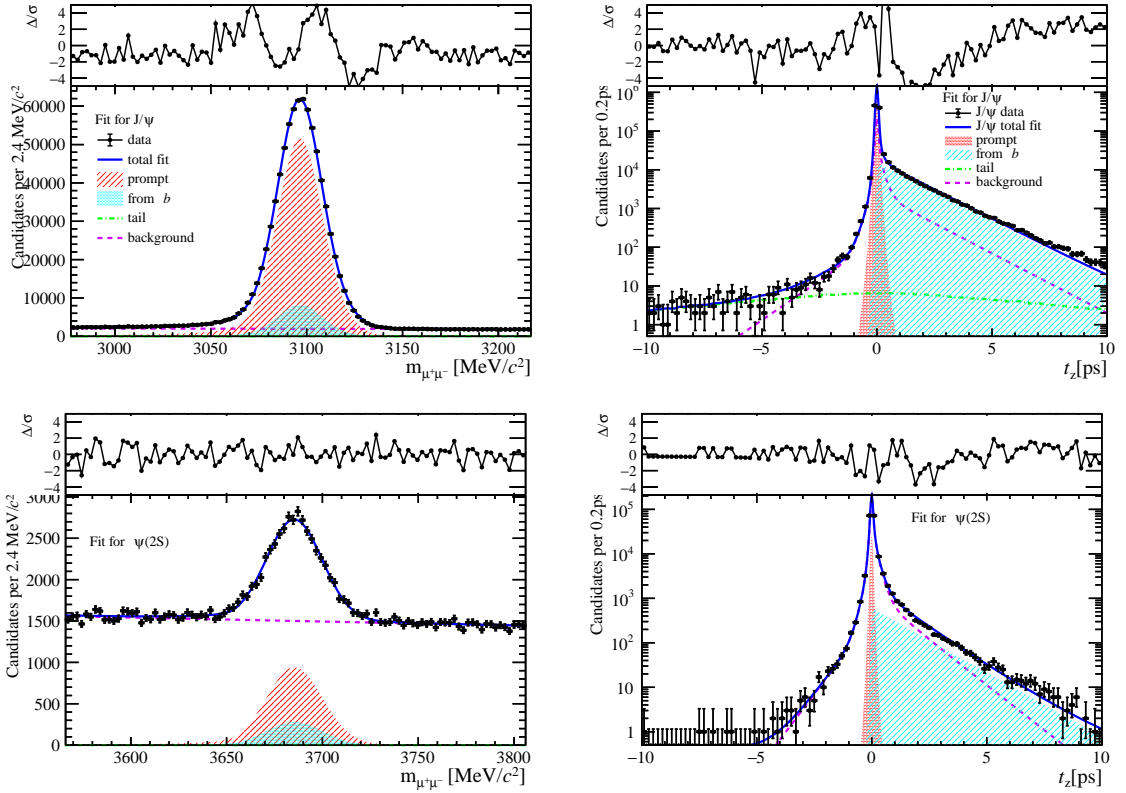


Figure 234: Fit results in  $2 \text{ GeV}/c < p_T < 4 \text{ GeV}/c$ ,  $2.8 < y < 3.5$  and  $36 \leq \text{nForwardTracks} < 48$ .

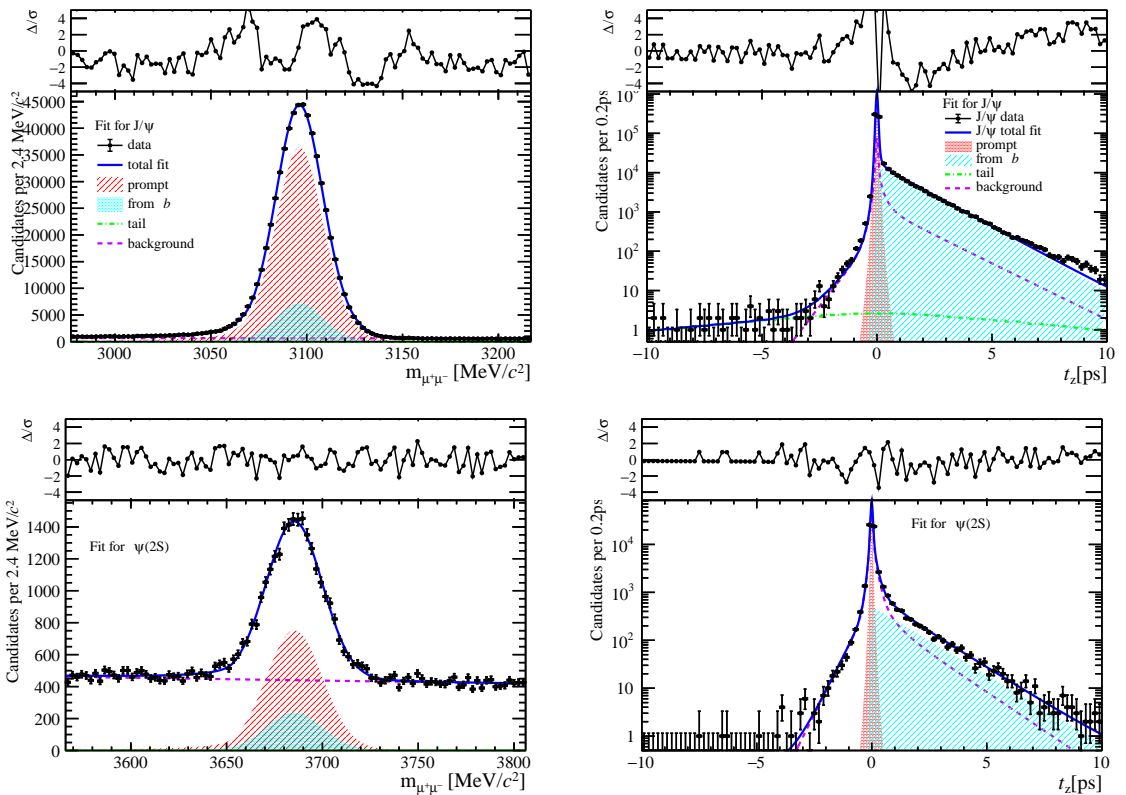


Figure 235: Fit results in  $4 \text{ GeV}/c < p_T < 6 \text{ GeV}/c$ ,  $2.8 < y < 3.5$  and  $36 \leq \text{nForwardTracks} < 48$ .

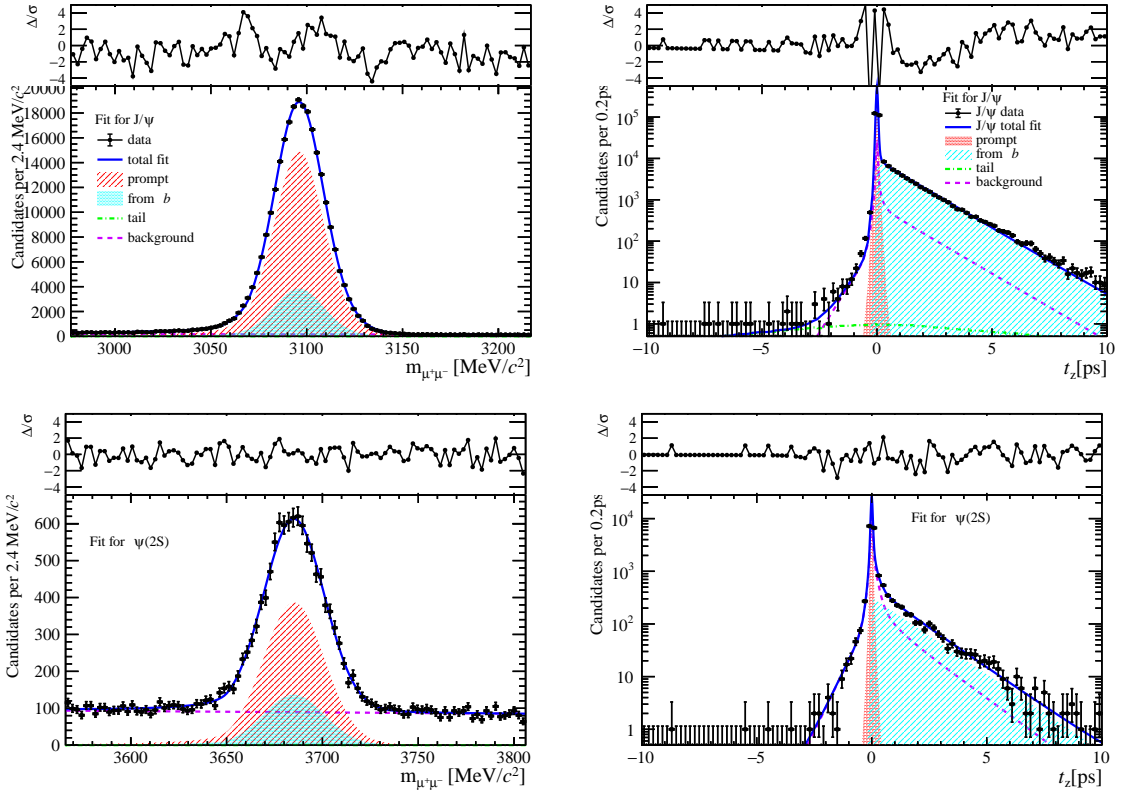


Figure 236: Fit results in  $6 \text{ GeV}/c < p_T < 8 \text{ GeV}/c$ ,  $2.8 < y < 3.5$  and  $36 \leq \text{nForwardTracks} < 48$ .

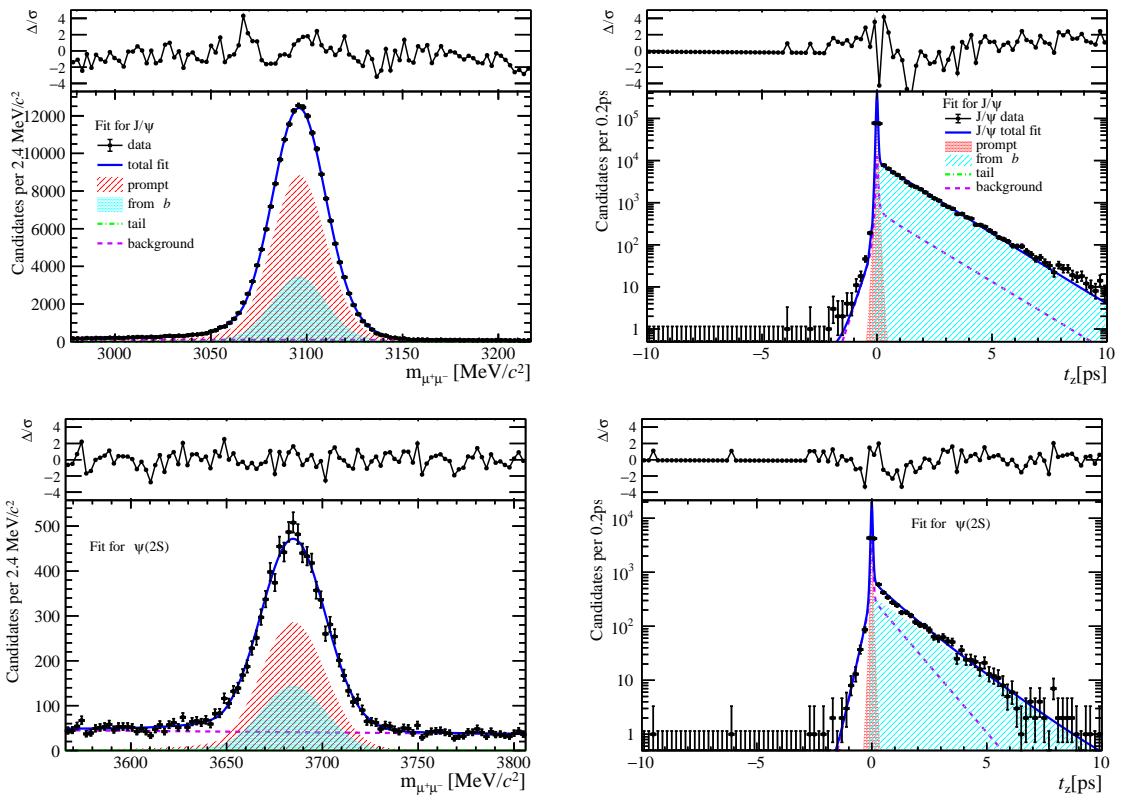


Figure 237: Fit results in  $8 \text{ GeV}/c < p_T < 20 \text{ GeV}/c$ ,  $2.8 < y < 3.5$  and  $36 \leq \text{nForwardTracks} < 48$ .

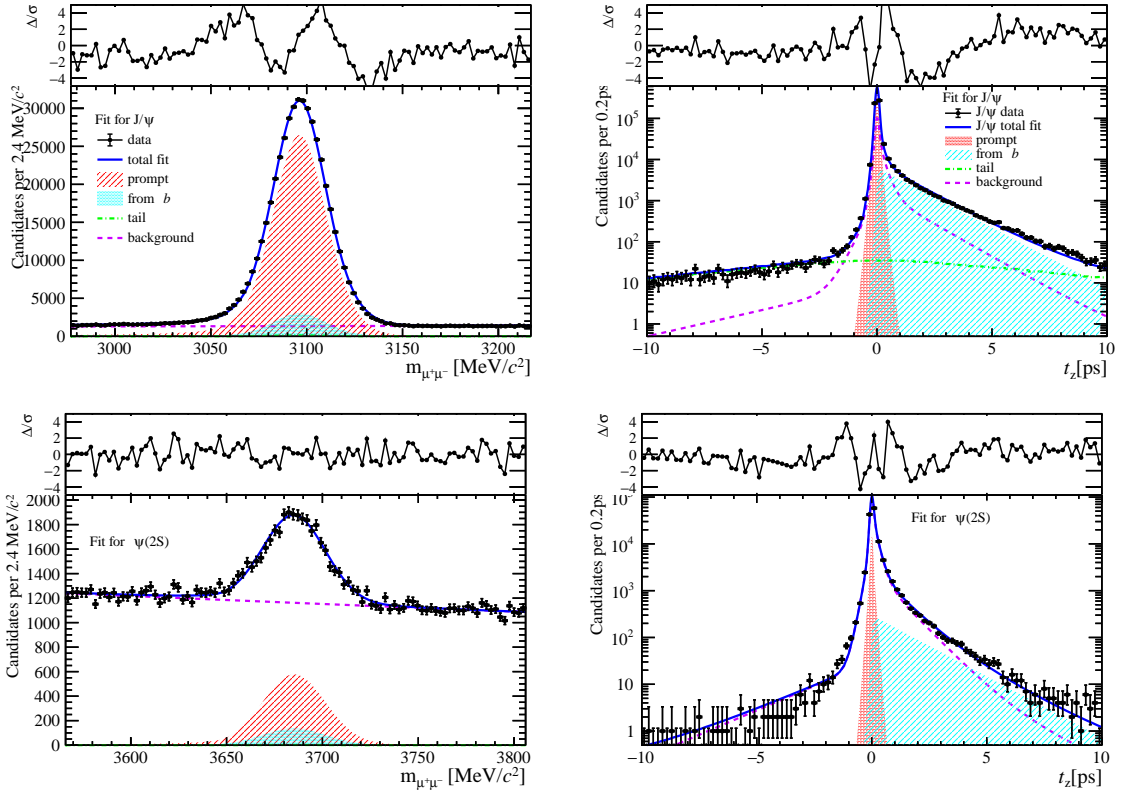


Figure 238: Fit results in  $0 \text{ GeV}/c < p_T < 2 \text{ GeV}/c$ ,  $3.5 < y < 4.5$  and  $36 \leq \text{nForwardTracks} < 48$ .

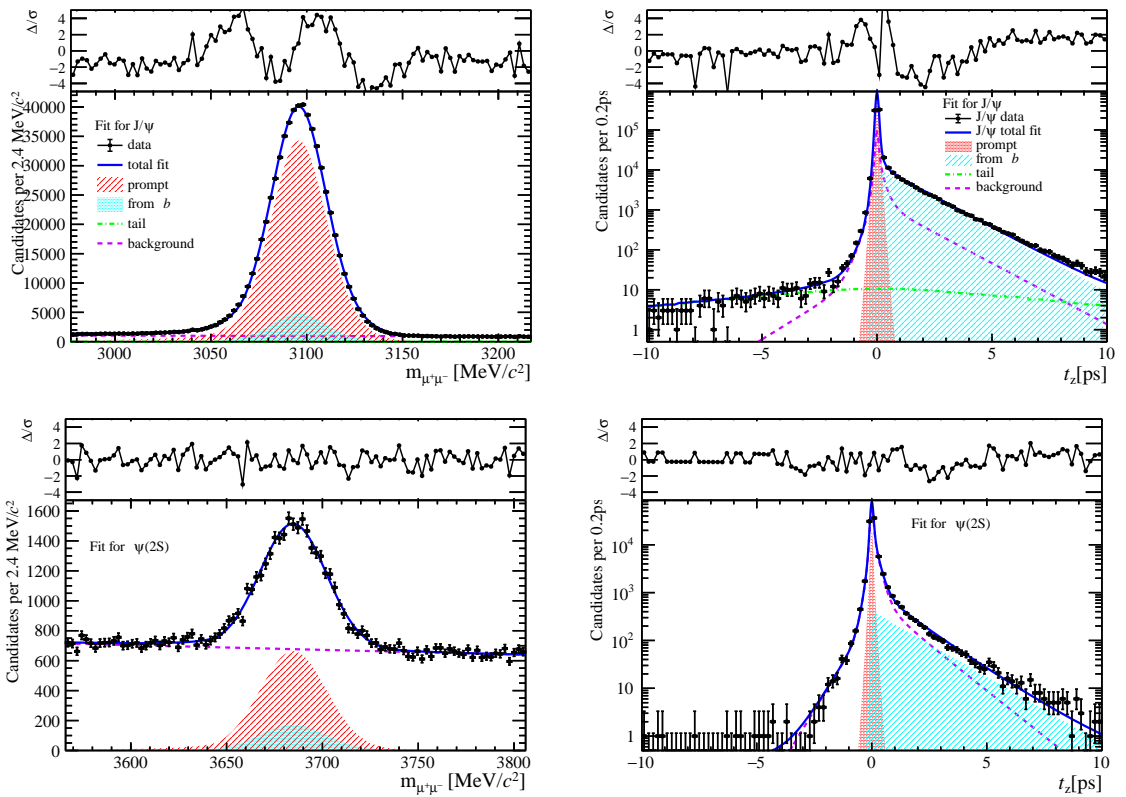


Figure 239: Fit results in  $2 \text{ GeV}/c < p_T < 4 \text{ GeV}/c$ ,  $3.5 < y < 4.5$  and  $36 \leq \text{nForwardTracks} < 48$ .

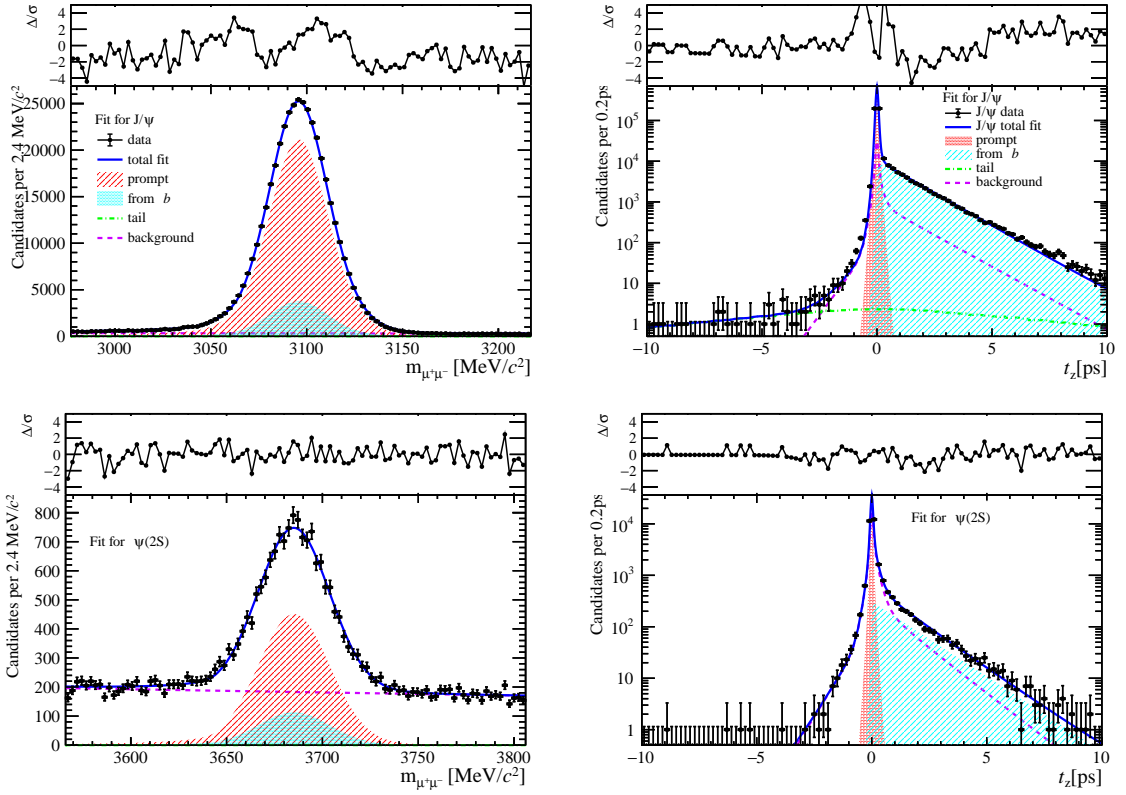


Figure 240: Fit results in  $4 \text{ GeV}/c < p_T < 6 \text{ GeV}/c$ ,  $3.5 < y < 4.5$  and  $36 \leq \text{nForwardTracks} < 48$ .

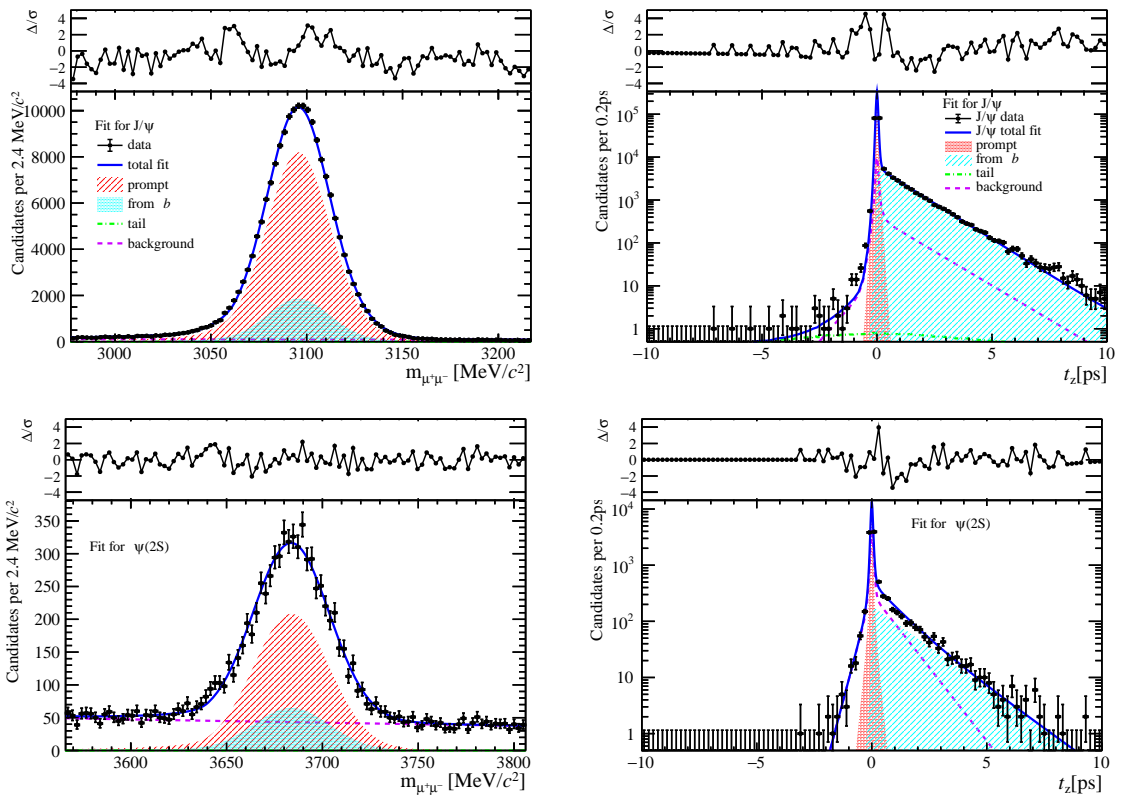


Figure 241: Fit results in  $6 \text{ GeV}/c < p_T < 8 \text{ GeV}/c$ ,  $3.5 < y < 4.5$  and  $36 \leq \text{nForwardTracks} < 48$ .

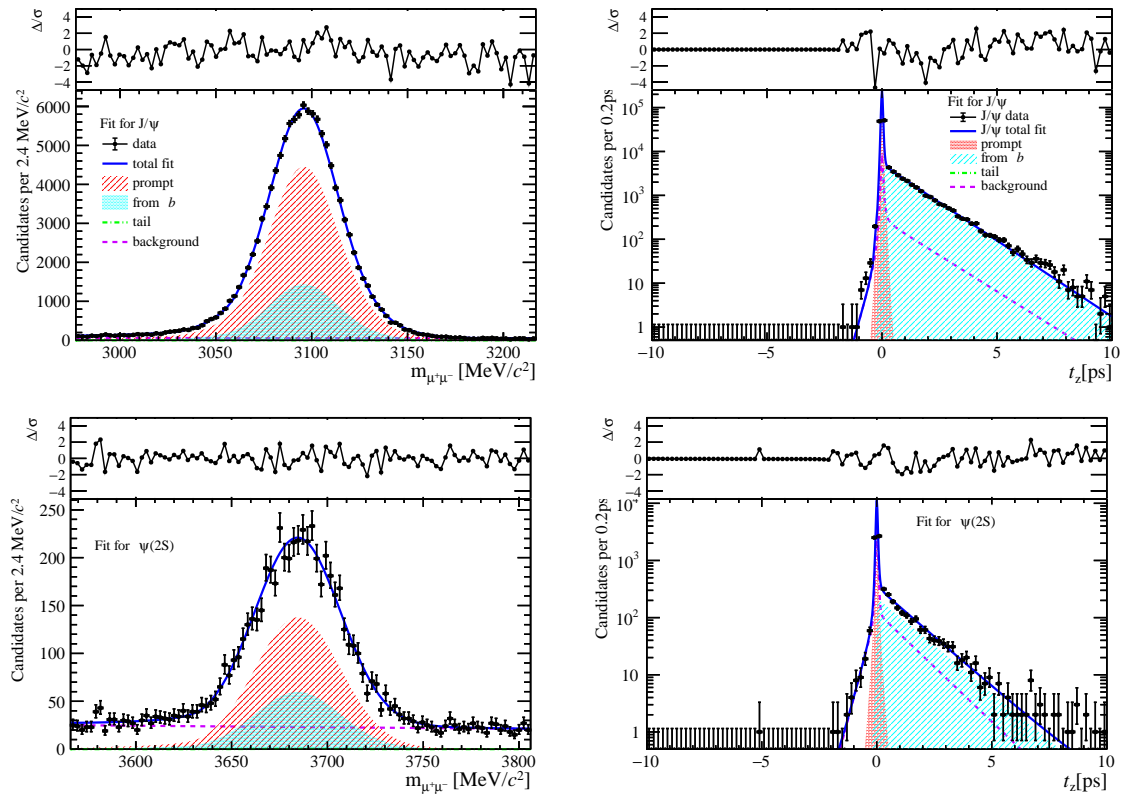


Figure 242: Fit results in  $8 \text{ GeV}/c < p_T < 20 \text{ GeV}/c$ ,  $3.5 < y < 4.5$  and  $36 \leq \text{nForwardTracks} < 48$ .

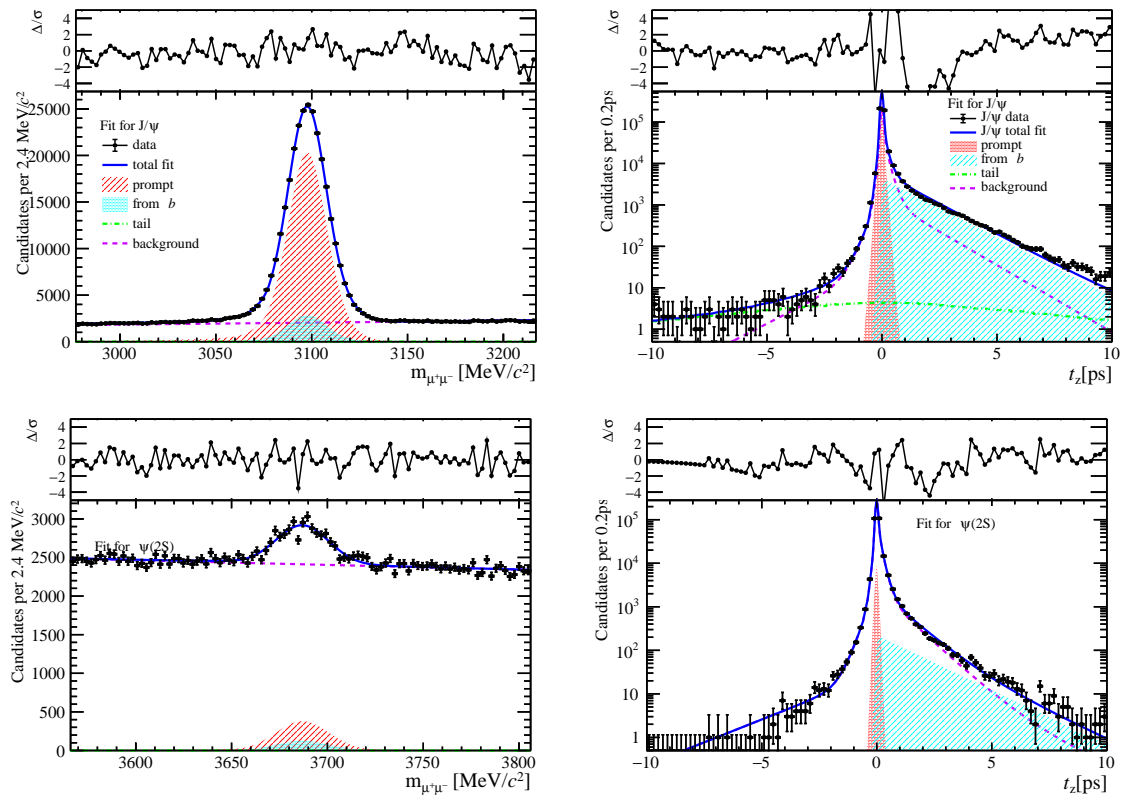


Figure 243: Fit results in  $0 \text{ GeV}/c < p_T < 2 \text{ GeV}/c$ ,  $2.0 < y < 2.8$  and  $48 \leq \text{nForwardTracks} < 130$ .

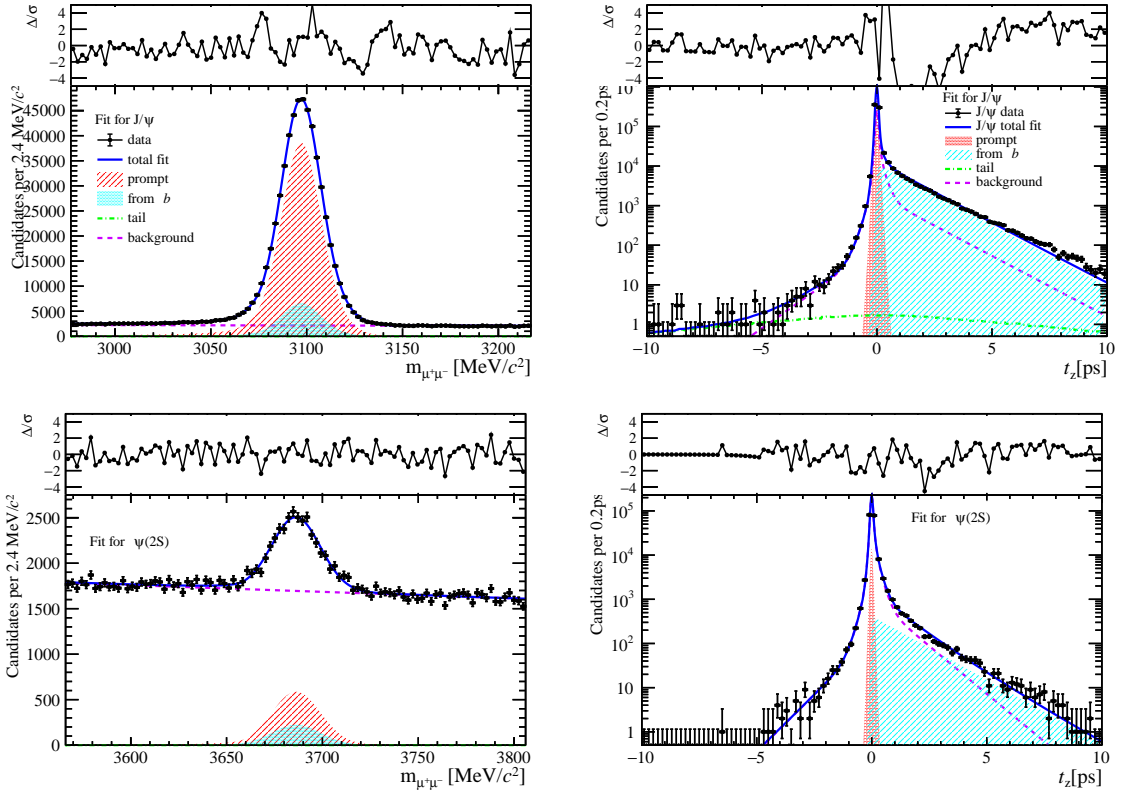


Figure 244: Fit results in  $2 \text{ GeV}/c < p_T < 4 \text{ GeV}/c$ ,  $2.0 < y < 2.8$  and  $48 \leq \text{nForwardTracks} < 130$ .

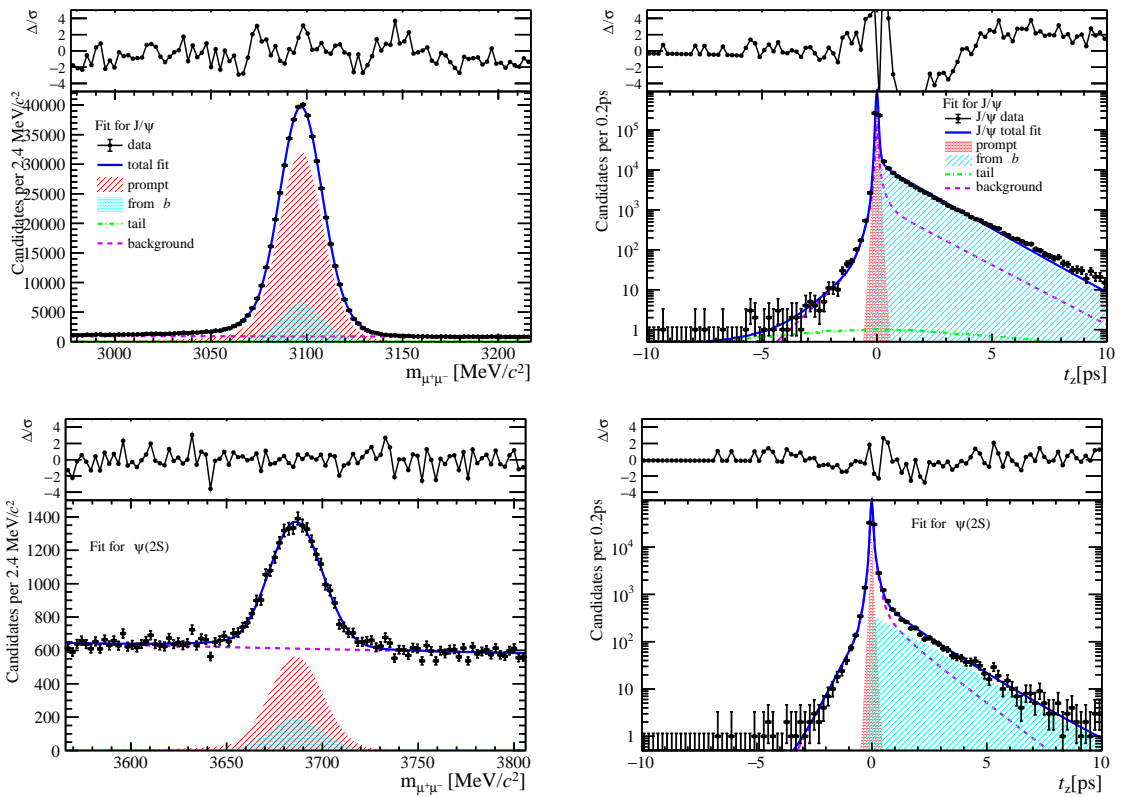


Figure 245: Fit results in  $4 \text{ GeV}/c < p_T < 6 \text{ GeV}/c$ ,  $2.0 < y < 2.8$  and  $48 \leq \text{nForwardTracks} < 130$ .

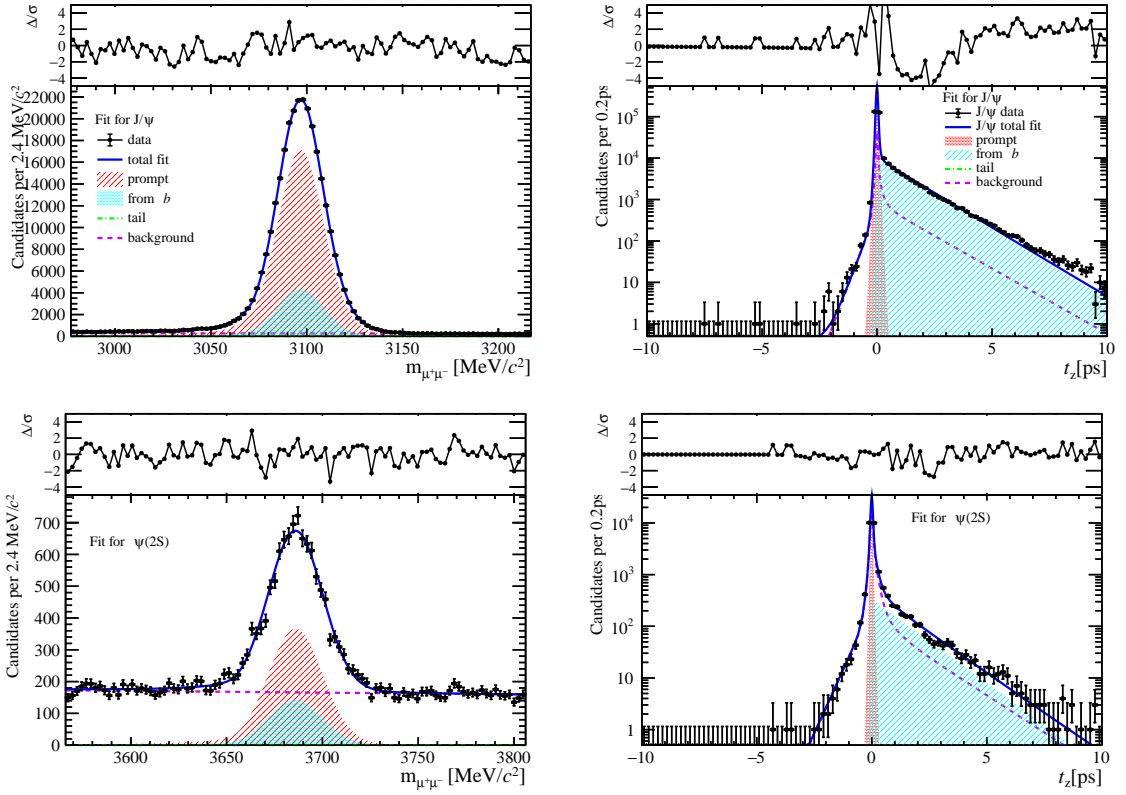


Figure 246: Fit results in  $6 \text{ GeV}/c < p_T < 8 \text{ GeV}/c$ ,  $2.0 < y < 2.8$  and  $48 \leq \text{nForwardTracks} < 130$ .

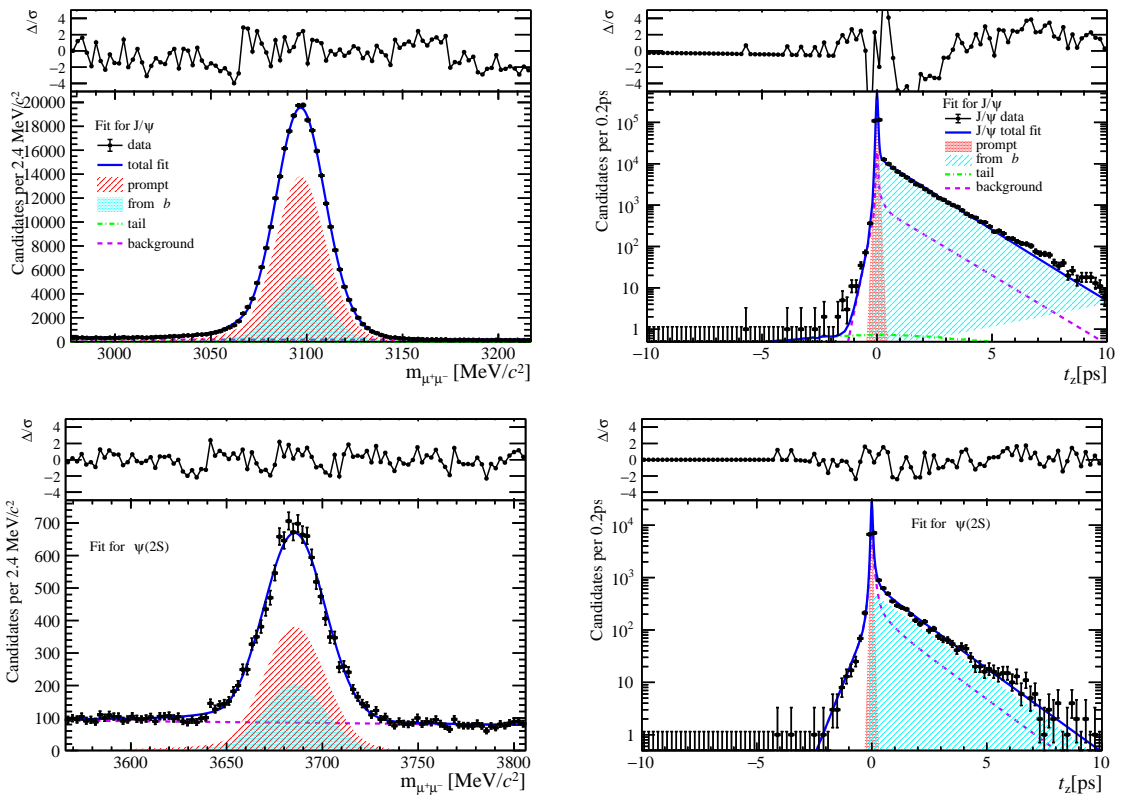


Figure 247: Fit results in  $8 \text{ GeV}/c < p_T < 20 \text{ GeV}/c$ ,  $2.0 < y < 2.8$  and  $48 \leq \text{nForwardTracks} < 130$ .

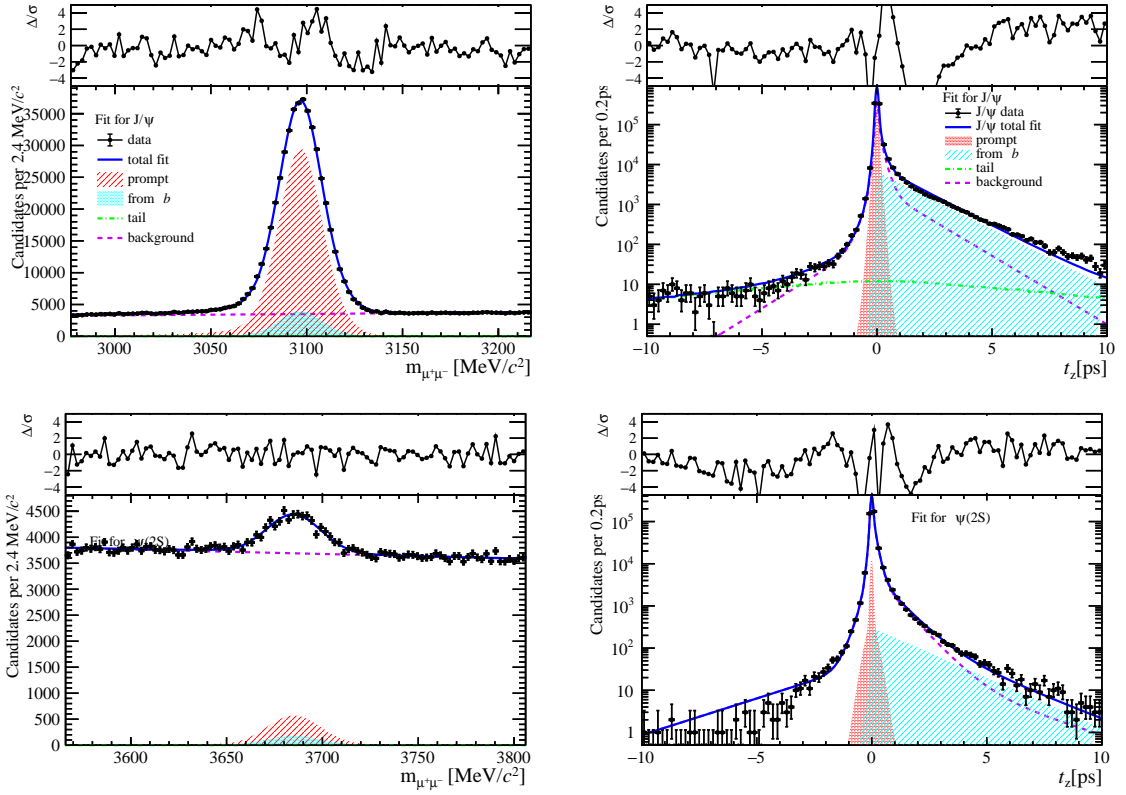


Figure 248: Fit results in  $0 \text{ GeV}/c < p_T < 2 \text{ GeV}/c$ ,  $2.8 < y < 3.5$  and  $48 \leq \text{nForwardTracks} < 130$ .

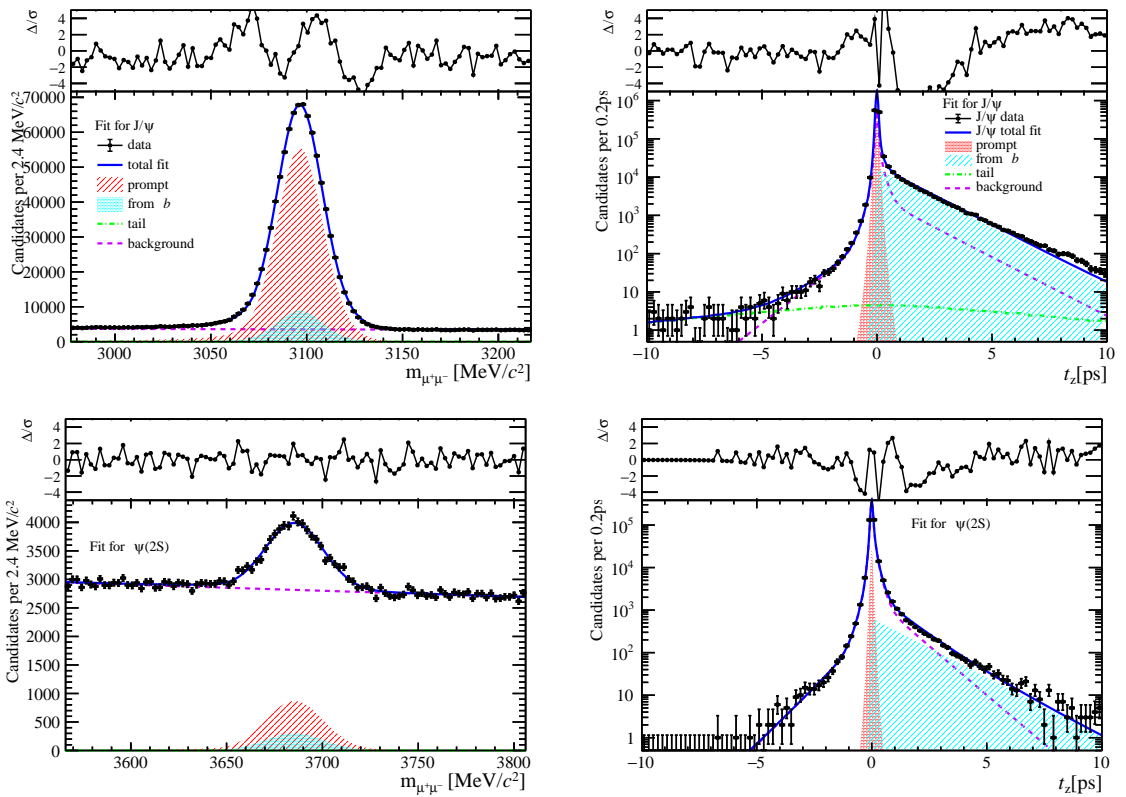


Figure 249: Fit results in  $2 \text{ GeV}/c < p_T < 4 \text{ GeV}/c$ ,  $2.8 < y < 3.5$  and  $48 \leq \text{nForwardTracks} < 130$ .

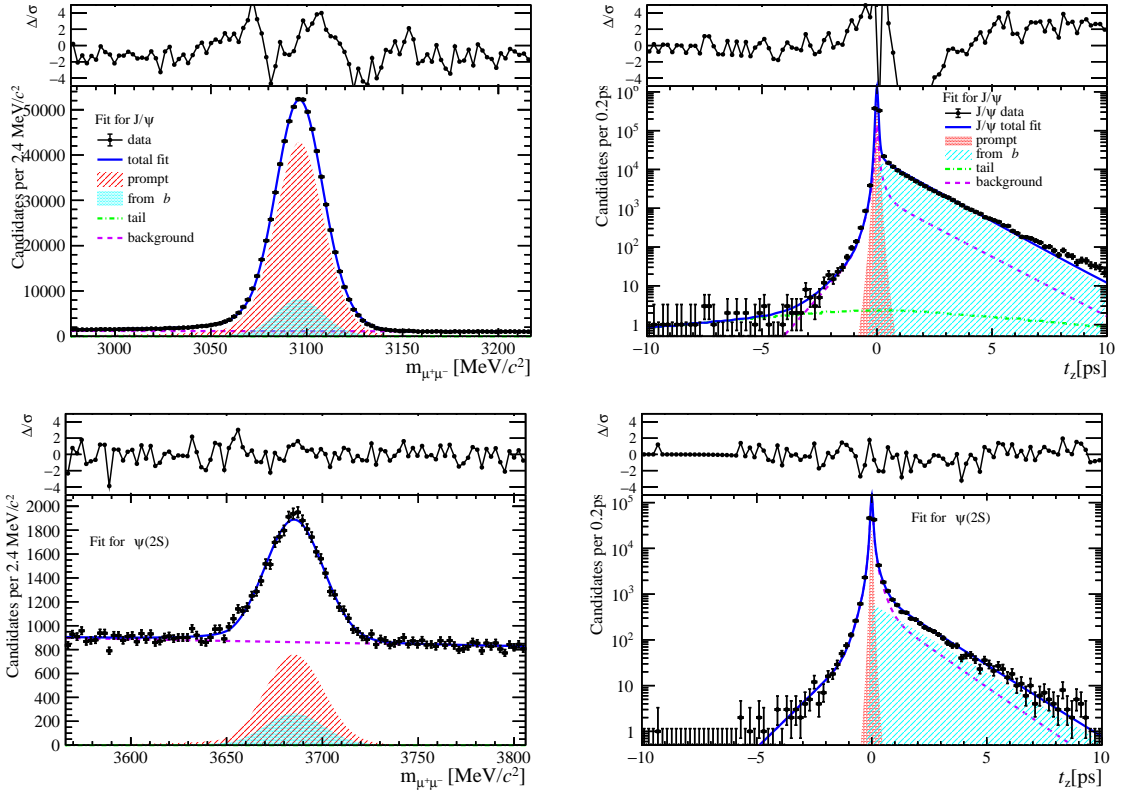


Figure 250: Fit results in  $4 \text{ GeV}/c < p_T < 6 \text{ GeV}/c$ ,  $2.8 < y < 3.5$  and  $48 \leq \text{nForwardTracks} < 130$ .

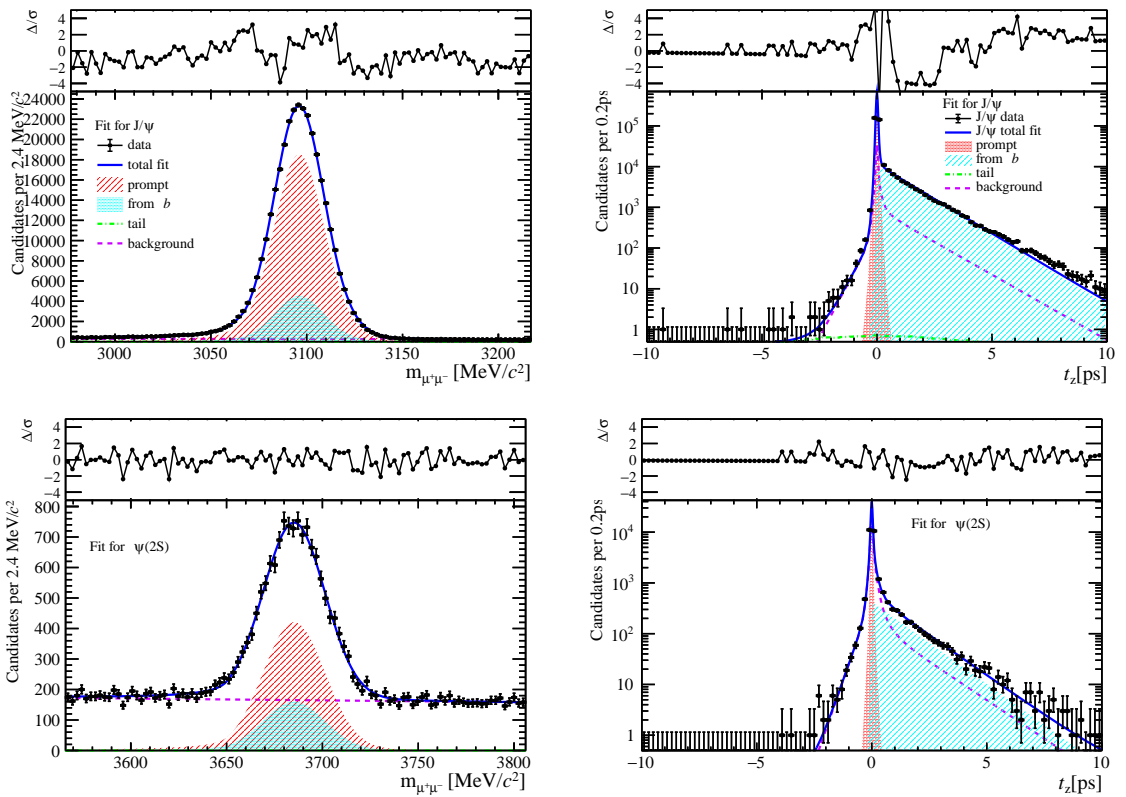


Figure 251: Fit results in  $6 \text{ GeV}/c < p_T < 8 \text{ GeV}/c$ ,  $2.8 < y < 3.5$  and  $48 \leq \text{nForwardTracks} < 130$ .

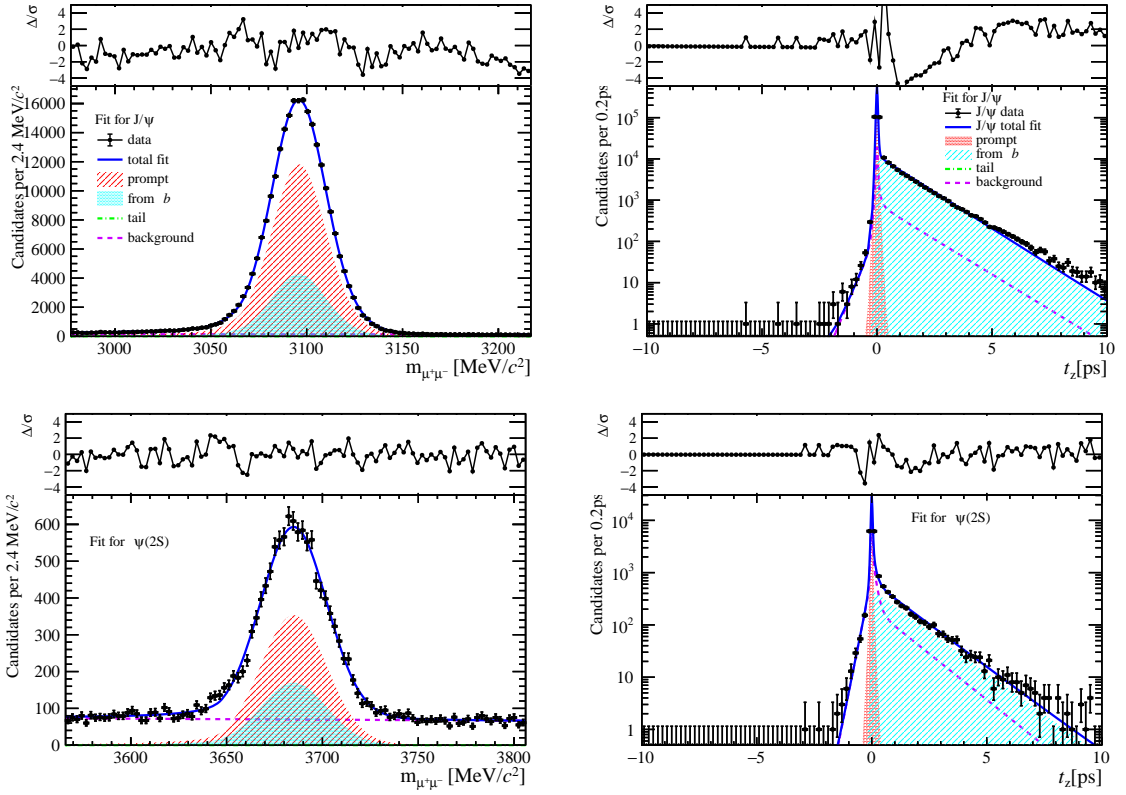


Figure 252: Fit results in  $8 \text{ GeV}/c < p_T < 20 \text{ GeV}/c$ ,  $2.8 < y < 3.5$  and  $48 \leq \text{nForwardTracks} < 130$ .

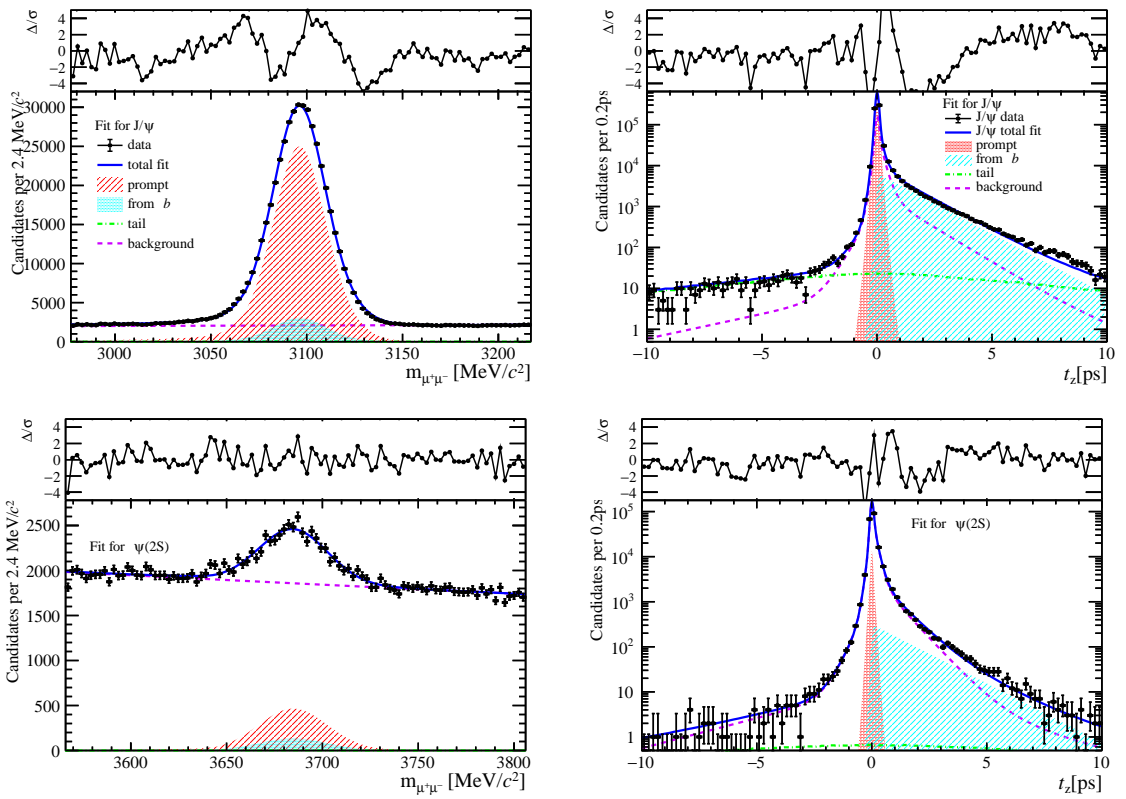


Figure 253: Fit results in  $0 \text{ GeV}/c < p_T < 2 \text{ GeV}/c$ ,  $3.5 < y < 4.5$  and  $48 \leq \text{nForwardTracks} < 130$ .

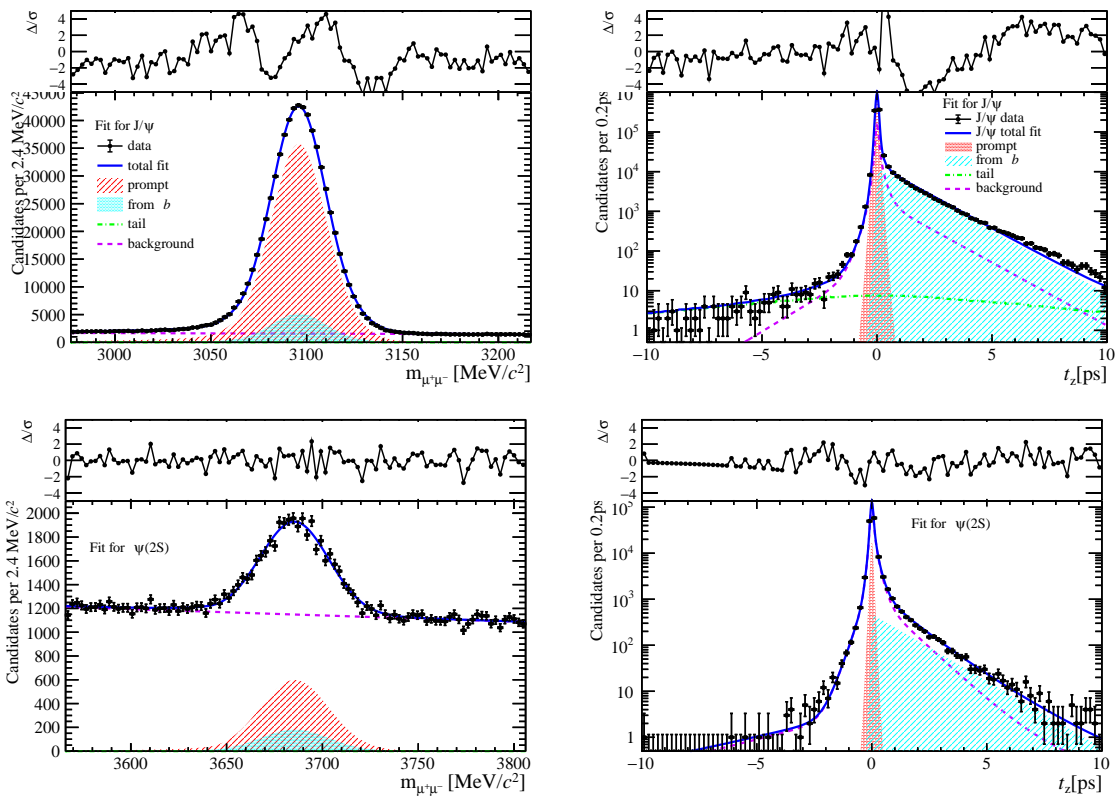


Figure 254: Fit results in  $2 \text{ GeV}/c < p_T < 4 \text{ GeV}/c$ ,  $3.5 < y < 4.5$  and  $48 \leq \text{nForwardTracks} < 130$ .

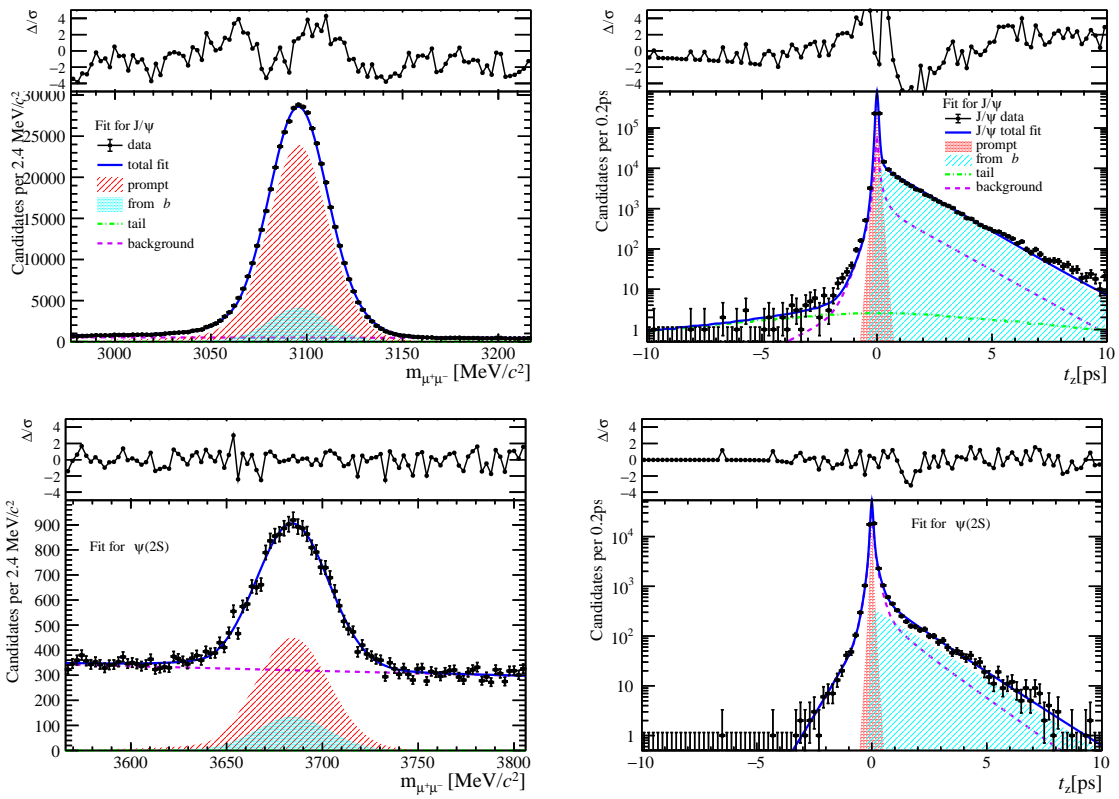


Figure 255: Fit results in  $4 \text{ GeV}/c < p_T < 6 \text{ GeV}/c$ ,  $3.5 < y < 4.5$  and  $48 \leq \text{nForwardTracks} < 130$ .

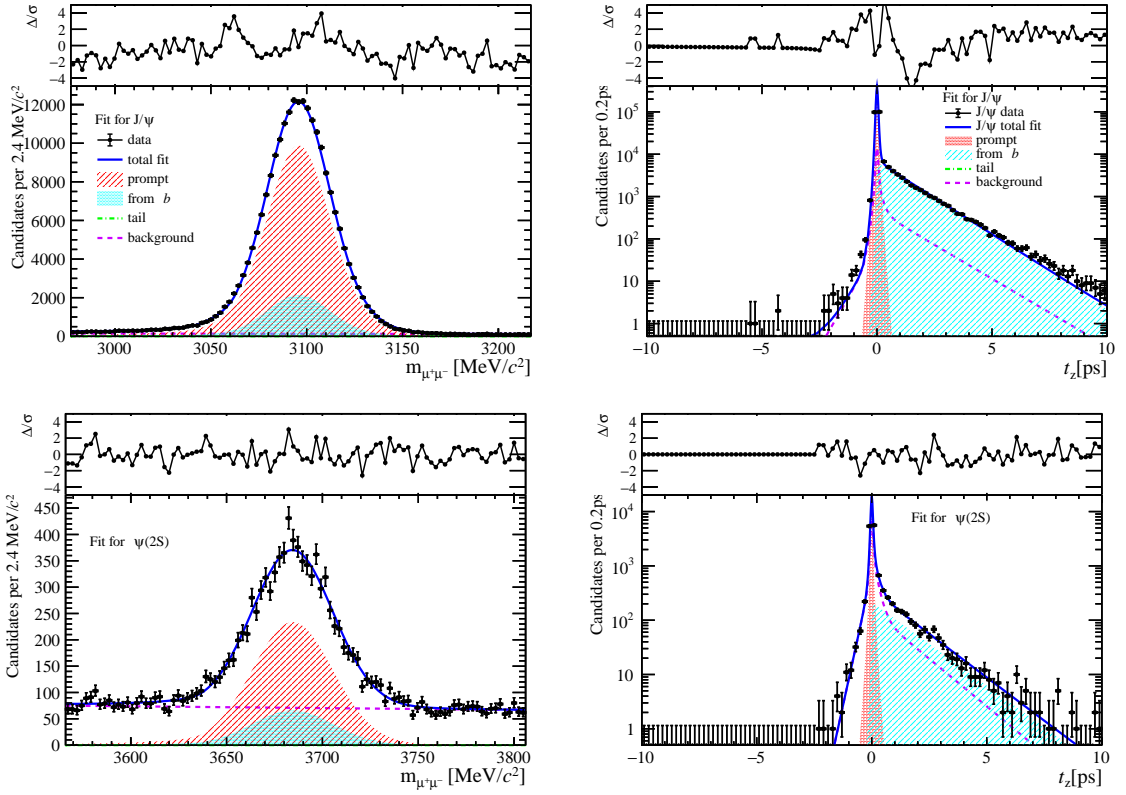


Figure 256: Fit results in  $6 \text{ GeV}/c < p_T < 8 \text{ GeV}/c$ ,  $3.5 < y < 4.5$  and  $48 \leq \text{nForwardTracks} < 130$ .

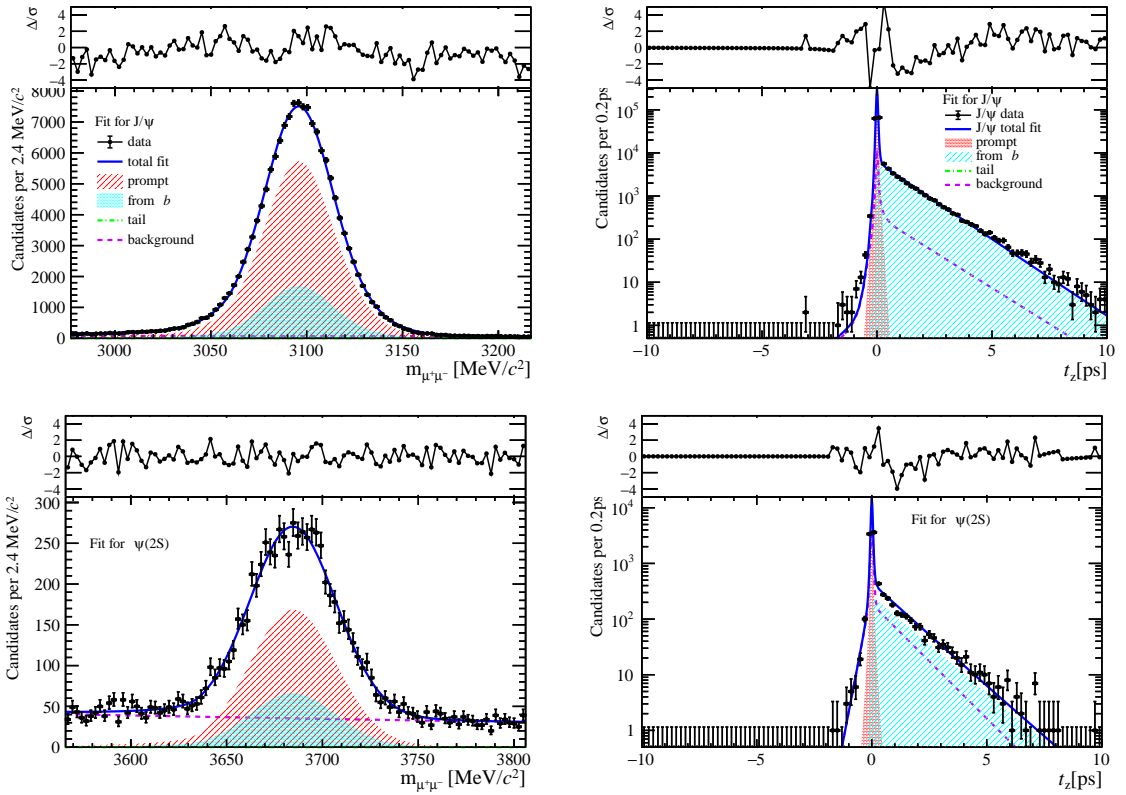


Figure 257: Fit results in  $8 \text{ GeV}/c < p_T < 20 \text{ GeV}/c$ ,  $3.5 < y < 4.5$  and  $48 \leq \text{nForwardTracks} < 130$ .

681 **References**

- 682 [1] T. Matsui and H. Satz, *J/psi suppression by quark-gluon plasma formation*, Physics  
683 Letters B **178** (1986) 416.
- 684 [2] PHENIX collaboration, A. Adare *et al.*, *Cold Nuclear Matter Effects on J/Psi as*  
685 *Constrained by Deuteron-Gold Measurements at s(NN)\*\*(1/2) = 200-GeV*, Phys. Rev.  
686 C **77** (2008) 024912, arXiv:0903.4845, [Erratum: Phys.Rev.C 79, 059901 (2009)].
- 687 [3] LHCb collaboration, R. Aaij *et al.*, *Prompt and nonprompt J/ψ production and*  
688 *nuclear modification in pPb collisions at  $\sqrt{s_{NN}} = 8.16 \text{ TeV}$* , Phys. Lett. B **774** (2017)  
689 159, arXiv:1706.07122.
- 690 [4] F. Arleo and S. Peigné, *Quarkonium suppression in heavy-ion collisions from coherent*  
691 *energy loss in cold nuclear matter*, JHEP **10** (2014) 073, arXiv:1407.5054.
- 692 [5] E. G. Ferreiro, *Charmonium dissociation and recombination at LHC: Revisiting*  
693 *comovers*, Phys. Lett. B **731** (2014) 57, arXiv:1210.3209.
- 694 [6] ALICE collaboration, J. Adam *et al.*, *Enhanced production of multi-strange*  
695 *hadrons in high-multiplicity proton-proton collisions*, Nature Phys. **13** (2017) 535,  
696 arXiv:1606.07424.
- 697 [7] CMS collaboration, V. Khachatryan *et al.*, *Evidence for collectivity in pp collisions*  
698 *at the LHC*, Phys. Lett. B **765** (2017) 193, arXiv:1606.06198.
- 699 [8] P. Ball, V. M. Braun, and A. Lenz, *Higher-twist distribution amplitudes of the K*  
700 *meson in QCD*, JHEP **05** (2006) 004, arXiv:hep-ph/0603063.
- 701 [9] LHCb collaboration, I. Belyaev *et al.*, *Handling of the generation of primary events*  
702 *in Gauss, the LHCb simulation framework*, J. Phys. Conf. Ser. **331** (2011) 032047.
- 703 [10] D. J. Lange, *The EvtGen particle decay simulation package*, Nucl. Instrum. Meth.  
704 **A462** (2001) 152.
- 705 [11] P. Golonka and Z. Was, *PHOTOS Monte Carlo: A precision tool for QED corrections*  
706 *in Z and W decays*, Eur. Phys. J. **C45** (2006) 97, arXiv:hep-ph/0506026.
- 707 [12] GEANT4 collaboration, S. Agostinelli *et al.*, *GEANT4—a simulation toolkit*, Nucl.  
708 Instrum. Meth. A **506** (2003) 250.
- 709 [13] LHCb collaboration, M. Clemencic *et al.*, *The LHCb simulation application, Gauss:*  
710 *Design, evolution and experience*, J. Phys. Conf. Ser. **331** (2011) 032023.
- 711 [14] M. Bargiotti and V. Vagnoni, *Heavy quarkonia sector in PYTHIA 6.324: Tuning,*  
712 *validation and perspectives at LHCb*.
- 713 [15] Particle Data Group, R. L. Workman and Others, *Review of Particle Physics*, PTEP  
714 **2022** (2022) 083C01.
- 715 [16] LHCb collaboration, *Evidence for modification of b quark hadronization in high-*  
716 *multiplicity pp collisions at  $\sqrt{s} = 13 \text{ TeV}$* , arXiv:2204.13042.

- 717 [17] Z. Koba, H. B. Nielsen, and P. Olesen, *Scaling of multiplicity distributions in high-*  
718 *energy hadron collisions*, Nucl. Phys. B **40** (1972) 317.
- 719 [18] LHCb collaboration, R. Aaij *et al.*, *Measurement of forward  $J/\psi$  production cross-*  
720 *sections in  $pp$  collisions at  $\sqrt{s} = 13\text{ TeV}$* , JHEP **10** (2015) 172, Erratum *ibid.* **05**  
721 (2017) 063, [arXiv:1509.00771](https://arxiv.org/abs/1509.00771).
- 722 [19] LHCb collaboration, R. Aaij *et al.*, *Measurement of  $\psi(2S)$  production cross-sections*  
723 *in proton-proton collisions at  $\sqrt{s} = 7$  and  $13\text{ TeV}$* , Eur. Phys. J. C **80** (2020) 185,  
724 [arXiv:1908.03099](https://arxiv.org/abs/1908.03099).
- 725 [20] T. Skwarnicki, *A study of the radiative cascade transitions between the Upsilon-prime*  
726 *and Upsilon resonances*, PhD thesis, Institute of Nuclear Physics, Krakow, 1986,  
727 DESY-F31-86-02.
- 728 [21] J. Lefrancous, *Crystal ball fits*, [link](#).
- 729 [22] LHCb collaboration, R. Aaij *et al.*, *Measurement of the track reconstruction efficiency*  
730 *at LHCb*, JINST **10** (2015) P02007, [arXiv:1408.1251](https://arxiv.org/abs/1408.1251).
- 731 [23] *Tracking correction table*, <https://twiki.cern.ch/twiki/bin/view/LHCb/LHCbTrackingEfficiencies>.